Universidad de **Valladolid**

ESCUELA DE INGENIERÍAS INDUSTRIALES

DPTO. INGENIERÍA ENERGÉTICA Y FLUIDOMECÁNICA

PhD THESIS:

DEVELOPMENT OF AN ADVANCED TECHNIQUE BASED ON ACOUSTIC RESONANCE IN GASES FOR DETERMINING RELEVANT THERMODYNAMIC CONSTANTS AND PROPERTIES

Submitted by

FERNANDO JOSÉ PÉREZ SANZ

For the Partial Fulfilment of a Doctorate in Philosophy by the

University of Valladolid

Directed by:

Dr. JOSÉ JUAN SEGOVIA PURAS

Dra. MARÍA DEL CARMEN MARTÍN GONZALEZ

Valladolid, October 2014

“To measure is to know if you cannot measure it you cannot improve it”

Lord Kelvin

“It is not easy to be green”

Kermit the frog

Acknowledgements

The author wants to thank for the help on this thesis to:

José Juan Segovia Puras and María del Carmen Martín Gonzalez for helping me and guiding me, when doing the experimentation and the writing, also they were very helpful inside and outside of the working place.

All the colleagues In Termocal facilities, who are always willing to help, give a new point of view or idea and take a coffee break.

Roberto Gavioso from INRiM, for all the help during my stay in Torino. He was more a friend than a boss from the beginning.

My family, I would not be here without them.

Ana, for supporting me all this time.

For last to the Spanish Economy Ministry for provide the funding for this study.

Table of contents

NOMENCLATURE

ABBREVIATIONS

BAAS	British Association for the Advancement of Science
BIMP	Bureau International des Poids et Measures
BS	Bureau of Standards
CCT	Consultative Committee on Thermometry
CEM	Centro Español de Metrología
CGPM	Conférence Générale des poids et Mesures
CIPM	Comité International des Poids et Measures
cnam	Consrvatoire national des arts et métiers
EMRP	European Metrology Research Programme
EPT	1976 Provisional 0.5 K to 30 K Temperature Scale
EURAMET	European Association of National Metrology Institutes
GERG	Groupe Européen de Recherché Gaziéres
GUM	Guide to the Expression of Uncertainty in Measurement
InK	Implementing the New Kelvin
INM	Institut National de Métrologie
INRiM	Instituto Nazionale di Ricerca in Metrologia
IPTS	International Practical Temperature Scale
ITS	International Temperature Scale
JRP	Joint Research Project
LNE	Laboratoire Nationale de Métrologie et d'essais
NIST	National Institute of Standards and Technology
NPL	National Physical Laboratory
PRMI	Physicotechnical and Radiotechnical Measurements Institute
PTB	Physikalish-Technische Bundesanstalt
Termocal	Termodinámica y Calibración

SYMBOLS

a	Resonator Internal Radius, m
A_0	First Acoustic Virial Equation Coefficient, $m^2 \cdot s^{-2}$
A_1	Second Acoustic Virial Equation Coefficient, $m^2 \cdot s^{-2} Pa^{-1}$
A_2	Third Acoustic Virial Equation Coefficient, $m^2 \cdot s^{-2} Pa^{-2}$
Ag	Silver
$a_{T_{exp}P_{exp}}$	Resonator internal radius at experimental temperature and pressure, m
$a_{T_0P_0}$	Resonator internal radius at T=273.16K and specified pressure, m
Au	Gold
b	Resonator External radius, m
c	Speed of light, $m \cdot s^{-1}$
CO_2	Carbon Dioxide
C_P	Isobaric Heat Capacity, $J \cdot mol^{-1} k^{-1}$
C_V	Isochoric Heat Capacity, $J \cdot mol^{-1} k^{-1}$
D_{th}	Thermal Diffusivity, $m^2 s^{-1}$
D_v	Kinematic Viscosity, $m^2 s^{-1}$
E	Energy, J
	Young modulus, Pa
f_{breath}	Frequency of the radially-symmetric resonance of the empty spherical shell, Hz
f_{lm}	Frequency of resonance for mode lm, Hz
Δf_{lm}	Sum of frequency corrections, Hz
Δf^{skin}	Finite conductivity frequency correction, Hz
f_{shell}	Shell motion frequency correction, Hz
f_{th}	Thermal boundary layer frequency correction, Hz
f_{tube}	Tubes frequency correction, Hz

g_{bulk}	Viscous Boundary Layer Half-Width Contribution, Hz
Δg_{lm}	Sum of theoretical half-width contribution, Hz
$-g^{skin}$	Finite conductivity half-width contribution, Hz
g_{th}	Thermal Boundary Layer Half-Width Contribution, Hz
g_{tube}	Thermal Boundary Layer Half-Width Contribution, Hz
H	Hydrogen
h	Accommodation coefficient, dimensionless
He	Helium
k_B	Boltzmann's Constant
k_{KH}	Propagation constant, m^{-1}
L	Tube length, m
l	Resonance mode indicator, dimensionless
l_{th}	Thermal accommodation length, m
M	Molar Mass, $kg \cdot mol^{-1}$
m	mass, Kg Resonance mode indicator, dimensionless
N_A	Avogadro's Number
NO_x	Nitrogen Oxides
O	Oxygen
p	Pressure, Pa
Pt	Platinum
R	Ideal gas constant
r	Pressure and temperature correction factor, dimensionless
Rh	Rhodium
r_h	Hole radius, m
ΔS	Hole surface, m^2
Sb	Antimony
SO_x	Sulphur Oxides

T	Thermodynamic Temperature, K
T_0	Specific temperature, K
T_{90}	Temperature according ITS-90,K
t_{90}	Temperature according ITS-90, ^{o}C
T_{exp}	Experimental Temperature, K
T_{WTP}	Water Triple Point Temperature
u	Speed of sound, m·s^{-1}
$U(x)$	Expanded uncertainty of magnitude x
$u(x)$	Standard uncertaintyof magnitude x
u_{shell}	Speed of sound in resonator shell, m·s^{-1}
$u_{T_0P_0}$	Speed of sound at T=273.16K and specified pressure, m·s^{-1}
$u_{T_{exp}P_{exp}}$	Speed of sound at experimental temperature and pressure, m·s^{-1}
v	speed, m·s^{-1}
W	Resistance ratio, Ω·Ω^{-1}
X_{CO}	Carbon Monoxide Molar Fraction, mol·mol^{-1}
X_{N2}	Nitrogen Molar Fraction, mol·mol^{-1}
y_o	Specific acoustic admittance of the opening, dimensionless

GREEK SYMBOLS

α_{KH}	Kirchholff-Helmholtz absorption coefficient, m^{-1}
α_L	Thermal expansion coefficient, K^{-1}
β_a	Second Acoustic Virial Equation Coefficient, m^{3}mol^{-1}
γ	Adiabatic coefficient, dimensionless
γ_a	Third Acoustic Virial Equation Coefficient, m^{6}mol^{-2}
γ^{pg}	Adiabatic coefficient for a perfect gas, dimensionless
δ	Electromagnetic penetration length, m

δ_{shell}	Thermal Penetration Length in the resonator shell, m
δ_{th}	Thermal Penetration Length, m
δ_{v}	Viscous Penetration Length, m
ε_0	Electric permittivity in vacuum, $F \cdot m^{-1}$
ε_r	Relative electric permittivity, dimensionless
κ	Thermal Conductivity, $W \cdot m^{-1}k^{-1}$
κ_{316L}	Thermal Conductivity of the 316L steel, $W \cdot m^{-1}k^{-1}$
κ_{gas}	Thermal Conductivity of the gas, $W \cdot m^{-1}k^{-1}$
κ_T	Isothermal compressibility, Pa^{-1}
μ	Dynamic viscosity, Pa·s
μ_0	Magnetic permittivity in vacuum, $N \cdot A^{-2}$
ξ_{lm}	Eigen value for the resonance mode lm
π	Pi number,dimensionless
	Magnetic permeability, $N \cdot A^{-2}$
ρ	Density, $kg \cdot m^{-3}$ or $mol \cdot m^{-3}$
ρ_{shell}	Resonator shell density, $kg \cdot m^{-3}$
σ	Steel Poisson's ratio, dimensionless
	Electric conductivity, $\Omega^{-1}m^{-1}$

Chapter 1:

INTRODUCTION

1.1 MOTIVATION OF THE STUDY

Speed of sound determination in high and medium pressure gases using a spherical resonator is a procedure carried out to measure thermodynamic properties as ideal heat capacities of gases or gas mixtures [1], to compare equation of state deviation [1], to measure ideal gas properties, Boltzmann constant [2, 3], and other applications.

In this study, acoustic resonance is applied in two studies that have two different motivations: The new Kelvin definition and the determination of thermodynamic properties of gas mixtures.

1.1.1 New Kelvin Definition

1.1.1.1 Introduction

Units and measurements are being used by human beings since ancient times because people needed to inform others about places where collecting food, hunting expeditions, territory limits...

Those primitive units used to be related to human body, like inch, feet... or time periods related with people time cycles: seasons, moon cycles, etc. But when different populations started buying and selling products to each other they started to use common units so marketing became much easier. Therefore, people used mainly volumetric, superficial, weighty, time and space magnitudes. Temperature was not so important for ancient people. Besides they noticed temperature changes, and they used it to heat meals up with rocks that were placed close to fire, or fever in ill people. But they were subjective measurements and they did not need accurate results so they used vague temperature descriptions as “temperature of the hottest day in summer” or “the coldest day in winter”.

It was not until 1592 that Galileo made an artefact which could be used as thermometer, this apparatus was a bulb connected to a pipe tube. When the pipe is introduced in water or wine the fluid climb it up and the height it raises is proportional to the temperature difference between the air inside the bulb and the environment.

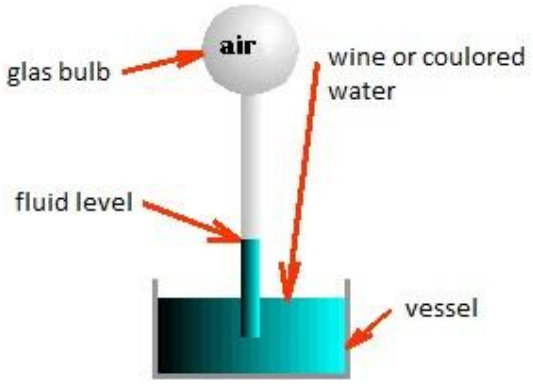

Figure 1.1 *Galileo thermometer*

The first thermometer, as it is known nowadays, was developed in 1614 by Duke of Toscana, it was a capillary closed pipe filled in with alcohol. This artefact could be made thanks to an improvement in glass production techniques. The first mercury thermometer was made by Fahrenheit in 1716, and it is just like mercury thermometers used today, a closed capillary pipe with a mercury-filled bulb.

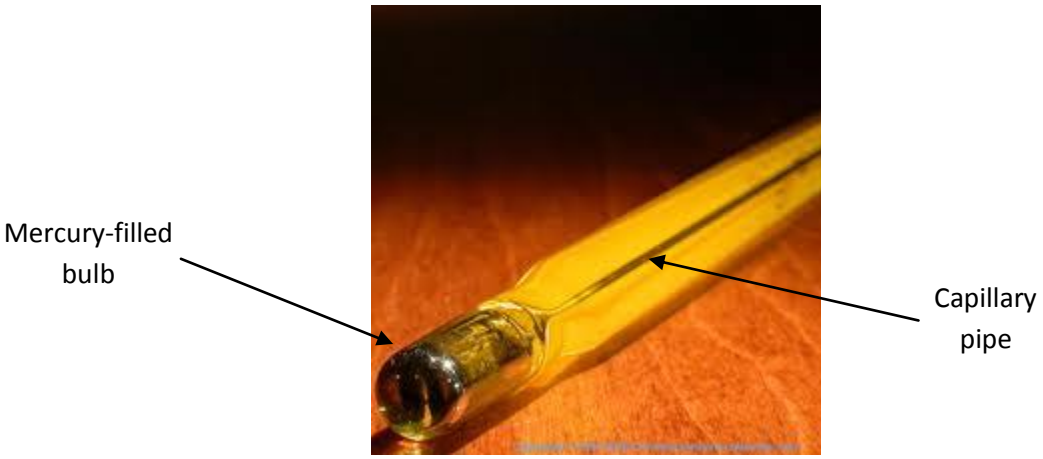

Figure 1.2 *Mercury thermometer*

Fahrenheit set fusion temperature of a common salt-water solution and human body temperature as fix points of the scale.

A Sweden scientific called Celsius set a new scale using ice melting and water boiling temperatures as fix points and he divided by one hundred the length between mercury levels.

Celsius' scale was wide used in scientific environment and was not change until 1967 when modern temperature scales started to take a form.

1.1.1.2 *Temperature Scales: From Normal Hydrogen Scale to International Temperature Scale of 1990 (ITS-90)*

Normal Hydrogen Scale

About 1878 metre prototypes were made and, with each one, two mercury-in-glass thermometers. Measurements of a few thousandths of a degree were possible using those apparatus.

Chappuis related mercury thermometers to thermodynamic temperatures using constant volume gas thermometers with hydrogen, nitrogen and carbon dioxide as working fluids. Thanks to these research Chappuis concluded that measurements better than one-hundredths of degree could be achieved[4].

After Chappuis study (1884-1887), Bureau International des Poids et Measures (BIMP) adopted Hydrogen scale for temperature measurements, this scale used freezing point and steam point of water as fix points of 0°C and 100°C respectively.

Meanwhile, Griffiths was working in Kew Observatory to measure higher temperatures using constant volume gas thermometers. Also, in collaboration with Callendar developed a platinum resistance thermometer which measured temperatures up to 600°C. They proposed sulphur boiling point (444.53°C) as a third fix point for calibration. When they finished this work in 1889 they proposed to compare platinum thermometer to Chappius' thermometer.

Chappuis in collaboration with Harker from Kew Observatory carried out the proposed comparison and he ended it in 1897. They developed a constant volume gas thermometer, using nitrogen as working gas, to reach sulphur boiling point. Chappuis and Harker determine sulphur boiling point to be 444.70°C. This result was in agreement with the one given by Griffiths and Callendar years before.

ITS-1927

Measurements of freezing and boiling points were carried out in the last years of the nineteenth century. British Association for the Advancement of Science (BAAS) set a meeting in 1899 where Callendar proposed a new scale of temperature using platinum resistances as measurement instrument. He also specified that resistances should be made using the same platinum batch to avoid differences in between apparatus. This scale used freezing and boiling point of water and boiling point of sulphur. Callendar idea was to call this scale British

Association Scale of Temperature and related constant volume gas thermometers to this scale, but BAAS did not accept Callendar's proposal.

In 1911 National Physical Laboratory (Teddington), Bureau of Standards (today known as National Institute of Standard Technology, Washington) and BIMP agreed to the initiative of Physikalish-Technische Reichanstalt (today Physikalish-Technische Bundesanstalt, Berlin) to adopt thermodynamic temperature as the International Scale of Temperature, and to use Callendar's 1899 proposal to carry out the "mise en practique".

Project of an international scale of temperature slowed down because of the World War I, but in 1923 all three laboratories involved had put into operation platinum thermometers which worked from mercury freezing point (-38°C) up to sulphur boiling point (444.5°C). It was during a visit in NPL and PTB from the BS, all three agreed to the basis of international scale. It consists in platinum resistance to the range up to 650°C calibrated at 0°C, 100°C and 444.5°C. They proposed a Pt 10%Rh/Pt thermocouple for the range from 650°C up to 1100°C using zinc, antimony, silver and gold freezing points as calibrating points. They also proposed optical pyrometry for temperatures above 1100°C.

The International Scale of Temperature of 1927 was launched, quite similar to the initial agreement but the lower limit was -193°C and the thermocouple range was adjusted by a quadratic equation with only three fix points, (Sb, Ag, and Au freezing points).

IPTS-1948

The ITS-27 was supposed to be presented and discussed at a congress in 1928, but this meeting never came out. Instead, the CIPM (Comité International des Poids et Measures, or International Committee for Weights and Measures, in English) creates the Consultative Committee on Thermometry and Calorimetry in 1937. Today the Consultative Committee on Thermometry (CCT) is taken all the initiatives about the ITS.

There were some important modifications in 1948. The extrapolation below the oxygen boiling point was removed, the junction between resistance and thermocouple range was from this moment the antimony fix point, silver point increased from 960.5ºC to 960.8ºC and they decided to finish calling the unit of temperature degree Centigrade and call it degree Celsius. The International Practical Temperature Scale of 1948 document included all this changes.

ITPS-1958

CIPM adopted a new scale based on ^{4}He vapour-liquid equilibrium, in such a way that measuring saturated vapour pressure you could determine temperature. This scale was useful for the range of 0.5 K to 5.23 K and it was known as 1958 ^{4}He Scale. Four years later a new improved scale was released using ^{3}He. The new scale was called 1962 ^{3}He Scale.

ITPS-1968

Kelvin was accepted as unit of the international thermodynamic temperature in 1954 during the 10th CGPM(Conférence Générale des poids et Mesures, General Conference on Weights and Measures), as it was suggested previously in 1948. This unit was defined as Kelvin did in 1854, using a scale between the absolute zero and the triple point of water (273.16).

The Physicotechnical and Radiotechnical Measurements Institute (PRMI), Moscow, and the NPL carried out a comparison of the platinum resistance used in the more important gas scales (NPL, PMRI, NIST and Pennsylvania State University). This comparison was made in 1961 and provided the bases scale for low temperatures.

CCT (Comité Consultatif de Thermométrie, Consultantive Committee for Thermometry) introduced the function *W* and made the "Provisional Reference Table CCT-64 of *W* against T for platinum resistance thermometers in the range 12 K to 273.15 K" in 1964. Only two years later CCT proposed the Provisional Scale 1966 including oxygen boiling point and triple point of hydrogen. Parameter W is the ratio of resistance at temperature of measurement and resistance at triple point of water temperature, this way any change suffer by the resistance should not change the W value.

Since the first meeting in 1899, thermodynamic temperature was defined in so many different ways from the International Practical Temperature that a second meeting was necessary to bring all efforts together and drive them to the same goals. In 1968 this meeting took place, they included numerical changes, designed to bring it more nearly in accord with thermodynamic temperatures, that were sufficiently large to be apparent to many users, they also resolved that the unit of temperature will be "the Kelvin" and no longer "degree Kelvin", its symbol shift from "°K" to "K" and its value was 1/273.16 the thermodynamic temperature of the triple point of water.

The new scale, IPTS-68, divided temperature in four ranges:

1. From 13.8 K to 273.15 K. The scale is defined by 6 fixed points and a reference function.
2. 0°C to 630.74°C. This range uses the Callendar equation corrected for some new values of gas thermometry.
3. 630.74°C-1064°C. Where the thermometer used must be a thermocouple Pt-10%Rh/Pt calibrated at 630.74°C and silver and gold freezing points.
4. Above 1064°C temperature is defined using Plank's law and the radiation of black bodies.

EPT-76

CIPM developed the 1976 Provisional 0.5 K to 30 K Temperature Scale (EPT-76). This scale was made to fulfil the necessities in the low temperature range (there was not a satisfactory scale for this range, but different scales used without standardization). It had 11 fix points and the text explained how to correlate the scales which were used before (IPST-68, ^{4}He-1958, ^{3}He1962, NPL1962, NBS-55) to EPT-78.

ITS-90

The current temperature scale came into effect the 1st of January of 1990.This scale establishes Kelvin as unit of temperature (as it was done before) but the definition is related by the triple point of water (273.16 K) and not any longer by water freezing point (273.15 K).

The lower limit of the ITS-90 is decreased from 13.8 K to 0.68 K. The upper limit is as high as it can be measured by radiation techniques according Plank's law.

The new scale is divided in ranges and sub-ranges to cover all temperatures, which overlap sometimes, and T_{90} is defined by two different ways for the same thermodynamic temperature. The overlapping is not a problem because definitions are made to be in agreement, and the possible difference between the values of T_{90} is negligible.

The difference between T_{90} and temperature of the systems is very low in comparison to older scales. The agreement with ITPS-68 is shown in figure 1.3. ITS-90 also improves continuity and precision on measurements.

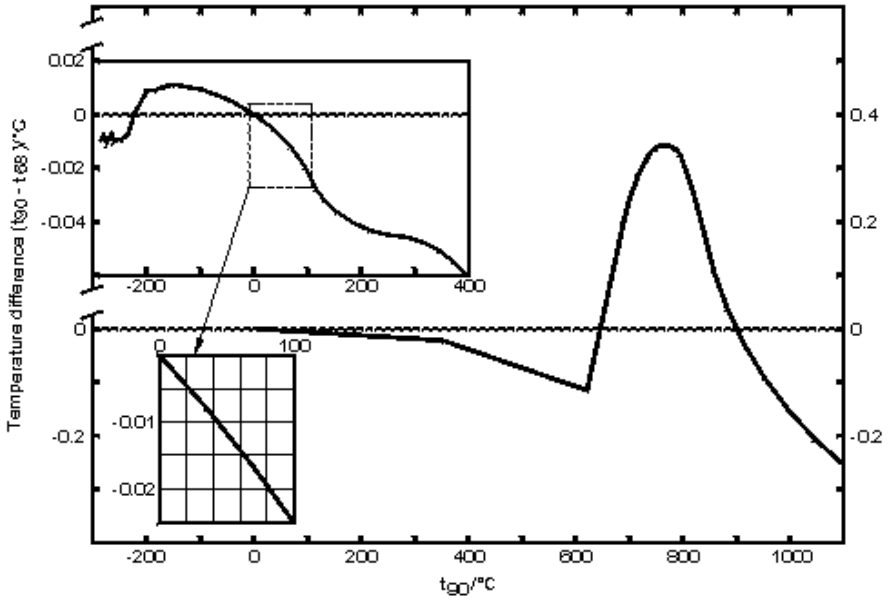

Figure 1.3 *The differences (t90 - t68) as a function of Celsius temperature[5]*

There are some important changes on the high temperature range. Thermocouple are no longer used, platinum resistances are used for 630°C to 962°C instead. And for higher temperatures Planck´s law is taking place.

ITS-90 is divided in four ranges:

- 0.65K to 5K, where temperature is defined by ^{3}He and ^{4}He vapour pressure.
- 3K to 24.5561 K, helium gas thermometry is used in this range.
- 13.8032 K to 961.78 K In this range temperature is measured by platinum resistances.
- Above 961.78 K where Planck's radiation law is used.

All those ranges and the fix points used for calibration are summarised in figure 1.4.

1.1.1.3 *Kelvin Definition, Issues and Disagreements.*

The current International System of Units establishes seven fundamental magnitudes and units: time (second, s), length (meter, m), mass (kilogram, kg), electric current (ampere, A), thermodynamic temperature (kelvin, K), amount of substance (mole, mol) and luminous intensity (candela, cd). Some of those units (kg, A, K and mol) were defined referencing artefacts or substances. This kind of definitions involve material related issues, in other words,

substances or artefacts change in long time periods, even when preservative methods are provide [6].

In order to procure a no-substantial dependent definition, several projects have been started. Main target of those projects is redefinition of those units. Those new definitions will change their dependence on material compounds or instruments for definition based on thermodynamic constants as speed of light in vacuum, Planck constant, etc. It is easy to understand that accuracy in determination of those constants is a critical factor, otherwise new units will not be accurate either.

In the particular case of the kelvin, its current definition is based in the temperature of the water triple point [5]:

$$K = \frac{1}{273.16} T_{WTP} \tag{1.1}$$

This definition makes the kelvin water dependent and, as it was said before, water properties can change because it might be contaminated from the envelope, after long time periods. Also, isotopic composition of water is different around the world; therefore triple point temperature will change while using different waters. Therefore it is necessary supplementary information about water composition, which was define as composition of ocean water, and according to Vienna Standard Mean Ocean Water[7] is:

0.00015576 mole of H^2 to H^1

0.0003799 mole of O^{17} to O^{16}

0.0020052 mole of O^{18} to O^{16}

Therefore the water isotopic composition of triple point cells must be specified and temperature measurement corrected accordingly.

To avoid these issues, European project named “New Determinations of the Boltzmann Constant” was started by Euramet and EMRP. The main objective of this project is to procure a new definition of kelvin which has not dependence with water or other material. TERMOCAL laboratory in collaboration with CEM (Centro Español de Metrología) is involved in this project carrying out acoustic resonance to measure speed of sound and determine Boltzmann

constant. There are many other partners as PTB, NPL, INRiM, LNE-INM/Cnam, University of Paris North, Second University of Naples and Polytechnic of Milan.

Once, the new definition of kelvin is achieved it musts be introduced in a new temperature scale.

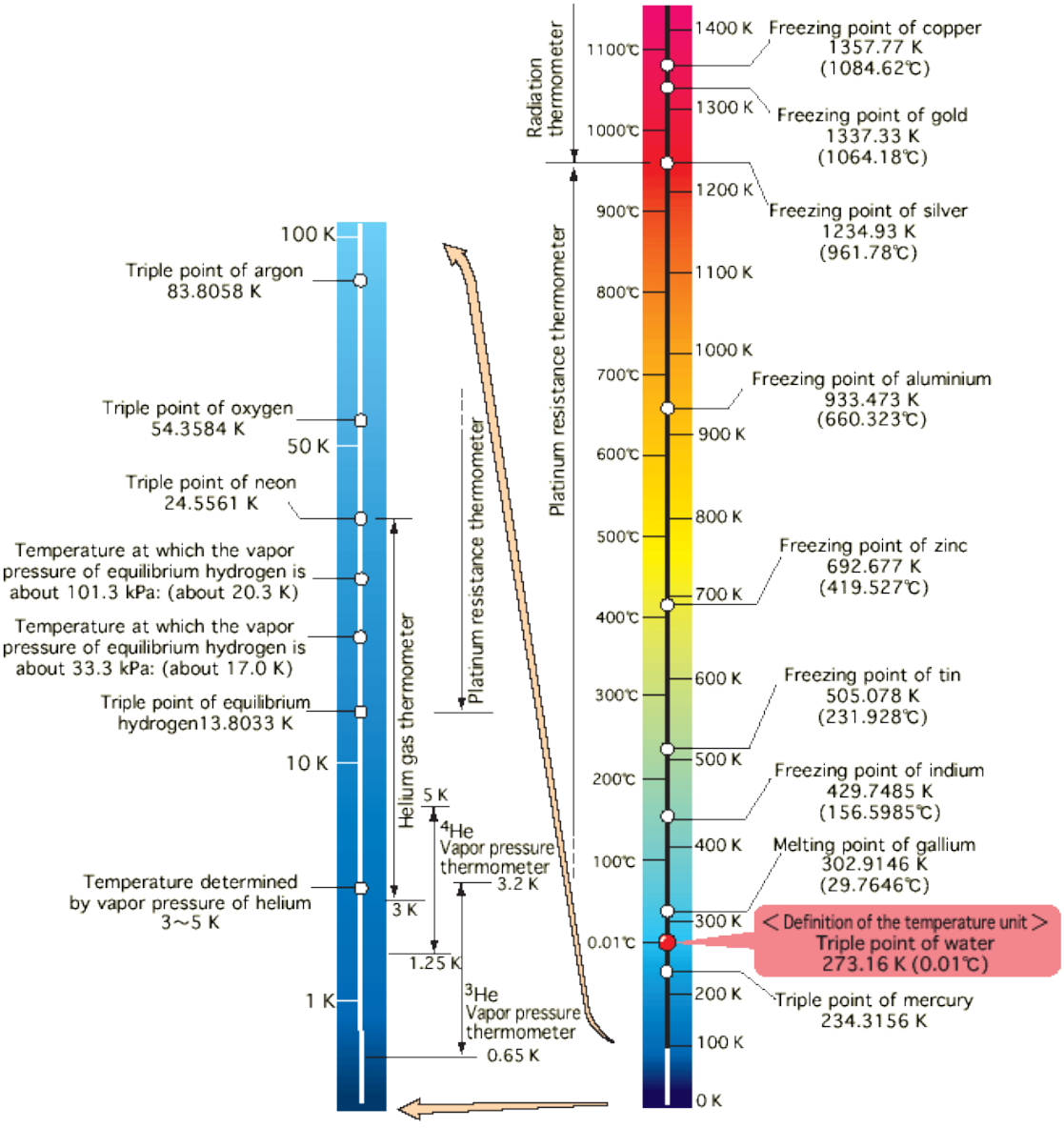

Figure 1.4 *ITS-90 in detail[8]*

In order to understand how this implementation will be done it is important to know what scale is being used and how it works:

The current scale is ITS90, the International Temperature Scale of 1990 is a thermodynamic scale based on the temperature of different thermodynamic fix points as triple points, melting

points, freezing points and vapour pressure of different materials from which we can measure from 0.65K to the highest temperature.

The purpose of the ITS-90 is to define procedures by which thermometers can be calibrated, this calibration will be precise and reproducible and as close as possible to the thermodynamic value. In other words, ITS-90 gives a well detailed “recipe” to set up thermometers by relating thermodynamic fixed points with its thermodynamic temperature.

As it was said, the whole scale pivots around triple point of water, as it is used to define the kelvin. Hence, the determination of very high or very low temperatures needs a water triple point measurement to be done accurately.

It is obvious that a new kelvin definition will change the scale used. So it will be necessary make a new one. EURAMET project JRP SIB01 “Implementing the new kelvin (InK)” is working in this new scale. Termocal research group, once again, in collaboration with CEM, is involved by measuring four fix points [5]:

Triple point of mercury (234.3156 K)

Triple point of water (273.16 K)

Melting point of gallium (302.9146 K)

Freezing point of indium (429.7485 K)

All these fix points will be measured using acoustic thermometry, same technique used for the present thesis

1.1.2 Measurement of Thermodynamic Properties of New Energy Gases.

Determination of speed of sound can also be used to measure thermodynamic properties as it was said before, this study uses speed of sound measurements to calculate isothermal and isochoric heat capacities when pressure is null as we will see forward in this thesis.

1.1.2.1 *Introduction*

It is obvious that, nowadays, human beings need energy for their usual activity; to take a hot shower, cook, drive a car, etc. Furthermore, production of food or elaborated goods, even water purification and distribution would not be possible without energy sources.

Before industrial revolution in the 18th century, wood and other kind of biomass were used as fuel (it was not the only energy source, wind and rivers were used to move mills but they are of less interest for the current work) for heating up houses, cooking... when cities grew, population energy needs grew as well. This fact caused important issues in the closest forests. Coal showed up as a solution for the increasing fuel demand.

Coal played an important role when the industrial revolution started. The new machinery developed during those years was powered mainly by coal. This also caused the growing of mining. Coal is cheap and easy to extract, so it is currently one of the fuels more often used as energy source, especially in developing countries.

Petroleum derivatives become of relevant interest when internal combustion engine was developed. Also European population started to use oil from petroleum instead from whales. Once again, it can be observed how humankind compromises a natural resource and must change it for a new one, wood in the case of coal and whales in the case of petroleum.

Awareness about environmental issues and the continuous development of gas industries and equipment have made possible the use of gas natural as a new energy source replacing some petroleum fractions in the use for house heating for the last decades. However, it is also used in several kinds of processes.

New sources of energy are more often developed solar, wind, nuclear... to fulfil our needs and reduce the human beings' environmental footprint, but fossil fuels are still the most important, as figure 1.5 shows [9].

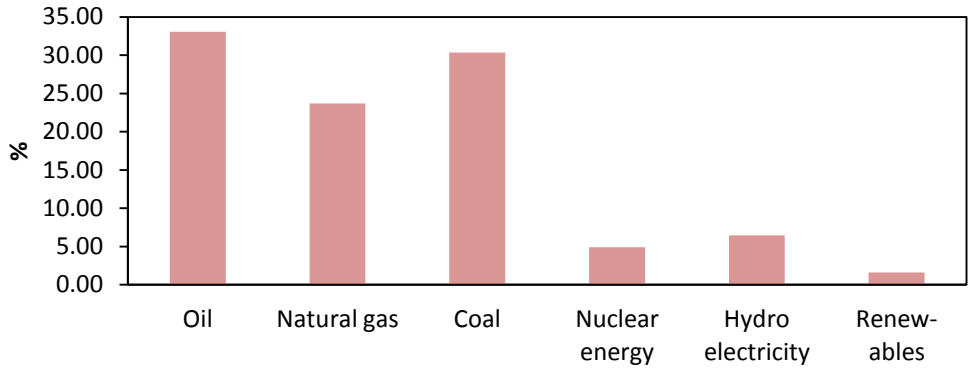

Figure 1.5 *Global Energy distributions by type of fuel during 2011*

1.1.2.2 *Fossil Fuels*

As it is said before, humankind development is very close related to the production and consumption of energy. In figures 1.6 it is shown the production and the consumption of the three more used fossil fuels, petroleum, coal and natural gas. Looking at those graphics it is easy to see that energy needs are growing higher every year[9].

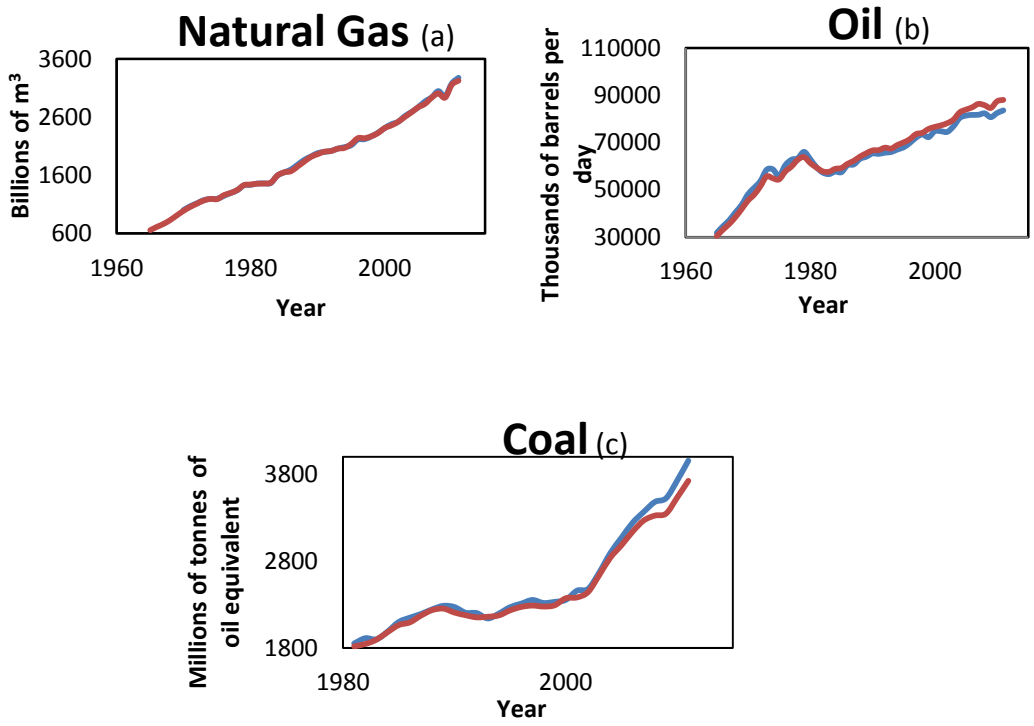

Figure 1.6 *The graphics show the evolution of the production (blue line) and the consumption (red line) of different fossil fuels: (a) the Billions of cubic meters of natural gas produced and consumed from 1965 to 2011; (b) the thousands of barrels of oil per day since 1965 to 2011; (c) the coal in millions of oil equivalent, from 1981 to 2011.*

These resources are not renewable; this means there is only a limited amount of coal, oil and natural gas. Fossil fuels are found in natural reservoirs which are classified according to their quality, quantity and accessibility. Therefore some reservoirs of good quality and large amount of fuel are not exploited because the extraction process is unviable; same happens when they have easy access and good quality but it is not large enough to be profitable or if fuel quality makes necessary an expensive purification process.

In figure 1.7 [9] it is observed an increment of the reservoirs. This fact is due to the development and improvement of extraction and purification process and to higher prices (as we can see in figure 1.8) of oil. This way, reservoirs that were not considered before because

of lack of quality, quantity or extraction issues; might be viable and profitable now a day or in a near future.

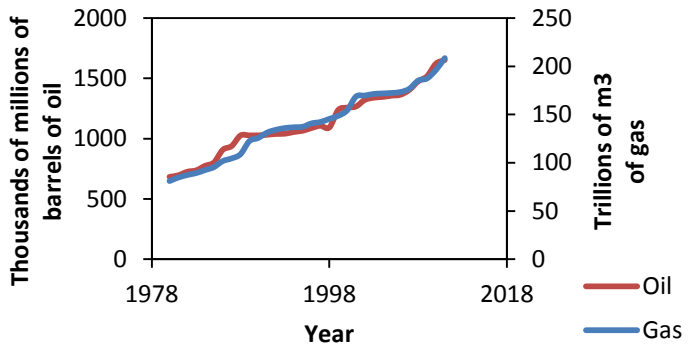

Figure 1.7 *Oil and Natural gas global reservoirs along years.*

Price of fuels matters, beside the obvious induced effect in the cost of energy, when one of the fuels become cheaper than the others, more energy is produced using this one. It is the case of coal, prices of gas and oil increased when coal remained cheap, that way coal production and consumption has grown faster than other fuels for the last 10 years, as can be observed in figures 1.6.

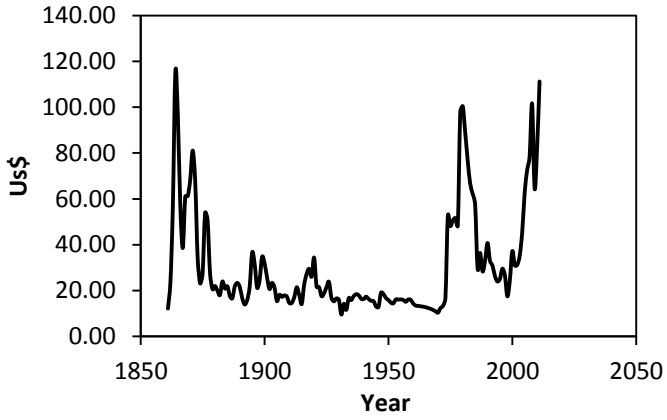

Figure 1.8 *Price of barrel of oil in today US$ since 1865 to 2011.*

1.1.2.3 *New Fuels*

Fossil fuels reservoirs are limited and they are not a renewable source of energy, this means humanity will run out of coal, gas and oil eventually, and other energy sources will be required, furthermore the current energy system based on fossil fuels produces large amount of gases as CO_2, SO_x, NO_x... which are deeply related with environmental issues as green house

effects, global warming or acid rain [10]. New fuels are being developed in order to avoid some of these issues.

New fuels are usually produced as a by-product of different process, like biogases, where methane and carbon dioxide are produced by anaerobic fermentation of organic wastes, cereals, or other raw material. There are other kinds of gases that reduce the environmental footprint besides they are no renewable. Gases like coal bed methane which main component is methane. Methane's greenhouse factor is about 23, this means 1 kg of methane released freely to the atmosphere will affect as much as 23 kilograms of carbon dioxide. Also it is important to remove it from carbon mines for safe procedures.

The use of this kind of new fuels will decrease the CO_2 production and, as they come from renewable sources, there is not a chance of depleting reservoirs.

1.1.2.4 *The Importance Thermodynamic Properties in New Gases.*

The knowledge of gas properties is necessary for a better production, storage, transport and use in general of gas itself. There are many studies for natural gas behaviour and quite accurate equations of state for multicomponent gas mixtures (natural gas alike) [11-13]. But the new energy gases need to be studied.

Producers, transporters, network operators and ultimately consumers interests require for a characterization of these new gases for an efficient and safe utilization of theses alternative fuels. Properties like humidity and dew point temperature to understand de condensation behaviour at high pressure and temperature conditions.

Other important thermodynamic property is the calorific value, because what eventually matters about energy gases it is the amount of energy that is possible to obtain from certain amount of gas. This property has a strong impact on economy and profits of that gas utilization.

Density of these gases in wide range of pressure and temperature is one of the most important parameters, in particular in transport and storage processes. It can be obtained using accurate equations of state.

Others useful thermodynamic properties are heat capacities because using one heat capacity and an accurate equation of state any other property like enthalpy, entropy, Gibbs free energy... might be determined, which are very useful when designing equipment. For

instance, how much energy must be removed after compressing these new gases, or expected temperature after expanding gases in a valve...

All these thermodynamic properties can be predicted using current equations of state but it is mandatory to check the right approximation of those equations of state to experimental data otherwise estimations might not be as good as expected.

1.2 OBJECTIVES OF THIS THESIS

The main objectives of this thesis are enumerated as follows:

As part of the European project “New Determination of the Boltzmann’s Constant” this work aims to determine the value of the Boltzmann constant with as low uncertainty as possible, for this purpose, some improvements have been performed in the acoustic spherical resonator which is used as an acoustic gas thermometer.

Adjustment of the equipment for thermodynamic characterization of gas mixtures. Acoustic resonance technique can be used for thermodynamic characterization of gas mixtures. This objective might be fulfilled by using a different resonating cavity and calibrating its internal radius with pressure.

Determination of adiabatic coefficient, heat capacities and acoustic virial parameters of gas mixtures through measurements of speeds of sound. This thesis aims to measure some parameters for a thermodynamic characterization of mixtures which components are usually present in non-conventional energy gases. Data of this kind of mixtures are required to predict and estimate behaviour of more complex mixtures. Synthetic mixtures of non-conventional energy gases like coal-bed methane will be measured.

Test of the current reference equation of state for natural gases. All the data acquired for all mixtures under study will be compared to GERG-2008 equation of state, which is extendedly used in the natural gas environment. It can be validated for the mixtures under study and the measurements performed can contribute to the thermodynamic properties data base.

1.3 STRUCTURE OF THE THESIS

This thesis explains the development of an advanced technique of acoustic and electromagnetic resonance in gases to determine thermodynamic constants and properties, collection of data and detailed theoretical explanation of the basis of the technique.

It consists in 8 chapters and 5 annexes which contains are detailed as follows:

Chapter 1 contains the introduction of this work describing the different motivations to carry out the study; it also explains the expected results of this thesis and an outline where the thesis contains are explained.

The main theoretical aspects related to the study are explained in **chapter 2**. This theoretic analysis includes how to determine the Boltzmann's constant and the thermodynamic properties from values of speed of sound. Also it is detailed the corrections applied to the frequency of resonance and the uncertainty calculation process.

Chapter 3 is a detailed description of the components of the equipment including controlling devices used to maintain pressure and temperature at the desired conditions; and a summary of all the steps required to obtain the measurements starting with the preparation previous to the filling process and finishing with the last obtained datum.

Some of the experimental results acquired for the determination of the Boltzmann's constant are in **chapter 4**. Data showed in this part include electromagnetic resonance results for determination of internal radius, some results of acoustic resonance measurements and all the frequency correction applied at both acoustic and electromagnetic resonance. This chapter shows values of speed of sound in argon and the uncertainty assessment performed.

Calibrate the internal radius of the resonator is a very important task. **Chapter 5** shows some of the measurements carried out to fulfil this calibration. Radius was measured at several pressures and temperatures. Some of the frequency corrections applied are displayed too. Data at different temperatures were modelled falling in a second order equation.

Chapter 6 shows some of the results obtained in the binary mixtures {CO (0.05)+ N_2 (0.95)} and {CO (0.1)+ N_2 (0.9)} at two different temperatures T = 273.16 K and T = 325.00 K in the pressure range from 0.1 MPa up to 10 MPa. It shows results like frequency corrections applied, speed of sound data adiabatic coefficient, heat capacities, and acoustic virial parameters. It also shows the uncertainty assessment performed.

Chapter 7 contains some of the results obtained in a synthetic coal mine methane Mixture at two different temperatures T=250.00K and T=273.16K in the pressure range from 0.1MPa up to 10MPa. It shows results like frequency corrections applied, speed of sound data adiabatic coefficient, heat capacities, and acoustic virial parameters. It also shows the uncertainty assessment performed.

And finally, the conclusions are summarized in **chapter 8**. All collected data of pressure temperature and pressure for all gas mixtures and all the frequency corrections, speed of sound and other calculated data can be found in the annexes.

1.4 REFERENCES

1. Estela-Uribe, J.F., Trusler, J.P.M., Chamorro, C.R., Segovia, J.J., Martín, M.C., and Villamañán, M.A. (2006) Speeds of sound in {(1 - x)CH4 + xN2} with x = (0.10001, 0.19999, and 0.5422) at temperatures between 170 K and 400 K and pressures up to 30 MPa. The Journal of Chemical Thermodynamics 38, 929-937.

2. Moldover, M.R., Trusler, J.P.M., Edwards, T.J., Mehl, J.B., and Davis, R.S. (1988) Measurement of the Universal Gas Constant R Using a Spherical Acoustic Resonator. Physical Review Letters 60, 249.

3. Moldover, M.R. (2009) Optimizing acoustic measurements of the Boltzmann constant. Comptes Rendus Physique 10, 815-827.

4. Watanabe, H. (1995) Chappuis' experiments and the "Ã‰chelle Normale". Metrologia 32, 397.

5. McGlashan M.L (1990) The international temperature scale of 1990 (ITS-90). The Journal of Chemical Thermodynamics 22, 653.

6. The current SI seen from the perspective of the proposed new SI. Journal of Research of the National Institute of Standards and Technology 116, 797.

7. Pavese, F. (2005) On problems in the definition of the International Temperature Scale arising from the variability of the isotopic composition of some substances used for the fixed-points. Metrologia 42, 194.

8. Japan, N.M.I.o. Standards of the Kelvin and the International Temperature Scale.

9. Petroleum, B. (2012) BP Statical Review of World Energy.

10. Nordell, B. (2003) Thermal Pollution causes global warming. Global and planetary Change, 7.

11. KLIMECK, R.S.a.W., W. (1999) Development of a Reference Equation of State for Thermal And Calorie Properties of Natural Gases. Phase1: Theoretical Results. Report to GERG WG 1.34 (Lehertuhl Für Thermodynamik, Ruhr-Iniversität Bochum).

12. KUNZ, O.e.a. (2007) The GERG-2004 Wide-Range Reference Equation of State for Natural Gases and Other Mixtures. GERG Technical Monograph Fortschr.

13. SPAN, R. (2000) Multiparameter Equations of State, an Acurate Source of Thermodynamic Property Data. Berlin: Springer.

Chapter 2

ACOUSTIC AND ELECTROMAGNETIC RESONANCE IN A QUASI-SPHERICAL CAVITY

2.1 INTRODUCTION

To understand the relation between the Boltzmann constant or the heat capacities and the speed of sound we need to review some point of the kinetic theory of gases. This theory explains that thermal energy of gases is related to the kinetic energy of the gas molecules according the next equation [1]

$$3E = \frac{1}{2} m v^2 = \frac{3}{2} k_B T \tag{2.1}$$

E represents the energy, m is the mass of the molecule, v is the average velocity of the molecules, k_B is the Boltzmann constant, and T is the thermodynamic temperature.

Kinetic theory also says that the mean speed of particles is related to the speed of sound by [2]:

$$u^2 = \frac{\gamma^{pg}}{3} v^2 \tag{2.2}$$

The speed of sound is represented by u, and the ratio between isobaric and isochoric heat capacities as perfect gas is γ^{pg}.

When implementing eq.2.2 in eq.2.1 and solving for the square of the speed of sound we obtain:

$$u^2 = \frac{\gamma^{pg} \cdot k_B T}{m} \tag{2.3}$$

If we use Boltzmann constant as $k_B = \frac{R}{N_A}$ (R and N_A are the ideal gas constant and Avogadro's constant) we obtain equation 2.4 where the mass of the molecule is replaced by the molar mass of the gas M.

$$u^2 = \frac{\gamma^{pg} \cdot R \cdot T}{M} \tag{2.4}$$

When the molar mass of the gas and the thermodynamic temperature are known Boltzmann constant can be obtained from equation 2.3, but for heat capacities it is necessary to look a bit farther in equation 2.4, from the adiabatic coefficient as perfect gas can be

measured. And thanks to Mayer's relation for perfect gas (equation 2.5) calculate isochoric (C_v) and isobaric molar heat capacities (C_p).

$$C_p - C_V = R \tag{2.5}$$

Equation 2.4 is obtained thanks to kinetic theory which is only valid for perfect gases, in other words, this expression is only true when the gas pressure is null. However, sound needs a material pathway to propagate, so we cannot satisfy both requirements at the same time. The solution for this inconvenient comes thanks to the acoustic virial equation. This equation can be presented as a function of density (equation 2.6-a) or pressure (equation 2.6-b). When it is presented in the second way and pressure takes the value of 0 Pa, the acoustic virial equation is equal to equation 2.4. Because, any term vanish away but the first term.

$$u^2 = \frac{\gamma^{pg} RT}{M}\left(1 + \beta_a \rho + \gamma_a \rho^2 + \ldots\right) \tag{2.6-a}$$

$$u^2 = \frac{\gamma^{pg} RT}{M} + A_1 p + A_2 p^2 + \ldots \tag{2.6-b}$$

Where p is the pressure and ρ is the density of the gas, A_1 and A_2 are the coefficients for the acoustic virial equation when square speed of sound is expressed as a function of pressure and β_a and γ_a, are acoustic virial coefficients as well but when it is expressed as a function of density. Pressure and density acoustic virial coefficient are related as equations 2.7 and 2.8

$$\beta_a = \frac{A_1}{A_0} RT \tag{2.7}$$

$$\gamma_a = \frac{A_2}{A_0}\left(RT\right)^2 \tag{2.8}$$

A_0 is the square speed of sound in the gas when pressure is null. It can be obtained from equation 2.6-b, it is shown in equation 2.9

$$A_0 = \frac{\gamma^{pg} RT}{M} \tag{2.9}$$

For calculating the Boltzmann constant we measure speed of sound in a gas which properties are well known (M and γ^{pg}), so keeping temperature constant we solve k_B. When we want to know the heat capacities the same equations are used but the unknown value this time is γ^{pg}, it is essential to know the molar mass of the gas.

2.2 ACOUSTIC RESONANCE

The set up for the measurement of the speed of sound in gases does not perform a direct measurement, this mean the magnitude which is truly measured is the frequency of resonance and from this frequency speed of sound is calculated.

The relation between frequencies of resonance and speed of sound is wide studied [1,3-5], for the particular case of a spherical cavity the relation is shown in equation 2.10

$$u = \frac{2\pi a f_{lm}}{\xi_{lm}} \tag{2.10}$$

Where a is the radius of the cavity, f_{lm} is the frequency of resonance for de mode lm, and ξ_{lm} is the eigenvalue for the acoustic mode of resonance lm.

As it was said before the frequency of resonance is the measured magnitude; the eigenvalue is a calculated as the m^{th} root for the l^{th} spherical Bessel equation [6]; and the radius must be determined for each pressure and temperature. This determination will be carried out by microwave resonance as section 2.2 will show.

2.2.1 Acoustic Corrections

Equation 2.7 is completely true for a perfect spherical cavity, which boundaries have infinite thermal conductivity, the structure is rigid (no motion or vibrations on the enclosure), etc. In other words, it gives the unperturbed eigenfrequencies. For the correct understanding and calculations of these phenomena it is necessary to introduce some corrections for the equation [1]; these contributions do not only affect the real component of the frequency but the imaginary part as well.

There are four corrections of relative importance: thermal contribution, bulk viscosity contribution, shell coupling and shell imperfections (inlet and outlet pipes, transducers...). When introducing all these corrections the eigenfrequencies shift in the way shown in equation 2.11.

$$F_{lm} = f_{lm} + \Delta f_{lm} + i\Delta g_{lm} = f_{lm} + f_{th} + f_{shell} + f_{tube} + i\left(g_{bulk} + g_{th} + g_{tube}\right) \qquad (2.11)$$

The frequency measured is f_{lm}, the sum of all the contributions for the real part is represented by Δf_{lm} and it includes the thermal contribution (f_{th}), the shell motion contribution (f_{sh}) and the imperfections on the shell contribution (f_{tube}). It is the same for the imaginary part; Δg_m represents the sum of contributions for the imaginary component, where g_{bulk}, g_{th} and g_{tube} are the bulk viscosity, thermal and imperfection contributions respectively. The shell motion does not have imaginary contribution and the bulk viscosity affects only the imaginary component. The real frequency of resonance F_{ml} is obtained when all these frequency corrections and half-width contributions are added to the theoretical frequency of resonance (f_{lm}). The imaginary part of the experimental measurements represents the energy that waves lose when travelling through a non ideal environment. Once the corrections are applied equation 2.10 turns into 2.12

$$u = \frac{2\pi a\left(f_{lm} + \Delta f_{lm}\right)}{\xi_{lm}} \qquad (2.12)$$

When there is not a perfect sphere (quasi-sphere or misaligned hemispheres) there is a small change in the frequencies, however since we are using radial modes the frequencies are not affected as long as the total volume stays unperturbed [6].

2.2.1.1 *Bulk Viscosity*

As waves theory can tell [7], the energy of plane waves decays with distance x proportional to Exp(-αx). Where α represents the media's absorption. In the particular case of low frequencies the absorption coefficient is zero, but it does not behave that way in high frequencies as the measurements were done.

Sound produces a variation on the local pressure of fluid along its pathway, and the changes in pressure make changes on the density and temperature, these small changes in pressure and density in local areas inside the resonator make the gas flow slightly from high pressure areas to lower pressure areas. The absorption coefficient changes because the pressure fluctuations, this means the frequencies of resonance shift, and it is necessary to introduce a correction. This correction is the one presented before as bulk viscosity correction (g_{bulk}) and it is calculated according equation 2.13 [8].

$$\frac{g_{bulk}}{f_{lm}} = f_{lm}^2 \frac{\pi^2}{u^2}\left(\frac{4}{3}\delta_v^2 + (\gamma-1)\delta_{th}^2\right) \quad (2.13)$$

Where γ is the adiabatic coefficient, δ_v and δ_{th} are the viscous and thermal penetration length:

$$\delta_v = \sqrt{\frac{D_v}{\pi f_{lm}}} = \sqrt{\frac{\mu}{\rho \pi f_{lm}}} \quad (2.14)$$

D_v is viscous diffusivity or kinematic viscosity ($D_v=\mu/\rho$) which is equal to the dynamic viscosity μ divided by the density ρ.

$$\delta_{th} = \sqrt{\frac{D_{th}}{\pi f_{lm}}} = \sqrt{\frac{\kappa}{\rho C_p \pi f_{lm}}} \quad (2.15)$$

D_{th} Is the thermal diffusivity of the gas ($D_{th}=\kappa/\rho C_p$) and it is calculated dividing the thermal conductivity, κ, by the density, ρ, and the isobaric heat capacity $C_{p.}$

2.2.1.2 *Thermal Boundary Layer*

The highest contribution on the corrections used is the thermal boundary layer correction. The boundary conditions on the resonator establish that the temperature fluctuations and the tangential fluid velocity, that are present in bulk of the fluid, vanish on the inner surface of the cavity. Hence, there is a gradient in temperature, as well as tangential velocity, between the interface and the bulk of the fluid. This gradient's length (the viscous and thermal penetration length, δ_v and δ_{th}, defined in equations 2.14 and 2.15 respectively) is quite shorter than the wavelength so the effect on the frequencies is larger than those that happen in the fluid (g_b). Non degenerate modes of resonance do not have tangential component in the speed of sound so for the measured modes there are not viscous boundary layer correction.

Equation 2.12 shows how to calculate the thermal boundary layer correction [1].

$$\frac{\Delta f_{th} + i g_{th}}{f_{lm}} = (-1+i)\frac{(\gamma-1)}{2a}\delta_{th}\frac{1}{1-l(l-1)/\xi_{lm}^2} + \frac{(\gamma-1)}{a}l_{th} - (1+i)\frac{(\gamma-1)}{2a}\delta_{316L}\frac{\kappa_{gas}}{\kappa_{316L}} \quad (2.16)$$

κ_{gas} and κ_{316L} are the thermal conductivities of the gas which is being measured and 316L stainless steel (the shell is made of this material) respectively. δ_{316L} is the thermal penetration length in steel shell, calculated from equation 2.15, using stainless steel properties (thermal

conductivity, density, and heat capacity) instead. The thermal accommodation length l_{th} is calculated according equation 2.17

$$l_{th} = \left(\frac{\kappa_{gas}}{p}\right)\left(\frac{\pi MT}{2R}\right)^{1/2}\left(\frac{C_v}{R}+\frac{1}{2}\right)^{-1}\left(\frac{2+h}{h}\right) \qquad (2.17)$$

The accommodation coefficient, h represents the ratio of the energy transported across the interface and the energy that would be transported in the ideal case of every molecules reaching equilibrium with the surface. Values of h between 0 and 1 are mandatory but they depend on the nature of the surface not only the material it is made of but the shape as well. Therefore during all studies and measurements carried out in the present thesis the accommodation coefficient remains constant at 0.85 as suggested in bibliography [9].

2.2.1.3 *Pipes and Tubes **C**orrection.*

We already talk about how shape imperfections over the inner surface of the resonator shift lightly the frequency of resonance. Some of these imperfections might be calculated so we can apply the proper corrections. Inlet pipes have special interest and it is easy to understand that sound wave travels along the pipe and this effect produces a small change in the resonance inside the spherical cavity.

The model for this correction is well known [3]:

$$\Delta f_{tube} + ig_{tube} = \left(\frac{u}{2\pi a}\right)\left(\frac{\Delta S}{4\pi a^2}\right) iy_o \qquad (2.18)$$

The surface of the hole is represented by ΔS and y_o is the specific acoustic input admittance of the opening. We consider the closure of pipe to have zero specific acoustic admittance, so y_o at the opening can be calculated according equation 2.19.

$$y_o = i\tan(k_{KH}L) \qquad (2.19)$$

L is the length from the opening to the closure and k_{KH} is the propagation constant according to the Kirchhoff-Helmholtz theory and it is calculated as:

$$k_{KH} = \left(\frac{2\pi f_{lm}}{u}\right) + (1-i)\alpha_{KH} \qquad (2.20)$$

The effective absorption coefficient α_{KH}, also known as the Kirchhoff-Helmholtz absorption coefficient, is calculated as expressed in equation 2.17

$$\alpha_{KH} = \left(\frac{\pi f_{lm}}{u r_h}\right)\left[\delta_v + (\gamma - 1)\delta_{th}\right] \tag{2.21}$$

Where, r_h is the opening radius.

2.2.1.4 *Shell Motion Correction.*

It does not matter what material we use to make the walls of the resonator, this material will have some elasticity, and the elasticity of the walls reduces the frequency of resonance. The reduction is calculated like equation 2.22 shows [10].

$$\left(\frac{\Delta f_{shell}}{f_{lm}}\right)^2 \approx \frac{2\kappa p}{1-\left(\frac{f_{breath}}{f_{lm}}\right)} \tag{2.22}$$

And κ is given by:

$$\kappa = \frac{5a}{6(b-a)\rho_{shell}u_{shell}^2} \tag{2.23}$$

Where b is the external radius of the resonator, ρ_{shell} is the density of the shell, 316L stainless steel in this case, and u_{shell} is the speed of sound in the shell. And f_{breath} is the frequency of the radially-symmetric resonance of the empty spherical shell and it is calculated by [11]:

$$f_{breath} = \left(\frac{u_{shell}}{2\pi a}\right)\left(\frac{2\left[\left(\frac{b}{a}\right)^3 - 1\right]}{\left[\left(\frac{b}{a}\right) - 1\right]\left[1 + 2\left(\frac{b}{a}\right)^3\right]}\right)^{1/2} \tag{2.24}$$

And the longitudinal speed of sound in steel is given by equation 2.25 [12].

$$u_{shell} = \sqrt{\frac{(1-\sigma)}{(1-2\sigma)(1+\sigma)}\frac{E}{\rho_{shelll}}} \tag{2.25}$$

Where σ is steel Poisson's ratio (0.27), E is the Young's modulus (193GPa) and ρ_{shell} is the steel density (8027kg·m^{-3}); all these data remain constant during all measurements in this thesis. They were obtained from bibliography [13]

2.3 MICROWAVE RESONANCE

As we said before we calculate the Boltzmann constant or the properties of the gases from the speed of sound, and this from the frequency of resonance, according equation 2.7. Looking into detail this equation we can see that the inner radius of the resonator is an important parameter and small changes in the radius make the uncertainty increase.

Small uncertainties are a requirement in the determination of the Boltzmann constant, but they are not so important for the thermodynamic properties, as we will see later. For this reason we used different techniques for each research, microwave resonance for the Boltzmann constant determination and acoustic resonance in argon for the thermodynamic properties of gas mixtures.

Researchers have been using different techniques for the determination of resonator internal radius as mercury pycnometry [1, 8], equation of state of a well known gas [14], or microwave resonance [2, 5, 15].

Mercury pycnometry is an excellent and accurate technique, and commonly used until mercury and its use was restricted, because environmental safety.

When the speed of sound of certain gas is well known in a temperature and pressure range we can turn around equation 2.7 and solve for *a* (inner radius). It seems obvious that the precision of this procedure is as good as the equation of state precision. This is good enough for measuring thermodynamic properties but quite inaccurate for determining the Boltzman constant.

Microwave resonance is quite similar to acoustic resonance but with electromagnetic waves instead of acoustic ones. This changes equation 2.10 into 2.26

$$a = \frac{2\pi c f_{lm}}{\xi_{lm}} \qquad (2.26)$$

Where, *c* is the speed of light in the gas and it is calculated according to Maxwell's equations [16] using equation 2.27

$$c = \left(\sqrt{\varepsilon_0 \varepsilon_r \mu_0}\right)^{-1} \tag{2.27}$$

The magnetic permittivity in vacuum, μ_0, is $1.2566 \cdot 10^{-6}$ $N \cdot A^{-2}$, ε_0 is the electric permittivity in vacuum and its value is $8.854 \cdot 10^{-12}$ $F \cdot m^{-1}$. Both magnetic and electric permittivities are physic constants. For last, ε_r is the relative electric permittivity taken form NIST database [17].

Electromagnetic resonance is more accurate than acoustic resonance because speed of light is quite stable with pressure and temperature, this means big changes in pressure and temperature does not produce big changes in speed of light. The main difference between electromagnetic and acoustic resonance is the use of degenerate modes of resonance in resonance of microwave. Degenerate modes come as triplets, this means they have three peaks of resonance, however then average frequency of all resonance peaks is the frequency value used to solve equation 2.26. Degenerate modes only split when the resonating cavity is not a perfect sphere. It often used a ellipsoidal cavity for this porpoises. The variations on the cavity surface do not affect acoustic resonance as long as its volume does not change. This study does not use a ellipsoidal cavity, it uses a misaligned sphere. This means it is composed of two separated hemispheres attached by the equatorial joint but slightly misaligned so they do not compose a sphere. As it was said these changes in the shape of the cavity do not affect the frequency of resonance but it has some effect on the width of the peak, enlarging them which has a negative effect on uncertainty determination, therefore it is important to induce a very small misalignment but enough to measure the triplets. This effect was obtained with an induced misaligned of 10μm for this resonator.

Measurements of speed of sound were taken at pressure and temperature points close to desired ones. These divergences are quite small; nevertheless they should be taken into account. This is the reason why the calculated speed of sound must be corrected. The correction factor (*r*) is calculated as:

$$r = \frac{u_{T_0,P_0} / a_{T_0,P_0}}{u_{T_{\exp},P_{\exp}} / a_{T_{\exp},P_{\exp}}} \tag{2.28}$$

Where $u_{P,T}$ is the speed of sound obtained from the NIST data base, P and T are the pressure and temperature. The suffix "0" indicates the desired measuring conditions and suffix

"exp" indicates the actual measuring conditions. The radius at experimental conditions($a_{T_{exp}P_{exp}}$) is obtained thanks to electromagnetic resonance and the values of the radius at the desired conditions are calculated using thermal expansion coefficient and isothermal compressibility (α_L and κ_T) shell factors:

$$a_{T_0,P_0} = a_{T_{exp},P_{exp}}\left[\left(1+\frac{\kappa_T}{3}\left(P_{exp}-P_0\right)\right)+\alpha_L\left(T_{exp}-T_0\right)\right] \qquad (2.29)$$

2.3.1 Electromagnetic Corrections

Microwave resonance needs, just like acoustic resonance, some corrections from the ideal case (Equation 2.26) to the real case.

2.3.1.1 *Finite Conductivity of the Walls*

In the microwave case, one of the applied corrections is the half wide factor (g), which also represents the imaginary magnitude of the wave. This value of the half width can be calculated using equation 2.30 [5]. Half-width of the resonance peaks is measured with the frequency of resonance and the differences between experimental and calculated factor g give one of the contributions to the uncertainty of the measurements.

$$\Delta f^{skin} = -g^{skin} = \frac{f_{lm}\delta}{2a}\left(1-\frac{l(l+1)}{\xi_{lm}^2}\right)^{-1} \qquad (2.30)$$

Where Δf^{skin} is the value of the different between ideal case and real case where the walls have a finite conductivity, g^{skin} is the value of the calculated imaginary component, a is the inner radius, ξ_{lm} is the eigenvalue for the resonance mode lm, l is the value of l in the mode lm, and δ is penetration depth of the field into the cavity walls calculated according equation 2.31

$$\delta = \frac{1}{\sqrt{\pi f_{lm}\mu\sigma}} \qquad (2.31)$$

Where μ is the magnetic permeability of the wall, and σ is the electric conductivity.

2.3.1.2 *Not a Spherical Surface*

It was proved that the eigenvalues of the non radial modes of a perfect spherical resonator change for a quasi-spherical resonator [18]. The first order correction does not affect the mean value of the three degenerate picks of resonance, but for ellipsoidal resonator second order corrections were obtained [19].

There are not studies for corrections when a misaligned resonator is used, however for first order approximation, as it happens to quasi-spherical resonators, the mean value of the frequency does not change; but we are not able to develop a model for second order approximations.

2.4 REFERENCES

1. Moldover, M.R., Trusler, J.P.M., Edwards, T.J., Mehl, J.B., and Davis, R.S. (1988) Measurement of the Universal Gas Constant R Using a Spherical Acoustic Resonator. Physical Review Letters 60, 249.

2. Moldover, M.R. (2009) Optimizing acoustic measurements of the Boltzmann constant. Comptes Rendus Physique 10, 815-827.

3. Trusler, J.P.M. (1991) Physical acoustics and metrology of fluids. Adam Hilger.

4. Trusler, J.P.M., and Zarari, M. (1992) The speed of sound and derived thermodynamic properties of methane at temperatures between 275 K and 375 K and pressures up to 10 MPa. The Journal of Chemical Thermodynamics 24, 973-991.

5. Benedetto, G., and et al. (2004) Acoustic measurements of the thermodynamic temperature between the triple point of mercury and 380 K. Metrologia 41, 74.

6. Mehl, J.B., and et al. (2004) Designing quasi-spherical resonators for acoustic thermometry. Metrologia 41, 295.

7. P. M. Morse, H.F. (1953) Methods of Theoretical physics. McGraw-Hill.

8. Moldover, M.R., and Trusler, J.P.M. (1988) Accurate Acoustic Thermometry I: The Triple Point of Gallium. Metrologia 25, 165.

9. M.B. Ewing, M.L.M., and J.P.M. Trusler. (1986) The Temperature-Jump Effect and the Theory of the Therma Boundary Layer for Spherical Resonator. Speeds of Sound in Argon at 273.16K. Metrologia 22, 9.

10. Pitre, L., Guianvarc'h, C.c., Sparasci, F., Guillou, A., Truong, D., Hermier, Y., and Himbert, M.E. (2009) An improved acoustic method for the determination of the Boltzmann constant at LNE-INM/CNAM. Comptes Rendus Physique 10, 835-848.

11. Mehl, J.B. (1985) Spherical acoustic resonator: Effects of shell motion. J. Acoust. Soc. Am. 78.

12. G.W.C. Kaye, T.H.L., . (1985) Tables of Physical and Chemical Constants.

13. eFunda. (2013) eFunda: properties of stainless steel AISI 316.

14. Estela-Uribe, J.F., Trusler, J.P.M., Chamorro, C.R., Segovia, J.J., Martín, M.C., and Villamañán, M.A. (2006) Speeds of sound in {(1 - x)CH4 + xN2} with x = (0.10001, 0.19999, and 0.5422) at temperatures between 170 K and 400 K and pressures up to 30 MPa. The Journal of Chemical Thermodynamics 38, 929-937.

15. Pitre, L., and et al. (2006) Acoustic thermometry: new results from 273 K to 77 K and progress towards 4 K. Metrologia 43, 142.

16. Mahmoud, S.F. (1991) Electromagnetic Waveguides: Theory and Applications. 221.

17. Tegeler, C.S., R.; Wagner,W. (1999) A New Equation of State for Argon Covering the Fluid Region for Temperatures From ther Melting Line to 700K at Presures up to 1000MPa. Journal of Physical and Chemical Reference Data 28, 71.

18. Mehl, J.B. (1982) Acoustic Resonaces Frecuencies of Deformated Spherical resonators. J. Acoust. Soc. Am. 71, 1109-1113.

19. Mehl, J.B. (2009) Second-oder electromagnetic eigenfrequencies of a triaxial ellipsoid. Metrologia, 6.

Chapter 3

EXPERIMENTAL SET UP AND PROCEDURE

3.1 EXPERIMENTAL SET UP.

3.1.1 Introduction.

A high accurate technique, based on a spherical resonator, has been developed for the measurement of speed of sound in gases at a wide range of temperatures and pressures. This chapter describes the equipment used for controlling both magnitudes, also the required apparatus for measuring acoustic and electromagnetic resonance and how are they displayed across the resonator. It also describes the filling and measuring processes carried out for better, faster and more accurate measurements.

3.1.2 Resonator

Two different spherical resonators were used in this study. Both of them were made of 360L steel because of their mechanical properties.

Both resonators are made from two different hemispheres and they are attached together by the equator. One of them is joined by welding, the other by several screws around the equatorial ring, the can be seen in figure 3.1.

A)  B) 

Figure 3.1 *A) Spherical resonator made by welding together two hemispheres. B) Misaligned resonator made attaching together two hemispheres using screws.*

The resonator A was used for measuring heat capacities and other thermodynamic properties; on the other hand, resonator B was used for the determination of the Boltzmann constant.

The welded resonator is completely spherical, therefore only acoustic resonance was carried out in it, because electromagnetic resonance needs little deviations from perfect spherical shape to split degenerate resonance modes, according to electromagnetic resonance theory [1]. This Resonator was designed by J.T.M. Trusler at the imperial College in London. Internal radius of this resonator is about 40mm.

Electromagnetic resonance was carried out in the screwed resonator, which, in order to accomplice shape requirements, is misaligned. This resonator was designed based on Tursler's resonator but a few changes were implemented: the misalignment system and the two new ports for microwave antennae. The internal radius of this resonator is about 40mm too.

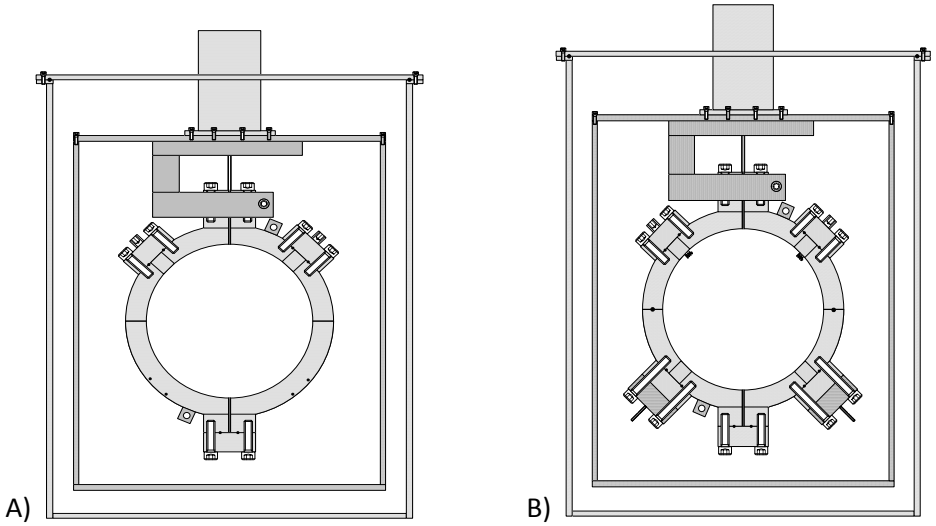

Figure 3.2 *Schematic view of welded resonator (A) and the misaligned resonator (B), both inside the temperature and pressure controlling vessels*

The resonator is assembled to the supporting structure, and several mechanisms to control temperature and pressure are placed around (figure 3.3). The first controller is a steel vessel wired on sides and bottom to heat it up and transfer heat to the sphere.

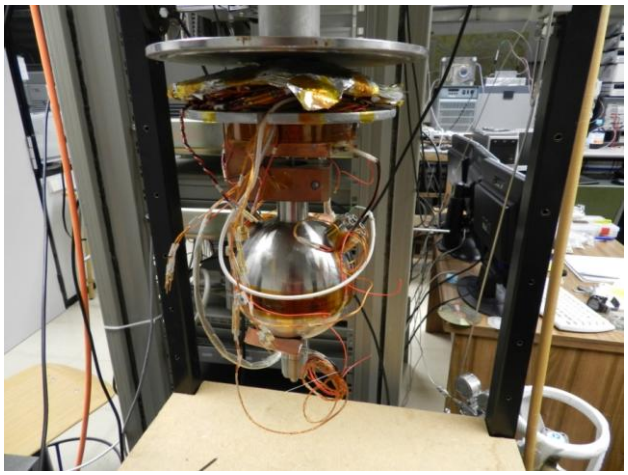

Figure 3.3 *Resonator A assembled to copper block and supporting structure.*

3.1.3 Temperature Measurement and Control

The temperature on the resonator is measured by two capsule-type platinum resistance thermometer CSPRT Rosemount 162D using an ac bridge ASLF18, which can measure variations in temperature of 2.5 µK, thermometer and bridge can be seen in figure 3.3. The sensors were placed across the resonator in opposite hemispheres and separated as much as possible on the outer surface of the sphere. If there is a temperature gradient across the resonator it will be observed when thermometers are placed like this. These resistance thermometers were calibrated in Termocal facilities and they are traceable to national standards; their uncertainties are detailed in table 3.1 both thermometers.

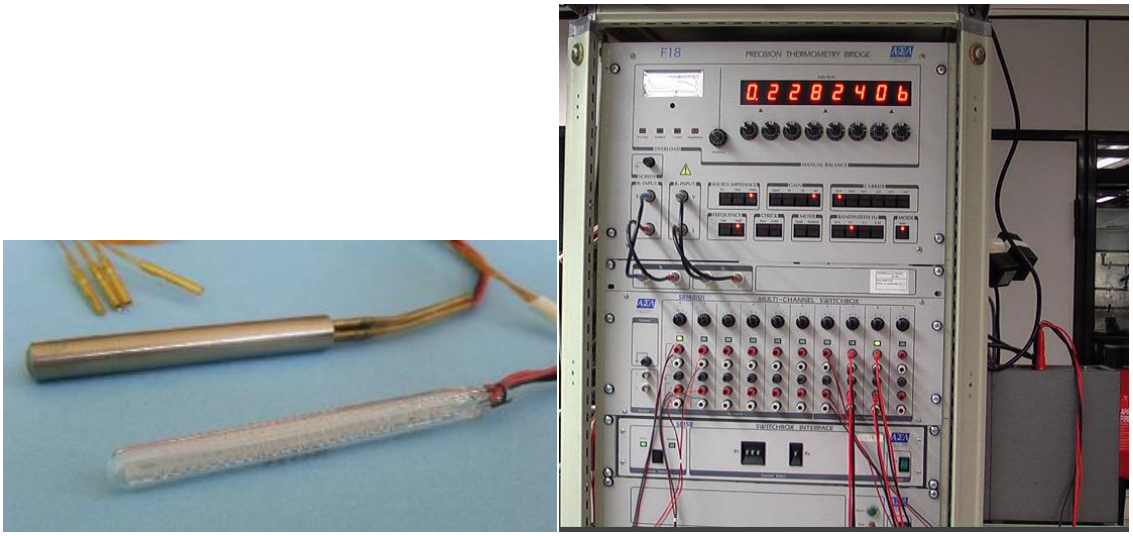

Figure 3.3 *Capsule-type platinum resistance thermometer CSPRT Rosemount 162D (top left) and Hart Scientific (bottom left) and the AC bridge ASLF18 used to measure resonator temperature (right).*

Table 3.1 *Calibration extended uncertainties (k=2) for thermometer PT-25 in fix points.*

T ºC	U (mK)
231.928	6
156.598	5
29.765	4
0.01	2
-38.833	4

Resonator temperature is controlled in three steeps: by heat transfer by conduction trough the copper block, radiation losses is minimized by an aluminium cylinder that works as a radiation tramp and vacuum around the resonator prevent convection losses. This thermostat has been designed for operation in a temperature range from T=123K to T=523K.

The resonator is assembled to a copper block which function is double; it is a supporting structure from where resonator hangs, and a temperature controller using heat flow by conduction across itself to heat the resonator. Wires and inlet pipes are attached to this copper block so their temperature is also controlled and heat flux along them is avoided.

When the resonator is attached to this copper block, it is surrounded for several layers which function is to control temperature and pressure. The first layer consists on a cylindrical aluminium vessel. This vessel is used to control temperature by radiation heat flux. It is completely covered (inside and outside) with aluminium foil and fibreglass tissue layers. Figure 3.5 shows this vessel form to different views, so the internal fibreglass can be appreciated. Figure 3.6 shows this vessel assembled to the structure with and without the radiation trap cover.

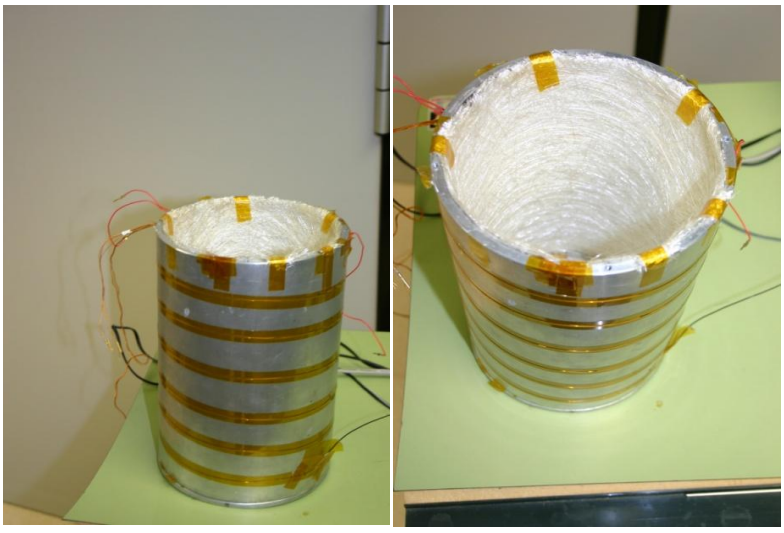

Figure 3.5 *Vessel used to control resonator temperature thanks to radiation heat flux.*

This “radiation” vessel is inside another vessel, which keeps vacuum conditions thanks to an indium shield. Vacuum is induced so convection heat flux to the resonator is avoided and conduction through the upper copper block and radiation from the other internal vessel are the only heat flux to the resonator.

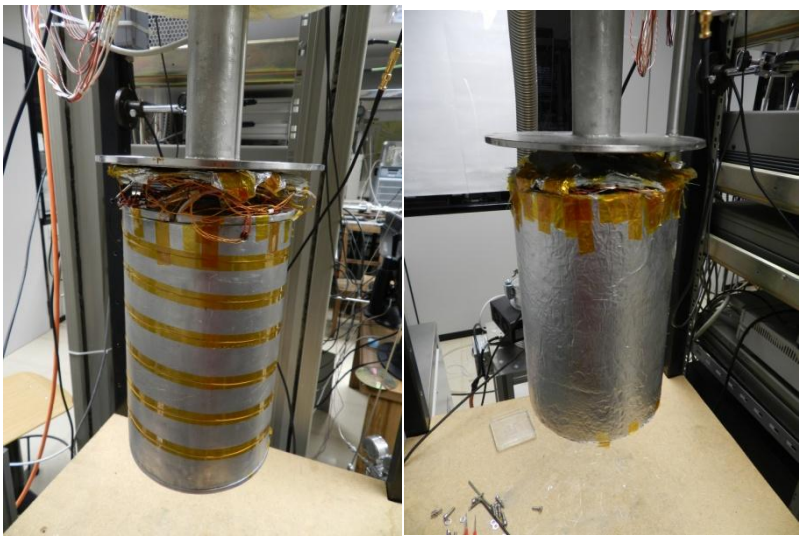

Figure 3.6 *Vessel used to control resonator temperature thanks to radiation heat flux assembled, with and without the radiation trap cover.*

This resonator is made in steel and screwed to the structure by sixteen screws, to assure the shield. This shield uses indium instead o-ring elastomeric material because elastomeric material is not appropriate for low temperatures. Figure 3.7 shows this vessel before and after assembling.

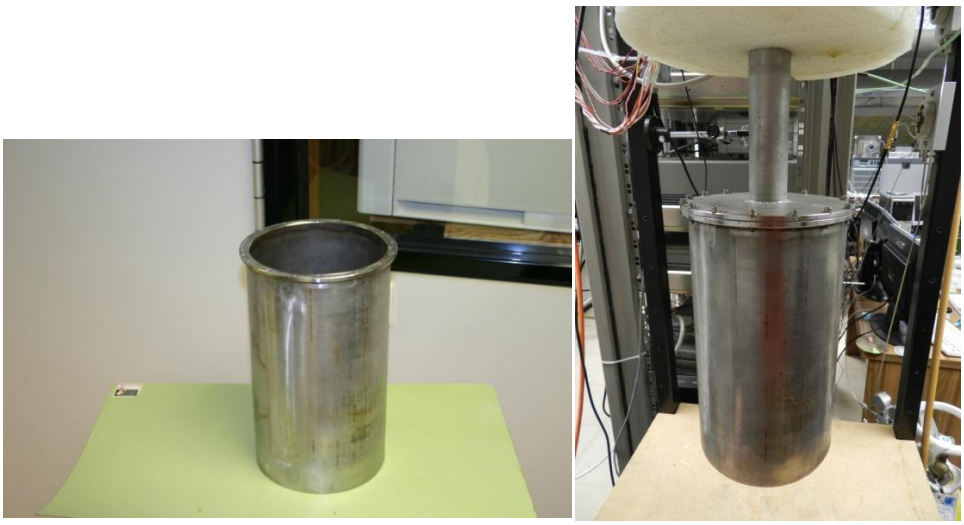

Figure 3.7 *Pressure vessel before and after assembled to the structure.*

This “pressure” vessel keeps pressure at low levels using two vacuum tandem pumps. They can be seen in figure 3.8. The first one (a centrifuge pump model Leybold Trivac B8B) is just to reduce pressure and the second one is a turbo molecular pump (model Leybold Turbovac SL300) which is able to decrease pressure to 10^{-4}Pa.

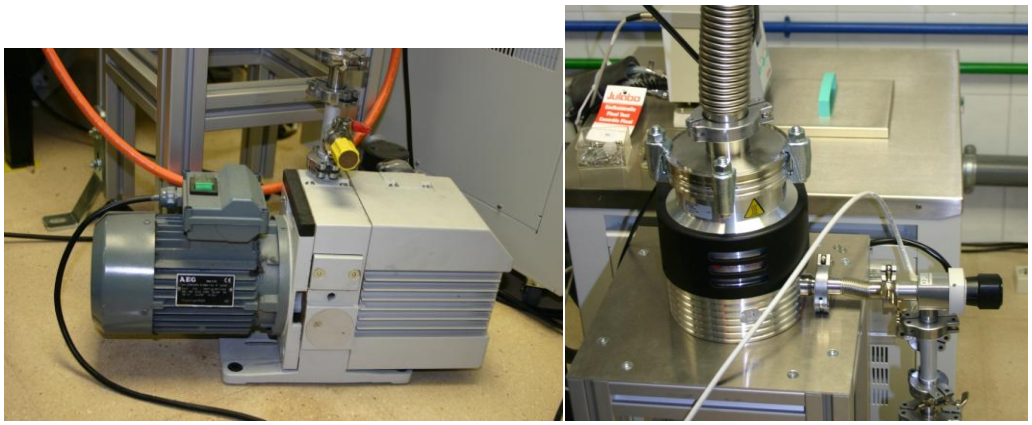

Figure 3.8 *Centrifuge pump Leybold Trivac B8B (left) and Turbo molecular vacuum pump model Leybold Turbovac SL300 (right)*

Resonator and vessels are immersed in a thermal bath, a Deward vessel filled with ethanol, to cool the entire equipment down the working temperature, and then by radiation and conduction heat flux control to the set up temperature(figure 3.9). The ethanol is cooled thanks to a Julabo FP89 thermal bath which extracts heat by a coil pipe (figure 3.10).

Figure 3.9 *Dewar vessel to cool resonator, pressure vessel and radiation vessel.*

Figure 3.10 *Thermostatic bath model Julabo FP89*

The copper block is only able to heat the resonator; therefore it is necessary to keep the temperature surrounding the equipment below the measuring temperature. The Julabo thermal bath and Dewar vessel are in charge of this issue. It is important set the temperature in the Dewar vessel at least 10K below the measuring Temperature to assure the right behaviour of the other temperature controlling systems. The lower the bath temperature the easier control, but it takes longer to reach the set up temperature after any change. So it is important to get an agreement on the bath temperature.

The temperature on the resonator is controlled indirectly, it is measured by means of two different thermometers as explained previously but the control is realized on the copper block, where the resonator is hanging from, and on the side and base of the radiation vessel. The temperature on the copper block is measured by one thermometer capsule-type platinum resistance, CSRT Rosemount 162D Pt-25 and by two Hart Scientific Pt-25 on the side and base of the isothermal shield. They were calibrated in Termocal facilities and results are shown in tables 3.1. The thermometers are read every five second using a Hewlett-Packard HP3458A multimeter and an Angilent Technologies 3499B switch control unit. The copper block, side and base of isothermal vessel temperature is separately controlled, to do so they hace

attached copper wires that are heated when electric current pass through them by joules effect. These wires are fed by three Hewllet Packard 3632A power suppliers that supply up to 7A of electric current, they can be seen in figure 3.11 Control loops were developed at Termocal facilities.

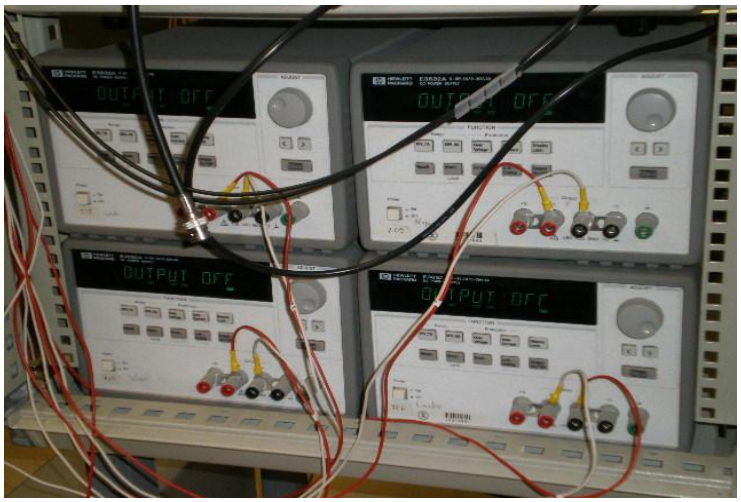

Figure 3.11 *Electric current sources HP3632A*

The radiation vessel was designed to avoid temperature gradient across the resonator by reducing energy loses by radiation from resonator surface to internal surface of the vessel. The way to reduce these radiation losses is by heating the radiation vessel to a temperature close to resonator surface temperature so there is not heat flux or if there is some heat flux is always to compensate possible temperature discrepancies.

The uncertainty budget achieved using the explained control steps is visible in table 3.2

Table 3.2 *Temperature uncertainty budget at 273.16K*

	Estimate (mK)	Distribution	Contribution to the standard uncertainty $u_i(T)$ (mK)
Stability	0.2	√12	0.06
Uniformity	0.5	√12	0.16
Calibration	0.07	1	0.07
Temperature		**k=1**	**0.19**

3.1.4 Pressure Measurement

The pressure is measured using two transducers, one for the range of high pressures (form 1MPa up to 20MPa) and the other one for low pressure range (up to 2MPa). The high pressure transducer is a Digiquartz Model 43RK-101 and model 2300A-101 for pressure lower than 2MPa. Thanks to these transducers the pressure accuracy is ±2Pa/Pa. Both transducers can be seen in figures 3.12 and 3.13.

Figure 3.12 *Pressure transducer Digiquartz 2003A-101*

Both transducers were calibrated in Termocal facilities, and are traceable to national standards. Calibration results are visible on table 3.3 for model 2300A-101 and in 3.4 for model 43RK-101

Figure 3.13 *Pressure transducer Digiquartz 43RK-101*

Table 3.3 *Calibration results for pressure transducer model 2300A-101.*

Reference pressure (kPa)	Read Pressure (kPa)	Uncertainty (kPa)
0.00	-0.70	± 0.07
51.02	50.32	± 0.07
103.57	102.88	± 0.08
107.26	106.57	± 0.07
504.39	503.73	± 0.10
1006.62	1005.86	± 0.13
1508.83	1507.93	± 0.16
1999.47	1998.51	± 0.19

Table 3.4 *Calibration results for pressure transducer model 43RK-101*

Reference pressure (kPa)	Read pressure (kPa)	Uncertainty (kPa)
1092.50	1098.80	±0.20
5089.60	5096.10	±0.50
10086.00	10093.30	±0.90
15082.40	15090.30	±1.30
20078.80	20087.50	±1.70

The measurements were taken from higher pressure reducing it by steps until the lower pressure measurements are possible.

The highest pressure is usually provided from the gas bottle, but when this pressure is not enough, a cylinder and piston is used to increase it to the desired conditions. The gas is expelled to the ambient from inside the resonator or through a vacuum pump when pressure is low.

To adjust pressure for measurements it is necessary to bring pressure close to the desired one, and after let some time to achieve thermal equilibrium, a smaller piston and cylinder system is used to make a fine adjustment. This adjusting cylinder is in figure 3.14

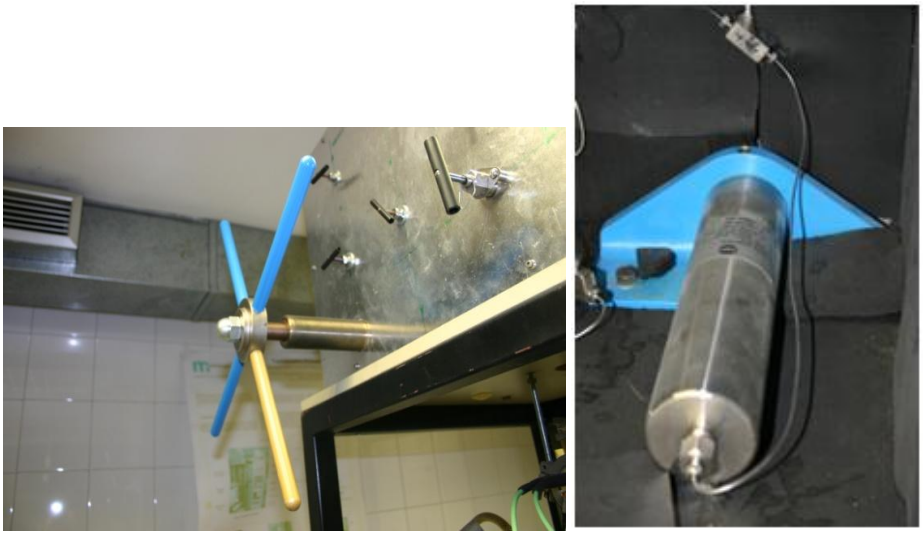

Figure 3.14 *Piston and cylinder pressure adjuster*

3.1.5 Acoustic Resonance Measurements.

Two capacitive acoustic transducers were designed to measure acoustic frequency of resonance. A detailed picture of one of them is displayed in figure 3.15. These transducers are capacitors made of two conductive surfaces (steel and a gold layer) separated by a dielectric polyimide membrane. When electric signal is supplied to one of these transducers induce the membrane to vibrate in such a way that it makes sound. And vice versa, if acoustic pressure vibrations impact on the membrane it produces an electrical signal which may be measured and quantified.

Figure 3.15 *Detailed view of acoustic transducer components*

One transducer acts as acoustic source, incoming signal is provided by HP synthesizer model 3225B which accuracy is $1X10^{-7}$Hz/Hz but it is attached to a rubidium frequency standard, Standford Research System FS725, , which improves this accuracy to $\pm5x10^{-11}$Hz/Hz.

Signal frequency is controlled digitally by computer software developed in Termocal facilities. The other acoustic transducer vibrates and produce electrical signal which is measured by a lock in, model SRS SR850-100kHzDSP (both apparatus are in figure 3.16) , after pass through a preamplifier designed by Ángel Gómez in Termocal facilities, figure 3.17 shows a schematic view of this preamplifier. This preamplifier is placed inside thermostatically isolated vessel but far enough to reduce heat dissipation from preamplifier to resonator.

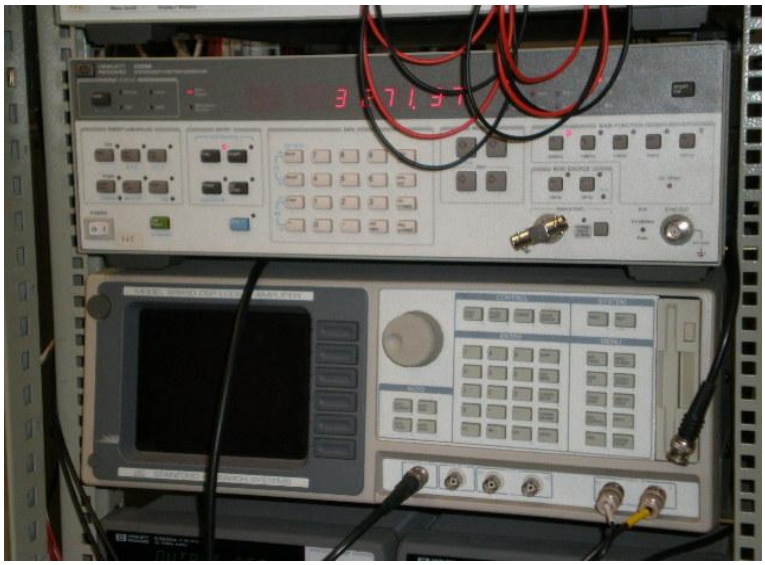

Figure 3.16 *Acoustic synthesizer model 3225B (on top) and lock in, model SRS SR850-100kHzDSP (at the bottom)*

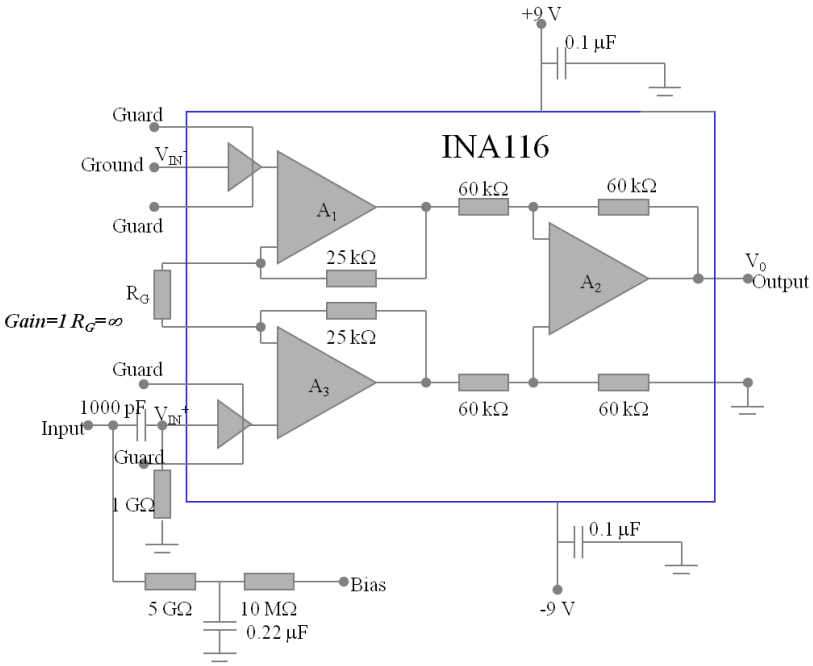

Figure 3.17 *Schematic view of the preamplifier design by Ángel Gómez*

3.1.6 Microwave Resonance Measurements.

The microwave resonance measurements were taken in the resonator B which is the misaligned one, and as it can be seen in figure 3.1 B, it has four transducer holders, two of them on the north hemisphere for the microwave transducers and two of them on the south for acoustic ones. Resonator A only has 2 holders for acoustic or microwave transducers, therefore to measure acoustic and microwave resonance it is necessary to dissemble and reassemble the transducer. That is why resonator B is used when microwave resonance is required and resonator A is used for other cases.

The microwave transducers are built using an OFHC copper loops (0.125 mm diameter) for which electrical and magnetic fields are excited. Figure 3.16 shows a microwave transducer.

Figure 3.16 *Microwave transducer into detail.*

A Network Analyzer Agilent N5230C PNA-L is used to measure frequency of resonance; it can be seen in figure 3.17. This Network Analyzer has a frequency range up to 13.5 GHz.

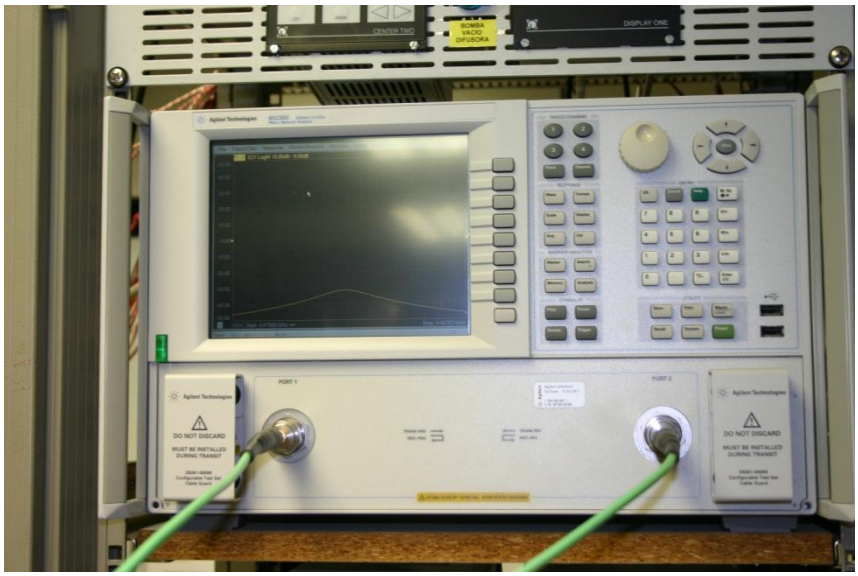

3.17 Figure *Network analyzer Agilent N523CPNA-L*

It is necessary to orientate the antennae before attach them to the resonator because antennae orientation has strong influence in microwave resonance peaks, when placed correctly and internal shape is smooth and high conductive, three separated peaks are detected. However, this study using stainless steel, hand polished resonator only two peaks are detected.

3.2 EXPERIMENTAL PROCEDURE.

The internal resonator radius is the first parameter measured because of its importance to calculate speed of sound as it is explained in chapter 2. It was measured by two different techniques, microwave resonance and acoustic resonance.

3.2.1 Radius Measurements Using Microwave Resonance.

Microwave resonance is carried on to measure internal radius with high accuracy, so it was used for the Boltzmann constant determination.

Boltzmann constant project requires measurements at only one temperature (273.16 K), in other words only one isotherm was defined. The process of measurement begins by filling the resonator with argon up to the maximum pressure, 0.9MPa. This top pressure was provided directly from the bottle, it was not need of compressor.

Once pressure has reached the desired conditions, the temperature needs to be adjusted. Two thermometers were placed across resonator surface to measure its temperature and

avoid temperature gradient. As it was explained in section before temperature in resonator was controlled indirectly by three more thermometers and PID software. Before measuring it is necessary to wait until thermal equilibrium is reached. Usually after this first process of filling and temperature adjustment, pressure shift and needs to be corrected. The cylinder and piston described before are used for this purpose, once again as it always happens when working with gases changes in pressure induce changes in temperature, therefore the process of adjusting pressure, waiting for thermal equilibrium and readjust pressure is carried on as many times as necessary to set desired pressure and temperature.

Radius is measured once temperature and pressure are set. Network analyzer feed microwave signal to one of the microwave transducer and read signal from the other one. Measured data are collected by a computer and processed by software which calculates degenerate modes peaks of resonance. This process is critical because microwave resonance is different for each mode and antennae orientation makes important changes in different modes, those changes affect directly to overall uncertainty. Even small changes on seeds for the calculation can make important changes on the results. These measurements require special attention and many times repetitions in order to obtain a reliable data. An example of microwave resonance measurements is shown in figure 3.18

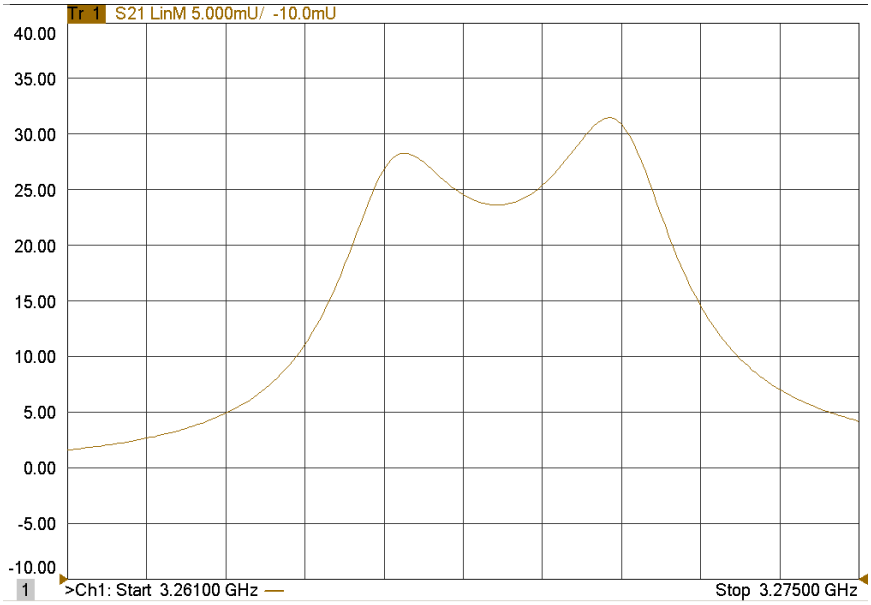

Figure 3.18 *Microwave resonance mode TM11 at P=0.9MPa and T=273.16K in argon*

Even when measurements shows results as those visible in figure 3.18, software is able to get three peaks, where two of them are very close. Nevertheless radius determination is possible even when only two peaks are detected, but modes dispersion increases and so it does the uncertainty.

Five electromagnetic modes were measured successfully, two electric modes TE11 and TE12, and three magnetic modes TM11, TM12, TM13.

Acoustic measurements are carried out immediately after microwave resonance to assure pressure and temperature changes are avoid or lower to 1mK.

After acoustic measurements are done pressure is reduced 0.2MPa. Once again thermal equilibrium must be reached and pressure readjusts. And measurements can be carried on again at the new pressure.

This whole process is done over again from 0.9MPa down to 0.2MPa and when pressure is lower than 0.2MPa, pressure steps were decreased, this way it is possible to obtain more information at lower pressures and increase accuracy when zero pressure extrapolation is done; the experimental results are given in the next chapters.

3.2.2 Acoustic Resonance.

Acoustic resonance was used for two purposes: measuring resonator internal radius at several pressures and temperatures; and to measure carrier gas properties. This last point includes the determination of the Boltzmann's constant.

Experimental procedures to measure internal radius or gas properties are quite similar, but changing pressure values according to the viability (cylinder pressure, gas amount...)

This chapter explains how internal radius was measured using argon, but this technique is also used two determine gas properties and Boltzmann's constant.

Radius was measured using acoustic resonance for the heat capacities determination since it does not need to be as accurate as Boltzmann's constant determination. Determine internal radius by acoustic resonance is also faster and easier. The speed of sound in the gas must be well known therefore argon, which equation of state is well known, is used.

These measurements are done in similar way than microwave resonance. Pressure and temperature are set. But five different isotherms (T=250.00K, T=273.16K, T=300.00K,

T=325.00K and T=350.00K) were measured and the procedure was the same for each one. (carbon monoxide and nitrogen mixtures were measured at, T=273.16K and T=325.00K; coal mine methane at T=250.00K and 273.16K).

First, the resonator is filled with working gas up to the highest pressure, when using argon this pressure was 20MPa, but for CO-N_2 mixtures it was 10MPa and for CMM 8MPa. For some of measured isotherms it was necessary to increase pressure manually, because the highest pressure provided by the gas bottle was not enough to reach the maximum pressure required inside the resonator. The manual compressor consists in a piston and cylinder system which can be isolated from the feeding bottle or the resonator independently therefore it can be feed from the bottle and compress the gas into the resonator and repeating this process several times it is possible to rise gas pressure in the resonator higher than that provided by the bottle.

Just like when using microwave it is necessary let the gas reach thermal equilibrium, and readjust pressure. Measurements are done once the temperature and pressure are set

Four acoustic modes were measured, (0,2), (0,3), (0,4) and (0,5), using two software programs were developed. One swipes frequency in range near theoretical frequencies of resonance, so it locates acoustic modes frequency of resonance and peak width. The other software program is run using frequency and peak width data obtained thanks to the first software. Figure 3.19 shows swiping program interface, and locating programs interface is shown in figure 3.20.

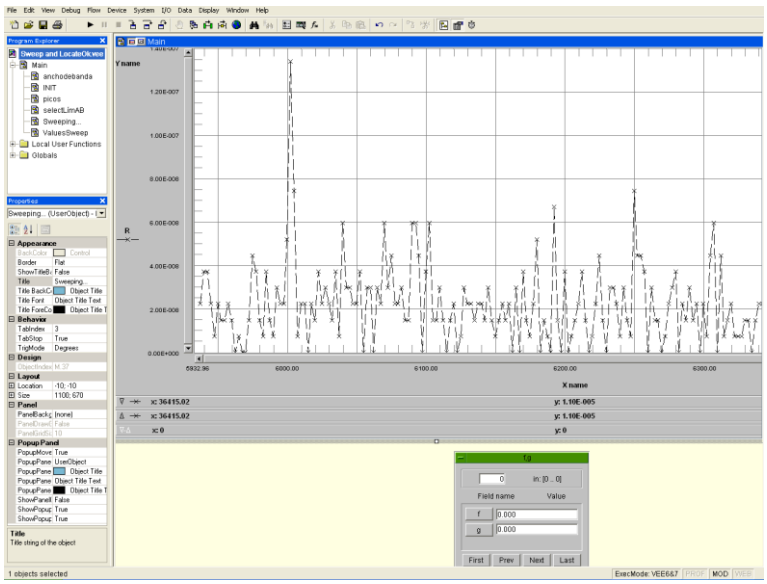

Figure 3.19 *Screen caption of the frequency gross location software*

Once all four modes are measured the pressure is changed by evacuating little amount of gas to the air or moving some gas to free volumes in the pipe circuit, like the manual compressor cylinder. Pressure changes affect temperature, therefore it is necessary to wait for thermal equilibrium, same procedure that at the beginning or when measuring microwave resonance.

Pressure changes are done by 1MPa steps (or 0.5MPa is more points are required to obtain a reliable isotherm) until 1MPa, after that a final measure at 0,1MPa was done.

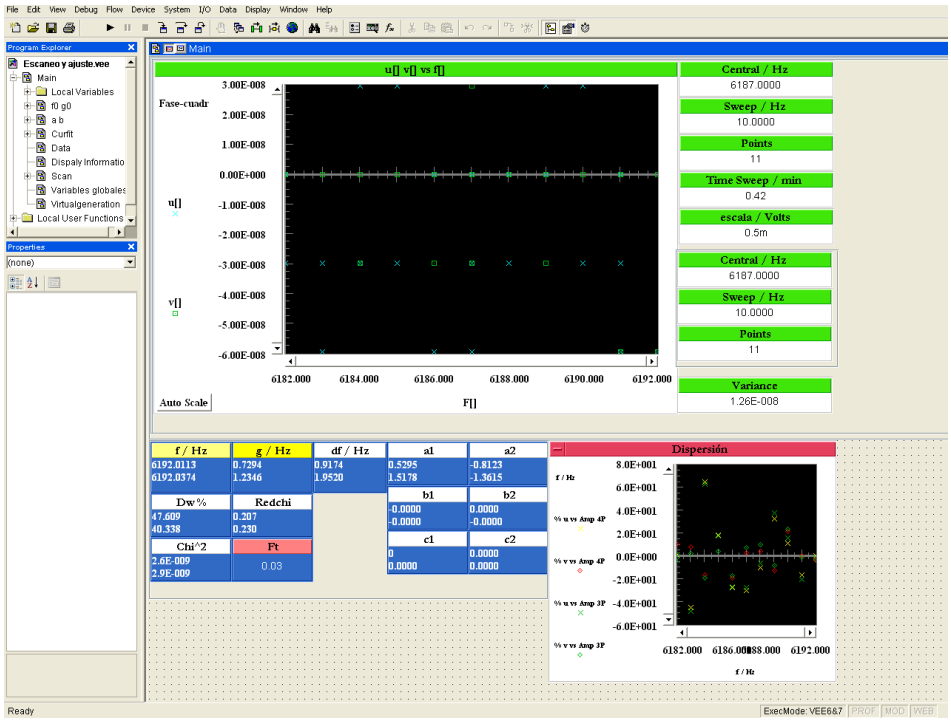

Figure 3.20 *Screen caption of the resonance frequency fine adjustment software*

Once the first isotherm is complete, the resonator is filled again and temperature is set for the next isotherm, and the whole process is repeated for each isotherm.

3.3 UNCERTAINTY BUDGET

Uncertainty is calculated following the Guide to the expression of Uncertainty in Measurement (GUM).

Acoustic resonance measurements were carried out in argon to obtain the Boltzmann's constant and in several gas mixtures for the determination of their thermodynamic properties. Two different uncertainty analyses were performed.

3.3.1 Boltzmann Constant Uncertainty Budget.

This uncertainty analysis was developed by Roberto Gavioso at the Metrologic Research National Institution (INRiM) in Torino, Italy [2]. The purpose of this analysis is made an equal standard in uncertainty calculations for all involved laboratories so they can be compared.

As it was described previously Boltzmann constant might be defined by equation 3.1:

$$k_B = \frac{M}{T\gamma^{pg}N_A}u_0^2 = \frac{M}{T\gamma^{pg}N_A}A_0 \tag{3.1}$$

The uncertainties are separated in two different sources, those which origin is because of the acoustic measurement, and those which origin is anything else. This second kind includes molar fraction, temperature and Avogadro's number uncertainty. All uncertainties in this section are obtained for a covering factor k=1.

Avogadro's constant value and uncertainty are detailed as follows:

$$N_A = 6.02214129\cdot10^{23}\ mol^{-1} \pm 2.7\cdot10^{16}\ mol^{-1}$$

If Avogadro's number uncertainty is expressed in relative it becomes [3]:

$$u(N_A) = 4.5\cdot10^{-8} mol^{-1} mol$$

Sensitivity for Avogadro's number is necessary to know how this relative uncertainty affects the overall Boltzmann constant relative uncertainty. It is calculated as indicated in equation 3.2

$$\frac{N_A}{k_B}\frac{\partial k_B}{\partial N_A} = 1 \tag{3.2}$$

Temperature sources of uncertainty are well known for this study. There are three sources of uncertainty: the sensors uncertainty, dispersion of the measurements and that due to the temperature gradient across the spherical resonator. The propagated temperature uncertainty is calculated using equation 3.3.

$$u(T)=\sqrt{u_{sensor}^2(T)+u_{disp}^2(T)+u_{grad}^2(T)} \tag{3.3}$$

Sensor uncertainty as it was described previously is lower than 1mK. Uncertainty due to temperature gradient across the resonator is calculated from experimental data considering temperature as a rectangular distribution which limit values are those measured at both hemispheres. And dispersion in temperature is equal to zero, because all temperature measurements were corrected from the measured value to the desired one. There are two different sources of uncertainty but in both cases sensitivity is calculated in the same way (equation 3.4):

$$\frac{T}{k_B}\frac{\partial k_B}{\partial T}=1 \tag{3.4}$$

Next parameter to take into account is molar composition of the gas. Argon composition was provided by "Air liquide", however, as it will be explained in chapter 4, argon was purified thanks to two chromatographic filters. Impurities were reduced to levels specified in table 4.1. All sensitivities for any impurity is calculated as it explains equation 3.5

$$\frac{M_i}{k_B}\frac{\partial k_B}{\partial M_i}=1 \tag{3.5}$$

The argon isotopic composition must be taken into consideration (isotopic average composition argon mola mass is M_{Ar}=39.948 g·mol^{-1}). Air liquide does not provide such information and it was not possible to compute, however, argon molar mass uncertainty provided includes this contribution.

Uncertainties related to the acoustic model are divided in two kinds of contributions: those related to acoustic frequency of resonance measurements themselves and those related to the determination of the internal radius length.

The uncertainty contributions which come from internal radius calculations are those related to microwave resonance. They are relative excess half-widths and relative modal dispersion [4].

Relative excess half-widths are calculated like shown in equation (3.6)

$$\frac{\Delta g}{f} = \frac{\left(g_{\exp} - g_{calc}\right)}{f} \tag{3.6}$$

The excess half-width taken into account for the measurement is that obtained at zero pressure. And its sensitivity is calculated as shown in equation 3.7

$$\frac{\Delta g}{k_B}\frac{\partial k_B}{\partial \Delta g} = 2 \tag{3.7}$$

The relative modal dispersion uncertainty is due to measuring internal radius by different microwave resonance modes, it is calculated according to equation 3.8

$$\frac{\Delta f}{f} = \frac{\left(f_i - \langle f \rangle\right)}{\langle f \rangle} \tag{3.8}$$

Where f_i is the peak frequency and $<f>$ is the frequency average of the three peaks. This dispersion must be evaluated at zero pressure. The sensitivity applied is shown by equation 3.9

$$\frac{\Delta f}{k_B}\frac{\partial k_B}{\partial \Delta f} = 2 \tag{3.9}$$

Other uncertainty sources are caused by acoustic resonance, which are described as follows.

The most important contributions to uncertainty due to acoustic resonance are those caused by modal inconsistency and extrapolation to zero pressure uncertainty.

Modal inconsistency has two contributions, excess half-widths that is calculated according equation 3.6 and relative modal dispersion calculated according equation 3.8

Relative modal dispersion is not required to apply when other uncertainties are added. Those uncertainties that must be added are due to thermal boundary layer, surface roughness, thermal accommodation, shell vibration, geometrical perturbations, ducts and microphones compliances.

These seven contributions were studied in previous works, some of them are null when the measurement of speed of sound is obtained by extrapolation to zero pressure. These uncertainties are those due to thermal boundary layer [5-9], thermal accommodation [10, 11], shell vibration [12-14] and microphone compliance [15]. The other 3 contributions are not

null. They are surface roughness [9, 16], geometry perturbations [17-21] and ducts compliance[22-24].

Chapter 4 shows the uncertainty calculations from the modal relative modal dispersion instead of the contribution of the other uncertainty sources described above.

Extrapolation to zero pressure, or the fitting uncertainty was computed using different analytical schemes. Four different fitting schemes were carried out according to bibliography[10] and the variation of the A_0 value gives the uncertainty .

Chapter 4 shows some of the most significant values of uncertainty contributions according equation 3.1 to 3.9. Other required values for the uncertainty calculations are detailed in the appendixes.

3.3.2 Gas Mixtures Properties Uncertainties.

In this case uncertainty analysis was carried out following "The guide to the expression of uncertainty in measurements" [25].

Speed of sound is the first property under study. Equation 3.10 describes how speed of sound is calculated from acoustic frequency of resonance, and from this equation using uncertainty propagation law, equation 3.11 is achieved and the speed of sound uncertainty might be computed.

$$u = \frac{2\pi a}{n}\sum_{i=1}^{n}\frac{f_i}{\upsilon_i} \tag{3.10}$$

$$u(u) = \sqrt{u^2(u) + \left(\frac{\partial u}{\partial a}\right)^2 u^2(a) + \sum_{i=1}^{n}\left(\frac{\partial u}{\partial f_i}\right)^2 u^2(f_i)}$$

$$u(u) = \sqrt{u^2(u) + \left(\frac{2\pi}{n}\sum_{i=1}^{n}\frac{f_i}{\upsilon_i}\right)^2 u^2(a) + \left(\frac{1}{n}\sum_{i=1}^{n}\frac{2\pi a}{\upsilon_i}\right)^2 u^2(f_i)} \tag{3.11}$$

Speed of sound uncertainty refers to experimental dispersion of all measured modes, and it is calculated as the mean standard deviation of the measured data.

Frequency of resonance uncertainty is calculated as mean standard deviation of the frequency measurements carried out. The detail of the results can be seen in the appendixes C, D and E.

Inner radius is calculated using acoustic resonance in a well-known gas, argon in this work. If speed of sound in the gas is known, equation 3.10 can be changed to equation 3.12. And using uncertainty propagation law it is easy to get equation 3.13

$$a = \frac{1}{n}\frac{u}{2\pi}\sum_{i=1}^{n}\frac{\upsilon_i}{f_i} \tag{3.12}$$

$$u(a) = \sqrt{u^2(a)_{disp} + \sum_{i=1}^{n}\left(\frac{\partial a}{\partial f_i}\right)^2 u^2(f_i) + \sum_{i=1}^{n}\left(\frac{\partial a}{\partial u}\right)^2 u^2(u)}$$

$$u(a) = \sqrt{u^2(a)_{disp} + \sum_{i=1}^{n}\left(\frac{1}{n}\frac{u}{2\pi}\frac{\upsilon_i}{f_i^2}\right)^2 u^2(f_i) + \sum_{i=1}^{n}\left(\frac{1}{n}\frac{\upsilon_i}{2\pi f_i}\right)^2 u^2(u)} \tag{3.13}$$

Resonance mode dispersion contributes to overall uncertainty just like it does in speed of sound measurements. It is calculated as an A type uncertainty. Also, frequencies of resonance have some uncertainty acquired during measuring process. Speed of sound is calculated according bibliographic equation of states, and uncertainty of this equation of state[26] is provided as well and it is lower than 0.02%.

Other thermodynamic properties are calculated using equation 3.14, and when uncertainty propagation law is applied to equation 3.10 to calculate uncertainty in the adiabatic coefficient, the equation 3.15 is obtained.

$$\gamma^{pg} = \frac{MA_0}{RT} \tag{3.14}$$

$$u(\gamma^{pg}) = \sqrt{\left(\frac{\partial \gamma^{pg}}{\partial M}\right)^2 u^2(M) + \left(\frac{\partial \gamma^{pg}}{\partial R}\right)^2 u^2(R) + \left(\frac{\partial \gamma^{pg}}{\partial T}\right)^2 u^2(T) + \left(\frac{\partial \gamma^{pg}}{\partial A_0}\right)^2 u^2(A_0)}$$

$$u(\gamma^{pg}) = \sqrt{\left(\frac{u_0^2}{RT}\right)^2 u^2(M) + \left(\frac{Mu_0^2}{R^2T}\right)^2 u^2(R) + \left(\frac{Mu_0^2}{RT^2}\right)^2 u^2(T) + \left(\frac{M}{RT}\right)^2 u^2(A_0)} \tag{3.15}$$

Molar mass uncertainty is obtained from individual component molar composition uncertainties which are detailed in each chapter of experimental measurements. Equations 3.16 and 3.17 are used to calculate molar composition contribution to overall uncertainty.

$$M = \sum_i x_i M_i \tag{3.16}$$

$$u(M)=\sqrt{\sum_i\left(\frac{\partial M}{\partial x_i}\right)^2 u^2(x_i)+\sum_i\left(\frac{\partial M}{\partial M_i}\right)^2 u^2(M_i)}$$
$$u(M)=\sqrt{\sum_i (M_i)^2 u^2(x_i)+\sum_i (x_i)^2 u^2(M_i)} \qquad (3.17)$$

Where suffix *i* refers to any component in the gas mixture.

The next uncertainty source is that due to the uncertainty on the ideal gas constant, this value was obtained from NIST data base[3].

$$R=8.3144621\ J\cdot mol^{-1}K^{-1} \pm 0.0000075\ J\cdot mol^{-1}K^{-1}$$

Temperature uncertainty is calculated as explained before for Boltzmann constant determination. Equation 3.3 was used, but in this case temperature dispersion is not null. It is calculated as type A uncertainty, the mean standard deviation of the collected temperature data.

One of the most important and complex calculation to measure these thermodynamic properties is the square of speed of sound at zero pressure which cannot be measured directly. It is necessary to calculate it by a polynomial regression as it was explained in chapter 2. Uncertainty in this parameter was calculated using Monte Carlo estimation, using experimental measurements of speed of sound at several different pressures and the uncertainty of those measurements. Pressure measurements uncertainties were explained in section 3.4.1 and uncertainty in speed of sound calculations was described previously in this section.

Isochoric molar heat capacities are calculated from adiabatic factor using Mayer's relation (equation 3.18). When uncertainty propagation law is applied to this relation equation 3.19 is obtained.

$$C_v=\frac{R}{\gamma^{pg}-1} \qquad (3.18)$$

$$u(C_v)=\sqrt{\left(\frac{\partial C_v}{\partial R}\right)^2 u^2(R)+\left(\frac{\partial C_v}{\partial \gamma^{pg}}\right)^2 u^2(\gamma^{pg})}$$
$$u(C_v)=\sqrt{\left(\frac{1}{\gamma^{pg}-1}\right)^2 u^2(R)+\left(\frac{R}{(\gamma^{pg}-1)^2}\right)^2 u^2(\gamma^{pg})} \qquad (3.19)$$

The ideal gas constant uncertainty was explained previously, and adiabatic coefficient uncertainty calculations are explained in equations 3.10 to 3.13.

Isobaric heat capacity is calculated when adiabatic coefficient and isochoric heat capacity are know by equation 3.20, and its uncertainty thanks to equation 3.21.

$$C_p = \gamma^{pg} C_v \tag{3.20}$$

$$u(C_p) = \sqrt{\left(\frac{\partial C_p}{\partial \gamma^{pg}}\right)^2 u^2(\gamma^{pg}) + \left(\frac{\partial C_p}{\partial C_v}\right)^2 u^2(C_v)}$$

$$u(C_p) = \sqrt{C_v^2 u^2(\gamma^{pg}) + \gamma^{pg^2} u^2(C_v)} \tag{3.21}$$

All required uncertainties to compute isobaric uncertainty were explained previously.

Two more thermodynamic properties are obtained in this study, first and second acoustic virial parameters, for this calculation it is important to refresh how they are obtained. Acoustic virial equation is defined as a density polynomial function which is truncated in the third term for our measurement (equation 3.22). However, as the density measurements were not taken, equation 3.22 may be modified in to equation 3.23 where it becomes function of pressure which was properly measured. The acoustic virial parameters from equation 3.22 are related to parameters in equation 3.23. These relations are shown in 3.24 and 3.25

$$u^2 = A_0\left(1 + \beta_a \rho + \gamma_a \rho^2\right) \tag{3.22}$$

$$u^2 = A_0 + A_1 p + A_2 p^2 \tag{3.23}$$

$$\beta_a = \frac{A_1}{A_0} RT \tag{3.24}$$

$$\gamma_a = \frac{A_2}{A_0}(RT)^2 \tag{3.25}$$

Second acoustic virial coefficient uncertainty therefore was calculated according to equation 3.26 and in similar way equation 3.27 was used for third acoustic virial coefficient.

$$u(\beta_a)=\sqrt{\left(\frac{\partial\beta_a}{\partial A_1}\right)^2 u^2(A_1)+\left(\frac{\partial\beta_a}{\partial A_0}\right)^2 u^2(A_0)+\left(\frac{\partial\beta_a}{\partial R}\right)^2 u^2(R)+\left(\frac{\partial\beta_a}{\partial T}\right)^2 u^2(T)}$$

$$u(\beta_a)=\sqrt{\left(\frac{RT}{A_0}\right)^2 u^2(A_1)+\left(\frac{A_1RT}{A_0^2}\right)^2 u^2(A_0)+\left(\frac{A_1T}{A_0}\right)^2 u^2(R)+\left(\frac{A_1R}{A_0}\right)^2 u^2(T)} \quad (3.26)$$

$$u(\gamma_a)=\sqrt{\left(\frac{\partial\gamma_a}{\partial A_2}\right)^2 u^2(A_2)+\left(\frac{\partial\gamma_a}{\partial A_0}\right)^2 u^2(A_0)+\left(\frac{\partial\gamma_a}{\partial R}\right)^2 u^2(R)+\left(\frac{\partial\gamma_a}{\partial T}\right)^2 u^2(T)} \quad (3.27)$$

$$u(\gamma_a)=\sqrt{\left(\frac{(RT)^2}{A_0}\right)^2 u^2(A_2)+\left(\frac{A_2(RT)^2}{A_0^2}\right)^2 u^2(A_0)+\left(\frac{2A_1RT^2}{A_0}\right)^2 u^2(R)+\left(\frac{2A_1R^2T}{A_0}\right)^2 u^2(T)}$$

Parameters A_0, A_1 and A_2 uncertainties were calculated using Monte Carlo simulation; ideal gas constant and temperature uncertainties were explained before.

Uncertainties values of thermodynamic parameters are in the results section of each gas mixture. Other uncertainties as frequencies or speed of sound are in appendixes.

3.4 REFERENCES

1. Mehl, J.B., and Moldover, M.B. (1986) Measurement of the ratio of the speed of sound to the speed of light. Phys. Rev. 34, 3341-3344.

2. Moldover, M.R., Gavioso, R.M., Mehl, J.B., Pitre, L., Podesta, M.d., and Zhang, J.T. Acoustic gas thermometry. Metrologia 51, R1-R19.

3. NIST. (2010) NIST Database. NIST.

4. Albo, P.A.G., Gavioso, R.M., and Benedetto, G. (2010) Modeling Steady Acoustic Fields Bounded in Cavities with Geometrical Imperfections. International Journal of Thermophysics 31, 1248-1258.

5. Mehl, J.B. (2009) Ab initio properties of gaseous helium. Comptes Rendus Physique 10, 859-865.

6. G. C. Maitland, R.R., E. B. Smith, W. A. Wakeham. (1981) Intermolecular Forces: Their Origin and Determination. Oxford.

7. Sutton, G. (2009) Uncertainty in the TBLC and bulk dissipation corrections for TCU1 / Argon. NPL Report ENG 20.

8. May, E.F., Moldover, M.R., Berg, R.F., and Hurly, J.J. (2006) Transport properties of argon at zero density from viscosity-ratio measurements. Metrologia 43, 247-258.

9. Moldover, M.R. (2009) Optimizing acoustic measurements of the Boltzmann constant. Comptes Rendus Physique 10, 815-827.

10. Sutton, G., Underwood, R., Pitre, L., Podesta, M., and Valkiers, S. Acoustic Resonator Experiments at the Triple Point of Water: First Results for the Boltzmann Constant and Remaining Challenges. International Journal of Thermophysics 31, 1310-1346.

11. F. O. Goodman, H.Y.W. (1967) Formula for Thermal Accommodation Coefficients. J. Chem. Phys. 49, 107-115.

12. Mehl, J.B. (1985) Spherical acoustic resonator: Effects of shell motion. The Journal of the Acoustical Society of America 78, 782-788.

13. Gavioso, R.M., Madonna Ripa, D., Guianvarc'h, C., Benedetto, G., Giuliano Albo, P.A., Cuccaro, R., Pitre, L., and Truong, D. Shell Perturbations of an Acoustic Thermometer Determined from Speed of Sound in Gas Mixtures. International Journal of Thermophysics 31, 1739-1748.

14. Truong, D., Sparasci, F., Foltête, E., Ouisse, M., and Pitre, L. Measuring Shell Resonances of Spherical Acoustic Resonators. International Journal of Thermophysics 32, 427-440.

15. Guianvarc'h, C.c., Gavioso, R.M., Benedetto, G., Pitre, L., and Bruneau, M. (2009) Characterization of condenser microphones under different environmental conditions for accurate speed of sound measurements with acoustic resonators. Review of Scientific Instruments 80, -.

16. Mehl, J.B. Thermal Viscous Boundary Layer Near Corrugated Surface.

17. Mehl, J.B. (2007) Acoustic Eigenvalues of a Quasispherical Resonator: Second Order Shape Perturbation Theory for Arbitrary Modes. J. Res. Natl. Inst. Stand. Technl. 112, 11.

18. Mehl, J. Acoustic Eigenvalues of Quasispherical Resonators: Beyond the Triaxial Ellipsoid Approximation. International Journal of Thermophysics 31, 163-173.

19. Albo, P.A.G., Gavioso, R.M., and Benedetto, G. Modeling Steady Acoustic Fields Bounded in Cavities with Geometrical Imperfections. International Journal of Thermophysics 31, 1248-1258.

20. Podesta, M.d., May, E.F., Mehl, J.B., Pitre, L., Gavioso, R.M., Benedetto, G., Albo, P.A.G., Truong, D., and Flack, D. Characterization of the volume and shape of quasi-spherical resonators using coordinate measurement machines. Metrologia 47, 588-604.

21. Underwood, R., Flack, D., Morantz, P., Sutton, G., Shore, P., and Podesta, M.d. Dimensional characterization of a quasispherical resonator by microwave and coordinate measurement techniques. Metrologia 48, 1-15.

22. K. A. Gillis, H.L., M. R. Moldover. (2009) Perturbation From Ducts on the Modes of Acoustic Thermometers. J. Res. Natl. Inst. Stand. Technol. 114, 263-285.

23. Rodrigues, D., Guianvarc'h, C., Durocher, J.N., Bruneau, M., and Bruneau, A.M. (2008) A method to measure and interpret input impedance of small acoustic components. Journal of Sound and Vibration 315, 890-910.

24. Matula, R.A. (1979) Electrical resistivity of copper, gold, palladium, and silver. Journal of Physical and Chemical Reference Data 8, 1147-1298.

25. Evaluation of measurment data - Guide to the expression of uncertainty in measurement BIMP, 2008.

26. Tegeler, C.S., R.; Wagner,W. (1999) A New Equation of State for Argon Covering the Fluid Region for Temperatures From ther Melting Line to 700K at Presures up to 1000MPa. Journal of Physical and Chemical Reference Data 28, 779-850.

Chapter 4

ARGON MEASUREMENTS, DETERMINATION OF BOLTZMANN'S CONSTANT

4.1 INTRODUCTION

As it was said before this thesis has two different sets of measurements for two different purposes. Argon measurements were carried out to determine the Boltzmann constant.

As explained in section 2 for these measurements it is necessary to use monatomic gases. Argon and helium are useful for this purpose because they are non reactive gases and this way assures low or null contamination from the pipes and resonator shell. This experiment was carried out using argon to fill the acoustic cavity.

4.2 GAS SAMPLE

The argon was purchased to air liquid. Molar mass is 39.948 g·mol-1 which purity is certified to be 99.9999% and impurities are lower than specifications detailed in table 4.1

Argon goes through two chromatographic filters before entering the cavity; these filters assure reduction of humidity and other possible impurities lower than specifications in table 4.1

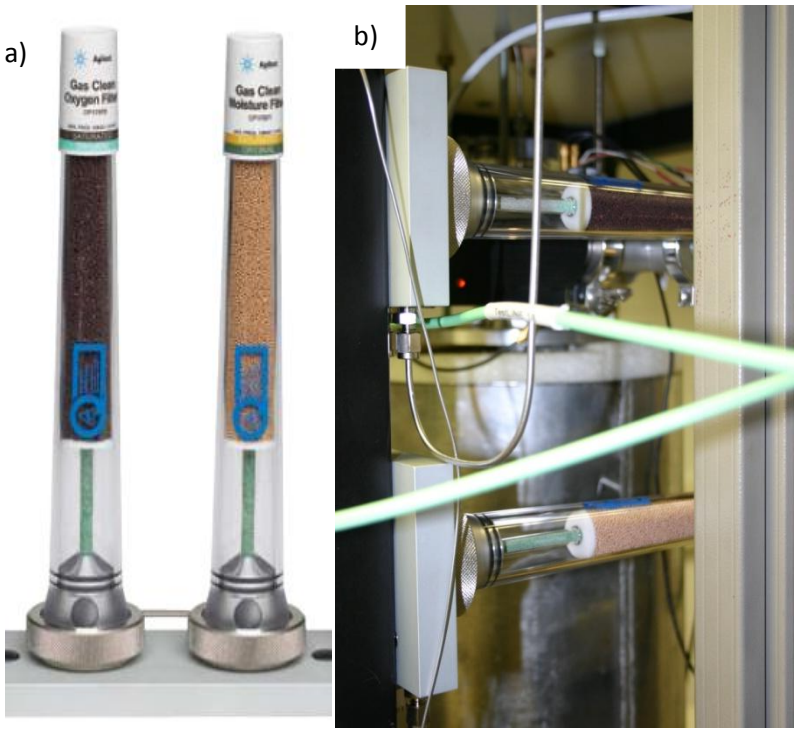

Figure 4.1 *a) Picture of the two chromatographic filters used to assure low impurities in argon. b) Detailed view of the filters set up.*

However isotopic composition of argon in the bottle was not provided which could increase uncertainty on overall result.

Table 4.1 *Argon impurities especifications before and after chromatographic filters.*

Compound	**Concentration according air liquid /ppb**	**Concentration after chromatographic filter /ppb**
Oxygen	<100	<50
Water	<500	<100
Carbon dioxide	<100	<100
Carbon monoxide	<100	<100
Hydrogen	<100	<100
Other organic compounds	<100	<100

Microwave resonance measurements were carried out in order to get inner radius values for different pressures and temperatures. Acoustic and microwave resonance measurements were taken consecutively so changes of pressure or temperature were reduced to the minimum and therefore lower corrections are needed and lower uncertainty is obtained.

Five electromagnetic modes of resonance were measured: TM11, TE11, TM12, TE12 and TM13. They were measured at the temperature of the triple point of water, 273.16K for several different pressures from 78.2 kPa up to 901.3kPa.

4.3 MICROWAVE MEASUREMENTS, DETERMINATION OF RADIUS

Electromagnetic mode resonance frequencies are degenerated into triplets, but the set up displayed for this study was in such a way that two of them were mixed together as it is visible in figure 4.2

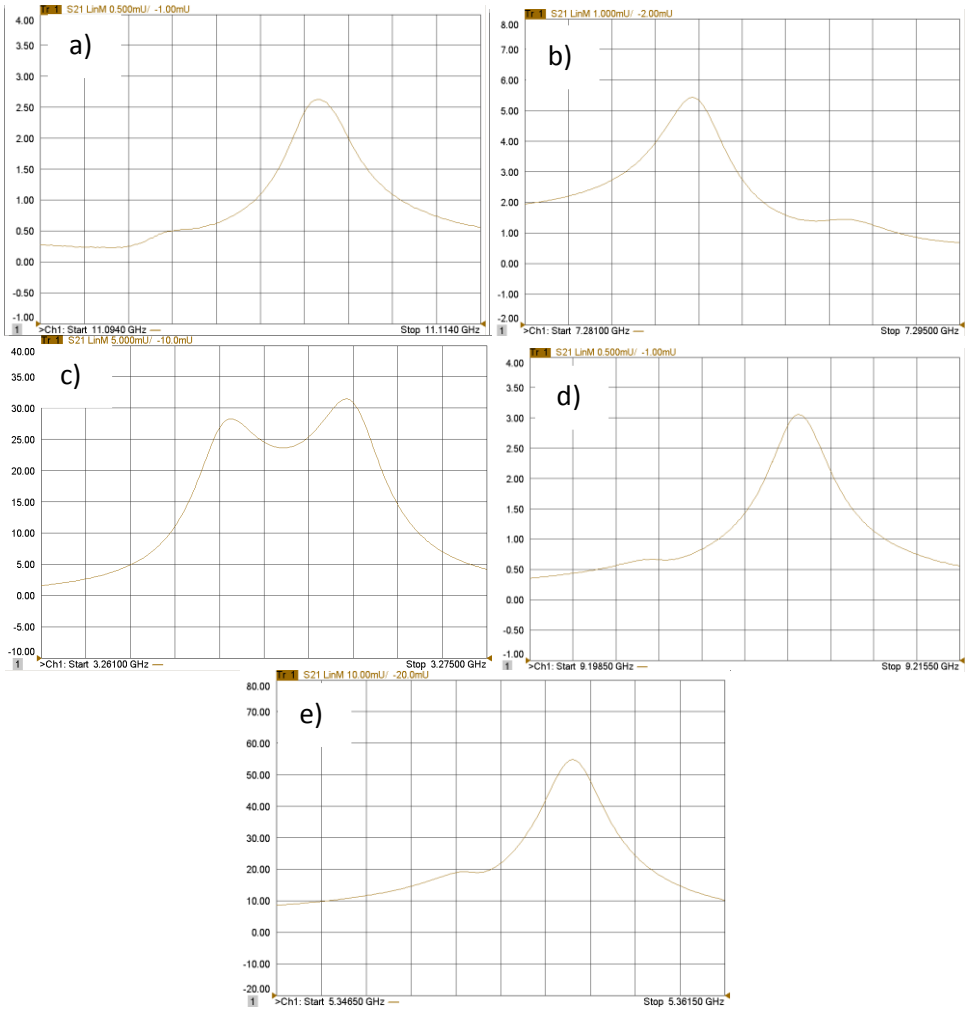

Figure 4.2 *Measurements for the electromagnetic modes a) TM11, b) TE11, c) TM12, d) TE12 and e) TM13.*

Resonance peaks are found thanks to a Labview program developed by Prof. Eric May at University of Western Australia using Levenberg-Mardquardt algorithm. This programme is able to locate the three peaks and their half-width factors, even when the shape of the measurements looks like figure 4.2. Table 4.2 shows values of some of the taken measurements; the values of each measured peak are in appendix A.

Table 4.2 *Resonance frequency peaks and half-width of the resonance peaks for modes TM11, TE11, TM12, TE12 and TM13 at T=273.16K and p=0.9MPa*

mode	1st peak frequency (Hz)	2nd peak frequency (Hz)	3rd peak frequency (Hz)	1st peak halfwidth (Hz)	2nd peak halfwidth (Hz)	3rd peak halfwidth (Hz)
TM11	3260.171	3263.861	3264.120	1.001	1.088	1.017
TE11	5341.894	5345.292	5345.607	0.942	1.092	1.135
TM12	7271.564	7271.781	7276.464	1.070	1.782	1.241
TE12	9184.416	9189.971	9190.449	1.102	1.097	1.129
TM13	11076.424	11083.314	11084.143	1.118	1.187	1.162

As it was said before some corrections must be applied. The values of these corrections are shown in appendix B, some of these data are shown in the following table 4.3. The thermal penetration length decreases with pressure, and it is just the opposite when we observe the thermal boundary layer correction for microwaves, these behaviours are shown in figure 4.3 and 4.4

Table 4.3 *Thermal penetration length and thermal boundary layer corrections for electromagnetic modes TM11, TE11, TM12, TE12 and TM13 at p=0.9MPa and T=273.16K*

Mode	$\delta_{TH}(m)$	$\Delta f(Hz)$
TM11	3.95×10^{-6}	0.219
TE11	3.08×10^{-6}	0.229
TM12	2.64×10^{-6}	0.254
TE12	2.35×10^{-6}	0.279
TM13	2.14×10^{-6}	0.304

.

We can calculate the radius of the sphere according equation 2.17, after applying the proper corrections explained previously.

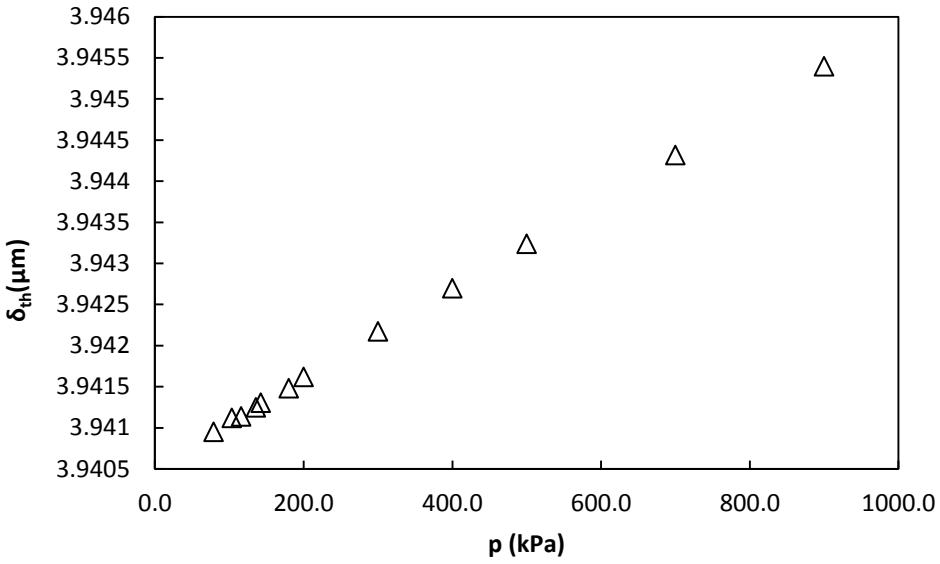

Figure 4.3 *Thermal penetration lengths for electromagnetic mode TM11 at T=273.16K and pressure range from p=0.078MPa up to p= 0.9MPa*

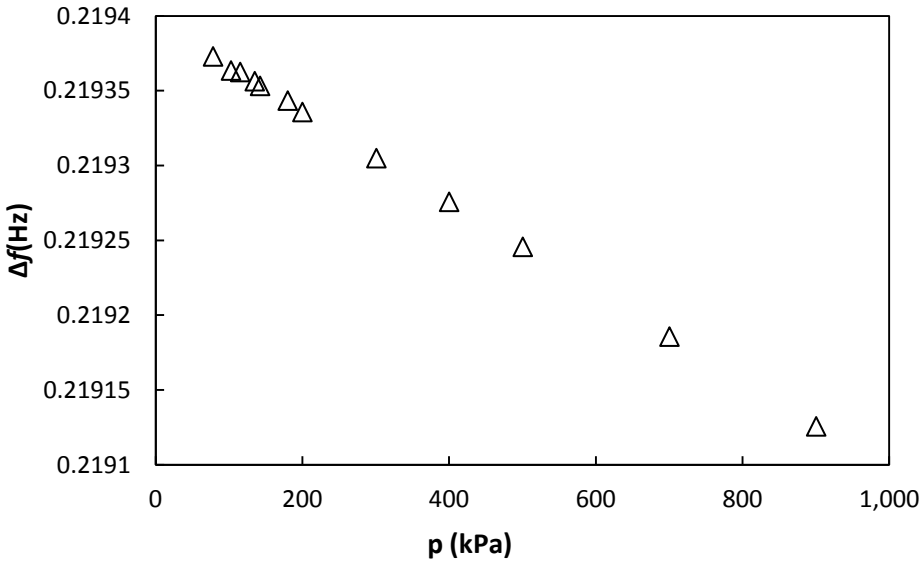

Figure 4.4 *Thermal boundary later corrections for Electromagnetic mode TM11 at T=273.16K and pressure from p = 0.078MPa up to p = 0.9MPa*

Table 4.4 *Calculated radii for electromagnetic mode TE11 at T=273.16K at several pressures.*

p (kPa)	a(mm)
901.3	40.01616
701. 3	40.01611
501.2	40.01598
400.8	40.01595
301. 6	40.01591
200.7	40.01586
180.7	40.01586
143.0	40.01584
135.7	40.01577
102.7	40.01584
78.2	40.01583

As an example the calculated radii for mode TM13 are shown in table 4.4, and all the values of radius for each mode are shown in appendix B.

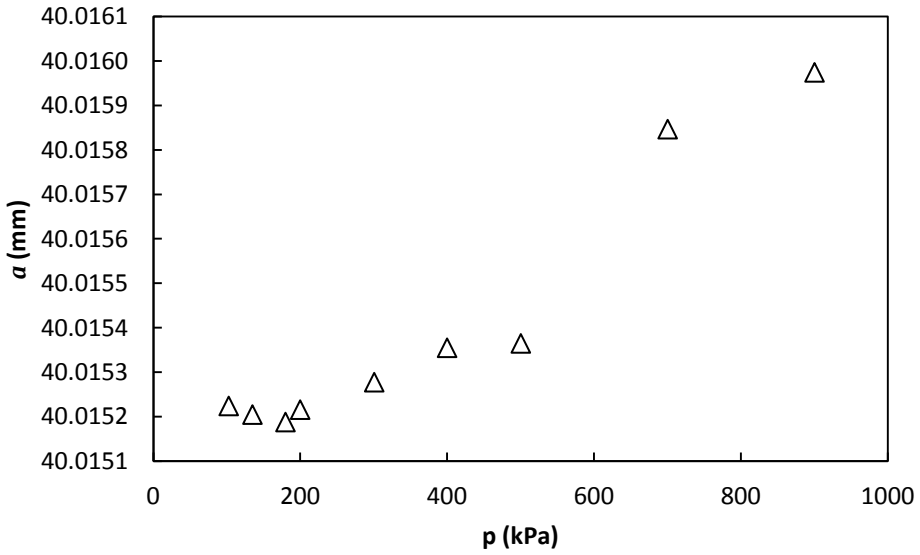

Figure 4.5 *Average radius values at T=273.16K in the pressure range from p = 0.078MPa up to p = 0.9MPa*

Each resonance mode gives a different radius value and because of that, figure 4.5 shows the average of the calculated radii at each pressure, these values are obtained from the average of the frequency of the three peaks of the modes TE11, TM12, TE12 and TM13. TM11 mode does not have a good accordance with the other measured modes, and this is the reason why it was not taken into account to calculate the average radius, however, the data were

taken, calculated and displayed in table 4.5 therefore a comparison could be made. As it can be seen in figure 4.6 and table 4.5 radius values decreases with frequency. This variation with frequency is a consequence of the shell imperfections, it should be necessary develop and apply second order corrections for misaligned resonators.

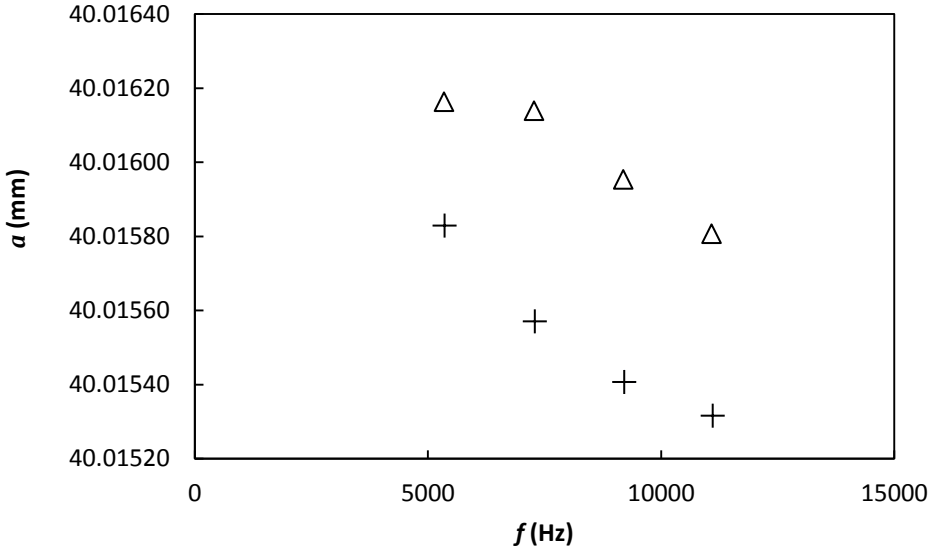

Figure 4.6 *Radius values for modes TE11 (5,3MHz), TM12 (7.2MHZ), TE12 (9.2MHz) and TM13 (11.0MHz) at two different pressures (Δ) p = 0.9MPa and (+) p = 0.078MPa.*

Table 4.5 *Radius values for electromagnetic resonance modes TM11, TE11, TM12, TE12 and TM13 at T=273.16K and p=0.9MPa*

Mode	*a* (mm)
TM11	40.02057
TE11	40.01616
TM12	40.01613
TE12	40.01595
TM13	40.01581

Temperature and pressure are not exactly the same for each experimental data. The setup and experimental procedure are designed to take the measurements as close as possible to the desired conditions but it is not possible to achieve an exact control at the desired temperature with the required precision. Therefore the calculated value of the radius needs correction. Equation 2.29 is used to apply this temperature and pressure correction for the average radius. We can look the effect of this correction into detail in table 4.6, where the values of the radius before and after the correction are reported.

$$a_{T_0,P_0} = a_{T_{\exp},P_{\exp}}\left[\left(1+\frac{\kappa_T}{3}\left(P_{\exp}-P_0\right)\right)+\alpha_L\left(T_{\exp}-T_0\right)\right] \quad (2.29)$$

Table 4.6 *Radius average value before and after the pressure and temperature correction*

p (kPa)	***a*(mm)**	***a* corrected (mm)**
901	40.01597	40.01599
701	40.01585	40.01586
501	40.01536	40.01538
401	40.0154	40.01537
302	40.01528	40.01530
201	40.01522	40.01523
181	40.01519	40.01520
143	40.01563	40.01564
136	40.01520	40.01520
116	40.01738	40.01738
103	40.01522	40.01523
79	40.01552	40.01552

In order to get the highest accuracy of the measurements, acoustic and microwave resonance must be done at the same pressure and temperature conditions.

4.4 ACOUSTIC MEASUREMENTS.

Just after measuring electromagnetic frequency of resonance we took data for acoustic frequencies this way measuring conditions are equal for both processes, and the uncertainty is reduced.

The set of measurements were taken at the conditions of several different pressures from 78.2 kPa up to 901.3 kPa, and the temperature of 273.16K. Seven acoustic resonance modes were measured: (0,2); (0,3); (0,4); (0,5); (0,6); (0,7) and (0,8). Some of these measurements are shown in tables 4.7 and 4.8. In the first one we can see all the modes frequencies of resonance (f) and the half-width factor (g) when pressure is set to 0.901MPa; the second of these tables presents the same data (f and g) but in this case only for the mode (0,2) and for the complete range of pressure.

Table 4.7 *Acoustic frequency of resonance (f) and half-width of the resonance peaks (g) for modes (0,2) to (0,8) at T = 273.16K and p = 0.9MPa*

Mode	*f*(Hz)	*g*(Hz)
(0,2)	5507.74	0.775
(0,3)	9469.72	0.941
(0,4)	13366.29	1.049
(0,5)	17241.06	1.629
(0,6)	21106.18	5.824
(0,7)	24809.90	3.901
(0,8)	28692.45	2.623

Table 4.8 *Acoustic resonance frequencies (f) and half-width of the resonance peak for mode (0,2) at 273.16K and the range of pressure from p = 0.078MPa up to p = 0.9MPa*

p (kPa)	*f*(Hz)	*g*(Hz)
901.3	5507.74	0.775
701. 3	5505.93	0.848
501.2	5504.20	0.960
400.8	5503.34	1.043
301. 6	5502.53	1.169
200.7	5501.63	1.388
180.7	5501.43	1.433
143.0	5501.05	1.572
135.7	5500.94	1.609
115.3	5500.71	1.711
102.7	5500.58	1.785
78.2	5500.21	1.995

The frequency of resonance change with pressure and temperature but this part of the study was carried out only at T = 273.16K, therefore no changes with temperature are present and only pressure shifts will be shown. We can see in figure 4.7 one of these changes with pressure, in particular the acoustic frequency of resonance. This change happens because the speed of sound behaves in the same way with pressure and according equation 2.10 frequency of resonance and speed of sound are linearly dependent.

$$u = \frac{2\pi a f_{lm}}{\xi_{lm}} \tag{2.10}$$

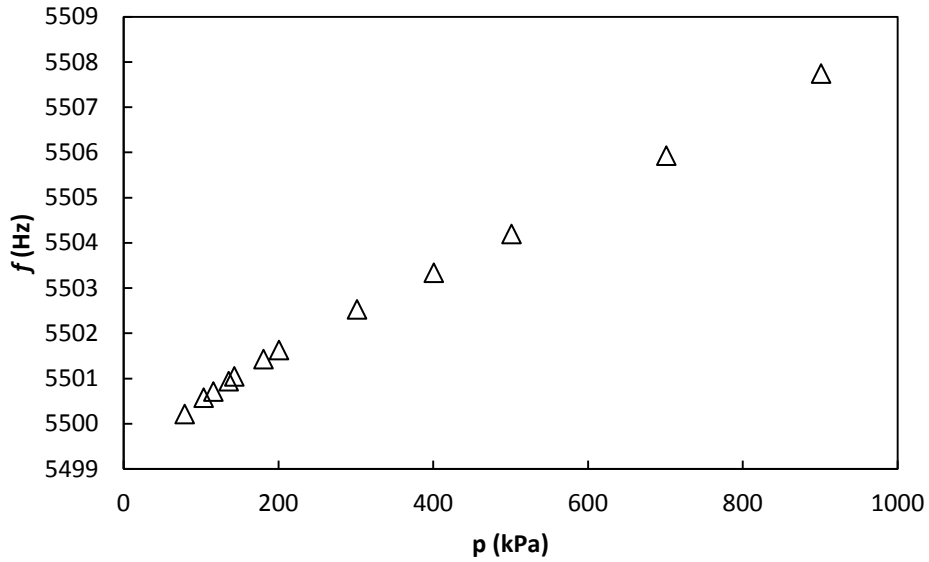

Figure 4.7 *Acoustic frequency of resonance for acoustic mode (0,2) at T = 273.16Kfor the pressure range from p = 0.078MPa up to p=0.9MPa.*

The resonance peak half-width tendency is shown in figure 4.8. It increases when pressure decreases this is a normal effect because acoustic waves need a material pathway for their propagation, and at low pressure the density decreases and it became harder to propagate, in other words, it loses more energy for its propagation, and as it was explained in chapter 2 resonance peak half-widths is the quality factor that represents the lost of acoustic energy.

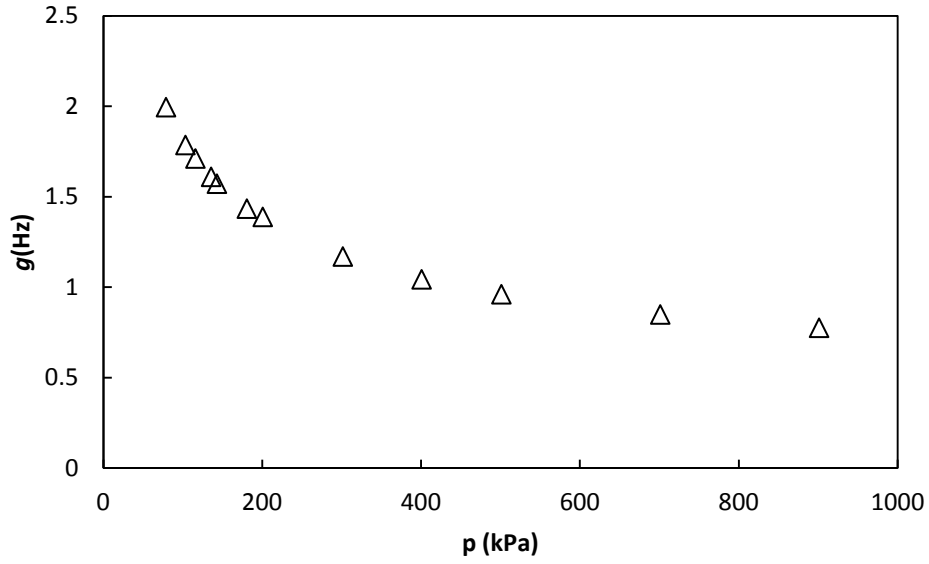

Figure4.8 *Half-width of resonance peak for acoustic mode (0,2) at T = 273.16K for the pressure range p = 0.078MPa up to p = 0.9MPa*

4.4.1 Frequency corrections

Once the data are taken some calculations must be done, as it was said in chapter 2 acoustic frequency of resonance needs corrections. These corrections are function of pressure, temperature and frequency of resonance itself. Therefore no corrections might be applied before measure the frequencies. The following sections will resume the calculations carried out and some of the final results.

4.4.1.1 *Thermal boundary layer correction*

The thermal boundary layer correction is the most important. But in order to get these corrections it is necessary to calculate some other parameters first, like the thermal penetration length. Figure 4.9 shows thermal penetration length for modes (0,2) to (0,8) in the pressure range from p=0.078MPa to p=0.9MPa and table 4.9 shows variation of this parameter with resonance mode

Table 4.9 *Thermal penetration length at p= 0.9MPa for acoustic modes (0,2) to (0,8) in argon*

Mode	δ_{TH}(m)
(0,2)	1.07×10^{-5}
(0,3)	8.13×10^{-6}
(0,4)	6.84×10^{-6}
(0,5)	6.02×10^{-6}
(0,6)	$5.44E \times 10^{-6}$
(0,7)	5.02×10^{-6}
(0,8)	4.67×10^{-6}

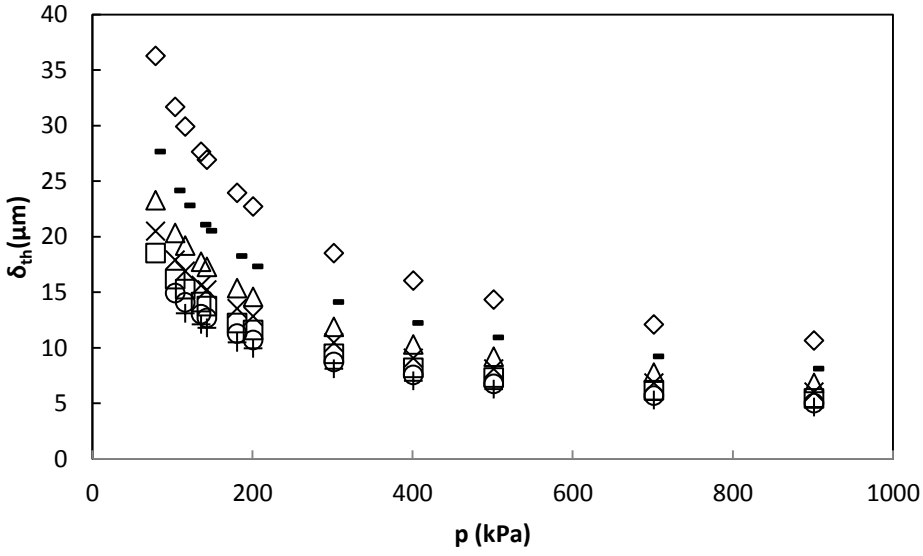

Figure 4.9 *Thermal penetration lengths in the pressure range from p=78kPa to p= 900kPa for acoustics modes (0,2) (◊), (0,3) (-), (0,4) (Δ), (0,5) (X), (0,6) (□), (0,7) (o) and (0,8)(+) at 273.16K*

It is also necessary to calculate the thermal accommodation length (l_{th}) to determine the thermal boundary layer correction as it was explained in chapter 2. This parameter changes with temperature and pressure. Frequency of resonance does not affect this parameter. Figure 4.10 represents the thermal accommodation length versus pressure for mode (0,2).

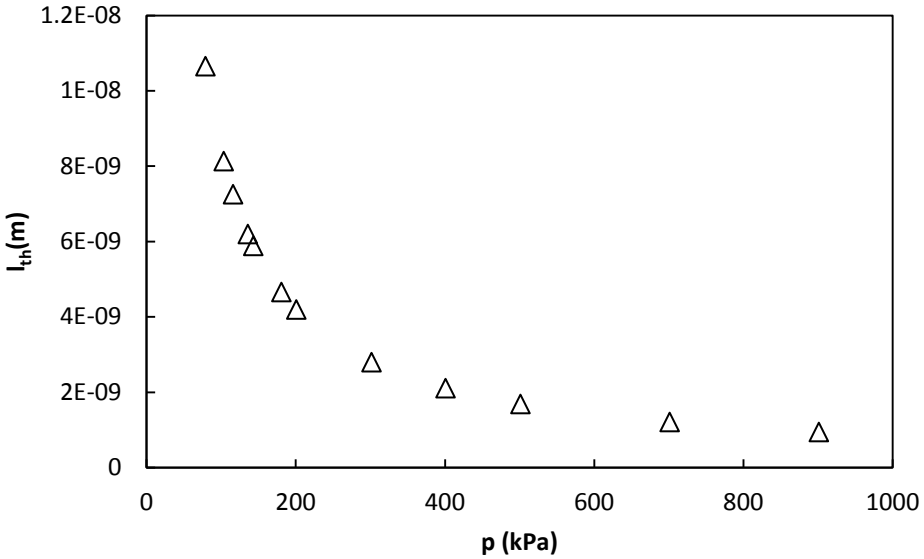

Figure 4.10 *Thermal accommodation length at T=273.6K in the pressure range from p=78kPa up to p= 901kPa.*

Finally, the thermal penetration length of the shell is the last parameter needed to calculate the thermal boundary layer correction. This parameter depends on frequency and on the material properties, 316L steel properties, in this case, which are thermal conductivity (κ_{316L}=14.6W·m^{-1}K^{-1}), isobaric heat capacity (C_{p316L}=450J·kg^{-1}K^{-1}) and density (ρ_{316L}=8027kg·m^{-3}) according to bibliographic references [1]. As it depends on frequency, the pressure and resonance mode also influence on the thermal penetration length. Table 4.10 gives the mode dependence at one pressure and the variations with pressure are shown in figure 4.11.

Table 4.10 *Shell thermal penetration length values for acoustic modes (0,2) to (0,8) at p = 0.9MPa in argon*

Mode	δ_{shell}(m)
(0,2)	1.53 x10^{-5}
(0,3)	1.17 x10^{-5}
(0,4)	9.81 x10^{-6}
(0,5)	8.64 x10^{-6}
(0,6)	7.81 x10^{-6}
(0,7)	7.20 x10^{-6}
(0,8)	6.70 x10^{-6}

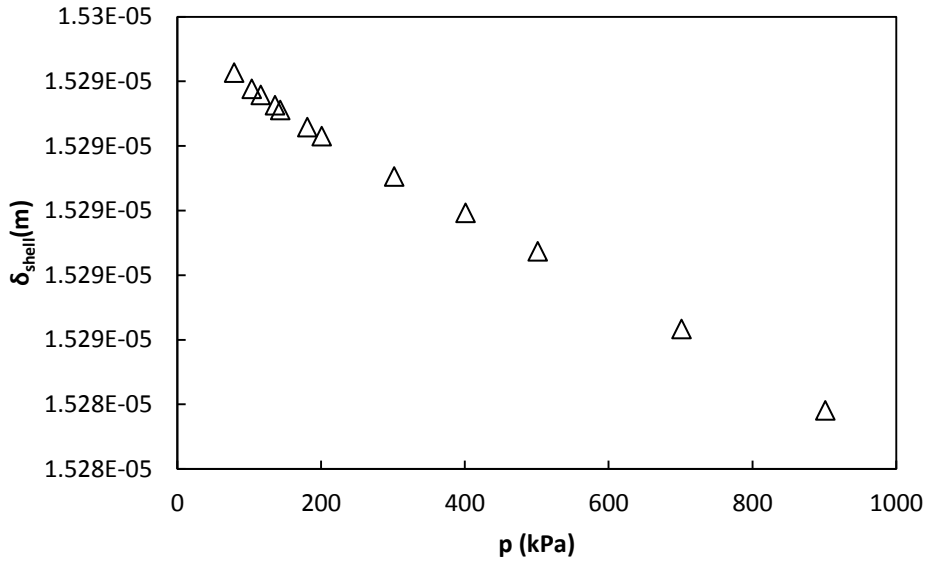

Figure 4.11 *Shell thermal penetration length for acoustic mode (0,2) at T = 273.16K in the pressure range from p = 78kPa up to p = 901kPa.*

It is possible to estimate the frequency correction and the contribution to the acoustic energy lost using those parameters. The frequency corrections for acoustic modes (0,2) to (0,8) at 0.9MPa are in table 4.11, which also shows the theoretical thermal contribution to the peak half-width.

Table 4.12 *Thermal boundary layer frequency correction and half-width contribution for acoustic modes (0,2) to (0,8) at p = 0.9MPa and T = 273.16Kin argon.*

Mode	Δf_{th} (Hz)	g_{th} (Hz)
(0,2)	-0.512	0.513
(0,3)	-0.671	0.673
(0,4)	-0.797	0.800
(0,5)	-0.905	0.908
(0,6)	-1.001	1.005
(0,7)	-1.086	1.090
(0,8)	-1.168	1.172

It is obvious that this correction will be pressure and mode dependant as all of the parameters used to calculate it. The variation with pressure of the thermal boundary layer correction and the half-width contribution are represented in figure 4.12 and in figure 4.13, respectively.

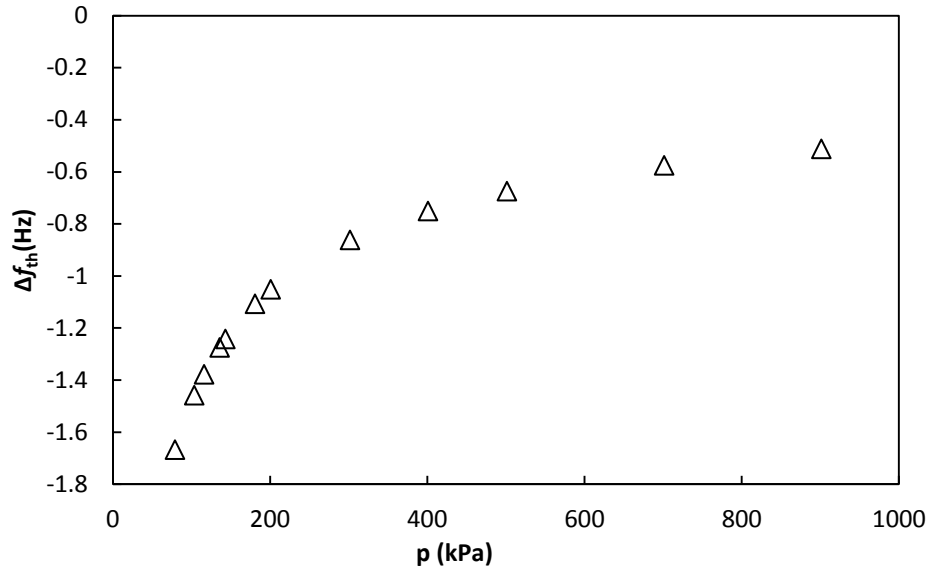

Figure 4.12 *Thermal boundary layer frequency correction for acoustic mode (0,2) at T = 273.16K in the pressure range from p = 78kPa up to p = 901kPa.*

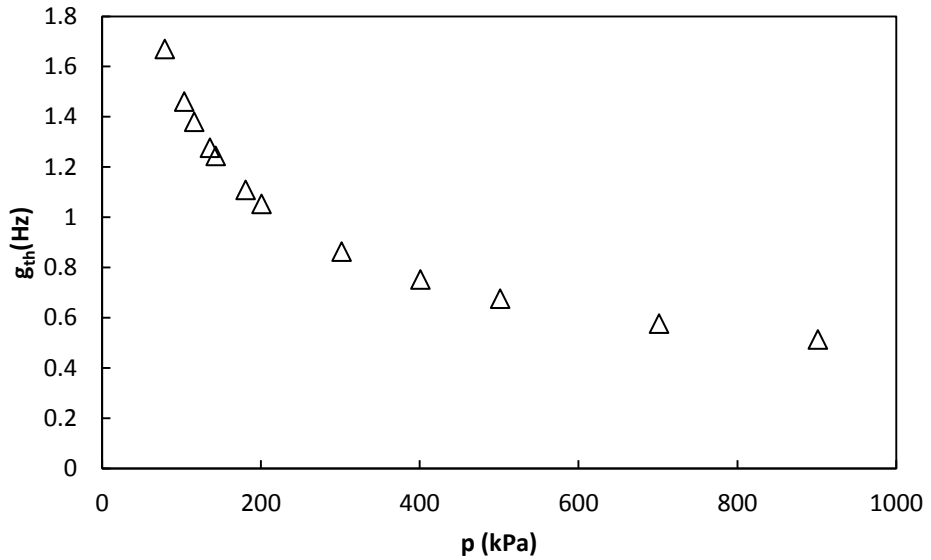

Figure 4.13 *Thermal boundary layer half-width contribution for acoustic mode (0,2) at T= 273.16K in the pressure range from p = 78kPa up to p = 901kPa.*

The thermal boundary layer correction is the most important one (about 0.01% of the measured frequency) but there are some others for consideration.

4.4.1.2 *Bulk viscosity contribution*

This correction is due to the density gradient in the bulk of the fluid caused by the acoustic wave pressure and it takes into account the acoustic energy dissipation in the gas. This correction does not affect the frequency but the half-width factor *g*.

Some of the parameters needed to calculate the bulk dissipation are taken from the experimental data like the frequency of resonance and the speed of sound, and the others need some calculation, for instance the thermal penetration length which was calculated for the thermal boundary layer correction and which values and tendency with pressure are visible at figure 4.9.

There is other parameter that is necessary to get this correction, such as the viscous penetration length (δ_v). Table 4.12 shows the frequency dependence of this parameter ordered by mode, and in figure 4.14 the pressure tendency for the acoustic mode (0,2) is represented.

Table 4.12 *Viscous penetration length (δ_v) for acoustic modes (0,2) to (0,8) at p = 901K and T = 273.16Kin argon*

Mode	δ_V(μm)
(0,2)	8.75
(0,3)	6.67
(0,4)	5.62
(0,5)	4.95
(0,6)	4.47
(0,7)	4.12
(0,8)	3.83

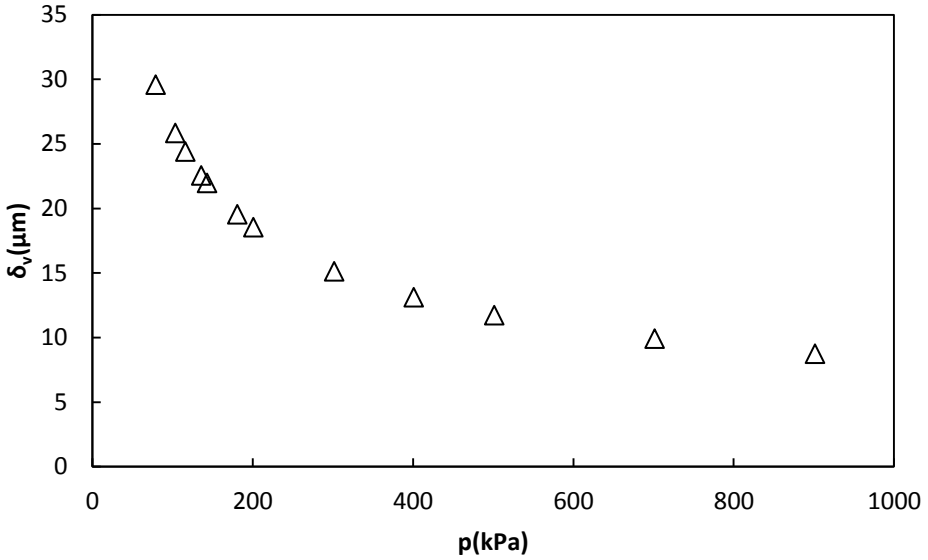

Figure 4.14 *Viscous penetration length for acoustic mode (0,2) in the pressure range from p = 78kPa up to p = 901kPa.*

It is possible to obtain the bulk dissipation (g_b) using this parameter and those previously mentioned. The results are shown in table 4.13 (for each mode at the same pressure, 901kPa) and figure 4.15 (for mode (0,2)in the range of pressure under study).

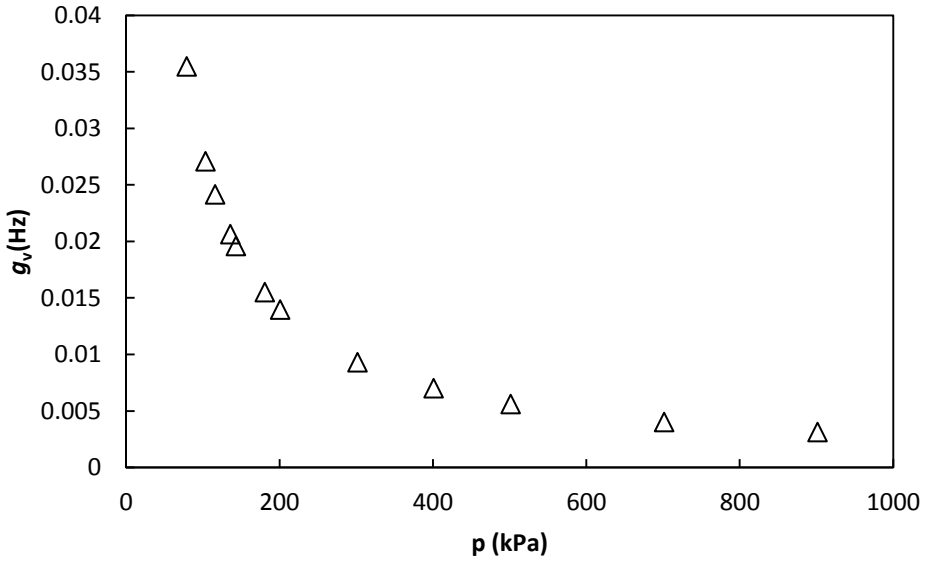

Figure 4.15 *Bulk viscosity half-with contribution for acoustic mode (0,2) at T = 273.16K in the pressure range from p = 78kPa up to p = 900kPa*

Table 4.13 *Bulk viscosity half-width contribution for acoustic modes (0,2) to (0,8) at p=0.9MPa and T=273.16Kin argon*

Mode	g_b(Hz)
(0,2)	3.15×10^{-3}
(0,3)	9.31×10^{-3}
(0,4)	18.55×10^{-3}
(0,5)	30.87×10^{-3}
(0,6)	46.26×10^{-3}
(0,7)	63.91×10^{-3}
(0,8)	85.48×10^{-3}

4.4.1.3 *Shell motion correction*

This correction needs only two parameters the speed of sound in the shell, which is made of 316L steel and the breathing mode frequency. The speed of sound in steel is constant as we saw in earlier chapters and the breathing mode frequency depends only on the internal radius of the cavity which might be considerate constant for the corrections, therefore they are constant and they have the following values:

$$u_{shell} = 5481 m \cdot s^{-1}$$

$$f_{breath} = 26488 Hz$$

The next table (4.14) reports the values of the shell motion correction at 901kPa for modes (0,2) to (0,7). The frequency correction for mode (0,8) cannot be calculated by the proposed model, however, as we will see later this mode is not useful for the purpose of Boltzmann constant determination.

Table 4.14 *Shell motion correction for acoustic modes (0,2) to (0,7) at p = 901kPa and T = 273.16K in argon*

Mode	Δf_{shell} (Hz)
(0,2)	-0.02567873
(0,3)	-0.04623559
(0,4)	-0.0705788
(0,5)	-0.1034748
(0,6)	-0.15894613
(0,7)	-0.32002753

This correction shifts in pressure, we can see this shifting for mode (0,2) in figure 4.16

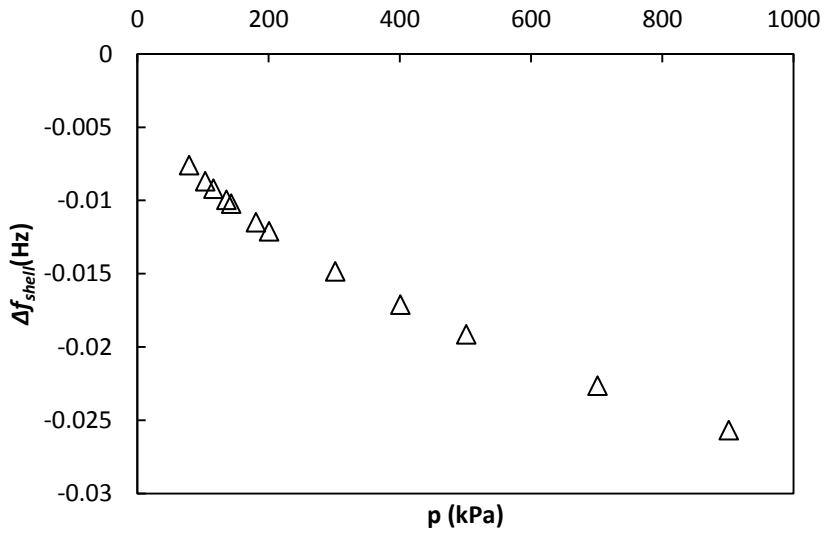

Figure 4.16 *Shell motion correction for acoustic mode (0,2) at T=273.16K in the pressure range form p=78kPa up to p=900kPa*

4.4.1.4 *Tubes and holes correction.*

The last correction applied was the one due to the holes in the shape of the cavity and the inlet and outlet tubes. For the experimental set up used, where there was not gas coming into or out of the resonator during the measuring, there are two holes connected to closed pipes. Those pipes work as gas inlet and outlet for other setup, however the corrections described in chapter 2 must be applied. These frequency corrections are function of temperature and pressure, as every correction described before, and obviously this one is also dependent on the radius and length of the pipe. There are two connections to the resonator the gas inlet and blind connection no longer used. The radius and length of these pipes 1 and 2 are:

$r_{h1}=5x10^{-4}m$ $r_{h2}=1x10^{-3}m$

$L_1=3.8x10^{-2}m$ $L_2=0.8m$

There are some previous calculations that we need for the final correction. Those calculations are for two parameters, the propagation constant according Kirchhoff-Helmholtz theory (k_{KH}) and the effective absorption coefficient (α_{KH}). These parameters must be calculated separately for each pipe. Both propagation constant and absorption coefficient for pipe 1 are shown in table 4.15 and for pipe 2 in table 4.16. In order to see the tendency of these parameters with pressure figure 4.17 shows the values of α_{KH} for the range of pressure

of the study, for both pipes. And figure 4.18 shows the real and imaginary component of the propagation coefficient for mode (0,2) for pipes 1 and 2.

Table 4.15 *Kirchhoff-Helmholtz absorption coefficient α_{KH} and propagation coefficient k_{KH} for modes (0,2) to (0,8) for tube 1 at p = 901kPa and T = 273.16K in argon*

Mode	α_{KH1} (m^{-1})	k_{KH1}(m^{-1})
(0,2)	0.2662	112.5412-0.2662i
(0,3)	0.3490	193.3887-0.3490i
(0,4)	0.4146	272.8856-0.4147i
(0,5)	0.4710	351.9291-0.4710i
(0,6)	0.5211	430.7694-0.5211i
(0,7)	0.5650	506.3134-0.5650i
(0,8)	0.6075	585.5015-0.6075i

Table 4.16 *Kirchhoff-Helmholtz absorption coefficient α_{KH} and propagation coefficient k_{KH} for modes (0,2) to (0,8) for pipe 2 at p = 901kPa and T = 273.16K in argon*

Mode	α_{KH2} (m^{-1})	k_{KH2}(m^{-1})
(0,2)	0.1331	112.4081-0.1331i
(0,3)	0.1745	193.2141-0.1745i
(0,4)	0.2073	272.6783-0.2073i
(0,5)	0.2355	351.6936-0.2355i
(0,6)	0.2606	430.5088-0.2606i
(0,7)	0.2825	506.0309-0.2825i
(0,8)	0.3038	585.1977-0.3038i

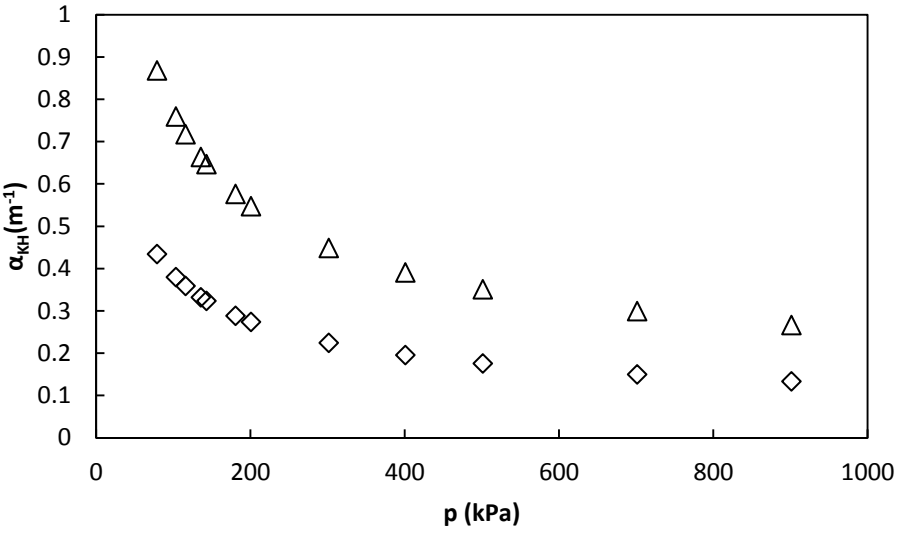

Figure 4.17 *Kirchhoff-Helmholtz absorption coefficient for acoustic mode (0,2) at T = 273.16K in the pressure range from p = 78kPa up to p = 901kPa for pipe 1(Δ) and pipe 2(◊)*

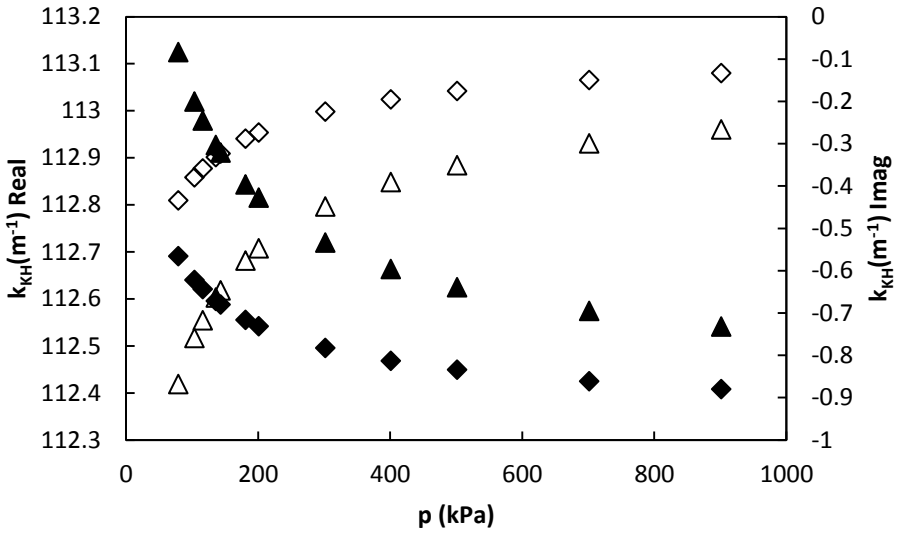

Figure 4.18 *Propagation coefficient for acoustic mode (0,2) for tube 1 (Δ) and tube 2(◊) at T=273.16K in the pressure range from p = 78kPa up to p = 901kPa. Empty symbols are the imaginary component (secondary axe) and filled marks are the real part (primary axis).*

Once these calculations are done it is possible to obtain the correction for the frequency and the contribution to the half-width factor. We can see the values for different modes at the same pressure in table 4.17 and for mode (0,2) at all the pressures considered for measurement in figures 4.19 and 4.20.

Table 4.17 *Tubes frequency correction and half-width contribution for acoustic modes (0,2) to (0,8) at T=273.16K and p=0.9MPa in argon*

Mode	Δf_{tubes}	g_{tubes}
(0,2)	0.0408	0.0312
(0,3)	0.0286	0.1291
(0,4)	0.1449	0.0630
(0,5)	0.0629	0.0003
(0,6)	0.0407	0.0038
(0,7)	0.0249	0.0196
(0,8)	0.0322	0.0333

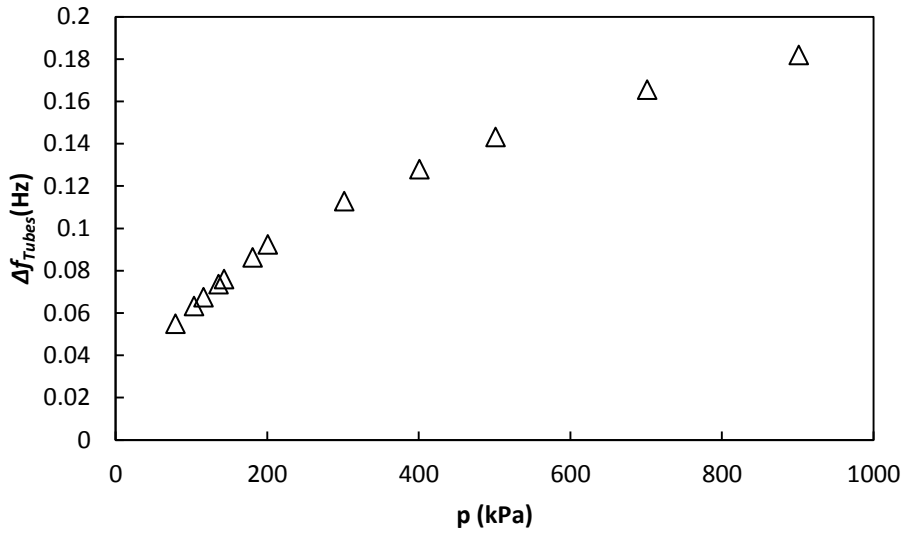

Figure 4.19 *Tubes frequency correction for acoustic mode (0,2) at T = 273.16K in the pressure range from p = 78kPa up to p = 901kPa.*

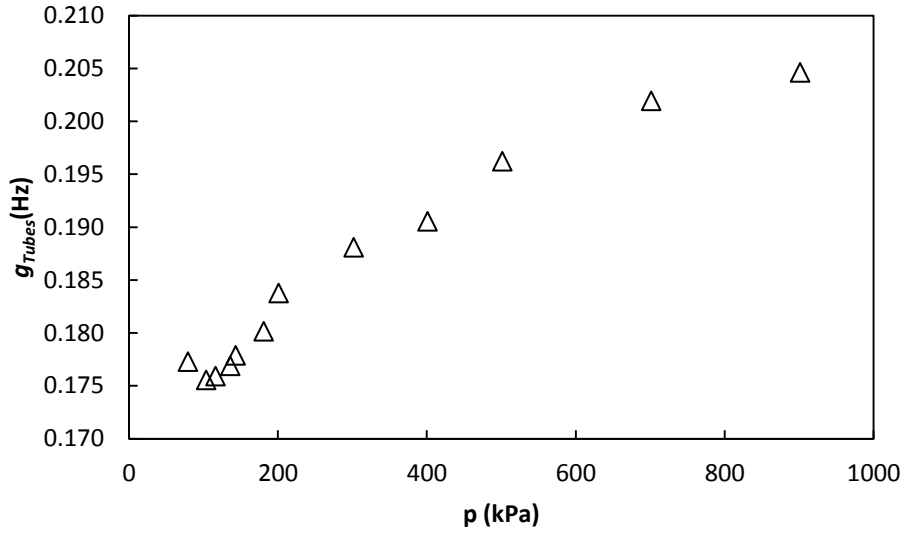

Figure 4.20 *Tubes half-width contribution for the acoustic mode (0,2) at T = 273.16K in the range of pressure from p = 78kPa up to p = 901kPa.*

After all these calculations we have all the required data for the determination of the speed of sound

4.4.2 Determination of Speed of Sound

Once all the frequency corrections are calculated it is possible to obtain the speed of sound. These values of the speed of sound must be corrected for pressure and temperature because of the small fluctuations while measuring is done. This correction is made by

multiplying the value by a factor calculated according equation 2.28 in chapter 2. Some of these factor values are shown in table 4.18

$$r = \frac{u_{T_0,P_0} / a_{T_0,P_0}}{u_{T_{exp},P_{exp}} / a_{T_{exp},P_{exp}}} \qquad (2.28)$$

Table 4.18 *Values of temperature and pressure correction factor for acoustic modes (0,2) to (0,8) at p=901kPa in argon*

Mode	Correction factor
(0,2)	0.99998995
(0,3)	0.99999004
(0,4)	0.99998994
(0,5)	0.99999006
(0,6)	0.99999015
(0,7)	0.99999024
(0,8)	0.99999013

As each mode has its own frequency it is obvious that each mode provides different speed of sound.

Another set of calculations were carried out in order to specify which modes should be taken into account and which ones should not. We compared experimental half-width factor to the one we calculated. The final uncertainty decreases when discrepancy between experimental and calculated half-width decreases too. Figure 4.21 is a view into detail of this comparison for modes (0,2), (0,3), (0,4) and (0,5). Modes (0,6), (0,7) and (0,8) were dismissed because of their high discrepancy.

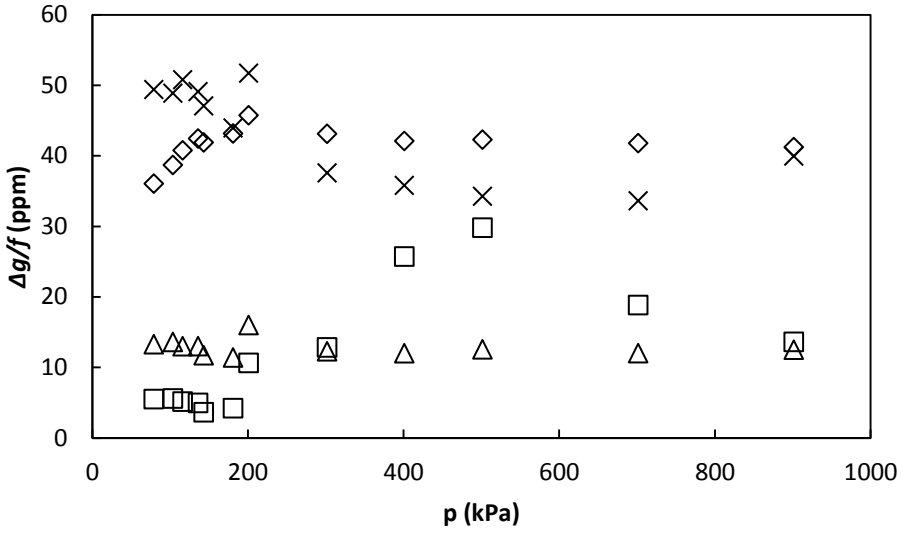

Figure 4.21 *Excess half-width of resonance peaks for acoustic modes (0,2) (◊), (0,3) (□), (0,4) (Δ) and (0,5) (X) at T = 273.16K in the pressure range from p = 78kPa up to p = 901kPa*

Taking into consideration the data shown in figure 4.21, the model developed to calculate Boltzmann constant only used experimental results for modes (0,2) to (0,4) because excess half-width decreases with pressure. This model offers a relation between the square of the speed of sound and pressure. The measurements of the speed of sound of these modes are shown in figure 4.22

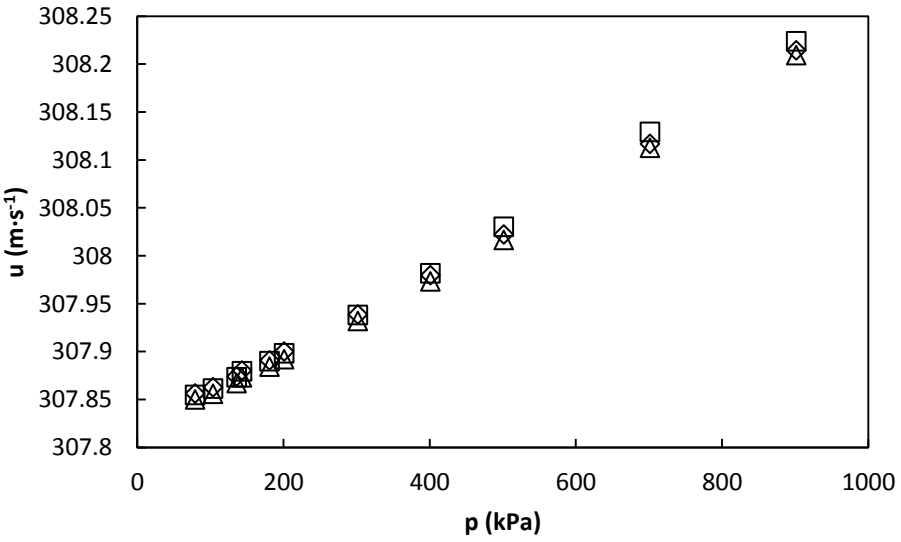

Figure 4.22 *Experimental speed of sound for acoustic modes (0,2) (Δ), (0,3) (□) and (0,4) (◊) at T=273.16K in the pressure range from p = 78kPa up to p = 900kPa.*

The model developed using the three cited modes is not exactly that shown in equation 2.6-b. In order to compare these results to previous studies the model was slightly different, including a new term that multiplies the inverse of pressure, as it is detailed in equation 4.1. The value of all these parameters is shown in table 4.19. The graphic representation of this model and the experimental points used for its development are in figure 4.23.

$$u^2 = A_0 + A_{-1}p^{-1} + A_1 p + A_2 p^2 + A_3 p^3 \qquad (4.1)$$

Table 4.19*First four parameters for the acoustic virial equation of state as function of pressure.*

A_0 (m^2s^{-2})	94755.3304
A_{-1}($m^2s^{-2}Pa$)	2.0150 x10^{-4}
A_1($m^2s^{-2}Pa^{-1}$)	9.0324 x10^{-11}
A_2($m^2s^{-2}Pa^{-2}$)	1.8035 x10^{5}
A_3($m^2s^{-2}Pa^{-3}$)	-1.9228 x10^{-17}

The first parameter, A_0, is the value of the speed of sound when pressure is zero or in other words is the required data in order to get the Boltzmann's constant.

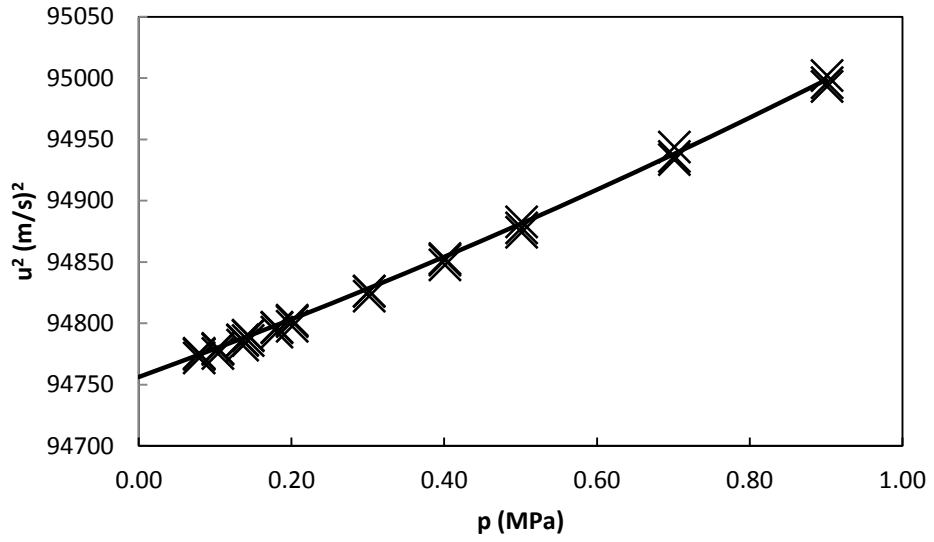

Figure 4.23 *Experimental square speed of sound (X) and acoustic equation of state developed in this study (──)*

Equation 2.4 is solved for obtaining the universal gas constant, R, using the square speed of sound at zero pressure (A_0) from table 4.19, and the Boltzmann constant is obtained when the ideal gas constant is divided by the Avogadro constant:

R=8.314470 J·mol^{-1}K^{-1} and k_B=1.380650·10^{-23}J·K^{-1}

4.5 UNCERTAINTY ASSESMENT.

Overall uncertainty in Boltzmann constant determination is calculated according section 3.3.1. However some calculations need to be explained in this section.

Uncertainty due to the presence of impurities in the gas must be obtained this calculation is done according to equation 3.13 using data from table 4.1 and specifications provided by the supplier uncertainty on molar fraction are calculated and showed in table 4.20. Impurities specifications from table 4.1 were considered a rectangular distribution and its uncertainties calculated according GUM.

Table 4.20 *Molar fraction uncertainties of the argon according to supplier specifications*

Compound	$u(x_i)/mol \cdot mol^{-1} \cdot 10^{-6}$	$M\ (g \cdot mol^{-1})$
Ar	0.29	39.948
O_2	0.014	31.998
H_2O	0.029	18.015
CO_2	0.029	44.009
CO	0.029	28.010
H_2	0.029	2.016
C_nH_m	0.029	58.124

Molar mass of all the components were calculated using IUPAC values of atomic mass. The organic fraction was considered as butane to calculate the uncertainty contribution.

Other source of uncertainty that requires further details is that due to extrapolation to zero pressure. As it was explained in chapter 3 to obtain uncertainty due to extrapolation to zero pressure, different fitting models were done. The fitting models are in agreement with previous studies [2-4]. The four models fitted are: when all 4 parameters are fitted, when A_{-1} is fixed to value of 0, when $A_3=1.45x10^{-18}$, and the combination of both A-1= 0 and A3=1.45 x10-18. Values af all parameters for each fitted model are shown in table 4.21

Table 4.21 *Parameter values when different adjustment models are applied*

	all fittted	$A_{-1}=0$	$A_3=1.45x10^{-18}$	$A_3=1.45x10^{-18}$; $A_{-1}=0$
$A_0\ (m^2s^{-2})$	94755.3304	94756.1367	94754.7955	94756.8196
$A_{-1}(m^2s^{-2}Pa)$	2.0150×10^{-4}	2.1006×10^{-4}	2.1000×10^{-4}	2.0420×10^{-4}
$A_1(m^2s^{-2}Pa^{-1})$	9.0324×10^{-11}	5.85518×10^{-11}	6.36492×10^{-11}	6.7662×10^{-11}
$A_2(m^2s^{-2}Pa^{-2})$	1.8035×10^{5}	0	1.6787×10^{5}	0
$A_3(m^2s^{-2}Pa^{-3})$	-1.9228×10^{-17}	4.9798×10^{-18}	1.4500×10^{-18}	1.4500×10^{-18}

The contribution to overall uncertainty because of these two sources (molar mass and zero pressure extrapolation) and other 5 contributions explained in chapter 3 are in table 4.22. All required data for the calculation of these uncertainties are in appendix A.

Table 4.22 *Uncertainty contribution to overall uncertainty for determination of Boltzmann's constant*

		u in $k_B/10^{-6}$ $(k_{Bexp}-k_B)/k_B$
Microwave Radius	Dispersion of radii determined from 3 different modes	12
	Relative excess halfwidths	11
Corrected acoustics frequencies	Dispersion of the frequencies from 3 radial modes	6
	Relative excess halfwidths	10
	Extrapolation to zero pressure	2
Temperature	Gradient across resonator	0,5
	Repeteability of calibrations	1
Mollar mass		3
Sum		**20**

This chapter concludes that the Boltzmann constant value and uncertainty is:

$$k_B=1.380650\cdot10^{-23}\ J\cdot K^{-1} \pm 28\cdot10^{-29}\ J\cdot K^{-1}$$

This result was compared to results obtained by other laboratories involved in the determination of the Boltzmann constant for the redefinition of the Kelvin. This comparison is represented in figure 4.24

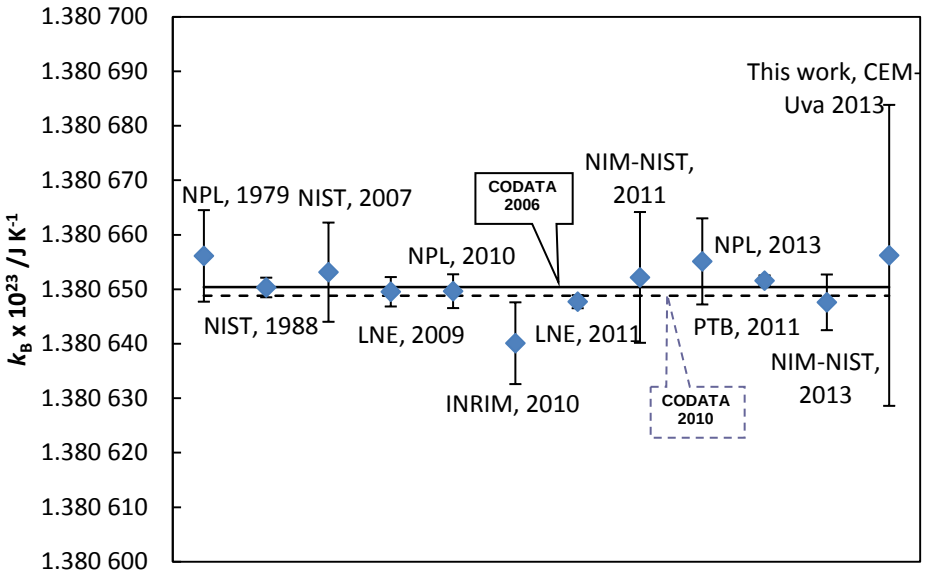

Figure 4.24 *Comparison of the determination of k_B with the CODATA 2006 y 2010 recommended values and other authors [2,5-13].*

4.6 REFERENCES

1. eFunda. (2013) eFunda: properties of stainless steel AISI 316.

2. Sutton, G., Underwood, R., Pitre, L., Podesta, M., and Valkiers, S. Acoustic Resonator Experiments at the Triple Point of Water: First Results for the Boltzmann Constant and Remaining Challenges. International Journal of Thermophysics 31, 1310-1346.

3. Gavioso, R.M., Madonna Ripa, D., Guianvarcâ€™h, C., Benedetto, G., Giuliano Albo, P.A., Cuccaro, R., Pitre, L., and Truong, D. Shell Perturbations of an Acoustic Thermometer Determined from Speed of Sound in Gas Mixtures. International Journal of Thermophysics 31, 1739-1748.

4. Truong, D., Sparasci, F., FoltÃªte, E., Ouisse, M., and Pitre, L. Measuring Shell Resonances of Spherical Acoustic Resonators. International Journal of Thermophysics 32, 427-440.

5. R.M. Gavioso, G. Benedetto, P.A. Fiuliano Albo, D. Madonna Ripa, A. Merlone, C. Guianvarc'h, F. Moro, R. Cuccaro, A determination of the Boltzmann constant from speed of

sound measurements in helium at a single thermodynamic state, Metrologia 47 (2010) 387-409.

6. A.R. Colclough, T.J. Quinn, T.R.D. Chandler, An acoustic redetermination of the gas constant, Proc. R. Soc. Lond. A (1979) 368: 125-139.

7. M.R. Moldover, J.P.M. Trusler, T.J. Edwards, J.B. Mehl, R.S. Davis, Measurement of the universal gas constant R using a spherical acoustic resonator. J. Res. Natl. Bur. Stand. (1988) 93: 85-144.

8. L. Pitre, C. Guianvarc'h, F. Sparasci, A. Guillou, L D. Truong, Y. Hermier, M.E. Himbert, An improved acoustic method for the determination of the Boltzmann constant at LNE-INM/CNAM, C.R. Phys. (2009) 10: 835-848.

9. L. Pitre, F. Sparasci, D. Truong, A. Guillou, L Risegari, M.E. Himbert, Measurement of the Boltzmann constant kB using a quasi-spherical acoustic resonator, Int. J. Thermophys. (2011) 32: 1825-1886.

10. P.J. Mohr, B.N. Taylor, D.B. Newell, CODATA recommended values of the fundamental physical constants: 2010. Rev. Mod. Phys. (2012) 84: 1527-1605.

11. J.T. Zhang, H. Lin, X.J. Feng, J.P. Sun, K.A. Gillis, M.R. Moldover, Y.Y. Duan, Progress toward redetermining the Boltzmann constant with a fixed-path-length cylindrical resonator, Int. J. Thermophys. 32 (2011) 1297-1331.

12. M. de Podesta, R. Underwood, G. Sutton, P. Morantz, P. Harris, D.F. Mark, F.M. Stuart, G. Vargha, G. Machin, A low-uncertainty measurement of the Boltzmann constant, Metrologia 50 (2013) 354-376.

13. H. Lin, X.J. Feng, K.A. Gillis, M.R. Moldover, J.T. Zhang, J.P. Sun, Y.Y. Duan, Improved determination of the Boltzmann constant using a single, fixed-length cylindrical cavity, Metrologia 50 (2013) 417-432.

Chapter 5

RADIUS MEASUREMENTS USING ACOUSTIC RESONANCE IN ARGON FOR THERMODYNAMIC PROPERTIES DETERMINATION

5.1 INTRODUCTION.

The inertial radius of the sphere depends on the temperature and pressure. When determining thermodynamic properties of gases, like speed of sound using acoustic resonators, the degree of accuracy required allows characterizing the resonator by a reference gas so microwave resonance is not necessary. The resonator B, which was built at Imperial College and which only has two acoustic transducers was used for this purpose as it was used in previous studies[1-5].

The reference gas used was argon. The radius can be calculated using equation 2.22, measuring acoustic frequency of resonance when speed of sound is known, as it was in this case thanks to NIST database[6, 7].

The internal radius was measured not only for the cases under study but also for some other conditions in perspective of future work. Measurements were taken from 0.1 MPa up to 20 MPa in 1 MPa intervals and five isotherms at 250.10 K, 273.16 K, 299.72 K, 324.99 K and 350.02 K

5.2 RADIUS MEASUREMENTS.

The resonance frequency data of four acoustic modes (0,2), (0,3), (0,4) and (0,5) were collected at each pressure at each temperature. All the collected data are in the appendix B, but for a better understanding of the research this chapter will include only the data and calculations for 250.10K isotherm.

The equipment provides both frequency of resonance and quality factor named half-width as well. Those parameters are different for each mode and they change with pressure. The value of frequency of resonance and half-width for modes (0,2) to (0,5) are shown in table 5.2; and figure 5.1 represents the frequency of resonance in the range of pressure under study for mode (0,3), therefore it is possible to appreciate the frequency change along the pressure range. Along this chapter there are more parameters that are dependents on the mode, as a representative example mode (0,3) was selected for all acoustic modes.

Table 5.1 *Frequency of resonance and half-width of the resonance peaks for acoustic modes (0,2) to (0,5) at p = 20MPa and T = 250.10K in argon.*

Mode	*f*(Hz)	*g*(Hz)
(0,2)	6294.34	0.333
(0,3)	10820.46	0.496
(0,4)	15271.44	0.737
(0,5)	19695.86	1.372

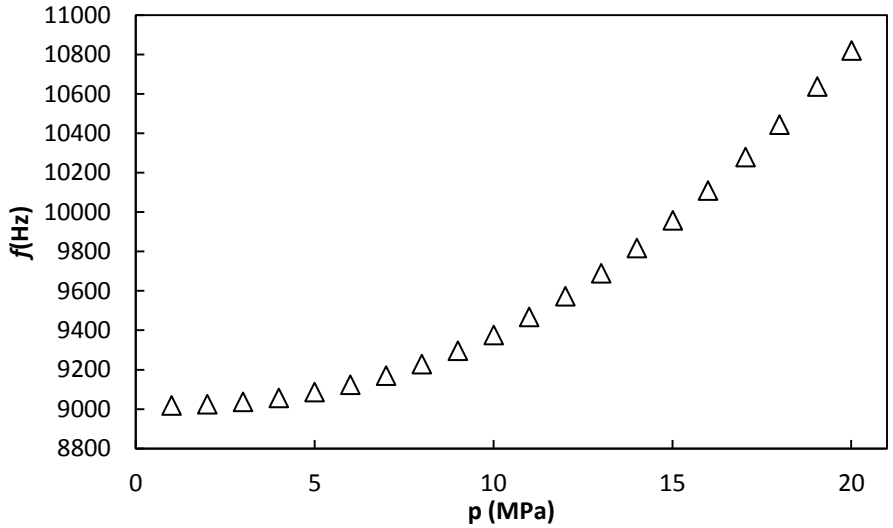

Figure 5.1 *Frequency of resonance for acoustic mode (0,3) at T = 250.10K in the pressure range from p = 1MPa up to p = 20MPa in Argon.*

The value of the half-width of the resonance peaks also changes with pressure, as it can be seen in figure 5.2

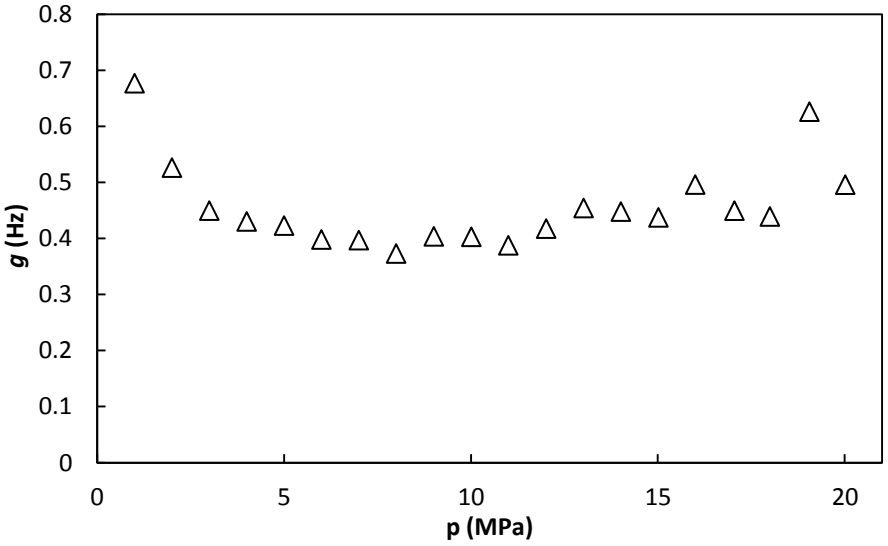

Figure 5.2 *Half-width of the resonance peak for acoustic mode (0,3) at T = 250.10 K in the range pressure from p = 1 MPa up to p = 20 MPa in Argon.*

Just like it happened in the acoustic part of the Boltzmann constant determination, it is necessary to calculate and apply some corrections.

5.2.1 Frequency Corrections.

5.2.1.1 *Thermal Boundary Layer Correction.*

This is the most important contribution. It is necessary to calculate some parameters before the final calculation of the thermal boundary layer correction. The first of these parameters is the thermal penetration length (δ_{th}) which depends on pressure and frequency or in other words the resonance mode. Some values of this parameter at the highest pressure for each measured mode are in table 5.2.

Table 5.2 *Thermal penetration length for acoustic mode (0,2) to (0,5) at T = 250.10 K and p = 20 MPa in argon.*

Mode	δ_{TH}(m)
(0,2)	1.90×10^{-6}
(0,3)	1.45×10^{-6}
(0,4)	1.22×10^{-6}
(0,5)	1.07×10^{-6}

The thermal penetration length is also dependant on pressure; this behaviour is visible in figure 5.3

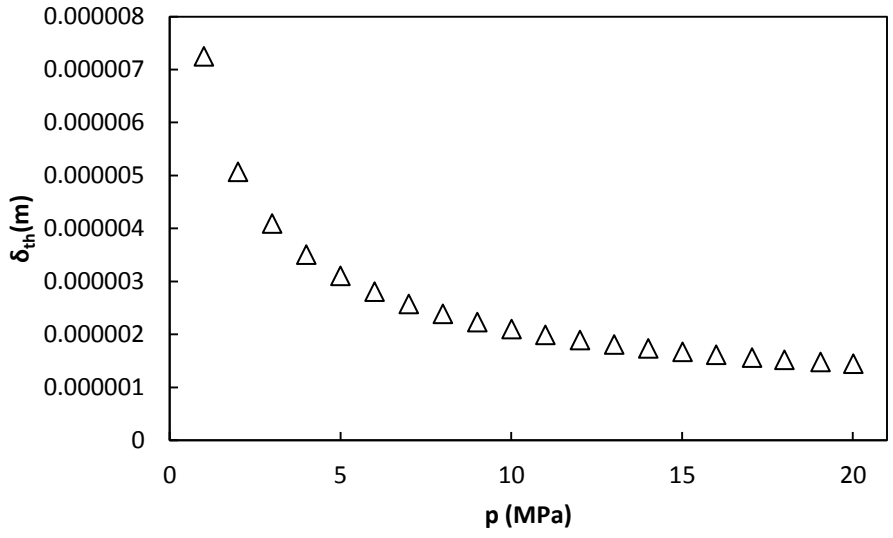

Figure 5.3 *Thermal penetration length for acoustic mode (0,3) at T = 250.10 K for the pressure range from p = 1MPa up to p = 20MPa in Argon.*

Other of the needed parameters to calculate internal radius is the thermal accommodation length (l_{th}). Just like the thermal penetration length, it depends on the pressure but not on the resonance mode. This variation with pressure is shown in figure 5.4

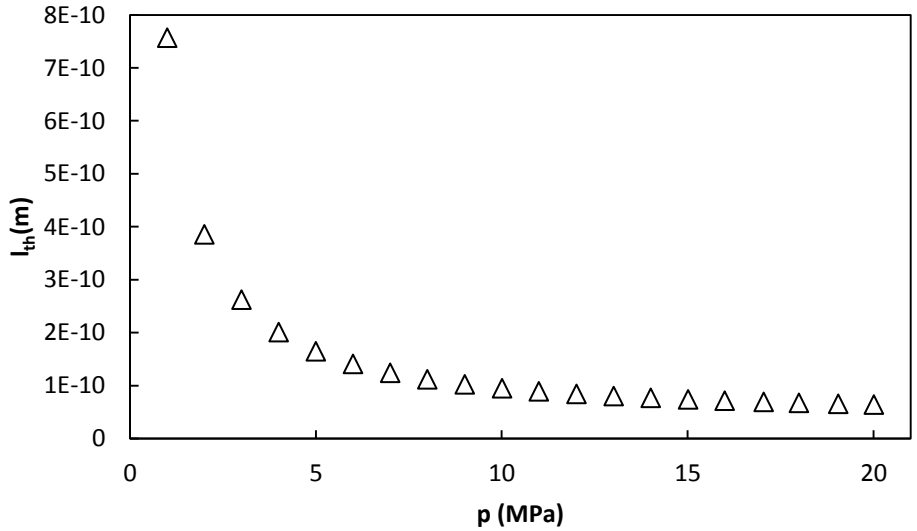

Figure 5.4 *Thermal accommodation length at T = 250.10 K in the range pressure from p = 1 MPa up to p = 20 MPa in Argon.*

The last parameter necessary to calculate the thermal boundary layer correction is the shell thermal penetration length (δ_{316L}), or the thermal boundary layer in the shell side of the interface. This correction depends on the frequency as it was explained in chapter 2. As it is already known frequency shifts with pressure, therefore this parameter changes for modes and pressure. Table 5.3 shows the values at p=20MPa for the different modes at 250.10K.

Table 5.3 *Shell thermal penetration length at p = 20 MPa for acoustic modes (0,2) to (0,5) at T = 250.10 K in argon.*

Modo	δ_{shell}(m)
(0,2)	1.43×10^{-5}
(0,3)	1.09×10^{-5}
(0,4)	9.18×10^{-5}
(0,5)	8.08×10^{-5}

Variation against pressure of the shell thermal penetration length for mode (0,3) at T=250.10K is represented in figure 5.5

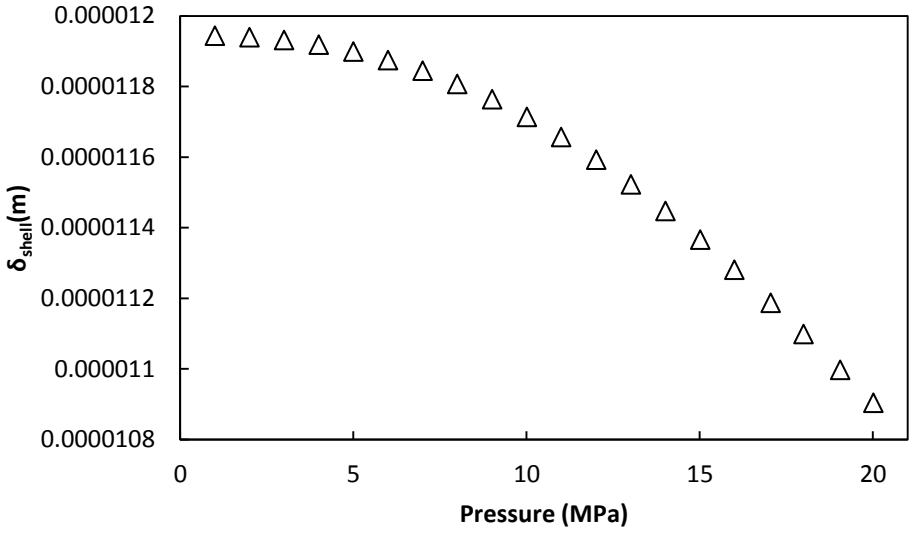

Figure 5.5 *Shell thermal penetration length for acoustic mode (0,3) at T = 250.10 K in the range pressure from p = 1 MPa up to p = 20 MPa in Argon.*

Once all the required parameters are calculated, it is possible to quantify the thermal boundary layer correction to the frequency of resonance and the contribution to the half-width. Both frequency corrections and half-width contributions are different for each mode and change with pressure. The changes for different modes of the frequency correction and half-width can be seen in table 5.4 at 250.10K and the highest and lowest pressures (p = 1 MPa and p = 20 MPa).

Table 5.4 *Thermal boundary layer frequency correction and half-width contribution for modes (0,2) to (0,5) at p = 20MPa and p = 1 MPa and T = 250.10K in argon.*

	p = 20 MPa		**p = 1MPa**	
Mode	**Δf_{th} (Hz)**	**g_{th}(Hz)**	**Δf_{th} (Hz)**	**g_{th}(Hz)**
(0,2)	-0.241	0.248	-0.441	0.442
(0,3)	-0.315	0.325	-0.578	0.580
(0,4)	-0.375	0.387	-0.687	0.689
(0,5)	-0.425	0.439	-0.780	0.783

The variation that this frequency correction and the half-width contribution suffer when the pressure changes can be observed in figures 5.6 and 5.7 for mode (0,3)

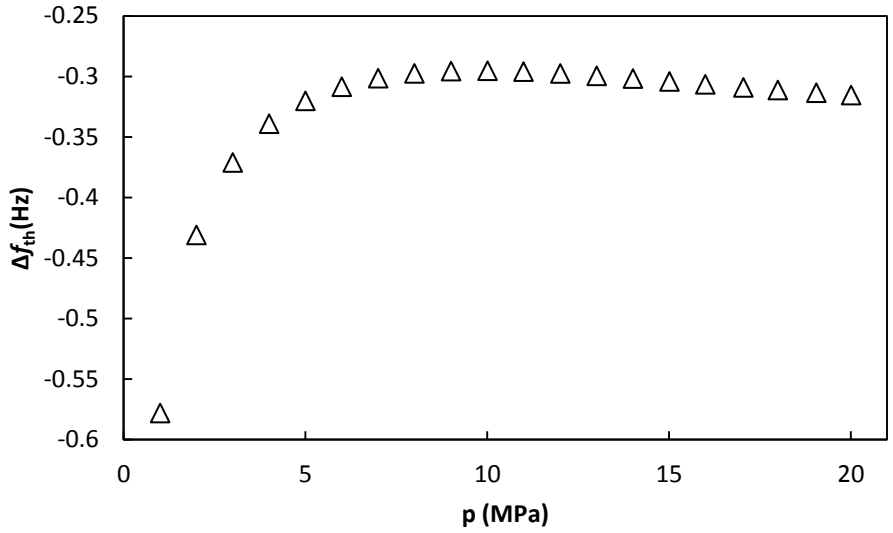

Figure 5.6 *Thermal boundary layer frequency correction for acoustic mode (0,3) at T = 250.10 K in the pressure range from p = 1 MPa up to p = 20 MPa in Argon.*

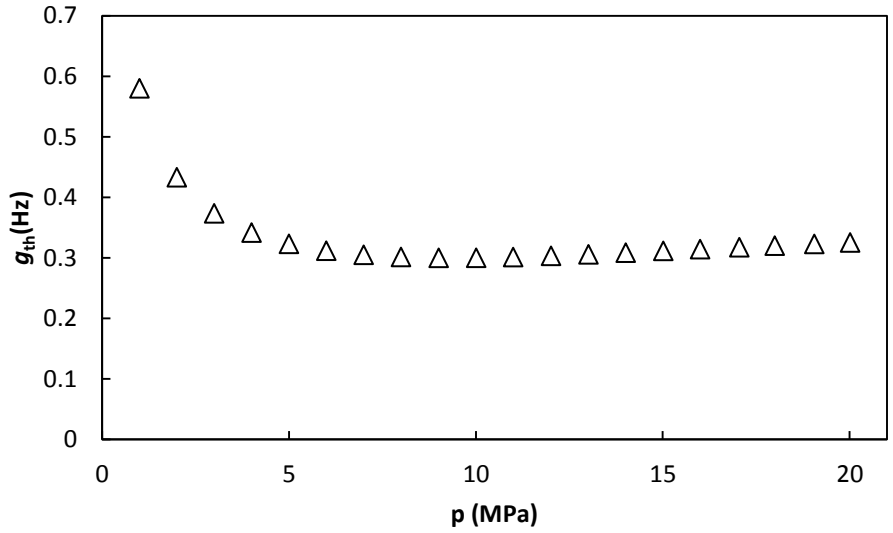

Figure 5.7 *Values of thermal boundary layer half-width contribution for mode (0,3) at T = 250.10 K in the range pressure from p = 1 MPa up to p = 20 MPa in Argon.*

5.2.1.2 *Bulk Viscosity Correction.*

The bulk viscosity correction is not a frequency correction. It is only the contribution to the half-width due to the viscosity change in the bulk of the fluid.

This contribution needs some previous calculation one of them is the thermal penetration length (δ_{th}) which was calculated previously and values can be seen in table 5.3 and figure 5.3. The other required factor is the viscous penetration length, which changes for modes and pressure. Change for modes (0,2) to (0,5) at the same pressure can be seen in table 5.5, and the variation with pressure in figure 5.8

Table 5.5 *Viscous penetration length for acoustic modes (0,2) to (0,5) at T = 250.10 K and p = 20 MPa in argon.*

Mode	δ_V(m)
(0,2)	1.88 x10^{-6}
(0,3)	1.43 x10^{-6}
(0,4)	1.21 x10^{-6}
(0,5)	1.06 x10^{-6}

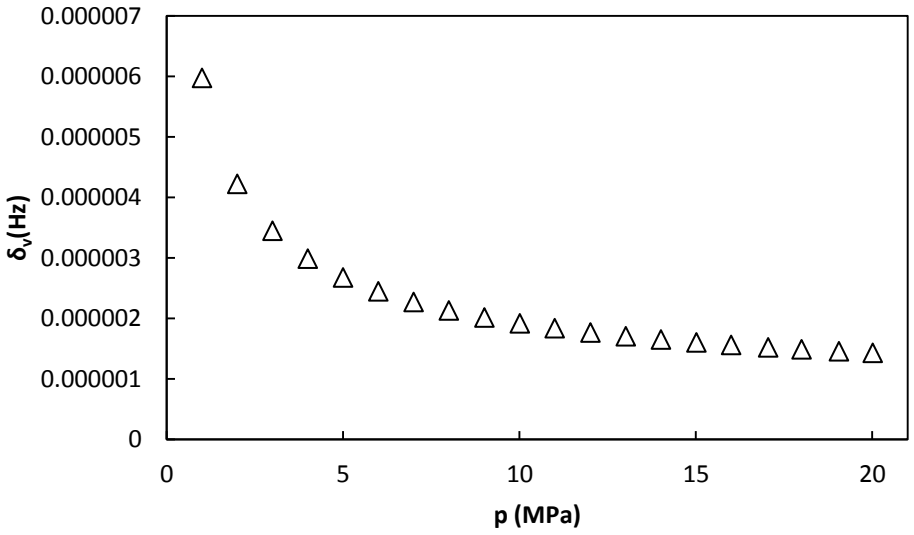

Figure 5.8 *Viscous penetration length for acoustic mode (0,3) at T = 250.10 K in the pressure range from p = 1 MPa up to p = 20 MPa in Argon.*

After these parameters are calculated the bulk viscosity half-width contribution (g_b) may be computed. Table 5.6 shows the values of g_b for different modes at the same pressure.

Table 5.6 *Bulk viscosity half-width contribution for acoustic modes (0,2) to (0,5) at p = 20 MPa and T = 250.10 K in argon*

Mode	g_b(Hz)
(0,2)	2.09 x10^{-4}
(0,3)	6.195 x10^{-4}
(0,4)	12.32 x10^{-4}
(0,5)	20.50 x10^{-4}

The variation with pressure of the half-width contribution due to the bulk viscosity is shown in figure 5.9

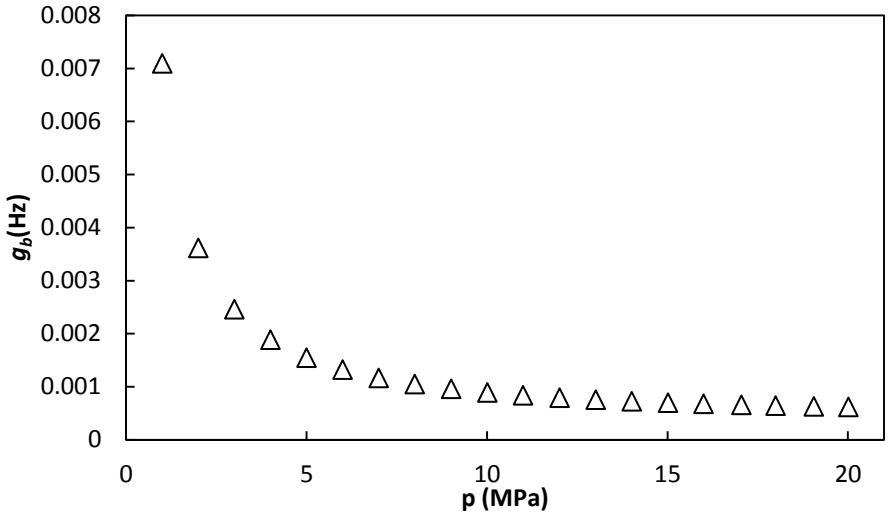

Figure 5.9 *Bulk viscosity half-width contribution for acoustic mode (0,3) at T=250.10 in the range pressure from p = 1 MPa up to p = 20 MPa in argon.*

5.2.1.3 *Shell Motion Correction.*

Shell motion correction is other necessary correction applied before computing the internal radius of the cavity. How to calculate this correction is explained in chapter 2.

The breathing frequency is needed for this calculation, it is obtained according to equation 2.24 and it is constant:

$$f_{breath} = \left(\frac{u_{shell}}{2\pi a}\right)\left(\frac{2\left[\left(\frac{b}{a}\right)^3 - 1\right]}{\left[\left(\frac{b}{a}\right) - 1\right]\left[1 + 2\left(\frac{b}{a}\right)^3\right]}\right)^{1/2} \qquad (2.24)$$

f_{breath}=26488 Hz

The shell motion correction depends on frequency therefore it is different for each mode and it is changing with pressure. These variations are detailed in table 5.7 for resonance modes and in figure 5.10 for pressure.

Table 5.7 *Shell motion frequency correction for acoustic modes (0,2) to (0,5) at p = 20 MPa and T = 250.10 K in argon.*

Mode	Δf_{Shell} (Hz)
(0,2)	-0.140
(0,3)	-0.257
(0,4)	-0.405
(0,5)	-0.639

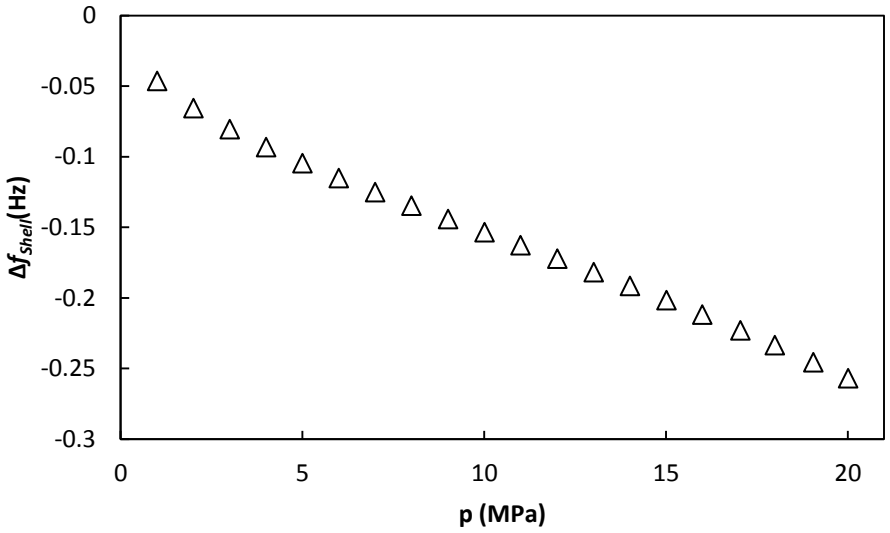

Figure 5.10 *Shell motion frequency correction for acoustic mode (0,3)) at T = 250.10K in the range pressure from p = 1 MPa up to p = 20 MPa in argon.*

5.2.1.4 *Tubes and Holes Correction.*

The inlets and outlets of the cavity make a disturbance on the frequency of resonance that has to be corrected, but as the current set up has two tubes all the calculations must be done for each pipe. Radius (r_h) and longitude (L) of pipes are:

$r_{h1}=5x10^{-4}m$ $r_{h2}=1x10^{-3}m$

$L_1=3.8x10^{-2}m$ $L_2=0.8m$

This correction needs previous calculations. The first of the calculated parameters is the effective absorption coefficient (α_{KH}). This parameter is function of frequency so it will change

with pressure and resonance mode. Table 5.8 shows the variation of the effective absorption coefficient at the same pressure (20MPa) for different modes.

Table 5.8 *Kirchhoff-Helmholtz absorption coefficient for acoustic modes (0,2) to (0,5) at T = 250.10 K and p = 20 MPa in argon.*

Mode	$\alpha_{KH1}(m^{-1})$	$\alpha_{KH2}(m^{-1})$
(0,2)	0.111	0.056
(0,3)	0.146	0.073
(0,4)	0.173	0.087
(0,5)	0.196	0.098

Figure 5.11 shows the effective absorption coefficient for both pipes at 250.10K in the range of pressure under study for mode (0,3)

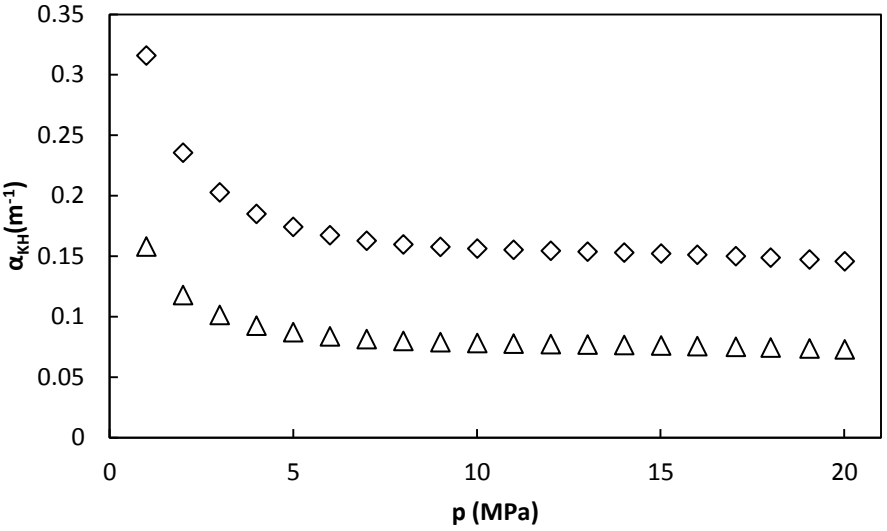

Figure 5.11 *Kirchhoff-Helmholtz absorption coefficient for acoustic mode (0,3) at T = 250.10K in the range of pressure from p = 1MPa up to p = 20 MPa for tube 1 (◊) and tube 2 (Δ) in argon.*

The next parameter calculated is the propagation coefficient (k_{KH}) which has real and imaginary components; fortunately the imaginary component occurs to be the effective absorption coefficient with opposite sign. Therefore, only values of the real component are detailed. Table 5.9 shows the values for different modes at the same pressure.

Table 5.9 *Real component of the propagation constant for tubes 1 and 2 at T = 250.10 K and p = 20 MPa for acoustic modes (0,2) to (0,5) in argon.*

Mode	$k_{KH1}(m^{-1})$	$k_{KH2}(m^{-1})$
(0,2)	111.970	0.273
(0,3)	192.440	0.290
(0,4)	271.568	0.303
(0,5)	350.220	0.315

Variation with pressure for this parameter is shown in figures 5.12 for pipe 1 and 5.13 for pipe 2, for the mode (0,3)

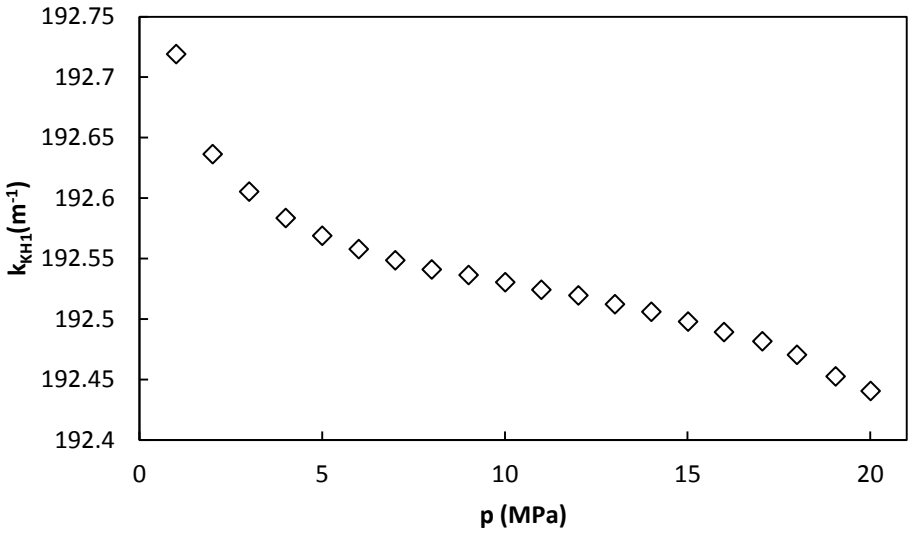

Figure 5.12 *Propagation constant real component for acoustic mode (0,3) and tube 1 at T = 250.10 K for the pressure range from p = 1MPa up to p = 20MPa in argon.*

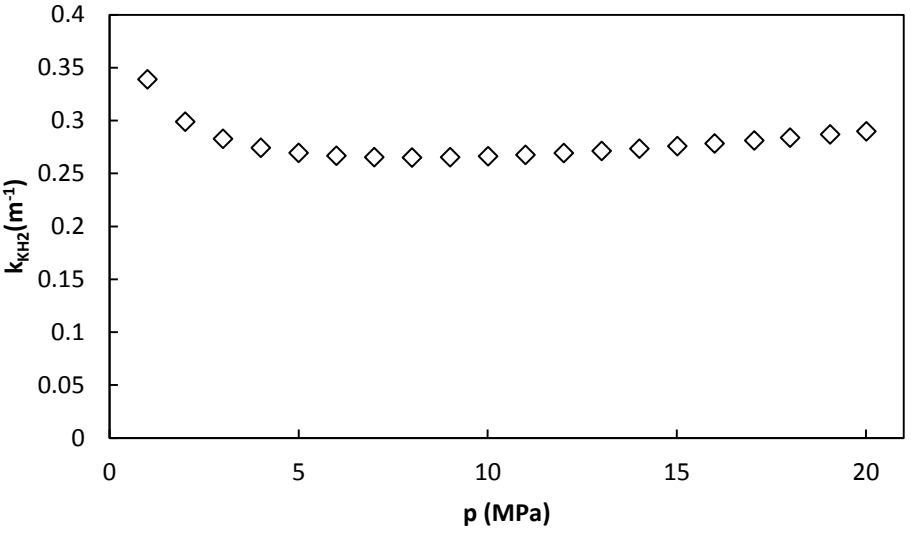

Figure 5.13 *Propagation constant real component for acoustic mode (0,3) and pipe 2 at T = 250.10 K for the pressure range from p = 1MPa up to p = 20MPa in argon.*

The last parameter before the final correction is the specific acoustic admittance (y_0), which is an imaginary number. Table 5.10 shows this parameter for each mode and pipe.

Table 5.10 *Specific acoustic admittance of the opening for tubes 1 and 2 at T = 250.10 K and p = 20 MPa for acoustic modes (0,2) to (0,5) in argon.*

Mode	y_{01}	y_{02}
(0,2)	0.026+2.040i	20.906-1.69i
(0,3)	0.030+1.684i	0.067-0.022i
(0,4)	0.029+1.275i	0.109+0.490i
(0,5)	0.029+0.951i	0.153+0.629i

Figures 5.14 to 5.17 show the values of real and imaginary components for both pipes for mode (0,3)

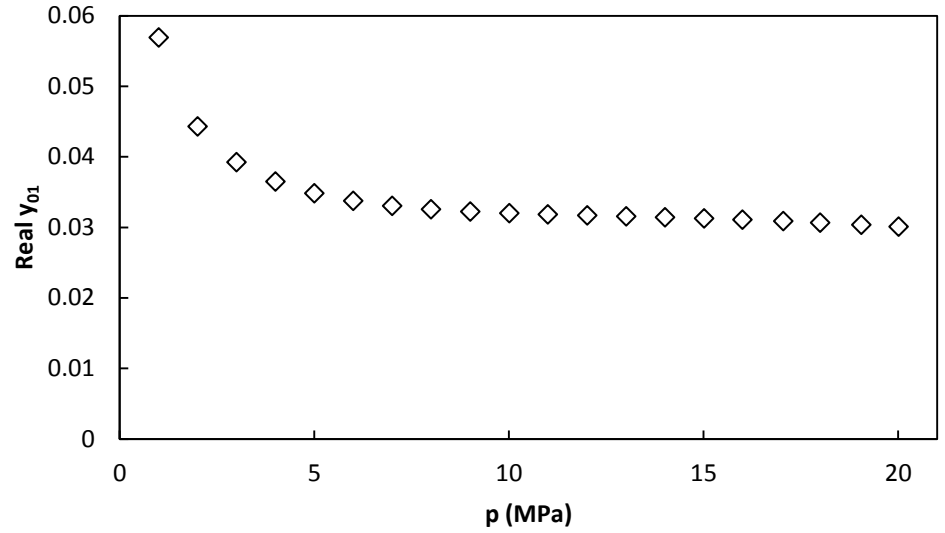

Figure 5.14 *Specific acoustic admittance of the opening real component for tube 1, acoustic mode (0,3) at T = 250.10 K for the pressure range from p = 1 MPa up to p = 20 MPa in argon.*

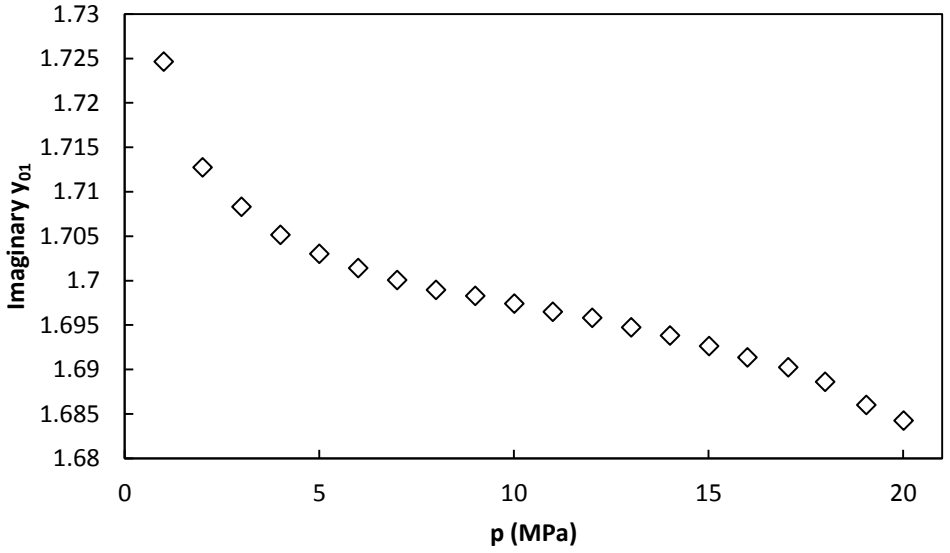

Figure 5.15 *Specific acoustic admittance of the opening imaginary component for tube 1 and acoustic mode (0,3) at T = 250.10 K for the range on pressure from p = 1 MPa up to p = 20 MPa in argon.*

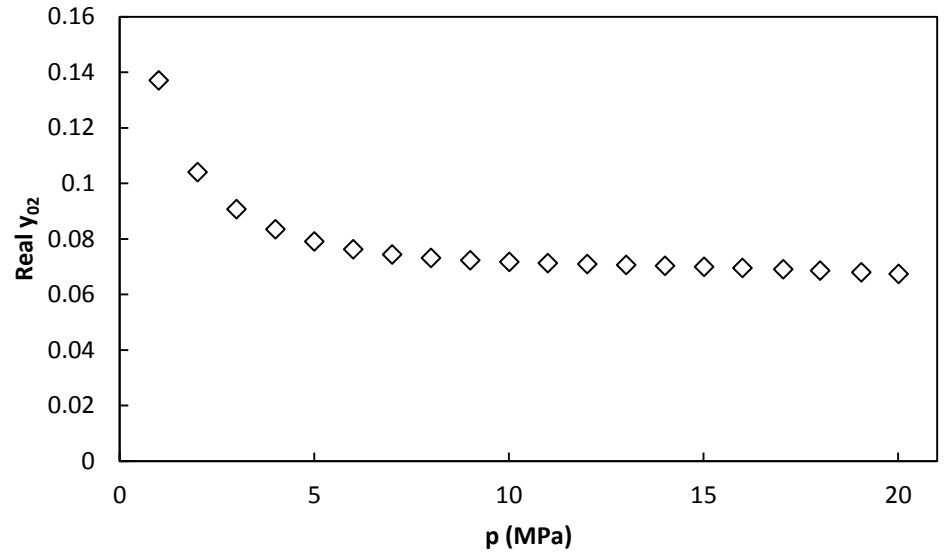

Figure 5.16 *Specific acoustic admittance of the opening real component for tube 2 and acoustic mode (0,3) at T = 250.10 K for the range on pressure from p = 1 MPa up to p = 20 MPa in argon.*

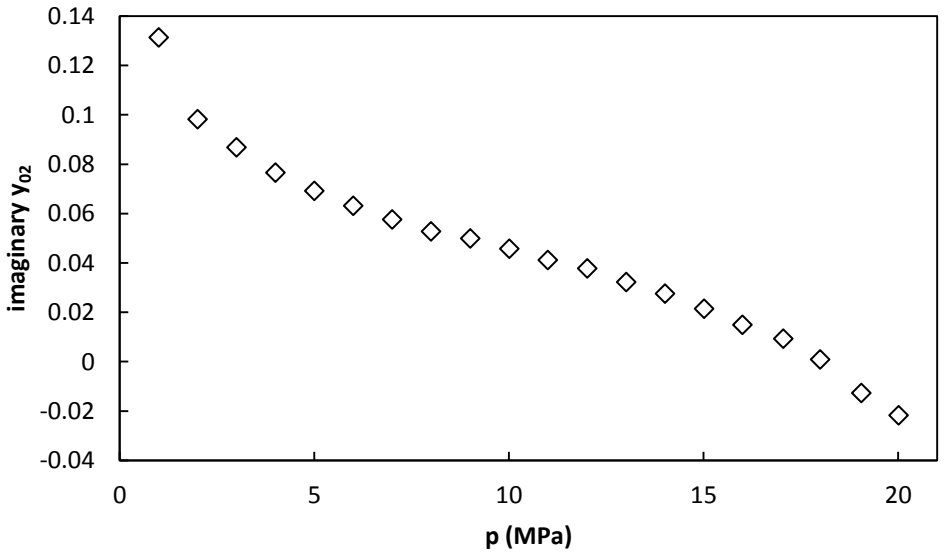

Figure 5.17 *Specific acoustic admittance of the opening imaginary component for tube 2 and acoustic mode (0,3) at T = 250.10 K for the range on pressure from p = 1 MPa up to p = 20 MPa in argon..*

Using all the parameters calculated in this section it is possible to quantify the frequency correction and the half-width contribution. Table 5.11 shows both ones for modes (0,2) to (0,5) at 250.10K and p = 20 MPa.

Table 5.11*Tubes frequency correction and half-width contribution for acoustic modes (0,2) to (0,5) at T = 250.10 K and p = 20MPa in argon.*

Mode	Δf_{tubes}(Hz)	g_{tubes}(Hz)
(0,2)	0.218	2.42
(0,3)	0.004	0.097
(0,4)	-0.032	0.077
(0,5)	-0.031	0.060

The variation with pressure of the frequency correction and the half-width contribution for mode (0,3) are detailed in figure 5.18 and in figure 5.19 respectively.

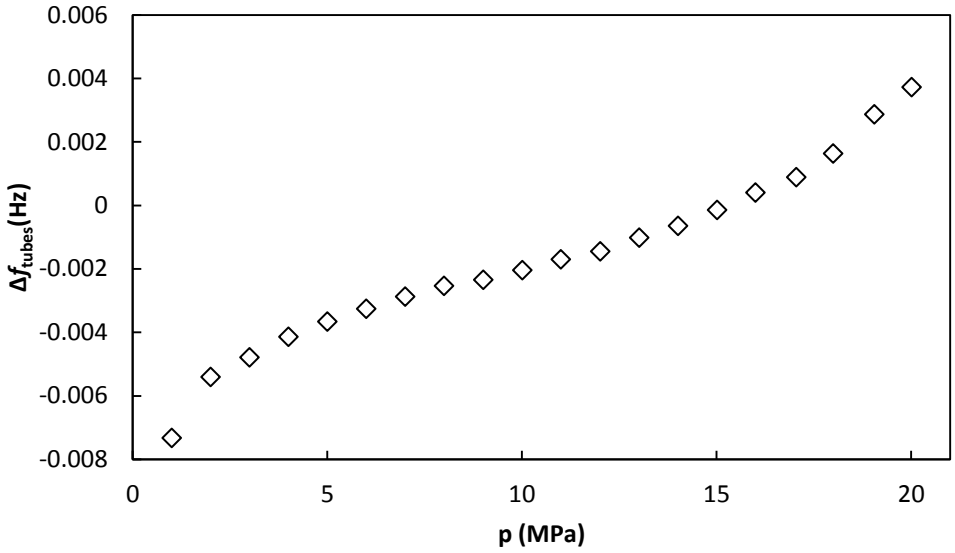

Figure 5.18 *Tubes frequency correction for the acoustic mode (0,3) at T = 250.10 K in Argon for the pressure range from p = 1 MPa up to p = 20 MPa.*

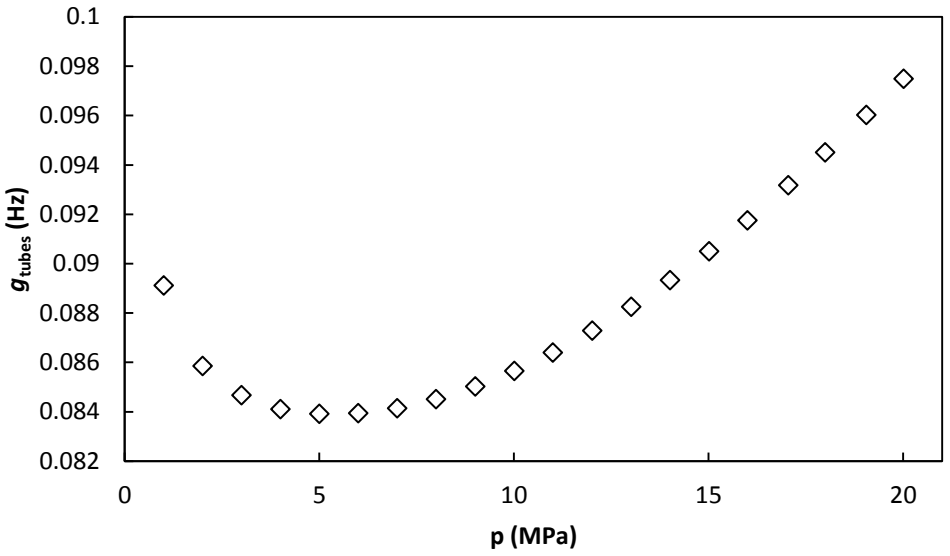

Figure 5.19 *Tubes half-width contribution for acoustic mode (0,3) at T = 250.10 K for the range on pressure from p = 1 MPa up to p = 20 MPa in argon.*

5.2.2 Radius Model

Once all the corrections for the five isotherms under study are computed, the different values of the inner cavity radius for each pressure and temperature may be calculated. But once again for each mode a different radius value is obtained as shown in table 5.12.

Table 5.12 *Radius values for acoustic modes (0,2) to (0,5) at T=250.10K and p=20MPa in argon.*

Mode	a(m)
(0,2)	0.040166
(0,3)	0.040171
(0,4)	0.040176
(0,5)	0.040184

Before farther calculations in radius determination it is necessary to identify which of these modes are suitable for the study purposes. The experimental half-width was compared to the calculated one to check the modes. As figure 5.20 shows, the excess half-width tends to be lower than 10 ppm for three modes (0,2), (0,3), and (0,4); and lower than 20 ppm for mode (0,5) them. Therefore the four modes are good enough for this work purposes.

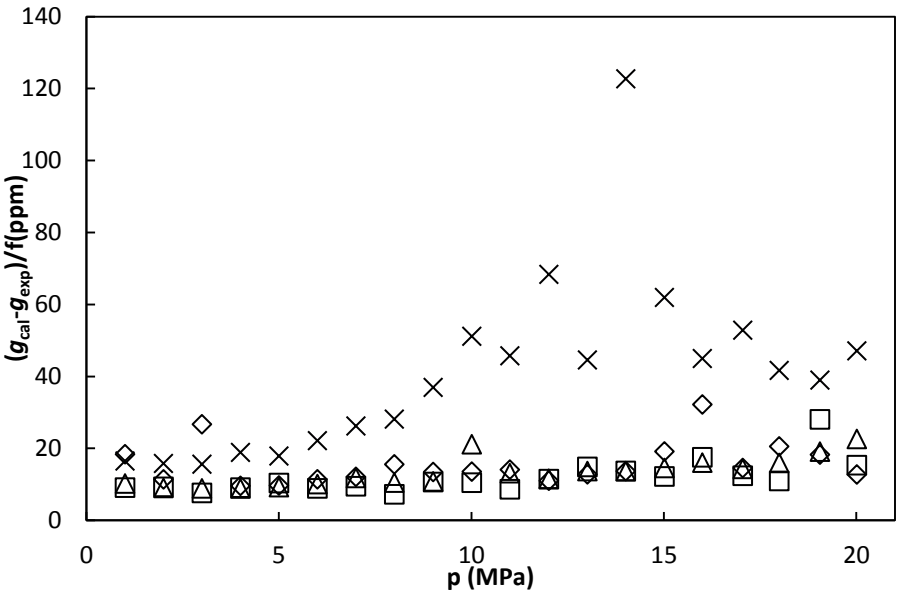

Figure 5.20 *Excess half-width at T = 250.10 K for acoustic modes (0,2) (◊),(0,3) (□),(0,4) (Δ) and (0,5) (X) for the pressure range from p = 1 MPa up to p = 20 MPa in argon.*

Data from the four modes were used for all the temperatures and a second order model for each of them was developed. Models and experimental data are shown in figure 5.21

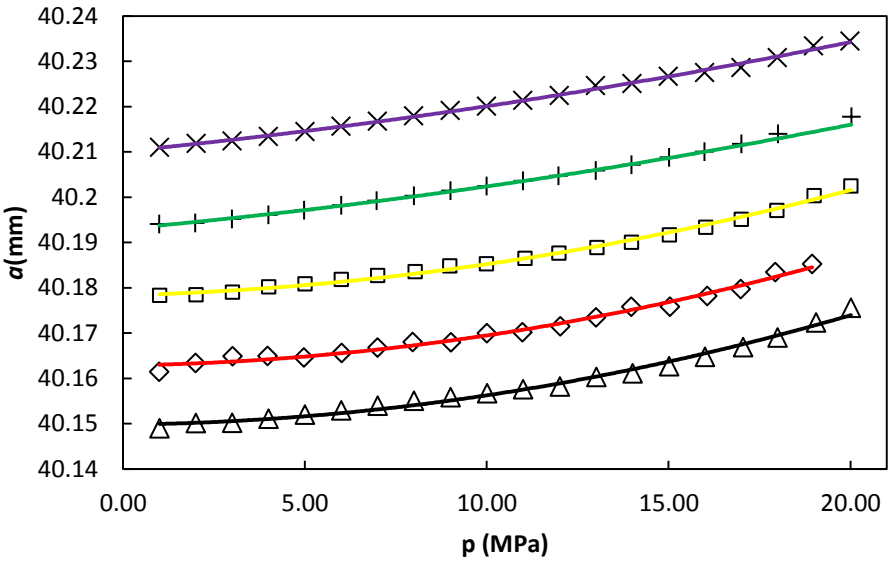

Figure 5.21 *Experimental data and fitted second order equation of the internal radius of the cavity in the pressure range from p = 1 MPa up to p = 20MPa at T = 250.10 K (Δ, experimental; —model), T = 273.15 K (◊, experimental; —model), T = 299.72 K (□, experimental; —model), T = 324.99 K (+, experimental;—model), T = 350.02 K (X, experimental; —model).*

The parameters of each model are shown in table 5.13 these parameters are adjusted to second order polynomial function (equation 2.6-b). Models give the radius results in millimetres.

$$u^2 = \frac{\gamma^{pg} RT}{M} + A_1 p + A_2 p^2 + \ldots \qquad (2.6\text{-b})$$

Table 5.13 *Experimental coefficients for second order equation modelling radius behaviour at different temperatures in a pressure range from p = 1 MPa up to p = 20 MPa.*

	Model				
Temperature	**250.10K**	**273.15K**	**299.72K**	**324.99K**	**350.02K**
A_2 (mm·MPa^{-2})	5.59959	5.36953	4.73185	2.11921	2.08493
A_1 (mm·MPa^{-1})	0.86341	1.27646	2.15376	7.25200	7.89101
A_0 (mm)	40.14981	40.16285	40.17834	40.19301	40.21011
σ(mm)	$1.320 \cdot 10^{-4}$	$2.0064 \cdot 10^{-4}$	$9.4318 \cdot 10^{-4}$	$9.3474 \cdot 10^{-4}$	$4.0297 \cdot 10^{-4}$

A comparison was made between the experimental radii obtained and the model radii; this comparison is a residual analysis which can be seen in figure 5.22

All residuals are inside the interval ±50x10^{-6} relative deviation from the measured data. This gives the idea of the reliability of the model.

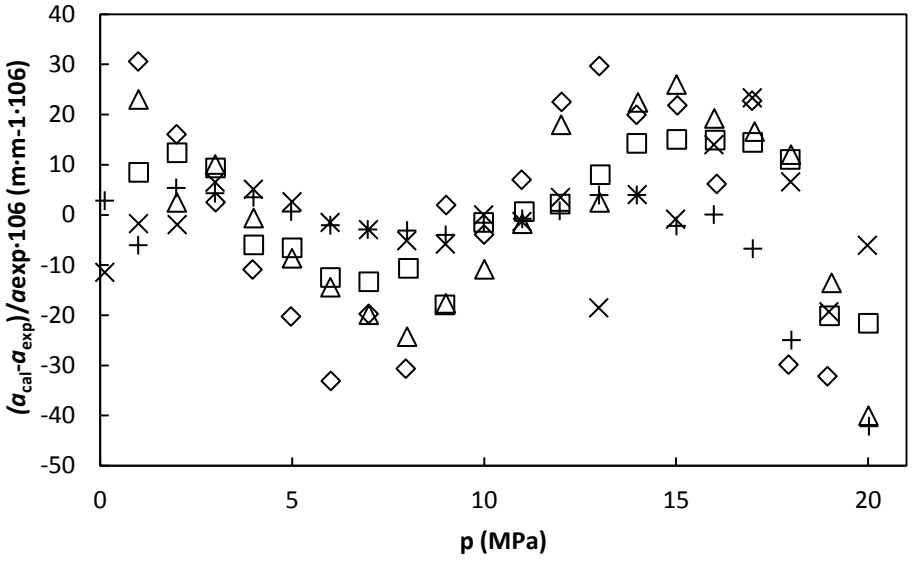

Figure 5.22 *Residual analysis for developed models at T = 250.10 K (Δ), T = 273.15 K (◊),T = 299.74 K (□),T = 324.99 K (+) and T = 350.02 K (X) in the pressure range from p = 1 MPa up to p = 20MPa.*

5.3 UNCERTAINTY ASSESMENT.

Radius uncertainty is calculated according equations 3.12 and 3.13. It has three main sources: acoustic modal dispersion, frequency uncertainty and speed of sound uncertainty. Mass molar contribution and pressure and temperature contributions were not taken into account because they are negligible against the uncertainty sources cited before.

$$a = \frac{1}{n}\frac{u}{2\pi}\sum_{i=1}^{n}\frac{\upsilon_i}{f_i} \tag{3.12}$$

$$u(a) = \sqrt{u^2(a)_{disp} + \sum_{i=1}^{n}\left(\frac{\partial a}{\partial f_i}\right)^2 u^2(f_i) + \sum_{i=1}^{n}\left(\frac{\partial a}{\partial u}\right)^2 u^2(u)}$$

$$u(a) = \sqrt{u^2(a)_{disp} + \sum_{i=1}^{n}\left(\frac{1}{n}\frac{u}{2\pi}\frac{\upsilon_i}{f_i^2}\right)^2 u^2(f_i) + \sum_{i=1}^{n}\left(\frac{1}{n}\frac{\upsilon_i}{2\pi f_i}\right)^2 u^2(u)} \tag{3.13}$$

5.3.1 Radius Dispersion.

Four acoustic modes were measured, (0,2), (0,3), (0,4) and (0,5) and all of them were taken into consideration for the radius calculations. The uncertainty contribution due to this dispersion was calculated as the average standard deviation of the four measurements. Table 5.14 shows the values of the radius modal dispersion uncertainties at each pressure for the isotherm at T=250K, other isotherms uncertainties are displayed in the appendix B.

Table 5.14 *Radius modal dispersion absolute and relative uncertainty at T = 250 K and in the pressure range pressure under study.*

p (MPa)	$u_{disp}(a)$ (m·10^6)	$u_r(a)$ (m·m^{-1} x10^6)
20.01	3.4	85
19.05	2.8	69
17.99	2.3	58
17.05	1.9	48
16.00	2.1	52
15.01	1.0	25
14.01	0.98	24
13.01	1.4	35
12.01	0.97	24
11.00	0.98	24
10.01	0.9.7	24
9.00	0.79	20

Table 5.14 *(Continuation) Radius modal dispersion absolute and relative uncertainty at T = 250 K and in the pressure range pressure under study.*

p (MPa)	$u_{disp}(a)$ (m·10^6)	$u_r(a)$ (m·m^{-1} x10^6)
8.00	0.66	16
7.00	0.54	13
6.00	0.59	15
5.00	0.41	10
4.00	0.28	7
3.00	0.19	5
2.00	0.16	4
1.00	1.1	28

5.3.2 Speed of Sound.

Speed of sound data were taken using REFPROP software [1,2], where according to bibliography the speed of sound data uncertainty is lower than 0.02%. Therefore every value of speed of sound uncertainty was calculated as the 0.02% of the speed of sound value at its corresponding pressure and temperature.

5.3.3 Frequency Measurement.

The frequency of resonance uncertainty was provided by the measurement software and collected during measuring process. Therefore each resonance mode has its own frequency uncertainty. Table 5.15 shows uncertainties of each measured acoustic mode at p=20MPa.

Table 5.15 *Frequency of resonance absolute and relative uncertainties for acoustic modes (0,2) to (0,5) at T = 250 K and p = 20 MPa.*

Mode	$u(f_i)$ (Hz)	$u_r(f)$ (Hz·Hz^{-1}x10^{-6})
0.2	0.15	25
0.3	0.98	90
0.4	0.44	29
0.5	4.2	210

Excess half-width is other source of uncertainty that might be considered as frequency uncertainty. Excess half-width values are different for each acoustic mode and they change with pressure as detailed in figure 5.20

The final frequency uncertainty is that obtained as the square sum of two contributions, frequency and excess half-widths. The sensitivity factor is equal for both contributions. It is

obtained from equation 3.12 which was shown previously in this chapter. Equation 5.1 shows how this sensitivity factor is obtained.

$$\left(\frac{\partial a}{\partial f_i}\right)=\left(\frac{\partial a}{\partial g_i}\right)=\left(\frac{1}{n}\frac{u}{2\pi}\frac{\upsilon_i}{f_i^{\,2}}\right) \qquad (5.1)$$

5.3.4 Overall Uncertainty

The overall uncertainty is calculated according to GUM [8] adding the squares of the uncertainties times their sensitivities as indicated in equation 3.17.

The overall standard uncertainty values of radius determination at T=250K in the range of pressure from p =1 MPa up to p = 20MPa are in table 5.16. Radius uncertainties at T = 273 K, T = 300 K, T = 325 K and T = 350 K are found in Appendix B. The radius relative uncertainty is higher than $100\cdot10^{-6}$ and lower $220\cdot10^{-6}$ at any temperature and pressure under study.

Table 5.16 *Radius standard uncertainty and relative standard uncertainty at T = 250 K in the range of pressure under study.*

p (MPa)	u(*a*)(m)	$u_r(a)$ ($m\cdot m^{-1}$ x10^6)
20.01	5.5 x10^{-6}	130
19.05	5.3 x10^{-6}	120
17.99	5.1 x10^{-6}	120
17.05	5.0 x10^{-6}	110
16.00	5.5 x10^{-6}	110
15.01	4.7 x10^{-6}	110
14.01	4.8 x10^{-6}	110
13.01	5.0 x10^{-6}	110
12.01	4.7 x10^{-6}	100
11.00	4.8 x10^{-6}	100
10.01	4.8 x10^{-6}	100
9.00	4.7 x10^{-6}	100
8.00	4.7 x10^{-6}	100
7.00	4.6 x10^{-6}	100
6.00	4.6 x10^{-6}	100
5.00	4.5 x10^{-6}	100
4.00	4.4 x10^{-6}	100
3.00	4.3 x10^{-6}	100
2.00	4.3 x10^{-6}	100
1.00	4.2 x10^{-6}	100

The uncertainty in the radius determination is an important value because it will be used as uncertainty source in next chapters for determination of thermodynamic properties and their uncertainties.

The radius uncertainty using developed models for studying radius dependence on pressure from parameters obtained in table 5.13 is computed as the square sum of uncertainty in the point and the uncertainty of the regression, which is calculated as shown in equation 5.2

$$u\left(a_{reg}\right)=\sqrt{\frac{\sum_{i}^{n}\left(a_i^{calc}-a_i^{\exp}\right)^2}{n-m}} \qquad (5.2)$$

Where $u(a_{reg})$ is the regression uncertainty, a_i^{calc} and a_i^{exp} are the value of a calculated according the model and the value of a measured respectively at the point i. The total number of measurements is n and m is the number of parameters

Values of regression uncertainties at T = 250 K,T = 273 K, T = 300 K, T = 325 K and T = 350K are in table 5.17.

Table 5.17 *Regressions uncertainties at several different temperatures*

T(K)	u(a_{reg}) (m)	$u_r(a_{reg})$ ($m \cdot m^{-1} x10^6$)
250	7.8×10^{-7}	19
273	9.5×10^{-7}	24
300	5.4×10^{-7}	13
325	8.6×10^{-7}	21
350	4.1×10^{-7}	10

When measurement uncertainties and regression uncertainties are compared it is obvious that the main contribution is due to the measurements. Therefore regression uncertainty might be neglected.

5.4 REFERENCES

1. Trusler, J.P.M., and Zarari, M. (1992) The speed of sound and derived thermodynamic properties of methane at temperatures between 275 K and 375 K and pressures up to 10 MPa. The Journal of Chemical Thermodynamics 24, 973-991.

2. Estela-Uribe, J.F., Trusler, J.P.M., Chamorro, C.R., Segovia, J.J., Martín, M.C., and Villamañán, M.A. (2006) Speeds of sound in {(1 - x)CH4 + xN2} with x = (0.10001, 0.19999, and

0.5422) at temperatures between 170 K and 400 K and pressures up to 30 MPa. The Journal of Chemical Thermodynamics 38, 929-937.

3. Costa Gomes, M.F., and Trusler, J.P.M. (1998) The speed of sound in two methane-rich gas mixtures at temperatures between 250 K and 350 K and at pressures up to 20 MPa. The Journal of Chemical Thermodynamics 30, 1121-1129.

4. Estrada-Alexanders, A.F., and Trusler, J.P.M. (1998) Speed of sound in carbon dioxide at temperatures between (220 and 450) K and pressures up to 14 MPa. The Journal of Chemical Thermodynamics 30, 1589-1601.

5. Estrada-Alexanders, A.F., and Trusler, J.P.M. (1999) Speed of sound in (0.4C2H6+0; 0.6CO2) at temperatures betweenT = 220 K andT = 450 K and pressures up to p = 1.2 MPa. The Journal of Chemical Thermodynamics 31, 685-695.

6. Lemmon, E.W., Huber, M.L., McLinden, M.O. NIST Standard Reference Database 23: Reference Fluid Thermodynamic and Transport Properties-REFPROP, Version 9.1, National Institute of Standards and Technology, Standard Reference Data Program, Gaithersburg, 2013.

7. Tegeler, C., Span, R., and Wagner, W. (1999) A New Equation of State for Argon Covering the Fluid Region for Temperatures From the Melting Line to 700 K at Pressures up to 1000 MPa. Journal of Physical and Chemical Reference Data 28, 779-850.

8. Evaluation of measurement data - Guide to the expression of uncertainty in measurement BIMP, 2008.

Chapter 6

MEASUREMENTS OF THE MIXTURES OF CARBON MONOXIDE AND NITROGEN

6.1 INTRODUCTION

Working with multicomponent gas mixtures is a hard task, in order to make it easier it is necessary to know some of their thermodynamic properties, but in order to get a suitable prediction it is necessary to understand the behavior of their components in binary mixtures at different compositions.

Nitrogen and carbon monoxide are compounds usually found in unconventional energy gases and in this study, two nitrogen + carbon monoxide mixtures have been characterized measuring the speed of sound and calculating some thermodynamic properties from it

The gas mixtures were prepared gravimetrically by the Spanish Center of Metrology (CEM) at their facilities. The composition and purity were specified by them at the values shown in table 6.1

Table 6.1 *Molar compositions of the gas mixture under study.*

Cylinder	x_{CO}	Specified purity of N_2 (x_{N_2})	Specified Purity of CO (x_{CO})	Pressure (bar)
92337	0.04999±0.00001	0.999995	0.999985	80
01163	0.10018 ± 0.00002	0.99995	0.9997	90

The filling process was carried out using a manual 100 cm^3 piston and cylinder compressor. The resonator temperature was set about 25 K lower than the ambient temperature to make lower the cavity pressure and make easier the gas flow. The 100 cm^3 cylinder was charged with the gas mixture from the bottle. Once it was full, the valves were set to ensure no gas was going back to the bottle and it was flowing to the sphere, this process was repeated several times. Once the pressure was the appropriated, it was changed the spherical resonator temperature set up to the measuring conditions. If necessary, pressure was adjusted by a piston and cylinder pressure adjuster, smaller than the one used during the filling process.

The measurements were carried out at two different temperatures: 273 K and 325 K in range of pressure from 0.1 MPa up to 10 MPa Once the spherical resonator is full of gas at the higest pressure, the pressure is reduce in 1 Mpa steps until the point p = 1 MPa is reached and the last one is taken at p = 0.1 MPA.

Acoustic resonance frequencies and the half-width of the resonance peaks were measured for four different acoustic modes (0,2), (0,3), (0,4) and (0,5) at each pressure for both binary mixtures.

The following sections contain the experimental measurements with the details of the applied corrections and the calculations of the speed of sound and the derived data such as heat capacities and virial acoustic coefficients which have been compared with those calculated from the literature [1-3].

6.2 EXPERIMENTAL MEASUREMENTS OF THE MIXTURE (0.05 CO + 0.95 N_2) AT T=273.15K

The acoustic frequencies of resonance and their half-width of resonance peaks for the acoustic modes (0,2), (0,3), (0,4) and (0,5) from 0.1 MPa to 9.99 MPa pressure range have been measured, as an example, the results at the highest pressure are detailed in table 6.2

Table 6.2 *Frequency of resonance and half-widths of resonance peaks for acoustic modes (0,2) to (0,5) at p=9.99MPa and T=273.15K for the binary mixture x_{CO} = 0.05 and x_{N2} = 0.95.*

Mode	***f*** **(Hz)**	***g*** **(Hz)**
(0,2)	6444.64	0.382
(0,3)	11079.56	0.409
(0,4)	15638.01	0.577
(0,5)	20171.55	0.776

According to the theory explained in chapter 2 the acoustic frequency of resonance must decrease when pressure decreases as it can be observed in figure 6.1 for the resonance mode (0,2) as an example.

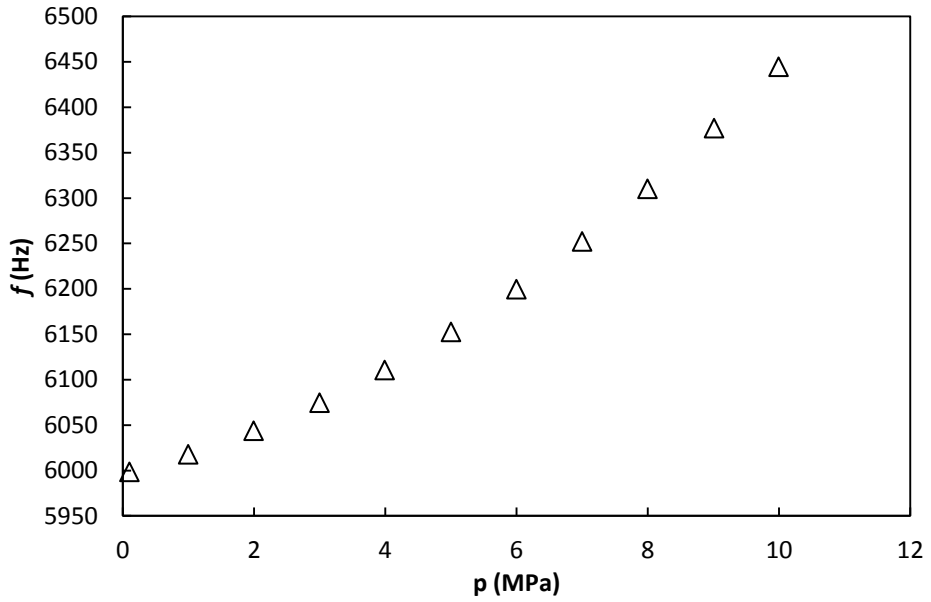

Figure 6.1 *Frequency of resonance for acoustic mode (0,2) at T = 273.15 K as a function of pressure from for the binary mixture x_{CO} = 0.05 and x_{N2} = 0.95.*

The half-widths also change with pressure but their tendency is different, it is quite constant for high pressure but, at lower pressures this factor grows quickly. This effect is easily observed in figure 6.2. This is because half-width represents in some way the energy loses, and as sound needs a material pathway to spread itself when this material pathway's density is decreasing the energy loses increase.

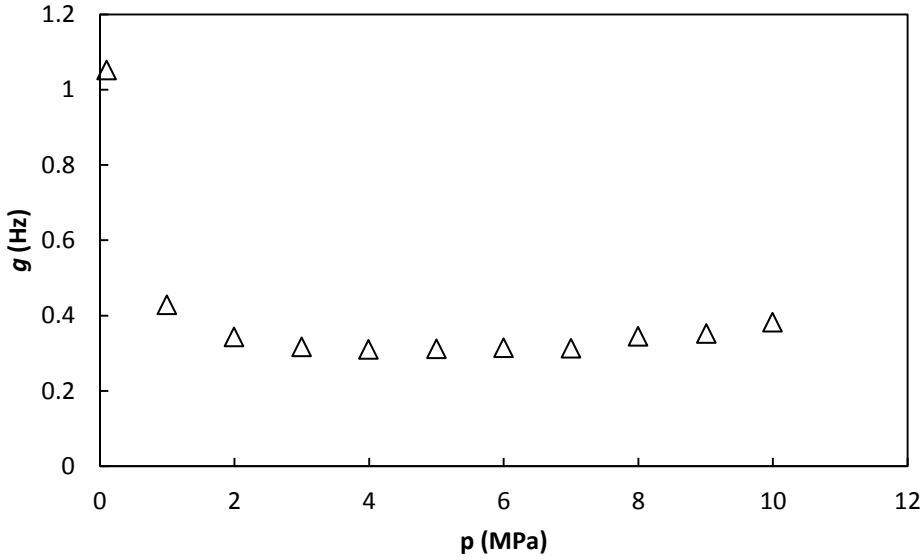

Figure 6.2 *Half-widths of resonance peaks for acoustic mode (0,2) at T = 273.15 K as a function of pressure for the binary mixture x_{CO} = 0.05 and x_{N2} = 0.95.*

6.2.1 Frequency Corrections

As it was explained in chapter 2, the data showed in the previous section (directly measured) need some corrections before they can be used to determine speed of sound from them.

These frequency corrections, half-width contributions and the parameters required to calculate them are usually dependent on frequency and pressure. Therefore this chapter summarize these values by showing the values of these parameters for all acoustic modes at the highest pressure and the variation width pressure for one representative acoustic mode of resonance.

6.2.1.1 *Thermal Boundary Layer Correction***.**

The most important contribution of the applied corrections is the thermal boundary layer correction. Just like it was done in previous chapters, some parameters are required to obtain the value for the thermal boundary layer correction. The first one is the thermal penetration length, which is dependent on frequency, so it will be different for each mode at the same pressure, this effect can be seen in table 6.3.

Table 6.3 *Thermal penetration length for acoustic modes (0,2) to (0,5) at T = 273.15 K and p = 9.99 MPa for the binary mixture* $x_{CO} = 0.05$ *and* $x_{N2} = 0.95$

Mode	δ_{TH}(m)
(0,2)	3.08×10^{-6}
(0,3)	2.35×10^{-6}
(0,4)	1.98×10^{-6}
(0,5)	1.74×10^{-6}

Also, as it is frequency dependent and figure 6.1 shows that the frequency of resonance changes with pressure, thermal penetration length changes with pressure too. This variation is shown in figure 6.3

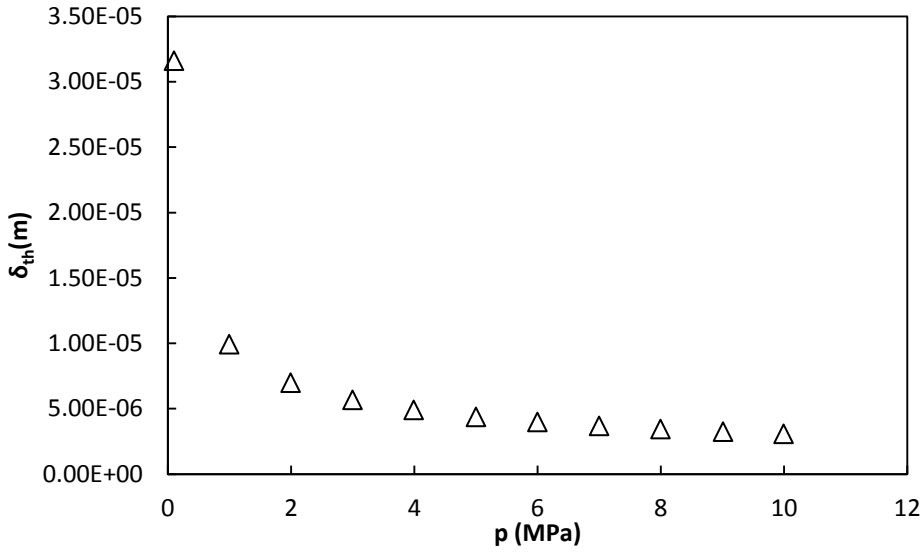

Figure 6.3 *Thermal penetration length for acoustic mode (0,2) at T = 273.15 K as a function of pressure for the binary mixture x_{CO} = 0.05 and x_{N2} = 0.95.*

The second parameter to calculate is the thermal accommodation length l_{th} which is only function af pressure, therefore at the same pressure and temperature the thermal accommodation length is equal for all modes. The variation of this parameter with pressure is shown in figure 6.4.

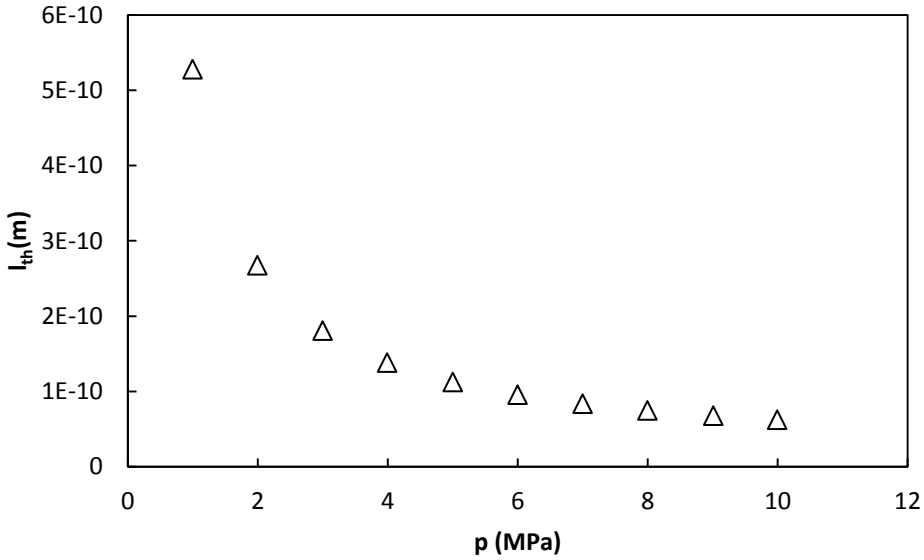

Figure 6.4 *Thermal accommodation length at T = 273.15 K as a function of pressure for the binary mixture x_{CO} = 0.05 and x_{N2} = 0.95.*

And for last, it was calculated the thermal penetration length in the shell surface. This parameter, just like the normal penetration length is function of frequency. Hence it is different for each mode as displayed in table 6.4

Table 6.4 *Shell thermal penetration length for acoustic modes (0,2) to (0,5) at T = 273.15 K and p = 9.99 MPa for the binary mixture x_{CO} = 0.05 and x_{N2} = 0.95.*

Mode	$\delta_{shell\delta}$(m)
(0,2)	1.41×10^{-5}
(0,3)	1.08×10^{-5}
(0,4)	9.07×10^{-6}
(0,5)	7.99×10^{-6}

This dissertation has shown that frequency of resonance change with pressure therefore a parameter like the thermal penetration length, which is frequency dependent, changes its value with pressure. This change can be seen in figure 6.5 for the acoustic mode (0,2).

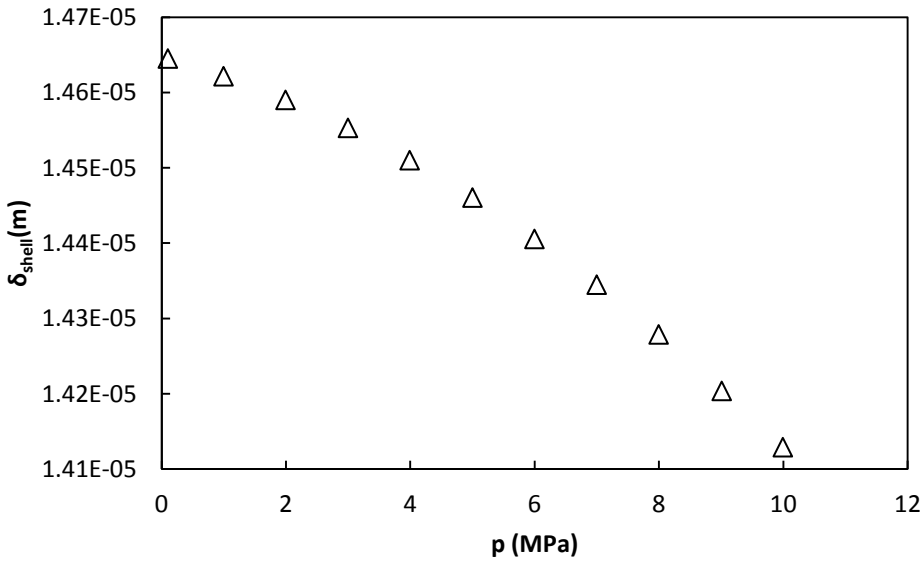

Figure 6.5 *Shell thermal penetration length for acoustic mode (0,2) at T = 273.15 K as a function of pressure for the binary mixture x_{CO} = 0.05 and x_{N2} = 0.95.*

Once all this parameters are calculated the values for the thermal boundary layer correction and the contribution to de half-width can be obtained. This parameters are in table 6.5 for the modes (0,2) to(0,5) at T = 273.15 K and p = 9.99 MPa.

Table 6.5 *Thermal boundary layer frequency correction and half-width contribution for acoustic modes (0,2) to (0,5) at T = 273.15 K and p = 9.99 MPa for the binary mixture x_{CO} = 0.05 and x_{N2} = 0.95.*

Mode	Δf_{th} (Hz)	g_{th} (Hz)
(0,2)	-0.150	0.153
(0,3)	-0.197	0.201
(0,4)	-0.234	0.238
(0,5)	-0.266	0.271

Both parameters tendency with pressure are shown in figures 6.6 for frequency and 6.7 for haft-width contribution.

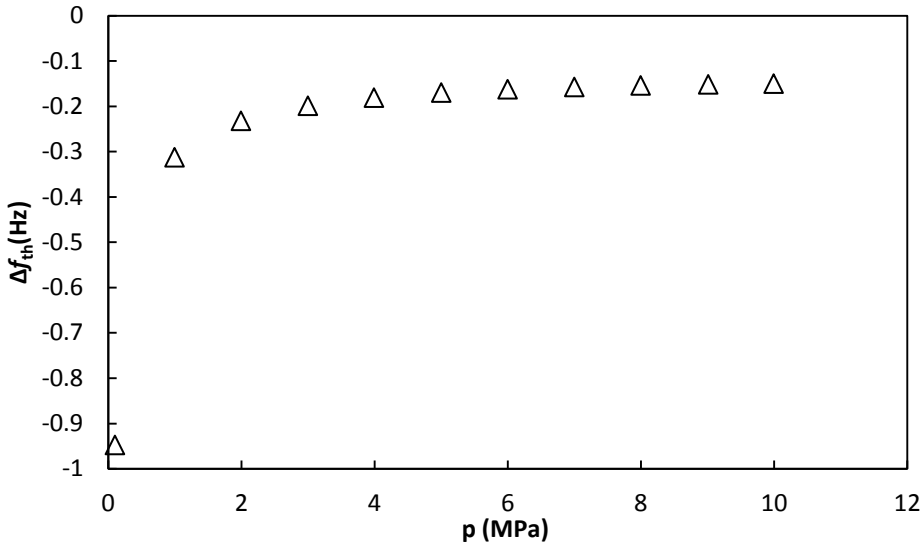

Figure 6.6 *Thermal boundary layer frequency correction for acoustic mode (0,2) at T = 273.15 K as a function of pressure for the binary mixture x_{CO} = 0.05 and x_{N2} = 0.95.*

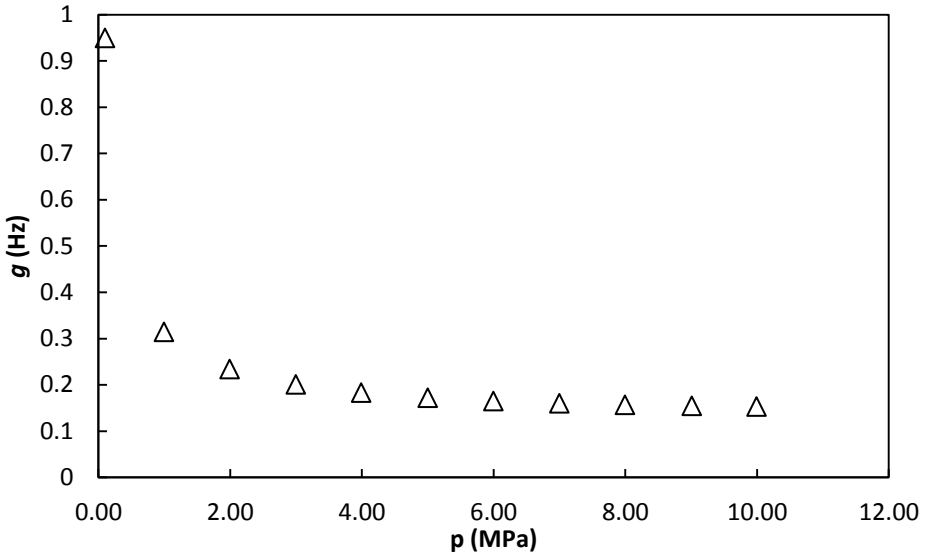

Figure 6.7 *Thermal boundary layer half-width contribution for acoustic mode (0,2) at T = 273.15 K as a function of pressure for the binary mixture x_{CO} = 0.05 and x_{N2} = 0.95.*

6.2.1.2 *Bulk Viscosity Contribution*

This parameter only affects to the half-width contribution.

Once again, it is required to compute some parameters before obtaining the actual bulk viscosity contribution to the half-width of the resonance peaks. One of the parameters required is already calculated and exposed in table 6.3 and figure 6.3, it is the thermal penetration length (δ_{th}). The last required parameter is the viscous penetration length (δ_v) which also depends on the frequency as many other parameters calculated until now. This dependency makes viscous penetration length change for each mode and with pressure. As it is displayed in table 6.6 and figure 6.8

Table 6.6 *Viscous penetration length for acoustic modes (0,2) to (0,5) at T = 273.15 K and p = 9.99 MPa, for the binary mixture x_{CO} = 0.05 and x_{N2} = 0.95.*

Mode	δ_V(m)
(0,2)	2.74 x10^{-6}
(0,3)	2.09 x10^{-6}
(0,4)	1.76 x10^{-6}
(0,5)	1.55 x10^{-6}

.

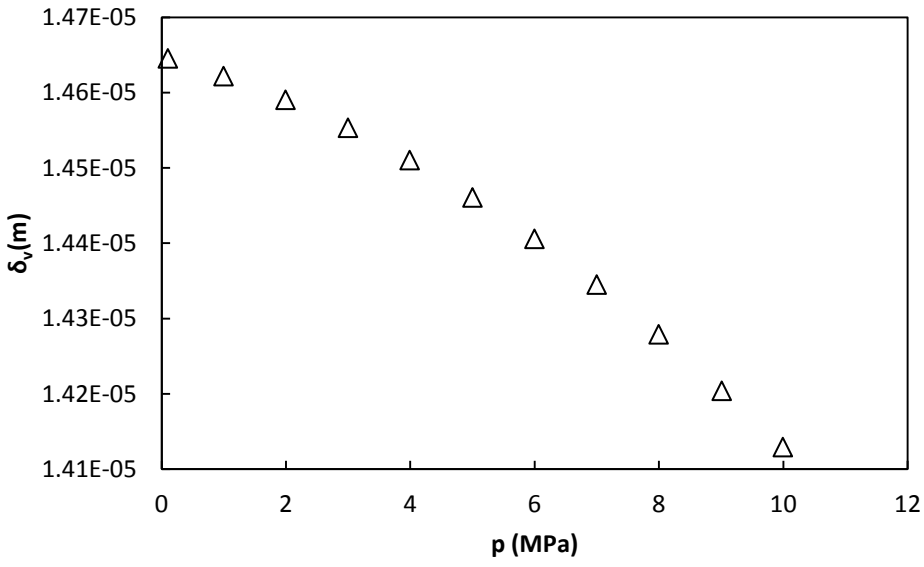

Figure 6.8 *Viscous penetration length for acoustic mode (0,2) at T = 273.15 K as a function of pressure for the binary mixture x_{CO} = 0.05 and x_{N2} = 0.95.*

Bulk viscosity contribution to the half-width is different for each mode and for each pressure; the variation for mode can be observed in table 6.7.

Table 6.7 *Bulk viscosity half-width contribution for acoustic modes (0,2) to (0,5) at T = 273.15 K and p = 10 MPa for the binary mixture x_{CO} = 0.05 and $x_{N\,2}$= 0.95.*

Mode	g_b(Hz)
(0,2)	3.20 x10^{-4}
(0,3)	9.45 x10^{-4}
(0,4)	1.88 x10^{-3}
(0,5)	3.13 x10^{-3}

The bulk viscosity contribution to the half-width dependence with pressure is shown in figure 6.9.

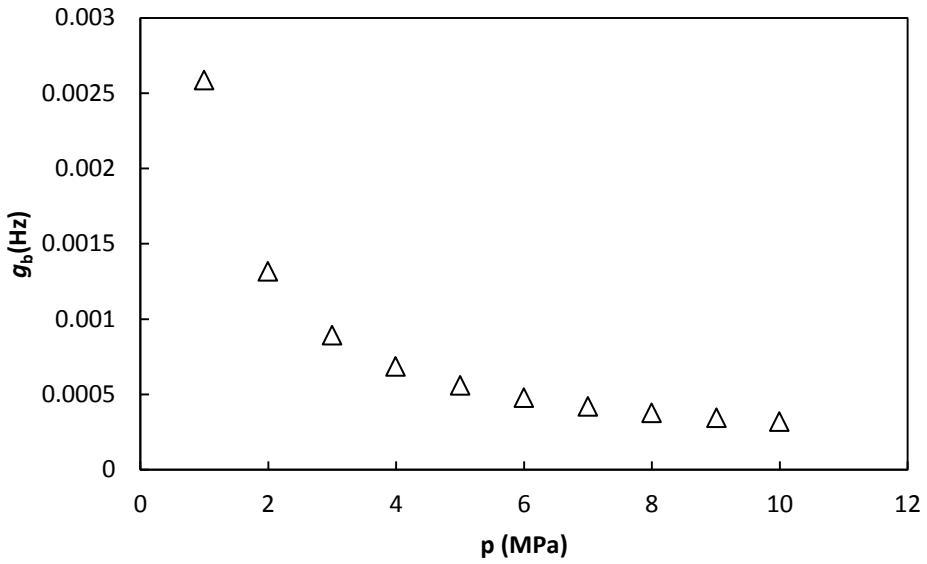

Figure 6.9 *Bulk viscosity half-width contribution for acoustic mode (0,2) at T = 273.15 K as a function of pressure for the binary mixture x_{CO} = 0.05 and x_{N2} = 0.95.*

6.2.1.3 *Shell Motion Correction*

This correction is due to the interactions between the acoustic waves and the inner cavity surface, which produces the cavity to vibrate and the frequency of resonance shifts.

The shell motion frequency correction is calculated using the breathing frequency (equation 2.24) which is constant for the resonator. It was already calculated in chapter 5.

$$f_{breath}=26488\text{Hz}$$

Shell motion frequency correction is function of the frequency, so this correction is dependent on mode and pressure. The mode dependence can be seen in table 6.8 and the pressure dependant for mode (0,2) in figure 6.10.

Table 6.8 *Shell motion frequency correction for acoustic modes (0,2) to (0,5) at T = 273.15 K and p = 9.99 MPa for the binary mixture x_{CO} = 0.05 and x_{N2} = 0.95.*

Mode	Δf_{shell} (Hz)
(0,2)	-0.102
(0,3)	-0.187
(0,4)	-0.297
(0,5)	-0.477

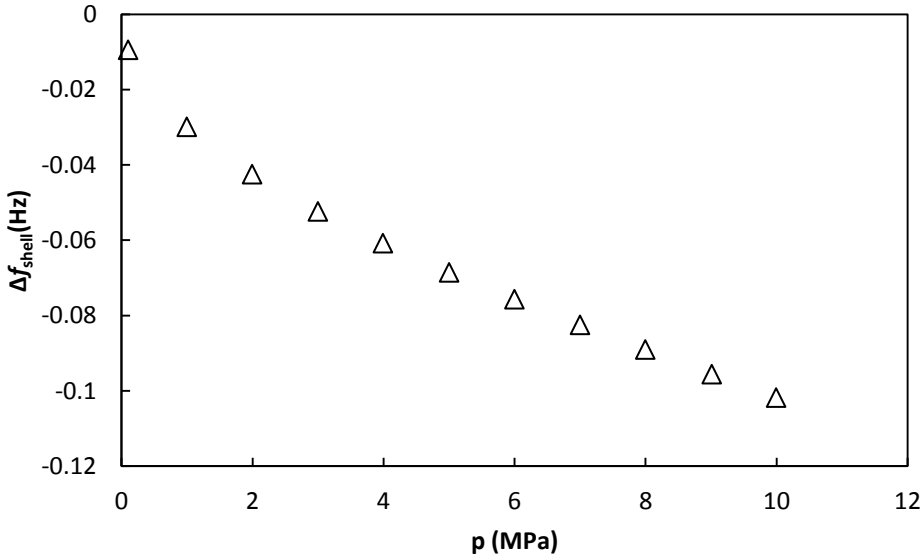

Figure 6.10 *Shell motion frequency correction for acoustic mode (0,2) at T = 273.15 K as a function of pressure for the binary mixture x_{CO} = 0.05 and x_{N2} = 0.95.*

6.2.1.4 *Tubes and Holes Correction*

The waves that travel through pipes or tubes connected to the cavity make the frequency of resonance change. This change can be calculated and corrected. But before that it is necessary to perform some complex calculations. First it is required to calculate the effective absorption coefficient (α_{KH}).

This coefficient depends on the wave frequency, the speed of sound, the radius of the pipe and the thermal and viscous penetration lengths calculated previously. As the current set up

has 2 pipes connected on the cavity, there are two different absorption coefficients, one for each tube. The dimensions of these tubes are:

$r_{h1} = 5x10^{-4}$ m $r_{h2} = 1x10^{-3}$ m

$L_1 = 3.8x10^{-2}$ m $L_2 = 0.8$ m

The frequency of resonance is different for each mode, therefore the effective absorption coefficient changes for each mode, as we can see in table 6.9.

Table 6.9 *Kirchhoff-Helmholtz absorption coefficient for tubes 1 and 2 for acoustic modes (0,2) to (0,5) at T = 273.15 K and p = 9.99MPa for the binary mixture $x_{CO} = 0.05$ and $x_{N2} = 0.95$.*

Mode	α_{KH1} (m^{-1})	α_{KH2} (m^{-1})
(0,2)	0.518	0.259
(0,3)	0.679	0.340
(0,4)	0.807	0.404
(0,5)	0.917	0.458

The effective absorption coefficient changes with pressure because it depends on speed of sound and frequency of resonance, and both magnitudes change on pressure. Figure 6.11 shows these changes for mode (0,2).

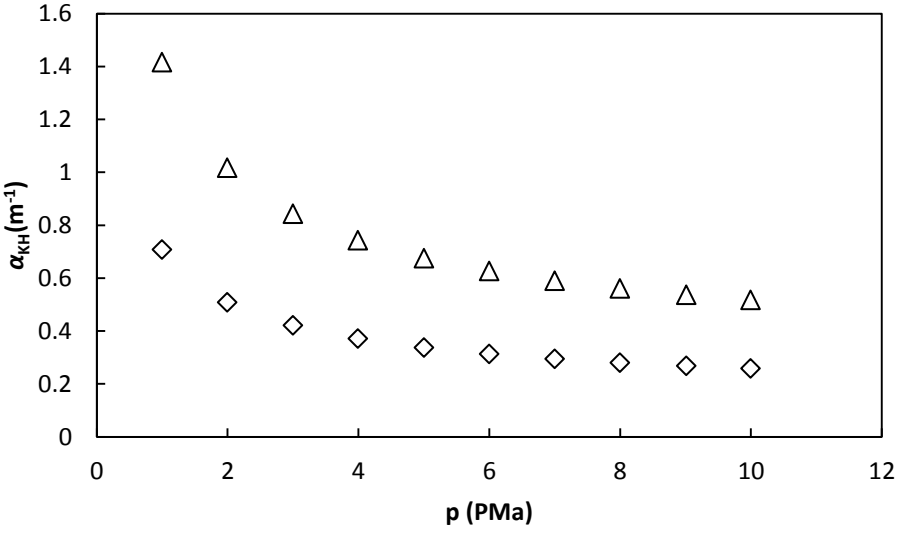

Figure 6.11 *Kirchhoff-Helmholtz absorption coefficients for tubes 1(Δ) and 2(◊) for acoustic mode (0,2) at T = 273.15 K as a function of pressure for the binary mixture $x_{CO} = 0.05$ and $x_{N2} = 0.95$.*

It is also necessary to calculate the propagation constant. This parameter changes for resonance modes and for each pressure, because it depends on frequency of resonance and speed of sound, just like the effective absorption coefficient, in fact, propagation constant is a complex number which imaginary component is α_{KH} changing the sign. As displayed in table 6.10.

Table 6.10 *Propagation constant for tubes 1 and 2 for acoustic modes (0,2) to (0,5) at T = 273.15 K and p = 9.99 MPa for the binary mixture x_{CO} = 0.05 and x_{N2} = 0.95*

Mode	k_{KH1} (m^{-1})	k_{KH2} (m^{-1})
(0,2)	112.368-0.518i	112.109-0.259i
(0,3)	192.971-0.679i	192.632-0.340i
(0,4)	272.213-0.807i	271.810-0.404i
(0,5)	351.005-0.917i	350.547-0.458i

The variation with pressure is shown in figure 6.12 only for the real component because the imaginary component can be seen in figure 6.11.

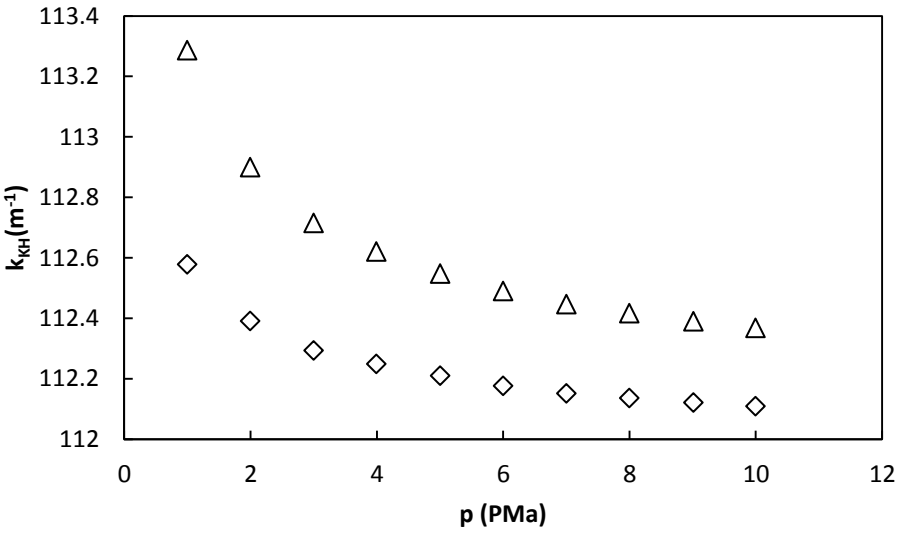

Figure 6.12 *Propagation constant real component for tubes 1 (Δ) and 2(◊)for acoustic mode (0,2) at T = 273.15 K as a function of pressure for the binary mixture x_{CO} = 0.05 and x_{N2} = 0.95.*

For last it is necessary to calculate the specific acoustic input admittance (y_o). This parameter as it was explained in chapter 2 depends only on propagation coefficient and the length of the tube. It is changing for modes and for pressure as k_{KH} does. The variation of this parameter for both conductions for modes (0,2) to (0,5) is in table 6.11.

Table 6.11 *Specific acoustic admittance of the opening for tubes 1 and 2 for modes (0,2) to (0,5) at T = 273.15 K and p = 10MPa for the binary mixture x_{CO} = 0.05 and x_{N2} = 0.95.*

Mode	y_{01}	y_{02}
(0,2)	0.112+2.116i	0.070+2.096i
(0,3)	0.115+1.759i	0.092+1.777i
(0,4)	0.099+1.337i	0.099+1.388i
(0,5)	0.086+1.006i	0.105+1.083i

Specific acoustic admittance is a complex parameter which changes with pressure; these variations can be seen in figures 6.13 for the real part, and 6.14 for the imaginary component.

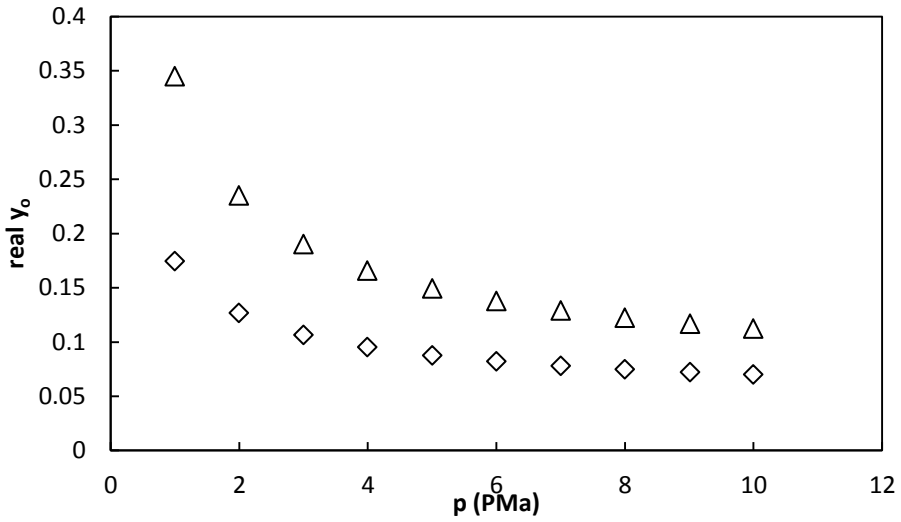

Figure 6.13 *Specific acoustic admittance of the opening real component for tubes 1 (Δ) and 2(◊) for acoustic mode (0,2) at T = 273.15 K as a function of pressure for the binary mixture x_{CO} = 0.05 and x_{N2} = 0.95.*

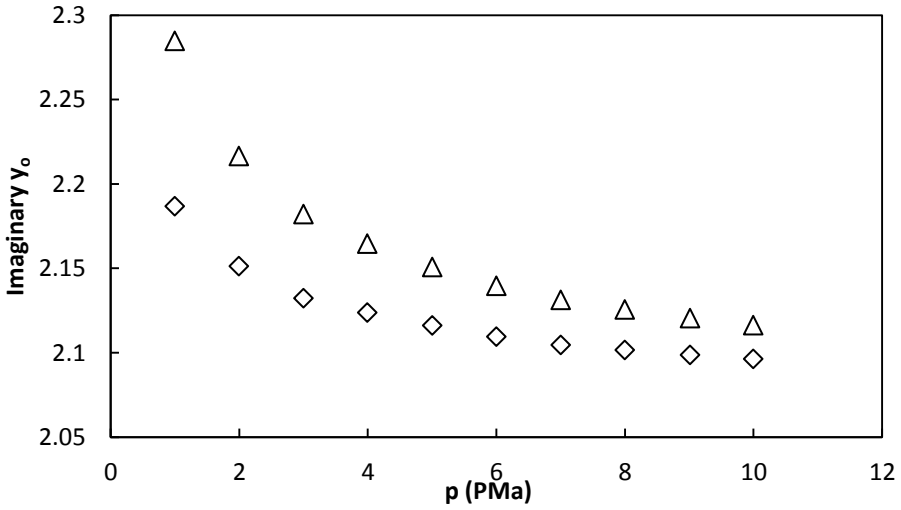

Figure 6.14 *Specific acoustic admittance of the opening imaginary component for tubes 1 (Δ) and 2(◊) for acoustic mode (0,2) at T = 273.15 K as a function of pressure for the binary mixture x_{CO} = 0.05 and x_{N2} = 0.95.*

The tubes frequency correction and half-width contribution can be calculated using all the parameters shown. As many parameters used to calculate this correction the frequency shift must be dependent on the resonance mode and pressure. The variation for different modes is visible in table 6.12.

Table 6.12 *Tubes frequency correction and half-width contribution for acoustic modes (0,2) to (0,5) at T = 273.15 K and p = 9.99MPa for the binary mixture x_{CO} = 0.05 and x_{N2} = 0.95.*

Mode	Δf_{tubes} (Hz)	g_{tubes} (Hz)
(0,2)	-0.240	0.139
(0,3)	-0.167	0.118
(0,4)	-0.097	0.089
(0,5)	-0.055	0.067

The variation with pressure of those parameters is displayed in figures 6.15 and 6.16.

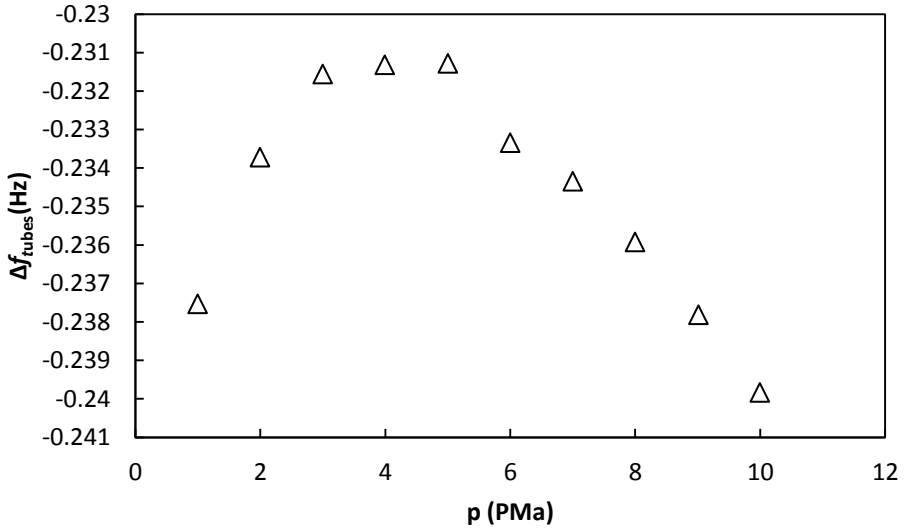

Figure 6.15 *Tubes frequency correction for acoustic mode (0,2) at T = 273.15 K as a function of pressure for the binary mixture x_{CO} = 0.05 and x_{N2} = 0.95.*

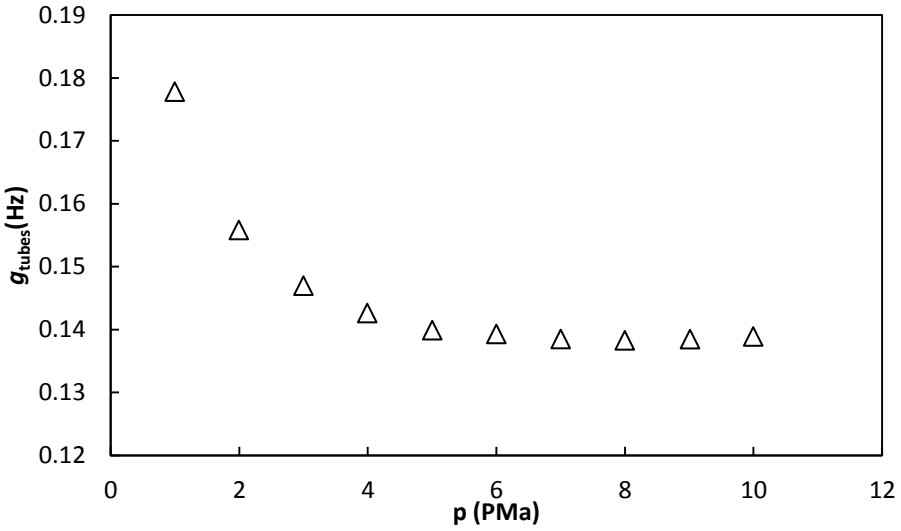

Figure 6.16 *Tubes half-width contribution for acoustic mode (0,2) at T = 273.15 K as a function of pressure for the binary mixture x_{CO} = 0.05 and x_{N2} = 0.95.*

6.2.2 Speed of Sound Determination

The frequency corrections applied and the calculated half-width contributions must conduce to the ideal case values from experimental results, then the excess half-width must tend to zero when performing an extrapolation to zero pressure. Otherwise the difference affects to the overall uncertainty. Therefore it is necessary to check the excess half-width. Difference between the calculated and experimental half-width must be divided by the measured frequency so they can be compared for different modes and pressure. This comparison is shown in figure 6.17.

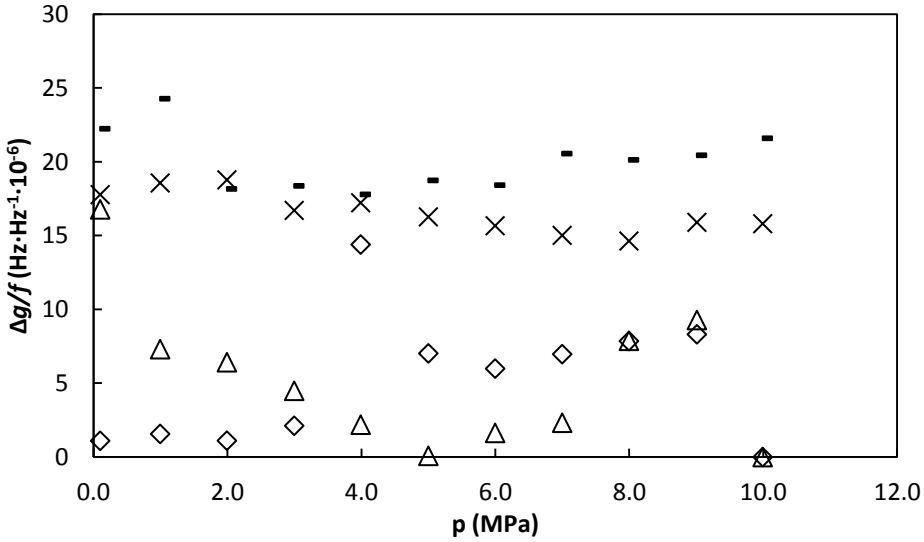

Figure 6.17 *Excess half-width for the acoustics modes (0,2) (**Δ**), (0,3) (**◊**), (0,4) (**x**) and (0,5) (-) at T = 273.15 K as a function of pressure for the binary mixture x_{CO} = 0.05 and x_{N2} = 0.95.*

Speed of sound is calculated as the average of the four acoustic modes measured but, if the excess half-width extrapolated to zero pressure for one of the acoustic modes is very high then this mode should not be taken into account to obtain of speed of sound. However, in this case excess half-width extrapolation is lower than 25 $Hz \cdot Hz^{-1} \cdot 10^{-6}$ for all acoustic modes, therefore they all were taken into account for the calculation of the speed of sound.

The speeds of sound obtained using all four modes of resonance are shown in figure 6.18. Table 6.13 shows a comparison between the measured data and the theoretical speed of sound calculated according GERG-2008 equation of state, which widely used for these mixtures [2] the calculations were done using the REFPRP 9.0 application developed by NIST[1]

Table 6.13 *Speed of sound values from experimental data and according to GERG-2008 equation of state, and the comparison between them for the binary mixture $x_{CO} = 0.05$ and $x_{N2} = 0.95$.*

p (MPa)	T (K)	u_{exp} ($m \cdot s^{-1}$)	u_{GERG} ($m \cdot s^{-1}$)	$(u_{exp} - u_{GERG})/ u_{GERG} x10^6$
9.99	273.2359	361.993	362.01	-46
9.01	273.2347	358.189	358.21	-58
7.99	273.0406	354.430	354.42	28
7.00	273.0465	351.175	351.19	-42
6.00	273.0451	348.210	348.22	-29
5.00	273.0425	345.566	345.56	16
3.99	273.0503	343.202	343.19	36
3.00	273.0478	341.180	341.17	28
1.99	273.1076	339.444	339.44	12
0.99	273.0461	337.991	337.96	91
0.10	273.0542	336.945	336.91	103

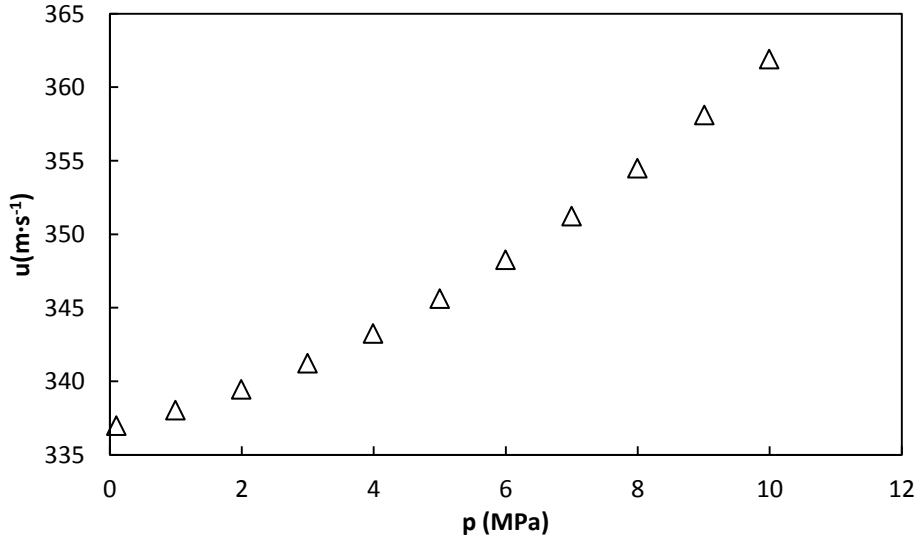

Figure 6.18 *Experimental speed of sound at T = 273.15 K as a function of pressure for the binary mixture $x_{CO} = 0.05$ and $x_{N2} = 0.95$.*

The acoustic equation of state as it was explained in chapter 2 gives the square speed of sound. That can be expressed as a polynomial function of the pressure. In this work, the expression given by equation 6.1 has been used:

$$u^2 = A_0 + A_1 p + A_2 p^2 \qquad (6.1)$$

Figure 6.19 shows the experimental values of the speed of sound and the model according equation 6.1

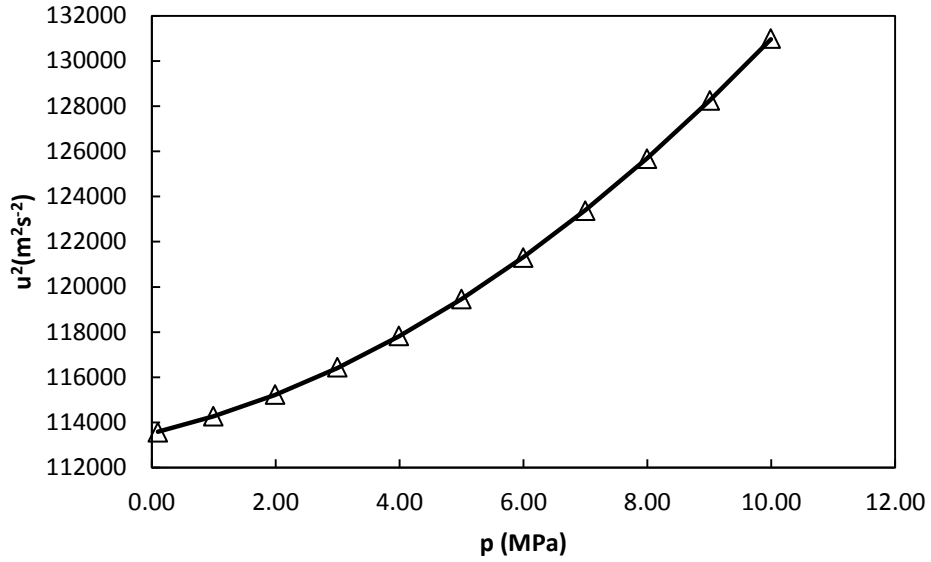

Figure 6.19 *Experimental square speed of sound (Δ) and developed acoustic virial model (—) at T = 273.15 K as a function of pressure for the binary mixture x_{CO} = 0.05 and x_{N2} = 0.95.*

Table 6.14 contains the values of the parameters for the model according equation 6.1 and the standard deviation of the adjustment (σ) defined as

$$\sigma = \sqrt{\sum \left(u_{exp}^2 - u_{calc}^2\right)^2 / (n-3)} \qquad (6.2)$$

Table 6.14 *Experimental acoustic virial equation of state parameters and standard deviation at T=273.15K for the binary mixture x_{CO}=0.05 and x_{N2}=0.95.*

A_0(m^2s^{-2})	A_1($m^2 \cdot s^{-2}MPa^{-1}$)	A_2 ($m^2 \cdot s^{-2}MPa^{-2}$)	σ ($m^2 \cdot s^{-2}$)
113544	624	112.1	25

A comparison between the developed model and the GERG-2008 equation of state was done and it is reported in table 6.15

Table 6.15 *Comparison between speed of sound according the developed model and according GERG-2008 equation of state for the binary mixture x_{CO} = 0.05 and x_{N2} = 0.95.*

p (MPa)	T (K)	u_{model}(m·s^{-1})	u_{GERG}(m·s^{-1})	(u_{model}-u_{GERG})/u_{GERG}x10^6
9.99	273.2359	361.903	362.01	295
9.01	273.2347	358.143	358.21	187
7.99	273.0406	354.540	354.42	-338
7.00	273.0465	351.286	351.19	-272
6.00	273.0451	348.306	348.22	-248
5.00	273.0425	345.639	345.56	-229
3.99	273.0503	343.246	343.19	-162
3.00	273.0478	341.205	341.17	-102
1.99	273.1076	339.458	339.44	-54
0.99	273.0461	338.047	337.96	-258
0.10	273.0542	337.057	336.91	-437

Acoustic virial coefficients (β_a, γ_a), isochoric and isobaric heat capacities (C_v^{pg} and C_p^{pg}) and the adiabatic coefficient (γ^{pg}) at zero pressure can be calculated from the parameters of the polynomial model (equation 6.1), as it has been explained in chapter 3, through the following equations:

$$\beta_a = \frac{A_1}{A_0} RT \qquad (3.24)$$

$$\gamma_a = \frac{A_2}{A_0} (RT)^2 \qquad (3.25)$$

$$\gamma^{pg} = \frac{MA_0}{RT} \qquad (3.10)$$

$$C_v^{pg} = \frac{R}{\gamma^{pg} - 1} \qquad (3.18)$$

$$C_p^{pg} = \gamma^{pg} C_v^{pg} \qquad (3.20)$$

These values were compared to those obtained from GERG-2008 equation of state. The results of this comparison are detailed in table 6.16.

Table 6.16 *Comparison between the calculated values of the isochoric and isobaric heat capacities (C_v^{pg} and C_p^{pg}) and the adiabatic coefficient (γ^{pg}) at zero pressure and the acoustic virial coefficients (β_a, γ_a) obtained from equation 6.1 and those calculated usingGERG-2008 EoS for the binary mixture $x_{CO} = 0.05$ and $x_{N2} = 0.95$ at T = 273.15 K.*

	Equation 6.1	**GERG-2008**	**Deviation (Eq. 6.1-GERG)/GERGx10^2**
γ^{pg}	1.4014	1.3997	0.0432
C_v^{pg}(J·mol^{-1}K^{-1})	20.716	20.801	0.1475
C_p^{pg}(J·mol^{-1}K^{-1})	29.030	29.116	0.1072
β_a(m^3·mol^{-1})	1.223 x10^{-5}	1.394 x10^{-5}	9.9729
γ_a(m^6·mol^{-2})	5.129 x10^{-9}	3.926 x10^{-9}	0.2937
u_0 (m·s^{-1})	336.964	336.87	0.2779

6.3 EXPERIMENTAL MEASURMENTS OF THE MIXTURE (0.05 CO +0.95 N_2) AT T=325.00K

Now the experimental results for the mixture (0.05 CO + 0.95 N_2)at T = 325.00 K are presented the methodology has been explained in section 6.2 and the tables and figures with the results are reported following the same order and at the end of the chapter a discussion of all the results for both mixtures is given.

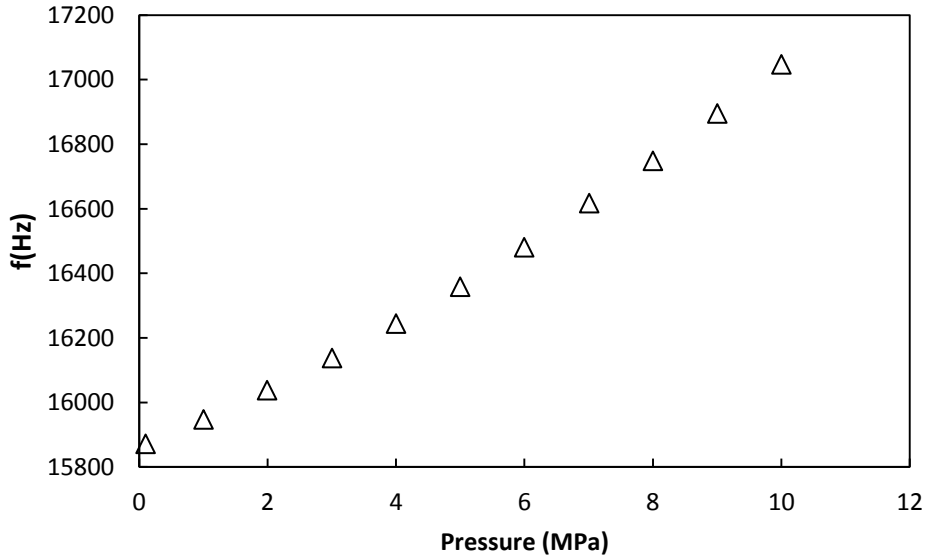

Figure 6.20 *Frequency of resonance for acoustic mode (0,4) at T = 325 K as a function of pressure for the binary mixture $x_{CO} = 0.05$ and $x_{N2} = 0.95$.*

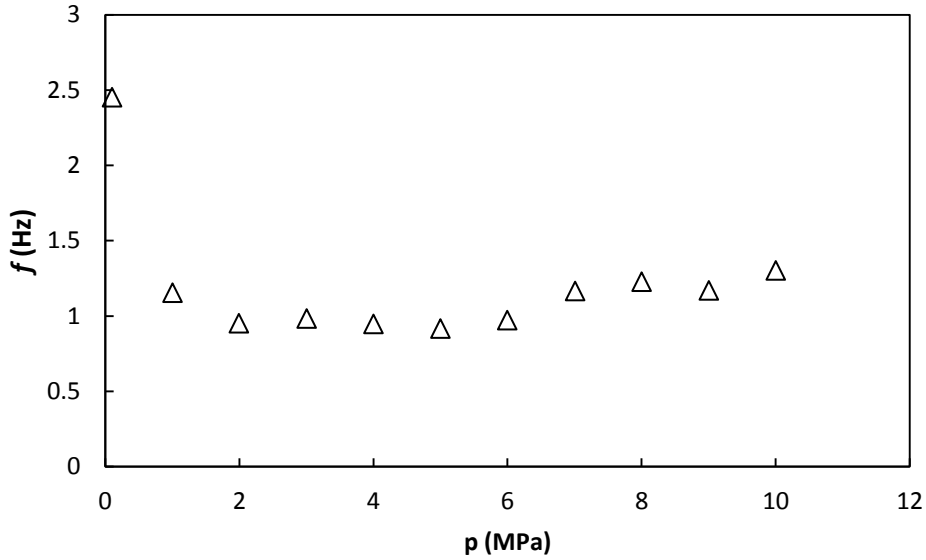

Figure 6.21 *Half-width of the resonance peaks for acoustic mode (0,4) at T = 325 K as a function of pressure for the binary mixture x_{CO} = 0.05 and x_{N2} = 0.95.*

Table 6.17 *Frequency of resonance and half-width contribution of resonance peaks for acoustic modes (0,2) to (0,5) at T = 325 K and p = 10 MPa.for the binary mixture x_{CO} = 0.05 and x_{N2} = 0.95.*

Mode	*f*(Hz)	*g*(Hz)
(0,2)	7025.72	0.704
(0,3)	12078.72	0.912
(0,4)	17047.72	1.303
(0,5)	21987.84	1.533

6.3.1 Frequency Corrections.

6.3.1.1 *Thermal Boundary Layer Correction*

Table 6.18 *Thermal penetration length for acoustic modes (0,2) to (0,5) at T = 325 K and p = 10 MPa for the binary mixture x_{CO} = 0.05 and x_{N2} = 0.95.*

Mode	δ_{TH}(m)
(0,2)	3.51×10^{-6}
(0,3)	2.68×10^{-6}
(0,4)	2.26×10^{-6}
(0,5)	1.99×10^{-6}

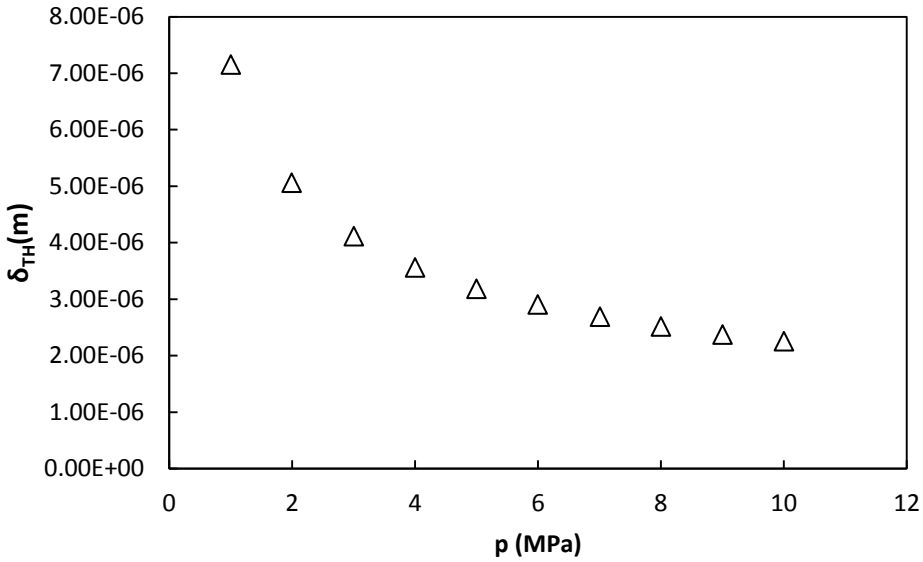

Figure 6.22 *Thermal penetration length for acoustic mode (0,4) at T = 325 K as a function of pressure for the binary mixture $x_{CO} = 0.05$ and $x_{N2} = 0.95$.*

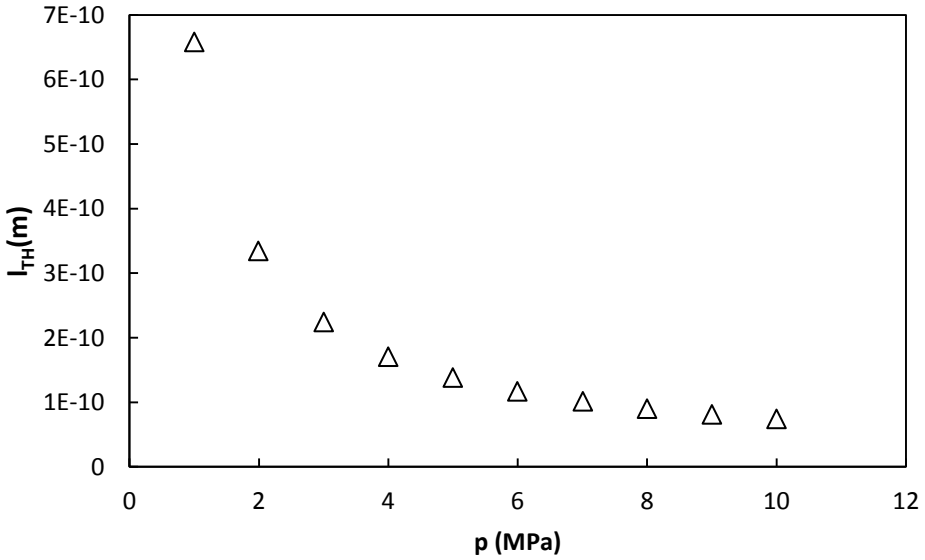

Figure 6.23 *Thermal accommodation length at T = 325 K as a function of pressure for the binary mixture $x_{CO} = 0.05$ and $x_{N2} = 0.95$.*

Table 6.19 *Shell thermal penetration length for acoustic modes (0,2) to (0,5) at T = 325 K and p = 10 MPa for the binary mixture x_{CO} = 0.05 and x_{N2} = 0.95.*

Mode	δ_{316L}(m)
(0,2)	1.35 x10^{-5}
(0,3)	1.03 x10^{-5}
(0,4)	8.69 x10^{-5}
(0,5)	7.65 x10^{-5}

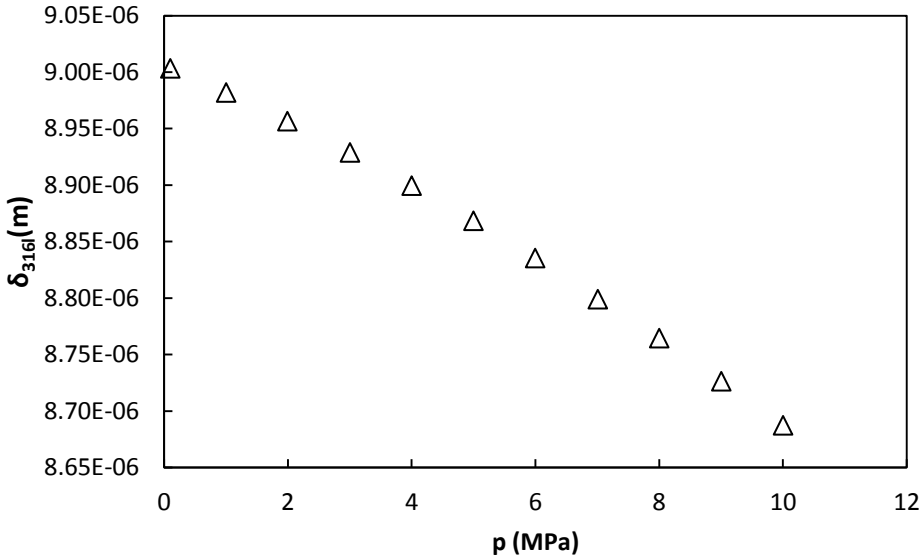

Figure 6.24 *Shell thermal penetration length for acoustic mode (0,4) at T = 325 K as a function of pressure for the binary mixture x_{CO} = 0.05 and x_{N2} = 0.95.*

Table 6.20 *Thermal boundary layer frequency correction and half-width contribution for acoustic modes (0,2) to (0,5) at T = 325 K and p = 10 MPa for the binary mixture x_{CO} = 0.05 and x_{N2} = 0.95.*

Mode	Δf_{TH} (Hz)	g_{TH}(Hz)
(0,2)	-0.162	0.164
(0,3)	-0.212	0.216
(0,4)	-0.252	0.256
(0,5)	-0.286	0.291

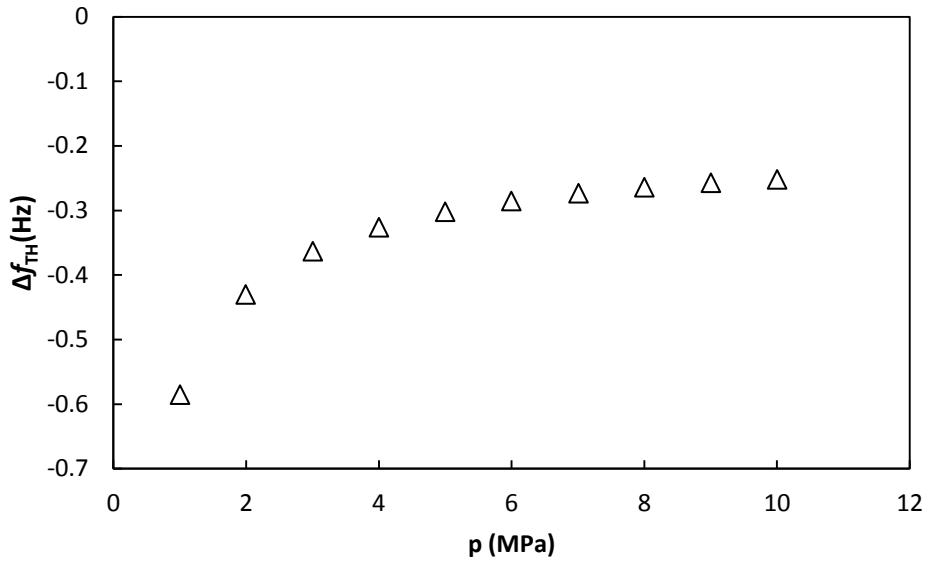

Figure 6.25 *Thermal boundary layer frequency correction for acoustic mode (0,4) at T = 325 K as a function of pressure for the binary mixture $x_{CO} = 0.05$ and $x_{N2} = 0.95$.*

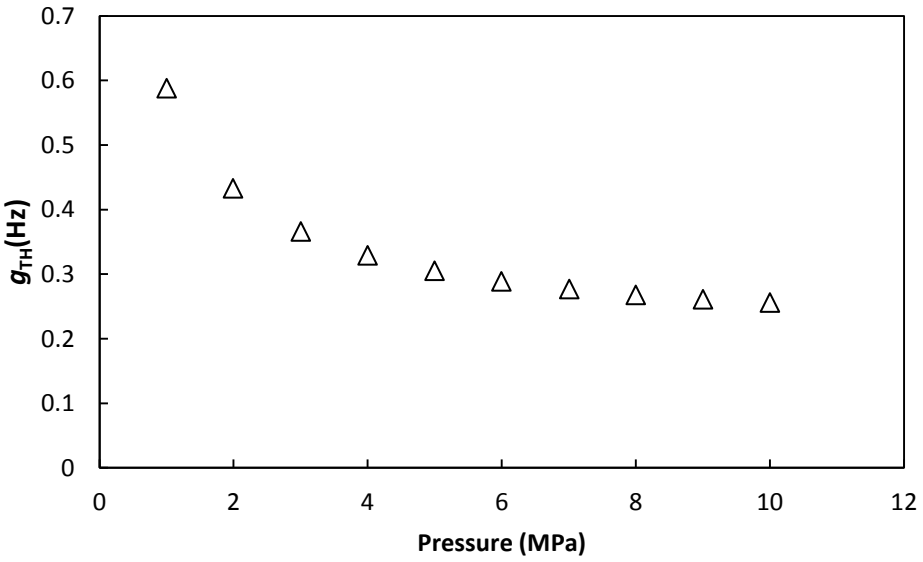

Figure 6.26 *Thermal boundary layer half-width contribution for acoustic mode (0,4) at T = 325 K as a function of pressure for the binary mixture $x_{CO} = 0.05$ and $x_{N2} = 0.95$.*

6.3.1.2 *Bulk Viscosity Contribution*

Table 6.21 *Viscous penetration length for acoustic modes (0,2) to (0,5) at T = 325 K and p = 10 MPa for the binary mixture x_{CO} = 0.05 and x_{N2} = 0.95.*

Mode	δ_v(m)
(0,2)	3.04 x10^{-6}
(0,3)	2.32 x10^{-6}
(0,4)	1.96 x10^{-6}
(0,5)	1.72 x10^{-6}

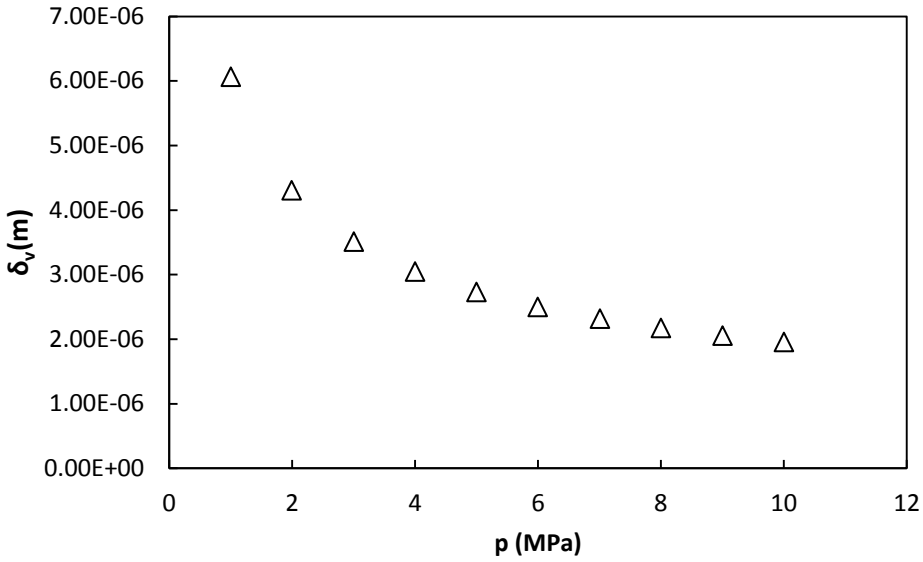

Figure 6.27 *Viscous penetration length for acoustic mode (0,4) at T = 325 K as a function of pressure for the binary mixture x_{CO} = 0.05 and x_{N2} = 0.95.*

Table 6.22 *Bulk viscosity half-width contribution for modes (0,2) to (0,5) at T = 325 K and p = 10 MPa for the binary mixture x_{CO} = 0.05 and x_{N2} = 0.95.*

Mode	g_b(Hz)
(0,2)	4.15 x10^{-4}
(0,3)	1.23 x10^{-3}
(0,4)	2.45 x10^{-3}
(0,5)	4.07 x10^{-3}

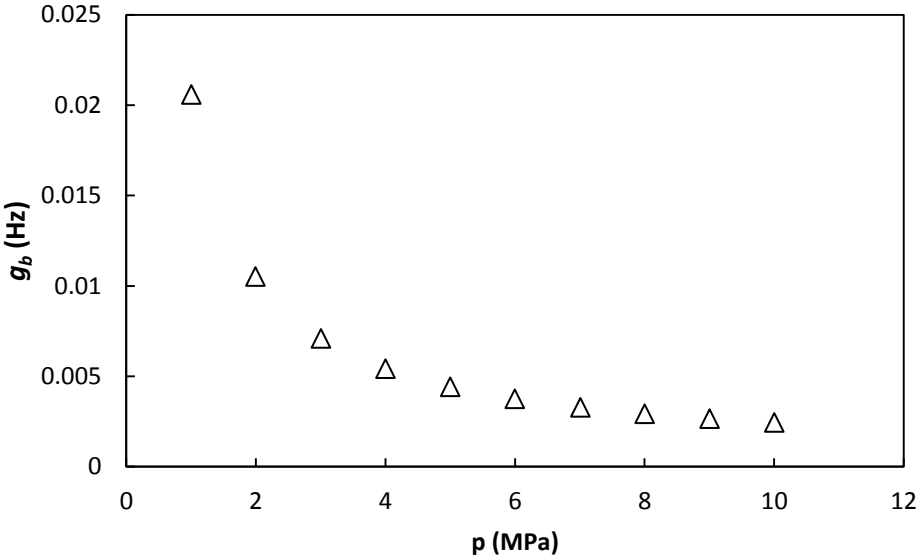

Figure 6.28 *Bulk viscosity half-width contribution for acoustic mode (0,4) at T = 325 K as a function of pressure for the binary mixture x_{CO} = 0.05 and x_{N2} = 0.95.*

6.3.1.3 *Shell Motion Correction.*

Table 6.23 *Shell motion frequency correction for acoustic modes (0,2) to (0,5) at T = 325 K and p = 10 MPa for the binary mixture x_{CO} = 0.05 and x_{N2} = 0.95.*

Mode	Δf_{sh}
(0,2)	-0.112
(0,3)	-0.208
(0,4)	-0.341
(0,5)	-0.605

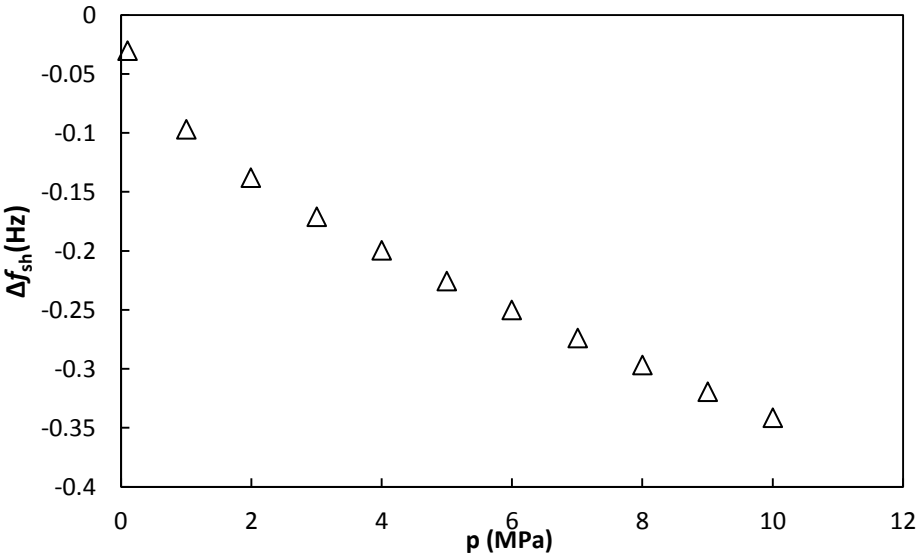

Figure 6.29 *Shell motion frequency correction for acoustic mode (0,4) at T = 325 K as a function of pressure for the binary mixture x_{CO} = 0.05 and x_{N2} = 0.95.*

6.3.1.4 *Tubes and Holes Correction.*

Table 6.24 *Kirchhoff-Helmholtz absorption coefficient for tubes 1 and 2, for modes (0,2) to (0,5) at T = 325 K and p = 10 MPa for the binary mixture x_{CO} = 0.05 and x_{N2} = 0.95.*

Mode	$\alpha_{KH1}(m^{-1})$	$\alpha_{KH2}(m^{-1})$
(0,2)	67.187	33.593
(0,3)	88.094	44.047
(0,4)	104.734	52.367
(0,5)	118.858	59.429

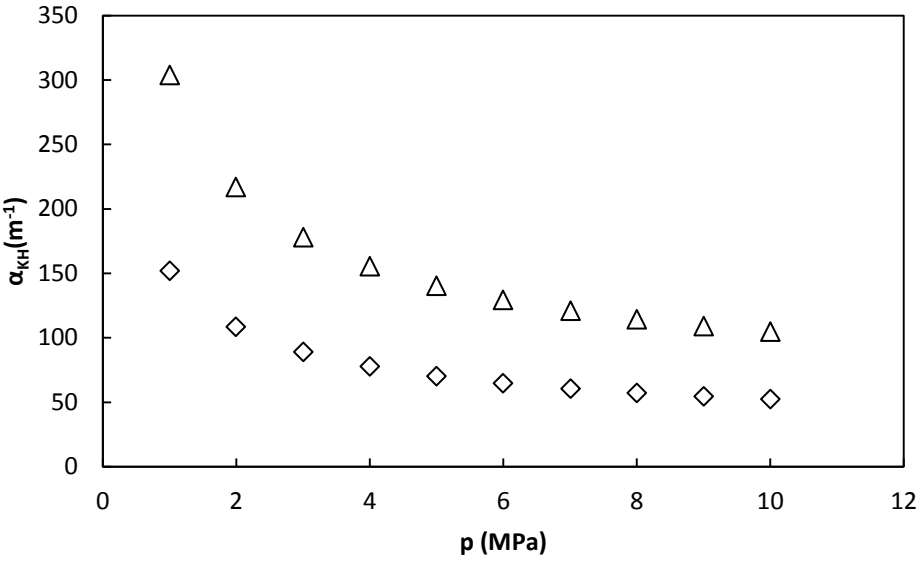

Figure 6.30 *Kirchhoff-Helmholtz absorption coefficient for acoustic mode (0,4) for tube 1(Δ) and tube 2(◊)at T = 325 K as a function of pressure for the binary mixture x_{CO} = 0.05 and x_{N2} = 0.95.*

Table 6.25 *Propagation constant for tubes 1 and 2, for acoustic modes (0,2) to (0,5) at T = 325 K and p = 10 MPa for the binary mixture x_{CO} = 0.05 and x_{N2} = 0.95.*

Mode	$k_{KH1}(m^{-1})$	$k_{KH2}(m^{-1})$
(0,2)	178.975-67.1870i	145.381-33.593i
(0,3)	280.281-88.0941i	236.234-44.047i
(0,4)	375.869-104.734i	323.502-52.367i
(0,5)	468.711-118.858i	409.282-59.429i

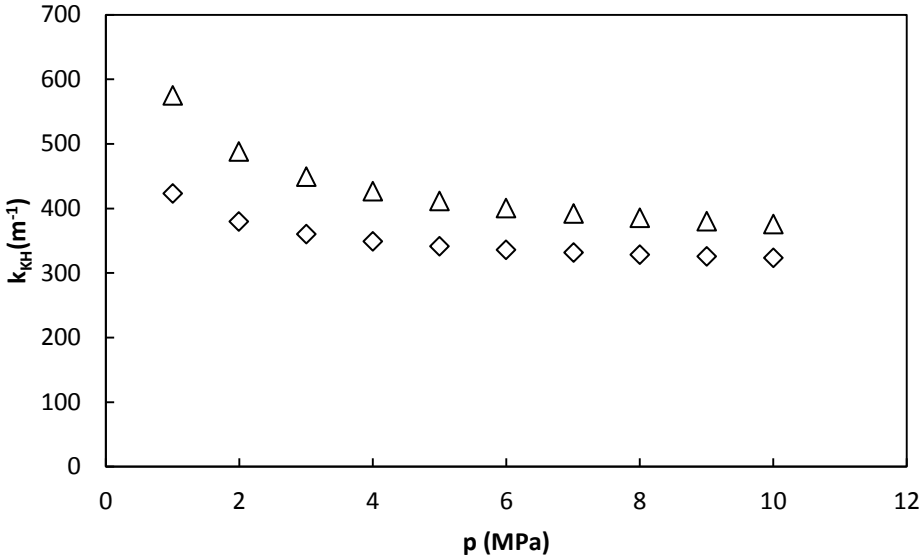

Figure 6.31 *Propagation constant real component for acoustic mode (0,4) for tube 1(Δ) and tube 2(◊)at T = 325 K as a function of pressure for the binary mixture x_{CO} = 0.05 and x_{N2} = 0.95.*

Table 6.26 *Specific acoustic admittance of the opening for tubes 1 and 2 for modes (0,2) to (0,5) at T = 325 K and p = 10 MPa for the binary mixture x_{CO} = 0.05 and x_{N2} = 0.95.*

Mode	y_{01}	y_{02}
(0,2)	0.994+0.0104i	0.978-0.15183i
(0,3)	1.002+0.0015i	0.954-0.04963i
(0,4)	1.001-0.00021i	0.968-0.01544i
(0,5)	1.000-0.00021i	0.980-0.00328i

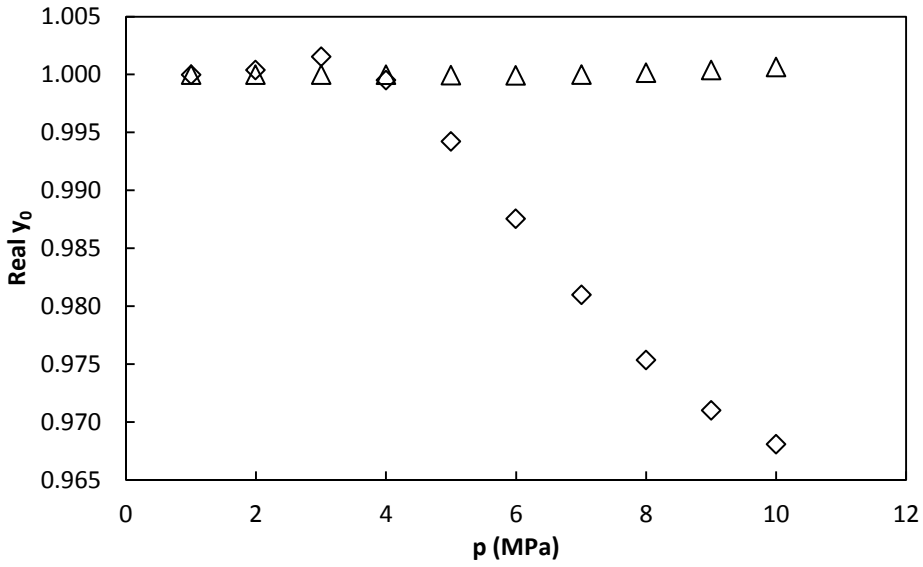

Figure 6.32 *Specific acoustic admittance real component for tube 1(Δ) and tube 2(◊)for acoustic mode (0,4) at T = 325 K as a function of pressure for the binary mixture x_{CO} = 0.05 and x_{N2} = 0.95.*

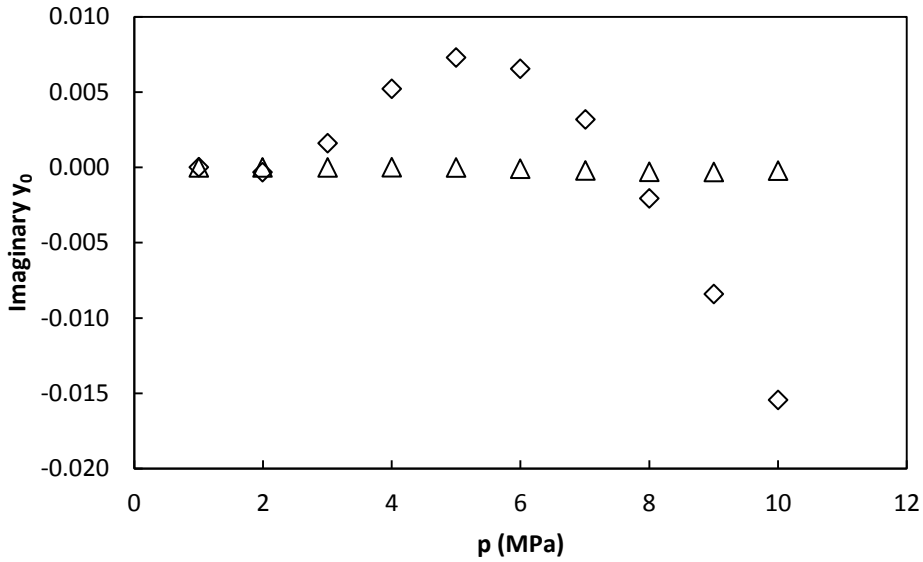

Figure 6.33 *Specific acoustic admittance Imaginary component for tube 1(Δ) and tube 2(◊)for acoustic mode (0,4) at T = 325 K as a function of pressure for the binary mixture x_{CO} = 0.05 and x_{N2} = 0.95.*

Table 6.27 *Tubes frequency correction and half-width contribution for acoustic modes (0,2) to (0,5) at T = 325 K and p = 10 MPa for the binary mixture x_{CO} = 0.05 and x_{N2} = 0.95.*

Mode	Δf_{tubes} (Hz)	g_{tubes} (Hz)
(0,2)	0.119	-0.008
(0,3)	0.118	-0.003
(0,4)	0.119	-0.001
(0,5)	0.120	-0.0002

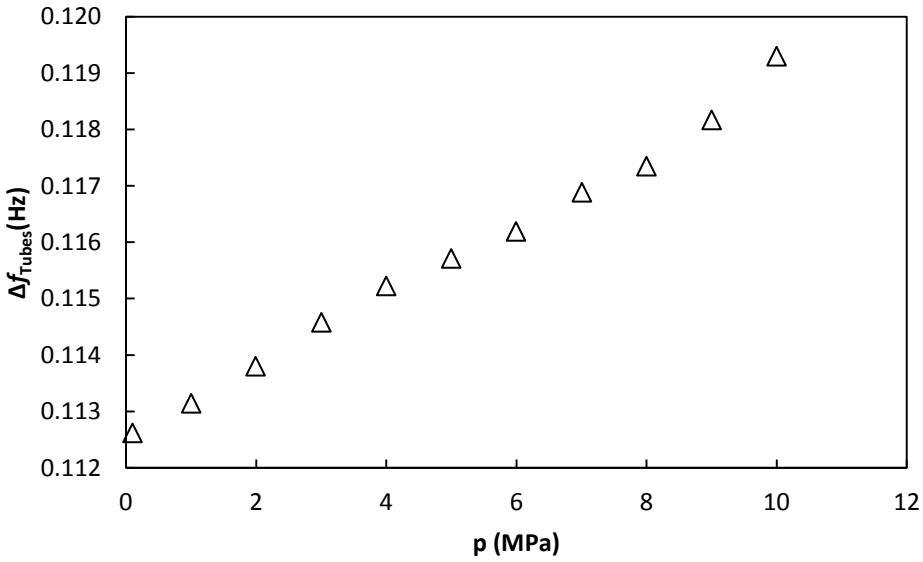

Figure 6.34 *Tubes motion frequency correction for acoustic mode (0,4) at T = 325 K as a function of pressure for the binary mixture x_{CO} = 0.05 and x_{N2} = 0.95.*

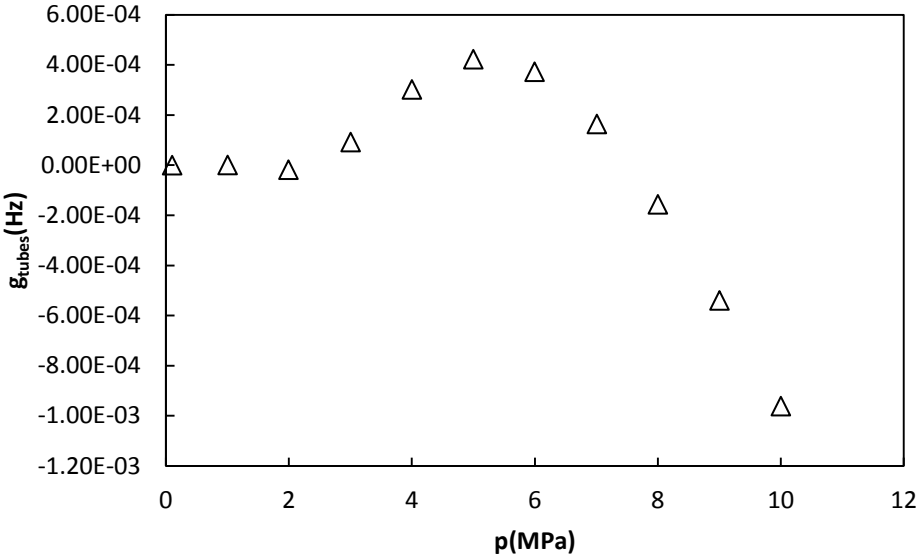

Figure 3.35 *Tubes half-width contribution for acoustic mode (0,4) at T = 325 K as a function of pressure for the binary mixture x_{CO} = 0.05 and x_{N2} = 0.95.*

6.3.2 Speed of Sound Determination

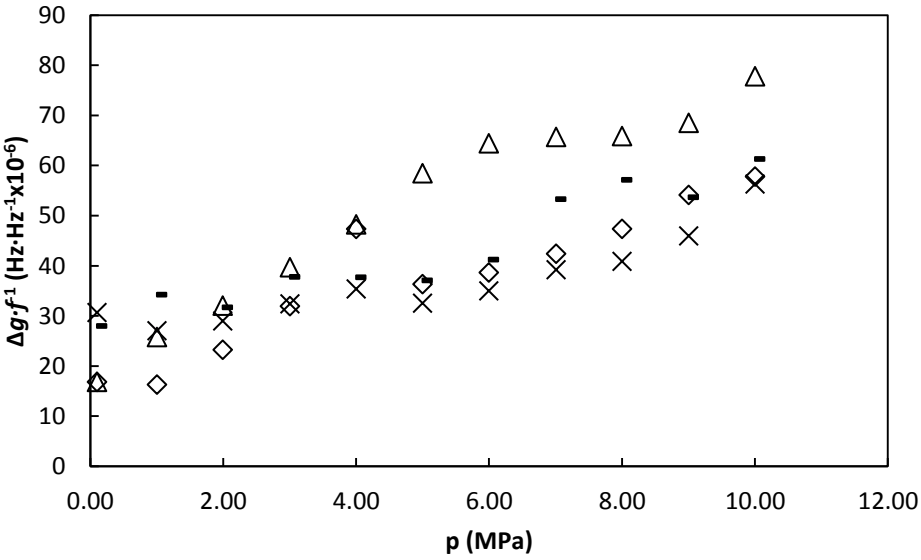

Figure 6.36 *Excess half-widths for acoustic modes (0,2) (Δ),(0,3) (◊),(0,4) (-) and (0,5) (x) at T = 325 K as a function of pressure for the binary mixture x_{CO} = 0.05 and x_{N2} = 0.95.*

Table 6.28 *Speed of sound values from experimental data and according to GERG-2008 equation of state, and the comparison between them at T = 325 K for the binary mixture x_{CO} = 0.05 and x_{N2} = 0.95.*

P(Mpa)	T (K)	u_{exp}(m·s^{-1})	u_{GERG} (m·s^{-1})	$(u_{exp}-u_{GERG})/u_{GERG}$ x10^{6}
10.00	325.1298	394.935	394.94	-13
9.00	325.0447	391.398	391.36	97
8.00	324.9912	387.989	387.94	127
7.01	325.2273	384.949	384.9	127
5.99	325.0288	381.773	381.72	140
5.00	325.0137	378.930	378.87	159
4.00	325.0267	376.278	376.21	181
3.00	325.0126	373.796	373.73	175
1.99	325.0040	371.483	371.4	223
1.00	325.0024	369.381	369.31	192
0.10	325.0061	367.645	367.57	204

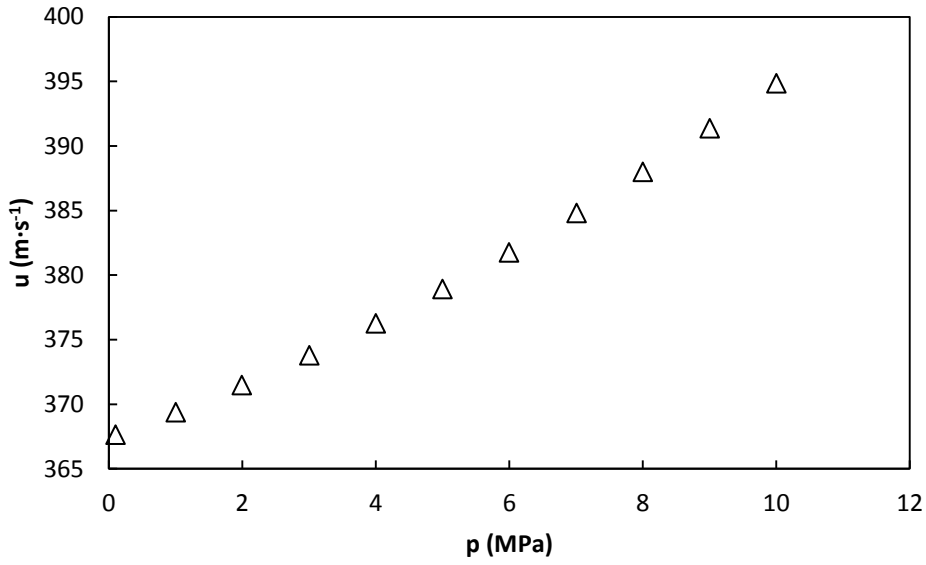

Figure 6.37 *Experimental speed of sound at T = 325 K as a function of pressure for the binary mixture x_{CO} = 0.05 and x_{N2} = 0.95.*

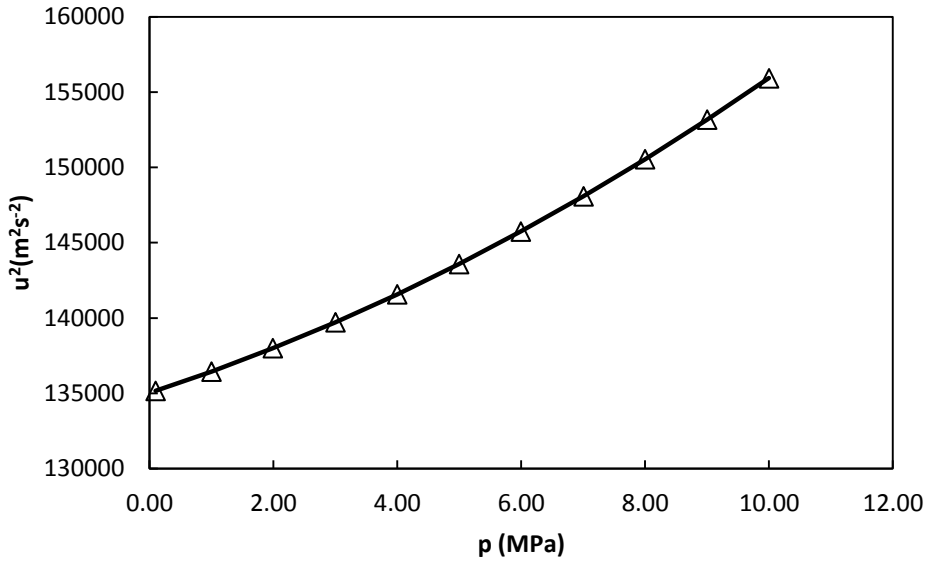

Figure 6.38 *Experimental square speed of sound (Δ) and developed acoustic virial model (—) at T = 325 K as a function of pressure for the binary mixture x_{CO} = 0.05 and x_{N2} = 0.95.*

Table 6.29 *Experimental acoustic virial equation of state parameters at T = 325 K for the binary mixture x_{CO} = 0.05 and x_{N2} = 0.95*

$A_0(m^2 \cdot s^{-2})$	$A_1(m^2 \cdot s^{-2}MPa^{-1})$	$A_2(m^2 \cdot s^{-2}MPa^{-2})$	$\sigma\ (m^2 \cdot s^{-2})$
135030	1335	75.4	11

Table 6.30 *Speed of sound according to developed model, and according to GERG-2008 equation of state and a comparison between them at T = 325 K for the binary mixture x_{CO} = 0.05 and x_{N2} = 0.95.*

P(Mpa)	T (K)	$u_{model}\ (m \cdot s^{-1})$	$u_{GERG}\ (m \cdot s^{-1})$	$(u_{model} - u_{GERG})/u_{GERG} x10^6$
10.00	325.1298	394.868	394.94	-182
9.00	325.0447	391.354	391.36	-16
8.00	324.9912	387.988	387.94	123
7.01	325.2273	384.821	384.9	-206
5.99	325.0288	381.762	381.72	111
5.00	325.0137	378.927	378.87	151
4.00	325.0267	376.264	376.21	145
3.00	325.0126	373.790	373.73	160
1.99	325.0040	371.466	371.4	179
1.00	325.0024	369.382	369.31	194
0.10	325.0061	367.646	336.97	205

Table 6.31 *Comparison between the calculated values of the isochoric and isobaric heat capacities (C_v^{pg} and C_p^{pg}) and the adiabatic coefficient (γ^{pg}) at zero pressure and the acoustic virial coefficients (β_a, γ_a) obtained from equation 6.1 and those calculated using GERG-2008 EoS for the binary mixture x_{CO} = 0.05 and x_{N2} = 0.95 at T = 325 K.*

	Experimental results	GERG-2008	Deviation (Exp-GERG)/GERGx10^2
γ^{pg}	1.3997	1.3992	0.05
C_v^{pg}(J·mol^{-1}K^{-1})	20.802	20.827	-0.15
C_p^{pg}(J·mol^{-1}K^{-1})	29.116	29.142	-0.11
β_a(m^3·mol^{-1})	2.671 x10^{-5}	2.6972 x10^{-5}	-0.95
γ_a(m^6·mol^{-2})	4.077x10^{-9}	3.7655x10^{-9}	8.26
u_0 (m·s^{-1})	367.464	367.38	0.023

6.4 EXPERIMENTAL MEASURMENTS OF THE MIXTURE (0.10 CO +0.90 N_2) AT T = 273.16 K

Now the experimental results for the mixture (0.10 CO + 0.90 N_2) at T = 273.16 K are presented. The methodology has been explained in section 6.2 and the tables and figures with the results are reported following the same order and a discussion of all the results for both mixtures is given at the end of the chapter.

Table 6.32 *Frequency of resonance and half-width of resonance peaks for acoustic modes (0,2), to (0,5) at p = 9.96 MPa and T = 273.16K for the binary mixture x_{CO} = 0.10 and x_{N2} = 0.90.*

Mode	*f* (Hz)	*g* (Hz)
(0,2)	6441.00	0.420
(0,3)	11073.37	0.512
(0,4)	15629.29	0.702
(0,5)	20160.46	0.897

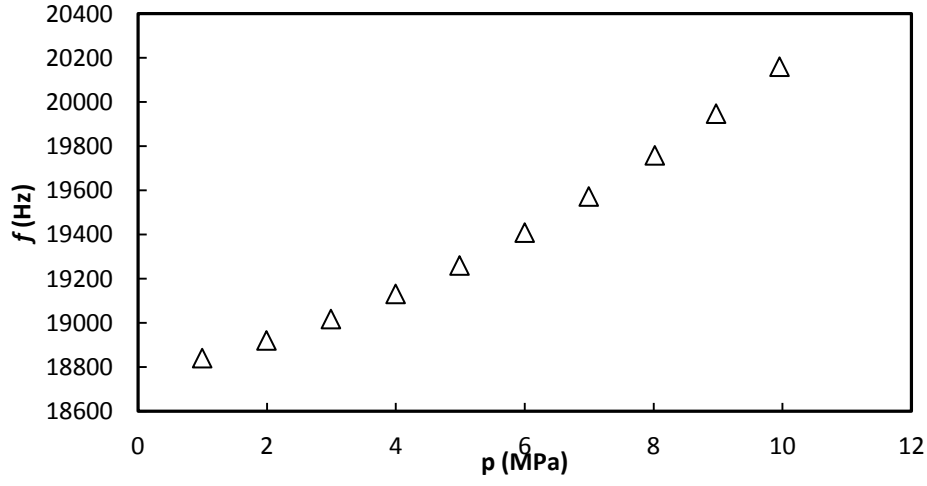

Figure 6.39 *Frequency of resonance for acoustic mode (0,5) at T = 273.16 K as a function of pressure for the binary mixture x_{CO} = 0.10 and x_{N2} = 0.90.*

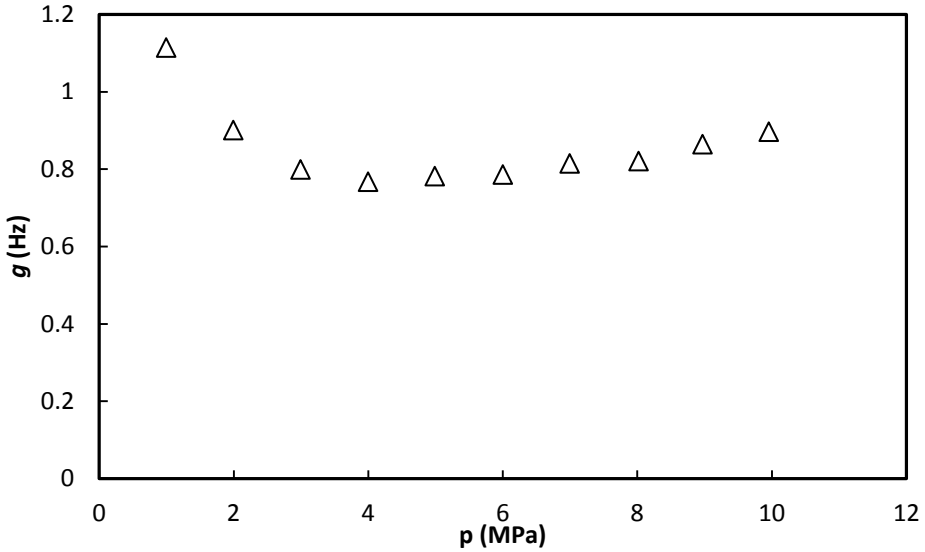

Figure 6.40 *Half-width of the resonance peaks for acoustic mode (0,5)) at T = 273.16 K as a function of pressure for the binary mixture x_{CO} = 0.10 and x_{N2} = 0.90.*

6.4.1 Frequency Corrections

6.4.1.1 *Thermal Boundary Layer Correction*

Table 6.33 *Thermal penetration length for acoustic modes (0,2) to (0,5) at T = 273.16 K and p = 9.96 MPa for the binary mixture x_{CO} = 0.10 and x_{N2} = 0.90.*

Mode	δ_{th}(μm)
(0,2)	3.087
(0,3)	2.354
(0,4)	1.982
(0,5)	1.745

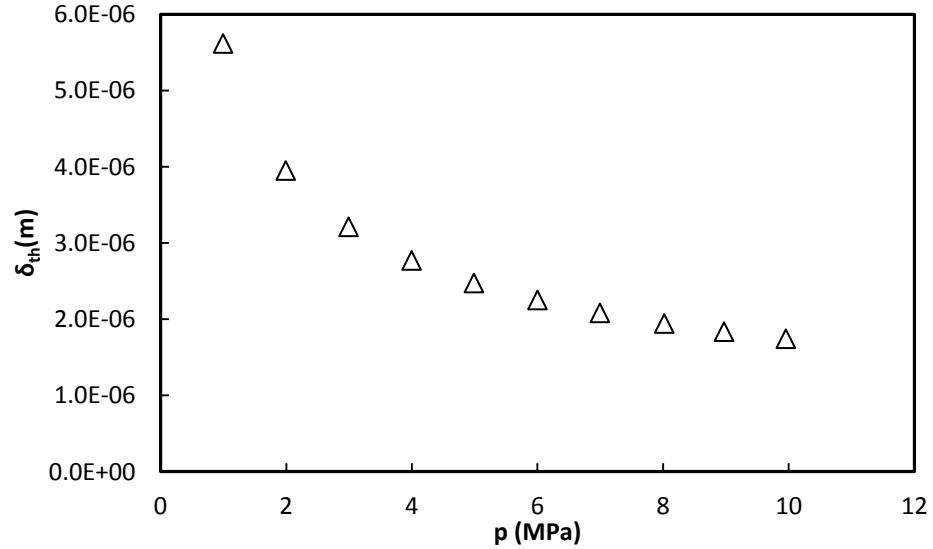

Figure 6.41 *Thermal penetration length for acoustic mode (0,5) at T = 273.16 K as a function of pressure for the binary mixture x_{CO} = 0.10 and x_{N2} = 0.90.*

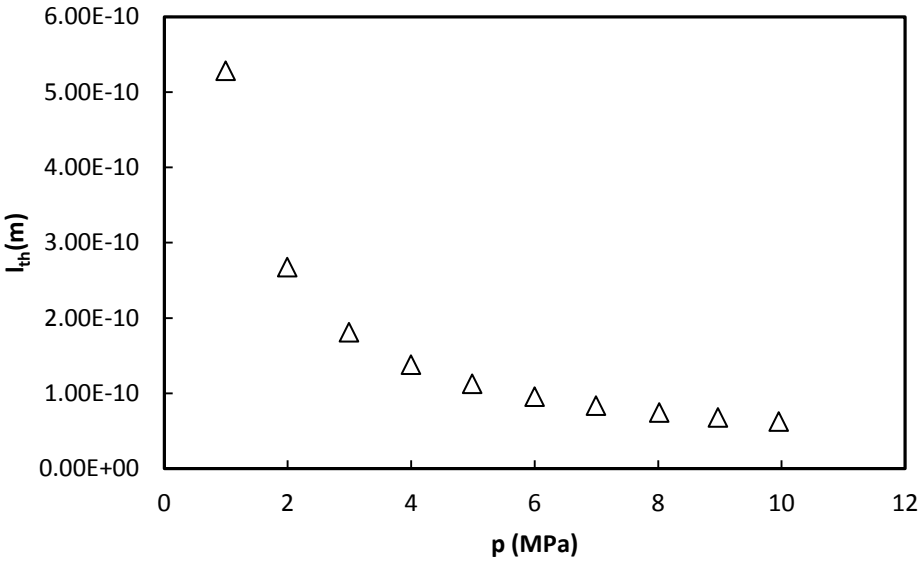

Figure 6.42 *Thermal accommodation length at T = 273.16 K as a function of pressure for the binary mixture x_{CO} = 0.10 and x_{N2} = 0.90.*

Table 6.34 *Shell thermal penetration length for acoustic modes (0,2) to (0,5) at T = 273.16K and p = 9.96 MPa for the binary mixture x_{CO} = 0.10 and x_{N2} = 0.90.*

Mode	δ_{shell}(m)
(0,2)	1.41 x10^{-5}
(0,3)	1.08 x10^{-5}
(0,4)	9.07 x10^{-5}
(0,5)	7.99 x10^{-5}

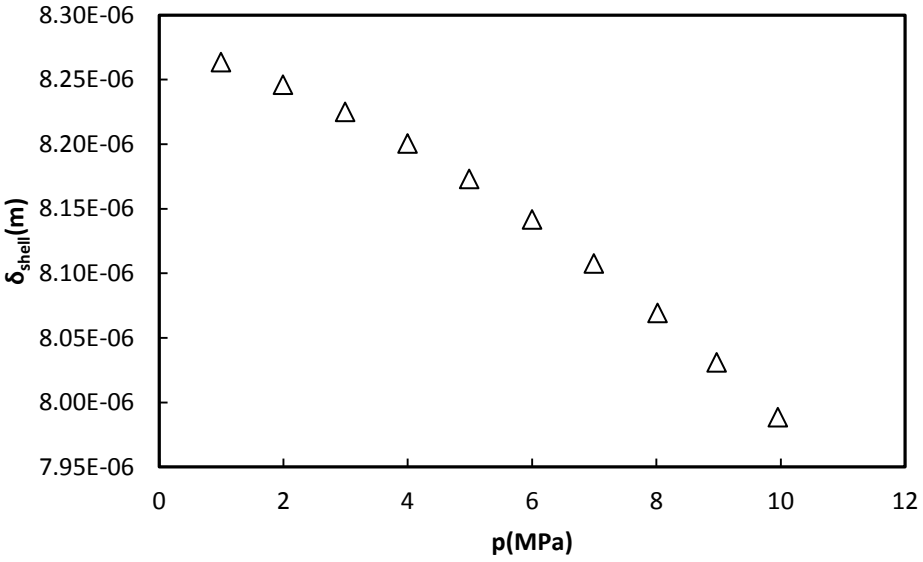

Figure 6.43 *Shell thermal penetration length for acoustic mode (0,5) at T = 273.16 K as a function of pressure for the binary mixture x_{CO} = 0.10 and x_{N2} = 0.90.*

Table 6.35 *Thermal boundary layer frequency correction and half-width contribution for acoustic modes (0,2) to (0,5) at T = 273.16 K and p = 9.96MPa for the binary mixture x_{CO} = 0.10 and x_{N2} = 0.90.*

Mode	Δf_{th}(Hz)	Δg_{th}(Hz)
(0,2)	-0.150	0.153
(0,3)	-0.197	0.201
(0,4)	-0.234	0.239
(0,5)	-0.266	0.271

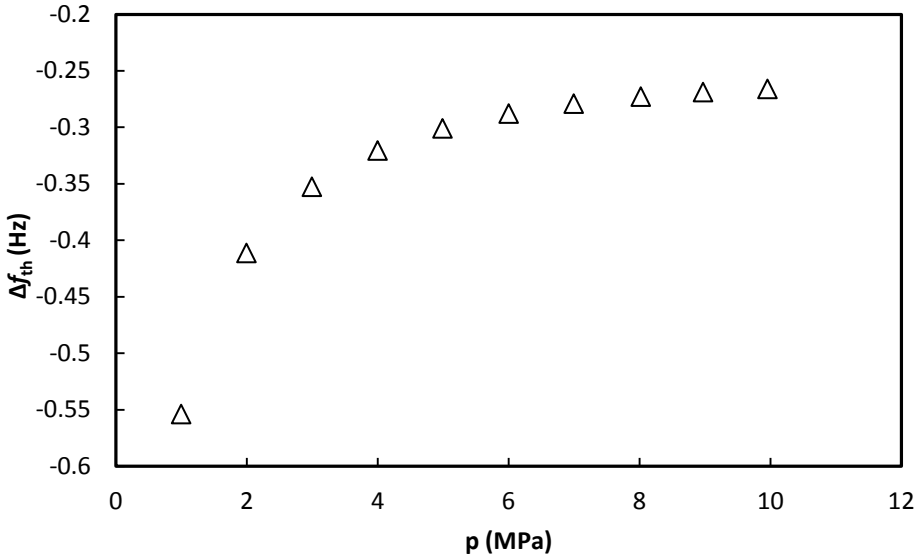

Figure 6.44 *Thermal boundary layer frequency correction for acoustic mode (0,5) at T = 273.16 K as a function of pressure for the binary mixture x_{CO} = 0.10 and x_{N2} = 0.90.*

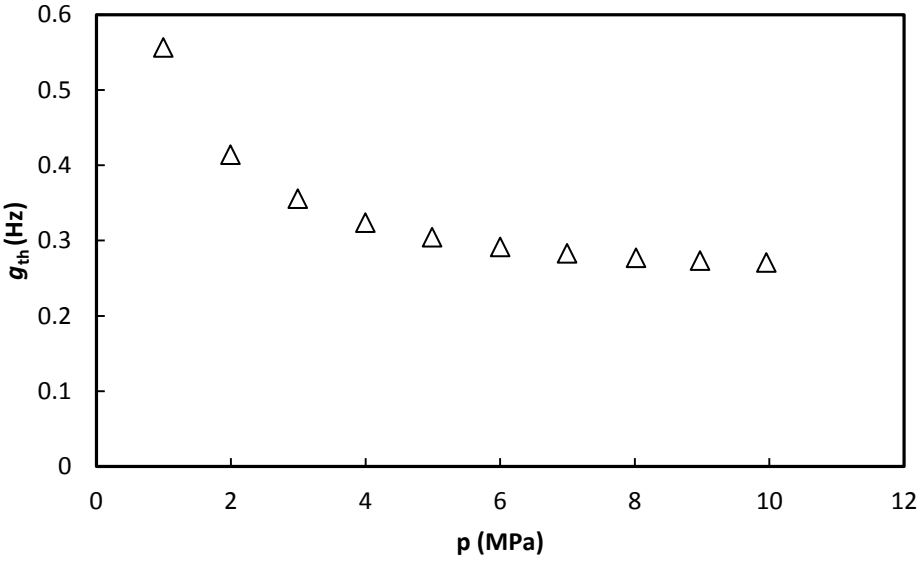

Figure 6.45 *Thermal boundary layer half-width contribution for acoustic mode (0,5) at T = 273.16 K as a function of pressure for the binary mixture x_{CO} = 0.10 and x_{N2} = 0.90.*

6.4.1.2 *Bulk Viscosity Contribution*

Table 6.36 *Viscous penetration length for acoustic modes (0,2) to (0,5) at T = 273.16 K and p = 9.96 MPa for the binary mixture x_{CO} = 0.10 and x_{N2} = 0.90*

Mode	δ_v(μm)
(0,2)	2.75
(0,3)	2.09
(0,4)	1.76
(0,5)	1.55

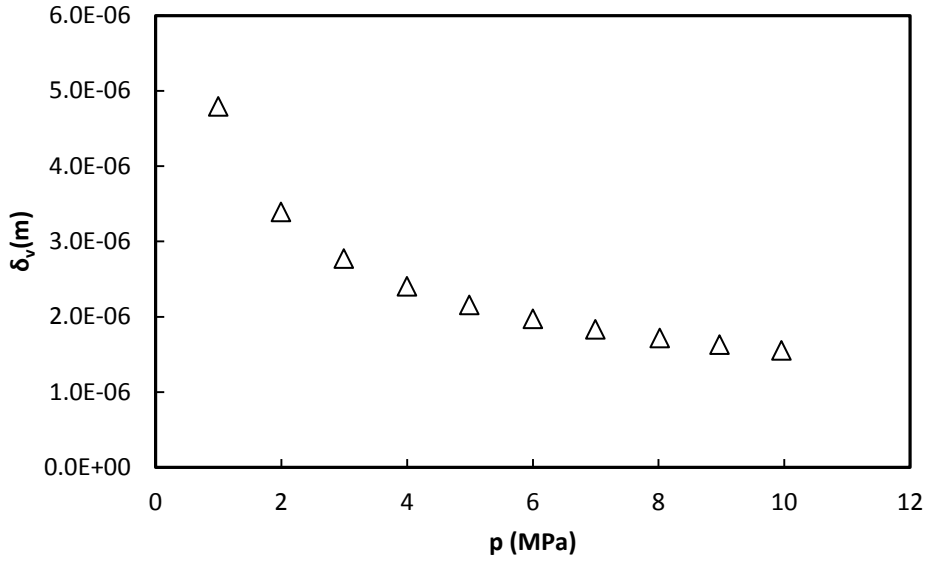

Figure 6.46 *Viscous penetration length for acoustic mode (0,5) at T = 273.16 K as a function of pressure for the binary mixture x_{CO} = 0.10 and x_{N2} = 0.90.*

Table 6.37 *Bulk viscosity half-width contribution for acoustic modes (0,2) to (0,5) at T = 273.16 K and p = 9.96 MPa for the binary mixture x_{CO} = 0.10 and x_{N2} = 0.90.*

Mode	g_b(Hz)
(0,2)	3.20×10^{-4}
(0,3)	9.47×10^{-4}
(0,4)	1.89×10^{-3}
(0,5)	3.14×10^{-3}

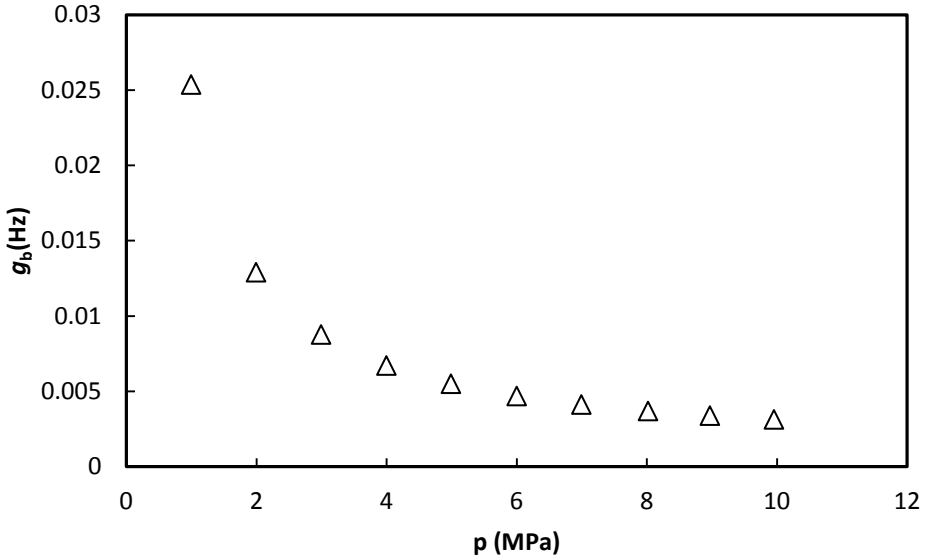

Figure 6.47 *Bulk viscosity half-width contribution for acoustic mode (0,5) at T = 273.16 K as a function of pressure for the binary mixture x_{CO} = 0.10 and x_{N2} = 0.90.*

6.4.1.3 *Shell Motion Correction.*

Table 6.38 *Shell motion frequency correction for acoustic modes (0,2) to (0,5) at T = 273.16 K and p = 9.96 MPa for the binary mixture x_{CO} = 0.10 and x_{N2} = 0.90.*

Mode	Δf_{shell}(Hz)
0.2	-0.101
0.3	-0.186
0.4	-0.296
0.5	-0.475

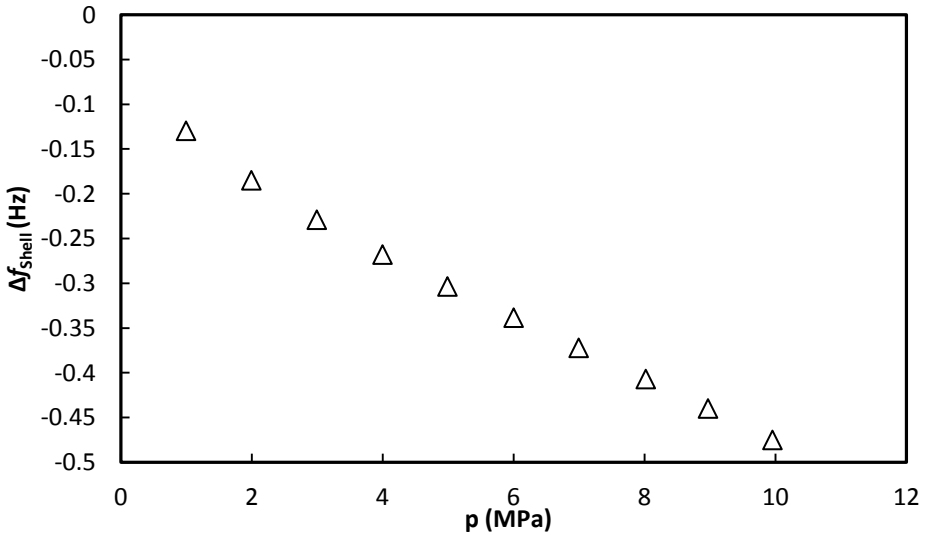

Figure 6.48 *Shell motion frequency correction for acoustic mode (0,5) at T = 273.16 K as a function of pressure for the binary mixture x_{CO} = 0.10 and x_{N2} = 0.90.*

6.4.1.4 *Tubes and Holes Correction.*

Table 6.39 *Kirchhoff-Helmholtz absorption coefficient for tubes 1 and 2 for acoustic modes (0,2) to (0,5) at T = 273.16 K and p = 9.96 MPa for the binary mixture x_{CO} = 0.10 and x_{N2} = 0.90.*

Mode	$\alpha_{KH1}(m^{-1})$	$\alpha_{KH2}(m^{-1})$
(0,2)	0.212	0.259
(0,3)	0.278	0.340
(0,4)	0.330	0.404
(0,5)	0.375	0.459

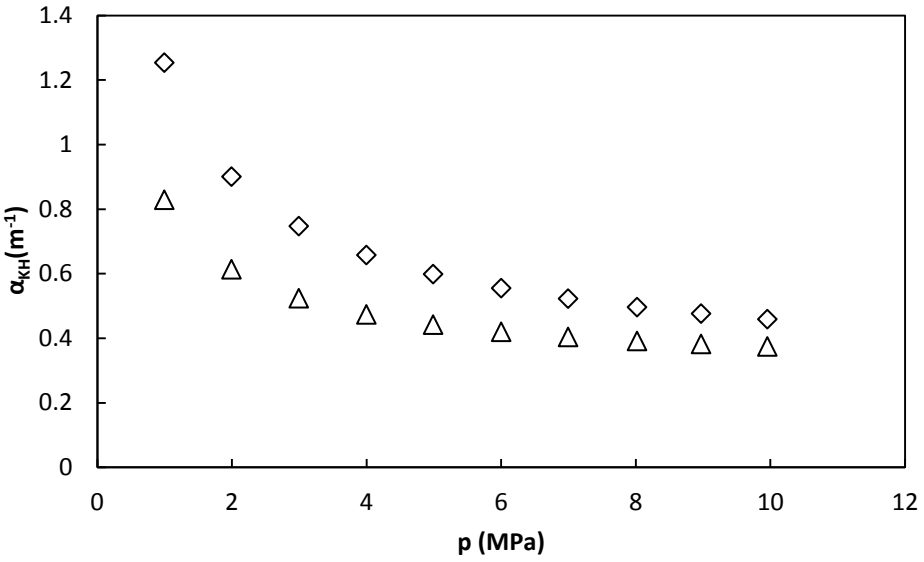

Figure 6.49 *Kirchhoff-Helmholtz absorption coefficient for tubes 1 (Δ) and 2 (◊) for the acoustic mode (0,5) at T = 273.16 K as a function of pressure for the binary mixture x_{CO} = 0.10 and x_{N2} = 0.90.*

Table 6.40 *Propagation constant for tubes 1 and 2 for acoustic modes (0,2) to (0,5) at T = 273.16 K and p = 9.96 MPa for the binary mixture x_{CO} = 0.10 and x_{N2} = 0.90.*

Mode	$k_{KH1}(m^{-1})$	$k_{KH2}(m^{-1})$
(0,2)	112.05-0.211i	112.09+0.259i
(0,3)	192.54-0.277i	192.60+0.340i
(0,4)	271.70-0.330i	271.77+0.404i
(0,5)	350.42-0.375i	350.50+0.459i

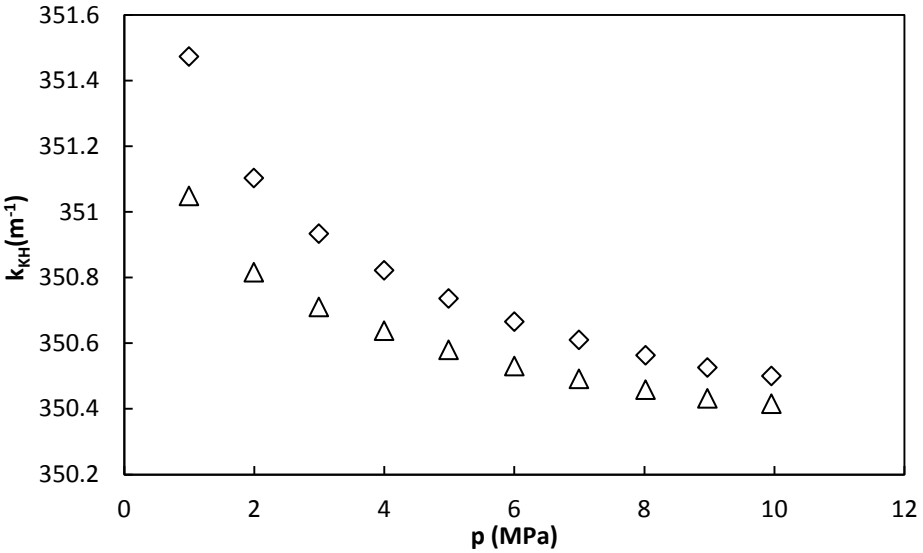

Figure 6.50 *Propagation constant real component for tubes 1 (Δ) and 2 (◊) for the acoustic mode (0,5) at T = 273.16 K as a function of pressure for the binary mixture x_{CO} = 0.10 and x_{N2} = 0.90.*

Table 6.41 *Specific acoustic admittance of the opening for tubes 1 and 2 for acoustic modes (0,2) to (0,5) at T = 273.16 K and p = 9.96 MPa for the binary mixture x_{CO} = 0.10 and x_{N2} = 0.90.*

Mode	y_{01}	y_{02}
(0,2)	0.0461+2.05i	3.2662-2.178i
(0,3)	0.0500+1.70i	0.2815+0.157i
(0,4)	0.0456+1.29i	0.5167+0.688i
(0,5)	0.0423+0.96i	0.7598+0.848i

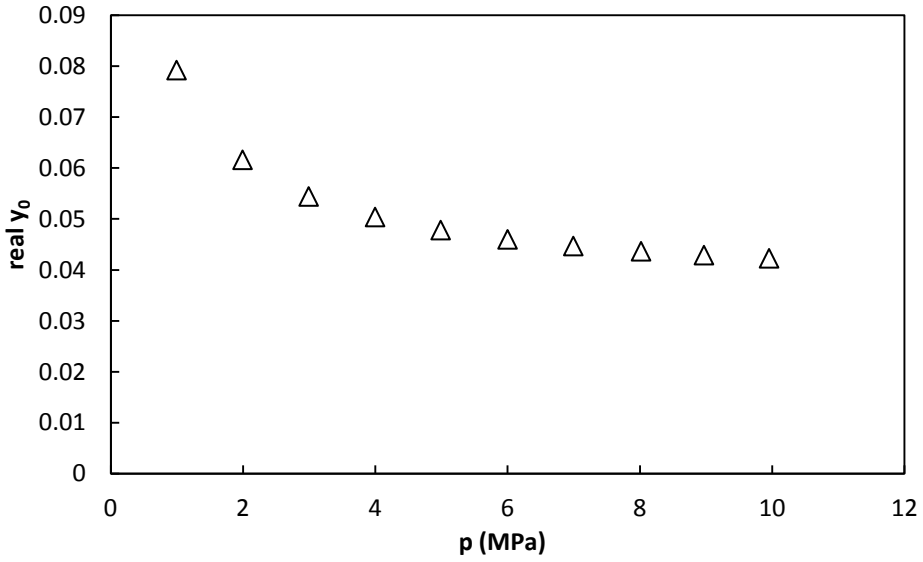

Figure 6.51 *Specific admittance of the opening real component for tube 1 for the acoustic mode (0,5) at T = 273.16 K as a function of pressure for the binary mixture x_{CO} = 0.10 and x_{N2} = 0.90.*

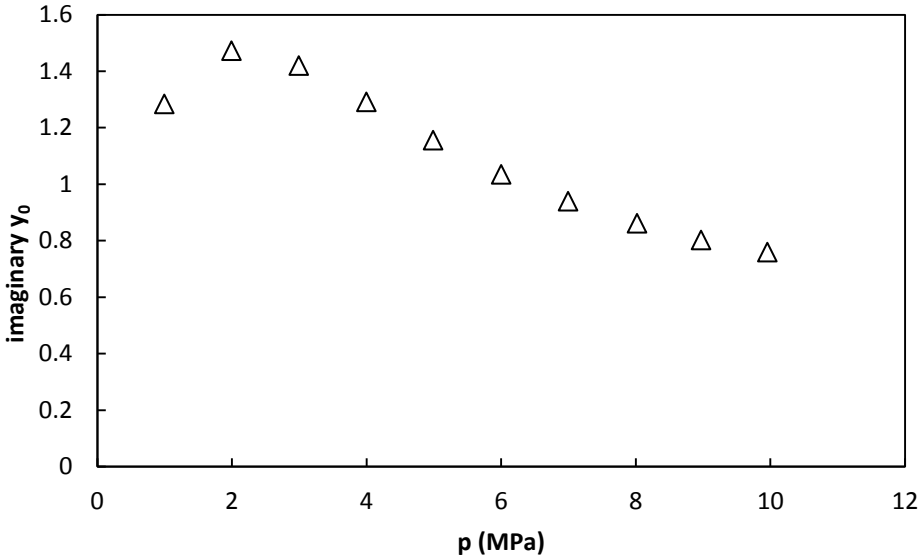

Figure 6.52 *Specific input admittance of the opening imaginary component for tube 1 for the acoustic mode (0,5) at T = 273.16 K as a function of pressure for the binary mixture x_{CO} = 0.10 and x_{N2} = 0.90.*

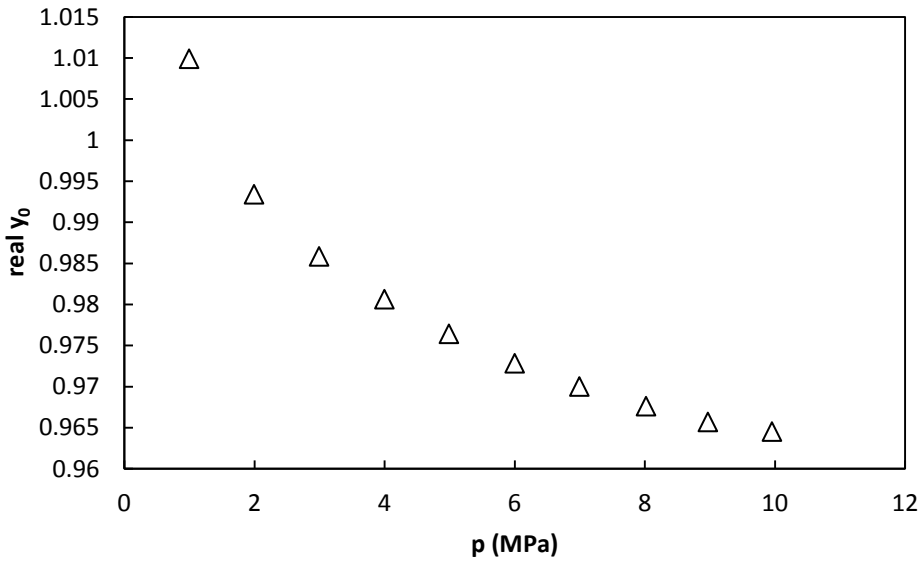

Figure 6.53 *Specific input admittance of the opening real component for tube 2 for the acoustic mode (0,5) at T = 273.16 K as a function of pressure for the binary mixture x_{CO} = 0.10 and x_{N2} = 0.90.*

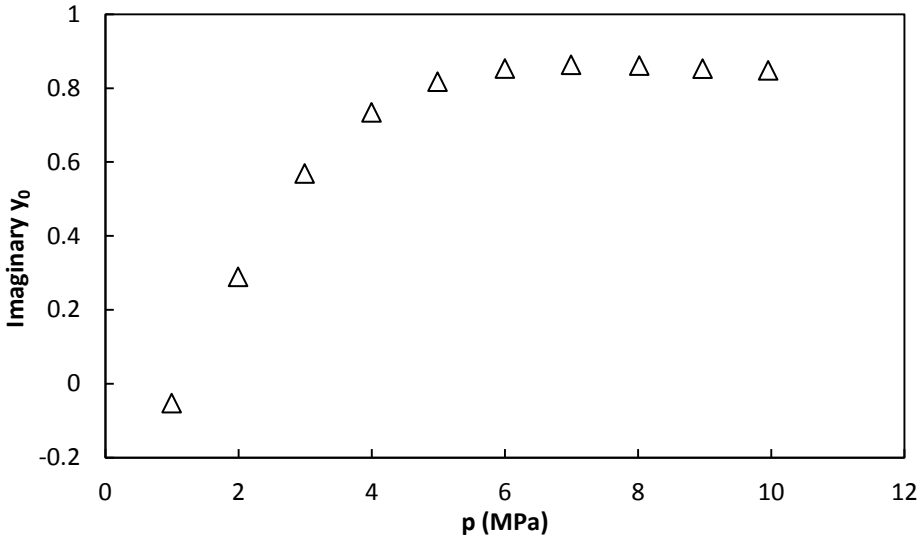

Figure 6.54 *Specific input admittance of the opening imaginary component of tube 2 for the acoustic mode (0,5) at T = 273.16 K as a function of pressure for the binary mixture x_{CO} = 0.10 and x_{N2} = 0.90.*

Table 6.42 *Tubes frequency correction and half-width contribution for acoustic modes (0,2) to (0,5) at T = 273.16 K and p = 9.96 MPa for the binary mixture x_{CO} = 0.10 and x_{N2} = 0.90.*

Mode	Δf_{tubes}(Hz)	g_{tubes}(Hz)
(0,2)	0.259	0.481
(0,3)	-0.011	0.121
(0,4)	-0.045	0.110
(0,5)	-0.041	0.096

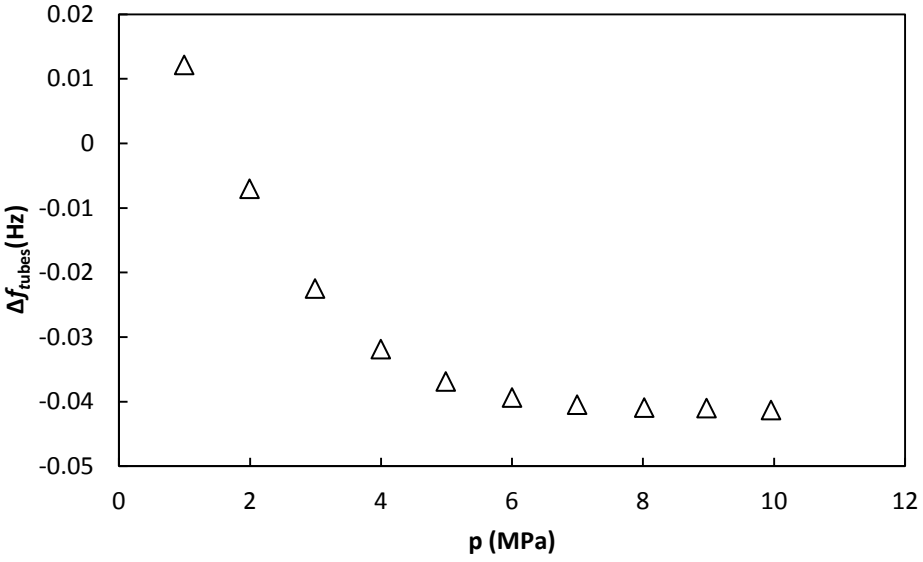

Figure 6.55 *Tubes frequency correction for the acoustic mode (0,5) at T = 273.16 K as a function of pressure for the binary mixture x_{CO} = 0.10 and x_{N2} = 0.90.*

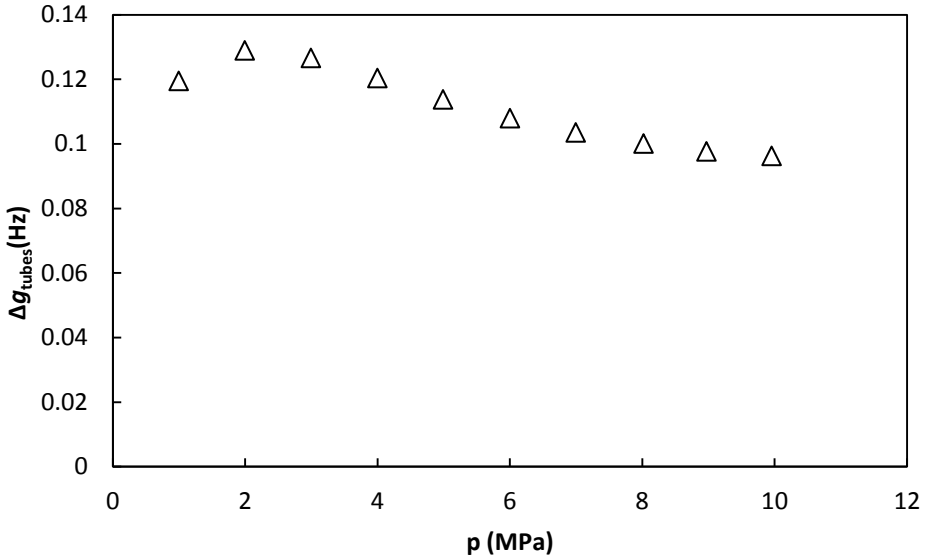

Figure 6.56 *Tubes half-width contribution for acoustic mode (0,5) at T = 273.16 K as a function of pressure for the binary mixture x_{CO} = 0.10 and x_{N2} = 0.90.*

6.4.2 Speed of Sound Determination.

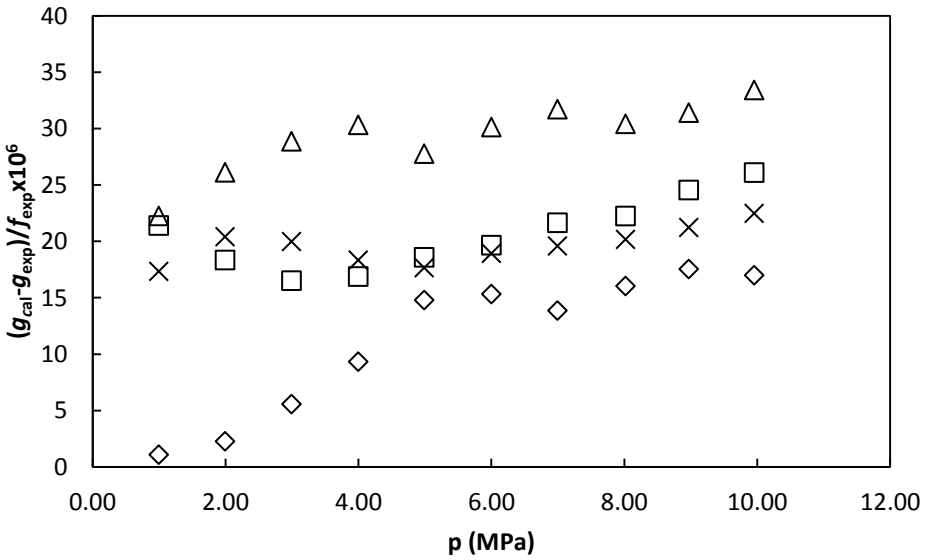

Figure 6.57 *Excess half-width for acoustic modes (0,2) (Δ),(0,3) (◊),(0,4) (x) and (0,5) (□)at T = 273.16 K as a function of pressure for the binary mixture x_{CO} = 0.10 and x_{N2} = 0.90.*

Table 6.43 *Speed of sound values from experimental data and according to GERG-2008 equation of state, and the comparison between them at T = 273.16 K for the binary mixture x_{CO} = 0.10 and x_{N2} = 0.90.*

p (Mpa)	T (K)	u_{exp} (m·s^{-1})	$u_{GERG-2008}$ (m·s^{-1})	$(u_{exp} - u_{GERG})/ u_{GERG} x10^6$
9.96	273.2048	361.782	361.83	-131
8.97	273.1775	357.953	358.02	-188
8.02	273.1751	354.551	354.62	-195
6.99	273.1750	351.197	351.25	-151
6.00	273.1721	348.252	348.30	-139
4.99	273.1721	345.573	345.60	-79
4.00	273.1759	343.255	343.27	-44
2.99	273.1735	341.207	341.22	-38
1.99	273.1669	339.464	339.47	-18
1.00	273.1592	338.027	338.03	-10

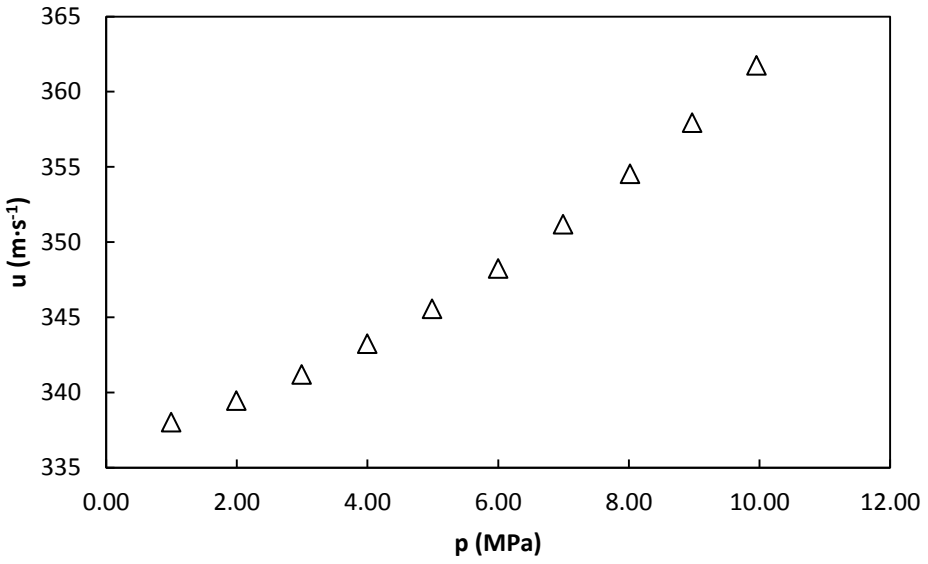

Figure 6.59 *Experimental speed of sound at T = 273.16 K as a function of pressure for the binary mixture x_{CO} = 0.10 and x_{N2} = 0.90.*

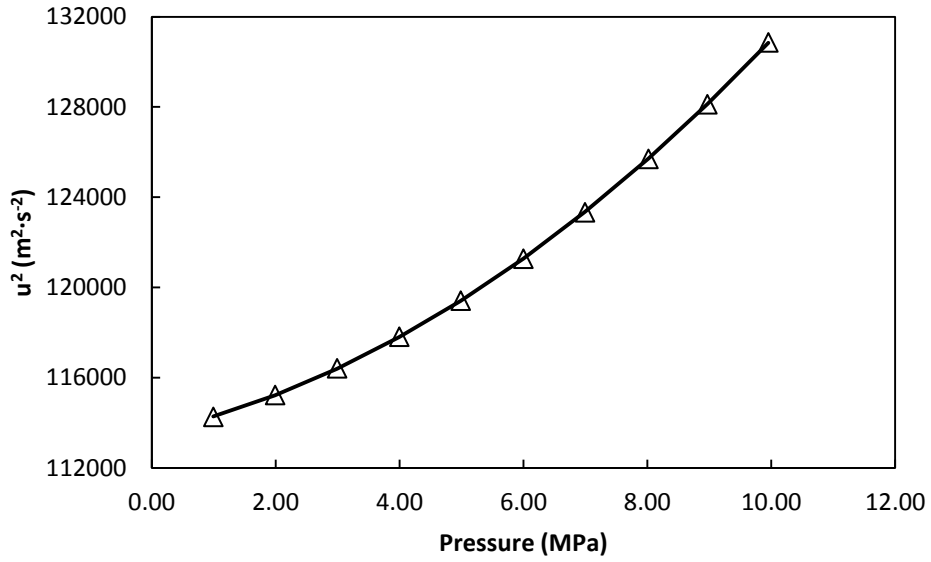

Figure 6.60 *Experimental square of speed of sound (Δ) and developed acoustic virial model (—) at T = 273.16 K as a function of pressure for the binary mixture x_{CO} = 0.10 and x_{N2} = 0.90.*

Table 6.44 *Experimental acoustic virial equation of state parameters at T = 273.16 K for the binary mixture x_{CO} = 0.10 and x_{N2} = 0.90.*

$A_0(m^2s^{-2})$	$A_1(m^2s^{-2}MPa^{-1})$	$A_2(m^2s^{-2}MPa^{-2})$	$\sigma\ (m^2s^{-2})$
113575	601	114.0	0.036

Table 6.45 *Speed of sound according developed model, and according GERG-2008 equation of state and a comparison between them at T = 273.16 K for the binary mixture x_{CO} = 0.10 and x_{N2} = 0.90.*

p (Mpa)	T (K)	$u_{model}\ (m{\cdot}s^{-1})$	$u_{GERG}\ (m{\cdot}s^{-1})$	$(u_{model}-u_{GERG})/u_{GERG}x10^6$
9.95	273.2048	361.721	361.83	-302
8.97	273.1775	357.951	358.02	-193
8.02	273.1751	354.567	354.62	-149
6.99	273.1750	351.213	351.25	-104
6.00	273.1721	348.257	348.30	-124
4.99	273.1721	345.557	345.60	-126
4.00	273.1759	343.217	343.27	-154
2.99	273.1735	341.167	341.22	-155
1.99	273.1669	339.449	339.47	-60
1.00	273.1592	338.062	338.03	96

Table 6.46 *Comparison between the calculated values of the isochoric and isobaric heat capacities (C_v^{pg} and C_p^{pg}) and the adiabatic coefficient (γ^{pg}) at zero pressure and the acoustic virial coefficients (β_a, γ_a) obtained from equation 6.1 and those calculated using GERG-2008 EoS for the binary mixture x_{CO} = 0.10 and x_{N2} = 0.90 at T = 273.16 K.*

	Eq 6.1	GERG-2008 EoS	Deviation (Eq.6.1-GERG)/GERGx10^2
γ^{pg}	1.4008	1.3997	0.0416
C_v^{pg}(J·mol^{-1}K^{-1})	20.744	20.802	0.0826
C_p^{pg}(J·mol^{-1}K^{-1})	29.059	29.116	0.2895
β_a(m^3·mol^{-1})	1.201E-05	1.3784E-05	0.2052
γ_a(m^6·mol^{-2})	5.177E-09	4.0306E-09	12.6819
u_0 (m·s^{-1})	337.008	336.87	0.0409

6.5 EXPERIMENTAL MEASUREMENTS OF THE MIXTURE (0.10 CO +0.90 N_2) AT T=325.00K

Table 6.47 *Frequency of resonance and half-width of the resonance peaks for acoustic modes (0,2) to (0,5) at T = 325 K and p = 10 .00 MPa for the binary mixture x_{CO} = 0.10 and x_{N2} = 0.90.*

Mode	*f* (Hz)	*g* (Hz)
(0,2)	7024.08	1.017
(0,3)	12076.13	1.289
(0,4)	17044.33	1.885
(0,5)	21983.42	2.034

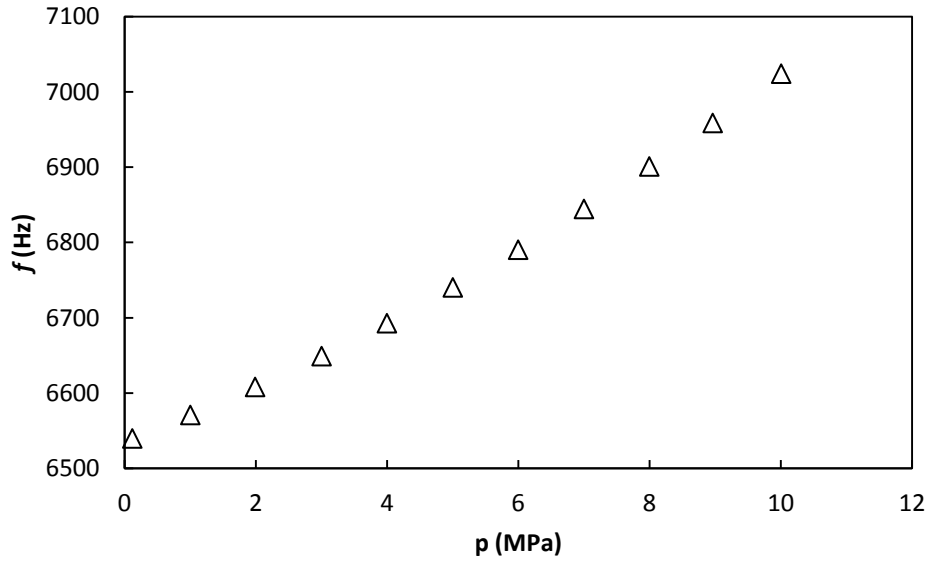

Figure 6.61 *Frequency of resonance for acoustic mode (0,2) at T = 325 K as a function of pressure for the binary mixture x_{CO} = 0.10 and x_{N2} = 0.90.*

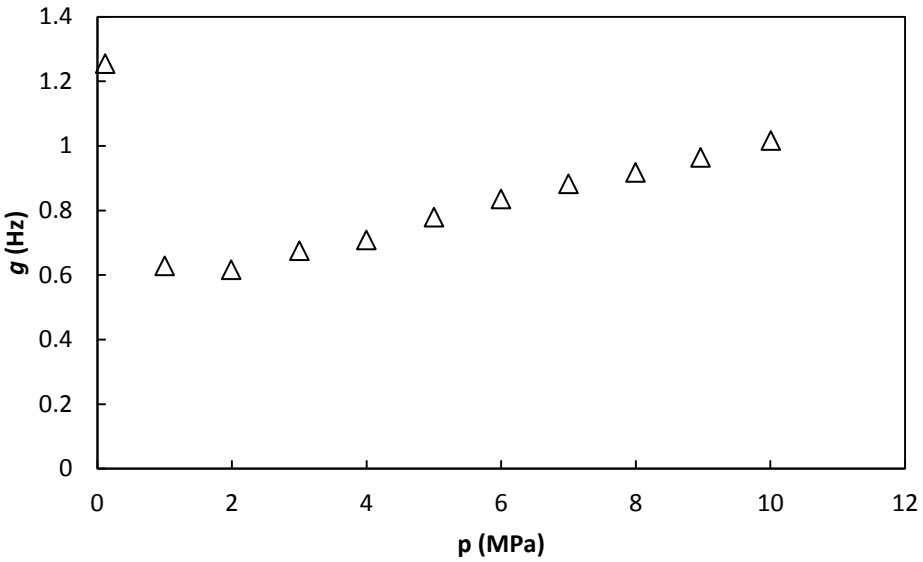

Figure 6.62 *Half-width of resonance peaks for acoustic mode (0,2) at T = 325 K as a function of pressure for the binary mixture x_{CO} = 0.10 and x_{N2} = 0.90.*

6.5.1 Frequency Corrections

6.5.1.1 *Thermal Boundary Layer Correction*

Table 6.49 *Thermal penetration length for acoustic modes (0,2) to (0,5) at T = 325 K and p = 10.00 MPa for the binary mixture x_{CO} = 0.10 and x_{N2} = 0.90.*

Mode	δ_{th} (m)
(0,2)	3.51×10^{-6}
(0,3)	2.68×10^{-6}
(0,4)	2.25×10^{-6}
(0,5)	1.98×10^{-6}

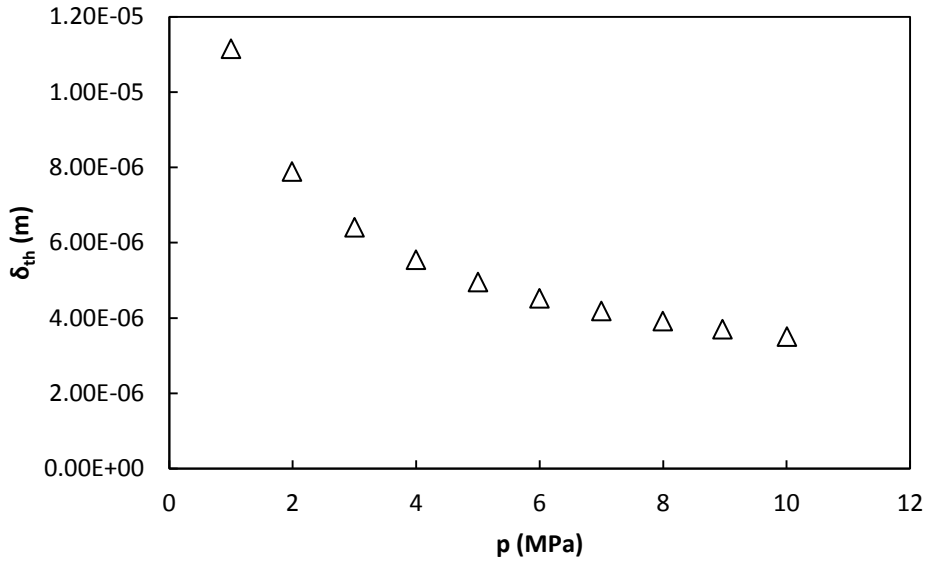

Figure 6.63 *Thermal penetration length for acoustic mode (0,2) at T = 325 K as a function of pressure for the binary mixture x_{CO} = 0.10 and x_{N2} = 0.90.*

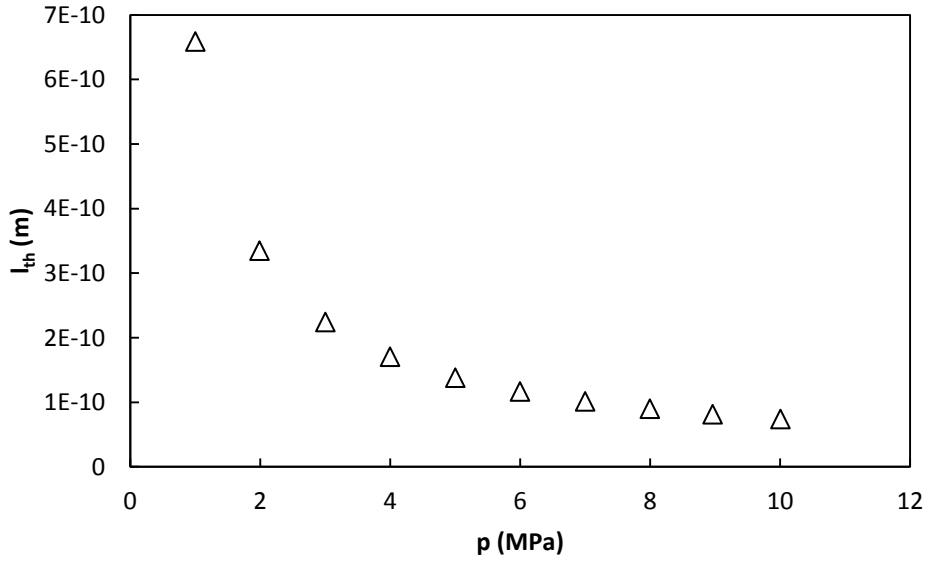

Figure 6.64 *Thermal accommodation length at T = 325 K as a function of pressure for the binary mixture x_{CO} = 0.10 and x_{N2} = 0.90.*

Table 6.50 *Shell thermal penetration length for acoustic modes (0,2) to (0,5) at T =325 K and p = 10.00 MPa for the binary mixture x_{CO} = 0.05 and x_{N2} = 0.95.*

Mode	δ_{Shell} (m)
(0,2)	1.35 x10^{-5}
(0,3)	1.03 x10^{-5}
(0,4)	8.69 x10^{-6}
(0,5)	7.65 x10^{-6}

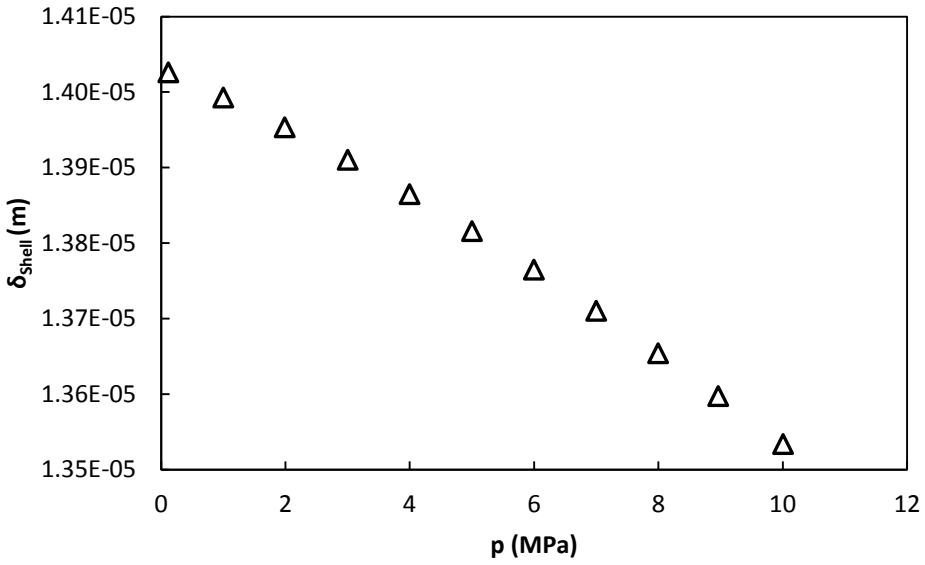

Figure 6.65 *Shell thermal penetration length for acoustic mode (0,2) at T = 325 K as a function of pressure for the binary mixture x_{CO} = 0.10 and x_{N2} = 0.90.*

Table 6.51 *Thermal boundary layer frequency correction and half-width contribution for acoustic modes (0,2) to (0,5) at T = 325 K and p = 10.00 MPa for the binary mixture x_{CO} = 0.10 and x_{N2} = 0.90.*

Mode	Δf_{th}(Hz)	g_{th}(Hz)
(0,2)	-0.162	0.164
(0,3)	-0.212	0.215
(0,4)	-0.252	0.256
(0,5)	-0.286	0.291

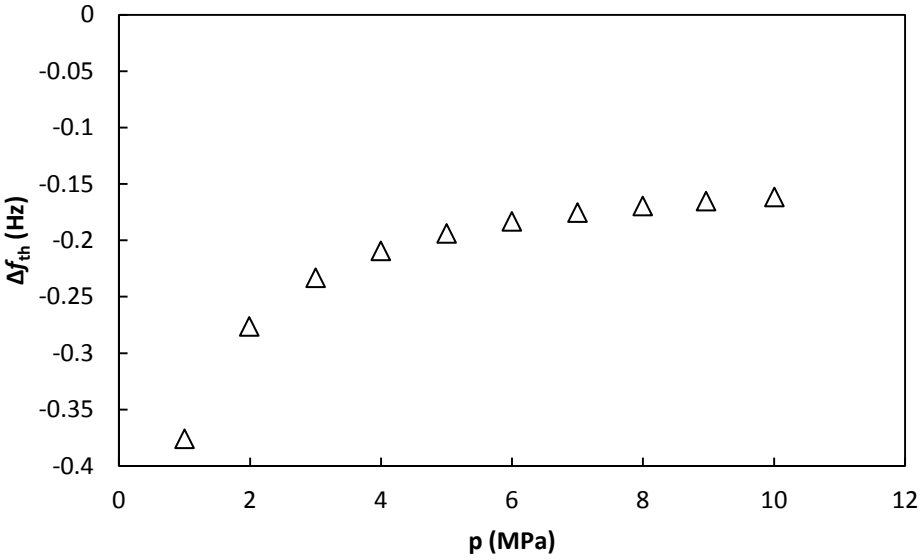

Figure 6.66 *Thermal boundary layer frequency correction for acoustic mode (0,2) at T = 325 K as a function of pressure for the binary mixture $x_{CO} = 0.10$ and $x_{N2} = 0.90$.*

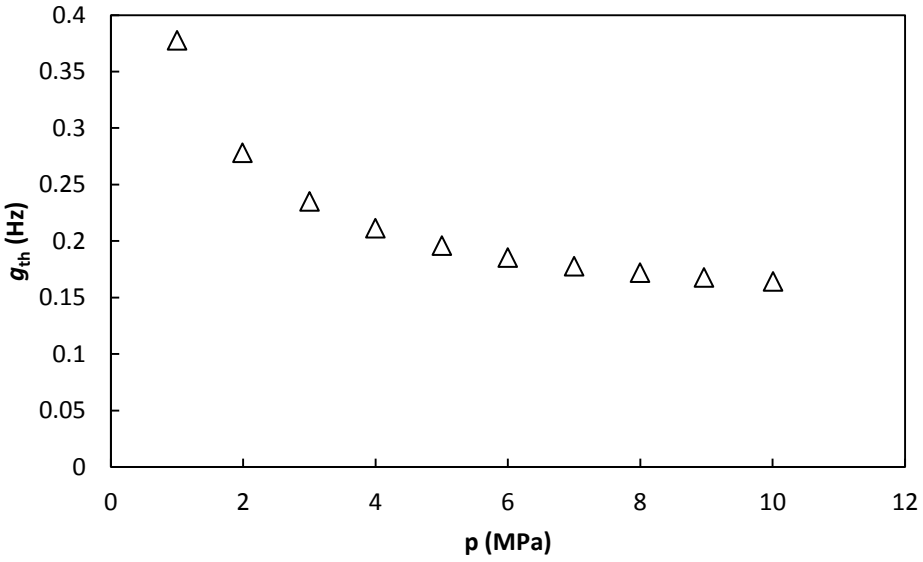

Figure 6.67 *Thermal boundary layer half-width contribution for acoustic mode (0,2) at T = 325 K as a function of pressure for the binary mixture $x_{CO} = 0.10$ and $x_{N2} = 0.90$.*

6.5.1.2 *Bulk Viscosity Contribution.*

Table 6.52 *Viscous penetration length for acoustic modes (0,2) to (0,5) at T = 325 K and p = 10.00 MPa for the binary mixture x_{CO} = 0.10 and x_{N2} = 0.90.*

Mode	δ_v (m)
(0,2)	3.04 x10^{-6}
(0,3)	2.32 x10^{-6}
(0,4)	1.95 x10^{-6}
(0,5)	1.72 x10^{-6}

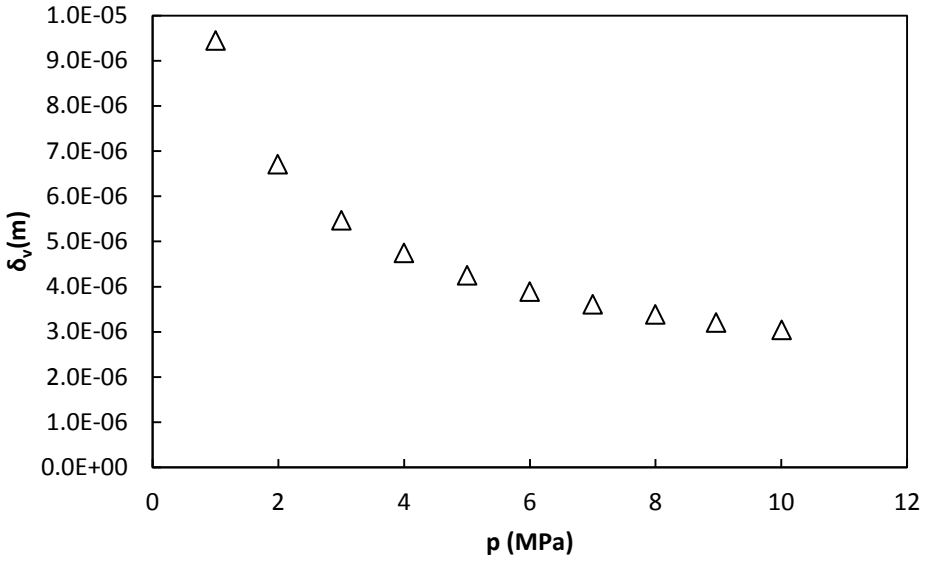

Figure 6.68 *Viscous penetration length for acoustic mode (0,2) at T = 325 K as a function of pressure for the binary mixture x_{CO} = 0.10 and x_{N2} = 0.90.*

Table 6.53 *Bulk viscosity half-width contribution for acoustic modes (0,2) to (0,5) at T=325.00K and p=10MPa for the binary mixture x_{CO}=0.10 and x_{N2}=0.90.*

Mode	g_b (Hz)
0.2	4.14 x10^{-4}
0.3	1.22 x10^{-3}
0.4	2.44 x10^{-3}
0.5	4.06 x10^{-3}

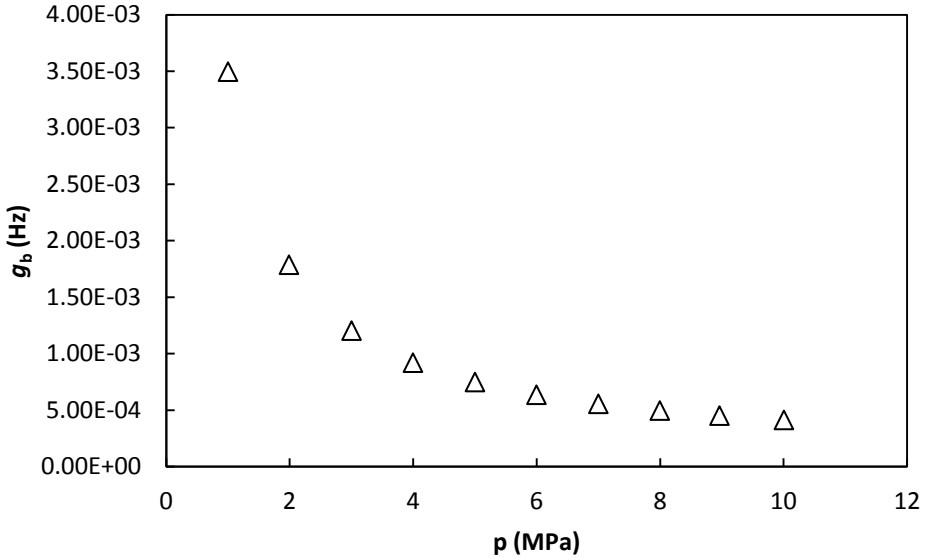

Figure 6.69 *Bulk viscosity half-width contribution to for acoustic mode (0,2) at T = 325 K as a function of pressure for the binary mixture x_{CO} = 0.10 and x_{N2} = 0.90.*

6.5.1.3 *Shell Motion Correction.*

Table 6.54 *Shell motion frequency correction for acoustic modes (0,2) to (0,5) at T = 325 K and p = 10.00 MPa for the binary mixture x_{CO} = 0.10 and x_{N2} = 0.90*

Mode	Δf_{shell} (Hz)
(0,2)	-0.112
(0,3)	-0.208
(0,4)	-0.342
(0,5)	-0.606

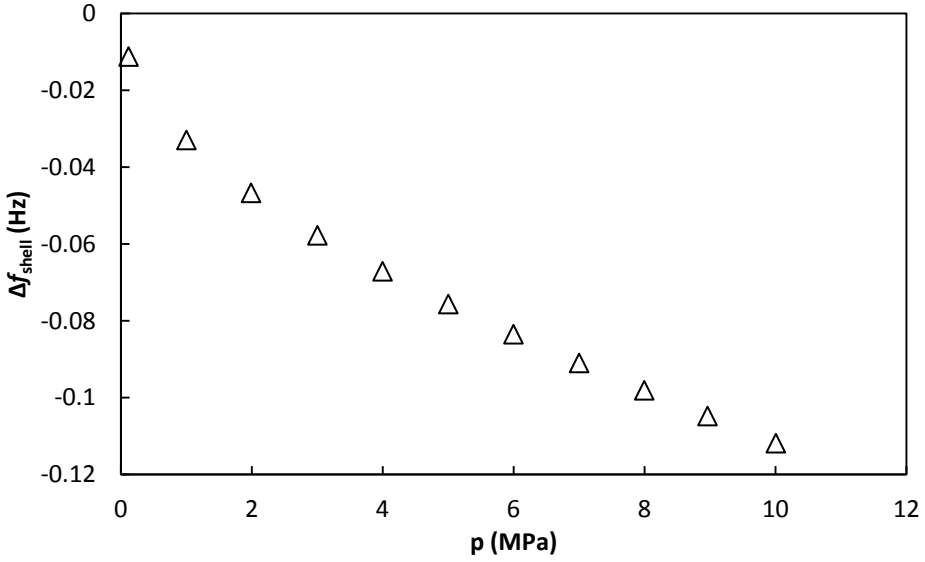

Figure 6.70 *Shell motion Frequency correction for acoustic mode (0,2) at T = 325 K as a function of pressure for the binary mixture x_{CO} = 0.10 and x_{N2} = 0.90.*

6.5.1.4 *Tubes and Holes Correction.*

Table 6.55 *Kirchhoff-Helmholtz absorption coefficient for tubes 1 and 2 for acoustic modes (0,2) to (0,5) at T = 325 K and p = 10.00 MPa for the binary mixture x_{CO} = 0.10 and x_{N2} = 0.90.*

Mode	$\alpha_{KH1}(m^{-1})$	$\alpha_{KH2}(m^{-1})$
(0,2)	0.548	0.274
(0,3)	0.719	0.360
(0,4)	0.854	0.427
(0,5)	0.970	0.485

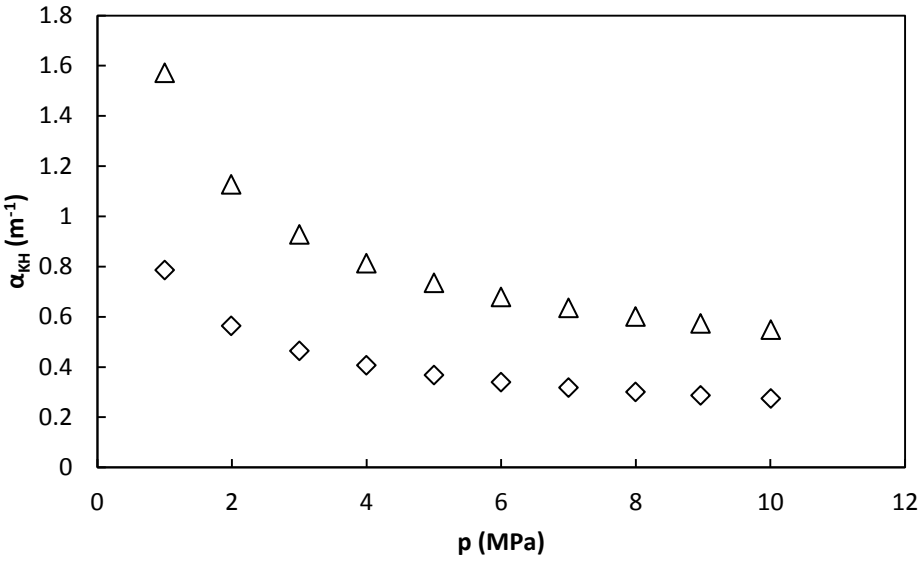

Figure 6.71 *Kirchhoff-Helmholtz absorption coefficient for tubes 1 (Δ) and 2 (◊) for acoustic mode (0,2) at T = 325 K as a function of pressure for the binary mixture x_{CO} = 0.10 and x_{N2} = 0.90.*

Table 6.65 *Propagation constant for tubes 1 and 2 for acoustic modes (0,2) to (0,5) at T = 325 K and p = 10.00 MPa for the binary mixture x_{CO} = 0.10 and x_{N2} = 0.90.*

Mode	$k_{KH1}(m^{-1})$	$k_{KH2}(m^{-1})$
(0,2)	112.317-0.548i	112.043-0.274i
(0,3)	192.878-0.719i	192.519-0.360i
(0,4)	272.069-0.854i	271.642-0.427i
(0,5)	350.778-0.970i	350.293-0.485i

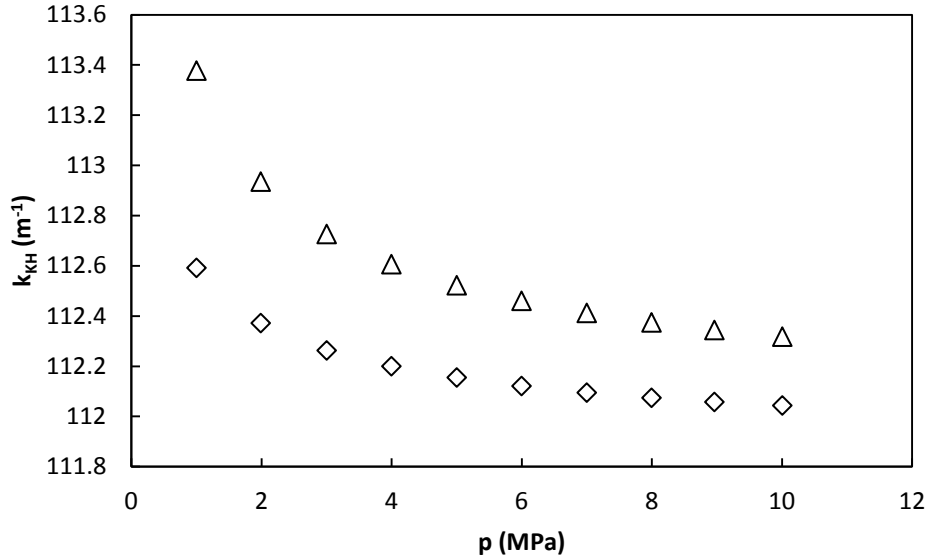

Figure 6.72 *Propagation constant real component for tubes 1 (Δ) and 2 (◊) for acoustic mode (0,2) at T = 325 K as a function of pressure for the binary mixture x_{CO} = 0.10 and x_{N2} = 0.90.*

Table 6.66 *Specific acoustic admittance of the opening for tubes 1 and 2 for acoustic modes (0,2) to (0,5) at T = 325 K and p = 10.00 MPa for the binary mixture x_{CO} = 0.10 and x_{N2} = 0.90.*

Mode	y_{01}	y_{02}
(0,2)	0.118+2.105i	3.723-1.721i
(0,3)	0.120+1.744i	0.291+0.091i
(0,4)	0.102+1.322i	0.474+0.558i
(0,5)	0.088+0.988i	0.614+0.646i

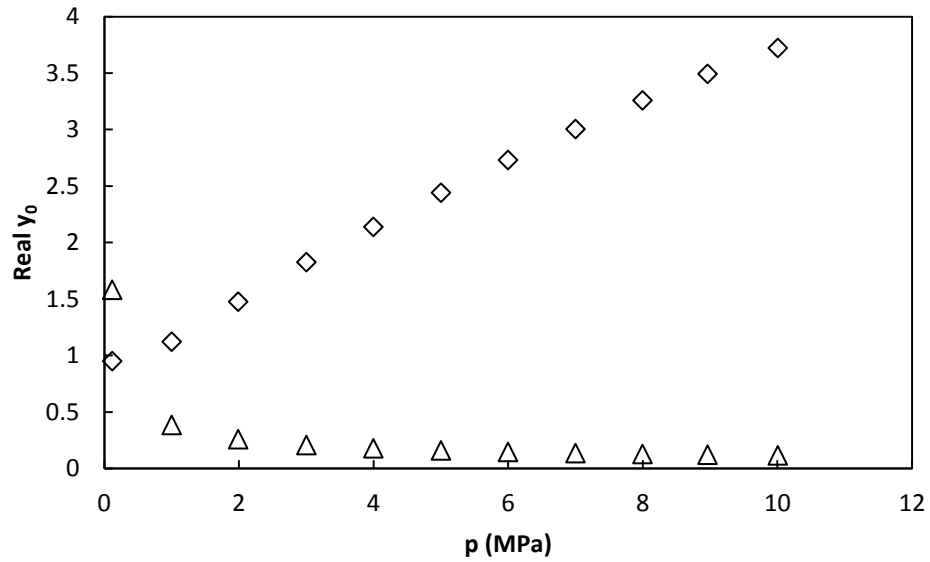

Figure 6.73 *Specific acoustic admittance of the opening real component for tubes 1 (Δ) and 2 (◊) for acoustic mode (0,2) at T = 325 K as a function of pressure for the binary mixture x_{CO} = 0.10 and x_{N2} = 0.90.*

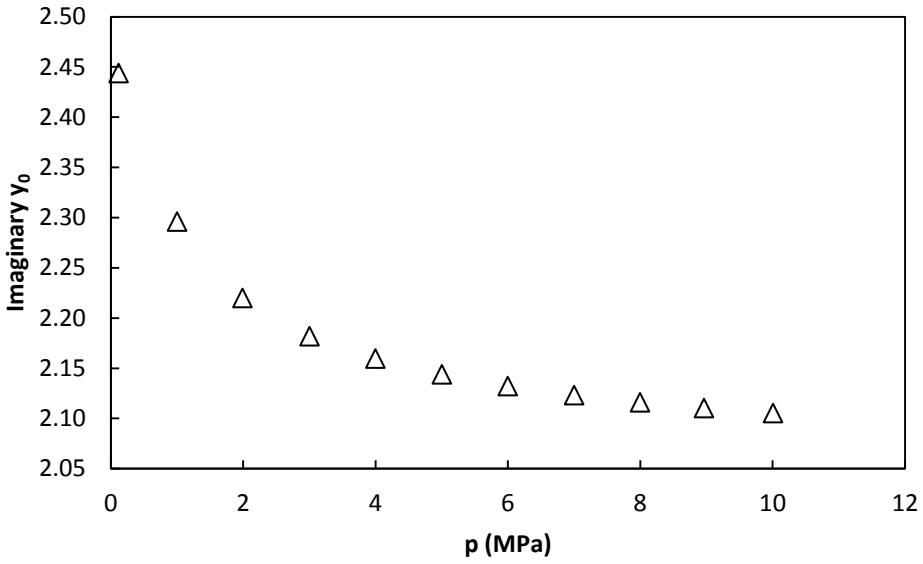

Figure 6.74 *Specific acoustic admittance of the opening imaginary component for tube 1 for acoustic mode (0,2) at T = 325 K as a function of pressure for the binary mixture x_{CO} = 0.10 and x_{N2} = 0.90.*

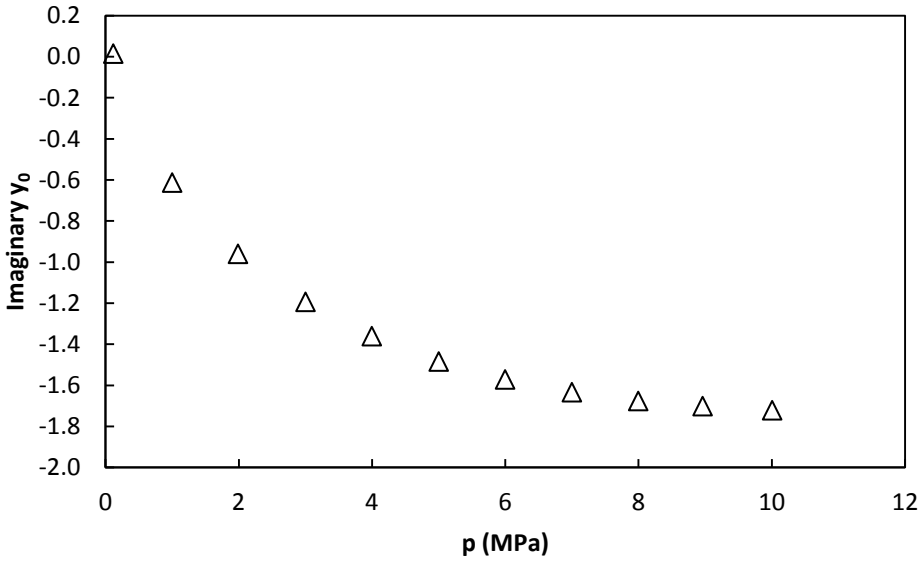

Figure 6.75 *Specific acoustic admittance of the opening for tube 2 for acoustic mode (0,2) at T = 325 K as a function of pressure for the binary mixture x_{CO} = 0.10 and x_{N2} = 0.90.*

Table 6.67 *Tubes frequency correction and half-width contribution for acoustic modes (0,2) to (0,5) at T = 325 K and p = 10.00 MPa for the binary mixture x_{CO} = 0.10 and x_{N2} = 0.90.*

Mode	Δf_{tubes} (Hz)	g_{tubes} (Hz)
(0,2)	0.253	0.589
(0,3)	-0.0003	0.137
(0,4)	-0.035	0.121
(0,5)	-0.030	0.100

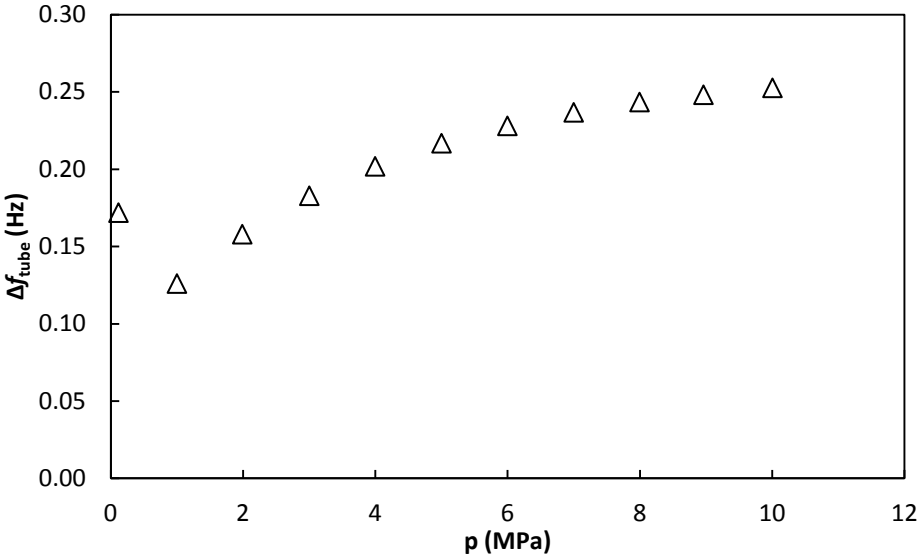

Figure 6.74 *Tubes frequency correction for acoustic mode (0,2) at T = 325 K as a function of pressure for the binary mixture x_{CO} = 0.10 and x_{N2} = 0.90.*

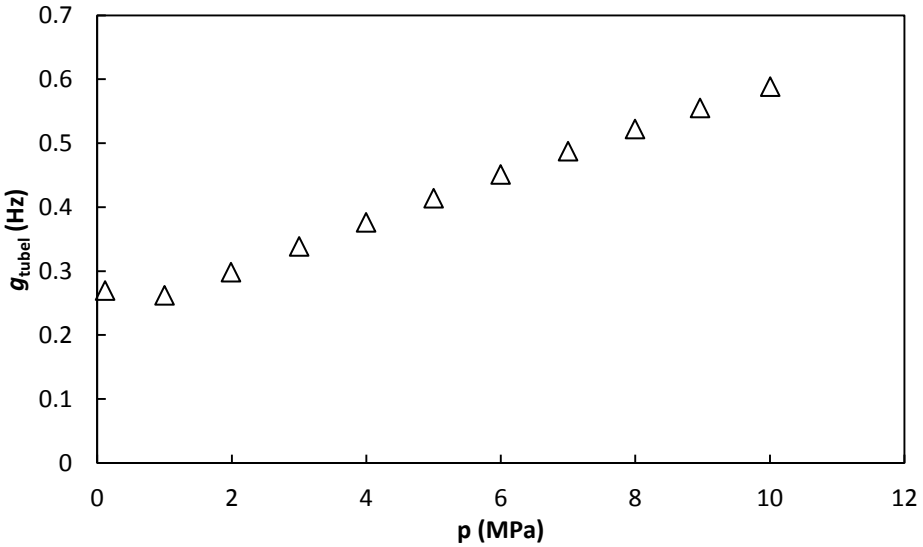

Figure 6.75 *Tubes half-width contribution for acoustic mode (0,2) at T = 325 K as a function of pressure for the binary mixture x_{CO} = 0.10 and x_{N2} = 0.90.*

6.5.2 Speed of Sound Determination.

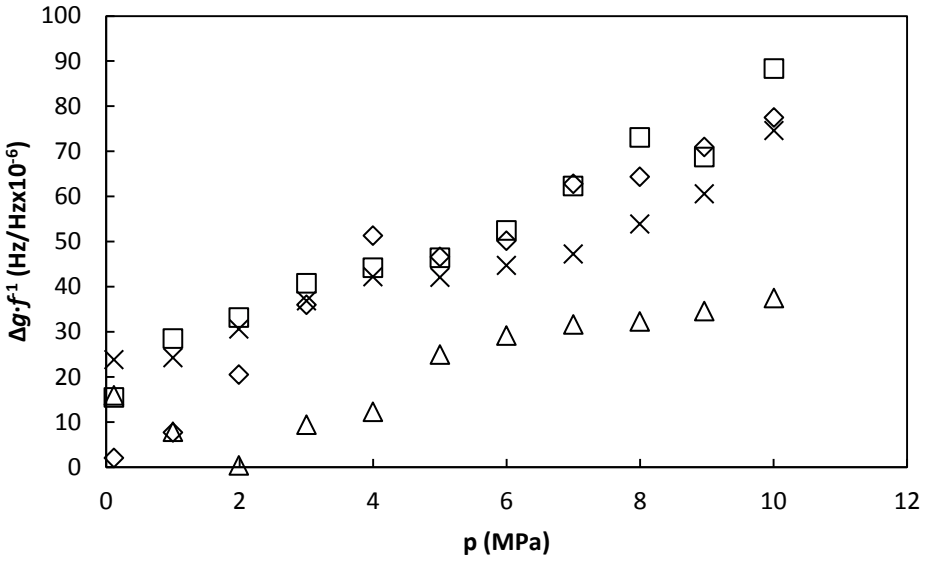

Figure 6.76 *Excess half-width for modes (0,2) (Δ), (0,3) (◊), (0,4) (□), (0,5) (X) at T = 325 K as a function of pressure for the binary mixture x_{CO} = 0.10 and x_{N2} = 0.90.*

Table 6.69 *Speed of sound values from experimental data and according to GERG-2008 equation of state, and the comparison between them at T = 325 K for the binary mixture x_{CO} = 0.10 and x_{N2} = 0.90.*

p (Mpa)	T (K)	u_{exp}(m·s^{-1})	u_{GERG} (m·s^{-1})	(u_{exp}-u_{GERG})/u_{GERG} x10^6 (m·s^{-1}/m·s^{-1} x10^6)
10.01	324.9377	394.851	394.87	48
8.96	324.9461	391.166	391.18	37
8.00	324.9553	387.916	387.92	11
7.00	324.9616	384.733	384.73	-7
6.00	324.9393	381.687	381.68	-18
5.00	324.9564	378.867	378.85	-45
4.00	324.9498	376.190	376.16	-81
3.00	324.9529	373.725	373.69	-94
1.99	324.9556	371.420	371.36	-161
1.00	324.9534	369.327	369.28	-127
0.12	324.9375	367.616	367.56	-152

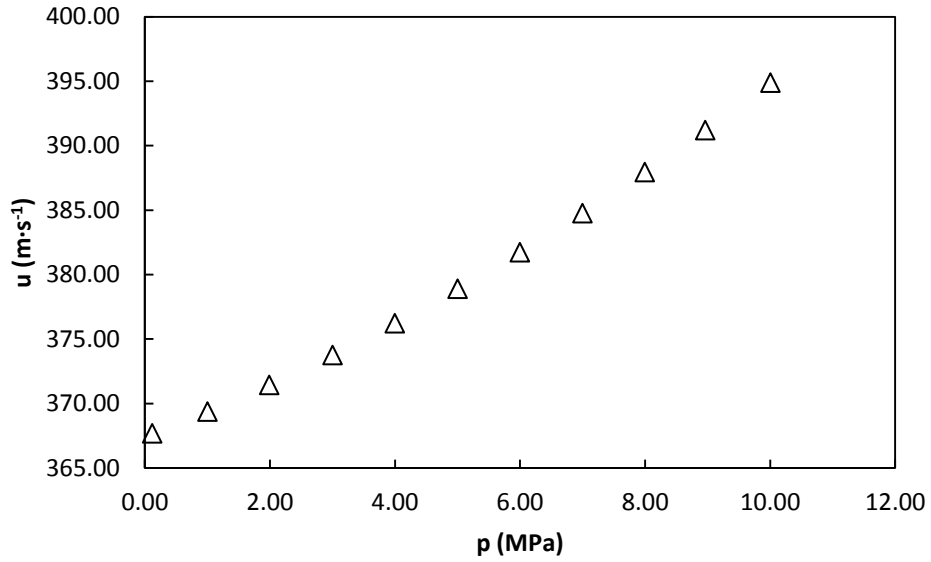

Figure 6.77 *Experimental speed of sound at T = 325 K as a function of pressure for the binary mixture x_{CO} = 0.10 and x_{N2} = 0.90.*

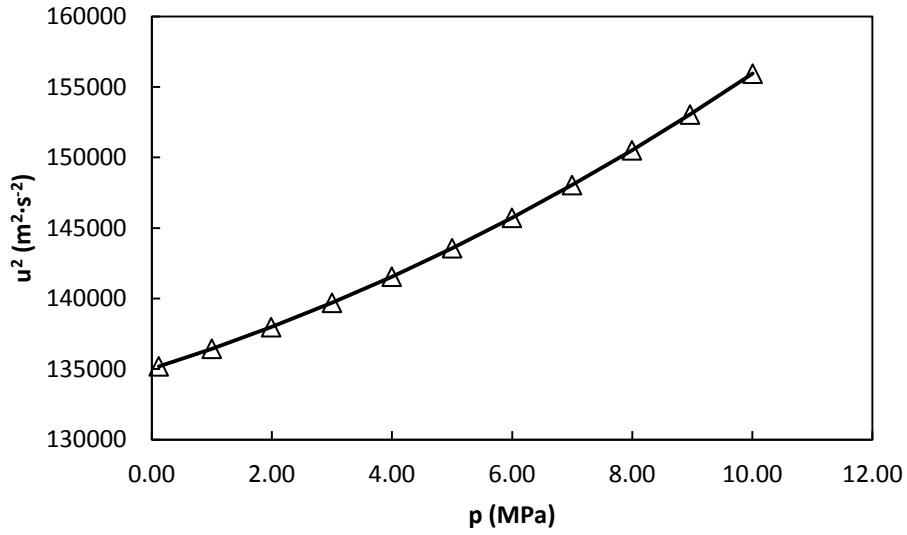

Figure 6.78 *Experimental square speed of sound (Δ) and developed acoustic virial model (—) at T = 325 K as a function of pressure for the binary mixture x_{CO} = 0.10 and x_{N2} = 0.90.*

Table 6.70 *Experimental acoustic virial equation of state parameters at T = 325K for the binary mixture x_{CO} = 0.10 and x_{N2} = 0.90.*

A_0 ($m^2 \cdot s^{-2}$)	A_1 ($m^2 \cdot s^{-2} MPa^{-1}$)	A_2 ($m^2 \cdot s^{-2} MPa^{-2}$)	σ ($m^2 s^{-2}$)
135017	1327	76.2	6.6

Table 6.71 *Speed of sound according to developed model, and according to GERG-2008 equation of state and a comparison between them at T = 325 K for the binary mixture x_{CO} = 0.10 and x_{N2} = 0.90.*

p (MPa)	T (k)	u_{model}	u_{GERG} ($m \cdot s^{-1}$)	$(u_{model}-u_{GERG})/u_{GERG-}$ x10^6 ($m \cdot s^{-1}/m \cdot s^{-1}$ x10^6)
10.01	324.9377	394.882	394.87	-30
8.96	324.9461	391.199	391.18	-49
8.00	324.9553	387.947	387.92	-69
7.00	324.9616	384.758	384.73	-73
6.00	324.9393	381.730	381.68	-132
5.00	324.9564	378.895	378.85	-119
4.00	324.9498	376.217	376.16	-152
3.00	324.9529	373.749	373.69	-157
1.99	324.9556	371.427	371.36	-180
1.00	324.9534	369.355	369.28	-203
0.12	324.9375	367.662	367.56	-278

Table 6.72 *Comparison between the calculated values of the isochoric and isobaric heat capacities (C_v^{pg} and C_p^{pg}) and the adiabatic coefficient (γ^{pg}) at zero pressure and the acoustic virial coefficients (β_a, γ_a) obtained from equation 6.1 and those calculated using GERG-2008 EoS for the binary mixture x_{CO} = 0.10 and x_{N2} = 0.90 at T = 325 K.*

	Eq. 6.1	GERG-2008	Deviation10^2 (Eq. 6.1-GERG)/GERG
γ^{pg}	1.3999	1.3992	0.0508
C_v^{pg}($J \cdot mol^{-1}K^{-1}$)	20.790	20.829	0.1833
C_p^{pg}($J \cdot mol^{-1}K^{-1}$)	29.104	29.143	0.1294
β_a($m^3 \cdot mol^{-1}$)	2.655 x10^{-5}	2.6905 x10^{-5}	1.7048
γ_a($m^3 \cdot mol^{-2}$)	2.912 x10^{-9}	3.8465 x10^{-9}	0.0778
u_0 ($m \cdot s^{-1}$)	367.450	367.38	-0.0190

6.6 UNCERTAINTY ASSESMENT

This section covers the computing of the measured properties uncertainties, these properties are speed of sound, adiabatic coefficient, isobaric and isochoric heat capacities and first and second acoustic birial coefficients. The calculations are done for both isotherms.

6.6.1 Speed of Sound Extrapolation to Zero Pressure

Speed of sound at zero pressure is an extrapolated value obtained by a polynomial regression using pressure and square speed of sound measurements. This analysis was done

using Monte Carlo method. This method requires uncertainties for both, square speed on sound and pressure at each point of study.

Pressure uncertainties are easily calculated as it is 0.01% of the measurement as it was explained in section 2.

Square speed of sound uncertainty determination requires some more complex calculations. For instance, speed of sound uncertainty is calculated first and then the square speed of sound uncertainty according GUM as shown in equation 6.2.

$$u\left(u^2\right)=\sqrt{\left(\frac{\partial u^2}{\partial u}\right)^2 u^2(u)}=2u\cdot u(u) \tag{6.2}$$

Therefore before computing any other uncertainty it is necessary to calculate speed of sound uncertainty at each pressure. The main uncertainty sources of speed of sound are those due to the radius calculation, modal dispersion and from the frequency measurements. Chapter 3 shows how sensitivity factors are calculated and how all uncertainty sources are added to obtain speed of sound uncertainty, equations 3.10 and 3.11.

$$u=\frac{2\pi a}{n}\sum_{i=1}^{n}\frac{f_i}{\upsilon_i} \tag{3.10}$$

$$u(u)=\sqrt{u^2(u)+\left(\frac{\partial u}{\partial a}\right)^2 u^2(a)+\sum_{i=1}^{n}\left(\frac{\partial u}{\partial f_i}\right)^2 u^2(f_i)}$$

$$u(u)=\sqrt{u^2(u)+\left(\frac{2\pi}{n}\sum_{i=1}^{n}\frac{f_i}{\upsilon_i}\right)^2 u^2(a)+\left(\frac{1}{n}\sum_{i=1}^{n}\frac{2\pi a}{\upsilon_i}\right)^2 u^2(f_i)} \tag{3.11}$$

6.6.1.1 *Radius Uncertainty*

Radius is obtained thanks to the polynomial equations computed in chapter 5, for determining resonator inner radius at each pressure. Two isotherms were measured for this gas mixture, therefore the polynomial equations used to calculate the internal radius must be chosen accordingly. The polynomial parameters for each measured temperature are displayed in table 5.13.

Radius uncertainties are calculated using regression uncertainty (calculated previously and detailed in table 5.18) and the experimental radius measurement nearest to current measuring

conditions. Inner radius values and uncertainties are in table 6.35 for T=273K T=325K isotherms.

Table 6.73 *Resonator inner radius uncertainties for both isotherms T = 273 K and T = 325K.*

	u(a) (m)	
p (MPa)	**T=273K**	**T=325K**
10	1.1×10^{-6}	4.3×10^{-6}
9	1.1×10^{-6}	4.3×10^{-6}
8	1.1×10^{-6}	4.2×10^{-6}
7	4.7×10^{-6}	4.2×10^{-6}
6	1.2×10^{-6}	4.2×10^{-6}
5	1.1×10^{-6}	4.2×10^{-6}
4	1.0×10^{-6}	4.2×10^{-6}
3	1.0×10^{-6}	4.1×10^{-6}
2	9.9×10^{-6}	4.2×10^{-6}
1	4.2×10^{-6}	4.2×10^{-6}
0.1	N/A	8.5×10^{-6}

6.6.1.2 *Frequency Uncertainty*

Frequency uncertainty has two contributions, one due to the frequency measurement itself and other due to the discrepancy between measured and calculated half-width of the resonance peaks, named excess half-width.

Both contributions are different for each acoustic mode. Excess half-width are dependent on pressure, but frequency uncertainty has no tendency with pressure, therefore an example of these uncertainty values are table 6.74 at the highest working pressure p = 10 MPa and all measured values can be found in appendix C for the mixture x_{CO}=0.05 and x_{N2}=0.95 and appendix D the mixture x_{CO}=0.10 and x_{N2}=0.90.

Table 6.74 *Frequency measurements uncertainty of acoustic modes (0,2), (0,3), (0,4) and (0,5) at p = 10 MPa for both binary mixtures.*

	u(f) (Hz)			
	x_{CO}=0.05		**x_{CO}=0.10**	
Mode	**T=273K**	**T=325K**	**T=273K**	**T=325K**
(0,2)	0.20	0.060	0.031	0.069
(0,3)	0.035	0.18	0.028	0.38
(0,4)	0.10	0.79	0.085	0.58
(0,5)	0.29	0.44	0.12	0.61

6.6.1.3 *Modal Dispersion Uncertainty.*

This uncertainty is due to the differences on the calculated speed of sound values for each acoustic mode. It is calculated as an A type uncertainty. Table 6.75 shows modal dispersion uncertainty values for each isotherm.

Table 6.75 *Modal dispersion uncertainty at each pressure for both isotherms, T = 273 K and T = 325 K. for the binary mixture $x_{CO} = 0.05$ and $x_{N2} = 0.95$*

	$u(u_{disp})$ ($m \cdot s^{-1}$)			
	$x_{CO} = 0.05$		**$x_{CO}=0.10$**	
p (MPa)	**T = 273 K**	**T = 325 K**	**T = 273 K**	**T = 325 K**
10	0.017	0.050	0.015	0.023
9	0.015	0.017	0.014	0.018
8	0.014	0.015	0.012	0.015
7	0.010	0.012	0.011	0.014
6	0.011	0.0093	0.0094	0.010
5	0.010	0.0071	0.0083	0.0086
4	0.0094	0.0052	0.0077	0.0075
3	0.0091	0.0042	0.0066	0.0067
2	0.0086	0.0033	0.0055	0.0056
1	0.0082	0.0026	0.0041	0.0040
0.1	0.0062	0.00078	N/A	0.0016

6.6.1.4 *Speed of Sound Uncertainty.*

Speed of sound uncertainty was computed using data shown in tables 6.73 to 6.75. Calculation was done according equations 3.10 and 3.11. Results of this calculation are in table 6.76 for isotherm T = 273 K and in table 6.39 for isotherm T = 325 K.

Table 6.76 *Measured speed of sound values, standard uncertainties and relative standard uncertainties for the binary mixture x_{CO} = 0.05 and x_{N2} = 0.95.*

	T = 273 K			T = 325 K		
p (MPa)	**u ($m \cdot s^{-1}$)**	**u(u) ($m \cdot s^{-1}$)**	**u_r(u) ($m \cdot s^{-1} \cdot m^{-1} \cdot s \cdot 10^6$)**	**u ($m \cdot s^{-1}$)**	**u(u) ($m \cdot s^{-1}$)**	**u_r(u) ($m \cdot s^{-1} \cdot m^{-1} \cdot s \cdot 10^6$)**
10	361.993	0.045	120	394.935	0.052	130
9	358.189	0.042	120	391.398	0.047	120
8	354.430	0.043	120	387.989	0.045	120
7	351.175	0.040	120	384.949	0.044	120
6	348.210	0.040	120	381.773	0.042	110
5	345.566	0.039	110	378.930	0.041	110
4	343.202	0.039	120	376.278	0.040	110
3	341.180	0.039	110	373.796	0.039	110
2	339.444	0.041	120	371.483	0.039	100
1	337.991	0.051	150	369.381	0.039	110
0.1	336.945	0.052	150	367.645	0.079	220

Table 6.77 *Measured speed of sound values, standard uncertainties and relative standard uncertainties for the binary mixture x_{CO} = 0.10 and x_{N2} = 0.90.*

	T = 273 K			T = 325 K		
p (MPa)	**u ($m \cdot s^{-1}$)**	**u(u) ($m \cdot s^{-1}$)**	**u_r(u) ($m \cdot s^{-1} \cdot m^{-1} \cdot s \cdot 10^6$)**	**u ($m \cdot s^{-1}$)**	**u(u) ($m \cdot s^{-1}$)**	**u_r(u) ($m \cdot s^{-1} \cdot m^{-1} \cdot s \cdot 10^6$)**
10	361.782	0.047	130	394.851	0.056	140
9	357.953	0.045	130	391.166	0.051	130
8	354.551	0.044	120	387.916	0.049	130
7	351.197	0.043	120	384.733	0.048	130
6	348.252	0.043	120	381.687	0.045	120
5	345.573	0.042	120	378.867	0.044	110
4	343.255	0.042	120	376.190	0.044	120
3	341.207	0.041	120	373.725	0.042	110
2	339.464	0.041	120	371.420	0.041	110
1	338.027	0.040	120	369.327	0.040	110
0.1	N/A	N/A	N/A	367.616	0.082	220

Values from tables 6.76 and 6.77 were used to obtain square speed of sound values and their uncertainties according equation 6.2. These values are in tables 6.40 and 6.41

Table 6.78 *Square speed of sound values absolute standard uncertainty for isotherm both mixtures.*

	$u(u^2)$ ($m^2 \cdot s^{-2}$)			
	x_{CO} = 0.05		x_{CO}=0.10	
p (MPa)	T = 273 K	T = 325 K	T = 273 K	T = 325 K
10	32	41	34	44
9	30	37	32	40
8	31	35	31	38
7	28	34	30	37
6	28	32	30	35
5	27	31	29	33
4	27	30	28	33
3	27	29	28	32
2	28	29	28	30
1	35	29	27	30
0.1	35	58		60

Values of pressure and speed of sound and their corresponding uncertainties were used in a Monte Carlo simulation. This simulation was carried out by doing a polynomial regression using pressure and square speed of sound as input data. Then new values of pressure and square speed of sound were used for a new regression, this new data were obtained randomly falling in a normal distribution which averages are the pressure and square speed of sound data; and the standard deviations are their standard uncertainties. The results of the new polynomial regression were storage for latter use.

This procedure was repeated 10^6 times and the results for each parameter were analyzed and fitted to a normal distribution which standard deviation is the resulting uncertainty. Results of this analysis are in table 6.79.

Table 6.79 *Experimental acoustic virial equation of state parameters and uncertainties for both mixtures*

Parameters	x_{CO} = 0.05		x_{CO} = 0.10		Units
	T =273 K	T = 325 K	T =273 K	T = 325 K	
A_0	113582	135030	113575	134995	m^2s^{-2}
A_1	611	1335	601	1327	$m^2s^{-2}MPa^{-1}$
A_2	113.0	75.4	114.0	76.13	$m^2s^{-2}MPa^{-2}$
$u(A_0)$	28	38	27	39	m^2s^{-2}
$u(A_1)$	12	17	12	18	$m^2s^{-2}MPa^{-1}$
$u(A_2)$	1.1	1.7	1.1	1.7	$m^2s^{-2}MPa^{-2}$
$u_r(A_0)$	245	281	234	290	$10^6 m^2s^{-2} \cdot (m^2s^{-2})^{-1}$
$u_r(A_1)$	2.0	1.3	2.0	1.3	$10^2 m^2s^{-2}MPa^{-1}(m^2s^{-2}MPa^{-1})^{-1}$
$u_r(A_2)$	0.99	2.3	0.96	2.2	$10^2 m^2s^{-2}MPa^{-2}(m^2s^{-2}MPa^{-2})^{-1}$

6.6.2 Adiabatic Coefficient Uncertainty.

Adiabatic coefficient uncertainty is calculated according equations 3.14 and 3.15. From that equation is easy to understand that it is necessary to obtain four other uncertainties previously, molar mass uncertainty, ideal gas constant uncertainty, temperature uncertainty and square speed of sound at zero pressure uncertainty.

$$\gamma^{pg} = \frac{MA_0}{RT} \tag{3.14}$$

$$u\left(\gamma^{pg}\right) = \sqrt{\left(\frac{\partial \gamma^{pg}}{\partial M}\right)^2 u^2(M) + \left(\frac{\partial \gamma^{pg}}{\partial R}\right)^2 u^2(R) + \left(\frac{\partial \gamma^{pg}}{\partial T}\right)^2 u^2(T) + \left(\frac{\partial \gamma^{pg}}{\partial A_0}\right)^2 u^2(A_0)}$$

$$u\left(\gamma^{pg}\right) = \sqrt{\left(\frac{u_0^2}{RT}\right)^2 u^2(M) + \left(\frac{Mu_0^2}{R^2T}\right)^2 u^2(R) + \left(\frac{Mu_0^2}{RT^2}\right)^2 u^2(T) + \left(\frac{M}{RT}\right)^2 u^2(A_0)} \tag{3.15}$$

Square speed of sound at zero pressure uncertainty, $u(A_0)$, was calculated previously, and ideal gas constant uncertainty was discussed in chapter 3. The other contributions calculations are detailed as follows.

6.6.2.1 *Molar Mass Uncertainty.*

Calculation of molar mass uncertainty was carried according equation 3.17. Data of molar mass uncertainty and composition uncertainties were taken from table 6.1. Molar mass standard uncertainty for the mixture x_{co} = 0.05 and x_{N2} = 0.95 is:

$$M = 28.01380\ g\cdot mol^{-1} \qquad u(M) = 5.6 \times 10^{-4}\ g\cdot mol^{-1}$$

Molar mass standard uncertainty for the mixture x_{co}=0.10 and x_{N2}=0.90 is:

$$M = 28.01360\ g\cdot mol^{-1} \qquad u(M) = 8.8 \times 10^{-4}\ g\cdot mol^{-1}$$

$$u(M) = \sqrt{\sum_i \left(\frac{\partial M}{\partial x_i}\right)^2 u^2(x_i) + \sum_i \left(\frac{\partial M}{\partial M_i}\right)^2 u^2(M_i)}$$

$$u(M) = \sqrt{\sum_i (M_i)^2 u^2(x_i) + \sum_i (x_i)^2 u^2(M_i)} \tag{3.17}$$

6.6.2.2 *Temperature Uncertainty.*

As it was explained in chapter 3 temperature has 3 different uncertainty sources. They are thermometer resolution, gradient across resonator and temperature measurement dispersion. The first one, as explained in chapter 3, is lower than 1mK. The gradient across the resonator is considered a rectangular probability distribution between the two measured temperatures across the resonator at the same time. The highest difference was taken as the uncertainty value. Gradient uncertainty values for both isotherms are in table 6.80. The temperature dispersion uncertainty was computed as the temperature measurements average standard deviation. Calculated values for both isotherms are in table 6.80. Overall temperature uncertainty was calculated from adding in terms of uncertainty the three values described in this section. Table 6.80 shows temperature overall uncertainty for both isotherms.

Table 6.80 *Temperature uncertainty contributions and final sum for both mixtures.*

	x_{CO} = 0.05		x_{CO} = 0.10	
	T = 273K	**T = 325K**	**T = 273K**	**T = 325K**
$u(T_{grad})$ (mK)	1.6	1.1	1.1	5.2
$u(T_{disp})$ (mK)	11	9.6	1.8	1.2
u(T) (mK)	**20**	**9.6**	**2.8**	**5.4**

Adiabatic coefficient for both mixtures at T = 273 K and T = 325 K and standard uncertainty may be calculated used this previous calculations. Their values are in table 6.81

Table 6.81 *Adiabatic coefficient values, standard uncertainty and relative standard uncertainty for both mixtures.*

x_{CO}	T (K)	γ^{pg}	$u(\gamma^{pg})$	$u_r(\gamma^{pg})\cdot 10^6$
0.05	**273**	1.40136	$3.6 \cdot 10^{-4}$	260
0.05	**325**	1.39970	$4.0 \cdot 10^{-4}$	280
0.10	**273**	1.40081	$3.3 \cdot 10^{-4}$	240
0.10	**325**	1.39994	$2.2 \cdot 10^{-4}$	290

6.6.3 Heat Capacities Uncertainties.

Heat capacities are calculated using adiabatic coefficient and Meyer's equation, as it was explained in chapter 3.

Calculation of isochoric heat capacities was done according equations 3.18 and 3.19. It was required ideal gas constant and adiabatic coefficient values and uncertainties. All data were calculated or detailed previously and results are displayed in table 6.82.

$$C_v = \frac{R}{\gamma^{pg} - 1} \tag{3.18}$$

$$u(C_v) = \sqrt{\left(\frac{\partial C_v}{\partial R}\right)^2 u^2(R) + \left(\frac{\partial C_v}{\partial \gamma^{pg}}\right)^2 u^2\left(\gamma^{pg}\right)}$$

$$u(C_v) = \sqrt{\left(\frac{1}{\gamma^{pg} - 1}\right)^2 u^2(R) + \left(\frac{R}{\left(\gamma^{pg} - 1\right)^2}\right)^2 u^2\left(\gamma^{pg}\right)} \tag{3.19}$$

Table 6.82*Isochoric heat capacity values, standard uncertainty and relative standard uncertainty at T = 273 K and T = 325 K.*

x_{CO}	T (K)	C_v ($J \cdot K^{-1} mol^{-1}$)	$u(C_v)$ ($J \cdot K^{-1} mol^{-1}$)	$u_r(C_v) \cdot 10^6$
0.05	**273K**	20.716	$1.9 \cdot 10^{-2}$	900
0.05	**325K**	20.802	$2.1 \cdot 10^{-2}$	990
0.10	**273K**	20.744	$1.7 \cdot 10^{-2}$	830
0.10	**325K**	20.789	$1.1 \cdot 10^{-2}$	1000

Isobaric and isochoric heat capacities are related to each other by the adiabatic coefficient. Hence until both of them and their uncertainties are not obtained it is not possible to calculate isobaric heat capacity and its uncertainty. These calculations were done using equations 3.20 and 3.21. Results are in table 6.83.

$$C_p = \gamma^{pg} C_v \tag{3.20}$$

$$u(C_p) = \sqrt{\left(\frac{\partial C_p}{\partial \gamma^{pg}}\right)^2 u^2\left(\gamma^{pg}\right) + \left(\frac{\partial C_p}{\partial C_v}\right)^2 u^2(C_v)}$$

$$u(C_p) = \sqrt{C_v^2 u^2\left(\gamma^{pg}\right) + \gamma^{pg^2} u^2(C_v)} \tag{3.21}$$

Table 6.83 *Isobaric heat capacity values and uncertainties at T=273K and T=325K for the mixture x_{CO}=0.05 and x_{N2}=0.95*

x_{CO}	T (K)	C_P ($J \cdot K^{-1} mol^{-1}$)	$u(C_P)$ ($J \cdot K^{-1} mol^{-1}$)	$u_r(C_P) \cdot 10^6$
0.05	**273**	29.030	$2.7 \cdot 10^{-2}$	930
0.05	**325**	29.116	$3.0 \cdot 10^{-2}$	1000
0.10	**273**	29.059	$2.5 \cdot 10^{-2}$	860
0.10	**325**	29.104	$1.6 \cdot 10^{-2}$	1100

6.6.4 Acoustic Virial Coefficients Uncertainty.

First and second acoustic virial coefficients are obtained according equations 3.24 and 3.25. The uncertainty calculations are detailed in equations 3.26 and 3.27. Those equations reveal the necessity of knowing temperature uncertainty (table 6.44) ideal gas constant uncertainty (chapter 3), and polynomial fitting parameters A_0, A_1 and A_2 uncertainties (tables 6.42 and 6.43). Uncertainty results for acoustic virial parameters are in tables 6.48 and 6.49.

$$\beta_a = \frac{A_1}{A_0} RT \tag{3.24}$$

$$\gamma_a = \frac{A_2}{A_0} (RT)^2 \tag{3.25}$$

$$u(\beta_a) = \sqrt{\left(\frac{\partial \beta_a}{\partial A_1}\right)^2 u^2(A_1) + \left(\frac{\partial \beta_a}{\partial A_0}\right)^2 u^2(A_0) + \left(\frac{\partial \beta_a}{\partial R}\right)^2 u^2(R) + \left(\frac{\partial \beta_a}{\partial T}\right)^2 u^2(T)}$$

$$u(\beta_a) = \sqrt{\left(\frac{RT}{A_0}\right)^2 u^2(A_1) + \left(\frac{A_1 RT}{A_0^2}\right)^2 u^2(A_0) + \left(\frac{A_1 T}{A_0}\right)^2 u^2(R) + \left(\frac{A_1 R}{A_0}\right)^2 u^2(T)} \tag{3.26}$$

$$u(\gamma_a) = \sqrt{\left(\frac{\partial \gamma_a}{\partial A_2}\right)^2 u^2(A_2) + \left(\frac{\partial \gamma_a}{\partial A_0}\right)^2 u^2(A_0) + \left(\frac{\partial \gamma_a}{\partial R}\right)^2 u^2(R) + \left(\frac{\partial \gamma_a}{\partial T}\right)^2 u^2(T)}$$

$$u(\gamma_a) = \sqrt{\left(\frac{(RT)^2}{A_0}\right)^2 u^2(A_2) + \left(\frac{A_2 (RT)^2}{A_0^2}\right)^2 u^2(A_0) + \left(\frac{2A_1 RT^2}{A_0}\right)^2 u^2(R) + \left(\frac{2A_1 R^2 T}{A_0}\right)^2 u^2(T)} \tag{3.27}$$

Table 6.84 *Second acoustic virial parameter values and uncertainties at T=273K and T=325K for the mixture x_{CO}=0.05 and x_{N2}=0.95.*

x_{CO}	T (K)	β_a ($m^3 \cdot mol^{-1}$)	$u(\beta_a)$ ($m^3 \cdot mol^{-1}$)	$u_r(\beta_a) \cdot 10^2$
0.05	**273**	$1.223 \cdot 10^{-5}$	$2.4 \cdot 10^{-7}$	2.0
0.05	**325**	$2.672 \cdot 10^{-5}$	$3.5 \cdot 10^{-7}$	1.3
0.10	**273**	$1.201 \cdot 10^{-5}$	$2.4 \cdot 10^{-7}$	2.0
0.10	**325**	$2.449 \cdot 10^{-5}$	$2.4 \cdot 10^{-7}$	1.3

Table 6.85 *Third acoustic virial parameter values and uncertainties at T=273K and T=325K for the mixture x_{CO}=0.05 and x_{N2}=0.95.*

x_{CO}	T (K)	γ_a ($m^6 \cdot mo^{l-2}$)	$u(\gamma_a)$ ($m^6 \cdot mo^{l-2}$)	$u_r(\gamma_a) \cdot 10^2$
0.05	**273**	$5.129 \cdot 10^{-9}$	$5.1 \cdot 10^{-11}$	0.99
0.05	**325**	$4.077 \cdot 10^{-9}$	$9.2 \cdot 10^{-11}$	2.3
0.10	**273**	$5.177 \cdot 10^{-9}$	$5.0 \cdot 10^{-11}$	0.96
0.10	**325**	$4.121 \cdot 10^{-9}$	$7.2 \cdot 10^{-11}$	2.2

6.7 DISCUSSION

Speed of sound was measured for two different mixtures (0.05 CO + 0.95 N_2 and 0.10 CO + 0.90 N_2) at two different temperatures, T = 273.16 K and T =325 K. Results of both mixtures at both temperatures were compared to data obtained according to GERG-2008 equation of state.

Speed of sound relative standard uncertainty for both mixtures is about $\pm 150 \cdot 10^{-6}$ $m \cdot s^{-1}/m \cdot s^{-1}$ at both temperatures.

Other properties like perfect gas adiabatic coefficient, ideal heat capacities and acoustic virial coefficients were computed using speed of sound data. Relative standard uncertainties of these properties were obtained: lower than $\pm 300 \cdot 10^{-6}$ for adiabatic coefficient, about $\pm 1000 \cdot 10^{-6}$ $J \cdot mol^{-1}K^{-1}$/ $J \cdot mol^{-1}K^{-1}$ for ideal heat capacities and lower than 2.3% for the acoustic virial parameters.

The standard deviation of the equation 6.1 is always lower than 25 m^2s^{-2}. This value is lower than the parameters uncertainties for both mixtures at all temperatures.

All thermodynamic properties measured were compared to predictions according GERG-2008 equation of state. Speed of sound in the (0.05 CO + 0.95 N_2) is underestimated by GERG-2008 EoS at T = 325 K, but at T = 273.16 K deviations are negative above 5 MPa and positive below 5 MPa. The speed of sound of the second mixture (0.10 CO + 0.90 N_2) is usually overestimated by GERG-2008. However, all these relative deviations are always within $\pm 200\ 10^{-6}$ $m \cdot s^{-1}/m \cdot s^{-1}$. Adiabatic coefficient deviation is lower than 0.05% for both mixtures at any temperature. The largest deviation in heat capacities comparison was 0.28%. Acoustic virial coefficients obtained from GERG-2008 EoS differ from the experimental values in more than 10%. These deviations are so high because some software malfunction in REFPROP 9.0 [1, 2] when implement GERG-2008 EoS.

The results of speed of sound obtained for the two mixtures are very similar at both temperatures. There is not a significant variation of speed of sound in this range of concentration. In the other hand, variations of temperature induce significant variations in speed of sound (around 9%).

Adiabatic coefficient and heat capacities do not suffer a significant variation with temperature either. These parameters are obtained by using speed of sound data, therefore variation with composition or temperature must be in agreement.

Acoustic virial coefficients do not vary significantly either composition or temperature. The small changes suffered are always inside the uncertainty limits for both acoustic virial coefficients.

Molar mass of both mixtures are very similar. This might be one of the reasons all these parameters do not suffer significant variations when molar composition changes.

REFERENCES

1. Lemmon, E.W., Huber, M.L., McLinden, M.O. NIST Standard Reference Database 23: Reference Fluid Thermodynamic and Transport Properties-REFPROP, Version 9.1, National Institute of Standards and Technology, Standard Reference Data Program, Gaithersburg, 2013.

2. Kunz, O., and Wagner, W. The GERG-2008 Wide-Range Equation of State for Natural Gases and Other Mixtures: An Expansion of GERG-2004. Journal of Chemical & Engineering Data 57, 3032-3091.

3. Tegeler, C., Span, R., and Wagner, W. (1999) A New Equation of State for Argon Covering the Fluid Region for Temperatures From the Melting Line to 700 K at Pressures up to 1000 MPa. Journal of Physical and Chemical Reference Data 28, 779-850.

Chapter 7

MEASUREMENTS IN A SYNTHETIC COAL MINE METHANE GAS MIXTURE

7.1 INTRODUCTION

Coal mine methane (CMM) is an unconventional energy gas, which has gained significance lately. In order to improve efficiency in any process where coal mine methane is involved, it is required to know accurate data of its equation of state and at least one heat capacity. And they are provided by this study.

A synthetic coal mine methane mixture was prepared gravimetrically by the Bundesanstalt für Material forschung und prüfung (BAM), which composition is detailed in table 7.1

Table 7.1 *Molar composition (mole fraction) of the synthetic CMM mixture supplied by BAM laboratory, relative extended uncertainty (k = 2) and purity of the component.*

Component	Concentration (x_i)	U(x_i)	Specified purity of the component
Methane	0.65401	0.008	99.999 vol.-%
Nitrogen	0.16400	0.011	99.9995 mol-%
Oxygen	0.00500	0.026	99.9995 vol.-%
Carbon dioxide	0.16700	0.010	99.9995 vol.-%
Ethane	0.00900	0.053	99.990 vol.-%
Propane	0.00080	0.052	99.990 vol.-%
i-Butane	0.00010	0.052	99.95 vol.-%
n-Butane	0.00006	0.053	99.98 vol.-%
i-Pentane	0.00002	0.200	>99.7%(GC)
n-Pentane	0.00001	0.200	>99.8% (GC)

Coal mine methane was storage in cylinder at p = 8 bar. The amount of gas and pressure provided by the cylinder allowed measurements of two different isotherms at T = 250 K and T = 273 K. The results of the measurements are reported in the following sections, the details of the experimental procedure and the calculations are the same that those given in the previous chapter for the binary mixtures.

7.2 EXPERIMENTAL MEASUREMENTS AT T=250K.

The isotherm at 250K was measured in the pressure range from 0.1MPa up to 10MPa.

Speed of sound is not measured directly. It is necessary to measure acoustic frequency of resonance first, and calculate speed of sound as it was explained in chapter 3. Four acoustic modes were measured at each pressure. Acoustic modes

(0,2), (0,3), (0,4) and (0,5) were under study. Their frequency of resonance and half-width of the peaks were measured and used to calculate speed of sound. Frequencies of resonance at p = 7.93 MPa are visible in table 7.2 as an example.

Table 7.2 *Frequency of resonance and half-width of resonance peaks for acoustic modes (0,2) to (0,5) at p = 10.01 MPa and T = 250K for the synthetic CMM mixture.*

Mode	*f*(Hz)	*g*(Hz)
(0,2)	7024.08	1.017
(0,3)	12076.13	1.289
(0,4)	17044.33	1.885
(0,5)	21983.42	2.034

The frequency of resonance of all modes changes with pressure, these variations are in proportion of the initial frequency of resonance, therefore acoustic mode of resonance was selected as a representative mode to explain pressure dependence of the parameters computed in this chapter. Figure 7.1 shows only mode (0,2) frequencies from p = 0.1 MPa up to p = 10.01 MPa

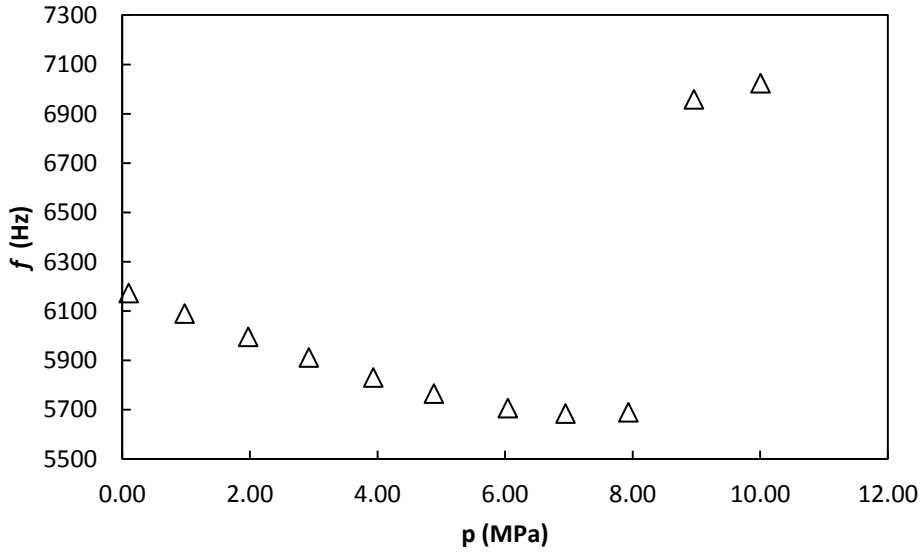

Figure 8.1 *Frequency of resonance for acoustic mode (0,2) at T = 250 K as function of pressure for the synthetic CMM mixture.*

Half-width of measurements presented in figure 7.1 are detailed in figure 7.2. In both figures it is obvious that the two measurements at the highest pressures are not in good agreement with the rest of the data. This deviation is produced by condensation of gas on resonator internal surface, condensation changes gas

composition and resonating volume. Therefore those points were measured but not taken into account for farther calculations.

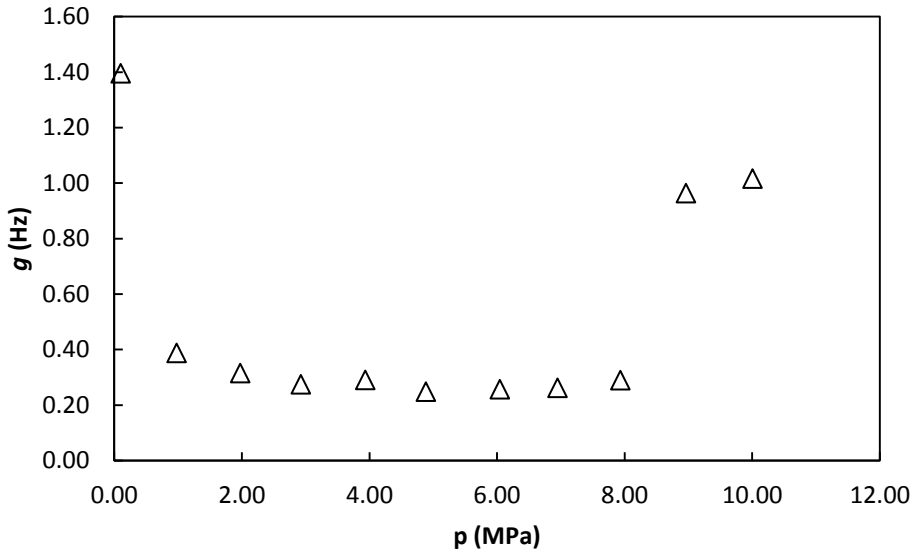

Figure 7.2 *Half-width of resonance peaks for acoustic mode (0,2) at T = 250 K as function of pressure for the synthetic CMM mixture.*

7.2.1 Frequency corrections.

As it was done in previous chapters (4 to 6), it is necessary to apply corrections to measured frequencies of resonance. These corrections are applied to lead measured frequency of resonance to the ideal frequency of resonance which is the data required to obtain speed of sound.

Contributions to this correction are detailed in the following sections.

7.2.1.1 *Thermal Boundary Layer Correction.*

Thermal boundary layer correction is due to temperature difference between shell internal surface, and the bulk of the fluid.

It is necessary to calculate some other parameters before computing the thermal boundary layer correction. First of this parameters is thermal penetration length (δ_{th}). This parameter depends on frequency of resonance. This means if 4 acoustic modes are measured at each pressure 4 different thermal penetration lengths must be calculated. Table 7.3 shows this parameter for each mode at the highest pressure considered p = 7.93 MPa, last two pressure points are not taken into account.

Table 7.3 *Thermal penetration length for acoustic modes (0,2) to (0,5) at p = 7.93 MPa and T = 250K for the synthetic CMM mixture.*

Mode	δ_{th}(m)
(0,2)	2.50 x10^{-6}
(0,3)	1.91 x10^{-6}
(0,4)	1.61 x10^{-6}
(0,5)	1.42 x10^{-6}

Thermal penetration length is dependent on some thermodynamic properties which are pressure dependent; therefore it changes whit pressure as well, as it can be seen in figure 7.3

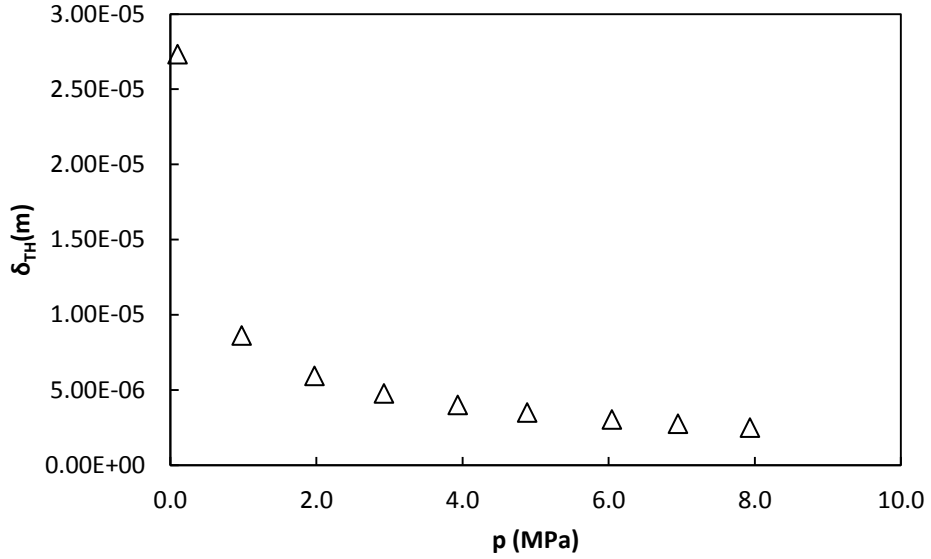

Figure 7.3 *Thermal penetration length for acoustic mode (0,2) at T = 250 K as function of pressure for the synthetic CMM mixture.*

Thermal accommodation length is another required parameter to calculate thermal boundary layer frequency correction. It is not dependant on frequency but depends on pressure, as figure 7.4 shows

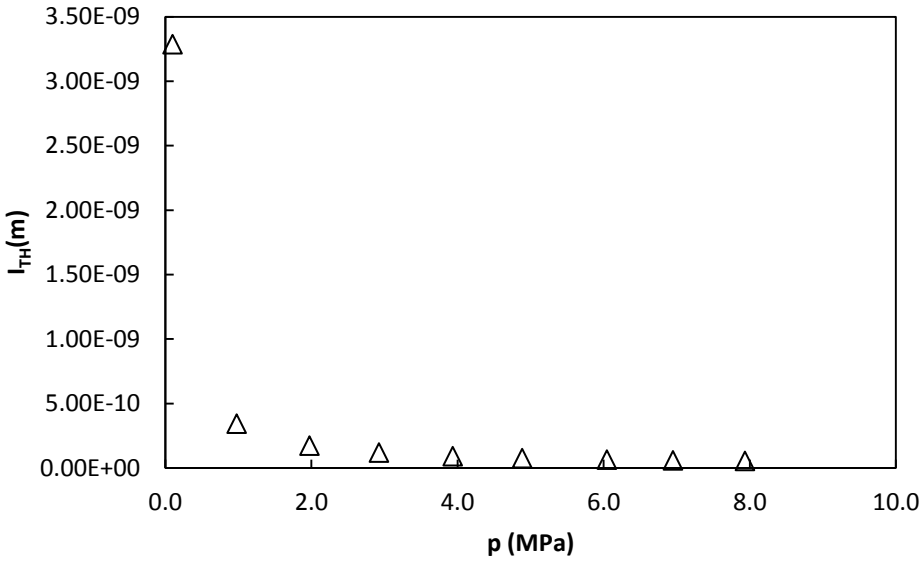

Figure 7.4 *Thermal accommodation length at T = 250 K as function of pressure for the synthetic CMM mixture.*

Thermal penetration length in shell internal surface is the last parameter required before computing the frequency correction. Just like thermal penetration length it changes for pressure and fore mode what is described thanks to table 7.4 and figure 7.5.

Table 7.4 *Shell thermal penetration length for acoustic modes (0,2) to (0,5) at p = 7.93 MPa and T = 250 K for the synthetic CMM mixture.*

Mode	δ_{shell}(m)
(0,2)	1.50×10^{-5}
(0,3)	1.15×10^{-6}
(0,4)	9.65×10^{-6}
(0,5)	8.50×10^{-6}

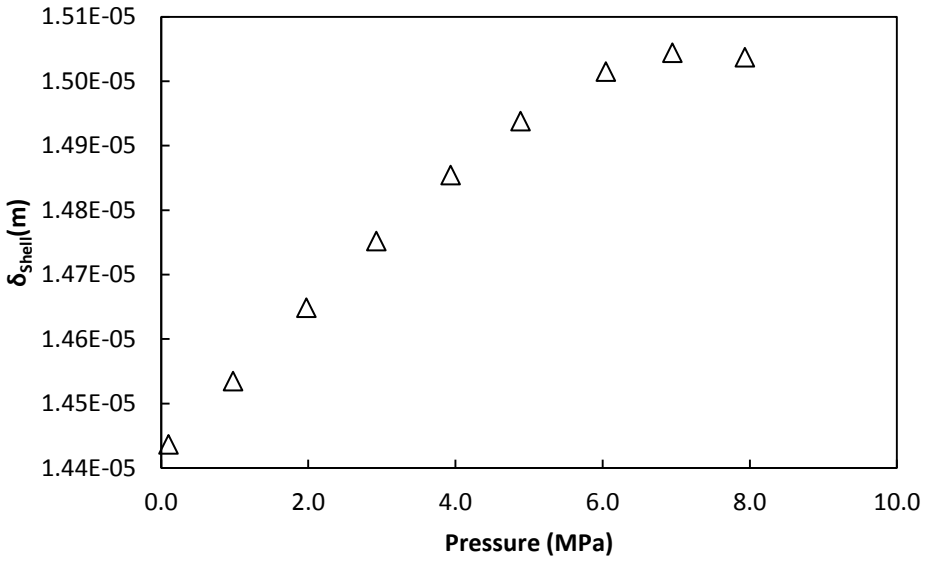

Figure 7.5 *Shell thermal penetration length for acoustic mode (0,2) at T = 250 K as function of pressure for the synthetic CMM mixture.*

Thermal boundary layer frequency correction and peaks half-width contribution can be calculated using parameters detailed previously. It is obvious that frequency correction and half-width contribution will change for mode and pressure as the parameters used to obtain them change as well. Different corrections and half-width contributions for each mode are shown in table 7.5, and changes along pressure range are detailed in figures 7.6 and 7.7.

Table 7.5 *Thermal boundary layer frequency corrections and half-width contribution for acoustic modes (0,2) to (0,5) at p = 7.93 MPa and T = 250 K for thesynthetic CMM mixture.*

Mode	Δf_{th} (Hz)	g_{th}(Hz)
(0,2)	-0.190	0.196
(0,3)	-0.249	0.257
(0,4)	-0.296	0.305
(0,5)	-0.336	0.346

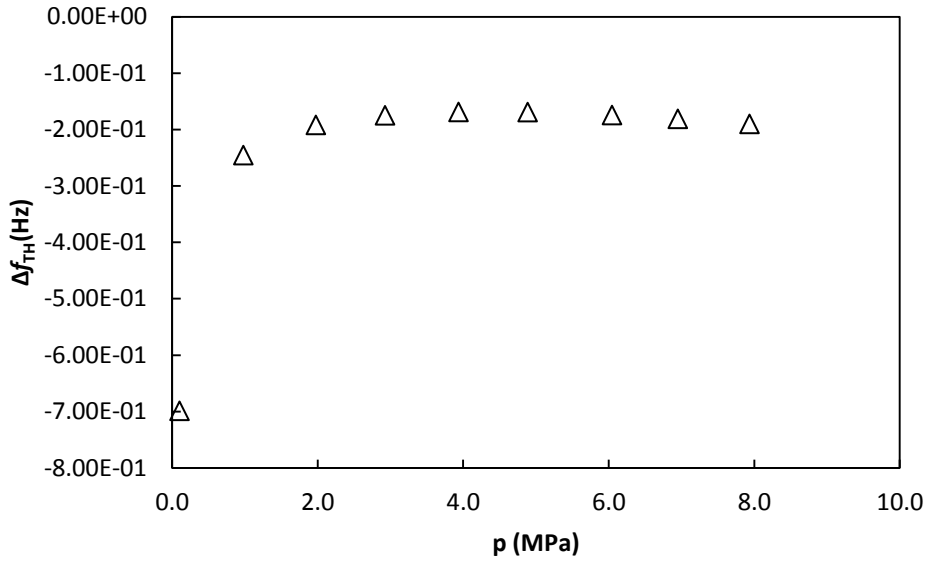

Figure 7.6 *Thermal boundary layer frequency correction for acoustic mode (0,2) at T = 250 K as function of pressure for the synthetic CMM mixture.*

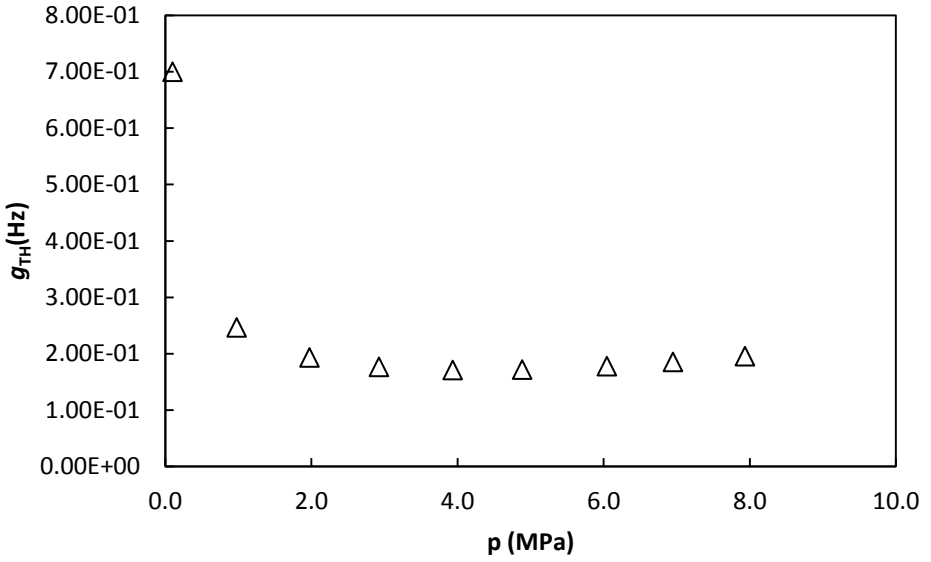

Figure 7.7 *Thermal boundary layer half-width contribution for acoustic mode (0,2) at T = 250 K as function of pressure for the synthetic CMM mixture.*

7.2.1.2 *Bulk Viscosity Contribution.*

This is not a correction to the frequency, but a contribution to the half-width of resonance peaks. However, it is necessary calculate it because this parameter will be used to determinate if acoustic mode is reliable to obtain speed of sound or if it must be dismissed. This is explained latter when discussing excess half-width in section 7.2.2

Calculation of the bulk viscosity contribution to peaks half-width needs to compute one more parameter, the viscous penetration length. It behaves like thermal penetration length, viscous penetration length changes for each resonance mode and for pressure, table 7.6 and figure 7.8 show this behaviour.

Table 7.6 *Viscous penetration length for acoustic modes (0,2) to (0,5) at p = 7.93 MPa and T = 250 K for the synthetic CMM mixture.*

Mode	δ_v(m)
(0,2)	2.61 x10^{-6}
(0,3)	1.99 x10^{-6}
(0,4)	1.67 x10^{-6}
(0,5)	1.47 x10^{-6}

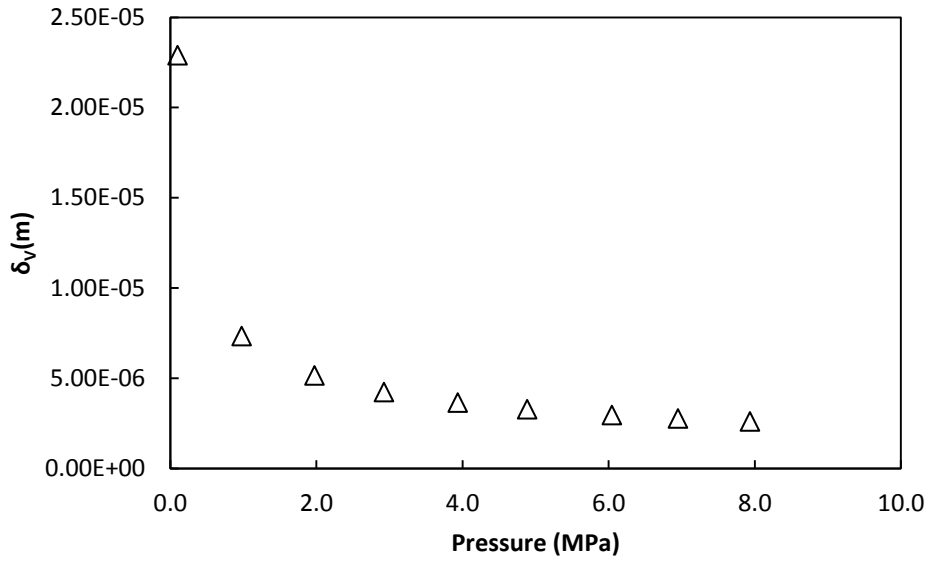

Figure 7.8 *Viscous penetration length for acoustic mode (0,2) at T = 250 K as function of pressure for the synthetic CMM mixture.*

Half-width contribution to resonance peaks depends on pressure and frequency as well as the parameters required for its calculation. Dependence on pressure is detailed in figure 7.9 and table 7.7 represnts variation for each mode at p = 793 MPa.

Figure 7.7 *Bulk viscosity half-width contribution for acoustic modes (0,2) to (0,5) at p = 7.93 MPa and T = 250 K for the synthetic CMM mixture.*

Mode	g_b(Hz)
(0,2)	$2.825 \cdot 10^{-4}$
(0,3)	$8.350 \cdot 10^{-4}$
(0,4)	$16.638 \cdot 10^{-4}$
(0,5)	$27.689 \cdot 10^{-4}$

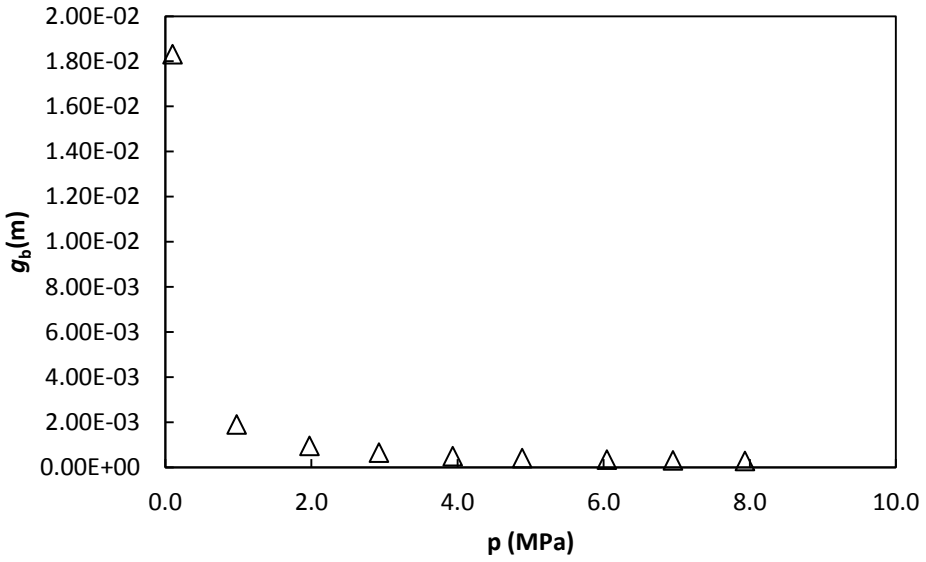

Figure 7.9 *Bulk viscosity half-width contribution for acoustic mode (0,2) at T = 250 K as function of pressure for the synthetic CMM mixture.*

7.2.1.3 *Shell Motion Correction.*

Coupling vibration between gas and shell induce frequency shifts. Therefore it is necessary to quantify this change so it can be corrected.

Breath frequency is required for this calculation, its value depends only on the resonator configuration, it was obtained in chapter 4:

$$f_{breath}=26488Hz$$

This correction changes with frequency and pressure, an example of those changes can be seen in table 7.8 for frequency and figure 7.10 for pressure.

Table 7.8 *Shell motion frequency correction for acoustic modes (0,2) to (0,5) at p = 7.93 MPa and T = 250 K for the synthetic CMM mixture.*

Mode	Δf_{shell} (Hz)
(0,2)	-0.079
(0,3)	-0.144
(0,4)	-0.221
(0,5)	-0.328

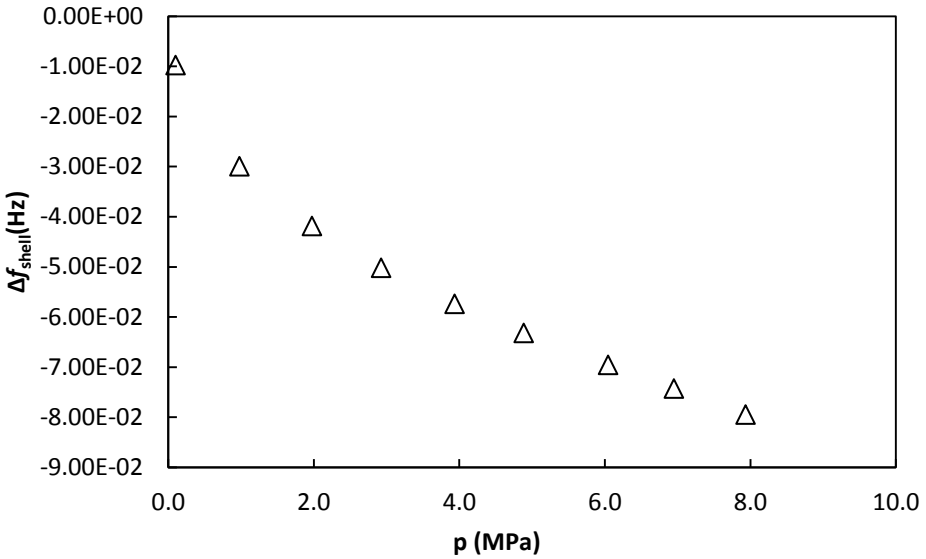

Figure 7.10 *Shell motion frequency correction for acoustic mode (0,2) at T = 250 K as function of pressure for the synthetic CMM mixture.*

There is not half-width contribution to resonance peaks due to shell motion.

7.2.1.4 *Tubes and Holes Correction.*

Pipes connected to resonance cavity changes frequency of resonance, this change depends on pipe diameter and length, frequency and pressure. Pipes length and diameter was detailed in chapter 6. Dependency on pipes dimensions, pressure and frequency is caused by the parameters required for its calculation. These parameters (Kirchhoff-Helmholtz absorption coefficient, propagation constant and specific acoustic admittance) are dependent on these properties too. The effective absorption coefficient is the first parameter obtained, table 7.9 and figure 7.11 show variations with frequency and pressure respectively.

Table 7.9 *Kirchhoff-Helmholtz absorption coefficient for tubes 1 and 2 for acoustic modes (0,2) to (0,5) at T = 250 Kand p = 7.93 MPa for the synthetic CMM mixture.*

Mode	α_{KH1} (m^{-1})	α_{KH2} (m^{-1})
(0,2)	0.597	0.298
(0,3)	0.783	0.391
(0,4)	0.930	0.465
(0,5)	1.056	0.528

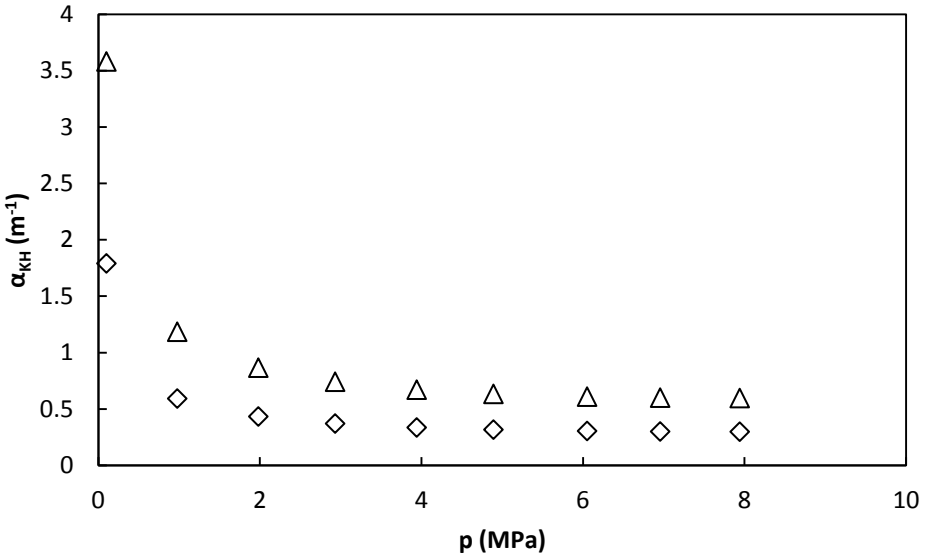

Figure 7.11 *Kirchhoff-Helmholtz absorption coefficient for tubes 1 (Δ) and 2 (◊) for acoustic mode (0,2) at T = 250 K as function of pressure for the synthetic CMM mixture.*

Next required parameter, propagation constant, depends on the effective absorption coefficient; therefore it changes with pressure and modes as it can be appreciated in table 7.10 and figure 7.12.

Table 8.11 *Propagation constant for tubes 1and 2 for acoustic modes (0,2) to (0,5) at p = 7.93 MPa and T = 250 K for the synthetic CMM mixture*

Mode	k_{KH1}	K_{KH2}
(0,2)	112.615-0.597i	112.316-0.298i
(0,3)	193.363-0.782i	192.972-0.391i
(0,4)	272.749-0.930i	272.284-0.465i
(0,5)	351.704-1.056i	351.176-0.528i

Propagation coefficient is an imaginary parameter; it is not possible to represent imaginary data in graphics, therefore figure 7.12 shows only the real component. Imaginary part is not detailed because it is the effective absorption coefficient with opposite sign.

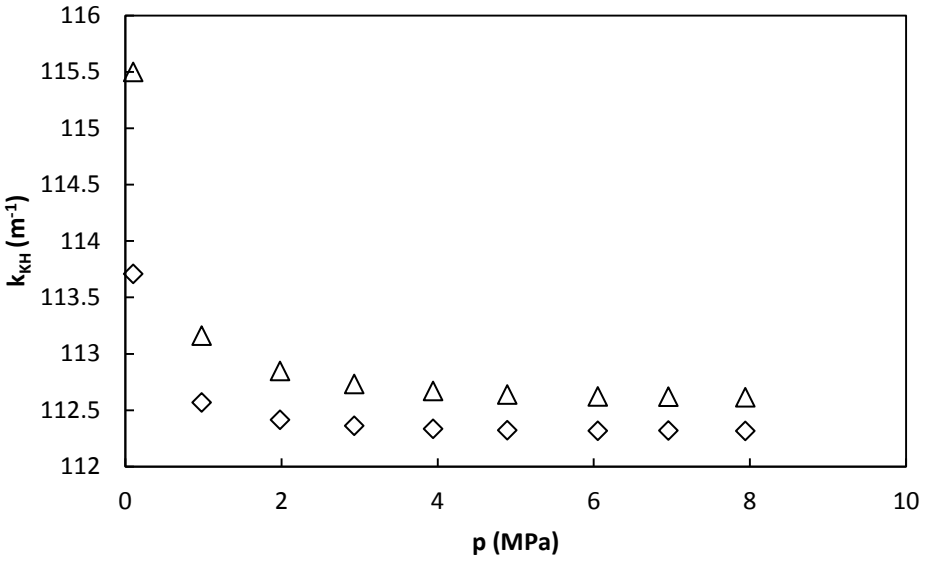

Figure 7.12 *Propagation constant real component for tubes 1 (Δ) and 2 (◊) for acoustic mode (0,2) at T = 250 K as function of pressure for the synthetic CMM mixture.*

The last parameter required for calculating tubes frequency correction and half-width contribution is specific acoustic admittance of the openings. As it needs of propagation coefficient to be calculated it is dependent on frequency and pressure as well. Specific acoustic admittance of openings is also an imaginary magnitude so imaginary and real components are graphed separately in figures 7.13 and 7.14 to present variation with pressure. Frequency variations are in table 7.11

Table 7.11 *Specific acoustic admittance of opening for pipes 1and 2 for acoustic modes (0,2) to (0,5) at p = 7.93 MPa and T = 250 K for the synthetic CMM mixture.*

Mode	y_{o1}	y_{o2}
(0,2)	0.134+2.167i	0.081+2.139i
(0,3)	0.139+1.820i	0.105+1.83i
(0,4)	0.118+1.394i	0.112+1.44i
(0,5)	0.102+1.060i	0.117+1.136i

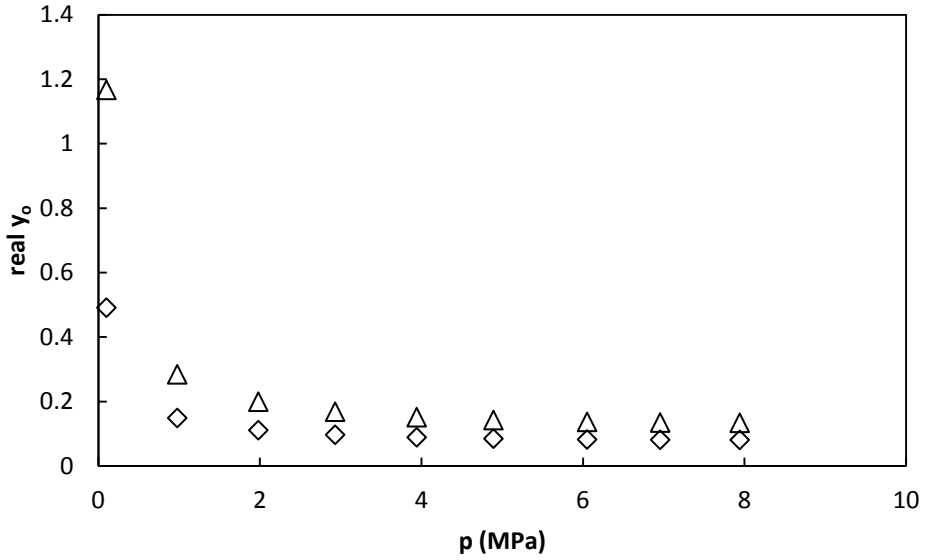

Figure 7.13 *Specific acoustic admittance of the opening real component for tubes 1 (Δ) and 2 (◊) for acoustic mode (0,2) at T = 250 K as function of pressure for the synthetic CMM mixture.*

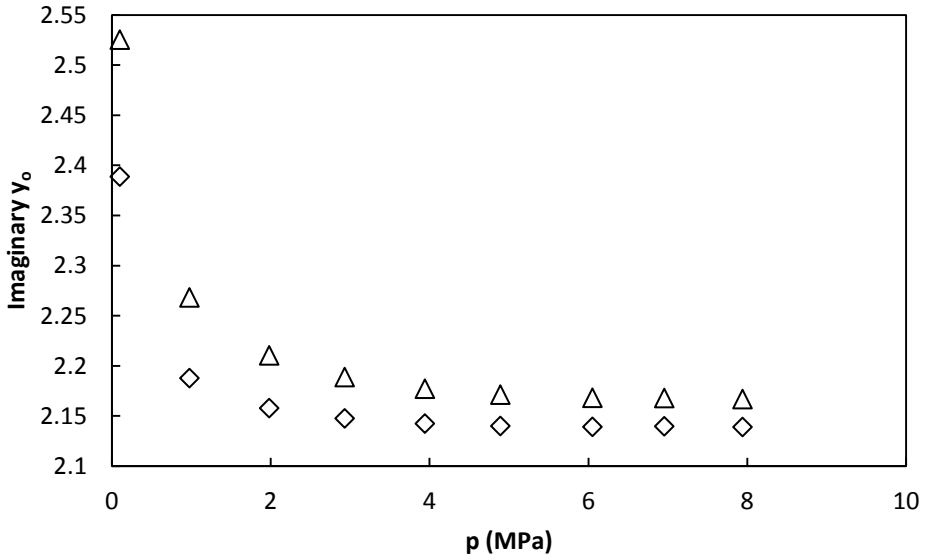

Figure 7.14 *Specific acoustic admittance of the opening imaginary component for tubes 1 (Δ) and 2 (◊) for acoustic mode (0,2) at T = 250 K as function of pressure for the synthetic CMM mixture.*

The tube correction and half width contribution is directly calculated from the specific acoustic admittance of each pipe and add them together. This means the correction and contribution depend on frequency and pressure, in similar way specific admittance does. It can be seen thanks to table 7.12 and figures 7.15 and 7.16.

Table 7.12 *Tubes frequency correction and half-width contribution for pipes 1and 2 for acoustic modes (0,2) to (0,5) at p = 7.93 MPa and T = 250 K for the synthetic CMM mixture.*

Mode	Δf_{Tube} (Hz)	g_{tube} (Hz)
(0,2)	-0.220	0.129
(0,3)	-0.156	0.111
(0,4)	-0.092	0.084
(0,5)	-0.053	0.064

Figure 7.15 *Tubes frequency correction for acoustic mode (0,2) at T = 250 K as function of pressure for the synthetic CMM mixture.*

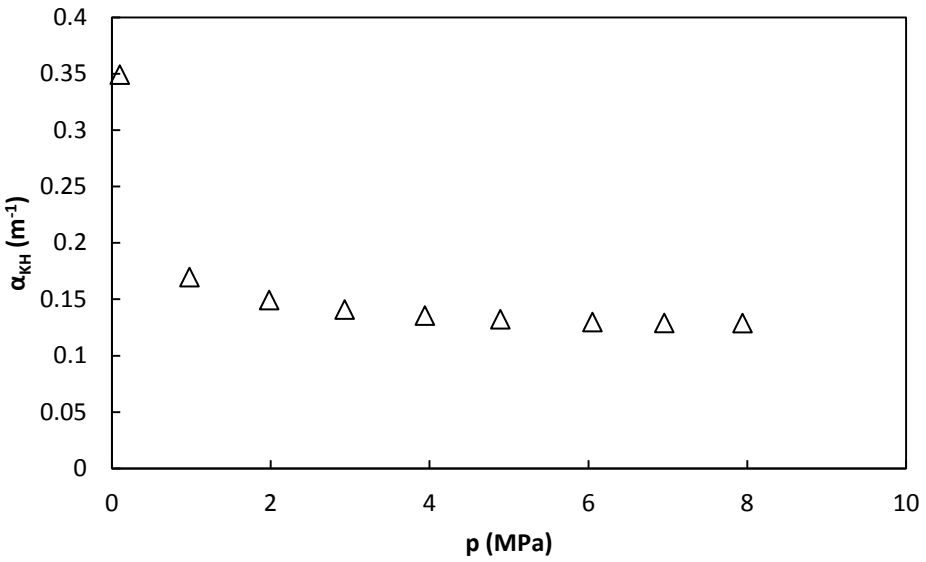

Figure 7.16 *Tubes half- width contribution for acoustic mode (0,2) at T = 250 K as function of pressure for the synthetic CMM mixture.*

7.2.2 Speed of Sound Determination.

Experimental and calculated half-width of resonance peaks are compared in the pressure range in order to determinate which modes are reliable for speed of sound determination. The excess half-width must decrease and it has to reach values close to zero, otherwise the acoustic mode will not be considered to obtain speed of sound, which is calculated as the average of the speed of sound obtained from each acoustic mode.

This comparison is presented in figure 7.17

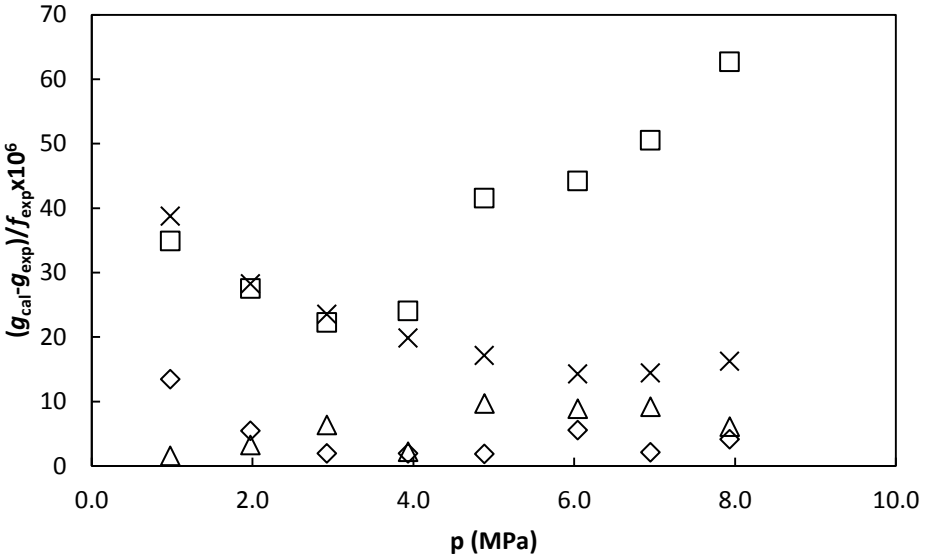

Figure 7.17 *Excess half-width for acoustic modes (0,2) (Δ),(0,3) (◊),(0,4) (x) and (0,5) (□)at T = 250 K as function of pressure for the synthetic CMM mixture.*

This analysis shows excess half-widths lower than 50 parts per million over the resonance frequency for any mode so it was concluded that all four modes can be used to calculate speed of sound.

Speed of sound calculated from experimental data was compared to speed of sound according GERG-2008 equation of state. The results of that comparison are shown in table 7.13.

Table 7.13 *Speed of sound according to developed model, and according to GERG-2008 equation of state and a comparison between them at T = 250 K for the synthetic CMM mixture.*

P(Mpa)	T (K)	u_{exp} (m·s^{-1})	u_{GERG} (m·s^{-1})	$(u_{exp} - u_{GERG})/u_{GERG}x10^6$
7.93	249.8875	319.541	319.21	1040
6.95	249.9286	319.214	318.87	1080
6.04	249.9232	320.459	320.10	1120
4.88	249.9733	323.723	323.41	967
3.93	249.9889	327.365	327.08	872
2.92	250.0115	331.905	331.67	710
1.97	249.9965	336.616	336.41	611
0.98	250.0106	341.901	341.73	500
0.10	250.0019	346.600	346.56	115

Speed of sound experimental data versus pressure are detailed in figure 7.18

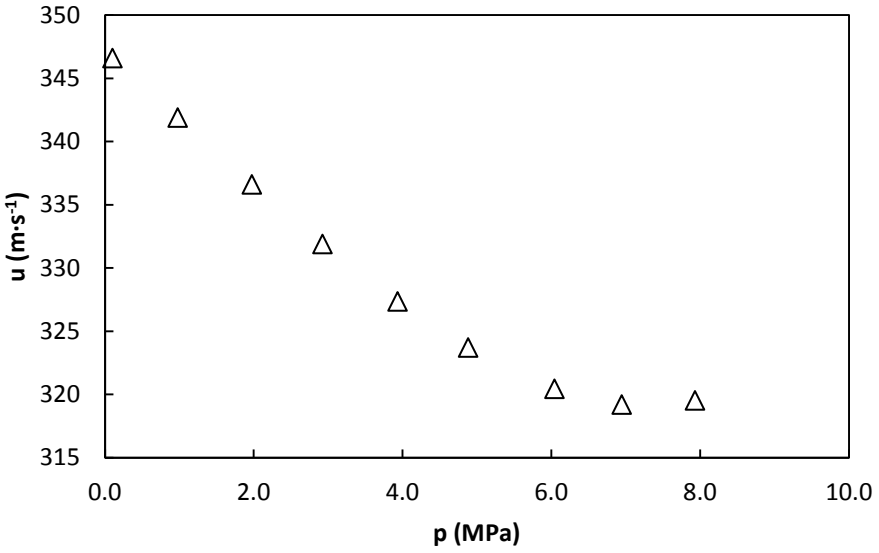

Figure 7.18 *Experimental speed of sound at T = 250 K as function of pressure for the synthetic CMM mixture.*

The acoustic virial equation of state uses square speed of sound as function of pressure, equation 2.6-b.Figure 7.19 shows experimental data and developed acoustic virial model.

$$u^2 = \frac{\gamma^{pg} RT}{M} + A_1 p + A_2 p^2 \qquad \text{(2.6-b)}$$

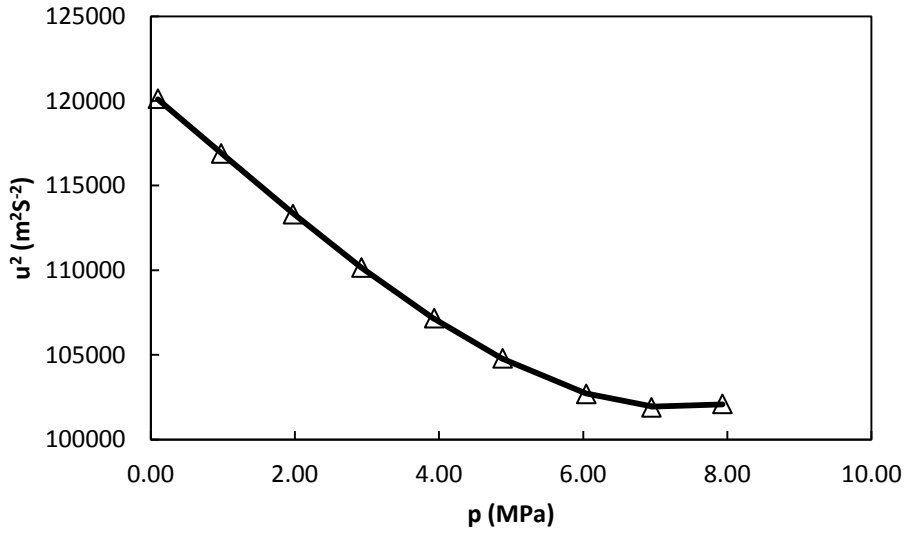

Figure 7.19 *Experimental square speed of sound data (Δ) and developed acoustic virial model (—) at T = 250 K as function of pressure for the synthetic CMM mixture.*

The fitting was done using three parameters; those are detailed in table 7.14

Table 7.14 *Experimental acoustic virial equation of state parameters at T = 250 K for the synthetic CMM mixture.*

A_0 (m^2s^{-2})	A_1 ($m^2s^{-2}\cdot MPa^{-1}$)	A_2 ($m^2s^{-2}\cdot MPa^{-2}$)	σ (m^2s^{-2})
121,748	-4970	309.5	290

Experimental model was compared to GERG-2008 equation of state in terms of speed of sound. Table 7.15 shows the results of this comparison.

Table 7.15 *Speed of sound according to developed model, and according to GERG-2008 equation of state and a comparison between them at T=250K for the synthetic CMM mixture.*

P(Mpa)	T (K)	u_{model} ($m\cdot s^{-1}$)	u_{GERG} ($m\cdot s^{-1}$)	$(u_{exp} - u_{GERG})/u_{GERG}x10^6$
7.93	249.8875	319.47	319.21	-463
6.95	249.9286	319.29	318.87	2370
6.04	249.9232	320.50	320.10	2700
4.88	249.9733	323.65	323.41	1280
3.93	249.9889	327.28	327.08	29
2.92	250.0115	331.89	331.67	-652
1.97	249.9965	336.68	336.41	-129
0.98	250.0106	341.93	341.73	1740
0.10	250.0019	346.55	346.56	4760

Once experimental and model are compared and probed to be in good agreement with theoretical data, the thermodynamic parameters isochoric heat capacity (C_v^{pg}), isobaric heat capacity (C_p^{pg}), adiabatic coefficient as perfect gas (γ^{pg}), first acoustic virial coefficient (β_a) and second acoustic virial coefficient (γ_a) are calculated and compared to those from GERG-2008 equation of state [1-2].

Table 7.16 *Comparison between the calculated values of the isochoric and isobaric heat capacities (C_v^{pg} and C_p^{pg}) and the adiabatic coefficient (γ^{pg}) at zero pressure and the acoustic virial coefficients (β_a, γ_a) obtained from equation 2.6-b and those calculated using GERG-2008 EoS for the synthetic CMM mixture.*

	Eq 2.6-b	GERG-2008	(eq 2.6-b - GERG)/GERGx10^2
γ^{pg}	1.3412	1.3283	0.965
C_v ($kJ\cdot mol^{-1}K^{-1}$)	24.3655	25.328	3.95
C_p ($kJ\cdot mol^{-1}K^{-1}$)	32.6800	33.642	2.94
β_a ($m^3\cdot mol^{-1}$)	-8.4438 x10^{-5}	-6.7083 x10^{-5}	-20.9
γ_a ($m^6\cdot mol^{-2}$)	1.0980x10^{-8}	1.1920 x10^{-2}	
u_0 ($m\cdot s^{-1}$)	348.925	347.13	0.517

Deviation from GERG-2008 equation of state for the second acoustic virial coefficient was not calculated because as table 7.16 shows GERG value is 10^6 larger, this must be a mistake on the software used for this calculation [1-2]. However, programmers were aware of this mistake. This mistake is only seen when GERG-2008 is used for other computational package available in this software values are in a better agreement.

7.3 EXPERIMENTAL MEASUREMENTS AT T = 273 K.

Procedure of measurement and calculation of the required parameters are already explained in this chapter in sections 7.1 and 7.2.

Section 7.3 shows only results and reliable information as an example of all the procedure performed using the coal mine methane at T = 273 K

The remaining gas in the bottle was enough to measure one more isotherm at 273.16K, which higher pressure was p = 5.51 MPa.

Table 7.17 *Frequency of resonance and half-width of resonance peaks of acoustic modes (0,2) to (0,5) at T = 273 K and p = 5.51 MPa for the synthetic CMM mixture.*

Mode	*f*(Hz)	*g*(Hz)
(0,2)	6154.95	0.261
(0,3)	10581.68	0.450
(0,4)	14935.82	0.613
(0,5)	19267.66	1.290

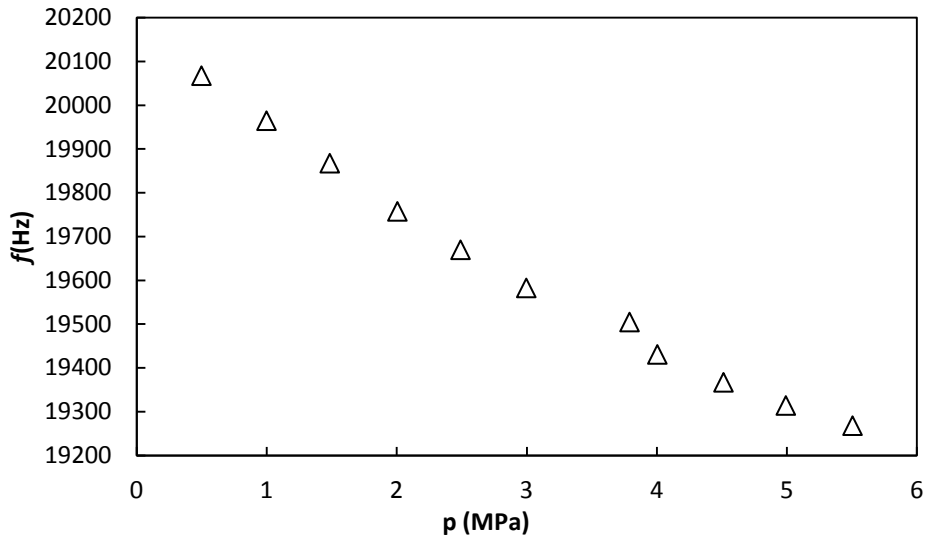

Figure 7.20 *Frequency of resonance for acoustic mode (0,2) at T = 273 K as function of pressure for the synthetic CMM mixture.*

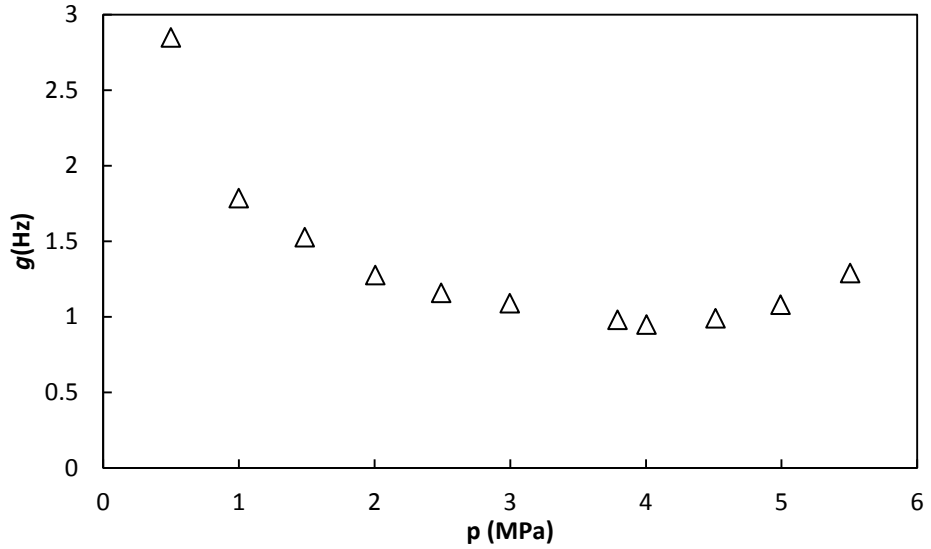

Figure 8.21 *Half-width of resonance peaks for acoustic mode (0,2) at T = 273 K as function of pressure for the synthetic CMM mixture.*

7.3.1 Frequency corrections

7.3.1.1 *Thermal boundary layer correction.*

Table 7.18 *Thermal penetration length for acoustic modes (0,2) to (0,5) at T = 273 K and p = 5.51 MPa for the synthetic CMM mixture.*

Mode	δ_{th} (m)
(0,2)	3.63×10^{-6}
(0,3)	2.77×10^{-6}
(0,4)	2.33×10^{-6}
(0,5)	2.05×10^{-6}

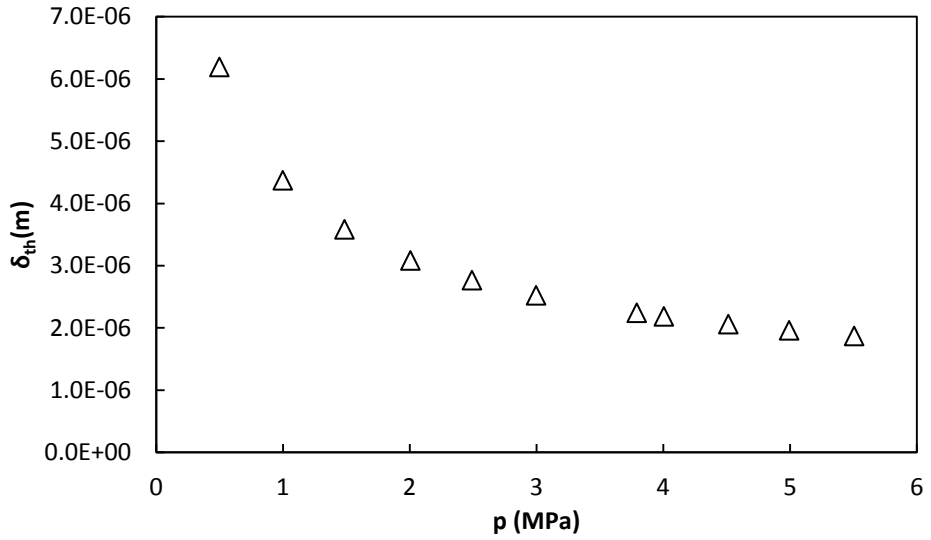

Figure 7.22 *Thermal penetration length for acoustic mode (0,2) at T = 273 K as function of pressure for the synthetic CMM mixture.*

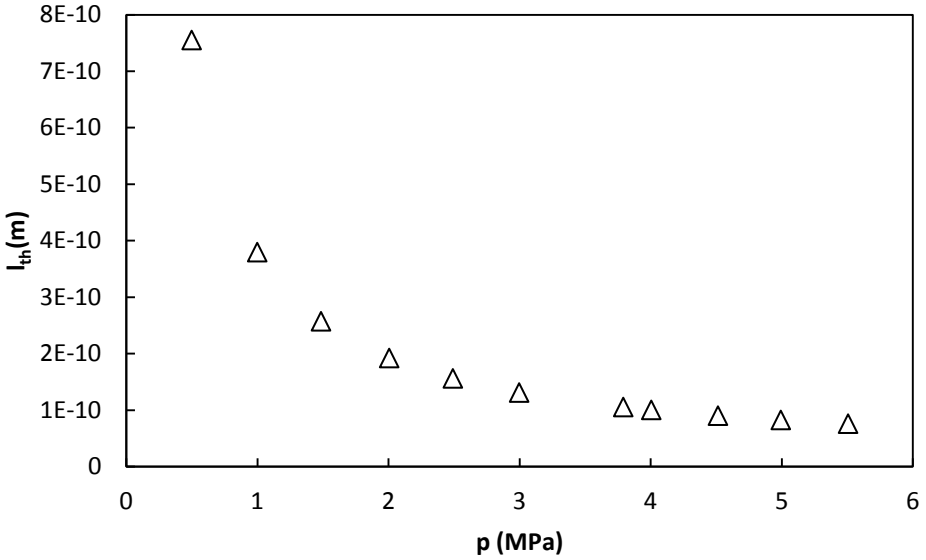

Figure 7.23 *Thermal accommodation length at T = 273 K as function of pressure for the synthetic CMM mixture.*

Table 7.19 *Shell thermal penetration length for acoustic modes (0,2) to (0,5) at T = 273 K and p = 5.51 MPa for the synthetic CMM mixture.*

Mode	δ_{shell} (m)
(0,2)	1.45×10^{-5}
(0,3)	1.10×10^{-5}
(0,4)	9.28×10^{-6}
(0,5)	8.17×10^{-6}

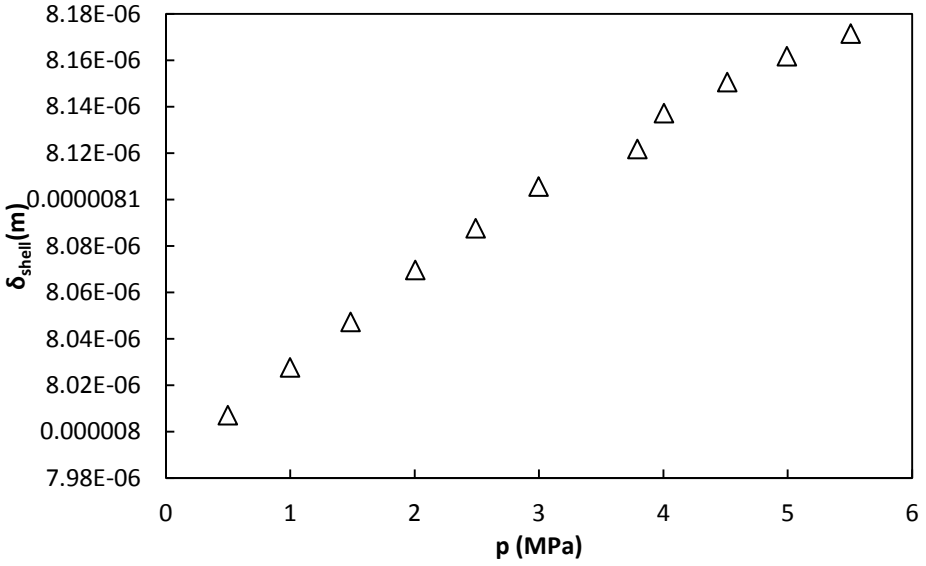

Figure 7.24 *Shell thermal penetration length for acoustic mode (0,2) at T = 273 K as function of pressure for the synthetic CMM mixture.*

Table 7.20 *Thermal boundary layer frequency correction and half-width contribution for acoustic modes (0,2) to (0,5) at T = 273 K and p = 5.51 MPa for the synthetic CMM mixture.*

Mode	Δf_{th} (Hz)	g_{th} (Hz)
0.2	-0.164	0.167
0.3	-0.215	0.219
0.4	-0.256	0.260
0.5	-0.290	0.295

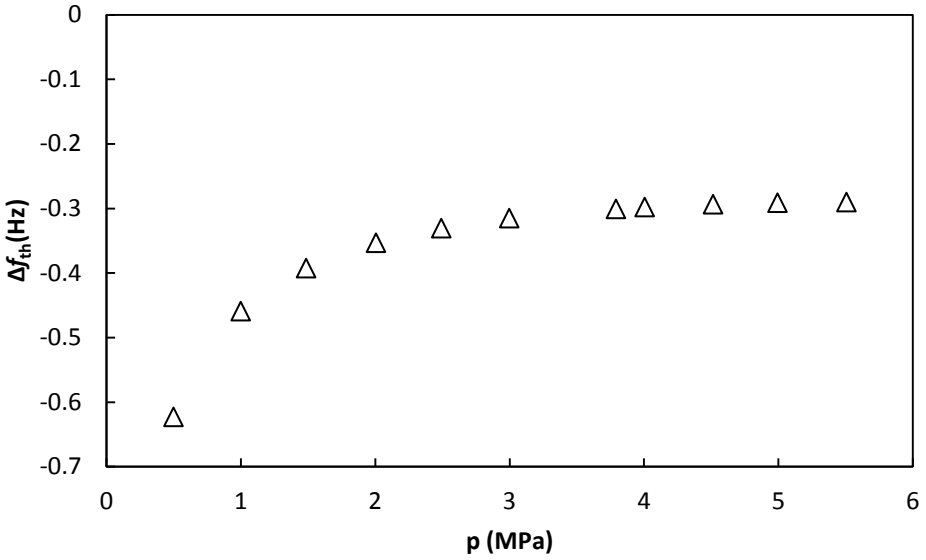

Figure 7.25 *Thermal boundary layer frequency correction for acoustic mode (0,2) at T = 273 K as function of pressure for the synthetic CMM mixture.*

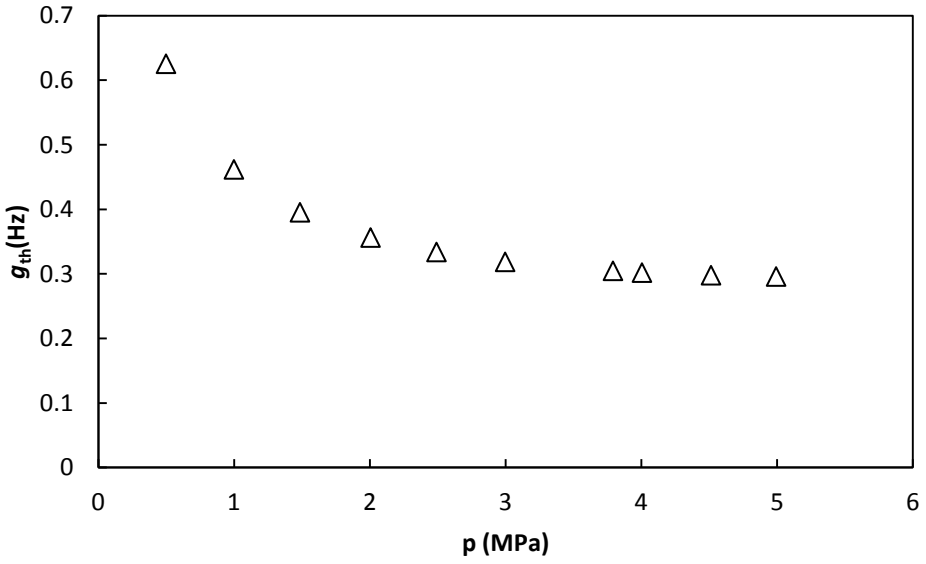

Figure 7.26 *Thermal boundary layer half-width contribution for acoustic mode (0,2) at T=273K in the range pressure from p=0.50MPa up to p=5.51MPa for the synthetic CMM mixture.*

7.3.1.2 *Bulk Viscosity Contribution.*

Table 7.21 *Viscous penetration length for acoustic modes (0,2) to (0,5) at T = 273 K and p = 5.51 MPa for the synthetic CMM mixture.*

Mode	δ_v(m)
(0,2)	3.31×10^{-6}
(0,3)	2.53×10^{-6}
(0,4)	2.13×10^{-6}
(0,5)	1.87×10^{-6}

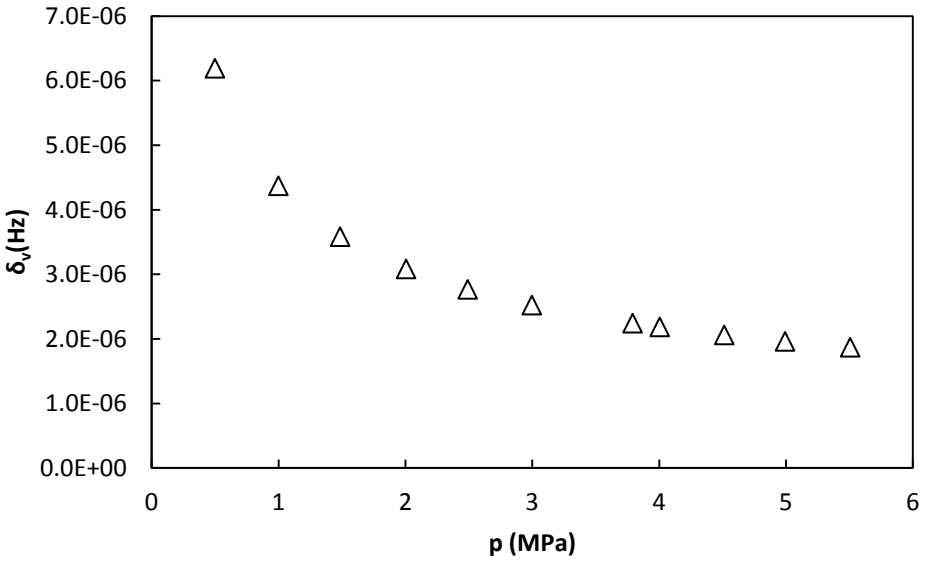

Figure 7.27 *Viscous penetration length for acoustic mode (0,2) at T = 273 K as function of pressure for the synthetic CMM mixture.*

Table 7.22 *Bulk viscosity half-width contribution for acoustic modes (0,2) to (0,5) at T = 273 K and p = 5.51 MPa for the synthetic CMM mixture.*

Mode	g_b(Hz)
(0,2)	$0.43 \cdot 10^{-3}$
(0,3)	$1.28 \cdot 10^{-3}$
(0,4)	$2.55 \cdot 10^{-3}$
(0,5)	$4.24 \cdot 10^{-3}$

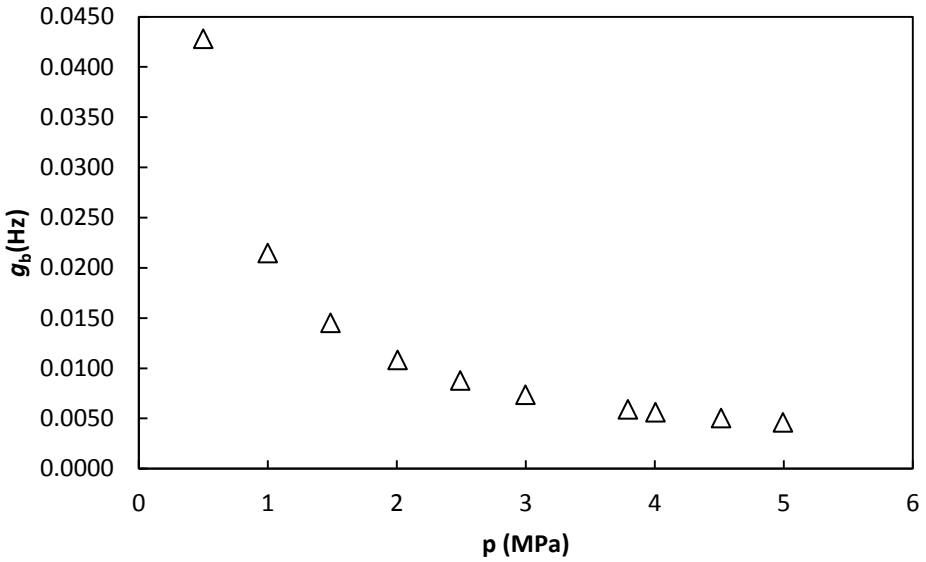

Figure 7.28 *Bulk viscosity half-width contribution for acoustic mode (0,2) at T = 273 K as function of pressure for the synthetic CMM mixture.*

7.3.1.3 *Shell Motion Correction.*

Table 7.23 *Shell motion frequency correction for acoustic modes (0,2) to (0,5) at T = 273 K and p = 5.51 MPa for the synthetic CMM mixture.*

Mode	Δf_{shell} (Hz)
(0,2)	-0.406
(0,3)	-0.785
(0,4)	-1.366
(0,5)	-2.553

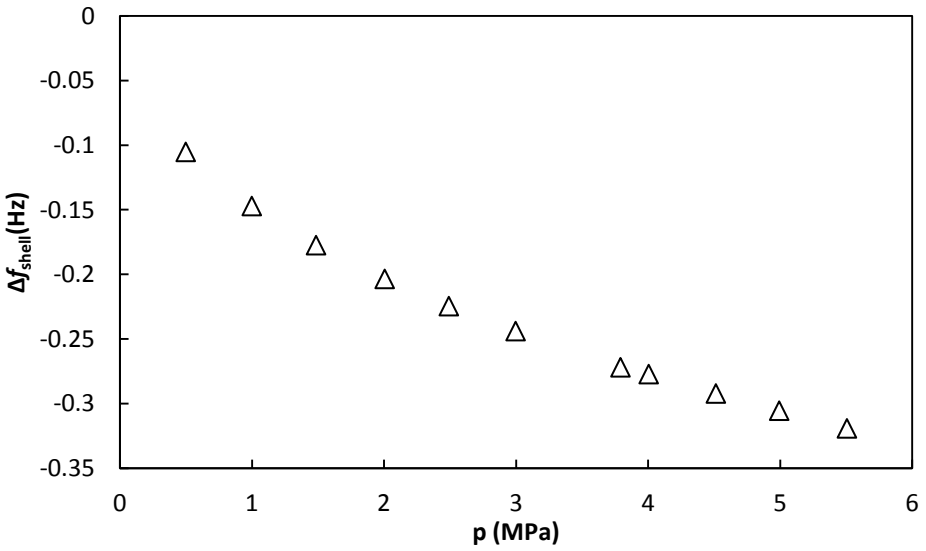

Figure 7.29 *Shell motion frequency correction for acoustic mode (0,2) at T = 273 K as function of pressure for the synthetic CMM mixture.*

7.3.1.4 *Tubes and Holes correction***.**

Table 7.24 *Kirchhoff-Helmholtz absorption coefficient for tubes 1 and 2 for acoustic modes (0,2) to (0,5) at T = 273 K and p = 5.51 MPa for the synthetic CMM mixture.*

Mode	$\alpha_{KH1}(m^{-1})$	$\alpha_{KH2}(m^{-1})$
(0,2)	0.61253	0.30626
(0,3)	0.80315	0.40157
(0,4)	0.95418	0.47709
(0,5)	1.08376	0.54188

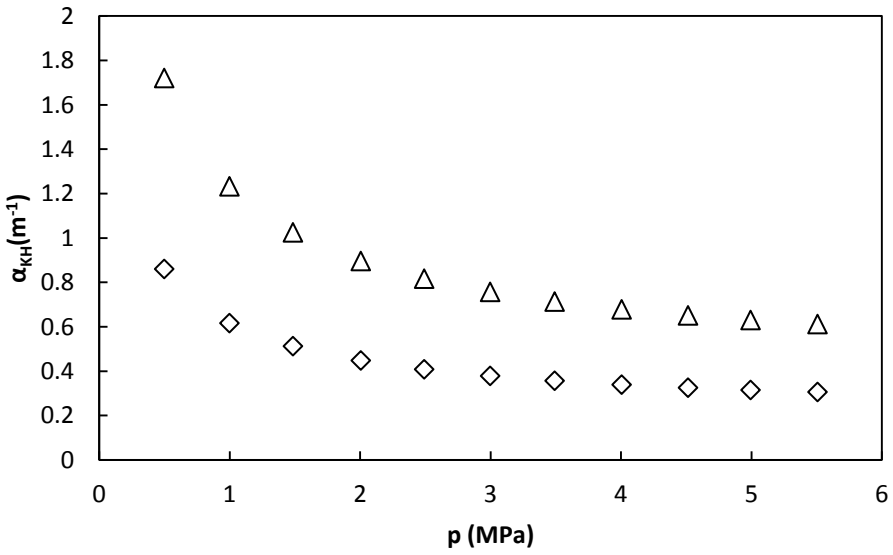

Figure 7.30 *Kirchhoff-Helmholtz absorption coefficient for tubes 1 (Δ) and 2 (◊) for acoustic mode (0,2) at T = 273 K as function of pressure for the synthetic CMM mixture.*

Table 7.25 *Propagation constant for tubes 1 and 2 for acoustic modes (0,2) to (0,5) at T = 273 K and p = 5.51 MPa for the synthetic CMM mixture*

Mode	k_{KH1} (m^{-1})	k_{KH2} (m^{-1})
(0,2)	112.57-0.61i	112.27-0.31i
(0,3)	193.29-0.80i	192.89-0.40i
(0,4)	272.64-0.95i	272.16-0.48i
(0,5)	351.57-1.08i	351.03-0.54i

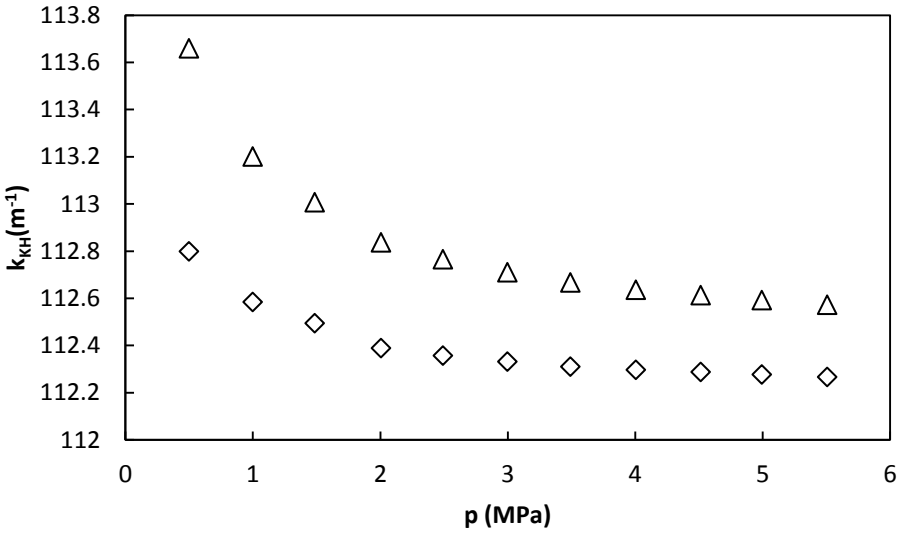

Figure 7.31 *Propagation constant real component for tubes 1 (Δ) and 2 (◊) for acoustic mode (0,2) at T = 273 K as function of pressure for the synthetic CMM mixture.*

Table 7.26 *Specific acoustic admittance of the opening for tubes 1 and 2 for acoustic modes (0,2) to (0,5) at T = 273 K and p = 5.51 MPa for the synthetic CMM mixture*

Mode	y_{01}	y_{02}
(0,2)	2.16-0.14i	0.08+2.13i
(0,3)	1.81-0.14i	0.11+1.82i
(0,4)	1.38-0.12i	0.11+1.43i
(0,5)	1.05-0.10i	0.12+1.12i

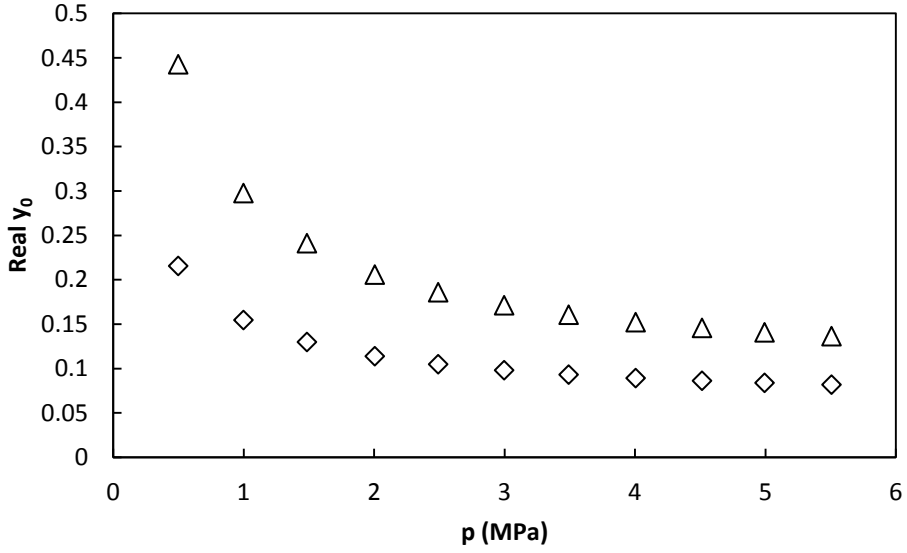

Figure 7.32 *Specific acoustic admittance of the opening real component for tubes 1 (Δ) and 2 (◊) for acoustic mode (0,2) at T = 273 K as function of pressure for the synthetic CMM mixture.*

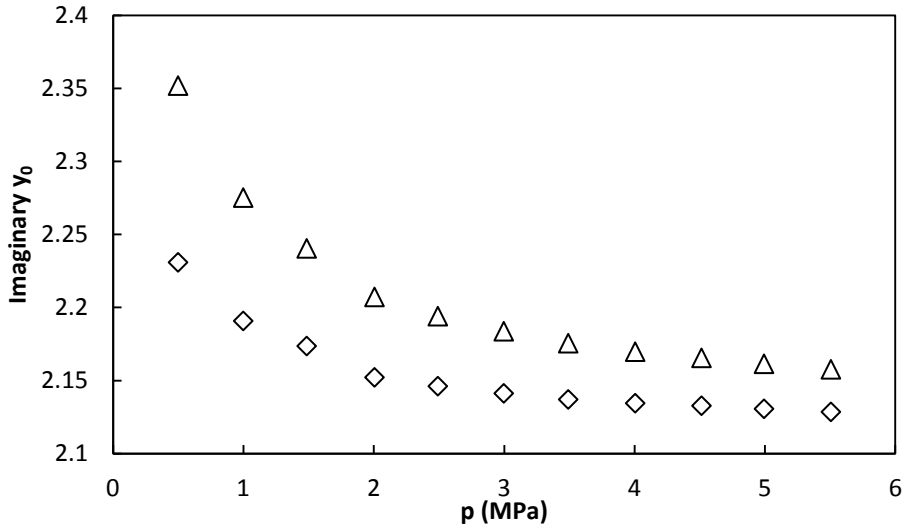

Figure 7.33 *Specific acoustic admittance of the opening imaginary component for tubes 1 (Δ) and 2(◊) for acoustic mode (0,2) at T = 273 K as function of pressure for the synthetic CMM mixture.*

Table 7.27 *Tubes frequency correction and half-width contribution for pipes 1 and 2 of acoustic modes (0,2) to (0,5) at T = 273 K and p = 5.51 MPa for the synthetic CMM mixture.*

Mode	Δf_{tube} (Hz)	g_{tube} (Hz)
(0,2)	-0.236	0.139
(0,3)	-0.166	0.119
(0,4)	-0.098	0.090
(0,5)	-0.056	0.068

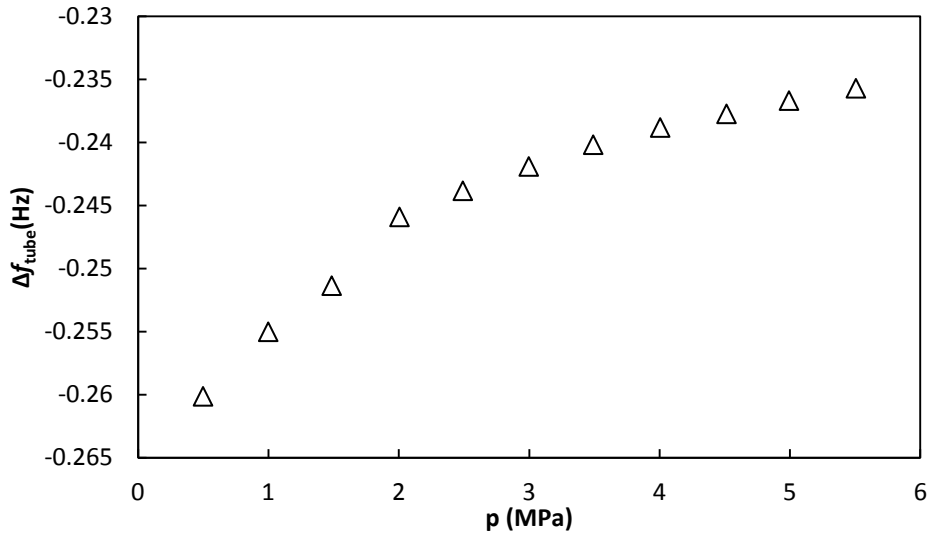

Figure 7.34 *Tubes frequency correction for acoustic mode (0,2) at T = 273 K as function of pressure for the synthetic CMM mixture.*

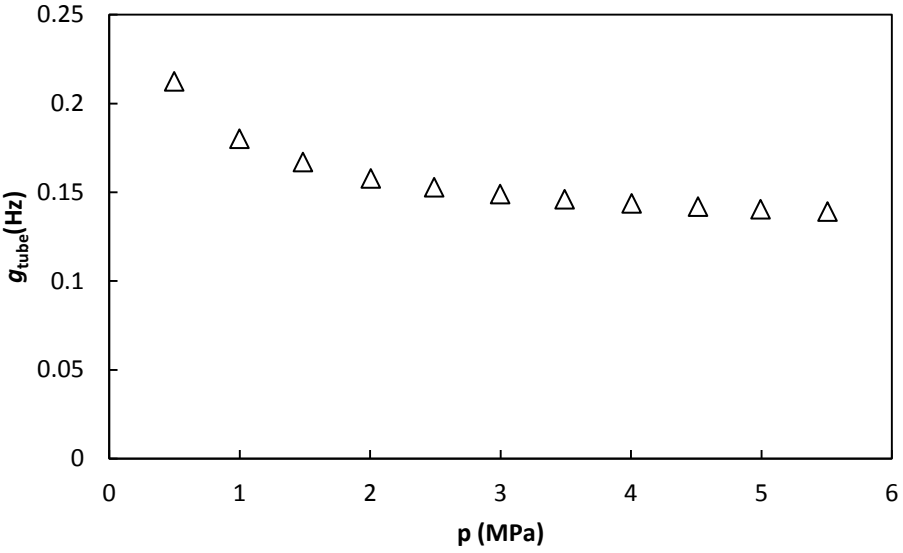

Figure 7.35 *Tubes half-width contribution for acoustic mode (0,2) at T=273K in the range pressure from 0 p=.50MPa up to p=5.51MPa for the CMM mixture.*

7.3.2 Speed of Sound Determination.

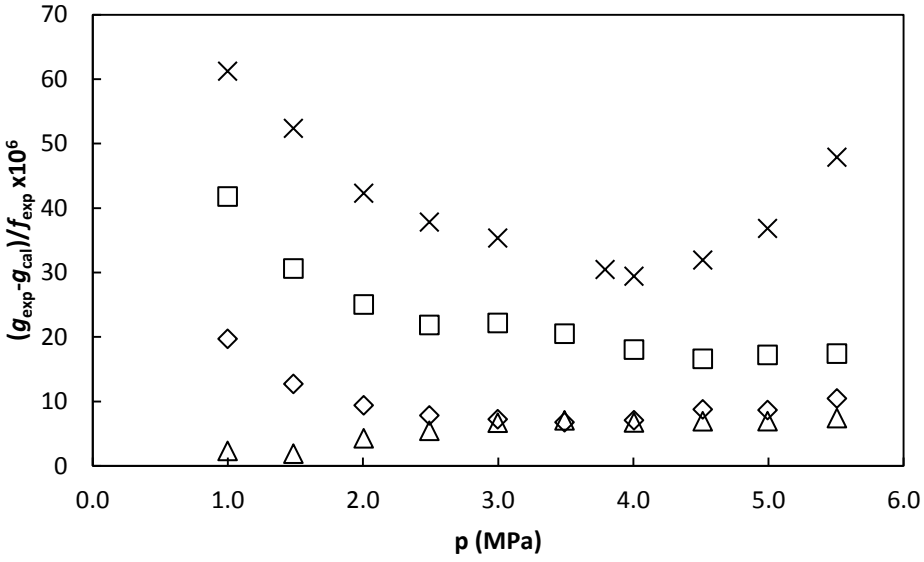

Figure 7.36 *Excess half-width for acoustic modes (0,2) (Δ), (0,3) (◊), (0,4) (□) and (0,5) (X) at T = 273 K as function of pressure for the synthetic CMM mixture.*

Table 7.28 *Speed of sound values from experimental data and according to GERG-2008 equation of state, and the comparison between them at T = 273 K for the synthetic CMM mixture.*

p (MPa)	T (K)	u_{exp}(m·s^{-1})	u_{GERG}(m·s^{-1})	$(u_{exp}-u_{GERG})/u_{GERG}$ x10^6 (m·s^{-1}/m·s^{-1} x10^6)
5.51	273.1572	345.694	345.38	910
4.99	273.1611	346.520	346.21	890
4.51	273.1688	347.462	359.82	780
4.01	273.1616	348.609	348.32	830
3.49	273.1720	349.927	349.67	740
3.00	273.1539	351.335	351.07	760
2.49	273.1623	352.890	352.65	680
2.01	273.1454	354.474	354.26	600
1.49	273.1688	356.432	356.11	900
1.00	273.1554	358.183	357.89	820
0.50	273.1707	360.015	359.82	540

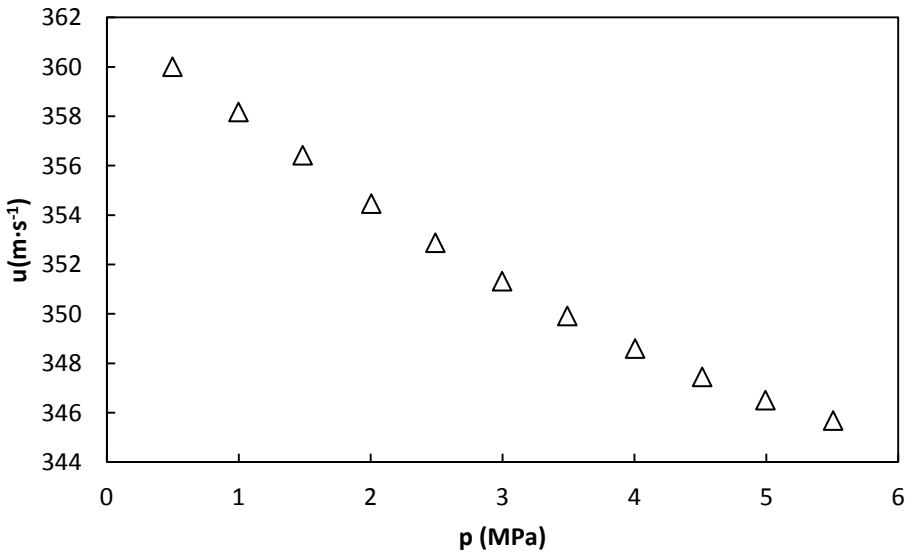

Figure 7.37 *Experimental speed of sound at T = 273 K as function of pressure for the synthetic CMM mixture.*

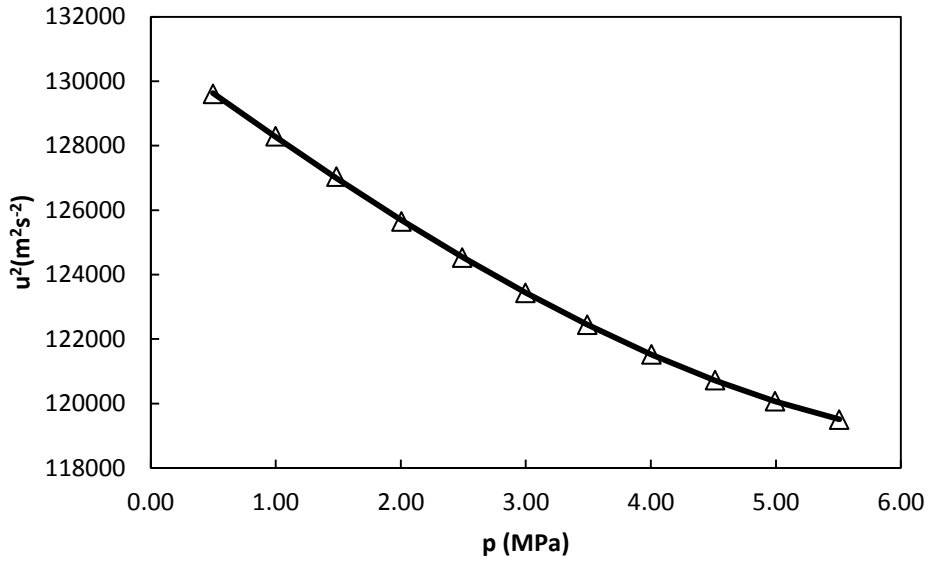

Figure 7.38 *Experimental square speed of sound (Δ) and developed acoustic virial model (—) at T = 273 K as function of pressure for the synthetic CMM mixture.*

Table 7.29 *Experimental acoustic virial equation of state parameters at T = 273K for the synthetic CMM mixture.*

A_0 (m^2s^{-2})	A_1 ($m^2s^{-2}\cdot MPa^{-1}$)	A_2 ($m^2s^{-2}\cdot MPa^{-2}$)	σ (m^2s^{-2})
131215	-3140	182.3	52

Table 7.30 *Speed of sound according to developed model and according to GERG-2008 equation of state and a comparison between them at T = 273 K for the synthetic CMM mixture.*

p(MPa)	u_{model} ($m\cdot s^{-1}$)	u_{GERG} ($m\cdot s^{-1}$)	$(u_{model}-u_{GERG})/u_{GERG}$ x10^6 ($m\cdot s^{-1}/m\cdot s^{-1}$ x10^6)
5.51	345.694	345.38	345.619
4.99	346.520	346.21	346.527
4.51	347.462	359.82	347.500
4.01	348.609	348.32	348.660
3.49	349.927	349.67	349.964
3.00	351.335	351.07	351.343
2.49	352.890	352.65	352.880
2.01	354.474	354.26	354.473
1.49	356.432	356.11	356.305
1.00	358.183	357.89	358.136
0.50	360.015	359.82	360.132

Table 7.31 *Comparison between the calculated values of the isochoric and isobaric heat capacities (C_v^{pg} and C_p^{pg}) and the adiabatic coefficient (γ^{pg}) at zero pressure and the acoustic virial coefficients (β_a, γ_a) obtained from equation 2.6-b and those calculated using GERG-2008 EoS for the synthetic CMM mixture.*

	Eq 2.6-b	**GERG-2008**	**(Eq2.6-b-GERG)/GERG x10^2**
γ^{pg}	1.3228	1.3205	0.1740
C_v^{pg}(J·mol^{-1}K^{-1})	25.7574	25.9400	0.7090
C_p^{pg}(J·mol^{-1}K^{-1})	34.0719	34.2540	0.5350
β_a(m^{3}mol^{-1})	-5.4349 x10^{-5}	-5.5120 x10^{-5}	-1.420
γ_a(m^{6}mol^2)	7.1651 x10^{-9}	7.6196 x10^{-2}	
u_0 (m·s^{-1})	360.237	361.79	0.1240

7.4 UNCERTAINTY ASSESMENT.

The procedure to obtain the uncertainty of the measurements was explained in chapter 6. This section shows the relevant uncertainty results for the two measured isotherms, T =250 K and T = 273 K, for the synthetic coal mine methane mixture.

7.4.1 Speed of Sound extrapolation to Zero Pressure Uncertainty.

7.4.1.1 *Resonator Internal Radius Uncertainty*.

Table 7.32 *Resonator inner radius standard uncertainties for both isotherms T = 250 K and T = 273 K for the synthetic CMM mixture.*

T = 250 K		**T = 273 K**	
p (MPa)	**u(a) (m)**	**p (MPa)**	**u(a) (m)**
7.93	4.1 x10^{-6}	5.51	1.2 x10^{-6}
6.95	4.1 x10^{-6}	4.99	1.1 x10^{-6}
6.04	4.1 x10^{-6}	4.51	1.1 x10^{-6}
4.88	4.1 x10^{-6}	4.01	1.0 x10^{-6}
3.93	4.1 x10^{-6}	3.49	1.0 x10^{-6}
2.92	4.1 x10^{-6}	3.00	1.0 x10^{-6}
1.97	4.1 x10^{-6}	2.49	1.0 x10^{-6}
0.98	4.1 x10^{-6}	2.01	9.9 x10^{-6}
		1.49	9.9 x10^{-6}
		1.00	4.2 x10^{-6}
		0.50	4.2 x10^{-6}

7.4.1.2 *Frequency of Resonance Uncertainty*.

Table 7.33 *Frequency measurements standard uncertainties for acoustic modes (0,2), (0,3), (0,4) and (0,5) at p = 5 MPa for the synthetic CMM mixture.*

	u(f) (Hz)	
Mode	**T = 250 K**	**T = 273 K**
(0,2)	0.064	0.037
(0,3)	0.12	0.063
(0,4)	0.15	0.11
(0,5)	0.17	0.72

7.4.1.3 *Modal Dispersion Uncertainty.*

Table 7.34 *Modal dispersion standard uncertainties for both isotherms T = 250 K and T = 273 K for the synthetic CMM mixture.*

T=250K		**T=273K**	
p (MPa)	**$u(u_{disp})$ ($m \cdot s^{-1}$)**	**p (MPa)**	**$u(u_{disp})$ ($m \cdot s^{-1}$)**
7.93	0.0071	5.51	0.0073
6.95	0.0056	4.99	0.0072
6.04	0.0051	4.51	0.0070
4.88	0.0044	4.01	0.0067
3.93	0.0038	3.49	0.0065
2.92	0.0043	3.00	0.0064
1.97	0.0040	2.49	0.0062
0.98	0.0031	2.01	0.0056
		1.49	0.0049
		1.00	0.0041
		0.50	0.0026

7.4.1.4 *Speed of Sound*

Table 7.35 *Measured speed of sound values and their and standard and relative uncertainties at T = 250 K for the synthetic CMM mixture*

p (MPa)	**u ($m \cdot s^{-1}$)**	**u(u) ($m \cdot s^{-1}$)**	**$u(u) \cdot 10^6$**
7.93	319.541	0.035	110
6.95	319.214	0.034	110
6.04	320.459	0.034	110
4.88	323.723	0.034	100
3.93	327.365	0.034	100
2.92	331.905	0.034	100
1.97	336.616	0.035	100
0.98	341.901	0.035	100

Table 7.36 *Measured speed of sound values and their uncertainties at T = 273 K for the synthetic CMM mixture*

p (MPa)	u (m·s^{-1})	u(u) (m·s^{-1})	$u_r(u)\cdot10^6$
5.51	345.694	0.013	37
4.99	346.520	0.012	35
4.51	347.462	0.012	35
4.01	348.609	0.011	32
3.49	349.927	0.011	32
3.00	351.335	0.011	32
2.49	352.890	0.011	32
2.01	354.474	0.011	30
1.49	356.432	0.010	29
1.00	358.183	0.038	110
0.50	360.015	0.038	110

Table 7.37 *Square speed of sound values and standard uncertainties at T = 250 K for the synthetic CMM mixture.*

p (MPa)	u^2 (m^2s^{-2})	$u(u^2)$ ($m^2\cdot s^{-2}$)
7.93	102106	23
6.95	101898	22
6.04	102694	22
4.88	104796	22
3.93	107168	22
2.92	110161	23
1.97	113310	23
0.98	116896	24

Table 7.38 *Square speed of sound values and standard uncertainties at T = 273 K for the synthetic CMM mixture.*

p (MPa)	u^2 ($m^2\cdot s^{-2}$)	$u(u^2)$ (m^2s^{-2})
5.51	119505	8.8
4.99	120076	8.4
4.51	120730	8.4
4.01	121528	7.9
3.49	122449	7.8
3.00	123436	7.8
2.49	124532	7.9
2.01	125652	7.4
1.49	127043	7.3
1.00	128295	27
0.50	129611	27

Table 7.39 *Experimental acoustic virial equation of state parameters and standard and relative uncertainties for the synthetic CMM mixture.*

Parameters	T = 250 K	T = 273 K	Units
A_0	121749	131216	m^2s^{-2}
A_1	-4970	-3140	$m^2s^{-2}MPa^{-1}$
A_2	309-5	182.3	$m^2s^{-2}MPa^{-2}$
$u(A_0)$	46	27	m^2s^{-2}
$u(A_1)$	23	17	$m^2s^{-2}MPa^{-1}$
$u(A_2)$	2.5	2.3	$m^2s^{-2}MPa^{-2}$
$u_r(A_0)$	380	200	$10^6m^2s^{-2}\cdot(m^2s^{-2})^{-1}$
$u_r(A_1)$	0.46	0.53	$10^2m^2s^{-2}MPa^{-1}(m^2s^{-2}MPa^{-1})^{-1}$
$u_r(A_2)$	0.90	1.3	$10^2m^2s^{-2}MPa^{-2}(m^2s^{-2}MPa^{-2})^{-1}$

7.4.2 Adiabatic coefficient uncertainty.

Molar mass uncertainty is calculated using molar composition data from table 7.1.

The results are:

$M=0.022896\ Kg\cdot mol^{-1}$ $u(M)=1.2\ x10^{-6}\ Kg\cdot mol^{-1}$

Table 7.40 *Temperature uncertainty contributions and final sum for two isotherms T = 250 K and T = 273 K for the synthetic CMM mixture.*

$T_{average}$ (K)	$u(T_{disp})$ (K)	$u(T_{grad})$ (K)	u(T) (K)
249.9691	0.0072	0.0052	0.0089
273.1615	0.0012	0.00064	0.0017

Table 7.41 *Adiabatic coefficient values and and standard and relative uncertainties at T = 250 K and T = 273 K for the synthetic CMM mixture.*

T (K)	γ^{pg}	$u(\gamma^{pg})$	$u_r(\gamma^{pg})\cdot10^6$
250	1.34124	0.00051	380
273	1.32280	0.00028	210

7.4.3 Heat Capacities Uncertainty.

Table 7.42 *Isochoric heat capacity and and standard and relative uncertainties at T = 250 K and T = 273 K for synthetic CMM mixture.*

T (K)	C_v ($J\cdot mol^{-1}K^{-1}$)	$u(C_v)$ ($J\cdot mol^{-1}K^{-1}$)	$u_r(C_v)\cdot10^6$
250	24.366	0.037	1500
273	25.757	0.022	860

Table 7.43 *Isobaric heat capacity and and standard and relative uncertainties at T = 250 K and T = 273 K for synthetic CMM mixture.*

T (K)	C_p (J·mol^{-1}K^{-1})	$u(C_p)$ (J·mol^{-1}K^{-1})	$u_r(C_p)\cdot10^6$
250	32.680	0.051	1500
273	34.072	0.030	890

7.4.4 Acoustic Virial parameters uncertainty.

Table 7.44 *Second acoustic virial parameter and and standard and relative uncertainties at T = 250 K and T = 273 K for the synthetic CMM mixture.*

T (K)	β_a(m^{3}mol^{-1})	$u(\beta_a)$(m^{3}mol^{-1})	$u_r(\beta_a)$(%)
250	-8.484E x10^{-5}	3.9 x10^{-7}	0.46
273	-5.435 x10^{-5}	2.9 x10^{-7}	0.53

Table 7.45 *Third acoustic virial parameter and standard and relative uncertainty at T = 250 K and T = 273 K for synthetic CMM mixture.*

T (K)	γ_a(m^{6}mol^{-2})	$u(\gamma_a)$(m^{6}mol^{-2})	$u_r(\gamma_a)$(%)
250	1.0980 x10^{-8}	8.7 x10^{-11}	0.80
273	7.1651 x10^{-9}	9.3 x10^{-11}	1.3

7.5 DISCUSSION

Speed of sound was measured in a synthetic coal mine methane mixture at two different temperatures T = 250 K and T = 273.16 K. The coldest one was measured in the pressure range up to 8 MPa and the other one up to 5.5 MPa.

Speed of sound uncertainties of both isotherms are always lower than 110·10^{-6} m·s^{-1}/m·s^{-1}. Adiabatic coefficient lower than 380·10^{-6} for both temperatures but slightly lower (230·10^{-6}) at T = 273.16 K. Heat capacities are calculated from adiabatic coefficient, therefore their uncertainties are lower for the T = 273.16 K isotherm, about 990·10^{-6} J·mol^{-1}K^{-1}/ J·mol^{-1}K^{-1}, while at T = 250 K heat capacities uncertainties are 1500·10^{-6} J·mol^{-1}K^{-1}/ J·mol^{-1}K^{-1}. Acoustic virial coefficient uncertainties are lower than 2.0 %.

The standard deviation of the equation 2.6-b is 52 m^{2}s^{-2} at T = 273.16 K which is in a good agreement with standard uncertainty of the second order polynomial parameters. At T = 250 K the standard deviation is much higher, 180 m^{2}s^{-2}. This

difference might be caused by the proximity to condensation condition at the higher pressures for this isotherm.

All measured thermodynamic properties, speed of sound, adiabatic coefficient, heat capacities and acoustic virial parameters, were compared to those predicted by GERG-2008 equation of state.

GERG-2008 EoS estimation of speed of sound is always lower than the experimental value this deviation is higher at higher pressure and it decreases when decreasing pressure. Deviations are lower than 1000 10^{-6} $m \cdot s^{-1}/m \cdot s^{-1}$ for both isotherms. Adiabatic coefficient estimation is 1% lower than the experimental result at T = 250 K and lower than 0.2 % at T = 273.16 K. Heat capacities deviations are lower than 4% at T = 250 K, and lower than 0.7% at T = 273.16 K. Comparison between acoustic virial coefficients probes that GERG-2008 EoS estimation is not in good agreement to experimental data with deviations too high to even be taken into consideration.

7.6 REFERENCES

1. Lemmon, E.W., Huber, M.L., McLinden, M.O. NIST Standard Reference Database 23: Reference Fluid Thermodynamic and Transport Properties-REFPROP, Version 9.1, National Institute of Standards and Technology, Standard Reference Data Program, Gaithersburg, 2013.

2. Kunz, O., and Wagner, W. The GERG-2008 Wide-Range Equation of State for Natural Gases and Other Mixtures: An Expansion of GERG-2004. Journal of Chemical & Engineering Data 57, 3032-3091.

Chapter 8:

CONCLUSIONS

8.1 CONCLUSIONS

1. An advanced technique for the measurement of speed of sound in gases was improved for the determination of the Boltzmann constant. New microwave antennae were implemented in a new misaligned resonator. These antennae are connected to a network analyzer, which cover the range up to 13.5 GHz, for measuring internal radius with a low uncertainty.

2. Chromatographic filters were implemented and the tubing was changed previous to the resonating cavity inlet to purify the argon, removing water and oxygen and assuring concentration of carbon monoxide, carbon dioxide, hydrogen and organic compounds.

3. A new preamplifier was designed, the implementation of this preamplifier reduced noise and improved the signal, it is also smaller than the previous one. The Boltzmann constant was determined, the value was k_B=1.380650·10^{-23} J·K^{-1} with a relative standard uncertainty of ± 20 10^{-6} J·K^{-1}/J·K^{-1}. The difference of this value to the codata 2010 value is -5.3 10^{-6} J·K^{-1}/J·K^{-1}

4. A different spherical cavity was used for determination of some thermodynamic properties like heat capacities, adiabatic factor and acoustic virial coefficients as well as the speed of sound of several gas mixtures.

5. The spherical resonator was characterized by using argon as a reference to measure internal radius at several different temperatures and pressures. The relative standard uncertainty was lower than ± 100·10^{-6} m·m^{-1}.

6. Different reference resistances were used in the bridge for temperature measurement enabling to work at higher temperatures and working temperature may be reduced below -40°C thanks to the new refrigeration equipment. It is possible increase the pressure from the cylinder to resonator by attaching new piston compressor.

7. Speeds of sound of the gas mixtures (5%CO and 95%N_2) and (10%CO and 90%N_2) were measured at two different temperatures, T = 273.16 K and T = 325.00 K starting at the higher pressure p = 10 MPa and decreasing in steps around 1MPa until the lower pressure was reached p = 0.10 MPa. The main uncertainty sources are the radius determination due to the speed of sound uncertainty in argon, and the dispersion

caused by the different acoustic modes measured. The relative standard uncertainty of the speed of sound measurements is better than ± 150 10^{-6} $m \cdot s^{-1}/m \cdot s^{-1}$

8. Values and uncertainties of speed of sound were used to solve the other thermodynamic properties. Their uncertainties were computed using a Monte Carlo method. One of these properties is the adiabatic coefficient which relative standard uncertainty was lower than ± 300 10^{-6} at both temperatures, the other properties depend on the value and uncertainty of the adiabatic coefficient, the heat capacities sensitivity to the adiabatic coefficient increases their uncertainties, isochoric and isobaric ideal heat capacities at both temperatures have relative standard uncertainties around ± 1000 10^{-6} $J \cdot mol^{-1}K^{-1}/J \cdot mol^{-1}\ K^{-1}$. The second and third acoustic virial coefficients were calculated as well, their relative standard uncertainties are lower than ± 2.5%

9. A set of measurements were carried out in synthetic coal mine methane at two different temperatures, T = 250 K and T = 273.16 K and pressures up to p = 8 MPa. The relative standard uncertainty of the speed of sound measurements is better than ± 110 10^{-6} $m \cdot s^{-1}/m \cdot s^{-1}$. Molar mass has an important role in the uncertainty contribution, this is due to the complexity of the mixture. The adiabatic coefficient relative standard uncertainty was lower than ± 380 10^{-6} at both temperatures. The isochoric and isobaric ideal heat capacities have relative standard uncertainties around ± 1500 10^{-6} $J \cdot mol^{-1}K^{-1}/J \cdot mol^{-1}\ K^{-1}$. The second and third acoustic virial coefficients were calculated as well, their relative standard uncertainties are lower than ± 1.3%

10. The behavior of all the mixtures was compared with those obtained from GERG-2008 equation of state and a good agreement was observed between the experimental values of the speeds of sound and those calculated by the equation. The relative deviations in the speed of sound for the CO +N_2 mixture are less than ± 250 10^{-6} $m \cdot s^{-1}/m \cdot s^{-1}$ and the relative deviations in the speed of sound for the synthetic coal mine methane mixture are less than ± 900 10^{-6} $m \cdot s^{-1}/m \cdot s^{-1}$

APPENDIX

Appendix A

ACOUSTIC AND ELECTROMAGNETIC MEASUREMENTS AND CORRECTIONS AND SPEED OF SOUND CALCULATION FOR DETERMINING BOLTZMANN'S CONSTANT.

A.1 Acoustic and electromagnetic resonance measurements

This appendix shows measurements of acoustic and electromagnetic frequencies of resonance in argon in a range of pressure from 0.078MPa up to 0.9MPa at T = 273.16 K and some calculations carried out as internal radius determination, speed of sound, frequency corrections…

Electromagnetic resonance output data are detailed in following tables A1.1 to 12. Three frequencies of resonance, their type A uncertainty and haft-width values are shown for modes TM11, TE11, TM12, TE12 and TM13 at the following pressures.

At p = 0.9 MPa:

Table A1.1 *Triplets frequencies of resonance, half-widths and uncertainties for modes TM11, TE11, TM12, TE12 and TM13 at T = 273.16 K and p = 0.9 MPa*

Mode	f_1/MHz	f_2/MHz	f_3/MHz	g_1/MHz	g_2/MHz	g_3/MHz	u(f_1)/MHz	u(f_2)/MHz	u(f_3)/MHz
TM11	3260.17	3263.86	3264.12	1.0013	1.0890	1.0174	3.2×10^{-5}	1.3×10^{-2}	1.6×10^{-3}
TE11	5341.89	5345.29	5345.60	0.9426	1.0928	1.1358	1.2×10^{-3}	6.5×10^{-3}	2.0×10^{-2}
TM12	7271.56	7271.78	7276.46	1.0707	7.7827	1.2413	6.3×10^{-4}	1.1×10^{-2}	2.3×10^{-3}
TE12	9184.41	9189.97	9190.44	1.1022	1.0971	1.1294	5.9×10^{-3}	5.5×10^{-3}	1.2×10^{-2}
TM13	11076.42	11083.31	11084.14	1.1180	1.1874	1.1624	3.3×10^{-3}	6.6×10^{-3}	1.1×10^{-2}

At p = 0.7 MPa:

Table A1.2 *Triplets frequencies of resonance, half-widths and uncertainties for modes TM11, TE11, TM12, TE12 and TM13 at T = 273.16 K and p = 0.7 MPa*

Mode	f_1/MHz	f_2/MHz	f_3/MHz	g_1/MHz	g_2/MHz	g_3/MHz	u(f_1)/MHz	u(f_2)/MHz	u(f_3)/MHz
TM11	3261.91	3265.69	3265.92	1.0018	1.3541	1.0313	5.3×10^{-5}	3.1×10^{-2}	1.3×10^{-3}
TE11	5344.89	5348.29	5348.50	0.9458	1.0361	0.9916	4.7×10^{-4}	4.1×10^{-3}	9.1×10^{-3}
TM12	7275.60	7275.66	7280.56	1.1492	1.1787	1.2426	2.9×10^{-1}	4.6×10^{-1}	2.5×10^{-3}
TE12	9189.55	9195.10	9195.65	1.0842	1.1247	1.1599	4.5×10^{-3}	4.4×10^{-3}	1.3×10^{-2}
TM13	11082.59	11089.49	11090.33	1.1082	1.1844	1.1956	2.9×10^{-3}	6.3×10^{-3}	9.5×10^{-3}

At p = 0.5 MPa:

Table A1.3 *Triplets frequencies of resonance, half-widths and uncertainties for modes TM11, TE11, TM12, TE12 and TM13 at T = 273.16 K and p = 0.5 MPa*

Mode	f_1/MHz	f_2/MHz	f_3/MHz	g_1/MHz	g_2/MHz	g_3/MHz	u(f_1)/MHz	u(f_2)/MHz	u(f_3)/MHz
TM11	3263.65	3267.48	3267.74	0.9991	1.0308	1.0111	2.70×10^{-5}	1.2×10^{-2}	1.4×10^{-3}
TE11	5347.85	5351.27	5351.64	0.9509	1.0784	1.0254	8.81×10^{-4}	2.8×10^{-3}	1.8×10^{-2}
TM12	7279.63	7279.70	7284.62	1.0759	1.6642	1.2614	2.59×10^{-3}	4.5×10^{-1}	3.0×10^{-3}
TE12	9194.65	9200.21	9200.77	1.0682	1.1304	1.1538	4.25×10^{-3}	4.1×10^{-3}	1.3×10^{-2}
TM13	11088.74	11095.65	11096.53	1.1169	1.1923	1.2089	2.84×10^{-3}	6.2×10^{-3}	9.3×10^{-3}

At p = 0.4 MPa:

Table A1.4 *Triplets frequencies of resonance, half-widths and uncertainties for modes TM11, TE11, TM12, TE12 and TM13 at T = 273.16 K and p = 0.4 MPa*

Mode	f_1/MHz	f_2/MHz	f_3/MHz	g_1/MHz	g_2/MHz	g_3/MHz	u(f_1)/MHz	u(f_2)/MHz	u(f_3)/MHz
TM11	3264.53	3268.39	3268.64	0.9969	1.0347	1.0117	2.8×10^{-5}	1.3×10^{-2}	1.4×10^{-3}
TE11	5349.34	5352.76	5353.20	0.9586	1.0797	0.9643	1.1×10^{-3}	2.3×10^{-3}	2.4×10^{-2}
TM12	7281.64	7282.14	7286.64	1.0700	1.1837	1.2738	7.3×10^{-4}	3.7×10^{-2}	3.1×10^{-3}
TE12	9197.25	9202.11	9202.88	1.0118	2.1790	1.2380	1.6×10^{-2}	1.6×10^{-1}	5.6×10^{-3}
TM13	11091.82	11098.76	11099.64	1.1200	1.2121	1.1873	2.5×10^{-3}	5.8×10^{-3}	9.7×10^{-3}

At p = 0.3 MPa

Table A1.5 *Triplets frequencies of resonance, half-widths and uncertainties for modes TM11, TE11, TM12, TE12 and TM13 at T = 273.16 K and p = 0.3 MPa*

Mode	f_1/MHz	f_2/MHz	f_3/MHz	g_1/MHz	g_2/MHz	g_3/MHz	u(f_1)/MHz	u(f_2)/MHz	u(f_3)/MHz
TM11	3265.40	3269.25	3269.52	0.9950	1.4335	1.0271	5.7×10^{-5}	3.7×10^{-2}	8.8×10^{-4}
TE11	5350.81	5354.24	5354.38	0.9535	1.0286	0.9121	6.3×10^{-4}	6.1×10^{-3}	1.9×10^{-2}
TM12	7283.61	7283.86	7288.64	1.0676	0.9055	1.2556	1.8×10^{-2}	4.6×10^{-1}	2.3×10^{-3}
TE12	9199.73	9205.24	9205.74	1.0420	1.1823	1.3316	7.0×10^{-3}	1.2×10^{-2}	2.5×10^{-2}
TM13	11094.87	11101.82	11102.67	1.1155	1.2054	1.1538	3.1×10^{-3}	6.7×10^{-3}	1.2×10^{-2}

At p = 0.2 MPa

Table A1.6 *Triplets frequencies of resonance, half-widths and uncertainties for modes TM11, TE11, TM12, TE12 and TM13 at T = 273.16 K and p = 0.2 MPa*

Mode	f_1/MHz	f_2/MHz	f_3/MHz	g_1/MHz	g_2/MHz	g_3/MHz	u(f_1)/MHz	u(f_2)/MHz	u(f_3)/MHz
TM11	3266.28	3270.20	3270.44	0.9919	1.0950	1.0174	3.4×10^{-5}	1.6×10^{-2}	1.6×10^{-3}
TE11	5352.30	5355.73	5355.92	0.9516	1.0403	0.8714	5.8×10^{-4}	2.8×10^{-3}	1.4×10^{-2}
TM12	7285.65	7285.69	7290.66	1.0289	1.0072	1.2638	3.7×10^{-1}	6.9×10^{-1}	2.0×10^{-3}
TE12	9202.28	9207.87	9208.43	1.0658	1.1263	1.1100	4.4×10^{-3}	4.0×10^{-3}	1.4×10^{-2}
TM13	11097.94	11104.89	11105.77	1.1165	1.2062	1.1918	2.5×10^{-3}	5.5×10^{-3}	8.6×10^{-3}

At p = 0.18 MPa:

Table A1.7 *Triplets frequencies of resonance, half-widths and uncertainties for modes TM11, TE11, TM12, TE12 and TM13 at T = 273.16 K and p = 0.18 MPa*

Mode	f_1/MHz	f_2/MHz	f_3/MHz	g_1/MHz	g_2/MHz	g_3/MHz	u(f_1)/MHz	u(f_2)/MHz	u(f_3)/MHz
TM11	3266.46	3270.54	3270.61	0.9913	1.2976	1.0354	4.8×10^{-5}	3.2×10^{-2}	2.2×10^{-3}
TE11	5352.60	5355.96	5356.13	0.9498	0.9790	1.0300	7.4×10^{-4}	1.4×10^{-2}	1.1×10^{-2}
TM12	7286.05	7287.21	7291.11	1.0652	5.2040	1.2778	1.1×10^{-3}	7.7×10^{-1}	4.4×10^{-3}
TE12	9202.78	9208.39	9208.94	1.0621	1.1226	1.0754	4.0×10^{-3}	3.8×10^{-3}	1.5E-02
TM13	11098.55	11105.49	11106.37	1.1165	1.1976	1.2138	3.0×10^{-3}	6.3×10^{-3}	9.3×10^{-3}

At p = 0.142 MPa:

Table A1.8 *Triplets frequencies of resonance, half-widths and uncertainties for modes TM11, TE11, TM12, TE12 and TM13 at T = 273.16 K and p = 0.142 MPa*

Mode	f_1/MHz	f_2/MHz	f_3/MHz	g_1/MHz	g_2/MHz	g_3/MHz	u(f_1)/MHz	u(f_2)/MHz	u(f_3)/MHz
TM11	3266.79	3270.75	3270.95	0.9930	1.2938	1.0364	2.1×10^{-4}	1.2×10^{-1}	7.0×10^{-3}
TE11	5353.14	5356.57	5356.93	0.9683	1.1195	1.4749	3.1×10^{-3}	7.0×10^{-3}	9.5×10^{-2}
TM12	7286.76	7286.83	7291.84	1.1938	1.1801	1.2842	3.7×10^{-1}	3.3×10^{-1}	2.9×10^{-3}
TE12	9203.76	9209.29	9209.67	1.1025	1.0349	1.0974	7.7×10^{-3}	1.7×10^{-2}	2.0×10^{-2}
TM13	11099.71	11106.65	11107.55	1.1313	1.2255	1.2172	5.7×10^{-3}	7.6×10^{-3}	1.2×10^{-2}

At p = 0.135 MPa:

Table A1.9 *Triplets frequencies of resonance, half-widths and uncertainties for modes TM11, TE11, TM12, TE12 and TM13 at T = 273.16 K and p = 0.135 MPa*

Mode	f_1/MHz	f_2/MHz	f_3/MHz	g_1/MHz	g_2/MHz	g_3/MHz	u(f_1)/MHz	u(f_2)/MHz	u(f_3)/MHz
TM11	3266.85	3270.87	3271.05	0.9931	0.9857	0.9984	1.5×10^{-4}	4.1×10^{-2}	1.5×10^{-2}
TE11	5353.26	5356.61	5356.91	0.9481	1.0585	1.0729	3.6×10^{-3}	1.7×10^{-2}	3.3×10^{-2}
TM12	7286.95	7287.13	7291.98	1.0821	8.5490	1.2923	9.0×10^{-4}	1.9	4.1×10^{-3}
TE12	9203.98	9209.13	9209.61	1.0543	1.9858	1.2870	1.6×10^{-2}	1.3×10^{-1}	9.9×10^{-3}
TM13	11099.89	11107.09	11107.30	1.2185	1.6793	2.6940	1.8×10^{-2}	3.9×10^{-2}	2.3×10^{-1}

At p = 0.115 MPa

Table A1.10 *Triplets frequencies of resonance, half-widths and uncertainties for modes TM11, TE11, TM12, TE12 and TM13 at T = 273.16 K and p = 0.115 MPa*

Mode	f_1/MHz	f_2/MHz	f_3/MHz	g_1/MHz	g_2/MHz	g_3/MHz	u(f_1)/MHz	u(f_2)/MHz	u(f_3)/MHz
TM11	3267.03	3271.07	3271.22	0.9891	0.9881	0.9866	3.4×10^{-5}	1.2×10^{-2}	5.3×10^{-3}
TE11	5353.55	5356.93	5357.16	0.9394	1.0276	1.0146	4.6×10^{-4}	3.1×10^{-3}	5.8×10^{-3}
TM12	7287.34	7287.45	7292.38	1.0759	5.3128	1.2988	1.7×10^{-3}	1.0	3.6×10^{-3}
TE12	9204.42	9210.02	9210.56	1.0684	1.1206	1.0932	4.5×10^{-3}	4.3×10^{-3}	1.5×10^{-2}
TM13	11100.54	11107.50	11108.33	1.1130	1.1829	1.1646	3.0×10^{-3}	6.4×10^{-3}	1.0×10^{-2}

At p = 0.102 MPa:

Table A1.11 *Triplets frequencies of resonance, half-widths and uncertainties for modes TM11, TE11, TM12, TE12 and TM13 at T = 273.16 K and p = 0.102 MPa*

Mode	f_1/MHz	f_2/MHz	f_3/MHz	g_1/MHz	g_2/MHz	g_3/MHz	u(f_1)/MHz	u(f_2)/MHz	u(f_3)/MHz
TM11	3267.14	3270.96	3271.31	0.9887	1.2708	1.0229	4.3×10^{-5}	3.0×10^{-2}	9.5×10^{-4}
TE11	5353.74	5357.14	5357.34	0.9453	1.0221	0.9501	4.4×10^{-4}	3.3×10^{-3}	8.7×10^{-3}
TM12	7287.60	7287.77	7292.66	1.0687	2.2107	1.2671	4.0×10^{-3}	5.4×10^{-1}	3.4×10^{-3}
TE12	9204.74	9210.34	9210.87	1.0727	1.1181	1.0817	3.9×10^{-3}	4.1×10^{-3}	1.4×10^{-2}
TM13	11100.91	11107.87	11108.76	1.1249	1.2096	1.1920	2.5×10^{-3}	5.8×10^{-3}	9.7×10^{-3}

At p = 0.078 MPa

Table A1.12 *Triplets frequencies of resonance, half-widths and uncertainties for modes TM11, TE11, TM12, TE12 and TM13 at T = 273.16 K and p = 0.078 MPa*

Mode	f_1/MHz	f_2/MHz	f_3/MHz	g_1/MHz	g_2/MHz	g_3/MHz	u(f_1)/MHz	u(f_2)/MHz	u(f_3)/MHz
TM11	3267.35	3271.36	3271.53	0.9875	1.2056	1.0300	4.0×10^{-5}	2.4×10^{-2}	2.3×10^{-3}
TE11	5354.10	5357.51	5357.71	0.9495	1.0307	0.8951	5.6×10^{-4}	3.2×10^{-3}	1.3×10^{-2}
TM12	7288.08	7288.47	7293.14	1.0693	6.4597	1.2920	1.0×10^{-3}	1.1	3.5×10^{-3}
TE12	9205.36	9211.49	9210.96	1.0768	1.0807	1.1199	4.5×10^{-3}	1.5×10^{-2}	4.4×10^{-3}
TM13	11101.66	11109.47	11108.63	1.1049	1.1819	1.1834	3.0×10^{-3}	8.9×10^{-3}	6.0×10^{-3}

Acoustic measurements are displayed in the followings tables:

Table A1.13 *Frequencies of resonance, haft-width of resonance peaks and frequency uncertainties for acoustic modes (0,2), (0,3), (0,4), (0,5), (0,6), (0,7) and (0,8) at T = 273.1 6K and p = 0.9 MPa*

Modo	T_N/K	T_S/K	P/MPa	f/Hz	g/Hz	u(f)/Hz
0.2	273.1635	273.1644	0.90051	5507.74391	0.77495	0.000798
0.3	273.1634	273.1644	0.90051	9469.716321	0.94070	0.000526
0.4	273.1634	273.1644	0.90057	13366.28687	1.04879	0.000757
0.5	273.1634	273.1644	0.9005	17241.0629	1.62861	0.000583
0.6	273.1633	273.1644	0.9005	21106.17716	5.82445	0.014183

Table A1.14 *Frequencies of resonance, haft-width of resonance peaks and frequency uncertainties for acoustic modes (0,2), (0,3), (0,4), (0,5), (0,6), (0,7) and (0,8) at T = 273.16 K and p = 0.7 MPa*

Modo	T_N/K	T_S/K	P/MPa	*f*/Hz	*g*/Hz	u(*f*)/Hz
0.2	273.1602	273.1628	0.70054	5505.92834	0.84844	0.00055
0.3	273.1602	273.1627	0.70056	9466.73443	1.07687	0.00070
0.4	273.1599	273.1625	0.70051	13361.9288	1.13490	0.00059
0.5	273.1597	273.1623	0.70057	17235.84650	1.64690	0.00065
0.6	273.1597	273.1622	0.70059	21098.81550	6.32015	0.0038

Table A1.15 *Frequencies of resonance, haft-width of resonance peaks and frequency uncertainties for acoustic modes (0,2), (0,3), (0,4), (0,5), (0,6), (0,7) and (0,8) at T = 273.16 K and p = 0.5 MPa*

Modo	T_N/K	T_S/K	P/MPa	*f*/Hz	*g*/Hz	u(*f*)/Hz
0.2	273.1614	273.1631	0.50051	5504.19614	0.96035	0.00075
0.3	273.1614	273.1631	0.50051	9463.71013	1.31590	0.0015
0.4	273.1613	273.1631	0.50051	13357.85401	1.29849	0.00066
0.5	273.1613	273.1631	0.50052	17230.66898	1.85742	0.00062
0.6	273.1612	273.1631	0.50051	21092.22058	6.63841	0.012

Table A1.16 *Frequencies of resonance, haft-width of resonance peaks and frequency uncertainties for acoustic modes (0,2), (0,3), (0,4), (0,5), (0,6), (0,7) and (0,8) at T = 273.16 K and p = 0.4 MPa*

Modo	T_N/K	T_S/K	P/MPa	*f*/Hz	*g*/Hz	u(*f*)/Hz
0.2	273.1601	273.1621	0.400100	5503.33879	1.04278	0.00051
0.3	273.1601	273.162	0.400100	9462.107789	1.38107	0.0013
0.4	273.1601	273.162	0.400115	13355.85615	1.41669	0.00087
0.5	273.1600	273.1619	0.400100	17228.11479	2.03817	0.00077
0.6	273.1600	273.1618	0.400105	21089.29411	7.20423	0.0023

Table A1.17 *Frequencies of resonance, haft-width of resonance peaks and frequency uncertainties for acoustic modes (0,2), (0,3), (0,4), (0,5), (0,6), (0,7) and (0,8) at T = 273.16 K and p = 0.3 MPa*

Modo	T_N/K	T_S/K	P/MPa	*f*/Hz	*g*/Hz	u(*f*)/Hz
0.2	273.1619	273.1637	0.30087	5502.52899	1.16885	0.00050
0.3	273.162	273.1637	0.30087	9460.70025	1.40979	0.0010
0.4	273.162	273.1637	0.30087	13353.98289	1.60740	0.00065
0.5	273.1621	273.1638	0.30087	17225.79721	2.29399	0.00077
0.6	273.1622	273.1639	0.30087	21086.59213	7.92680	0.0057

Table A1.18 *Frequencies of resonance, haft-width of resonance peaks and frequency uncertainties for acoustic modes (0,2), (0,3), (0,4), (0,5), (0,6), (0,7) and (0,8) at T = 273.16 K and p = 0.2 MPa*

Modo	T_N/K	T_S/K	P/MPa	*f*/Hz	*g*/Hz	u(*f*)/Hz
0.2	273.1613	273.1633	0.20004	5501.62982	1.38788	0.0020
0.3	273.1613	273.1635	0.20004	9459.23867	1.64602	0.0042
0.4	273.1613	273.1635	0.20004	13352.00117	1.98420	0.0092
0.5	273.1614	273.1635	0.20004	17223.29835	2.92736	0.023
0.6	273.1614	273.1634	0.20004	21083.94401	9.00307	0.056

Table A1.19 *Frequencies of resonance, haft-width of resonance peaks and frequency uncertainties for acoustic modes (0,2), (0,3), (0,4), (0,5), (0,6), (0,7) and (0,8) at T = 273.16 K and p = 0.18 MPa*

Modo	T_N/K	T_S/K	P/MPa	*f*/Hz	*g*/Hz	u(*f*)/Hz
0.2	273.1600	273.1623	0.18003	5501.42872	1.43351	0.0011
0.3	273.1599	273.1623	0.18003	9458.89999	1.66073	0.0015
0.4	273.1599	273.1623	0.18003	13351.48995	2.02005	0.00094
0.5	273.1599	273.1622	0.18003	17222.68869	2.90934	0.0017
0.6	273.1599	273.1622	0.18003	21084.07688	8.62493	0.010

Table A1.20 *Frequencies of resonance, haft-width of resonance peaks and frequency uncertainties for acoustic modes (0,2), (0,3), (0,4), (0,5), (0,6), (0,7) and (0,8) at T = 273.16 K and p = 0.14 MPa*

Modo	T_N/K	T_S/K	P/MPa	*f*/Hz	*g*/Hz	u(*f*)/Hz
0.2	273.1625	273.162	0.142343	5501.04734	1.57153	0.00066
0.3	273.1624	273.1621	0.142343	9458.32237	1.83902	0.0017
0.4	273.1622	273.1621	0.142343	13350.69620	2.26251	0.0010
0.5	273.162	273.1621	0.142341	17221.69400	3.24697	0.0017
0.6	273.1617	273.1621	0.142341	21083.54080	8.98193	0.012

Table A1.21 *Frequencies of resonance, haft-width of resonance peaks and frequency uncertainties for acoustic modes (0,2), (0,3), (0,4), (0,5), (0,6), (0,7) and (0,8) at T = 273.16 K and p = 0.135 MPa*

Modo	T_N/K	T_S/K	P/MPa	*f*/Hz	*g*/Hz	u(*f*)/Hz
0.2	273.1599	273.1607	0.135062	5500.94105	1.60936	0.00087
0.3	273.1597	273.1605	0.135062	9458.14424	1.89582	0.0016
0.4	273.1595	273.1604	0.13506	13350.45246	2.33737	0.00080
0.5	273.1592	273.1602	0.13506	17221.40703	3.35048	0.0010
0.6	273.1589	273.1601	0.135054	21083.35395	9.31745	0.012

Table A1.22 *Frequencies of resonance, haft-width of resonance peaks and frequency uncertainties for acoustic modes (0,2), (0,3), (0,4), (0,5), (0,6), (0,7) and (0,8) at T = 273.16 K and p = 0.115 MPa*

Modo	T_N/K	T_S/K	P/MPa	*f*/Hz	*g*/Hz	u(*f*)/Hz
0.2	273.1598	273.1603	0.115265	5500.71187	1.71072	0.0010
0.3	273.1598	273.1602	0.115263	9457.78721	2.03924	0.0015
0.4	273.1597	273.1604	0.115263	13349.97390	2.52146	0.0012
0.5	273.1597	273.1604	0.115261	17220.83420	3.59963	0.0016
0.6	273.1597	273.1604	0.115261	21083.13120	9.53054	0.0087

Table A1.23 *Frequencies of resonance, haft-width of resonance peaks and frequency uncertainties for acoustic modes (0,2), (0,3), (0,4), (0,5), (0,6), and (0,7) at T = 273.16 K and p = 0.103 MPa*

Modo	T_N/K	T_S/K	P/MPa	*f*/Hz	*g*/Hz	u(*f*)/Hz
0.2	273.1619	273.1621	0.102722	5500.57555	1.78530	0.0012
0.3	273.1621	273.1623	0.102719	9457.57751	2.15446	0.0016
0.4	273.1624	273.1624	0.102719	13349.73100	2.67391	0.0016
0.5	273.1624	273.1624	0.102716	17220.52100	3.73956	0.0033
0.6	273.1627	273.1626	0.102716	21083.20350	9.51157	0.020

Table A1.24 *Frequencies of resonance, haft-width of resonance peaks and frequency uncertainties for acoustic modes (0,2), (0,3), (0,4), (0,5), and (0,6) at T = 273.16 K and p = 0.078 MPa*

Modo	T_N/K	T_S/K	P/MPa	*f*/Hz	*g*/Hz	u(*f*)/Hz
0.2	273.1609	273.1614	0.078231	5500.21482	1.99458	0.0014
0.3	273.1609	273.1615	0.078228	9457.01456	2.44648	0.0021
0.4	273.1609	273.1616	0.078228	13348.99769	3.04957	0.0011
0.5	273.1610	273.1616	0.078228	17219.65019	4.20519	0.0050
0.6	273.1610	273.1616	0.078228	21082.78268	9.54403	0.017

A.2

Internal radius calculations, acoustic and electromagnetic frequency corrections and theoretical half-width of resonance peaks using argon for Boltzmann constant determination

Frequency of resonance must be corrected in both microwave and acoustic resonance as it was explained in chapter 2. Parameters required to apply those corrections are different for microwave and acoustic resonance. Tables A2.1 to A2.12 show electromagnetic frequency of the three peaks of each mode, thermal penetration length, the experimental and calculated half-width and a comparison between them.

Table A2.1 *Frequency of resonance, thermal penetration length, calculated and experimental half-width for electromagnetic modes , TM11, TE11, TM12, TE12 and TM13 at T = 273.16 K and p = 0.9 MPa.*

	f (Hz)	δ_{TH}(m)	g_{calc} (Hz)	g_{epx} (Hz)	$10^6 x(g_{exp}-g_{calc})/f$
TM11	3260.1712	7.75E-06	0.43022	0.50772	24
	3263.8613	7.75E-06	0.43046	0.46119	9
	3264.1202	7.75E-06	0.43048	0.54775	36
TE11	5341.8942	6.06E-06	0.44885	0.73316	53
	5345.2919	6.05E-06	0.44900	0.71149	49
	5345.6069	6.05E-06	0.44901	0.61052	30
TM12	7271.5640	5.19E-06	0.49846	0.54938	7
	7271.7809	5.19E-06	0.49847	0.64848	21
	7276.4638	5.19E-06	0.49863	0.58178	11
TE12	9184.4164	4.62E-06	0.54864	0.68175	14
	9189.9705	4.62E-06	0.54880	0.66738	13
	9190.4488	4.62E-06	0.54882	0.71827	18
TM13	11076.4244	4.21E-06	0.59605	0.72926	12
	11083.3146	4.20E-06	0.59623	0.72631	12
	11084.1427	4.20E-06	0.59625	0.66682	6

Table A2.2 *Frequency of resonance, thermal penetration length, calculated and experimental half-width for electromagnetic modes , TM11, TE11, TM12, TE12 and TM13 at T = 273.16 K and p = 0.7 MPa*

	f (Hz)	δ_{TH}(m)	g_{calc} (Hz)	g_{epx} (Hz)	$10^6 x(g_{exp}-g_{calc})/f$
TM11	3261.9063	7.75E-06	0.43033	0.51943	27
	3265.6890	7.75E-06	0.43058	0.42454	-2
	3265.9178	7.75E-06	0.43060	0.54830	36
TE11	5344.8881	6.05E-06	0.44898	0.76139	58
	5348.2948	6.05E-06	0.44912	0.67699	43
	5348.4994	6.05E-06	0.44913	0.61031	30
TM12	7275.5979	5.19E-06	0.49860	0.55352	8
	7275.6607	5.19E-06	0.49860	0.65170	21
	7280.5594	5.19E-06	0.49877	0.58190	11
TE12	9189.5515	4.62E-06	0.54879	0.68228	15
	9195.0972	4.62E-06	0.54896	0.66740	13
	9195.6464	4.62E-06	0.54897	0.71780	18
TM13	11082.5945	4.20E-06	0.59621	0.61609	2
	11089.4942	4.20E-06	0.59640	0.70543	10
	11090.3346	4.20E-06	0.59642	0.55685	-4

Table A2.3 *Frequency of resonance, thermal penetration length, calculated and experimental half-width for electromagnetic modes , TM11, TE11, TM12, TE12 and TM13 at T = 273.16 K and p = 0.5 MPa.*

	f (Hz)	δ_{TH}(m)	g_{calc} (Hz)	g_{epx} (Hz)	$10^6 x(g_{exp}-g_{calc})/f$
TM11	3263.6533	7.75E-06	0.43045	0.50758	24
	3267.4845	7.74E-06	0.43070	0.45874	9
	3267.7364	7.74E-06	0.43072	0.54803	36
TE11	5347.8496	6.05E-06	0.44910	0.73173	53
	5351.2655	6.05E-06	0.44925	0.69528	46
	5351.6369	6.05E-06	0.44926	0.60709	29
TM12	7279.6255	5.19E-06	0.49873	0.56359	9
	7279.7002	5.19E-06	0.49874	0.58914	12
	7284.6184	5.19E-06	0.49891	0.58189	11
TE12	9194.6528	4.62E-06	0.54894	0.68258	15
	9200.2093	4.61E-06	0.54911	0.66713	13
	9200.7740	4.61E-06	0.54913	0.71798	18
TM13	11088.7359	4.20E-06	0.59638	0.61180	1
	11095.6525	4.20E-06	0.59656	0.80325	19
	11096.5270	4.20E-06	0.59659	0.55651	-4

Table A2.4 *Frequency of resonance, thermal penetration length, calculated and experimental half-width for electromagnetic modes , TM11, TE11, TM12, TE12 and TM13 at T = 273.16 K and p = 0.4 MPa.*

	f (Hz)	δ_{TH}(m)	g_{calc} (Hz)	g_{epx} (Hz)	$10^6 x(g_{exp}-g_{calc})/f$
TM11	3264.5309	7.75E-06	0.43051	0.50763	24
	3268.3895	7.74E-06	0.43076	0.45830	8
	3268.6416	7.74E-06	0.43078	0.54810	36
TE11	5349.3389	6.05E-06	0.44917	0.72212	51
	5352.7645	6.05E-06	0.44931	0.72566	52
	5353.2013	6.05E-06	0.44933	0.61074	30
TM12	7281.6397	5.19E-06	0.49880	0.56458	9
	7282.1393	5.19E-06	0.49882	0.56610	9
	7286.6414	5.19E-06	0.49897	0.58216	11
TE12	9197.2519	4.62E-06	0.54902	0.68264	15
	9202.1138	4.61E-06	0.54917	0.66742	13
	9202.8843	4.61E-06	0.54919	0.71734	18
TM13	11091.8202	4.20E-06	0.59646	0.62251	2
	11098.7564	4.20E-06	0.59665	0.54502	-5
	11099.6419	4.20E-06	0.59667	0.55654	-4

Table A2.5 *Frequency of resonance, thermal penetration length, calculated and experimental half-width for electromagnetic modes , TM11, TE11, TM12, TE12 and TM13 at T = 273.16 K and p = 0.3 MPa.*

	f (Hz)	δ_{TH}(m)	g_{calc} (Hz)	g_{epx} (Hz)	$10^6 x(g_{exp}-g_{calc})/f$
TM11	3265.4005	7.75E-06	0.43056	0.50969	24
	3269.2495	7.74E-06	0.43082	0.45428	7
	3269.5220	7.74E-06	0.43084	0.55019	37
TE11	5350.8129	6.05E-06	0.44923	0.73799	54
	5354.2440	6.05E-06	0.44937	0.69657	46
	5354.3795	6.05E-06	0.44938	0.60456	29
TM12	7283.6148	5.19E-06	0.49887	0.55315	7
	7283.8627	5.19E-06	0.49888	0.66540	23
	7288.6424	5.18E-06	0.49904	0.58169	11
TE12	9199.7342	4.61E-06	0.54909	0.68218	14
	9205.2386	4.61E-06	0.54926	0.66748	13
	9205.7355	4.61E-06	0.54927	0.71757	18
TM13	11094.8650	4.20E-06	0.59654	0.61935	2
	11101.8238	4.20E-06	0.59673	0.59448	0
	11102.6731	4.20E-06	0.59675	0.55673	-4

Table A2.6 *Frequency of resonance, thermal penetration length, calculated and experimental half-width for electromagnetic modes , TM11, TE11, TM12, TE12 and TM13 at T = 273.16 K and p = 0.2 MPa.*

	f (Hz)	δ_{TH}(m)	g_{calc} (Hz)	g_{epx} (Hz)	$10^6 x(g_{exp}-g_{calc})/f$
TM11	3266.2849	7.74E-06	0.43062	0.50946	24
	3270.1986	7.74E-06	0.43088	0.46212	10
	3270.4439	7.74E-06	0.43090	0.55036	37
TE11	5352.3026	6.05E-06	0.44929	0.75386	57
	5355.7289	6.05E-06	0.44944	0.66748	41
	5355.9245	6.05E-06	0.44944	0.59837	28
TM12	7285.6475	5.19E-06	0.49894	0.56164	9
	7285.6879	5.19E-06	0.49894	0.58499	12
	7290.6627	5.18E-06	0.49911	0.58097	11
TE12	9202.2840	4.61E-06	0.54917	0.68116	14
	9207.8701	4.61E-06	0.54934	0.66803	13
	9208.4262	4.61E-06	0.54935	0.71981	19
TM13	11097.9412	4.20E-06	0.59662	0.62126	2
	11104.8934	4.20E-06	0.59681	0.51306	-8
	11105.7714	4.20E-06	0.59683	0.55652	-4

Table A2.7 *Frequency of resonance, thermal penetration length, calculated and experimental half-width for electromagnetic modes , TM11, TE11, TM12, TE12 and TM13 at T = 273.16 K and p = 0.18 MPa.*

	f (Hz)	δ_{TH}(m)	g_{calc} (Hz)	g_{epx} (Hz)	$10^6 x(g_{exp}-g_{calc})/f$
TM11	3266.4603	7.74E-06	0.43063	0.50970	24
	3270.5395	7.74E-06	0.43090	0.46150	9
	3270.6113	7.74E-06	0.43091	0.55050	37
TE11	5352.5968	6.05E-06	0.44930	0.74866	56
	5355.9556	6.05E-06	0.44944	0.66901	41
	5356.1333	6.05E-06	0.44945	0.59720	28
TM12	7286.0508	5.19E-06	0.49895	0.56084	8
	7287.2122	5.19E-06	0.49899	0.58586	12
	7291.1077	5.18E-06	0.49913	0.58099	11
TE12	9202.7825	4.61E-06	0.54919	0.68118	14
	9208.3860	4.61E-06	0.54935	0.66818	13
	9208.9419	4.61E-06	0.54937	0.71984	19
TM13	11098.5507	4.20E-06	0.59664	0.62119	2
	11105.4948	4.20E-06	0.59683	0.48494	-10
	11106.3737	4.20E-06	0.59685	0.55674	-4

Table A2.8 *Frequency of resonance, thermal penetration length, calculated and experimental half-width for electromagnetic modes , TM11, TE11, TM12, TE12 and TM13 at T = 273.16 K and p = 0.142 MPa.*

	f (Hz)	δ_{TH}(m)	g_{calc} (Hz)	g_{epx} (Hz)	$10^6 x(g_{exp}-g_{calc})/f$
TM11	3266.7888	7.74E-06	0.43066	0.51038	24
	3270.7478	7.74E-06	0.43092	0.45207	6
	3270.9527	7.74E-06	0.43093	0.55063	37
TE11	5353.1427	6.05E-06	0.44933	0.72216	51
	5356.5732	6.05E-06	0.44947	0.67935	43
	5356.9279	6.05E-06	0.44949	0.59284	27
TM12	7286.7616	5.19E-06	0.49898	0.56096	9
	7286.8324	5.19E-06	0.49898	0.59743	14
	7291.8445	5.18E-06	0.49915	0.58099	11
TE12	9203.7634	4.61E-06	0.54921	0.68122	14
	9209.2907	4.61E-06	0.54938	0.66825	13
	9209.6675	4.61E-06	0.54939	0.71964	18
TM13	11099.7132	4.20E-06	0.59667	0.62293	2
	11106.6504	4.20E-06	0.59686	0.50390	-8
	11107.5470	4.20E-06	0.59688	0.55665	-4

Table A2.9 *Frequency of resonance, thermal penetration length, calculated and experimental half-width for electromagnetic modes , TM11, TE11, TM12, TE12 and TM13 at T = 273.16 K and p = 0.135 MPa.*

	f (Hz)	δ_{TH}(m)	g_{calc} (Hz)	g_{epx} (Hz)	$10^6 x(g_{exp}-g_{calc})/f$
TM11	3266.8529	7.74E-06	0.43066	0.51040	24
	3270.8713	7.74E-06	0.43092	0.45193	6
	3271.0454	7.74E-06	0.43094	0.55069	37
TE11	5353.2616	6.05E-06	0.44933	0.71916	50
	5356.6130	6.05E-06	0.44947	0.67970	43
	5356.9094	6.05E-06	0.44948	0.59248	27
TM12	7286.9457	5.19E-06	0.49898	0.56170	9
	7287.1273	5.19E-06	0.49899	0.57440	10
	7291.9846	5.18E-06	0.49916	0.58099	11
TE12	9203.9802	4.61E-06	0.54922	0.68170	14
	9209.1336	4.61E-06	0.54938	0.66892	13
	9209.6092	4.61E-06	0.54939	0.71933	18
TM13	11099.8857	4.20E-06	0.59668	0.62109	2
	11107.0941	4.20E-06	0.59687	0.46852	-12
	11107.3021	4.20E-06	0.59688	0.55727	-4

Table A2.10 *Frequency of resonance, thermal penetration length, calculated and experimental half-width for electromagnetic modes , TM11, TE11, TM12, TE12 and TM13 at T = 273.16 K and p = 0.115 MPa.*

	f (Hz)	δ_{TH}(m)	g_{calc} (Hz)	g_{epx} (Hz)	$10^6 x(g_{exp}-g_{calc})/f$
TM11	3267.0266	7.74E-06	0.43067	0.51068	24
	3271.0747	7.74E-06	0.43094	0.44950	6
	3271.2176	7.74E-06	0.43095	0.55070	37
TE11	5353.5524	6.05E-06	0.44934	0.72482	51
	5356.9252	6.05E-06	0.44949	0.69228	45
	5357.1649	6.05E-06	0.44950	0.59719	28
TM12	7287.3366	5.19E-06	0.49900	0.56283	9
	7287.4451	5.19E-06	0.49900	0.61594	16
	7292.3824	5.18E-06	0.49917	0.58104	11
TE12	9204.4244	4.61E-06	0.54923	0.68171	14
	9210.0195	4.61E-06	0.54940	0.66887	13
	9210.5615	4.61E-06	0.54942	0.71876	18
TM13	11100.5353	4.20E-06	0.59669	0.62213	2
	11107.5027	4.20E-06	0.59688	0.45392	-13
	11108.3257	4.20E-06	0.59690	0.55725	-4

Table A2.11 *Frequency of resonance, thermal penetration length, calculated and experimental half-width for electromagnetic modes , TM11, TE11, TM12, TE12 and TM13 at T = 273.16 K and p = 0.102 MPa.*

	f (Hz)	δ_{TH}(m)	g_{calc} (Hz)	g_{epx} (Hz)	$10^6 x(g_{exp}-g_{calc})/f$
TM11	3267.1370	7.74E-06	0.43068	0.51086	25
	3270.9642	7.74E-06	0.43093	0.44762	5
	3271.3062	7.74E-06	0.43095	0.55070	37
TE11	5353.7361	6.05E-06	0.44935	0.71954	50
	5357.1394	6.05E-06	0.44949	0.69892	47
	5357.3382	6.05E-06	0.44950	0.59748	28
TM12	7287.5976	5.19E-06	0.49901	0.56080	8
	7287.7692	5.18E-06	0.49901	0.63665	19
	7292.6583	5.18E-06	0.49918	0.58104	11
TE12	9204.7415	4.61E-06	0.54924	0.68177	14
	9210.3419	4.61E-06	0.54941	0.66854	13
	9210.8681	4.61E-06	0.54943	0.71853	18
TM13	11100.9111	4.20E-06	0.59670	0.62059	2
	11107.8721	4.20E-06	0.59689	0.53450	-6
	11108.7558	4.20E-06	0.59692	0.55777	-4

Table A2.12 *Frequency of resonance, thermal penetration length, calculated and experimental half-width for electromagnetic modes , TM11, TE11, TM12, TE12 and TM13 at T = 273.16 K and p = 0.078 MPa.*

	f (Hz)	δ_{TH}(m)	g_{calc} (Hz)	g_{epx} (Hz)	$10^6 x(g_{exp}-g_{calc})/f$
TM11	3267.3521	7.74E-06	0.43069	0.51103	25
	3271.3646	7.74E-06	0.43096	0.44574	5
	3271.5339	7.74E-06	0.43097	0.55071	37
TE11	5354.0971	6.05E-06	0.44937	0.71930	50
	5357.5150	6.05E-06	0.44951	0.69824	46
	5357.7080	6.05E-06	0.44952	0.59787	28
TM12	7288.0832	5.18E-06	0.49902	0.56150	9
	7288.4720	5.18E-06	0.49904	0.64202	20
	7293.1417	5.18E-06	0.49920	0.58116	11
TE12	9205.3629	4.61E-06	0.54926	0.68179	14
	9211.4910	4.61E-06	0.54945	0.66808	13
	9210.9610	4.61E-06	0.54943	0.71832	18
TM13	11101.6629	4.20E-06	0.59672	0.72817	12
	11109.4654	4.20E-06	0.59693	0.68448	8
	11108.6279	4.20E-06	0.59691	0.76742	15

Tables A2.13 to A2.24 show measured frequencies of resonance and half-width of resonance peaks at each pressure, it shows all the frequency correction applied (thermal boundary layer, shell motion and tubes corrections) and the theoretical contributions to the half-width of resonance peaks (thermal boundary layer, bulk viscosity and tubes contributions). All these parameters are calculated according description in chapter 2.

Table A2.13 *Acoustic frequency of resonance and half-width measurements and computed thermal boundary layer, shell motion and ducts frequency corrections; and thermal boundary layer, bulk viscosity and ducts half-width theoretical contributions; at T = 273.16 K and p = 0.901 MPa.*

Mode	f (Hz)	g (Hz)	Δf_h (Hz)	Δf_{shell} (Hz)	Δf_{ducts} (Hz)	g_h (Hz)	g_{bulk} (Hz)	g_{ducts} (Hz)
0.2	5507.74	0.77	-0.51168	-0.02568	-0.15472	0.51346	0.00315	5.8216×10^{-8}
0.3	9469.72	0.94	-0.67090	-0.07435	-0.01716	0.67327	0.00931	5.4516×10^{-8}
0.4	13366.29	1.05	-0.79700	-0.08097	-0.39532	0.79986	0.01855	4.7238×10^{-8}
0.5	17241.06	1.63	-0.90518	-0.07368	-0.28524	0.90846	0.03087	3.9015×10^{-8}
0.6	21106.18	5.82	-1.00149	-0.05264	-0.15467	1.00514	0.04626	3.2096×10^{-8}

Table A2.14 *Acoustic frequency of resonance and half-width measurements and computed thermal boundary layer, shell motion and ducts frequency corrections; and thermal boundary layer, bulk viscosity and ducts half-width theoretical contributions; at T = 273.16 K and p = 0.701 MPa.*

Mode	f (Hz)	g (Hz)	Δf_h (Hz)	Δf_{shell} (Hz)	Δf_{ducts} (Hz)	g_h (Hz)	g_{bulk} (Hz)	g_{ducts} (Hz)
0.2	5505.93	0.85	-0.57495	-0.04135	-0.20093	0.57673	0.00403	6.5550×10^{-8}
0.3	9466.73	1.08	-0.75384	-0.05770	0.00599	0.75622	0.01193	6.1515×10^{-8}
0.4	13361.93	1.13	-0.89559	-0.06284	-0.21693	0.89846	0.02376	5.3404×10^{-8}
0.5	17235.85	1.65	-1.01708	-0.05720	-0.67527	1.02038	0.03954	4.4156×10^{-8}
0.6	21098.82	6.32	-1.12524	-0.04090	-0.09144	1.12894	0.05925	3.6288×10^{-8}

Table A2.15 *Acoustic frequency of resonance and half-width measurements and computed thermal boundary layer, shell motion and ducts frequency corrections; and thermal boundary layer, bulk viscosity and ducts half-width theoretical contributions; at T = 273.16 K and p = 0.501 MPa.*

Mode	f (Hz)	g (Hz)	Δf_h (Hz)	Δf_{shell} (Hz)	Δf_{ducts} (Hz)	g_h (Hz)	g_{bulk} (Hz)	g_{ducts} (Hz)
0.2	5504.20	0.96	-0.67409	-0.02948	-0.20633	0.67589	0.00563	7.7004×10^{-8}
0.3	9463.71	1.32	-0.88383	-0.04113	0.00677	0.88626	0.01664	7.2526×10^{-8}
0.4	13357.85	1.30	-1.04998	-0.04481	-0.21488	1.05292	0.03314	6.3153×10^{-8}
0.5	17230.67	1.86	-1.19245	-0.04079	-0.52625	1.19585	0.05514	5.2271×10^{-8}
0.6	21092.22	6.64	-1.31927	-0.02918	-0.08992	1.32309	0.08263	4.2922×10^{-8}

Table A2.16 *Acoustic frequency of resonance and half-width measurements and computed thermal boundary layer, shell motion and ducts frequency corrections; and thermal boundary layer, bulk viscosity and ducts half-width theoretical contributions; at T = 273.16 K and p = 0.401 MPa.*

Mode	f (Hz)	g (Hz)	Δf_h (Hz)	Δf_{shell} (Hz)	Δf_{ducts} (Hz)	g_h (Hz)	g_{bulk} (Hz)	g_{ducts} (Hz)
0.2	5503.34	1.04	-0.75048	-0.02354	-0.20465	0.75231	0.00703	8.5840×10^{-8}
0.3	9462.11	1.38	-0.98398	-0.03285	0.00607	0.98645	0.02077	8.1092×10^{-8}
0.4	13355.86	1.42	-1.16894	-0.03579	-0.21071	1.17195	0.04138	7.0776×10^{-8}
0.5	17228.11	2.04	-1.32757	-0.03259	-0.43676	1.33107	0.06885	5.8620×10^{-8}
0.6	21089.29	7.20	-1.46875	-0.02332	-0.09250	1.47269	0.10317	4.8115×10^{-8}

Table A2.17 *Acoustic frequency of resonance and half-width measurements and computed thermal boundary layer, shell motion and ducts frequency corrections; and thermal boundary layer, bulk viscosity and ducts half-width theoretical contributions; at T = 273.16 K and p = 0.302 MPa.*

Mode	f (Hz)	g (Hz)	Δf_h (Hz)	Δf_{shell} (Hz)	Δf_{ducts} (Hz)	g_h (Hz)	g_{bulk} (Hz)	g_{ducts} (Hz)
0.2	5502.53	1.17	-0.86143	-0.01769	-0.19335	0.86330	0.00932	9.8724×10^{-8}
0.3	9460.70	1.41	-1.12943	-0.02469	-0.01040	1.13199	0.02756	9.3724×10^{-8}
0.4	13353.98	1.61	-1.34174	-0.02689	-0.19998	1.34489	0.05491	8.2060×10^{-8}
0.5	17225.80	2.29	-1.52379	-0.02449	-0.34020	1.52747	0.09137	6.8023×10^{-8}
0.6	21086.59	7.93	-1.68584	-0.01753	-0.09942	1.69000	0.13691	5.5786×10^{-8}

Table A2.18 *Acoustic frequency of resonance and half-width measurements and computed thermal boundary layer, shell motion and ducts frequency corrections; and thermal boundary layer, bulk viscosity and ducts half-width theoretical contributions; at T = 273.16 K and p = 0.201 MPa.*

Mode	f (Hz)	g (Hz)	Δf_h (Hz)	Δf_{shell} (Hz)	Δf_{ducts} (Hz)	g_h (Hz)	g_{bulk} (Hz)	g_{ducts} (Hz)
0.2	5501.63	1.39	-1.05116	-0.01176	-0.15750	1.05315	0.01398	1.2098×10^{-7}
0.3	9459.24	1.65	-1.37816	-0.01641	-0.21154	1.38093	0.04134	1.1590×10^{-7}
0.4	13352.00	1.98	-1.63722	-0.01788	-0.17283	1.64066	0.08236	1.0200×10^{-7}
0.5	17223.30	2.93	-1.85933	-0.01628	-0.23107	1.86339	0.13705	8.4650×10^{-8}
0.6	21083.94	9.00	-2.05705	-0.01166	-0.10901	2.06168	0.20537	6.9328×10^{-8}

Table A2.19 *Acoustic frequency of resonance and half-width measurements and computed thermal boundary layer, shell motion and ducts frequency corrections; and thermal boundary layer, bulk viscosity and ducts half-width theoretical contributions; at T = 273.16 K and p = 0.181 MPa.*

Mode	f (Hz)	g (Hz)	Δf_h (Hz)	Δf_{shell} (Hz)	Δf_{ducts} (Hz)	g_h (Hz)	g_{bulk} (Hz)	g_{ducts} (Hz)
0.2	5501.43	1.43	-1.10684	-0.01058	-0.14588	1.10887	0.01553	1.2757×10^{-7}
0.3	9458.90	1.66	-1.45116	-0.01477	-0.35756	1.45400	0.04590	1.2255×10^{-7}
0.4	13351.49	2.02	-1.72392	-0.01609	-0.16581	1.72746	0.09145	1.0801×10^{-7}
0.5	17222.69	2.91	-1.95780	-0.01466	-0.20541	1.96198	0.15217	8.9666×10^{-8}
0.6	21084.08	8.62	-2.16602	-0.01049	-0.11155	2.17081	0.22805	7.3456×10^{-8}

Table A2.20 *Acoustic frequency of resonance and half-width measurements and computed thermal boundary layer, shell motion and ducts frequency corrections; and thermal boundary layer, bulk viscosity and ducts half-width theoretical contributions; at T = 273.16 K and p = 0.142 MPa.*

Mode	f (Hz)	g (Hz)	Δf_h (Hz)	Δf_{shell} (Hz)	Δf_{ducts} (Hz)	g_h (Hz)	g_{bulk} (Hz)	g_{ducts} (Hz)
0.2	5501.05	1.57	-1.24261	-0.00837	-0.12089	1.24421	0.01961	1.4372×10^{-7}
0.3	9458.32	1.84	-1.62937	-0.01168	-0.69238	1.63146	0.05796	1.3901×10^{-7}
0.4	13350.70	2.26	-1.93582	-0.01273	-0.15462	1.93830	0.11548	1.2294×10^{-7}
0.5	17221.69	3.25	-2.19864	-0.01160	-0.14889	2.20146	0.19215	1.0214×10^{-7}
0.6	21083.54	8.98	-2.43269	-0.00830	-0.11674	2.43582	0.28799	8.3622×10^{-8}

Table A2.21 *Acoustic frequency of resonance and half-width measurements and computed thermal boundary layer, shell motion and ducts frequency corrections; and thermal boundary layer, bulk viscosity and ducts half-width theoretical contributions; at T = 273.16 K and p = 0.135 MPa.*

Mode	f (Hz)	g (Hz)	Δf_h (Hz)	Δf_{shell} (Hz)	Δf_{ducts} (Hz)	g_h (Hz)	g_{bulk} (Hz)	g_{ducts} (Hz)
0.2	5500.94	1.61	-1.27509	-0.00794	-0.11595	1.27668	0.02065	1.4763×10^{-7}
0.3	9458.14	1.90	-1.67196	-0.01109	-0.70827	1.67405	0.06106	1.4302×10^{-7}
0.4	13350.45	2.34	-1.98643	-0.01208	-0.15303	1.98891	0.12166	1.2659×10^{-7}
0.5	17221.41	3.35	-2.25610	-0.01101	-0.13669	2.25892	0.20243	1.0519×10^{-7}
0.6	21083.35	9.32	-2.49634	-0.00788	-0.11788	2.49946	0.30342	8.6111×10^{-8}

Table A2.22 *Acoustic frequency of resonance and half-width measurements and computed thermal boundary layer, shell motion and ducts frequency corrections; and thermal boundary layer, bulk viscosity and ducts half-width theoretical contributions; at T = 273.16 K and p = 0.115 MPa.*

Mode	f (Hz)	g (Hz)	Δf_h (Hz)	Δf_{shell} (Hz)	Δf_{ducts} (Hz)	g_h (Hz)	g_{bulk} (Hz)	g_{ducts} (Hz)
0.2	5500.71	1.71	-1.37848	-0.00678	-0.10330	1.38007	0.02417	1.6014×10^{-7}
0.3	9457.79	2.04	-1.80754	-0.00947	-0.62341	1.80963	0.07146	1.5596×10^{-7}
0.4	13349.97	2.52	-2.14750	-0.01032	-0.14944	2.14998	0.14238	1.3841×10^{-7}
0.5	17220.83	3.60	-2.43907	-0.00940	-0.10180	2.44189	0.23692	1.1506×10^{-7}
0.6	21083.13	9.53	-2.69876	-0.00673	-0.12114	2.70188	0.35511	9.4149×10^{-8}

Table A2.23 *Acoustic frequency of resonance and half-width measurements and computed thermal boundary layer, shell motion and ducts frequency corrections; and thermal boundary layer, bulk viscosity and ducts half-width theoretical contributions; at T = 273.16 K and p = 0.102 MPa.*

Mode	f (Hz)	g (Hz)	Δf_h (Hz)	Δf_{shell} (Hz)	Δf_{ducts} (Hz)	g_h (Hz)	g_{bulk} (Hz)	g_{ducts} (Hz)
0.2	5500.58	1.79	-1.45891	-0.00605	-0.09661	1.46050	0.02710	1.6995×10^{-7}
0.3	9457.58	2.15	-1.91303	-0.00844	-0.51731	1.91511	0.08011	1.6621×10^{-7}
0.4	13349.73	2.67	-2.27283	-0.00920	-0.14704	2.27531	0.15962	1.4780×10^{-7}
0.5	17220.52	3.74	-2.58143	-0.00838	-0.07893	2.58425	0.26562	1.2292×10^{-7}
0.6	21083.20	9.51	-2.85632	-0.00600	-0.12323	2.85943	0.39814	1.0055×10^{-7}

Table A2.24 *Acoustic frequency of resonance and half-width measurements and computed thermal boundary layer, shell motion and ducts frequency corrections; and thermal boundary layer, bulk viscosity and ducts half-width theoretical contributions; at T = 273.16 K and p = 0.078 MPa.*

Mode	f (Hz)	g (Hz)	Δf_h (Hz)	Δf_{shell} (Hz)	Δf_{ducts} (Hz)	g_h (Hz)	g_{bulk} (Hz)	g_{ducts} (Hz)
0.2	5500.21	1.99	-1.66825	-0.00462	-0.08962	1.66984	0.03549	1.9587×10^{-7}
0.3	9457.01	2.45	-2.18755	-0.00644	-0.31409	2.18963	0.10493	1.9363×10^{-7}
0.4	13349.00	3.05	-2.59899	-0.00702	-0.13644	2.60146	0.20907	1.7305×10^{-7}
0.5	17219.65	4.21	-2.95184	-0.00639	-0.03867	2.95465	0.34789	1.4403×10^{-7}
0.6	21082.78	9.54	-3.26621	-0.00458	-0.12633	3.26932	0.52150	1.1769×10^{-7}

Some of the properties required to calculate the acoustic corrections displayed previously are shown in the following tables.

Table A2.25 *Thermal penetration length, viscous penetration length, and thermal penetration length in shell side for acoustic modes (0,2), (0,3), (0,4), (0,5), (0,6), (0,7) and (0,8) at T = 273.16 K and p = 0.901 MPa*

Mode	δ_{TH}/m	δ_V/m	$\delta_{TH,316L}$/m
0.2	1.0658×10^{-5}	8.7499×10^{-6}	1.5284×10^{-5}
0.3	8.1284×10^{-6}	6.6730×10^{-6}	1.1656×10^{-5}
0.4	6.8416×10^{-6}	5.6165×10^{-6}	9.8110×10^{-6}
0.5	6.0241×10^{-6}	4.9455×10^{-6}	8.6385×10^{-6}
0.6	5.4447×10^{-6}	4.4698×10^{-6}	7.8075×10^{-6}

Table A2.26 *Thermal penetration length, viscous penetration length, and thermal penetration length in shell side for acoustic modes (0,2), (0,3), (0,4), (0,5), (0,6), (0,7) and (0,8) at T = 273.16 K and p = 0.701 MPa*

Mode	δ_{TH}/m	δ_{V}/m	$\delta_{TH,316L}$/m
0.2	1.2104×10^{-5}	9.9204×10^{-6}	1.5286×10^{-5}
0.3	9.2304×10^{-6}	7.5655×10^{-6}	1.1658×10^{-5}
0.4	7.7697×10^{-6}	6.3682×10^{-6}	9.8126×10^{-6}
0.5	6.8407×10^{-6}	5.6068×10^{-6}	8.6398×10^{-6}
0.6	6.1828×10^{-6}	5.0676×10^{-6}	7.8089×10^{-6}

Table A2.27 *Thermal penetration length, viscous penetration length, and thermal penetration length in shell side for acoustic modes (0,2), (0,3), (0,4), (0,5), (0,6), (0,7) and (0,8) at T = 273.16 K and p = 0.501 MPa*

Mode	δ_{TH}/m	δ_{V}/m	$\delta_{TH,316L}$/m
0.2	1.4342×10^{-5}	1.1736×10^{-5}	1.5289×10^{-5}
0.3	1.0937×10^{-5}	8.9502×10^{-6}	1.1660×10^{-5}
0.4	9.2061×10^{-6}	7.5334×10^{-6}	9.8141×10^{-6}
0.5	8.1056×10^{-6}	6.6329×10^{-6}	8.6411×10^{-6}
0.6	7.3262×10^{-6}	5.9951×10^{-6}	7.8101×10^{-6}

Table A2.28 *Thermal penetration length, viscous penetration length, and thermal penetration length in shell side for acoustic modes (0,2), (0,3), (0,4), (0,5), (0,6), (0,7) and (0,8) at T = 273.16 K and p = 0.401 MPa*

Mode	δ_{TH}/m	δ_{V}/m	$\delta_{TH,316L}$/m
0.2	1.6052×10^{-5}	1.3125×10^{-5}	1.5290×10^{-5}
0.3	1.2242×10^{-5}	1.0010×10^{-5}	1.1661×10^{-5}
0.4	1.0304×10^{-5}	8.4249×10^{-6}	9.8148×10^{-6}
0.5	9.0723×10^{-6}	7.4180×10^{-6}	8.6417×10^{-6}
0.6	8.1998×10^{-6}	6.7046×10^{-6}	7.8107×10^{-6}

Table A2.29 *Thermal penetration length, viscous penetration length, and thermal penetration length in shell side for acoustic modes (0,2), (0,3), (0,4), (0,5), (0,6), (0,7) and (0,8) at T = 273.16 K and p = 0.301 MPa*

Mode	δ_{TH}/m	δ_{V}/m	$\delta_{TH,316L}$/m
0.2	1.8522×10^{-5}	1.5132×10^{-5}	1.5291×10^{-5}
0.3	1.4125×10^{-5}	1.1540×10^{-5}	1.1662×10^{-5}
0.4	1.1889×10^{-5}	9.7136×10^{-6}	9.8155×10^{-6}
0.5	1.0468×10^{-5}	8.5526×10^{-6}	8.6423×10^{-6}
0.6	9.4614×10^{-6}	7.7301×10^{-6}	7.8112×10^{-6}

Table A2.30 *Thermal penetration length, viscous penetration length, and thermal penetration length in shell side for acoustic modes (0,2), (0,3), (0,4), (0,5), (0,6), (0,7) and (0,8) at T = 273.16 K and p = 0.201 MPa*

Mode	δ_{TH}/m	δ_{V}/m	$\delta_{TH,316L}$/m
0.2	2.2722×10^{-5}	1.8549×10^{-5}	1.5292×10^{-5}
0.3	1.7329×10^{-5}	1.4146×10^{-5}	1.1662×10^{-5}
0.4	1.4586×10^{-5}	1.1907×10^{-5}	9.8162×10^{-6}
0.5	1.2842×10^{-5}	1.0484×10^{-5}	8.6429×10^{-6}
0.6	1.1607×10^{-5}	9.4754×10^{-6}	7.8116×10^{-6}

Table A2.31 *Thermal penetration length, viscous penetration length, and thermal penetration length in shell side for acoustic modes (0,2), (0,3), (0,4), (0,5), (0,6), (0,7) and (0,8) at T = 273.16 K and p = 0.180 MPa*

Mode	δ_{TH}/m	δ_{V}/m	$\delta_{TH,316L}$/m
0.2	2.3951×10^{-5}	1.9550×10^{-5}	1.5293×10^{-5}
0.3	1.8266×10^{-5}	1.4909×10^{-5}	1.1663×10^{-5}
0.4	1.5375×10^{-5}	1.2549×10^{-5}	9.8164×10^{-6}
0.5	1.3537×10^{-5}	1.1049×10^{-5}	8.6431×10^{-6}
0.6	1.2235×10^{-5}	9.9862×10^{-6}	7.8116×10^{-6}

Table A2.32 *Thermal penetration length, viscous penetration length, and thermal penetration length in shell side for acoustic modes (0,2), (0,3), (0,4), (0,5), (0,6), (0,7) and (0,8) at T = 273.16 K and p = 0.142 MPa*

Mode	δ_{TH}/m	δ_{V}/m	$\delta_{TH,316L}$/m
0.2	2.6932×10^{-5}	2.1976×10^{-5}	1.5293×10^{-5}
0.3	2.0539×10^{-5}	1.6759×10^{-5}	1.1663×10^{-5}
0.4	1.7288×10^{-5}	1.4106×10^{-5}	9.8167×10^{-6}
0.5	1.5221×10^{-5}	1.2420×10^{-5}	8.6433×10^{-6}
0.6	1.3757×10^{-5}	1.1225×10^{-5}	7.8117×10^{-6}

Table A2.33 *Thermal penetration length, viscous penetration length, and thermal penetration length in shell side for acoustic modes (0,2), (0,3), (0,4), (0,5), (0,6), (0,7) and (0,8) at T = 273.16 K and p = 0.135 MPa*

Mode	δ_{TH}/m	δ_{V}/m	$\delta_{TH,316L}$/m
0.2	2.7646×10^{-5}	2.2558×10^{-5}	1.5293×10^{-5}
0.3	2.1084×10^{-5}	1.7203×10^{-5}	1.1663×10^{-5}
0.4	1.7746×10^{-5}	1.4480×10^{-5}	9.8168×10^{-6}
0.5	1.5625×10^{-5}	1.2749×10^{-5}	8.6434×10^{-6}
0.6	1.4122×10^{-5}	1.1523×10^{-5}	7.8118×10^{-6}

Table A2.34 *Thermal penetration length, viscous penetration length, and thermal penetration length in shell side for acoustic modes (0,2), (0,3), (0,4), (0,5), (0,6), (0,7) and (0,8) at T = 273.16 K and p = 0.115 MPa*

Mode	δ_{TH}/m	δ_{V}/m	$\delta_{TH,316L}$/m
0.2	2.9919×10^{-5}	2.4408×10^{-5}	1.5294×10^{-5}
0.3	2.2817×10^{-5}	1.8614×10^{-5}	1.1663×10^{-5}
0.4	1.9205×10^{-5}	1.5668×10^{-5}	9.8170×10^{-6}
0.5	1.6910×10^{-5}	1.3795×10^{-5}	8.6435×10^{-6}
0.6	1.5283×10^{-5}	1.2468×10^{-5}	7.8118×10^{-6}

Table A2.35 *Thermal penetration length, viscous penetration length, and thermal penetration length in shell side for acoustic modes (0,2), (0,3), (0,4), (0,5), (0,6), (0,7) and (0,8) at T = 273.16 K and p = 0.102 MPa*

Mode	δ_{TH}/m	δ_{V}/m	$\delta_{TH,316L}$/m
0.2	3.1685×10^{-5}	2.5846×10^{-5}	1.5294×10^{-5}
0.3	2.4165×10^{-5}	1.9712×10^{-5}	1.1663×10^{-5}
0.4	2.0339×10^{-5}	1.6591×10^{-5}	9.8171×10^{-6}
0.5	1.7908×10^{-5}	1.4608×10^{-5}	8.6436×10^{-6}
0.6	1.6185×10^{-5}	1.3202×10^{-5}	7.8118×10^{-6}

Table A2.36 *Thermal penetration length, viscous penetration length, and thermal penetration length in shell side for acoustic modes (0,2), (0,3), (0,4), (0,5), (0,6), (0,7) and (0,8) at T = 273.16 K and p = 0.078 MPa*

Mode	δ_{TH}/m	δ_{V}/m	$\delta_{TH,316L}$/m
0.2	3.6279×10^{-5}	2.9587×10^{-5}	1.5294×10^{-5}
0.3	2.7668×10^{-5}	2.2565×10^{-5}	1.1664×10^{-5}
0.4	2.3288×10^{-5}	1.8992×10^{-5}	9.8173×10^{-6}
0.5	2.0504×10^{-5}	1.6722×10^{-5}	8.6438×10^{-6}
0.6	1.8530×10^{-5}	1.5113×10^{-5}	7.8119×10^{-6}

A.3

Speed of sound measurements and pressure and temperature corrections.

Table A3.1 *Average internal radius calculated and internal radius corrected in temperature for computing of correction ratio for speed of sound in argon for the determination of the Boltzman constant.*

p/Mpa	T/K	$a_{p,T}$/m	$a_{p,T=273.16K}$/m
0.901	273.164	0.040014681	0.040014701
0.701	273.162	0.040014436	0.040014454
0.501	273.162	0.040014072	0.040014090
0.401	273.161	0.040014063	0.040014074
0.302	273.163	0.040013985	0.040014008
0.201	273.162	0.040013924	0.040013935
0.181	273.161	0.040013896	0.040013906
0.143	273.162	0.040014218	0.040014229
0.136	273.160	0.040013913	0.040013913
0.103	273.162	0.040013932	0.040013934
0.079	273.161	0.040014225	0.040014226

Table A3.2 *Measured speed of sound at the measuring conditions correction ratio, speed of sound at the desired conditions, p = 0.90 MPa and T = 273.16 K.*

Mode	p/MPa	T/K	u_{exp}/m·s^{-1}	$\frac{u_0/a_0}{u_{exp}/a_{exp}}$	u_{PoTo}/m·s^{-1}
0.2	0.90127	273.1640	308.2134	0.99998995	308.2105
0.3	0.90127	273.1639	308.2184	0.99999004	308.2154
0.4	0.90133	273.1639	308.2199	0.99998994	308.2170
0.5	0.90126	273.1639	308.1900	0.99999006	308.1871
0.6	0.90126	273.1639	308.1637	0.99999015	308.1608

Table A3.3 *Measured speed of sound at the measuring conditions correction ratio, speed of sound at the desired conditions, p = 0.70 MPa and T = 273.16 K.*

Mode	p/MPa	T/K	u_{exp}/m·s^{-1}	$\frac{u_0/a_0}{u_{exp}/a_{exp}}$	u_{PoTo}/m·s^{-1}
0.2	0.70127	273.162	308.1169	0.99999474	308.1155
0.3	0.70129	273.161	308.1208	0.99999480	308.1194
0.4	0.70124	273.161	308.1153	0.99999535	308.1140
0.5	0.70130	273.161	308.1035	0.99999563	308.1023
0.6	0.70132	273.161	308.0550	0.99999569	308.0539

Table A3.4 *Measured speed of sound at the measuring conditions correction ratio, speed of sound at the desired conditions, p = 0.50 MPa and T = 273.16 K.*

Mode	P/MPa	T/K	u_{exp}/m·s^{-1}	$\frac{u_0/a_0}{u_{exp}/a_{exp}}$	u_{PoTo}/m·s^{-1}
0.2	0.50122	273.162	308.0224	0.99999359	308.0206
0.3	0.50122	273.162	308.0233	0.99999359	308.0214
0.4	0.50122	273.162	308.0216	0.99999368	308.0198
0.5	0.50123	273.162	308.0084	0.99999366	308.0065
0.6	0.50122	273.162	307.9586	0.99999377	307.9568

Table A3.5 *Measured speed of sound at the measuring conditions correction ratio, speed of sound at the desired conditions, p = 0.40 MPa and T = 273.16 K.*

Mode	p/MPa	T/K	u_{exp}/m·s^{-1}	$\frac{u_0/a_0}{u_{exp}/a_{exp}}$	u_{PoTo}/m·s^{-1}
0.2	0.40080	273.161	307.9782	0.99999654	307.9772
0.3	0.40080	273.161	307.9741	0.99999664	307.9731
0.4	0.40082	273.161	307.9779	0.99999662	307.9770
0.5	0.40080	273.161	307.9633	0.99999682	307.9624
0.6	0.40081	273.161	307.9179	0.99999691	307.9171

Table A3.6 *Measured speed of sound at the measuring conditions correction ratio, speed of sound at the desired conditions, p = 0.30 MPa and T = 273.16 K.*

Mode	p/MPa	T/K	u_{exp}/m·s^{-1}	$\frac{u_0/a_0}{u_{exp}/a_{exp}}$	u_{PoTo}/m·s^{-1}
0.2	0.30157	273.163	307.9376	0.99999214	307.9353
0.3	0.30157	273.163	307.9327	0.99999205	307.9304
0.4	0.30157	273.163	307.9377	0.99999205	307.9354
0.5	0.30157	273.163	307.9229	0.99999186	307.9206
0.6	0.30157	273.163	307.8811	0.99999168	307.8787

Table A3.7 *Measured speed of sound at the measuring conditions correction ratio, speed of sound at the desired conditions, p = 0.20 MPa and T = 273.16 K.*

Mode	p/MPa	T/K	u_{exp}/m·s^{-1}	$\frac{u_0/a_0}{u_{exp}/a_{exp}}$	u_{PoTo}/m·s^{-1}
0.2	0.20073	273.162	307.8951	0.99999453	307.8935
0.3	0.20073	273.162	307.8990	0.99999435	307.8974
0.4	0.20073	273.162	307.8975	0.99999435	307.8958
0.5	0.20073	273.162	307.8817	0.99999425	307.8800
0.6	0.20073	273.162	307.8474	0.99999435	307.8458

Table A3.8 *Measured speed of sound at the measuring conditions correction ratio, speed of sound at the desired conditions, p = 0.18 MPa and T = 273.16 K.*

Mode	p/MPa	T/K	u_{exp}/m·s^{-1}	$\frac{u_0/a_0}{u_{exp}/a_{exp}}$	u_{PoTo}/m·s^{-1}
0.2	0.18072	273.161	307.8860	0.99999669	307.8850
0.3	0.18072	273.161	307.8948	0.99999679	307.8939
0.4	0.18072	273.161	307.8873	0.99999679	307.8864
0.5	0.18072	273.161	307.8718	0.99999688	307.8710
0.6	0.18072	273.161	307.8508	0.99999688	307.8499

Table A3.9 *Measured speed of sound at the measuring conditions correction ratio, speed of sound at the desired conditions, p = 0.1403 MPa and T = 273.16 K.*

Mode	p/MPa	T/K	u_{exp}/m·s^{-1}	$\frac{u_0/a_0}{u_{exp}/a_{exp}}$	u_{PoTo}/m·s^{-1}
0.2	0.14303	273.162	307.8732	0.99999472	307.8717
0.3	0.14303	273.162	307.8951	0.99999472	307.8936
0.4	0.14303	273.162	307.8760	0.99999490	307.8745
0.5	0.14303	273.162	307.8598	0.99999509	307.8584
0.6	0.14303	273.162	307.8493	0.99999536	307.8480

Table A3.10 *Measured speed of sound at the measuring conditions correction ratio, speed of sound at the desired conditions, p = 0.136 MPa and T = 273.16 K.*

Mode	p/MPa	T/K	u_{exp}/m·s^{-1}	$\frac{u_0/a_0}{u_{exp}/a_{exp}}$	u_{PoTo}/m·s^{-1}
0.2	0.13575	273.160	307.8664	0.99999944	307.8663
0.3	0.13575	273.160	307.8889	0.99999981	307.8888
0.4	0.13575	273.160	307.8692	1.00000008	307.8692
0.5	0.13575	273.160	307.8531	1.00000054	307.8533
0.6	0.13575	273.160	307.8452	1.00000092	307.8455

Table A3.11 *Measured speed of sound at the measuring conditions correction ratio, speed of sound at the desired conditions, p = 0.116 MPa and T = 273.16 K.*

Mode	p/MPa	T/K	u_{exp}/m·s^{-1}	$\frac{u_0/a_0}{u_{exp}/a_{exp}}$	u_{PoTo}/m·s^{-1}
0.2	0.11596	273.160	307.8753	0.99999990	307.8753
0.3	0.11595	273.160	307.8955	1.00000000	307.8955
0.4	0.11595	273.160	307.8784	0.99999991	307.8784
0.5	0.11595	273.160	307.8622	0.99999991	307.8622
0.6	0.11595	273.160	307.8617	0.99999991	307.8616

Table A3.12 *Measured speed of sound at the measuring conditions correction ratio, speed of sound at the desired conditions, p = 0.103 MPa and T = 273.16 K.*

Mode	p/MPa	T/K	u_{exp}/m·s^{-1}	$\frac{u_0/a_0}{u_{exp}/a_{exp}}$	u_{PoTo}/m·s^{-1}
0.2	0.10341	273.162	307.8552	0.99999629	307.8541
0.3	0.10341	273.162	307.8721	0.99999593	307.8709
0.4	0.10341	273.162	307.8591	0.99999556	307.8577
0.5	0.10341	273.162	307.8422	0.99999556	307.8408
0.6	0.10341	273.163	307.8485	0.99999510	307.8470

Table A3.13 *Measured speed of sound at the measuring conditions correction ratio, speed of sound at the desired conditions, p = 0.079 MPa and T = 273.16 K.*

Mode	p/MPa	T/K	u_{exp}/m·s^{-1}	$\frac{u_0/a_0}{u_{exp}/a_{exp}}$	u_{PoTo}/m·s^{-1}
0.2	0.07892	273.161	307.8485	0.99999787	307.8479
0.3	0.07892	273.161	307.8583	0.99999778	307.8576
0.4	0.07892	273.161	307.8516	0.99999769	307.8509
0.5	0.07892	273.161	307.8347	0.99999760	307.8340
0.6	0.07892	273.161	307.8506	0.99999760	307.8499

Appendix B

ACOUSTIC RESONANCE MEASUREMENTS IN ARGON IN ORDER TO CALIBRATE RESONANTIG CAVITY INTERNAL RADIUS

B1

Frequency measurements, frequency corrections and radius measurements and uncertainties at T=250K

Table B1.1 *Pressure, north and south hemisphere and average temperature, frequency of resonance, half-width of the resonance peak and frequency measurement uncertainty using argon to calibrate internal radius at T = 250 K.*

Mode	p/MPa	T_N/K	T_S/K	T_{av}/K	*f*/Hz	*g*/Hz	u(*f*)/Hz
0.2	20.01876	250.1524	250.1560	250.1542	6294.3368	0.33276	0.15
0.3	20.01873	250.1524	250.1559	250.15415	10820.4612	0.49613	0.98
0.4	20.01871	250.1524	250.1559	250.15415	15271.4389	0.73694	0.44
0.5	20.01872	250.1524	250.1559	250.15415	19695.8680	1.37203	4.17
0.2	19.06063	250.1471	250.1505	250.1488	6188.0537	0.36371	0.50
0.3	19.06039	250.1471	250.1507	250.1489	10637.6599	0.62635	3.6
0.4	19.06021	250.1471	250.1509	250.1490	15013.8285	0.67541	0.14
0.5	19.0599	250.1471	250.1509	250.1490	19364.3549	1.19590	1.2
0.2	18.00176	250.0719	250.0805	250.0762	6075.12063	0.37332	0.44
0.3	18.00181	250.0819	250.0805	250.0812	10444.0687	0.43935	2.9
0.4	18.00188	250.0831	250.0170	250.0501	14740.4218	0.62056	0.46
0.5	18.00199	250.0843	250.0828	250.0836	19012.5917	1.22957	1.2
0.2	17.05411	250.081	250.0788	250.0799	5979.5392	0.33343	0.12
0.3	17.05421	250.0822	250.0501	250.0662	10279.6144	0.44975	2.3
0.4	17.05426	250.0834	250.0814	250.0824	14508.6960	0.58971	0.50
0.5	17.05434	250.0847	250.0826	250.0837	18714.3586	1.42276	0.95
0.2	16.00529	250.1706	250.1665	250.1686	5880.73549	0.43342	0.31
0.3	16.00501	250.1692	250.1680	250.1686	10109.6353	0.49636	3.8
0.4	16.00479	250.1692	250.1680	250.1686	14268.8338	0.60739	0.63
0.5	16.00470	250.1677	250.1687	250.1682	18404.9078	1.25743	1.6
0.2	15.01994	250.0844	250.0829	250.0836	5792.5810	0.35272	0.12
0.3	15.02003	250.0861	250.0850	250.0855	9958.4836	0.43772	3.6
0.4	15.02009	250.0869	250.0859	250.0864	14055.7451	0.57966	0.26
0.5	15.02021	250.0878	250.0869	250.0873	18131.1599	1.54908	2.4
0.2	14.01552	250.1212	250.1219	250.1216	5710.7844	0.31767	0.14
0.3	14.01552	250.1220	250.1225	250.1223	9817.8213	0.44813	1.8
0.4	14.01556	250.1228	250.1233	250.1231	13857.3040	0.56062	0.23
0.5	14.01559	250.1235	250.1239	250.1237	17875.0396	2.61556	3.0

Mode	p/MPa	T_N/K	T_S/K	T_{av}/K	*f*/Hz	*g*/Hz	u(*f*)/Hz
0.2	13.01852	250.1363	250.1370	250.1367	5636.3503	0.30946	0.15
0.3	13.01851	250.1362	250.1378	250.1370	9689.8296	0.45446	0.99
0.4	13.01852	250.1362	250.1384	250.1373	13676.7860	0.55561	0.40
0.5	13.01853	250.1364	250.1389	250.1377	17641.1610	1.20467	0.32
0.2	12.01688	250.1308	250.1319	250.1314	5568.4970	0.29683	0.053
0.3	12.01690	250.1316	250.1326	250.1321	9573.2517	0.41770	0.52
0.4	12.01391	250.1323	250.1333	250.1328	13512.2839	0.52154	0.27
0.5	12.01693	250.1330	250.1340	250.1335	17429.7584	1.60659	1.0
0.2	11.00380	250.1372	250.1404	250.1388	5507.3666	0.31155	0.16
0.3	11.00367	250.1412	250.1418	250.1415	9468.0984	0.38794	0.48
0.4	11.00370	250.1412	250.1425	250.1419	13363.9237	0.53841	0.62
0.5	11.00373	250.1407	250.1429	250.1418	17238.3241	1.20079	0.65
0.2	10.01454	250.0873	250.0867	250.0870	5453.8740	0.30691	0.13
0.3	10.01459	250.0873	250.0867	250.0870	9376.2745	0.40310	0.62
0.4	10.01464	250.0883	250.0876	250.0880	13234.5148	0.64179	0.36
0.5	10.01468	250.0893	250.0886	250.0890	17070.9959	1.28428	0.32
0.2	9.01102	250.1051	250.1036	250.1044	5407.4809	0.30563	0.14
0.3	9.01107	250.1062	250.1048	250.1055	9296.5746	0.40391	0.99
0.4	9.01109	250.1075	250.1060	250.1068	13121.8083	0.50390	0.16
0.5	9.01112	250.1087	250.1072	250.1080	16926.1746	1.03643	0.32
0.2	8.00243	250.1478	250.1516	250.1497	5367.9596	0.31771	0.15
0.3	8.00245	250.1478	250.1516	250.1497	9228.6021	0.37330	0.40
0.4	8.00243	250.1479	250.1517	250.1498	13025.9777	0.50041	0.41
0.5	8.00244	250.1480	250.1518	250.1499	16802.5790	0.88604	0.15
0.2	7.00423	250.0943	250.0930	250.0937	5333.9907	0.30151	0.057
0.3	7.00421	250.0955	250.0943	250.0949	9170.2301	0.39713	0.46
0.4	7.00421	250.0958	250.0954	250.0956	12943.6523	0.52080	0.33
0.5	7.00424	250.0963	250.0964	250.0964	16696.5740	0.85648	0.23
0.2	6.00370	250.1204	250.1222	250.1213	5307.0462	0.30278	0.087
0.3	6.00358	250.1246	250.1238	250.1242	9123.8797	0.39830	0.18
0.4	6.00356	250.1247	250.1250	250.1249	12878.2020	0.50644	0.10
0.5	6.00354	250.1247	250.1250	250.1249	16612.1658	0.79620	0.16
0.2	5.00406	250.1344	250.1369	250.1357	5285.4550	0.30236	0.11
0.3	5.00403	250.1344	250.1369	250.1357	9086.8007	0.42313	0.29
0.4	5.00402	250.1348	250.1373	250.1361	12825.9186	0.50917	0.11
0.5	5.00407	250.1344	250.1374	250.1359	16544.8408	0.74026	0.16
0.2	4.00431	250.0670	250.0617	250.0644	5268.0390	0.31623	0.072
0.3	4.00435	250.0685	250.0632	250.0659	9056.9656	0.43049	0.33
0.4	4.00437	250.0701	250.0649	250.0675	12783.8997	0.52686	0.15
0.5	4.00441	250.0714	250.0664	250.0689	16490.7716	0.78218	0.098

Mode	p/MPa	T_N/K	T_S/K	T_{av}/K	f/Hz	g/Hz	u(f)/Hz
0.2	3.00352	250.0798	250.0789	250.0794	5256.4721	0.43094	0.74
0.3	3.00355	250.0805	250.0799	250.0802	9037.1458	0.44984	0.57
0.4	3.00358	250.0813	250.0808	250.0811	12755.9009	0.56636	0.17
0.5	3.00362	250.0813	250.0808	250.0811	16454.6975	0.77265	0.12
0.2	1.997620	250.1176	250.1168	250.1172	5249.4937	0.39705	0.42
0.3	1.997382	250.1172	250.1166	250.1169	9025.0759	0.52653	0.53
0.4	1.997051	250.1164	250.1162	250.1163	12738.9232	0.64155	0.34
0.5	1.996817	250.1164	250.1162	250.1163	16432.8582	0.86064	0.066
0.2	0.998958	250.0802	250.0771	250.0787	5245.6717	0.54894	0.30
0.3	0.998830	250.0802	250.0771	250.0787	9018.6595	0.67708	2.3
0.4	0.998705	250.0813	250.0780	250.0797	12729.9199	0.84042	0.47
0.5	0.998563	250.0817	250.0787	250.0802	16421.3713	1.08274	0.11

Table B1.2 *Parameters required for computing frequency corrections, thermal boundary layer length, viscous boundary layer length accommodation length and thermal boundary layer in sell side length at T = 250 K.*

Mode	p/MPa	$10^6 \cdot \delta_{TH}$/m	$10^6 \cdot \delta_V$/m	$10^{11} \cdot l_{TH}$/m	$10^6 \cdot \delta_{TH,316L}$/m
0.2	20.01016	1.9001	1.8785	6.4427	14.2970
0.3	20.01013	1.4492	1.4327	6.4427	10.9042
0.4	20.01011	1.2199	1.2060	6.4427	9.1786
0.5	20.01012	1.0741	1.0619	6.4427	8.0822
0.2	19.05215	1.9429	1.9129	6.5867	14.4192
0.3	19.05191	1.4818	1.4590	6.5867	10.9975
0.4	19.05173	1.2473	1.2281	6.5868	9.2571
0.5	19.05142	1.0983	1.0813	6.5868	8.1511
0.2	17.99342	1.9961	1.9549	6.7654	14.5526
0.3	17.99347	1.5224	1.4910	6.7654	11.0990
0.4	17.99354	1.2813	1.2549	6.7652	9.3425
0.5	17.99365	1.1284	1.1051	6.7654	8.2262
0.2	17.04589	2.0510	1.9972	6.9468	14.6685
0.3	17.04599	1.5641	1.5232	6.9467	11.1874
0.4	17.04604	1.3167	1.2822	6.9468	9.4168
0.5	17.04612	1.1593	1.1289	6.9468	8.2915
0.2	15.99721	2.1208	2.0499	7.1763	14.7912
0.3	15.99693	1.6175	1.5634	7.1764	11.2811
0.4	15.99671	1.3615	1.3160	7.1764	9.4956
0.5	15.99662	1.1988	1.1587	7.1764	8.3609
0.2	15.01199	2.1935	2.1045	7.4223	14.9033
0.3	15.01208	1.6730	1.6050	7.4223	11.3664
0.4	15.01214	1.4082	1.3510	7.4223	9.5674
0.5	15.01226	1.2399	1.1895	7.4222	8.4238

Mode	p/MPa	$10^6 \cdot \delta_{TH}$/m	$10^6 \cdot \delta_V$/m	$10^{11} \cdot l_{TH}$/m	$10^6 \cdot \delta_{TH,316L}$/m
0.2	14.00770	2.2791	2.1676	7.7138	15.0097
0.3	14.00770	1.7382	1.6532	7.7138	11.4475
0.4	14.00774	1.4631	1.3915	7.7138	9.6356
0.5	14.00777	1.2882	1.2252	7.7138	8.4839
0.2	13.01083	2.3754	2.2383	8.0519	15.1084
0.3	13.01082	1.8117	1.7071	8.0519	11.5229
0.4	13.01083	1.5249	1.4369	8.0519	9.6990
0.5	13.01084	1.3427	1.2652	8.0519	8.5399
0.2	12.00932	2.4855	2.3188	8.4535	15.2002
0.3	12.00934	1.8956	1.7685	8.4535	11.5928
0.4	12.00635	1.5958	1.4887	8.4548	9.7579
0.5	12.00937	1.4049	1.3107	8.4535	8.5916
0.2	10.99637	2.6136	2.4124	8.9426	15.2843
0.3	10.99624	1.9934	1.8399	8.9428	11.6570
0.4	10.99627	1.6779	1.5487	8.9428	9.8119
0.5	10.99630	1.4773	1.3636	8.9428	8.6392
0.2	10.00724	2.7576	2.5180	9.5248	15.3591
0.3	10.00729	2.1031	1.9204	9.5247	11.7140
0.4	10.00734	1.7702	1.6164	9.5247	9.8597
0.5	10.00738	1.5587	1.4233	9.5247	8.6814
0.2	9.00385	2.9292	2.6445	10.2629	15.4249
0.3	9.00390	2.2340	2.0169	10.2629	11.7641
0.4	9.00392	1.8804	1.6976	10.2629	9.9020
0.5	9.00395	1.6557	1.4947	10.2630	8.7184
0.2	7.99539	3.1343	2.7968	11.2122	15.4815
0.3	7.99541	2.3905	2.1330	11.2122	11.8073
0.4	7.99539	2.0121	1.7954	11.2122	9.9383
0.5	7.99540	1.7716	1.5808	11.2122	8.7505
0.2	6.99732	3.3786	2.9801	12.4407	15.5308
0.3	6.99730	2.5768	2.2729	12.4408	11.8448
0.4	6.99730	2.1689	1.9131	12.4409	9.9699
0.5	6.99733	1.9096	1.6844	12.4409	8.7782
0.2	5.99692	3.6835	3.2112	14.1189	15.5701
0.3	5.99680	2.8093	2.4492	14.1193	11.8749
0.4	5.99678	2.3647	2.0615	14.1194	9.9952
0.5	5.99676	2.0820	1.8151	14.1194	8.8005
0.2	4.99741	4.0744	3.5110	16.5052	15.6019
0.3	4.99738	3.1075	2.6777	16.5053	11.8991
0.4	4.99737	2.6156	2.2539	16.5053	10.0155
0.5	4.99742	2.3029	1.9845	16.5052	8.8183

Mode	p/MPa	$10^6 \cdot \delta_{TH}$/m	$10^6 \cdot \delta_V$/m	$10^{11} \cdot l_{TH}$/m	$10^6 \cdot \delta_{TH,316L}$/m
0.2	3.99779	4.6008	3.9193	20.1271	15.6277
0.3	3.99783	3.5088	2.9891	20.1271	11.9187
0.4	3.99785	2.9534	2.5160	20.1272	10.0320
0.5	3.99789	2.6004	2.2152	20.1271	8.8328
0.2	2.99713	5.3705	4.5233	26.2514	15.6449
0.3	2.99716	4.0959	3.4497	26.2513	11.9317
0.4	2.99719	3.4475	2.9036	26.2511	10.0430
0.5	2.99723	3.0354	2.5565	26.2508	8.8425
0.2	1.99862	6.6500	5.5388	38.5783	15.6552
0.3	1.99838	5.0720	4.2245	38.5827	11.9397
0.4	1.99805	4.2695	3.5561	38.5887	10.0497
0.5	1.99781	3.7594	3.1312	38.5931	8.8483
0.2	0.99972	9.5086	7.8341	75.7058	15.6609
0.3	0.99959	7.2523	5.9751	75.7153	11.9439
0.4	0.99947	6.1047	5.0296	75.7250	10.0532
0.5	0.99933	5.3753	4.4287	75.7358	8.8514

Table B1.3 *Values of calculated thermal boundary layer, shell motion and holes and ducts frequency corrections; and thermal boundary layer, bulk viscosity and ducts and holes half width contributions to the resonance peaks at T = 250 K.*

Mode	p/MPa	Δf_{th}/Hz	Δf_{shell}/Hz	Δf_{hole}/Hz	g_{th}/Hz	g_b/Hz	g_{hole}/Hz
0.2	20.01016	-0.240570	-0.140403	0.113186	0.248230	0.000209	0.004096
0.3	20.01013	-0.315395	-0.256921	0.093761	0.325431	0.000619	0.004265
0.4	20.01011	-0.374650	-0.405176	0.071089	0.386574	0.001232	0.003728
0.5	20.01012	-0.425392	-0.638935	0.053130	0.438934	0.002050	0.003310
0.2	19.05215	-0.239108	-0.134533	0.111400	0.246382	0.000213	0.004072
0.3	19.05191	-0.313468	-0.245598	0.092312	0.323007	0.000629	0.004240
0.4	19.05173	-0.372370	-0.385413	0.070055	0.383705	0.001254	0.003707
0.5	19.05142	-0.422827	-0.600478	0.052449	0.435701	0.002086	0.003293
0.2	17.99342	-0.237391	-0.128209	0.109465	0.244243	0.000218	0.004043
0.3	17.99347	-0.311228	-0.233490	0.090808	0.320214	0.000643	0.004214
0.4	17.99354	-0.369747	-0.364549	0.068972	0.380428	0.001281	0.003684
0.5	17.99365	-0.419827	-0.561320	0.051675	0.431955	0.002132	0.003270
0.2	17.04589	-0.235733	-0.122708	0.107829	0.242197	0.000223	0.004015
0.3	17.04599	-0.309072	-0.223013	0.089494	0.317551	0.000658	0.004186
0.4	17.04604	-0.367136	-0.346805	0.067950	0.377210	0.001311	0.003654
0.5	17.04612	-0.416938	-0.528944	0.051023	0.428380	0.002181	0.003249
0.2	15.99721	-0.233804	-0.116787	0.106158	0.239830	0.000229	0.003983
0.3	15.99693	-0.306519	-0.211836	0.088098	0.314422	0.000678	0.004150
0.4	15.99671	-0.364127	-0.328060	0.066944	0.373519	0.001350	0.003625
0.5	15.99662	-0.413518	-0.495817	0.050286	0.424187	0.002246	0.003221

Mode	p/MPa	Δf_{th}/Hz	Δf_{shell}/Hz	Δf_{hole}/Hz	g_{th}/Hz	g_b/Hz	g_{hole}/Hz
0.2	15.01199	-0.232000	-0.111353	0.104598	0.237624	0.000237	0.003950
0.3	15.01208	-0.304170	-0.201618	0.086867	0.311548	0.000699	0.004118
0.4	15.01214	-0.361346	-0.311141	0.066043	0.370113	0.001393	0.003597
0.5	15.01226	-0.410401	-0.466638	0.049709	0.420361	0.002317	0.003201
0.2	14.00770	-0.230156	-0.105962	0.103189	0.235369	0.000245	0.003918
0.3	14.00770	-0.301755	-0.191547	0.085720	0.308593	0.000725	0.004086
0.4	14.00774	-0.358480	-0.294664	0.065194	0.366606	0.001444	0.003568
0.5	14.00777	-0.407167	-0.438884	0.049083	0.416400	0.002403	0.003174
0.2	13.01083	-0.228441	-0.100721	0.101901	0.233254	0.000256	0.003888
0.3	13.01082	-0.299506	-0.181811	0.084665	0.305820	0.000756	0.004054
0.4	13.01083	-0.355813	-0.278902	0.064418	0.363317	0.001505	0.003541
0.5	13.01084	-0.404072	-0.413077	0.048416	0.412597	0.002505	0.003142
0.2	12.00932	-0.226940	-0.095542	0.100726	0.231365	0.000268	0.003862
0.3	12.00934	-0.297541	-0.172243	0.083715	0.303345	0.000792	0.004027
0.4	12.00635	-0.353492	-0.263512	0.063762	0.360390	0.001579	0.003520
0.5	12.00937	-0.401460	-0.388334	0.047960	0.409298	0.002627	0.003124
0.2	10.99637	-0.225797	-0.090368	0.099676	0.229846	0.000283	0.003841
0.3	10.99624	-0.296037	-0.162734	0.082844	0.301347	0.000838	0.004005
0.4	10.99627	-0.351698	-0.248468	0.063062	0.358010	0.001669	0.003497
0.5	10.99630	-0.399425	-0.364485	0.047473	0.406596	0.002777	0.003105
0.2	10.00724	-0.225228	-0.085332	0.098741	0.228928	0.000302	0.003830
0.3	10.00729	-0.295299	-0.153511	0.082104	0.300154	0.000892	0.003994
0.4	10.00734	-0.350831	-0.233941	0.062530	0.356602	0.001777	0.003487
0.5	10.00738	-0.398424	-0.341899	0.047047	0.404980	0.002956	0.003093
0.2	9.00385	-0.225470	-0.080219	0.097956	0.228838	0.000325	0.003832
0.3	9.00390	-0.295619	-0.144192	0.081472	0.300037	0.000961	0.003996
0.4	9.00392	-0.351198	-0.219397	0.062029	0.356451	0.001914	0.003485
0.5	9.00395	-0.398859	-0.319622	0.046718	0.404827	0.003185	0.003092
0.2	7.99539	-0.226894	-0.075014	0.097301	0.229952	0.000355	0.003855
0.3	7.99541	-0.297484	-0.134742	0.080938	0.301497	0.001050	0.004018
0.4	7.99539	-0.353421	-0.204739	0.061646	0.358191	0.002092	0.003502
0.5	7.99540	-0.401382	-0.297486	0.046443	0.406803	0.003481	0.003105
0.2	6.99732	-0.229911	-0.069710	0.096778	0.232688	0.000394	0.003905
0.3	6.99730	-0.301442	-0.125138	0.080526	0.305087	0.001165	0.004068
0.4	6.99730	-0.358126	-0.189930	0.061347	0.362458	0.002321	0.003542
0.5	6.99733	-0.406730	-0.275357	0.046240	0.411654	0.003863	0.003137
0.2	5.99692	-0.235312	-0.064191	0.096424	0.237832	0.000448	0.003997
0.3	5.99680	-0.308523	-0.115176	0.080249	0.311830	0.001323	0.004159
0.4	5.99678	-0.366536	-0.174654	0.061145	0.370469	0.002635	0.003615
0.5	5.99676	-0.416282	-0.252769	0.046103	0.420752	0.004385	0.003195

Mode	p/MPa	Δf_{th}/Hz	Δf_{shell}/Hz	Δf_{hole}/Hz	g_{th}/Hz	g_b/Hz	g_{hole}/Hz
0.2	4.99741	-0.244197	-0.058348	0.096191	0.246485	0.000523	0.004148
0.3	4.99738	-0.320175	-0.104651	0.080097	0.323178	0.001547	0.004310
0.4	4.99737	-0.380381	-0.158581	0.061049	0.383953	0.003082	0.003737
0.5	4.99742	-0.432008	-0.229196	0.046054	0.436068	0.005128	0.003295
0.2	3.99779	-0.258601	-0.052006	0.096116	0.260680	0.000638	0.004395
0.3	3.99783	-0.339064	-0.093249	0.080084	0.341794	0.001886	0.004557
0.4	3.99785	-0.402825	-0.141224	0.061063	0.406072	0.003758	0.003937
0.5	3.99789	-0.457503	-0.203887	0.046090	0.461196	0.006253	0.003458
0.2	2.99713	-0.283032	-0.044923	0.096298	0.284924	0.000832	0.004820
0.3	2.99716	-0.371093	-0.080536	0.080301	0.373580	0.002460	0.004980
0.4	2.99719	-0.440875	-0.121924	0.061253	0.443835	0.004902	0.004280
0.5	2.99723	-0.500717	-0.175896	0.046267	0.504083	0.008157	0.003738
0.2	1.99862	-0.328672	-0.036635	0.096845	0.330401	0.001223	0.005626
0.3	1.99838	-0.430954	-0.065663	0.080842	0.433229	0.003616	0.005784
0.4	1.99805	-0.512029	-0.099375	0.061710	0.514739	0.007206	0.004930
0.5	1.99781	-0.581561	-0.143294	0.046656	0.584646	0.011992	0.004267
0.2	0.99972	-0.440867	-0.025889	0.098434	0.442461	0.002400	0.007694
0.3	0.99959	-0.578074	-0.046399	0.082408	0.580179	0.007094	0.007853
0.4	0.99947	-0.686821	-0.070215	0.062993	0.689335	0.014136	0.006596
0.5	0.99933	-0.780106	-0.101222	0.047733	0.782975	0.023527	0.005617

Table B1.4 *Uncertainty contributions and result of radius calibration at T = 250 K*

p/MPa	a/m	$10^{12}\cdot\sum_{i=1}^{4}\left(\frac{\partial a}{\partial f_i}\right)^2 u^2(f_i)\Big/m^2$	$10^{11}\cdot\left(\frac{\partial a}{\partial u}\right)^2 u^2(u)\Big/m^2$	$10^{12}\cdot u_{disp}^2(a)\Big/m^2$	$10^6\cdot u(a)/m$
20.0101	0.040175	5.7	1.6	12	5.8
19.0518	0.040172	13	1.6	7.7	6.1
17.9935	0.040169	9.2	1.6	5.4	5.5
17.0460	0.040167	5.9	1.6	3.7	5.1
15.9969	0.040165	15	1.6	4.3	6.0
15.0121	0.040162	33	1.6	0.99	7.1
14.0077	0.040161	7.8	1.6	0.96	5.0
13.0108	0.040160	1.5	1.6	1.9	4.4
12.0086	0.040158	1.2	1.6	0.93	4.3
10.9963	0.040157	0.96	1.6	0.95	4.2
10.0073	0.040156	0.94	1.6	0.95	4.2
9.0039	0.040156	1.4	1.6	0.63	4.3
7.9954	0.040155	0.49	1.6	0.43	4.1
6.9973	0.040154	0.45	1.6	0.29	4.1
5.9968	0.040153	0.16	1.6	0.34	4.1
4.9974	0.040152	0.22	1.6	0.17	4.1
3.9978	0.040151	0.23	1.6	0.081	4.1
2.9972	0.040150	2.5	1.6	0.037	4.3
1.9982	0.040150	1.1	1.6	0.027	4.2
0.9994	0.040149	7.0	1.6	1.3	4.9

B2

Frequency measurements, frequency corrections and radius measurements and uncertainties at 273K

Table B2.1 *Pressure, north and south hemisphere and average temperature, frequency of resonance, half-width of the resonance peak and frequency measurement uncertainty using argon to calibrate internal radius at T = 273 K.*

Mode	p/MPa	T_N/K	T_S/K	T_{ave}/K	*f*/Hz	*g*/Hz	u(*f*)/Hz
0.2	18.9435	273.1901	273.1933	273.1917	6344.6960	2.87993	8.6
0.3	18.9434	273.1898	273.1928	273.1913	10876.6206	0.64051	1.1
0.4	18.9433	273.1893	273.1923	273.1908	15350.9634	0.70187	0.38
0.5	18.9431	273.1891	273.1921	273.1906	19799.4254	0.08333	11
0.2	17.9305	273.1713	273.1735	273.1724	6260.5432	1.64028	3.6
0.3	17.9303	273.1713	273.1735	273.1724	10729.9189	0.60402	1.3
0.4	17.9303	273.1714	273.1736	273.1725	15144.1856	0.67758	0.17
0.5	17.9301	273.1714	273.1734	273.1724	19532.6331	1.18739	0.91
0.2	16.9795	273.1588	273.1603	273.1596	6165.1279	0.36148	0.47
0.3	16.9795	273.1588	273.1603	273.1596	10598.6448	0.53748	2.0
0.4	16.9794	273.1588	273.1604	273.1596	14958.9215	0.67901	0.37
0.5	16.9793	273.1589	273.1605	273.1597	19294.3291	1.19559	1.5
0.2	16.0595	273.1499	273.1735	273.1617	6094.7727	0.32036	0.15
0.3	16.0597	273.1502	273.1735	273.1619	10477.7260	0.49131	0.52
0.4	16.0596	273.1502	273.1736	273.1619	14788.4181	0.61831	0.10
0.5	16.0595	273.1504	273.1734	273.1619	19074.7746	1.10498	0.62
0.2	15.0335	273.1548	273.1564	273.1556	6020.7677	0.31789	0.045
0.3	15.0338	273.1548	273.1564	273.1556	10350.6069	0.47023	1.5
0.4	15.0336	273.1547	273.1564	273.1556	14609.0846	0.57860	0.14
0.5	15.0337	273.1547	273.1564	273.1556	18843.9231	1.07977	1.2
0.2	13.9705	273.1288	273.1245	273.1267	5948.8089	0.36556	0.47
0.3	13.9705	273.1296	273.1256	273.1276	10226.9182	0.43277	0.75
0.4	13.9706	273.1303	273.1267	273.1285	14434.6908	0.56253	0.16
0.5	13.9706	273.1303	273.1267	273.1285	18619.3872	1.05064	1.6
0.2	13.0005	273.1326	273.1279	273.1303	5888.0446	0.33635	0.11
0.3	13.0006	273.1336	273.1292	273.1314	10123.4088	0.01660	2.8
0.4	13.0006	273.1346	273.1304	273.1325	14287.3773	0.57528	0.24
0.5	13.0008	273.1363	273.1325	273.1344	18429.1743	1.25309	0.56

Mode	p/MPa	T_N/K	T_S/K	T_{ave}/K	f/Hz	g/Hz	u(f)/Hz
0.2	12.0189	273.1528	273.1279	273.1404	5831.2808	0.42939	0.058
0.3	12.0189	273.1527	273.1292	273.1410	10024.9281	0.43563	0.52
0.4	12.0188	273.1527	273.1304	273.1416	14149.7189	0.56551	0.15
0.5	12.0188	273.1527	273.1325	273.1426	18252.0039	0.98950	0.17
0.2	10.9776	273.1452	273.144	273.1446	5775.7275	0.33919	0.13
0.3	10.9774	273.1472	273.1454	273.1463	9929.5339	0.41985	0.45
0.4	10.9775	273.1472	273.1454	273.1463	14015.1946	0.55887	0.14
0.5	10.9774	273.1468	273.1461	273.1465	18078.8961	0.98300	0.29
0.2	10.0004	273.1373	273.1367	273.1370	5728.3154	0.31870	0.14
0.3	10.0004	273.1377	273.1373	273.1375	9848.1584	0.45548	1.2
0.4	10.0003	273.138	273.1377	273.1379	13900.3016	0.57119	0.20
0.5	10.0003	273.1384	273.1381	273.1383	17930.6315	1.42199	0.46
0.2	9.0122	273.1518	273.1367	273.1443	5685.2706	0.31023	0.16
0.3	9.0122	273.1518	273.1373	273.1446	9774.1214	0.41324	0.72
0.4	9.0122	273.1519	273.1377	273.1448	13795.8729	0.57039	0.48
0.5	9.0122	273.1519	273.1381	273.1450	17796.6131	1.30804	0.39
0.2	7.9594	273.1459	273.1467	273.1463	5644.1452	0.30725	0.14
0.3	7.9594	273.1461	273.1469	273.1465	9703.4173	0.42854	1.1
0.4	7.9594	273.1464	273.1472	273.1468	13696.1612	0.54327	0.098
0.5	7.9594	273.1466	273.1475	273.1471	17667.4354	2.36474	1.3
0.2	6.9935	273.1442	273.1444	273.1443	5610.8510	0.35935	0.43
0.3	6.9935	273.1446	273.1447	273.1447	9646.1941	0.41585	0.55
0.4	6.9935	273.1446	273.1447	273.1447	13615.4471	0.54859	0.17
0.5	6.9935	273.1447	273.1451	273.1449	17562.7682	1.36331	0.24
0.2	6.0072	273.1556	273.1574	273.1565	5581.2100	0.33185	0.14
0.3	6.0072	273.1556	273.1575	273.1566	9595.2880	0.40858	0.26
0.4	6.0072	273.1556	273.1574	273.1565	13543.5986	0.54368	0.13
0.5	6.0072	273.1556	273.1574	273.1565	17470.3304	1.10982	0.19
0.2	4.9690	273.1532	273.1541	273.1537	5554.2605	0.32812	0.19
0.3	4.9690	273.1535	273.1543	273.1539	9549.0045	0.43650	0.31
0.4	4.9690	273.1537	273.1545	273.1541	13478.3231	0.54736	0.12
0.5	4.9690	273.1539	273.1547	273.1543	17386.3201	0.96292	0.20
0.2	3.9695	273.1382	273.1394	273.1388	5532.2350	0.34070	0.10
0.3	3.9695	273.1382	273.1393	273.1388	9511.1606	0.45640	0.39
0.4	3.9695	273.1382	273.1393	273.1388	13424.9212	0.58214	0.094
0.5	3.9694	273.1382	273.1393	273.1388	17317.6266	1.00235	0.16
0.2	3.0072	273.1276	273.128	273.1278	5514.6743	0.37268	0.11
0.3	3.0072	273.1276	273.128	273.1278	9481.0022	0.49767	1.1
0.4	3.0072	273.1277	273.1281	273.1279	13382.4134	0.61253	0.11
0.5	3.0073	273.1277	273.1281	273.1279	17262.8283	1.00398	0.19

Mode	p/MPa	T_N/K	T_S/K	T_{ave}/K	f/Hz	g/Hz	u(f)/Hz
0.2	1.9902	273.1359	273.1363	273.1361	5499.9122	0.42173	0.18
0.3	1.9902	273.136	273.1365	273.1363	9455.7180	0.66291	1.9
0.4	1.9902	273.1363	273.1366	273.1365	13346.7067	0.70362	0.14
0.5	1.9903	273.1363	273.1366	273.1365	17216.8666	1.03855	0.16
0.2	0.9898	273.1517	273.1538	273.1528	5488.8237	0.56796	0.20
0.3	0.9898	273.1515	273.1536	273.1526	9436.6962	0.68720	3.9
0.4	0.9898	273.1515	273.1536	273.1526	13320.0050	0.91737	0.25
0.5	0.9898	273.1515	273.1535	273.1525	17182.5287	1.24116	0.12

Table B2.2 *Parameters required for computing frequency corrections, thermal boundary layer length, viscous boundary layer length accommodation length and thermal boundary layer in sell side length at T = 273 K.*

Mode	p/MPa	$10^6 \cdot \delta_{TH}$/m	$10^6 \cdot \delta_V$/m	$10^{11} \cdot l_{TH}$/m	$10^6 \cdot \delta_{TH,316L}$/m
0.2	18.9435	2.15328	2.01575	6.78936	14.24011
0.3	18.9434	1.64459	1.53955	6.78937	10.87606
0.4	18.9433	1.38432	1.29591	6.78938	9.15484
0.5	18.9431	1.21893	1.14108	6.78942	8.06106
0.2	17.9305	2.21210	2.06104	7.00328	14.33549
0.3	17.9303	1.68972	1.57433	7.00335	10.95016
0.4	17.9303	1.42230	1.32517	7.00335	9.21713
0.5	17.9301	1.25237	1.16685	7.00338	8.11593
0.2	16.9795	2.27716	2.11130	7.22855	14.44600
0.3	16.9795	1.73676	1.61026	7.22856	11.01776
0.4	16.9794	1.46189	1.35542	7.22857	9.27403
0.5	16.9793	1.28722	1.19346	7.22861	8.16589
0.2	16.0595	2.34336	2.16152	7.47331	14.52914
0.3	16.0597	1.78724	1.64856	7.47328	11.08116
0.4	16.0596	1.50438	1.38764	7.47331	9.32734
0.5	16.0595	1.32461	1.22183	7.47331	8.21276
0.2	15.0335	2.42550	2.22352	7.78337	14.61816
0.3	15.0338	1.84986	1.69582	7.78326	11.14899
0.4	15.0336	1.55709	1.42743	7.78331	9.38441
0.5	15.0337	1.37100	1.25684	7.78330	8.26291
0.2	13.9705	2.52121	2.29554	8.15492	14.70631
0.3	13.9705	1.92289	1.75077	8.15494	11.21621
0.4	13.9706	1.61854	1.47366	8.15492	9.44093
0.5	13.9706	1.42509	1.29753	8.15492	8.31258
0.2	13.0005	2.62014	2.36981	8.55111	14.78200
0.3	13.0006	1.99824	1.80733	8.55112	11.27341
0.4	13.0006	1.68204	1.52133	8.55112	9.48948
0.5	13.0008	1.48102	1.33952	8.55110	8.35537

Mode	p/MPa	$10^6 \cdot \delta_{TH}$/m	$10^6 \cdot \delta_V$/m	$10^{11} \cdot l_{TH}$/m	$10^6 \cdot \delta_{TH,316L}$/m
0.2	12.0189	2.73337	2.45482	9.02193	14.85377
0.3	12.0189	2.08469	1.87224	9.02195	11.32865
0.4	12.0188	1.75473	1.57591	9.02199	9.53553
0.5	12.0188	1.54501	1.38756	9.02206	8.39582
0.2	10.9776	2.87090	2.55832	9.62014	14.92503
0.3	10.9774	2.18959	1.95119	9.62030	11.38293
0.4	10.9775	1.84301	1.64234	9.62027	9.58118
0.5	10.9774	1.62271	1.44603	9.62029	8.43592
0.2	10.0004	3.01991	2.67088	10.30303	14.98667
0.3	10.0004	2.30320	2.03700	10.30304	11.42986
0.4	10.0003	1.93864	1.71458	10.30308	9.62070
0.5	10.0003	1.70692	1.50964	10.30310	8.47073
0.2	9.0122	3.19569	2.80427	11.15577	15.04330
0.3	9.0122	2.43726	2.13874	11.15578	11.47307
0.4	9.0122	2.05148	1.80020	11.15579	9.65704
0.5	9.0122	1.80623	1.58500	11.15582	8.50256
0.2	7.9594	3.41881	2.97463	12.31268	15.09800
0.3	7.9594	2.60743	2.26867	12.31269	11.51480
0.4	7.9594	2.19471	1.90957	12.31273	9.69213
0.5	7.9594	1.93236	1.68131	12.31272	8.53359
0.2	6.9935	3.66705	3.16545	13.69848	15.14273
0.3	6.9935	2.79675	2.41420	13.69850	11.54890
0.4	6.9935	2.35405	2.03205	13.69850	9.72081
0.5	6.9935	2.07269	1.78918	13.69848	8.55898
0.2	6.0072	3.98060	3.40818	15.59656	15.18289
0.3	6.0072	3.03587	2.59931	15.59652	11.57949
0.4	6.0072	2.55532	2.18786	15.59651	9.74656
0.5	6.0072	2.24989	1.92635	15.59651	8.58160
0.2	4.9690	4.40665	3.74058	18.43833	15.21968
0.3	4.9690	3.36083	2.85284	18.43862	11.60752
0.4	4.9690	2.82883	2.40125	18.43857	9.77014
0.5	4.9690	2.49070	2.11423	18.43855	8.60230
0.2	3.9695	4.96503	4.17977	22.61662	15.24995
0.3	3.9695	3.78665	3.18776	22.61657	11.63059
0.4	3.9695	3.18725	2.68316	22.61667	9.78955
0.5	3.9694	2.80627	2.36244	22.61683	8.61935
0.2	3.0072	5.74550	4.79848	29.31176	15.27421
0.3	3.0072	4.38186	3.65961	29.31149	11.64908
0.4	3.0072	3.68822	3.08030	29.31132	9.80509
0.5	3.0073	3.24732	2.71208	29.31095	8.63302

Mode	p/MPa	$10^6 \cdot \delta_{TH}$/m	$10^6 \cdot \delta_V$/m	$10^{11} \cdot l_{TH}$/m	$10^6 \cdot \delta_{TH,316L}$/m
0.2	1.9902	7.11974	5.89678	43.50450	15.29469
0.3	1.9902	5.42993	4.49723	43.50442	11.66464
0.4	1.9902	4.57040	3.78534	43.50436	9.81819
0.5	1.9903	4.02405	3.33283	43.50406	8.64453
0.2	0.9898	10.18051	8.36360	86.07665	15.31013
0.3	0.9898	7.76424	6.37856	86.07657	11.67639
0.4	0.9898	6.53517	5.36884	86.07657	9.82803
0.5	0.9898	5.75393	4.72703	86.07629	8.65317

Table B2.3 *Values of calculated thermal boundary layer, shell motion and holes and ducts frequency corrections; and thermal boundary layer, bulk viscosity and ducts and holes half width contributions to the resonance peaks at T = 273 K.*

Mode	p/MPa	Δf_{TH} /Hz	Δf_{shell} /Hz	Δf_{hole} /Hz	g_{TH} /Hz	g_b/HZ	g_{hole}/Hz
0.2	18.9435	-0.2323	-0.1369	-4.1016×10^{-3}	0.23826	0.00024	0.27226
0.3	18.9434	-0.3031	-0.2517	-4.3759×10^{-4}	0.31094	0.00069	0.27060
0.4	18.9433	-0.3601	-0.3976	2.3639×10^{-4}	0.36936	0.00138	0.27154
0.5	18.9431	-0.4088	-0.6295	2.7773×10^{-4}	0.41940	0.00229	0.27187
0.2	17.9305	-0.2313	-0.1313	-3.8571×10^{-3}	0.23702	0.00024	0.26862
0.3	17.9303	-0.3019	-0.2409	-3.5273×10^{-4}	0.30927	0.00071	0.26703
0.4	17.9303	-0.3586	-0.3789	2.6010×10^{-4}	0.36739	0.00142	0.26796
0.5	17.9301	-0.4072	-0.5940	2.7957×10^{-4}	0.41718	0.00236	0.26832
0.2	16.9795	-0.2294	-0.1266	-3.6735×10^{-3}	0.23474	0.00025	0.26286
0.3	16.9795	-0.3007	-0.2310	-2.6197×10^{-4}	0.30775	0.00073	0.26385
0.4	16.9794	-0.3572	-0.3621	2.8406×10^{-4}	0.36559	0.00146	0.26477
0.5	16.9793	-0.4056	-0.5627	2.8053×10^{-4}	0.41516	0.00242	0.26513
0.2	16.0595	-0.2286	-0.1216	-3.3996×10^{-3}	0.23366	0.00025	0.25985
0.3	16.0597	-0.2997	-0.2216	-1.6615×10^{-4}	0.30635	0.00075	0.26092
0.4	16.0596	-0.3560	-0.3462	3.0724×10^{-4}	0.36393	0.00150	0.26183
0.5	16.0595	-0.4043	-0.5342	2.7922×10^{-4}	0.41328	0.00250	0.26218
0.2	15.0335	-0.2278	-0.1161	-3.0607×10^{-3}	0.23260	0.00026	0.25671
0.3	15.0338	-0.2987	-0.2113	-5.1441×10^{-5}	0.30496	0.00078	0.25789
0.4	15.0336	-0.3548	-0.3291	3.3154×10^{-4}	0.36229	0.00156	0.25877
0.5	15.0337	-0.4030	-0.5040	2.7449×10^{-4}	0.41143	0.00259	0.25910
0.2	13.9705	-0.2272	-0.1105	-2.6749×10^{-3}	0.23171	0.00028	0.25367
0.3	13.9705	-0.2979	-0.2008	7.0110×10^{-5}	0.30379	0.00082	0.25495
0.4	13.9706	-0.3539	-0.3118	3.5101×10^{-4}	0.36090	0.00163	0.25579
0.5	13.9706	-0.4019	-0.4742	2.6384×10^{-4}	0.40986	0.00270	0.25611
0.2	13.0005	-0.2270	-0.1055	-2.2901×10^{-3}	0.23116	0.00029	0.25111
0.3	13.0006	-0.2976	-0.1913	1.8169×10^{-4}	0.30309	0.00085	0.25253
0.4	13.0006	-0.3535	-0.2964	3.6088×10^{-4}	0.36004	0.00170	0.25329
0.5	13.0008	-0.4015	-0.4483	2.4751×10^{-4}	0.40889	0.00283	0.25356

Mode	p/MPa	Δf_{TH} /Hz	Δf_{shell} /Hz	Δf_{hole} /Hz	g_{TH} /Hz	g_b/HZ	g_{hole}/Hz
0.2	12.0189	-0.2271	-0.1004	-1.8736×10^{-3}	0.23098	0.00030	0.24878
0.3	12.0189	-0.2977	-0.1819	2.8304×10^{-4}	0.30283	0.00090	0.25024
0.4	12.0188	-0.3536	-0.2811	3.5976×10^{-4}	0.35976	0.00179	0.25098
0.5	12.0188	-0.4016	-0.4231	2.2376×10^{-4}	0.40858	0.00298	0.25120
0.2	10.9776	-0.2277	-0.0950	-1.4112×10^{-3}	0.23132	0.00032	0.24650
0.3	10.9774	-0.2985	-0.1719	3.7379×10^{-4}	0.30329	0.00096	0.24805
0.4	10.9775	-0.3546	-0.2651	3.4224×10^{-4}	0.36031	0.00190	0.24870
0.5	10.9774	-0.4028	-0.3971	1.8981×10^{-4}	0.40922	0.00317	0.24889
0.2	10.0004	-0.2290	-0.0899	-9.6731×10^{-4}	0.23235	0.00035	0.24463
0.3	10.0004	-0.3002	-0.1625	4.3296×10^{-4}	0.30465	0.00102	0.24622
0.4	10.0003	-0.3566	-0.2502	3.0841×10^{-4}	0.36193	0.00203	0.24677
0.5	10.0003	-0.4051	-0.3732	1.5059×10^{-4}	0.41107	0.00339	0.24691
0.2	9.0122	-0.2312	-0.0846	-5.2398×10^{-4}	0.23435	0.00037	0.24303
0.3	9.0122	-0.3031	-0.1529	4.5673×10^{-4}	0.30726	0.00110	0.24459
0.4	9.0122	-0.3601	-0.2350	2.5616×10^{-4}	0.36504	0.00220	0.24502
0.5	9.0122	-0.4090	-0.3494	1.0586×10^{-4}	0.41462	0.00366	0.24513
0.2	7.9594	-0.2350	-0.0789	-8.8482×10^{-4}	0.23787	0.00041	0.24159
0.3	7.9594	-0.3081	-0.1425	4.3181×10^{-4}	0.31188	0.00122	0.24304
0.4	7.9594	-0.3660	-0.2187	1.8376×10^{-4}	0.37053	0.00242	0.24332
0.5	7.9594	-0.4157	-0.3240	5.8104×10^{-5}	0.42086	0.00403	0.24339
0.2	6.9935	-0.2402	-0.0735	2.4228×10^{-4}	0.24288	0.00046	0.24055
0.3	6.9935	-0.3149	-0.1327	3.5989×10^{-4}	0.31844	0.00135	0.24179
0.4	6.9935	-0.3741	-0.2033	1.1027×10^{-4}	0.37832	0.00269	0.24194
0.5	6.9935	-0.4249	-0.3005	2.0758×10^{-5}	0.42967	0.00448	0.24190
0.2	6.0072	-0.2480	-0.0678	4.6517×10^{-4}	0.25048	0.00052	0.23973
0.3	6.0072	-0.3251	-0.1222	2.4526×10^{-4}	0.32841	0.00154	0.24065
0.4	6.0072	-0.3863	-0.1871	4.1924×10^{-5}	0.39017	0.00306	0.24067
0.5	6.0072	-0.4387	-0.2759	-3.9192×10^{-6}	0.44313	0.00509	0.24062
0.2	4.9690	-0.2602	-0.0613	5.2061×10^{-4}	0.26252	0.00061	0.23906
0.3	4.9690	-0.3412	-0.1105	1.0819×10^{-4}	0.34421	0.00181	0.23955
0.4	4.9690	-0.4053	-0.1690	-4.4924×10^{-6}	0.40894	0.00361	0.23950
0.5	4.9690	-0.4603	-0.2488	-1.1127×10^{-5}	0.46445	0.00601	0.23945
0.2	3.9695	-0.2783	-0.0546	3.7852×10^{-4}	0.28043	0.00075	0.23849
0.3	3.9695	-0.3649	-0.0983	8.3902×10^{-6}	0.36769	0.00222	0.23859
0.4	3.9695	-0.4335	-0.1503	-1.4456×10^{-5}	0.43684	0.00443	0.23853
0.5	3.9694	-0.4923	-0.2208	-5.1494×10^{-6}	0.49615	0.00737	0.23851
0.2	3.0072	-0.3061	-0.0473	1.3262×10^{-4}	0.30814	0.00097	0.23790
0.3	3.0072	-0.4014	-0.0853	-1.9049×10^{-5}	0.40402	0.00288	0.23779
0.4	3.0072	-0.4769	-0.1302	-3.9795×10^{-6}	0.48000	0.00573	0.23777
0.5	3.0073	-0.5416	-0.1911	1.7230×10^{-7}	0.54516	0.00954	0.23777

Mode	p/MPa	Δf_{TH} /Hz	Δf_{shell} /Hz	Δf_{hole} /Hz	g_{TH} /Hz	g_b/HZ	g_{hole}/Hz
0.2	1.9902	-0.3595	-0.0384	-2.1198×10^{-5}	0.36137	0.00144	0.23720
0.3	1.9902	-0.4714	-0.0691	-1.2610×10^{-6}	0.47383	0.00426	0.23716
0.4	1.9902	-0.5600	-0.1055	5.2284×10^{-7}	0.56293	0.00850	0.23715
0.5	1.9903	-0.6361	-0.1548	4.9031×10^{-8}	0.63935	0.01414	0.23715
0.2	0.9898	-0.4876	-0.0270	9.5076×10^{-7}	0.48930	0.00285	0.23670
0.3	0.9898	-0.6393	-0.0487	-3.5891×10^{-8}	0.64156	0.00843	0.23669
0.4	0.9898	-0.7595	-0.0742	1.1301×10^{-10}	0.76223	0.01679	0.23669
0.5	0.9898	-0.8626	-0.1088	3.1048×10^{-10}	0.86572	0.02794	0.23669

Table B2.4 *Uncertainty contributions and result of radius calibration at T = 273 K*

p/MPa	a/m	$10^{11}\cdot\sum_{i=1}^{4}\left(\frac{\partial a}{\partial f_i}\right)^2 u^2(f_i)\Big/m^2$	$10^{12}\cdot\left(\frac{\partial a}{\partial u}\right)^2 u^2(u)\Big/m^2$	$10^{12}\cdot u_{disp}^2(a)\Big/m^2$	$10^6\cdot u(a)/m$
18.9433	0.040186	230	1.6	7.7	16
17.9303	0.040184	37	1.6	5.5	7.7
16.9794	0.040180	4.9	1.6	3.9	5.0
16.0596	0.040179	0.56	1.6	2.8	4.4
15.0336	0.040176	2.8	1.6	1.9	4.6
13.9706	0.040176	2.0	1.6	1.9	4.5
13.0006	0.040174	8.2	1.6	3.5	5.3
12.0188	0.040172	0.35	1.6	1.4	4.2
10.9775	0.040171	0.40	1.6	0.45	4.1
10.0003	0.040170	1.9	1.6	0.29	4.3
9.0122	0.040168	1.0	1.6	0.28	4.2
7.9594	0.040168	2.9	1.6	0.38	4.4
6.9935	0.040167	1.1	1.6	0.18	4.2
6.0072	0.040166	0.33	1.6	0.45	4.1
4.9690	0.040165	0.39	1.6	0.27	4.1
3.9695	0.040165	0.37	1.6	0.16	4.1
3.0072	0.040165	1.5	1.6	0.12	4.2
1.9902	0.040164	4.2	1.6	0.073	4.5
0.9898	0.040162	17	1.6	0.029	5.8

B3

Frequency measurements, frequency corrections and radius measurements and uncertainties at 300K

Table B3.1 *Pressure, north and south hemisphere and average temperature, frequency of resonance, half-width of the resonance peak and frequency measurement uncertainty using argon to calibrate internal radius at T = 300 K.*

Mode	p/MPa	T_N/K	T_S/K	T_{ave}/K	*f*/Hz	*g*/Hz	u(*f*)/Hz
0.2	20.0091	299.7104	299.7062	299.7083	6617.2580	0.33860	0.16
0.3	20.0091	299.7103	299.7062	299.7083	11375.9094	0.57462	0.32
0.4	20.0090	299.7101	299.7063	299.7082	16054.7654	0.81835	0.36
0.5	20.0090	299.7100	299.7063	299.7082	20704.7770	1.76804	2.0
0.2	18.9981	299.7039	299.7001	299.7020	6543.4658	0.33470	0.11
0.3	18.9981	299.7040	299.7002	299.7021	11249.1254	0.57283	0.33
0.4	18.9980	299.7040	299.7000	299.7020	15876.1292	0.75297	0.28
0.5	18.9979	299.7041	299.7002	299.7022	20473.8865	1.75304	0.38
0.2	17.9743	299.7153	299.7125	299.7139	6471.6410	0.33128	0.14
0.3	17.9742	299.7155	299.7125	299.7140	11125.6996	0.59482	0.41
0.4	17.9741	299.7156	299.7128	299.7142	15702.1930	0.70872	0.11
0.5	17.9741	299.7157	299.7129	299.7143	20251.6729	1.40063	0.94
0.2	16.9960	299.7083	299.7051	299.7067	6405.5212	0.32799	0.15
0.3	16.9960	299.7083	299.7050	299.7067	11012.0598	0.61046	0.40
0.4	16.9959	299.7084	299.7051	299.7068	15542.0744	0.65769	0.21
0.5	16.9959	299.7083	299.7051	299.7067	20045.7563	1.34497	5.0
0.2	16.0183	299.7125	299.7096	299.7111	6342.3596	0.32535	0.15
0.3	16.0184	299.7128	299.7098	299.7113	10903.4477	0.62564	0.59
0.4	16.0184	299.7131	299.7101	299.7116	15389.0578	0.64588	0.15
0.5	16.0184	299.7133	299.7105	299.7119	19848.7830	1.29835	1.4
0.2	15.0194	299.6961	299.6894	299.6928	6280.5773	0.32432	0.14
0.3	15.0194	299.6970	299.6905	299.6938	10797.2183	0.55603	0.25
0.4	15.0193	299.6981	299.6915	299.6948	15239.3690	0.70229	1.6
0.5	15.0193	299.6990	299.6926	299.6958	19656.1749	1.15812	1.3

Mode	p/MPa	T_N/K	T_S/K	T_{ave}/K	*f*/Hz	*g*/Hz	u(*f*)/Hz
0.2	13.9771	299.7237	299.7218	299.7228	6219.8890	0.32493	0.14
0.3	13.9770	299.7237	299.7218	299.7228	10692.9234	0.51506	0.70
0.4	13.9770	299.7236	299.7219	299.7228	15092.2990	0.60039	0.14
0.5	13.9770	299.7236	299.7219	299.7228	19466.8942	1.11080	0.31
0.2	13.0262	299.7096	299.7051	299.7074	6167.1199	0.32454	0.15
0.3	13.0263	299.7099	299.7058	299.7079	10602.2425	0.49704	0.85
0.4	13.0264	299.7106	299.7063	299.7085	14964.4594	0.60688	0.13
0.5	13.0264	299.7112	299.7069	299.7091	19302.3361	1.12186	0.33
0.2	11.9811	299.7032	299.6981	299.7007	6112.6235	0.32640	0.13
0.3	11.9811	299.7032	299.6981	299.7007	10508.6185	0.47096	0.65
0.4	11.9811	299.7038	299.6988	299.7013	14832.3450	0.61140	0.10
0.5	11.9811	299.7043	299.6996	299.7020	19132.0770	1.03216	0.28
0.2	11.0482	299.7152	299.7111	299.7132	6067.2268	0.37053	0.42
0.3	11.0482	299.7151	299.7116	299.7134	10430.5758	0.46876	0.25
0.4	11.0483	299.7151	299.7116	299.7134	14722.2789	0.57706	0.068
0.5	11.0483	299.7150	299.7119	299.7135	18990.4418	0.89444	0.26
0.2	9.9885	299.7061	299.7019	299.7040	6018.9235	0.39384	0.44
0.3	9.9885	299.7078	299.7028	299.7053	10347.5248	0.45712	0.87
0.4	9.9885	299.7078	299.7028	299.7053	14605.1465	0.58978	0.40
0.5	9.9885	299.7081	299.7036	299.7059	18839.6105	0.89962	0.27
0.2	8.9810	299.7220	299.7187	299.7204	5976.6453	0.35272	0.10
0.3	8.9810	299.7220	299.7187	299.7204	10274.9390	0.41702	0.40
0.4	8.9810	299.7225	299.7910	299.7568	14502.7768	0.61555	0.38
0.5	8.9809	299.7229	299.7195	299.7212	18707.8708	1.05092	0.22
0.2	8.0286	299.7276	299.7238	299.7257	5939.6272	0.38677	0.072
0.3	8.0286	299.7269	299.7236	299.7253	10211.4094	0.43972	0.40
0.4	8.0287	299.7269	299.7236	299.7253	14413.1057	0.57862	0.076
0.5	8.0287	299.7267	299.7240	299.7254	18592.1188	1.01542	0.45
0.2	6.9972	299.7466	299.7445	299.7456	5903.0675	0.36449	0.13
0.3	6.9971	299.7482	299.7455	299.7469	10148.5705	0.43437	1.4
0.4	6.9970	299.7477	299.7459	299.7468	14324.4671	0.58192	0.067
0.5	6.9971	299.7477	299.7459	299.7468	18478.0039	1.02879	0.13
0.2	5.9976	299.7322	299.7308	299.7315	5870.5196	0.38492	0.14
0.3	5.9976	299.7324	299.7310	299.7317	10092.7078	0.42870	0.70
0.4	5.9976	299.7322	299.7311	299.7317	14245.6392	0.60395	0.15
0.5	5.9976	299.7322	299.7311	299.7317	18376.3117	1.14924	0.23

Mode	p/MPa	T_N/K	T_S/K	T_{ave}/K	f/Hz	g/Hz	u(f)/Hz
0.2	5.0003	299.7150	299.7099	299.7125	5841.1589	0.35970	0.087
0.3	5.0003	299.7150	299.7099	299.7125	10042.2558	0.47634	0.52
0.4	5.0003	299.7156	299.7105	299.7131	14174.5309	0.59808	0.084
0.5	5.0003	299.7162	299.7110	299.7136	18284.5872	1.03422	0.14
0.2	4.0014	299.7193	299.7146	299.7170	5815.0578	0.39951	0.34
0.3	4.0014	299.7199	299.7510	299.7355	9997.4037	0.48441	0.42
0.4	4.0014	299.7205	299.7160	299.7183	14111.2896	0.63739	0.17
0.5	4.0014	299.7211	299.7161	299.7186	18203.1105	0.95197	0.087
0.2	3.0054	299.7302	299.7278	299.7290	5792.0449	0.40490	0.086
0.3	3.0054	299.7303	299.7277	299.7290	9957.8385	0.56824	1.5
0.4	3.0055	299.7303	299.7277	299.7290	14055.4995	0.67077	0.082
0.5	3.0055	299.7303	299.7277	299.7290	18131.2134	0.98737	0.20
0.2	2.0037	299.7112	299.7055	299.7084	5771.3843	0.48135	0.14
0.3	2.0037	299.7118	299.7062	299.7090	9922.3876	0.64686	1.1
0.4	2.0037	299.7118	299.7062	299.7090	14005.5007	0.77021	0.097
0.5	2.0037	299.7122	299.7068	299.7095	18066.8127	1.07470	0.13
0.2	1.0032	299.7262	299.7217	299.7240	5753.8128	0.63361	0.27
0.3	1.0032	299.7266	299.7222	299.7244	9892.3306	0.79670	7.1
0.4	1.0032	299.7266	299.7222	299.7244	13963.1313	1.00261	0.24
0.5	1.0032	299.7270	299.7523	299.7396	18012.2502	1.33522	0.21

Table B3.2 *Parameters required for computing frequency corrections, thermal boundary layer length, viscous boundary layer length accommodation length and thermal boundary layer in sell side length at T = 300 K.*

Mode	p/MPa	$10^5 \cdot \delta_{TH}$/m	$10^6 \cdot \delta_V$/m	$10^9 \cdot l_{TH}$/m	$10^6 \cdot \delta_{TH,316L}$/m
0.2	20.0091	7.27779	2.08456	5.28462	13.94375
0.3	20.0091	5.55067	1.58986	5.28462	10.63471
0.4	20.0090	4.67236	1.33829	5.28463	8.95193
0.5	20.0090	4.11437	1.17847	5.28463	7.88285
0.2	18.9981	7.46294	2.12991	5.44372	14.02215
0.3	18.9981	5.69187	1.62445	5.44373	10.69447
0.4	18.9980	4.79118	1.36739	5.44374	9.00215
0.5	18.9979	4.21906	1.20411	5.44376	7.92718
0.2	17.9743	7.66965	2.18028	5.62369	14.09975
0.3	17.9742	5.84951	1.66286	5.62370	10.75363
0.4	17.9741	4.92385	1.39972	5.62372	9.05187
0.5	17.9741	4.33566	1.23251	5.62374	7.97055

Mode	p/MPa	$10^5 \cdot \delta_{TH}$/m	$10^6 \cdot \delta_V$/m	$10^9 \cdot l_{TH}$/m	$10^6 \cdot \delta_{TH,316L}$/m
0.2	16.9960	7.88684	2.23305	5.81643	14.17233
0.3	16.9960	6.01515	1.70310	5.81643	10.80897
0.4	16.9959	5.06322	1.43358	5.81644	9.09838
0.5	16.9959	4.45831	1.26231	5.81646	8.01138
0.2	16.0183	8.12652	2.29112	6.03351	14.24273
0.3	16.0184	6.19795	1.74740	6.03350	10.86267
0.4	16.0184	5.21704	1.47085	6.03350	9.14350
0.5	16.0184	4.59371	1.29511	6.03348	8.05103
0.2	15.0194	8.39751	2.35671	6.28549	14.31261
0.3	15.0194	6.40467	1.79743	6.28551	10.91598
0.4	15.0193	5.39102	1.51295	6.28553	9.18830
0.5	15.0193	4.74687	1.33217	6.28555	8.09038
0.2	13.9771	8.71507	2.43348	6.58925	14.38226
0.3	13.9770	6.64683	1.85597	6.58926	10.96908
0.4	13.9770	5.59481	1.56222	6.58927	9.23296
0.5	13.9770	4.92623	1.37553	6.58927	8.12962
0.2	13.0262	9.03900	2.51189	6.91042	14.44367
0.3	13.0263	6.89386	1.91577	6.91041	11.01589
0.4	13.0264	5.80271	1.61254	6.91039	9.27231
0.5	13.0264	5.10924	1.41983	6.91039	8.16420
0.2	11.9811	9.44197	2.60959	7.32570	14.50791
0.3	11.9811	7.20119	1.99028	7.32571	11.06486
0.4	11.9811	6.06140	1.67526	7.32572	9.31352
0.5	11.9811	5.33701	1.47505	7.32573	8.20045
0.2	11.0482	9.85220	2.70926	7.76692	14.56208
0.3	11.0482	7.51406	2.06630	7.76693	11.10617
0.4	11.0483	6.32470	1.73924	7.76691	9.34827
0.5	11.0483	5.56878	1.53136	7.76690	8.23097
0.2	9.9885	10.38863	2.84005	8.37326	14.62040
0.3	9.9885	7.92324	2.16606	8.37332	11.15065
0.4	9.9885	6.66911	1.82320	8.37332	9.38568
0.5	9.9885	5.87200	1.60529	8.37334	8.26385
0.2	8.9810	10.98823	2.98681	9.09016	14.67202
0.3	8.9810	8.38045	2.27797	9.09019	11.18997
0.4	8.9810	7.05487	1.91761	9.09117	9.41874
0.5	8.9809	6.21079	1.68821	9.09023	8.29290

Mode	p/MPa	$10^5 \cdot \delta_{TH}$/m	$10^6 \cdot \delta_V$/m	$10^9 \cdot l_{TH}$/m	$10^6 \cdot \delta_{TH,316L}$/m
0.2	8.0286	11.65815	3.15150	9.94093	14.71767
0.3	8.0286	8.89126	2.40354	9.94084	11.22473
0.4	8.0287	7.48387	2.02309	9.94080	9.44800
0.5	8.0287	6.58932	1.78126	9.94078	8.31868
0.2	6.9972	12.53576	3.36828	11.13484	14.76317
0.3	6.9971	9.56074	2.56890	11.13498	11.25942
0.4	6.9970	8.04741	2.16228	11.13506	9.47719
0.5	6.9971	7.08545	1.90381	11.13504	8.34432
0.2	5.9976	13.59483	3.63128	12.69562	14.80404
0.3	5.9976	10.36834	2.76946	12.69566	11.29054
0.4	5.9976	8.72714	2.33109	12.69566	9.50337
0.5	5.9976	7.68395	2.05244	12.69570	8.36738
0.2	5.0003	14.95488	3.97086	14.89118	14.84120
0.3	5.0003	11.40553	3.02843	14.89110	11.31887
0.4	5.0003	9.60013	2.54905	14.89110	9.52718
0.5	5.0003	8.45255	2.24435	14.89103	8.38834
0.2	4.0014	16.79923	4.43393	18.20990	14.87447
0.3	4.0014	12.81298	3.38180	18.21122	11.34423
0.4	4.0014	10.78417	2.84633	18.21011	9.54850
0.5	4.0014	9.49506	2.50609	18.21014	8.40709
0.2	3.0054	19.48630	5.11247	23.74505	14.90399
0.3	3.0054	14.86146	3.89909	23.74490	11.36674
0.4	3.0055	12.50886	3.28186	23.74461	9.56743
0.5	3.0055	11.01357	2.88955	23.74468	8.42374
0.2	2.0037	23.99930	6.25885	34.90165	14.93065
0.3	2.0037	18.30336	4.77339	34.90166	11.38703
0.4	2.0037	15.40597	4.01777	34.90158	9.58450
0.5	2.0037	13.56428	3.53747	34.90143	8.43874
0.2	1.0032	34.12342	8.84618	68.38298	14.95343
0.3	1.0032	26.02442	6.74659	68.38292	11.40432
0.4	1.0032	21.90478	5.67861	68.38292	9.59903
0.5	1.0032	19.28709	5.00000	68.38732	8.45152

Table B3.3 *Values of calculated thermal boundary layer, shell motion and holes and ducts frequency corrections; and thermal boundary layer, bulk viscosity and ducts and holes half width contributions to the resonance peaks at T = 300 K.*

Mode	p/Mpa	Δf_{TH}/Hz	Δf_{Shell}/Hz	Δf_{ducts}/Hz	g_{th}/Hz	g_b/Hz	g_{hole}/Hz
0.2	20.0091	-7.3099	-1.8852	0.0290	7.31638	0.13379	0.00170
0.3	20.0091	-9.5843	-2.4649	0.0545	9.59228	0.39541	0.00170
0.4	20.0090	-11.3842	-2.4020	0.0078	11.39386	0.78755	0.00170
0.5	20.0090	-12.9248	-1.7165	0.0532	12.93601	1.30982	0.00170
0.2	18.9981	-7.2989	-1.7404	0.0232	7.30455	0.13698	0.00169
0.3	18.9981	-9.5692	-2.2861	0.0535	9.57687	0.40484	0.00169
0.4	18.9980	-11.3665	-2.2470	0.0080	11.37584	0.80638	0.00169
0.5	18.9979	-12.9043	-1.6420	0.0527	12.91510	1.34107	0.00168
0.2	17.9743	-7.2903	-1.6007	0.0229	7.29577	0.14062	0.00167
0.3	17.9742	-9.5581	-2.1121	0.0533	9.56544	0.41559	0.00167
0.4	17.9741	-11.3535	-2.0931	0.0083	11.36249	0.82781	0.00167
0.5	17.9741	-12.8914	-1.5605	0.0521	12.90177	1.37700	0.00167
0.2	16.9960	-7.2861	-1.4738	0.0227	7.29138	0.14452	0.00165
0.3	16.9960	-9.5526	-1.9526	0.0531	9.55975	0.42713	0.00165
0.4	16.9959	-11.3473	-1.9494	0.0086	11.35595	0.85082	0.00165
0.5	16.9959	-12.8849	-1.4794	0.0515	12.89493	1.41536	0.00165
0.2	16.0183	-7.2873	-1.3531	0.0225	7.29229	0.14894	0.00164
0.3	16.0184	-9.5541	-1.7996	0.0530	9.56091	0.44018	0.00164
0.4	16.0184	-11.3493	-1.8090	0.0089	11.35759	0.87686	0.00164
0.5	16.0184	-12.8875	-1.3954	0.0510	12.89712	1.45872	0.00164
0.2	15.0194	-7.2954	-1.2357	0.0223	7.30023	0.15408	0.00162
0.3	15.0194	-9.5647	-1.6497	0.0529	9.57123	0.45538	0.00162
0.4	15.0193	-11.3622	-1.6692	0.0092	11.37023	0.90717	0.00162
0.5	15.0193	-12.9025	-1.3074	0.0505	12.91179	1.50922	0.00162
0.2	13.9771	-7.3140	-1.1195	0.0220	7.31855	0.16032	0.00160
0.3	13.9770	-9.5890	-1.4999	0.0528	9.59528	0.47382	0.00160
0.4	13.9770	-11.3913	-1.5274	0.0096	11.39894	0.94391	0.00160
0.5	13.9770	-12.9360	-1.2136	0.0501	12.94488	1.57042	0.00160
0.2	13.0262	-7.3421	-1.0187	0.0219	7.34653	0.16692	0.00158
0.3	13.0263	-9.6260	-1.3692	0.0528	9.63198	0.49334	0.00158
0.4	13.0264	-11.4354	-1.4018	0.0100	11.44270	0.98280	0.00158
0.5	13.0264	-12.9863	-1.1273	0.0496	12.99489	1.63517	0.00158
0.2	11.9811	-7.3895	-0.9133	0.0217	7.39365	0.17549	0.00156
0.3	11.9811	-9.6881	-1.2314	0.0528	9.69383	0.51867	0.00156
0.4	11.9811	-11.5092	-1.2678	0.0105	11.51627	1.03329	0.00155
0.5	11.9811	-13.0703	-1.0319	0.0492	13.07854	1.71919	0.00155
0.2	11.0482	-7.4505	-0.8237	0.0215	7.45450	0.18463	0.00153
0.3	11.0482	-9.7680	-1.1137	0.0530	9.77354	0.54568	0.00153
0.4	11.0483	-11.6043	-1.1517	0.0109	11.61103	1.08711	0.00153
0.5	11.0483	-13.1785	-0.9465	0.0488	13.18646	1.80881	0.00153

Mode	p/Mpa	Δf_{TH}/Hz	Δf_{Shell}/Hz	Δf_{ducts}/Hz	g_{th}/Hz	g_b/Hz	g_{hole}/Hz
0.2	9.9885	-7.5473	-0.7269	0.0213	7.55112	0.19722	0.00151
0.3	9.9885	-9.8949	-0.9855	0.0532	9.90015	0.58289	0.00151
0.4	9.9885	-11.7551	-1.0240	0.0115	11.76160	1.16125	0.00151
0.5	9.9885	-13.3501	-0.8500	0.0484	13.35773	1.93222	0.00151
0.2	8.9810	-7.6754	-0.6393	0.0212	7.67903	0.21215	0.00149
0.3	8.9810	-10.0630	-0.8688	0.0536	10.06803	0.62702	0.00149
0.4	8.9810	-11.9545	-0.9066	0.0122	11.96079	1.24922	0.00149
0.5	8.9809	-13.5775	-0.7589	0.0481	13.58486	2.07861	0.00149
0.2	8.0286	-7.8395	-0.5601	0.0211	7.84303	0.22990	0.00146
0.3	8.0286	-10.2782	-0.7629	0.0541	10.28315	0.67949	0.00146
0.4	8.0287	-12.2106	-0.7987	0.0128	12.21671	1.35371	0.00146
0.5	8.0287	-13.8678	-0.6736	0.0478	13.87494	2.25251	0.00146
0.2	6.9972	-8.0823	-0.4782	0.0209	8.08567	0.25487	0.00144
0.3	6.9971	-10.5966	-0.6525	0.0548	10.60139	0.75331	0.00144
0.4	6.9970	-12.5890	-0.6856	0.0134	12.59492	1.50080	0.00144
0.5	6.9971	-14.2977	-0.5823	0.0475	14.30476	2.49732	0.00144
0.2	5.9976	-8.4081	-0.4021	0.0208	8.41138	0.28755	0.00142
0.3	5.9976	-11.0239	-0.5497	0.0558	11.02853	0.84991	0.00142
0.4	5.9976	-13.0966	-0.5793	0.0137	13.10240	1.69326	0.00142
0.5	5.9976	-14.8743	-0.4951	0.0472	14.88123	2.81758	0.00142
0.2	5.0003	-8.8669	-0.3292	0.0207	8.87012	0.33359	0.00139
0.3	5.0003	-11.6255	-0.4508	0.0578	11.63012	0.98599	0.00139
0.4	5.0003	-13.8113	-0.4764	0.0129	13.81719	1.96439	0.00139
0.5	5.0003	-15.6859	-0.4094	0.0470	15.69292	3.26873	0.00139
0.2	4.0014	-9.5421	-0.2590	0.0206	9.54536	0.40328	0.00137
0.3	4.0014	-12.5108	-0.3552	0.0587	12.51552	1.19203	0.00137
0.4	4.0014	-14.8632	-0.3762	0.0102	14.86920	2.37485	0.00137
0.5	4.0014	-16.8806	-0.3248	0.0468	16.88781	3.95179	0.00137
0.2	3.0054	-10.5990	-0.1914	0.0206	10.60236	0.51962	0.00135
0.3	3.0054	-13.8964	-0.2628	0.0608	13.90141	1.53585	0.00135
0.4	3.0055	-16.5093	-0.2790	0.0037	16.51567	3.05988	0.00135
0.5	3.0055	-18.7502	-0.2419	0.0466	18.75792	5.09175	0.00135
0.2	2.0037	-12.4905	-0.1257	0.0205	12.49433	0.75419	0.00132
0.3	2.0037	-16.3765	-0.1728	0.0634	16.38221	2.22923	0.00132
0.4	2.0037	-19.4557	-0.1838	-0.0081	19.46315	4.44138	0.00132
0.5	2.0037	-22.0964	-0.1599	0.0466	22.10561	7.39064	0.00132
0.2	1.0032	-16.9878	-0.0620	0.0206	16.99305	1.45849	0.00130
0.3	1.0032	-22.2728	-0.0854	0.0680	22.28106	4.31111	0.00130
0.4	1.0032	-26.4605	-0.0909	-0.0015	26.47160	8.58929	0.00130
0.5	1.0032	-30.0524	-0.0794	0.0464	30.06631	14.29367	0.00130

Table B3.4 *Uncertainty contributions and result of radius calibration at T = 300 K*

p/MPa	a/m	$10^{11}\cdot\sum_{i=1}^{4}\left(\frac{\partial a}{\partial f_i}\right)^2 u^2(f_i)\Big/m^2$	$10^{12}\cdot\left(\frac{\partial a}{\partial u}\right)^2 u^2(u)\Big/m^2$	$10^{11}\cdot u_{disp}^2(a)\Big/m^2$	$10^{6}\cdot u(a)/m$
20.0090	0.040165	1.2	1.6	9.8	11
18.9980	0.040163	0.18	1.6	9.5	11
17.9742	0.040160	0.41	1.6	7.5	9.5
16.9959	0.040158	6.3	1.6	6.6	9.4
16.0184	0.040156	0.85	1.6	8.1	9.9
15.0194	0.040154	1.7	1.6	5.5	8.5
13.9770	0.040153	0.52	1.6	5.0	8.2
13.0263	0.040151	0.74	1.6	4.6	7.9
11.9811	0.040150	0.46	1.6	4.4	7.8
11.0483	0.040149	0.57	1.6	4.1	7.6
9.9885	0.040147	1.4	1.6	4.0	7.6
8.9810	0.040146	0.27	1.6	4.0	7.5
8.0286	0.040144	0.23	1.6	3.7	7.3
6.9971	0.040142	2.1	1.6	3.7	7.4
5.9976	0.040140	0.57	1.6	3.8	7.4
5.0003	0.040137	0.30	1.6	4.0	7.5
4.0014	0.040133	0.54	1.6	4.4	7.8
3.0055	0.040126	2.2	1.6	5.2	8.4
2.0037	0.040116	1.2	1.6	6.9	9.3
1.0032	0.040103	52	1.6	9.0	13

B4

Frequency measurements, frequency corrections and radius measurements and uncertainties at 325K

Table B4.1 *Pressure, north and south hemisphere and average temperature, frequency of resonance, half-width of the resonance peak and frequency measurement uncertainty using argon to calibrate internal radius at T = 325 K.*

Mode	p/Mpa	T_N/K	T_S/K	T_{ave}/K	f/Hz	g/Hz	u(f)/Hz
0.2	20.0242	325.0000	324.9961	324.9980	6821.0819	0.39691	0.24
0.3	20.0243	325.0008	324.9959	324.9983	11726.7745	0.74730	0.56
0.4	20.0244	325.0008	324.9959	324.9983	16548.5937	2.97117	6.5
0.5	20.0244	325.0011	324.9959	324.9985	21340.6959	1.85923	3.4
0.2	18.9829	324.9944	324.9891	324.9918	6754.1857	0.37876	0.044
0.3	18.9829	324.9939	324.9893	324.9916	11611.6935	1.23002	2.0
0.4	18.9828	324.9937	324.9893	324.9915	16386.6827	1.12861	0.66
0.5	18.9828	324.9937	324.9893	324.9915	20473.8865	1.45619	2.6
0.2	18.0047	324.9932	324.9887	324.9910	6693.3555	0.37344	0.050
0.3	18.0047	324.9934	324.9890	324.9912	11506.2577	1.13307	2.0
0.4	18.0047	324.9936	324.9892	324.9914	16239.5050	0.90086	0.49
0.5	18.0047	324.9938	324.9894	324.9916	20944.5668	1.38043	0.69
0.2	16.9990	324.9799	324.9746	324.9773	6632.7781	0.36687	0.072
0.3	16.9989	324.9804	324.9749	324.9777	11402.3679	0.64064	0.32
0.4	16.9988	324.9808	324.9754	324.9781	16093.0231	0.73255	0.35
0.5	16.9987	324.9812	324.9758	324.9785	20756.1041	1.74480	0.74
0.2	15.9834	325.0039	325.0004	325.0021	6574.1838	0.36245	0.12
0.3	15.9834	325.0039	325.0004	325.0021	11301.8262	0.54672	0.66
0.4	15.9834	325.0039	325.0004	325.0021	15951.2505	0.73454	3.4
0.5	15.9835	325.0040	325.0004	325.0022	20573.1775	2.18060	7.2
0.2	15.0105	324.9827	324.9770	324.9798	6519.7614	0.36039	0.046
0.3	15.0105	324.9832	324.9774	324.9803	11208.3773	0.51351	0.12
0.4	15.0104	324.9836	324.9778	324.9807	15819.4535	0.66293	0.38
0.5	15.0103	324.9836	324.9778	324.9807	20403.2286	1.55293	1.7
0.2	13.9764	324.9949	324.9906	324.9928	6464.6558	0.35771	0.036
0.3	13.9764	324.9950	324.9906	324.9928	11113.7276	0.51253	0.22
0.4	13.9764	324.9949	324.9905	324.9927	15685.9919	0.64845	0.16
0.5	13.9764	324.9951	324.9905	324.9928	20231.8432	1.15007	0.31

Mode	p/Mpa	T_N/K	T_S/K	T_{ave}/K	*f*/Hz	*g*/Hz	u(*f*)/Hz
0.2	12.9943	325.0056	324.9996	325.0026	6414.6256	0.36037	0.039
0.3	12.9943	325.0056	324.9998	325.0027	11027.7879	0.51769	0.15
0.4	12.9943	325.0057	324.9999	325.0028	15564.8181	0.63475	0.10
0.5	12.9943	325.0057	324.9999	325.0028	20075.9807	1.26001	0.36
0.2	11.9689	325.0088	325.0050	325.0069	6364.8085	0.37307	0.25
0.3	11.9688	325.0087	325.0050	325.0069	10942.1827	0.51487	0.16
0.4	11.9687	325.0087	325.0048	325.0068	15444.1408	0.61740	0.15
0.5	11.9687	325.0087	325.0048	325.0068	19920.5987	1.06412	0.65
0.2	10.9935	325.0130	325.0084	325.0107	6319.8167	0.35683	0.056
0.3	10.9936	325.0131	325.0086	325.0109	10864.8826	0.50355	0.21
0.4	10.9936	325.0132	325.0088	325.0110	15335.1788	0.62455	0.40
0.5	10.9936	325.0133	325.0089	325.0111	19780.3878	0.98210	0.43
0.2	9.9930	325.0062	325.0017	325.0039	6276.0045	0.35954	0.036
0.3	9.9930	325.0062	325.0017	325.0039	10789.5931	0.49857	0.16
0.4	9.9930	325.0062	325.0017	325.0039	15229.0032	0.63775	0.32
0.5	9.9930	325.0062	325.0017	325.0039	19643.7482	0.90834	0.83
0.2	8.9994	325.0048	325.0012	325.0030	6235.0060	0.35780	0.035
0.3	8.9994	325.0051	325.0015	325.0033	10719.1554	0.49659	0.19
0.4	8.9994	325.0053	325.0018	325.0035	15129.6499	0.65281	0.19
0.5	8.9994	325.0054	325.0019	325.0036	19515.9190	0.93006	0.23
0.2	7.9949	324.9959	324.9923	324.9941	6195.9984	0.36328	0.045
0.3	7.9948	324.9960	324.9924	324.9942	10652.1202	0.50365	0.13
0.4	7.9947	324.9960	324.9924	324.9942	15035.1083	0.62282	0.11
0.5	7.9947	324.9960	324.9924	324.9942	19394.2062	0.91853	0.11
0.2	6.9686	324.9973	324.9937	324.9955	6158.8445	0.37376	0.061
0.3	6.9684	324.9975	324.9935	324.9955	10588.2870	0.51278	0.089
0.4	6.9687	324.9975	324.9935	324.9955	14945.1168	0.63205	0.22
0.5	6.9688	324.9976	324.9935	324.9955	19278.2078	0.95925	0.12
0.2	5.9954	325.0071	325.0026	325.0049	6126.0884	0.38217	0.11
0.3	5.9954	325.0072	325.0028	325.0050	10532.0248	0.52562	0.17
0.4	5.9954	325.0073	325.0029	325.0051	14865.7861	0.72000	0.97
0.5	5.9953	325.0073	325.0030	325.0052	19176.0384	0.95088	0.41
0.2	4.9746	325.0016	324.9968	324.9992	6094.1085	0.39590	0.082
0.3	4.9748	325.0016	324.9969	324.9992	10477.0892	0.53934	0.058
0.4	4.9749	325.0017	324.9969	324.9993	14788.2533	0.68260	0.19
0.5	4.9750	325.0018	324.9970	324.9994	19076.1946	0.97042	0.098
0.2	3.9933	325.0069	325.0026	325.0048	6065.8472	0.40734	0.11
0.3	3.9934	325.0071	325.0027	325.0049	10428.5082	0.56072	0.068
0.4	3.9935	325.0071	325.0027	325.0049	14719.7628	0.69315	0.27
0.5	3.9935	325.0072	325.0028	325.0050	18987.9905	0.98603	0.083

Mode	p/Mpa	T_N/K	T_S/K	T_{ave}/K	f/Hz	g/Hz	u(f)/Hz
0.2	2.9903	325.0049	325.0007	325.0028	6039.2332	0.45654	0.096
0.3	2.9903	325.0049	325.0007	325.0028	10382.8144	0.60047	0.12
0.4	2.9904	325.0049	325.0008	325.0028	14655.3006	0.75113	0.18
0.5	2.9905	325.0049	325.0007	325.0028	18904.9257	1.13672	0.10
0.2	1.9805	325.0069	325.0024	325.0047	6014.8529	0.54146	0.19
0.3	1.9805	325.0071	325.0028	325.0050	10340.9514	0.69061	0.21
0.4	1.9806	325.0076	325.0031	325.0054	14596.2792	0.85327	0.064
0.5	1.9807	325.0076	325.0031	325.0054	18828.8314	1.18975	0.098
0.2	0.9905	325.0061	325.0025	325.0043	5993.0264	0.70749	0.093
0.3	0.9905	325.0061	325.0025	325.0043	10303.5763	0.88930	0.63
0.4	0.9905	325.0060	325.0025	325.0042	14543.6099	1.11732	0.58
0.5	0.9905	325.0060	325.0024	325.0042	18760.9801	1.46991	0.27
0.2	0.1179	325.0061	325.0025	325.0043	5974.7708	1.75365	1.6
0.3	0.1179	325.0061	325.0025	325.0043	10272.6693	2.42533	4.6
0.4	0.1179	325.0060	325.0025	325.0042	14500.3607	3.02704	5.0
0.5	0.1179	325.0060	325.0024	325.0042	18705.7552	3.86744	6.3

Table B4.2 *Parameters required for computing frequency corrections, thermal boundary layer length, viscous boundary layer length accommodation length and thermal boundary layer in sell side length at T = 325 K.*

Mode	p/Mpa	$10^6 \cdot \delta_{TH}$/m	$10^6 \cdot \delta_V$/m	$10^{11} \cdot l_{TH}$/m	$10^6 \cdot \delta_{TH,316L}$/m
0.2	20.0242	2.4768	2.1852	7.24889	13.7338
0.3	20.0243	1.8890	1.6666	7.24887	10.4744
0.4	20.0244	1.5901	1.4030	7.24886	8.8173
0.5	20.0244	1.4003	1.2354	7.24884	7.7645
0.2	18.9829	2.5414	2.2356	7.51678	13.8017
0.3	18.9829	1.9382	1.7050	7.51679	10.5262
0.4	18.9828	1.6316	1.4352	7.51681	8.8608
0.5	18.9828	1.4597	1.2840	7.51683	7.9272
0.2	18.0047	2.6078	2.2872	7.79729	13.8643
0.3	18.0047	1.9890	1.7444	7.79730	10.5743
0.4	18.0047	1.6742	1.4684	7.79729	8.9009
0.5	18.0047	1.4742	1.2930	7.79730	7.8376
0.2	16.9990	2.6826	2.3453	8.11981	13.9274
0.3	16.9989	2.0460	1.7887	8.11985	10.6224
0.4	16.9988	1.7222	1.5057	8.11990	8.9413
0.5	16.9987	1.5165	1.3258	8.11995	7.8731

Mode	p/Mpa	$10^6 \cdot \delta_{TH}$/m	$10^6 \cdot \delta_V$/m	$10^{11} \cdot l_{TH}$/m	$10^6 \cdot \delta_{TH,316L}$/m

0.2	15.9834	2.7662	2.4101	8.48868	13.9894
0.3	15.9834	2.1097	1.8382	8.48868	10.6695
0.4	15.9834	1.7758	1.5472	8.48867	8.9809
0.5	15.9835	1.5637	1.3624	8.48864	7.9080
0.2	15.0105	2.8544	2.4786	8.88920	14.0476
0.3	15.0105	2.1770	1.8904	8.88924	10.7139
0.4	15.0104	1.8325	1.5912	8.88927	9.0183
0.5	15.0103	1.6136	1.4011	8.88930	7.9409
0.2	13.9764	2.9593	2.5600	9.37915	14.1074
0.3	13.9764	2.2570	1.9525	9.37916	10.7594
0.4	13.9764	1.8998	1.6435	9.37916	9.0565
0.5	13.9764	1.6728	1.4471	9.37915	7.9745
0.2	12.9943	3.0710	2.6468	9.91934	14.1623
0.3	12.9943	2.3422	2.0187	9.91934	10.8013
0.4	12.9943	1.9715	1.6992	9.91934	9.0917
0.5	12.9943	1.7359	1.4961	9.91932	8.0053
0.2	11.9689	3.2028	2.7494	10.58138	14.2176
0.3	11.9688	2.4427	2.0969	10.58143	10.8434
0.4	11.9687	2.0561	1.7651	10.58149	9.1272
0.5	11.9687	1.8104	1.5541	10.58154	8.0365
0.2	10.9935	3.3457	2.8610	11.33014	14.2681
0.3	10.9936	2.5517	2.1820	11.33013	10.8819
0.4	10.9936	2.1478	1.8366	11.33011	9.1596
0.5	10.9936	1.8911	1.6171	11.33008	8.0649
0.2	9.9930	3.5143	2.9929	12.25533	14.3178
0.3	9.9930	2.6803	2.2826	12.25535	10.9198
0.4	9.9930	2.2561	1.9213	12.25539	9.1914
0.5	9.9930	1.9864	1.6917	12.25541	8.0929
0.2	8.9994	3.7099	3.1463	13.38514	14.3648
0.3	8.9994	2.8294	2.3996	13.38512	10.9557
0.4	8.9994	2.3816	2.0198	13.38512	9.2216
0.5	8.9994	2.0969	1.7784	13.38507	8.1194
0.2	7.9949	3.9443	3.3309	14.82112	14.4100
0.3	7.9948	3.0082	2.5404	14.82133	10.9901
0.4	7.9947	2.5321	2.1383	14.82143	9.2505
0.5	7.9947	2.2294	1.8827	14.82139	8.1448
0.2	6.9686	4.2354	3.5608	16.72793	14.4534
0.3	6.9684	3.2303	2.7158	16.72833	11.0232
0.4	6.9687	2.7189	2.2859	16.72782	9.2783
0.5	6.9688	2.3939	2.0126	16.72761	8.1693
Mode	**p/Mpa**	**$10^6 \cdot \delta_{TH}$/m**	**$10^6 \cdot \delta_V$/m**	**$10^{11} \cdot l_{TH}$/m**	**$10^6 \cdot \delta_{TH,316L}$/m**

0.2	5.9954	4.5788	3.8331	19.15307	14.4920
0.3	5.9954	3.4921	2.9234	19.15308	11.0526
0.4	5.9954	2.9393	2.4606	19.15312	9.3030
0.5	5.9953	2.5880	2.1665	19.15318	8.1910
0.2	4.9746	5.0426	4.2023	22.73244	14.5299
0.3	4.9748	3.8458	3.2049	22.73181	11.0815
0.4	4.9749	3.2370	2.6976	22.73139	9.3274
0.5	4.9750	2.8501	2.3751	22.73106	8.2124
0.2	3.9933	5.6475	4.6857	27.92184	14.5637
0.3	3.9934	4.3071	3.5736	27.92133	11.1073
0.4	3.9935	3.6253	3.0079	27.92086	9.3491
0.5	3.9935	3.1919	2.6483	27.92041	8.2315
0.2	2.9903	6.5512	5.4110	36.77547	14.5958
0.3	2.9903	4.9963	4.1267	36.77464	11.1317
0.4	2.9904	4.2054	3.4735	36.77394	9.3696
0.5	2.9905	3.7026	3.0582	36.77334	8.2496
0.2	1.9805	8.0837	6.6464	54.79603	14.6253
0.3	1.9805	6.1650	5.0689	54.79448	11.1542
0.4	1.9806	5.1890	4.2664	54.79214	9.3885
0.5	1.9807	4.5687	3.7564	54.79133	8.2662
0.2	0.9905	11.4814	9.3977	108.22564	14.6520
0.3	0.9905	8.7563	7.1672	108.22554	11.1744
0.4	0.9905	7.3702	6.0327	108.22551	9.4055
0.5	0.9905	6.4892	5.3115	108.22517	8.2812
0.2	0.1179	33.4164	27.2441	899.78331	14.6743
0.3	0.1179	25.4843	20.7771	899.75283	11.1912
0.4	0.1179	21.4501	17.4881	899.77551	9.4195
0.5	0.1179	18.8856	15.3973	899.77532	8.2934

Table B4.3 *Values of calculated thermal boundary layer, shell motion and holes and ducts frequency corrections; and thermal boundary layer, bulk viscosity and ducts and holes half width contributions to the resonance peaks at T = 325 K.*

Mode	**p/Mpa**	**Δf_{TH} /Hz**	**Δf_{shell} /Hz**	**Δf_{hole} /Hz**	**g_{th}/Hz**	**g_b/Hz**	**g_{hole}/Hz**
0.2	20.0242	-0.2296	-0.1534	-1.5532×10^{-3}	0.23452	0.00028	0.85147
0.3	20.0243	-0.3010	-0.2842	4.4866×10^{-4}	0.30749	0.00083	0.85328
0.4	20.0244	-0.3575	-0.4607	3.8992×10^{-4}	0.36524	0.00165	0.85377
0.5	20.0244	-0.4058	-0.7845	2.1212×10^{-4}	0.41460	0.00274	0.85293
0.2	18.9829	-0.2299	-0.1477	-1.3467×10^{-3}	0.23469	0.00029	0.85104
0.3	18.9829	-0.3015	-0.2733	4.7396×10^{-4}	0.30773	0.00085	0.85296
0.4	18.9828	-0.3581	-0.4415	3.7405×10^{-4}	0.36549	0.00170	0.85309
0.5	18.9828	-0.3876	-0.7499	1.1634×10^{-4}	0.39569	0.00265	0.77513
Mode	**p/Mpa**	**Δf_{TH} /Hz**	**Δf_{shell} /Hz**	**Δf_{hole} /Hz**	**g_{th}/Hz**	**g_b/Hz**	**g_{hole}/Hz**

0.2	18.0047	-0.2304	-0.1425	-1.1419×10^{-3}	0.23501	0.00030	0.85069
0.3	18.0047	-0.3021	-0.2632	4.9314×10^{-4}	0.30811	0.00088	0.85239
0.4	18.0047	-0.3588	-0.4237	3.5553×10^{-4}	0.36599	0.00175	0.85270
0.5	18.0047	-0.4074	-0.7059	1.7554×10^{-4}	0.41556	0.00292	0.85238
0.2	16.9990	-0.2311	-0.1371	-9.2313×10^{-4}	0.23553	0.00031	0.85032
0.3	16.9989	-0.3030	-0.2529	5.0879×10^{-4}	0.30878	0.00091	0.85195
0.4	16.9988	-0.3599	-0.4057	3.3229×10^{-4}	0.36680	0.00182	0.85232
0.5	16.9987	-0.4087	-0.6696	1.5436×10^{-4}	0.41651	0.00303	0.85210
0.2	15.9834	-0.2321	-0.1317	-6.9416×10^{-4}	0.23630	0.00032	0.85008
0.3	15.9834	-0.3043	-0.2425	5.1700×10^{-4}	0.30980	0.00095	0.85171
0.4	15.9834	-0.3615	-0.3879	3.0385×10^{-4}	0.36802	0.00189	0.85205
0.5	15.9835	-0.4104	-0.6346	1.3110×10^{-4}	0.41790	0.00315	0.85184
0.2	15.0105	-0.2333	-0.1265	-4.7389×10^{-4}	0.23732	0.00034	0.84976
0.3	15.0105	-0.3058	-0.2327	5.1532×10^{-4}	0.31114	0.00099	0.85137
0.4	15.0104	-0.3633	-0.3711	2.7204×10^{-4}	0.36962	0.00197	0.85165
0.5	15.0103	-0.4125	-0.6024	1.0769×10^{-4}	0.41970	0.00328	0.85135
0.2	13.9764	-0.2349	-0.1209	-2.4045×10^{-4}	0.23880	0.00035	0.84956
0.3	13.9764	-0.3080	-0.2222	5.0124×10^{-4}	0.31308	0.00104	0.85112
0.4	13.9764	-0.3659	-0.3534	2.3317×10^{-4}	0.37193	0.00207	0.85134
0.5	13.9764	-0.4155	-0.5694	8.1959×10^{-5}	0.42234	0.00345	0.85105
0.2	12.9943	-0.2370	-0.1157	-2.7038×10^{-5}	0.24066	0.00037	0.84940
0.3	12.9943	-0.3107	-0.2122	4.7407×10^{-4}	0.31553	0.00110	0.85089
0.4	12.9943	-0.3691	-0.3367	1.9220×10^{-4}	0.37484	0.00219	0.85104
0.5	12.9943	-0.4191	-0.5389	5.7870×10^{-5}	0.42566	0.00364	0.85080
0.2	11.9689	-0.2397	-0.1101	1.7850×10^{-4}	0.24320	0.00039	0.84927
0.3	11.9688	-0.3143	-0.2018	4.2988×10^{-4}	0.31887	0.00117	0.85063
0.4	11.9687	-0.3733	-0.3193	1.4663×10^{-4}	0.37881	0.00232	0.85072
0.5	11.9687	-0.4239	-0.5079	3.4398×10^{-5}	0.43018	0.00386	0.85047
0.2	10.9935	-0.2430	-0.1047	3.4782×10^{-4}	0.24634	0.00042	0.84919
0.3	10.9936	-0.3186	-0.1917	3.7251×10^{-4}	0.32299	0.00124	0.85040
0.4	10.9936	-0.3785	-0.3027	1.0275×10^{-4}	0.38371	0.00248	0.85043
0.5	10.9936	-0.4298	-0.4789	1.5112×10^{-5}	0.43575	0.00412	0.85019
0.2	9.9930	-0.2473	-0.0991	4.8251×10^{-4}	0.25050	0.00045	0.84912
0.3	9.9930	-0.3242	-0.1812	2.9965×10^{-4}	0.32843	0.00134	0.85013
0.4	9.9930	-0.3852	-0.2856	6.0262×10^{-5}	0.39018	0.00267	0.85011
0.5	9.9930	-0.4374	-0.4495	-4.8890×10^{-8}	0.44311	0.00445	0.84989
0.2	8.9994	-0.2528	-0.0934	5.6375×10^{-4}	0.25584	0.00049	0.84911
0.3	8.9994	-0.3314	-0.1706	2.1730×10^{-4}	0.33543	0.00146	0.84989
0.4	8.9994	-0.3938	-0.2684	2.4282×10^{-5}	0.39850	0.00291	0.84981
0.5	8.9994	-0.4472	-0.4204	-9.2447×10^{-6}	0.45257	0.00484	0.84963

Mode	**p/Mpa**	**Δf_{TH} /Hz**	**Δf_{shell} /Hz**	**Δf_{hole} /Hz**	**g_{th}/Hz**	**g_b/Hz**	**g_{hole}/Hz**

0.2	7.9949	-0.2600	-0.0874	5.7906×10^{-4}	0.26286	0.00055	0.84910
0.3	7.9948	-0.3408	-0.1596	1.3174×10^{-4}	0.34464	0.00161	0.84961
0.4	7.9947	-0.4049	-0.2506	-1.8269×10^{-6}	0.40944	0.00321	0.84950
0.5	7.9947	-0.4599	-0.3909	-1.2171×10^{-5}	0.46501	0.00534	0.84936
0.2	6.9686	-0.2696	-0.0811	5.1611×10^{-4}	0.27236	0.00061	0.84912
0.3	6.9684	-0.3535	-0.1480	5.3787×10^{-5}	0.35710	0.00181	0.84935
0.4	6.9687	-0.4200	-0.2319	-1.4938×10^{-5}	0.42424	0.00361	0.84924
0.5	6.9688	-0.4769	-0.3603	-9.6177×10^{-6}	0.48181	0.00601	0.84912
0.2	5.9954	-0.2818	-0.0748	3.8653×10^{-4}	0.28444	0.00070	0.84912
0.3	5.9954	-0.3695	-0.1364	1.6058×10^{-6}	0.37294	0.00207	0.84912
0.4	5.9954	-0.4390	-0.2134	-1.4970×10^{-5}	0.44307	0.00412	0.84905
0.5	5.9953	-0.4986	-0.3304	-4.6666×10^{-6}	0.50320	0.00686	0.84895
0.2	4.9746	-0.2994	-0.0678	2.0616×10^{-4}	0.30190	0.00083	0.84901
0.3	4.9748	-0.3926	-0.1234	-2.0643×10^{-5}	0.39584	0.00245	0.84886
0.4	4.9749	-0.4664	-0.1929	-7.2111×10^{-6}	0.47027	0.00488	0.84880
0.5	4.9750	-0.5297	-0.2977	-5.1597×10^{-7}	0.53410	0.00812	0.84875
0.2	3.9933	-0.3238	-0.0604	4.8348×10^{-5}	0.32614	0.00102	0.84883
0.3	3.9934	-0.4245	-0.1100	-1.4188×10^{-5}	0.42761	0.00300	0.84865
0.4	3.9935	-0.5043	-0.1717	-5.4468×10^{-7}	0.50802	0.00598	0.84864
0.5	3.9935	-0.5728	-0.2641	5.0604×10^{-7}	0.57698	0.00995	0.84861
0.2	2.9903	-0.3622	-0.0520	-2.3763×10^{-5}	0.36442	0.00133	0.84858
0.3	2.9903	-0.4749	-0.0947	-1.0503×10^{-6}	0.47780	0.00394	0.84847
0.4	2.9904	-0.5641	-0.1476	5.3229×10^{-7}	0.56765	0.00786	0.84847
0.5	2.9905	-0.6407	-0.2265	4.0852×10^{-8}	0.64472	0.01307	0.84846
0.2	1.9805	-0.4306	-0.0422	-5.3321×10^{-6}	0.43278	0.00198	0.84839
0.3	1.9805	-0.5646	-0.0767	3.4404×10^{-7}	0.56744	0.00586	0.84833
0.4	1.9806	-0.6708	-0.1194	-2.9109×10^{-8}	0.67414	0.01168	0.84833
0.5	1.9807	-0.7618	-0.1828	-2.1135×10^{-9}	0.76566	0.01943	0.84831
0.2	0.9905	-0.5896	-0.0297	6.5891×10^{-9}	0.59168	0.00391	0.84822
0.3	0.9905	-0.7731	-0.0540	1.6726×10^{-9}	0.77580	0.01155	0.84817
0.4	0.9905	-0.9185	-0.0840	-5.5421×10^{-11}	0.92171	0.02301	0.84819
0.5	0.9905	-1.0431	-0.1283	7.4591×10^{-13}	1.04685	0.03829	0.84817
0.2	0.1179	-1.6613	-0.0102	0	1.66365	0.03241	0.84811
0.3	0.1179	-2.1781	-0.0186	0	2.18141	0.09581	0.84811
0.4	0.1179	-2.5877	-0.0289	0	2.59176	0.19091	0.84814
0.5	0.1179	-2.9390	-0.0440	3.1249×10^{-18}	2.94376	0.31770	0.84820

Table B4.4 *Uncertainty contributions and result of radius calibration at T = 325 K.*

p/MPa	a/m	$10^{11}\cdot\sum_{i=1}^{4}\left(\frac{\partial a}{\partial f_i}\right)^2 u^2(f_i)\Big/m^2$	$10^{11}\cdot\left(\frac{\partial a}{\partial u}\right)^2 u^2(u)\Big/m^2$	$10^{11}\cdot u_{disp}^2(a)/m^2$	$10^6\cdot u(a)/m$
20.0243	0.04022	2.3	1.6	2.8	8.2
18.9829	0.04021	0.65	1.6	0.81	5.6
18.0047	0.04021	0.47	1.6	1.2	5.7
16.9989	0.04021	0.18	1.6	0.89	5.2
15.9834	0.04021	2.01	1.6	1.1	6.9
15.0104	0.04021	0.26	1.6	0.73	5.1
13.9764	0.04021	0.19	1.6	0.51	4.8
12.9943	0.04021	0.19	1.6	0.38	4.7
11.9688	0.04021	0.21	1.6	0.29	4.6
10.9936	0.04020	0.21	1.6	0.22	4.5
9.9930	0.04020	0.23	1.6	0.15	4.5
8.9994	0.04020	0.21	1.6	0.11	4.4
7.9948	0.04020	0.22	1.6	0.075	4.4
6.9686	0.04020	0.22	1.6	0.058	4.4
5.9954	0.04020	0.28	1.6	0.036	4.4
4.9748	0.04020	0.23	1.6	0.027	4.4
3.9934	0.04020	0.24	1.6	0.018	4.3
2.9904	0.04020	0.24	1.6	0.011	4.3
1.9806	0.04019	0.25	1.6	0.0085	4.3
0.9905	0.04019	0.30	1.6	0.0023	4.4
0.1179	0.04019	5.8	1.6	0.0015	8.6

B5

Frequency measurements, frequency corrections and radius measurements and uncertainties at 350K

Table B5.1 *Pressure, north and south hemisphere and average temperature, frequency of resonance, half-width of the resonance peak and frequency measurement uncertainty using argon to calibrate internal radius at T = 350 K.*

Mode	p/MPa	T_N/K	T_S/K	T_{ave}/K	*f*/Hz	*g*/Hz	u(*f*)/Hz
0.2	19.9836	350.0273	350.0333	350.0303	7021.0686	0.49269	0.15
0.3	19.9834	350.0270	350.0331	350.0301	12070.1675	0.87821	0.19
0.4	19.9833	350.0267	350.0328	350.0298	17034.5269	1.24305	0.38
0.5	19.9831	350.0267	350.0328	350.0298	21965.2325	1.95165	1.5
0.2	18.9814	350.0150	350.0161	350.0156	6962.5110	0.46386	0.33
0.3	18.9814	350.0154	350.0170	350.0162	11969.6368	0.62337	0.32
0.4	18.9814	350.0154	350.0170	350.0162	16892.9019	1.08659	1.3
0.5	18.9813	350.0188	350.0196	350.0192	21781.7957	2.82005	5.2
0.2	17.9855	350.0239	350.0279	350.0259	6906.1270	0.40886	0.074
0.3	17.9852	350.0239	350.0279	350.0259	11872.7297	0.64227	0.12
0.4	17.9851	350.0249	350.0284	350.0267	16756.5766	1.01862	0.48
0.5	17.9850	350.0242	350.0287	350.0265	21607.4276	1.39914	1.2
0.2	16.9865	350.0040	350.0088	350.0064	6850.8646	0.38488	0.15
0.3	16.9864	350.0038	350.0090	350.0064	11777.8591	0.68216	0.16
0.4	16.9863	350.0047	350.0095	350.0071	16623.0629	1.81488	1.3
0.5	16.9863	350.0056	350.0098	350.0077	21436.4374	1.35768	0.39
0.2	15.9862	350.0261	350.0309	350.0285	6797.5544	0.38914	0.090
0.3	15.9863	350.0261	350.0309	350.0285	11686.2873	1.01795	0.41
0.4	15.9864	350.0266	350.0307	350.0287	16493.2693	2.55807	3.6
0.5	15.9864	350.0266	350.0307	350.0287	21270.7731	1.18554	0.44
0.2	14.9872	350.0147	350.0196	350.0172	6745.7499	0.37775	0.073
0.3	14.9871	350.0148	350.0198	350.0173	11596.8861	0.80038	0.30
0.4	14.9870	350.0150	350.0200	350.0175	16367.0477	1.07001	0.93
0.5	14.9870	350.0151	350.0202	350.0177	21109.7884	1.06826	0.37
0.2	13.9898	350.0228	350.0279	350.0254	6695.9892	0.38387	0.065
0.3	13.9898	350.0280	350.0292	350.0286	11511.2635	0.66175	0.27
0.4	13.9897	350.0269	350.0300	350.0285	16246.7345	0.87095	0.15
0.5	13.9896	350.0262	350.0304	350.0283	20955.2605	1.14583	0.22

Mode	p/MPa	T_N/K	T_S/K	T_{ave}/K	*f*/Hz	*g*/Hz	u(*f*)/Hz
0.2	12.9860	350.0087	350.1300	350.0694	6647.4580	0.39948	0.040
0.3	12.9860	350.0090	350.0137	350.0114	11427.9527	0.57662	0.36
0.4	12.9859	350.0093	350.0137	350.0115	16129.3697	0.76122	0.14
0.5	12.9859	350.0093	350.0137	350.0115	20803.9313	1.35845	0.34
0.2	11.9910	350.0340	350.0408	350.0374	6601.6608	0.39889	0.049
0.3	11.9908	350.0346	350.0410	350.0378	11349.1983	0.55744	0.32
0.4	11.9906	350.0344	350.0411	350.0378	16018.3204	0.72108	0.19
0.5	11.9905	350.0340	350.0410	350.0375	20661.0575	1.41129	0.71
0.2	10.9862	350.0262	350.0272	350.0267	6556.8993	0.41680	0.21
0.3	10.9861	350.0262	350.0272	350.0267	11272.3638	0.54436	0.25
0.4	10.9860	350.0304	350.0294	350.0299	15910.0535	0.67124	0.14
0.5	10.9860	350.0287	350.0304	350.0296	20521.3799	1.40383	0.47
0.2	9.9895	350.0146	350.0193	350.0170	6514.4554	0.40495	0.068
0.3	9.9893	350.0206	350.0211	350.0209	11199.4246	0.54650	0.17
0.4	9.9893	350.0198	350.0220	350.0209	15807.2424	0.66743	0.20
0.5	9.9892	350.0190	350.0224	350.0207	20389.1281	1.18981	3.53
0.2	8.9915	350.0042	350.0081	350.0062	6473.7271	0.39633	0.035
0.3	8.9915	350.0045	350.0083	350.0064	11129.5745	0.53953	0.13
0.4	8.9914	350.0047	350.0085	350.0066	15708.8000	0.67920	0.10
0.5	8.9914	350.0047	350.0085	350.0066	20262.5043	1.10125	0.21
0.2	7.9853	350.0140	350.0179	350.0160	6434.9547	0.38908	0.048
0.3	7.9853	350.0140	350.0180	350.0160	11062.9741	0.54322	0.19
0.4	7.9853	350.0140	350.0180	350.0160	15614.8823	0.66941	0.11
0.5	7.9853	350.0140	350.0180	350.0160	20141.6060	1.08754	0.14
0.2	6.9884	350.0065	350.0102	350.0084	6398.3549	0.40426	0.069
0.3	6.9884	350.0065	350.0102	350.0084	11000.0670	0.55612	0.14
0.4	6.9884	350.0068	350.0104	350.0086	15526.2203	0.67966	0.17
0.5	6.9884	350.0071	350.0107	350.0089	20027.4693	1.03314	0.17
0.2	5.9890	350.0143	350.0189	350.0166	6363.7460	0.41091	0.045
0.3	5.9889	350.0143	350.0189	350.0166	10940.6324	0.57118	0.12
0.4	5.9889	350.0143	350.0189	350.0166	15442.4132	0.70232	0.19
0.5	5.9889	350.0143	350.0189	350.0166	19919.5986	1.02163	0.18
0.2	4.9983	350.0114	350.0152	350.0133	6331.3000	0.42883	0.11
0.3	4.9983	350.0115	350.0153	350.0134	10884.8933	0.59726	0.099
0.4	4.9983	350.0116	350.0153	350.0135	15363.8231	0.73198	0.22
0.5	4.9983	350.0117	350.0155	350.0136	19818.4243	1.06317	0.20
0.2	3.9907	349.9989	350.0004	349.9997	6300.1819	0.44612	0.096
0.3	3.9907	349.9992	350.0008	350.0000	10831.3972	0.62094	0.098
0.4	3.9907	349.9994	350.0012	350.0003	15288.4185	0.76561	0.16
0.5	3.9907	349.9997	350.0015	350.0006	19721.3434	1.06219	0.15

Mode	p/MPa	T_N/K	T_S/K	T_{ave}/K	f/Hz	g/Hz	u(f)/Hz
0.2	2.9937	350.0104	350.0144	350.0124	6271.5512	0.48541	0.10
0.3	2.9937	350.0104	350.0144	350.0124	10782.2144	0.66202	0.11
0.4	2.9937	350.0104	350.0144	350.0124	15219.0588	0.83116	0.12
0.5	2.9937	350.0104	350.0144	350.0124	19632.0479	1.18686	0.092
0.2	2.0065	350.0264	350.0276	350.0270	6245.0391	0.55555	0.24
0.3	2.0065	350.0264	350.0276	350.0270	10736.6921	0.74101	0.12
0.4	2.0065	350.0265	350.0277	350.0271	15154.8613	0.94058	0.12
0.5	2.0066	350.0266	350.0278	350.0272	19549.3342	1.27766	0.18
0.2	0.9989	350.0132	350.0164	350.0148	6219.6002	0.75938	0.28
0.3	0.9989	350.0136	350.0168	350.0152	10693.1024	0.97835	0.50
0.4	0.9989	350.0140	350.0172	350.0156	15093.4291	1.19997	0.20
0.5	0.9989	350.0143	350.0176	350.0160	19470.2395	1.62426	0.69
0.2	0.1203	350.0312	350.0352	350.0332	6198.1880	1.90178	1.5
0.3	0.1203	350.0315	350.0354	350.0335	10656.7853	2.78726	5.0
0.4	0.1203	350.0315	350.0357	350.0336	15042.6152	3.30341	4.7
0.5	0.1203	350.0314	350.0358	350.0336	19405.1079	4.11196	5.6

Table B5.2 *Parameters required for computing frequency corrections, thermal boundary layer length, viscous boundary layer length accommodation length and thermal boundary layer in sell side length at T = 350 K.*

Mode	p/MPa	$10^6 \cdot \delta_{TH}$/m	$10^6 \cdot \delta_V$/m	$10^{11} \cdot l_{TH}$/m	$10^6 \cdot \delta_{TH,316L}$/m
0.2	19.9836	2.6398	2.2847	7.6870	13.5368
0.3	19.9834	2.0134	1.7425	7.6871	10.3243
0.4	19.9833	1.6948	1.4668	7.6871	8.6907
0.5	19.9831	1.4925	1.2917	7.6872	7.6533
0.2	18.9814	2.7056	2.3364	7.9764	13.5936
0.3	18.9814	2.0635	1.7819	7.9765	10.3676
0.4	18.9814	1.7370	1.5000	7.9765	8.7270
0.5	18.9813	1.5297	1.3210	7.9765	7.6855
0.2	17.9855	2.7771	2.3925	8.2970	13.6490
0.3	17.9852	2.1180	1.8247	8.2971	10.4098
0.4	17.9851	1.7829	1.5360	8.2972	8.7625
0.5	17.9850	1.5700	1.3526	8.2972	7.7164
0.2	16.9865	2.8554	2.4540	8.6565	13.7040
0.3	16.9864	2.1777	1.8716	8.6565	10.4517
0.4	16.9863	1.8331	1.5754	8.6566	8.7976
0.5	16.9863	1.6142	1.3873	8.6566	7.7472

Mode	p/MPa	$10^6 \cdot \delta_{TH}$/m	$10^6 \cdot \delta_V$/m	$10^{11} \cdot l_{TH}$/m	$10^6 \cdot \delta_{TH,316L}$/m
0.2	15.9862	2.9419	2.5219	9.0635	13.7576
0.3	15.9863	2.2437	1.9234	9.0635	10.4925
0.4	15.9864	1.8887	1.6190	9.0635	8.8321
0.5	15.9864	1.6631	1.4256	9.0635	7.7773
0.2	14.9872	3.0373	2.5968	9.5250	13.8103
0.3	14.9871	2.3165	1.9805	9.5250	10.5329
0.4	14.9870	1.9499	1.6671	9.5251	8.8661
0.5	14.9870	1.7170	1.4679	9.5251	7.8069
0.2	13.9898	3.1434	2.6801	10.0539	13.8615
0.3	13.9898	2.3974	2.0441	10.0540	10.5720
0.4	13.9897	2.0180	1.7206	10.0540	8.8989
0.5	13.9896	1.7769	1.5150	10.0541	7.8356
0.2	12.9860	3.2633	2.7744	10.6719	13.9120
0.3	12.9860	2.4885	2.1157	10.6701	10.6105
0.4	12.9859	2.0946	1.7809	10.6702	8.9312
0.5	12.9859	1.8444	1.5681	10.6702	7.8640
0.2	11.9910	3.3967	2.8795	11.3873	13.9602
0.3	11.9908	2.5906	2.1962	11.3874	10.6472
0.4	11.9906	2.1806	1.8486	11.3876	8.9621
0.5	11.9905	1.9201	1.6277	11.3876	7.8912
0.2	10.9862	3.5505	3.0009	12.2459	14.0078
0.3	10.9861	2.7079	2.2887	12.2460	10.6834
0.4	10.9860	2.2794	1.9265	12.2462	8.9925
0.5	10.9860	2.0070	1.6963	12.2463	7.9180
0.2	9.9895	3.7264	3.1399	13.2734	14.0533
0.3	9.9893	2.8421	2.3948	13.2737	10.7182
0.4	9.9893	2.3923	2.0157	13.2739	9.0217
0.5	9.9892	2.1064	1.7749	13.2739	7.9436
0.2	8.9915	3.9319	3.3027	14.5365	14.0975
0.3	8.9915	2.9988	2.5189	14.5365	10.7518
0.4	8.9914	2.5241	2.1202	14.5366	9.0500
0.5	8.9914	2.2225	1.8668	14.5366	7.9684
0.2	7.9853	4.1780	3.4981	16.1381	14.1399
0.3	7.9853	3.1864	2.6679	16.1382	10.7841
0.4	7.9853	2.6821	2.2456	16.1382	9.0771
0.5	7.9853	2.3615	1.9773	16.1382	7.9923
0.2	6.9884	4.4732	3.7332	18.1879	14.1803
0.3	6.9884	3.4116	2.8472	18.1880	10.8149
0.4	6.9884	2.8716	2.3965	18.1880	9.1030
0.5	6.9884	2.5284	2.1101	18.1880	8.0150

Mode	p/MPa	$10^6 \cdot \delta_{TH}$/m	$10^6 \cdot \delta_V$/m	$10^{11} \cdot l_{TH}$/m	$10^6 \cdot \delta_{TH,316L}$/m
0.2	5.9890	4.8414	4.0271	20.9406	14.2188
0.3	5.9889	3.6924	3.0713	20.9407	10.8442
0.4	5.9889	3.1079	2.5852	20.9407	9.1277
0.5	5.9889	2.7364	2.2762	20.9408	8.0367
0.2	4.9983	5.3110	4.4030	24.7687	14.2552
0.3	4.9983	4.0505	3.3580	24.7688	10.8719
0.4	4.9983	3.4094	2.8265	24.7688	9.1510
0.5	4.9983	3.0018	2.4886	24.7688	8.0572
0.2	3.9907	5.9585	4.9229	30.6290	14.2903
0.3	3.9907	4.5443	3.7545	30.6291	10.8987
0.4	3.9907	3.8250	3.1602	30.6292	9.1735
0.5	3.9907	3.3678	2.7825	30.6292	8.0770
0.2	2.9937	6.8988	5.6803	40.3407	14.3229
0.3	2.9937	5.2615	4.3322	40.3407	10.9236
0.4	2.9937	4.4286	3.6464	40.3409	9.1944
0.5	2.9937	3.8993	3.2105	40.3411	8.0954
0.2	2.0065	8.4526	6.9358	59.5040	14.3533
0.3	2.0065	6.4465	5.2897	59.5037	10.9467
0.4	2.0065	5.4260	4.4523	59.5035	9.2139
0.5	2.0066	4.7774	3.9201	59.5033	8.1125
0.2	0.9989	12.0202	9.8286	118.1898	14.3826
0.3	0.9989	9.1673	7.4958	118.1894	10.9690
0.4	0.9989	7.7161	6.3092	118.1899	9.2326
0.5	0.9989	6.7937	5.5550	118.1900	8.1289
0.2	0.1203	34.7586	28.3334	972.7330	14.4074
0.3	0.1203	26.5083	21.6081	972.7339	10.9877
0.4	0.1203	22.3120	18.1876	972.7587	9.2482
0.5	0.1203	19.6443	16.0130	972.7345	8.1426

Table B4.3 *Values of calculated thermal boundary layer, shell motion and holes and ducts frequency corrections; and thermal boundary layer, bulk viscosity and ducts and holes half width contributions to the resonance peaks at T = 325 K.*

Mode	p/MPa	Δf_{TH} /Hz	Δf_{Shell}/Hz	Δf_{hole}/Hz	g_{TH}/Hz	g_b/Hz	g_{hole}/Hz
0.2	19.9836	-0.23310	-0.15817	-9.5437E-03	0.23780	0.00031	0.30488
0.3	19.9834	-0.30562	-0.29461	-2.5530E-03	0.31177	0.00091	0.30156
0.4	19.9833	-0.36302	-0.48360	-8.8163E-04	0.37032	0.00182	0.30145
0.5	19.9831	-0.41206	-0.85631	-3.7626E-04	0.42035	0.00302	0.30118
0.2	18.9814	-0.23400	-0.15276	-8.9698E-03	0.23853	0.00032	0.30193
0.3	18.9814	-0.30679	-0.28412	-2.3324E-03	0.31273	0.00094	0.29900
0.4	18.9814	-0.36442	-0.46465	-7.9574E-04	0.37148	0.00187	0.29895
0.5	18.9813	-0.41364	-0.81267	-3.3806E-04	0.42166	0.00312	0.29870

Mode	p/MPa	Δf_{TH} /Hz	Δf_{Shell}/Hz	Δf_{hole}/Hz	g_{TH}/Hz	g_b/Hz	g_{hole}/Hz
0.2	17.9855	-0.23509	-0.14740	-8.3656E-03	0.23947	0.00033	0.29907
0.3	17.9852	-0.30822	-0.27373	-2.1078E-03	0.31397	0.00097	0.29655
0.4	17.9851	-0.36613	-0.44612	-7.0959E-04	0.37296	0.00194	0.29657
0.5	17.9850	-0.41560	-0.77176	-2.9951E-04	0.42335	0.00323	0.29632
0.2	16.9865	-0.23642	-0.14201	-7.7309E-03	0.24064	0.00034	0.29627
0.3	16.9864	-0.30997	-0.26335	-1.8809E-03	0.31551	0.00101	0.29417
0.4	16.9863	-0.36824	-0.42773	-6.2429E-04	0.37482	0.00202	0.29427
0.5	16.9863	-0.41800	-0.73241	-2.6148E-04	0.42548	0.00335	0.29404
0.2	15.9862	-0.23805	-0.13661	-7.0623E-03	0.24212	0.00036	0.29356
0.3	15.9863	-0.31212	-0.25297	-1.6523E-03	0.31746	0.00106	0.29189
0.4	15.9864	-0.37077	-0.40960	-5.4019E-04	0.37712	0.00210	0.29201
0.5	15.9864	-0.42091	-0.69478	-2.2402E-04	0.42812	0.00350	0.29180
0.2	14.9872	-0.24002	-0.13119	-6.3709E-03	0.24394	0.00037	0.29094
0.3	14.9871	-0.31468	-0.24263	-1.4275E-03	0.31983	0.00110	0.28962
0.4	14.9870	-0.37380	-0.39176	-4.5891E-04	0.37991	0.00220	0.28970
0.5	14.9870	-0.42443	-0.65850	-1.8787E-04	0.43138	0.00366	0.28963
0.2	13.9898	-0.24242	-0.12575	-5.6573E-03	0.24620	0.00039	0.28844
0.3	13.9898	-0.31783	-0.23228	-1.2083E-03	0.32278	0.00116	0.28747
0.4	13.9897	-0.37755	-0.37400	-3.8113E-04	0.38343	0.00231	0.28759
0.5	13.9896	-0.42872	-0.62351	-1.5326E-04	0.43541	0.00385	0.28756
0.2	12.9860	-0.24536	-0.12023	-4.9213E-03	0.24898	0.00042	0.28599
0.3	12.9860	-0.32169	-0.22179	-9.9783E-04	0.32645	0.00123	0.28540
0.4	12.9859	-0.38214	-0.35615	-3.0779E-04	0.38780	0.00244	0.28554
0.5	12.9859	-0.43395	-0.58922	-1.2062E-04	0.44037	0.00407	0.28552
0.2	11.9910	-0.24895	-0.11466	-4.1924E-03	0.25244	0.00044	0.28380
0.3	11.9908	-0.32639	-0.21131	-8.0135E-04	0.33096	0.00130	0.28346
0.4	11.9906	-0.38774	-0.33848	-2.4039E-04	0.39317	0.00260	0.28360
0.5	11.9905	-0.44031	-0.55610	-9.0513E-05	0.44649	0.00432	0.28360
0.2	10.9862	-0.25338	-0.10895	-3.4619E-03	0.25673	0.00047	0.28166
0.3	10.9861	-0.33220	-0.20058	-6.2045E-04	0.33659	0.00140	0.28158
0.4	10.9860	-0.39465	-0.32053	-1.7903E-04	0.39986	0.00278	0.28171
0.5	10.9860	-0.44816	-0.52319	-6.3238E-05	0.45408	0.00463	0.28171
0.2	9.9895	-0.25882	-0.10317	-2.7607E-03	0.26203	0.00051	0.27969
0.3	9.9893	-0.33933	-0.18975	-4.6063E-04	0.34354	0.00151	0.27980
0.4	9.9893	-0.40312	-0.30255	-1.2526E-04	0.40812	0.00301	0.27993
0.5	9.9892	-0.45779	-0.49089	-3.9687E-05	0.46348	0.00500	0.27992
0.2	8.9915	-0.26559	-0.09723	-2.1017E-03	0.26867	0.00056	0.27785
0.3	8.9915	-0.34822	-0.17865	-3.2266E-04	0.35226	0.00165	0.27810
0.4	8.9914	-0.41369	-0.28425	-7.9250E-05	0.41848	0.00328	0.27822
0.5	8.9914	-0.46980	-0.45866	-2.0417E-05	0.47525	0.00546	0.27821

Mode	p/MPa	Δf_{TH} /Hz	Δf_{Shell}/Hz	Δf_{hole}/Hz	g_{TH}/Hz	g_b/Hz	g_{hole}/Hz
0.2	7.9853	-0.27424	-0.09104	-1.5021E-03	0.27719	0.00062	0.27618
0.3	7.9853	-0.35956	-0.16712	-2.0692E-04	0.36343	0.00182	0.27649
0.4	7.9853	-0.42716	-0.26540	-4.1573E-05	0.43176	0.00363	0.27659
0.5	7.9853	-0.48511	-0.42604	-6.1467E-06	0.49033	0.00604	0.27659
0.2	6.9884	-0.28523	-0.08465	-9.9521E-04	0.28805	0.00069	0.27467
0.3	6.9884	-0.37397	-0.15526	-1.1607E-04	0.37767	0.00205	0.27498
0.4	6.9884	-0.44428	-0.24611	-1.4126E-05	0.44868	0.00408	0.27506
0.5	6.9884	-0.50455	-0.39322	2.1948E-06	0.50956	0.00679	0.27506
0.2	5.9890	-0.29968	-0.07791	-5.9006E-04	0.30238	0.00080	0.27328
0.3	5.9889	-0.39292	-0.14279	-4.8691E-05	0.39646	0.00235	0.27355
0.4	5.9889	-0.46680	-0.22595	2.3476E-06	0.47101	0.00468	0.27362
0.5	5.9889	-0.53014	-0.35944	4.8746E-06	0.53493	0.00779	0.27361
0.2	4.9983	-0.31906	-0.07079	-2.9731E-04	0.32164	0.00094	0.27201
0.3	4.9983	-0.41833	-0.12963	-6.2710E-06	0.42172	0.00277	0.27222
0.4	4.9983	-0.49698	-0.20482	7.5698E-06	0.50102	0.00552	0.27226
0.5	4.9983	-0.56443	-0.32453	3.4622E-06	0.56902	0.00919	0.27225
0.2	3.9907	-0.34704	-0.06292	-1.0403E-04	0.34952	0.00116	0.27080
0.3	3.9907	-0.45502	-0.11514	1.0853E-05	0.45827	0.00342	0.27093
0.4	3.9907	-0.54058	-0.18165	4.6802E-06	0.54445	0.00681	0.27095
0.5	3.9907	-0.61395	-0.28675	9.9291E-07	0.61835	0.01133	0.27093
0.2	2.9937	-0.38952	-0.05423	-4.2848E-06	0.39189	0.00152	0.26968
0.3	2.9937	-0.51071	-0.09918	6.8597E-06	0.51383	0.00449	0.26974
0.4	2.9937	-0.60675	-0.15625	7.1510E-07	0.61046	0.00894	0.26974
0.5	2.9937	-0.68911	-0.24583	1.2555E-08	0.69333	0.01488	0.26973
0.2	2.0065	-0.46259	-0.04420	1.2305E-05	0.46487	0.00223	0.26862
0.3	2.0065	-0.60652	-0.08079	3.0669E-07	0.60952	0.00660	0.26861
0.4	2.0065	-0.72058	-0.12712	-2.7925E-08	0.72415	0.01316	0.26861
0.5	2.0066	-0.81838	-0.19938	-3.4662E-09	0.82246	0.02189	0.26860
0.2	0.9989	-0.63702	-0.03105	-6.2476E-08	0.63923	0.00443	0.26756
0.3	0.9989	-0.83522	-0.05672	-1.2555E-09	0.83814	0.01308	0.26754
0.4	0.9989	-0.99228	-0.08915	2.5083E-11	0.99577	0.02606	0.26754
0.5	0.9989	-1.12698	-0.13943	2.8109E-12	1.13097	0.04337	0.26754
0.2	0.1203	-1.79079	-0.01073	-6.2115E-19	1.79335	0.03633	0.26669
0.3	0.1203	-2.34797	-0.01960	0.0000E+00	2.35153	0.10740	0.26670
0.4	0.1203	-2.78944	-0.03077	0.0000E+00	2.79387	0.21399	0.26670
0.5	0.1203	-3.16800	-0.04802	0.0000E+00	3.17322	0.35610	0.26670

Table B5.4 *Uncertainty contributions and result of radius calibration at T = 350 K*

p/MPa	a/m	$10^{12}\cdot\sum_{i=1}^{4}\left(\frac{\partial a}{\partial f_i}\right)^2 u^2(f_i)\Big/m^2$	$10^{11}\cdot\left(\frac{\partial a}{\partial u}\right)^2 u^2(u)\Big/m^2$	$10^{12}\cdot u_{disp}^2(a)/m^2$	$10^6\cdot u(a)/m$
19.9833	0.040235	1.1	1.6	30	6.9
18.9814	0.040234	8.3	1.6	33	7.6
17.9852	0.040231	0.66	1.6	23	6.3
16.9864	0.040229	1.4	1.6	17	5.9
15.9863	0.040228	7.2	1.6	17	6.4
14.9871	0.040227	0.65	1.6	9.1	5.1
13.9897	0.040225	0.20	1.6	6.2	4.8
12.9859	0.040225	0.29	1.6	3.3	4.4
11.9907	0.040223	0.40	1.6	4.1	4.6
10.9861	0.040222	0.38	1.6	3.7	4.5
9.9893	0.040220	3.5	1.6	2.8	4.7
8.9914	0.040220	0.13	1.6	1.7	4.2
7.9853	0.040218	0.15	1.6	1.3	4.2
6.9884	0.040217	0.14	1.6	0.91	4.2
5.9890	0.040216	0.13	1.6	0.58	4.1
4.9983	0.040215	0.17	1.6	0.38	4.1
3.9907	0.040214	0.15	1.6	0.25	4.1
2.9937	0.040213	0.16	1.6	0.14	4.1
2.0065	0.040212	0.31	1.6	0.099	4.1
0.9989	0.040211	0.71	1.6	0.029	4.1
0.1203	0.040211	51	1.6	0.0078	8.1

Appendix C

MEASUREMENTS, CORRECTIONS AND UNCERTAINTIES FOR X_{CO}=0.05 and X_{N_2}=0.95 MIXTURE

C1

Measurements, corrections and uncertainties X_{CO}=0.05 and X_{N_2}=0.95 mixture at T=273.16K.

Table C1.1 *Pressure, north and south hemisphere and average temperature, frequency of resonance, half-width of the resonance peak and frequency measured uncertainty in 0.05%CO-0.95%N_2 Mixture at T = 273 K.*

Mode	p/MPa	T_N/K	T_S/K	T_{ave}/K	*f*/Hz	*g*/Hz	u(*f*)/Hz
0.2	9.9926	273.2372	273.2355	273.2364	6444.6424	0.38245	0.20
0.3	9.9926	273.2369	273.2349	273.2359	11079.5685	0.40875	0.035
0.4	9.9926	273.2369	273.2349	273.2359	15638.0182	0.57662	0.10
0.5	9.9926	273.2366	273.2344	273.2355	20171.5501	0.77629	0.29
0.2	9.0096	273.2384	273.2309	273.2347	6377.0466	0.35244	0.024
0.3	9.0097	273.2385	273.2309	273.2347	10963.3704	0.41246	0.044
0.4	9.0097	273.2385	273.2309	273.2347	15474.1311	0.57762	0.072
0.5	9.0097	273.2385	273.2310	273.2348	19960.4402	0.75138	0.15
0.2	7.9948	273.0435	273.0375	273.0405	6310.2155	0.34501	0.024
0.3	7.9949	273.0436	273.0376	273.0406	10848.5053	0.40945	0.16
0.4	7.9949	273.0436	273.0377	273.0407	15312.0943	0.55919	0.14
0.5	7.9948	273.0436	273.0377	273.0407	19751.6651	0.74513	0.057
0.2	6.9984	273.0494	273.0434	273.0464	6252.2533	0.31337	0.076
0.3	6.9983	273.0494	273.0435	273.0465	10749.1434	0.40387	0.22
0.4	6.9984	273.0494	273.0436	273.0465	15171.9779	0.56847	0.17
0.5	6.9984	273.0494	273.0436	273.0465	19571.0796	0.75615	0.13
0.2	5.9968	273.0480	273.0422	273.0451	6199.6599	0.31469	0.010
0.3	5.9969	273.0480	273.0423	273.0452	10658.5236	0.40008	0.37
0.4	5.9968	273.0480	273.0423	273.0452	15044.0876	0.58472	0.32
0.5	5.9968	273.0480	273.0423	273.0452	19406.2582	0.72072	0.14
0.2	5.0000	273.0450	273.0389	273.0420	6152.6432	0.31185	0.012
0.3	5.0001	273.0454	273.0393	273.0424	10577.7552	0.42078	0.15
0.4	5.0000	273.0459	273.0397	273.0428	14930.1133	0.60393	0.30
0.5	5.0000	273.0459	273.0397	273.0428	19259.4090	0.73792	0.14
0.2	3.9893	273.0525	273.0480	273.0503	6110.6380	0.31019	0.011
0.3	3.9894	273.0526	273.0480	273.0503	10505.5091	0.51266	0.54
0.4	3.9894	273.0526	273.0481	273.0504	14828.2759	0.63444	0.51
0.5	3.9895	273.0527	273.0481	273.0504	19128.1402	0.73819	0.084

Mode	p/MPa	T_N/K	T_S/K	T_{ave}/K	*f*/Hz	*g*/Hz	u(*f*)/Hz
0.2	2.9968	273.0505	273.0448	273.0477	6074.6722	0.31701	0.013
0.3	2.9968	273.0506	273.0449	273.0478	10443.6887	0.40994	0.022
0.4	2.9968	273.0507	273.0451	273.0479	14741.0386	0.65591	0.13
0.5	2.9968	273.0507	273.0451	273.0479	19015.7443	0.78183	0.069
0.2	1.9920	273.1635	273.0517	273.1076	6043.7800	0.34336	0.0086
0.3	1.9919	273.1635	273.0517	273.1076	10390.6330	0.44788	0.017
0.4	1.9919	273.1636	273.0517	273.1077	14666.1678	0.74165	0.086
0.5	1.9919	273.1636	273.0518	273.1077	18919.2605	0.84068	0.089
0.2	0.9948	273.0484	273.0437	273.0461	6017.8393	0.42870	0.019
0.3	0.9948	273.0484	273.0437	273.0461	10346.1154	0.53725	0.021
0.4	0.9948	273.0485	273.0437	273.0461	14603.4075	0.87549	0.14
0.5	0.9948	273.0485	273.0437	273.0461	18838.2889	1.11272	0.53
0.2	0.0992	273.0566	273.0517	273.0542	5998.5116	1.05206	0.16
0.3	0.0992	273.0566	273.0517	273.0542	10313.2615	1.48497	0.37
0.4	0.0992	273.0566	273.0517	273.0542	14557.5305	2.00081	0.51
0.5	0.0992	273.0566	273.0517	273.0542	18779.1633	2.43069	0.28

Table C1.2*. Parameters required for computing frequency corrections, thermal boundary layer length, viscous boundary layer length accommodation length and thermal boundary layer in sell side length in the 0.05%CO-0.95%N_2 mixture at T = 273.16 K.*

Mode	p/MPa	$10^6 \cdot \delta_{TH}$(m)	$10^6 \cdot \delta_V$(m)	$10^{11} \cdot l_{TH}$(m)	$10^5 \cdot \delta_{TH,316L}$(m)
0.2	9.9926	3.08314	2.74303	6.24584	1.41293
0.3	9.9926	2.35142	2.09203	6.24583	1.07760
0.4	9.9926	1.97925	1.76091	6.24581	0.90704
0.5	9.9926	1.74270	1.55045	6.24583	0.79864
0.2	9.0096	3.24739	2.87737	6.78558	1.42039
0.3	9.0097	2.47669	2.19449	6.78556	1.08329
0.4	9.0097	2.08469	1.84715	6.78556	0.91183
0.5	9.0097	1.83552	1.62637	6.78557	0.80285
0.2	7.9948	3.44732	3.04158	7.48104	1.42790
0.3	7.9949	2.62916	2.31972	7.48102	1.08901
0.4	7.9949	2.21302	1.95256	7.48102	0.91665
0.5	7.9948	1.94851	1.71917	7.48105	0.80708
0.2	6.9984	3.68809	3.23979	8.37185	1.43450
0.3	6.9983	2.81276	2.47087	8.37187	1.09404
0.4	6.9984	2.36755	2.07977	8.37185	0.92087
0.5	6.9984	2.08454	1.83116	8.37177	0.81080
0.2	5.9968	3.98924	3.48884	9.57191	1.44057
0.3	5.9969	3.04246	2.66082	9.57190	1.09868
0.4	5.9968	2.56090	2.23966	9.57194	0.92477
0.5	5.9968	2.25479	1.97195	9.57204	0.81423

Mode	p/MPa	$10^6 \cdot \delta_{TH}$(m)	$10^6 \cdot \delta_V$(m)	$10^{11} \cdot l_{TH}$(m)	$10^5 \cdot \delta_{TH,316L}$(m)
0.2	5.0000	4.37605	3.81016	11.25324	1.44606
0.3	5.0001	3.33744	2.90586	11.25307	1.10286
0.4	5.0000	2.80919	2.44592	11.25322	0.92830
0.5	5.0000	2.47338	2.15354	11.25322	0.81733
0.2	3.9893	4.90962	4.25523	13.83141	1.45103
0.3	3.9894	3.74434	3.24527	13.83097	1.10665
0.4	3.9894	3.15165	2.73157	13.83094	0.93148
0.5	3.9895	2.77489	2.40503	13.83088	0.82013
0.2	2.9968	5.67940	4.89956	18.07972	1.45532
0.3	2.9968	4.33149	3.73673	18.07972	1.10992
0.4	2.9968	3.64586	3.14525	18.07974	0.93423
0.5	2.9968	3.21002	2.76925	18.07974	0.82255
0.2	1.9920	6.99129	6.00086	26.75200	1.45903
0.3	1.9919	5.33201	4.57664	26.75202	1.11275
0.4	1.9919	4.48801	3.85221	26.75203	0.93661
0.5	1.9919	3.95148	3.39169	26.75208	0.82464
0.2	0.9948	9.93453	8.47971	52.77509	1.46217
0.3	0.9948	7.57669	6.46716	52.77525	1.11514
0.4	0.9948	6.37736	5.44346	52.77521	0.93862
0.5	0.9948	5.61497	4.79271	52.77521	0.82641
0.2	0.0992	31.61392	26.82842	523.39041	1.46453
0.3	0.0992	24.11064	20.46093	523.40622	1.11692
0.4	0.0992	20.29377	17.22184	523.40622	0.94010
0.5	0.0992	17.86770	15.16301	523.40622	0.82771

Table C1.3 *Values of calculated thermal boundary layer, shell motion and holes and ducts frequency corrections; and thermal boundary layer, bulk viscosity and ducts and holes half-width contributions to the resonance peaks in the 0.05%CO-0.95%N_2 mixture at T = 273.16 K.*

Mode	p/MPa	Δf_{th} /Hz	Δfs_{hell} /Hz	Δf_{hole} /Hz	g_{th}/Hz	g_b/Hz	g_{hole}/Hz
0.2	9.9926	-0.1501	-0.1017	-0.5139	0.152941	0.000320	-0.060311
0.3	9.9926	-0.1968	-0.1868	-0.3012	0.200534	0.000945	-0.055960
0.4	9.9926	-0.2338	-0.2967	-0.1133	0.238241	0.001882	-0.037922
0.5	9.9926	-0.2655	-0.4766	-0.0167	0.270580	0.003132	-0.024990
0.2	9.0096	-0.1517	-0.0955	-0.5106	0.154397	0.000345	-0.061873
0.3	9.0097	-0.1989	-0.1751	-0.2996	0.202443	0.001020	-0.057145
0.4	9.0097	-0.2363	-0.2772	-0.1130	0.240510	0.002032	-0.038537
0.5	9.0097	-0.2684	-0.4415	-0.0170	0.273159	0.003382	-0.025291
0.2	7.9948	-0.1541	-0.0890	-0.5077	0.156623	0.000378	-0.063925
0.3	7.9949	-0.2021	-0.1629	-0.2984	0.205361	0.001118	-0.058739
0.4	7.9949	-0.2401	-0.2570	-0.1129	0.243978	0.002227	-0.039380
0.5	7.9948	-0.2726	-0.4060	-0.0174	0.277099	0.003705	-0.025713

Mode	p/MPa	Δf_{th} /Hz	Δfs_{hell} /Hz	Δf_{hole} /Hz	g_{th}/Hz	g_b/Hz	g_{hole}/Hz
0.2	6.9984	-0.1576	-0.0824	-0.5056	0.159909	0.000421	-0.066569
0.3	6.9983	-0.2066	-0.1507	-0.2980	0.209673	0.001244	-0.060874
0.4	6.9984	-0.2454	-0.2372	-0.1132	0.249101	0.002478	-0.040544
0.5	6.9984	-0.2787	-0.3721	-0.0180	0.282919	0.004124	-0.026304
0.2	5.9968	-0.1625	-0.0756	-0.5053	0.164750	0.000479	-0.070246
0.3	5.9969	-0.2131	-0.1381	-0.2983	0.216018	0.001415	-0.063769
0.4	5.9968	-0.2532	-0.2168	-0.1138	0.256640	0.002820	-0.042123
0.5	5.9968	-0.2876	-0.3382	-0.0186	0.291483	0.004693	-0.027118
0.2	5.0000	-0.1698	-0.0685	-0.5033	0.171889	0.000560	-0.074833
0.3	5.0001	-0.2227	-0.1249	-0.2983	0.225379	0.001657	-0.067471
0.4	5.0000	-0.2646	-0.1957	-0.1146	0.267762	0.003301	-0.044179
0.5	5.0000	-0.3005	-0.3038	-0.0196	0.304116	0.005493	-0.028203
0.2	3.9893	-0.1811	-0.0607	-0.5033	0.182998	0.000686	-0.074833
0.3	3.9894	-0.2374	-0.1107	-0.2983	0.239942	0.002028	-0.067471
0.4	3.9894	-0.2821	-0.1731	-0.1146	0.285065	0.004041	-0.044179
0.5	3.9895	-0.3204	-0.2675	-0.0196	0.323768	0.006724	-0.028203
0.2	2.9968	-0.1990	-0.0523	-0.5064	0.200771	0.000894	-0.082230
0.3	2.9968	-0.2609	-0.0953	-0.3011	0.263249	0.002641	-0.073459
0.4	2.9968	-0.3100	-0.1487	-0.1163	0.312755	0.005263	-0.047503
0.5	2.9968	-0.3521	-0.2290	-0.0206	0.355220	0.008758	-0.029948
0.2	1.9920	-0.2322	-0.0424	-0.5109	0.233905	0.001317	-0.093329
0.3	1.9919	-0.3045	-0.0772	-0.3044	0.306695	0.003894	-0.082331
0.4	1.9919	-0.3618	-0.1204	-0.1180	0.364371	0.007759	-0.052345
0.5	1.9919	-0.4109	-0.1848	-0.0213	0.413845	0.012911	-0.032415
0.2	0.9948	-0.3127	-0.0298	-0.5236	0.314270	0.002588	-0.114486
0.3	0.9948	-0.4100	-0.0543	-0.3142	0.412071	0.007649	-0.099707
0.4	0.9948	-0.4871	-0.0845	-0.1232	0.489565	0.015240	-0.062082
0.5	0.9948	-0.5533	-0.1294	-0.0237	0.556037	0.025362	-0.037561
0.2	0.0992	-0.9478	-0.0094	-0.5487	0.949369	0.025540	-0.167199
0.3	0.0992	-1.2427	-0.0171	-0.3312	1.244852	0.075507	-0.142900
0.4	0.0992	-1.4763	-0.0266	-0.1315	1.478984	0.150445	-0.086120
0.5	0.0992	-1.6767	-0.0406	-0.0266	1.679801	0.250361	-0.050112

Table C1.4 *Uncertainty contributions and result of speed of sound measurements in the 0.05%CO-0.95%N_2 mixture at T = 273.16 K.*

p/MPa	$u/m\cdot s^{-1}$	$10^3\cdot\left(\sum_{i=1}^{4}\frac{2\pi f_i}{4\upsilon_i}\right)^2 u^2(a)\Big/m^2\cdot s^{-2}$	$10^4\cdot\sum_{i=1}^{4}\left(\frac{2\pi a}{4\upsilon_i}\right)^2 u^2(f_i)\Big/m^2\cdot s^{-2}$	$10^4\cdot u_{disp}^2(u)/m^2\cdot s^{-2}$	$10^2\cdot u(u)/m\cdot s^{-1}$
9.99	361.9933	1.6	1.5	2.9	4.5
9.01	358.1892	1.5	1.1	2.3	4.2
7.99	354.4298	1.6	1.1	1.8	4.3
7.00	351.1751	1.4	1.1	1.1	4.0
6.00	348.2098	1.3	1.4	1.3	4.0
5.00	345.5656	1.3	1.1	1.0	3.9
3.99	343.2024	1.3	1.9	0.89	3.9
3.00	341.1797	1.3	0.80	0.81	3.9
1.99	339.4439	1.5	0.84	0.73	4.1
0.99	337.9906	2.4	1.2	0.67	5.1
0.10	336.9446	2.4	2.2	0.39	5.2

C2

Measurements, corrections and uncertainties for X_{CO}=0.05 and X_{N_2}=0.95 mixture at T=325K.

Table C2.1 *Pressure, north and south hemisphere and average temperature, frequency of resonance, half-width of the resonance peak and frequency measured uncertainty in 0.05%CO-0.95%N_2 Mixture at T = 325 K.*

Mode	p/MPa	T_N/K	T_S/K	T_{ave}/K	*f*/Hz	*g*/Hz	u(*f*)/K
0.2	10.0005	325.0623	325.0562	325.0593	7025.7219	0.70362	0.060
0.3	10.0006	325.0623	325.0562	325.0593	12078.7219	0.91211	0.18
0.4	10.0005	325.0626	325.0564	325.0595	17047.7289	1.30299	0.79
0.5	10.0006	325.0628	325.0565	325.0597	21987.8407	1.53297	0.44
0.2	9.0022	325.0480	325.0405	325.0443	6962.8904	0.63844	0.11
0.3	9.0021	325.0480	325.0405	325.0443	11970.5545	0.86718	0.12
0.4	9.0022	325.0489	325.0413	325.0451	16895.6466	1.17038	0.42
0.5	9.0022	325.0491	325.0415	325.0453	21792.3696	1.30289	0.26
0.2	7.9995	324.9942	324.9879	324.9911	6902.3727	0.62155	0.040
0.3	7.9996	324.9944	324.9880	324.9912	11866.5617	0.78778	0.089
0.4	7.9996	324.9944	324.9880	324.9912	16748.8605	1.22805	0.46
0.5	7.9996	324.9945	324.9881	324.9913	21603.6610	1.19292	0.14
0.2	7.0073	325.2259	325.2286	325.2273	6848.4395	0.62387	0.041
0.3	7.0073	325.2259	325.2286	325.2273	11773.8380	0.73349	0.19
0.4	7.0073	325.2260	325.2288	325.2274	16617.9071	1.16634	0.74
0.5	7.0073	325.2260	325.2288	325.2274	21435.5819	1.16133	0.51
0.2	5.9945	325.0289	325.0285	325.0287	6792.0054	0.62051	0.029
0.3	5.9945	325.0289	325.0285	325.0287	11676.9093	0.69651	0.062
0.4	5.9946	325.0292	325.0287	325.0290	16481.2099	0.97291	0.18
0.5	5.9946	325.0292	325.0287	325.0290	21259.6022	1.07907	0.094
0.2	4.9979	325.0141	325.0131	325.0136	6741.4942	0.58901	0.027
0.3	4.9979	325.0142	325.0132	325.0137	11590.1643	0.68096	0.053
0.4	4.9978	325.0142	325.0133	325.0138	16358.9039	0.91716	0.10
0.5	4.9979	325.0142	325.0133	325.0138	21102.0674	1.04138	0.16
0.2	3.9991	325.0265	325.0266	325.0266	6694.3895	0.53346	0.020
0.3	3.9991	325.0266	325.0267	325.0267	11509.2459	0.82537	0.070
0.4	3.9991	325.0266	325.0267	325.0267	16244.7695	0.94790	0.058
0.5	3.9991	325.0267	325.0268	325.0268	20955.1701	1.12499	0.082

Mode	p/MPa	T_N/K	T_S/K	T_{ave}/K	f/Hz	g/Hz	u(f)/K
0.2	3.0027	325.0125	325.0114	325.0120	6650.3353	0.49985	0.020
0.3	3.0027	325.0137	325.0126	325.0132	11433.4228	0.67781	0.11
0.4	3.0027	325.0129	325.0118	325.0124	16137.9891	0.98374	0.26
0.5	3.0027	325.0133	325.0122	325.0128	20817.5067	1.10281	0.079
0.2	1.9912	325.0045	325.0036	325.0041	6609.2690	0.49215	0.034
0.3	1.9912	325.0045	325.0035	325.0040	11362.8296	0.63446	0.10
0.4	1.9912	325.0044	325.0035	325.0040	16038.4345	0.95246	0.21
0.5	1.9912	325.0044	325.0035	325.0040	20689.2445	1.10956	0.23
0.2	1.0017	325.0028	325.0020	325.0024	6571.8701	0.55118	0.026
0.3	1.0017	325.0028	325.0019	325.0024	11298.6373	0.68976	0.071
0.4	1.0017	325.0028	325.0019	325.0024	15947.8609	1.15500	0.13
0.5	1.0017	325.0028	325.0019	325.0024	20572.5522	1.25898	0.51
0.2	0.0994	325.0066	325.0052	325.0059	6540.2083	1.30258	0.23
0.3	0.0994	325.0069	325.0054	325.0062	11244.6667	1.81005	0.37
0.4	0.0994	325.0070	325.0055	325.0063	15872.2507	2.45263	0.44
0.5	0.0994	325.0070	325.0055	325.0063	20475.1278	3.01733	0.44

Table C2.2*. Parameters required for computing frequency corrections, thermal boundary layer length, viscous boundary layer length accommodation length and thermal boundary layer in sell side length in the 0.05%CO-0.95%N_2 mixture at T = 325 K.*

Mode	p/MPa	$10^6 \cdot \delta_{TH}$/m	$10^6 \cdot \delta_V$/m	$10^{11} \cdot l_{TH}$/m	$10^6 \cdot \delta_{TH,316L}$/m
0.2	10.0005	3.51298	3.04393	7.44121	13.53235
0.3	10.0006	2.67923	2.32150	7.44116	10.32068
0.4	10.0005	2.25522	1.95410	7.44121	8.68731
0.5	10.0006	1.98577	1.72064	7.44119	7.64940
0.2	9.0022	3.69967	3.19897	8.14543	13.59327
0.3	9.0021	2.82164	2.43977	8.14547	10.36720
0.4	9.0022	2.37504	2.05361	8.14542	8.72632
0.5	9.0022	2.09125	1.80823	8.14542	7.68363
0.2	7.9995	3.92202	3.38400	9.03098	13.65273
0.3	7.9996	2.99120	2.58087	9.03093	10.41253
0.4	7.9996	2.51776	2.17238	9.03092	8.76448
0.5	7.9996	2.21689	1.91278	9.03091	7.71711
0.2	7.0073	4.19134	3.60834	10.17053	13.70638
0.3	7.0073	3.19661	2.75198	10.17051	10.45345
0.4	7.0073	2.69066	2.31641	10.17048	8.79894
0.5	7.0073	2.36908	2.03955	10.17045	7.74731
0.2	5.9945	4.52931	3.89078	11.70938	13.76321
0.3	5.9945	3.45436	2.96737	11.70938	10.49675
0.4	5.9946	2.90761	2.49770	11.70935	8.83536
0.5	5.9946	2.56008	2.19916	11.70937	7.77931

Mode	p/MPa	$10^6 \cdot \delta_{TH}$/m	$10^6 \cdot \delta_V$/m	$10^{11} \cdot l_{TH}$/m	$10^6 \cdot \delta_{TH,316L}$/m
0.2	4.9979	4.96143	4.25230	13.84914	13.81467
0.3	4.9979	3.78391	3.24308	13.84915	10.53595
0.4	4.9978	3.18500	2.72977	13.84920	8.86832
0.5	4.9979	2.80429	2.40347	13.84915	7.80829
0.2	3.9991	5.54998	4.74530	17.07688	13.86319
0.3	3.9991	4.23276	3.61905	17.07685	10.57293
0.4	3.9991	3.56281	3.04624	17.07705	8.89942
0.5	3.9991	3.13692	2.68210	17.07706	7.83561
0.2	3.0027	6.41153	5.46774	22.45443	13.90903
0.3	3.0027	4.88986	4.17007	22.45453	10.60793
0.4	3.0027	4.11583	3.50998	22.45432	8.92882
0.5	3.0027	3.62387	3.09043	22.45471	7.86148
0.2	1.9912	7.88623	6.70558	33.45950	13.95217
0.3	1.9912	6.01454	5.11410	33.45941	10.64083
0.4	1.9912	5.06251	4.30460	33.45962	8.95649
0.5	1.9912	4.45734	3.79003	33.45983	7.88581
0.2	1.0017	11.14549	9.44536	65.83233	13.99182
0.3	1.0017	8.50022	7.20360	65.83231	10.67101
0.4	1.0017	7.15471	6.06333	65.83225	8.98188
0.5	1.0017	6.29939	5.33848	65.83205	7.90814
0.2	0.0994	35.49031	29.96904	658.32914	14.02564
0.3	0.0994	27.06612	22.85541	658.30994	10.69659
0.4	0.0994	22.78161	19.23746	658.32345	9.00325
0.5	0.0994	20.05813	16.93767	658.32345	7.92693

Table C1.3 *Values of calculated thermal boundary layer, shell motion and holes and ducts frequency corrections; and thermal boundary layer, bulk viscosity and ducts and holes half-width contributions to the resonance peaks in the 0.05%CO-0.95%N_2 mixture at T = 273.16 K.*

Mode	p/PMa	Δf_{th}/Hz	Δf_{shell}/Hz	Δf_{hole}/Hz	g_{th}/Hz	g_b/Hz	g_{hole}/Hz
0.2	10.0005	-0.16157	-0.11183	-0.06008	0.16435	0.00041	0.24244
0.3	10.0006	-0.21184	-0.20830	-0.06057	0.21550	0.00123	0.24191
0.4	10.0005	-0.25167	-0.34192	-0.06049	0.25601	0.00244	0.24180
0.5	10.0006	-0.28582	-0.60564	-0.06046	0.29075	0.00406	0.24180
0.2	9.0022	-0.16505	-0.10507	-0.05973	0.16772	0.00045	0.24022
0.3	9.0021	-0.21641	-0.19539	-0.06002	0.21991	0.00133	0.23971
0.4	9.0022	-0.25710	-0.31948	-0.05994	0.26126	0.00266	0.23965
0.5	9.0022	-0.29199	-0.55859	-0.05992	0.29671	0.00442	0.23966

Mode	p/MPa	Δf_{th}/Hz	Δf_{shell}/Hz	Δf_{hole}/Hz	g_{th}/Hz	g_b/Hz	g_{hole}/Hz
0.2	7.9995	-0.16953	-0.09812	-0.05937	0.17208	0.00050	0.23805
0.3	7.9996	-0.22228	-0.18217	-0.05948	0.22562	0.00147	0.23760
0.4	7.9996	-0.26407	-0.29677	-0.05941	0.26805	0.00293	0.23758
0.5	7.9996	-0.29991	-0.51276	-0.05940	0.30443	0.00487	0.23759
0.2	7.0073	-0.17540	-0.09106	-0.05902	0.17784	0.00056	0.23607
0.3	7.0073	-0.22998	-0.16883	-0.05899	0.23318	0.00165	0.23574
0.4	7.0073	-0.27322	-0.27414	-0.05894	0.27702	0.00328	0.23575
0.5	7.0073	-0.31030	-0.46895	-0.05894	0.31463	0.00546	0.23576
0.2	5.9945	-0.18320	-0.08347	-0.05859	0.18552	0.00064	0.23399
0.3	5.9945	-0.24021	-0.15454	-0.05847	0.24326	0.00189	0.23380
0.4	5.9946	-0.28537	-0.25013	-0.05845	0.28900	0.00376	0.23382
0.5	5.9946	-0.32411	-0.42362	-0.05845	0.32823	0.00625	0.23382
0.2	4.9979	-0.19387	-0.07561	-0.05814	0.19608	0.00075	0.23214
0.3	4.9979	-0.25419	-0.13981	-0.05802	0.25711	0.00222	0.23208
0.4	4.9978	-0.30199	-0.22563	-0.05802	0.30545	0.00442	0.23209
0.5	4.9979	-0.34299	-0.37887	-0.05802	0.34692	0.00736	0.23209
0.2	3.9991	-0.20929	-0.06712	-0.05814	0.21140	0.00092	0.23214
0.3	3.9991	-0.27441	-0.12398	-0.05802	0.27719	0.00272	0.23208
0.4	3.9991	-0.32601	-0.19956	-0.05802	0.32931	0.00542	0.23209
0.5	3.9991	-0.37027	-0.33253	-0.05802	0.37402	0.00903	0.23209
0.2	3.0027	-0.23313	-0.05775	-0.05767	0.23514	0.00121	0.23046
0.3	3.0027	-0.30567	-0.10655	-0.05762	0.30832	0.00356	0.23048
0.4	3.0027	-0.36315	-0.17110	-0.05762	0.36630	0.00710	0.23048
0.5	3.0027	-0.41245	-0.28315	-0.05762	0.41603	0.01181	0.23048
0.2	1.9912	-0.27610	-0.04672	-0.05724	0.27802	0.00179	0.22895
0.3	1.9912	-0.36202	-0.08611	-0.05724	0.36454	0.00528	0.22897
0.4	1.9912	-0.43010	-0.13797	-0.05724	0.43310	0.01052	0.22897
0.5	1.9912	-0.48849	-0.22690	-0.05724	0.49190	0.01751	0.22897
0.2	1.0017	-0.37573	-0.03293	-0.05689	0.37757	0.00350	0.22756
0.3	1.0017	-0.49265	-0.06065	-0.05689	0.49507	0.01034	0.22756
0.4	1.0017	-0.58529	-0.09698	-0.05689	0.58817	0.02059	0.22756
0.5	1.0017	-0.66475	-0.15862	-0.05689	0.66803	0.03427	0.22756
0.2	0.0994	-1.15563	-0.01032	-0.05657	1.15758	0.03477	0.22629
0.3	0.0994	-1.51518	-0.01899	-0.05657	1.51783	0.10278	0.22629
0.4	0.0994	-1.80009	-0.03032	-0.05657	1.80332	0.20478	0.22629
0.5	0.0994	-2.04443	-0.04937	-0.05657	2.04818	0.34078	0.22629

Table C1.4 *Uncertainty contributions and result of speed of sound measurements in the 0.05%CO-0.95%N_2 mixture at T = 273.16 K.*

p/MPa	$u/m\cdot s^{-1}$	$10^3\cdot\left(\sum_{i=1}^{4}\frac{2\pi f_i}{4\upsilon_i}\right)^2 u^2(a)\Big/m^2\cdot s^{-2}$	$10^4\cdot\sum_{i=1}^{4}\left(\frac{2\pi a}{4\upsilon_i}\right)^2 u^2(f_i)\Big/m^2\cdot s^{-2}$	$10^4\cdot u^2_{disp}(u)/m^2\cdot s^{-2}$	$10^2\cdot u(u)/m\cdot s^{-1}$
10.0006	394.9350	1.8	3.9	5.2	5.2
9.0022	391.3979	1.7	2.3	3.0	4.7
7.9996	387.9894	1.7	1.9	2.1	4.5
7.0073	384.9489	1.6	2.2	1.4	4.4
5.9946	381.7733	1.6	0.96	0.85	4.2
4.9979	378.9301	1.5	0.69	0.51	4.1
3.9991	376.2780	1.5	0.72	0.27	4.0
3.0027	373.7956	1.5	0.45	0.17	3.9
1.9912	371.4830	1.5	0.29	0.11	3.9
1.0017	369.3810	1.5	0.39	0.067	3.9
0.0994	367.6451	6.1	1.5	0.0062	7.9

Appendix D

MEASUREMENTS, CORRECTIONS, AND UNCERTAINTIES FOR X_{CO}=0.10 and X_{N_2}=0.90 MIXTURE

D1

Measurements, corrections and uncertainties for X_{CO}=0.10 and X_{N_2}=0.90 mixture at T=273.16K.

Table D1.1 *Pressure, north and south hemisphere and average temperature, frequency of resonance, half-width of the resonance peak and frequency measured uncertainty in 0.10%CO-0.90%N_2 Mixture at T = 273 K.*

Mode	p/MPa	T_N/K	T_S/K	T_{ave}/K	*f*/Hz	*g*/Hz	u(*f*)/K
0.2	9.9546	273.2043	273.2038	273.2041	6440.9985	0.41953	0.031
0.3	9.9546	273.2048	273.2048	273.2048	11073.3739	0.51151	0.028
0.4	9.9546	273.2048	273.2048	273.2048	15629.2903	0.70232	0.085
0.5	9.9546	273.2054	273.2058	273.2056	20160.4618	0.89685	0.12
0.2	8.9700	273.1740	273.1806	273.1773	6372.9555	0.41462	0.025
0.3	8.9700	273.1742	273.1808	273.1775	10956.4186	0.51729	0.024
0.4	8.9700	273.1744	273.1809	273.1777	15464.2975	0.68238	0.071
0.5	8.9700	273.1744	273.1809	273.1777	19947.8557	0.86460	0.094
0.2	8.0190	273.1715	273.1786	273.1751	6312.5021	0.40085	0.032
0.3	8.0189	273.1716	273.1787	273.1752	10852.5212	0.50219	0.035
0.4	8.0189	273.1716	273.1787	273.1752	15317.7580	0.66814	0.051
0.5	8.0189	273.1717	273.1787	273.1752	19759.0389	0.82092	0.052
0.2	6.9945	273.1709	273.1798	273.1754	6252.9097	0.37070	0.019
0.3	6.9945	273.1706	273.1794	273.1750	10750.1092	0.48243	0.047
0.4	6.9944	273.1706	273.1794	273.1750	15173.2561	0.66439	0.039
0.5	6.9944	273.1703	273.1791	273.1747	19572.7808	0.81487	0.051
0.2	6.0005	273.1688	273.1752	273.1720	6200.5731	0.35935	0.034
0.3	6.0005	273.1688	273.1752	273.1720	10660.1518	0.50452	0.063
0.4	6.0005	273.1689	273.1754	273.1722	15046.3487	0.66337	0.035
0.5	6.0005	273.1689	273.1754	273.1722	19409.2369	0.78619	0.042
0.2	4.9890	273.1688	273.1749	273.1719	6152.9688	0.35367	0.033
0.3	4.9891	273.1690	273.1751	273.1721	10578.2732	0.50960	0.071
0.4	4.9891	273.1692	273.1753	273.1723	14930.9199	0.65925	0.18
0.5	4.9891	273.1692	273.1753	273.1723	19260.4729	0.78203	0.17
0.2	3.9972	273.1722	273.1800	273.1761	6111.7710	0.35028	0.042
0.3	3.9972	273.1719	273.1797	273.1758	10507.4495	0.46587	0.030
0.4	3.9972	273.1719	273.1797	273.1758	14831.0165	0.68526	0.11
0.5	3.9972	273.1718	273.1797	273.1758	19131.7092	0.76761	0.098

Mode	p/MPa	T_N/K	T_S/K	T_{ave}/K	f/Hz	g/Hz	u(f)/K
0.2	2.9930	273.1699	273.1766	273.1733	6075.3490	0.34997	0.037
0.3	2.9930	273.1699	273.1766	273.1733	10444.8745	0.45370	0.016
0.4	2.9931	273.1703	273.1769	273.1736	14742.7294	0.74444	0.053
0.5	2.9931	273.1704	273.1770	273.1737	19017.9416	0.79928	0.037
0.2	1.9934	273.1635	273.1702	273.1669	6044.3350	0.37170	0.039
0.3	1.9933	273.1635	273.1702	273.1669	10391.5932	0.46942	0.074
0.4	1.9932	273.1636	273.1702	273.1669	14667.5068	0.81308	0.094
0.5	1.9932	273.1636	273.1702	273.1669	18921.0635	0.90105	0.11
0.2	0.9957	273.1561	273.1622	273.1592	6018.7010	0.44665	0.025
0.3	0.9957	273.1561	273.1622	273.1592	10347.6048	0.55411	0.031
0.4	0.9957	273.1562	273.1623	273.1593	14605.5068	0.91278	0.12
0.5	0.9954	273.1562	273.1624	273.1593	18841.0066	1.11441	0.53

***Table D1.2**. Parameters required for computing frequency corrections, thermal boundary layer length, viscous boundary layer length accommodation length and thermal boundary layer in sell side length in the 0.10%CO-0.90%N_2 mixture at T = 273.16 K.*

Mode	p/MPa	$10^6 \cdot \delta_{TH}$/m	$10^6 \cdot \delta_V$/m	$10^{11} \cdot l_{TH}$/m	$10^6 \cdot \delta_{TH,316L}$/m
0.2	9.9546	3.07287	2.73921	6.28004	14.13325
0.3	9.9546	2.34360	2.08912	6.28006	10.77900
0.4	9.9546	1.97266	1.75846	6.28006	9.07296
0.5	9.9546	1.73689	1.54829	6.28006	7.98856
0.2	8.9700	3.22947	2.87556	6.78726	14.20850
0.3	8.9700	2.46302	2.19311	6.78729	10.83638
0.4	8.9700	2.07318	1.84599	6.78729	9.12123
0.5	8.9700	1.82538	1.62535	6.78727	8.03102
0.2	8.0190	3.41277	3.03183	7.41648	14.27637
0.3	8.0189	2.60282	2.31229	7.41652	10.88813
0.4	8.0189	2.19084	1.94630	7.41650	9.16476
0.5	8.0189	1.92898	1.71366	7.41652	8.06930
0.2	6.9945	3.65633	3.23617	8.30993	14.34424
0.3	6.9945	2.78857	2.46813	8.30998	10.93987
0.4	6.9944	2.34720	2.07747	8.31001	9.20829
0.5	6.9944	2.06664	1.82915	8.31007	8.10760
0.2	6.0005	3.95530	3.48424	9.49419	14.40465
0.3	6.0005	3.01657	2.65731	9.49419	10.98593
0.4	6.0005	2.53910	2.23670	9.49419	9.24705
0.5	6.0005	2.23558	1.96934	9.49419	8.14169

Mode	p/MPa	$10^6 \cdot \delta_{TH}$/m	$10^6 \cdot \delta_V$/m	$10^{11} \cdot l_{TH}$/m	$10^6 \cdot \delta_{TH,316L}$/m
0.2	4.9890	4.35206	3.81134	11.21256	14.46026
0.3	4.9891	3.31916	2.90677	11.21247	11.02837
0.4	4.9891	2.79378	2.44666	11.21244	9.28272
0.5	4.9891	2.45981	2.15419	11.21244	8.17307
0.2	3.9972	4.88364	4.24848	13.77487	14.50892
0.3	3.9972	3.72459	3.24017	13.77485	11.06547
0.4	3.9972	3.13502	2.72728	13.77479	9.31393
0.5	3.9972	2.76025	2.40126	13.77478	8.20053
0.2	2.9930	5.67521	4.89991	18.13963	14.55235
0.3	2.9930	4.32827	3.73698	18.13952	11.09857
0.4	2.9931	3.64309	3.14540	18.13890	9.34178
0.5	2.9931	3.20759	2.76940	18.13909	8.22502
0.2	1.9934	6.99973	5.99366	26.90939	14.58963
0.3	1.9933	5.33856	4.57125	26.91058	11.12699
0.4	1.9932	4.49362	3.84775	26.91164	9.36570
0.5	1.9932	3.95641	3.38776	26.91164	8.24605
0.2	0.9957	9.97878	8.46813	53.33577	14.62067
0.3	0.9957	7.61037	6.45827	53.33498	11.15061
0.4	0.9957	6.40565	5.43593	53.33410	9.38556
0.5	0.9954	5.64070	4.78677	53.34930	8.26355

Table D1.3 *Values of calculated thermal boundary layer, shell motion and holes and ducts frequency corrections; and thermal boundary layer, bulk viscosity and ducts and holes half-width contributions to the resonance peaks in the 0.10%CO-0.90%N_2 mixture at T = 273.16 K.*

Mode	p/PMa	Δf_{th}/Hz	Δf_{shell}/Hz	Δf_{hole}/Hz	g_{th}/Hz	g_b/Hz	g_{hole}/Hz
0.2	9.9546	-0.15241	-0.10149	-0.38280	0.15532	0.00032	0.67027
0.3	9.9546	-0.19983	-0.18630	0.13603	0.20366	0.00095	0.06626
0.4	9.9546	-0.23741	-0.29587	0.23640	0.24195	0.00189	0.12517
0.5	9.9546	-0.26964	-0.47509	0.25605	0.27479	0.00314	0.18925
0.2	8.9700	-0.15357	-0.09525	-0.36546	0.15630	0.00035	0.61675
0.3	8.9700	-0.20136	-0.17458	0.13938	0.20493	0.00102	0.06829
0.4	8.9700	-0.23922	-0.27633	0.24045	0.24347	0.00203	0.13316
0.5	8.9700	-0.27169	-0.43989	0.25869	0.27652	0.00339	0.20568
0.2	8.0190	-0.15552	-0.08915	-0.34575	0.15807	0.00038	0.56332
0.3	8.0189	-0.20391	-0.16318	0.14364	0.20726	0.00111	0.07093
0.4	8.0189	-0.24226	-0.25753	0.24553	0.24624	0.00222	0.14369
0.5	8.0189	-0.27514	-0.40695	0.26018	0.27967	0.00369	0.22690

Mode	p/MPa	Δf_{th}/Hz	Δf_{shell}/Hz	Δf_{hole}/Hz	g_{th}/Hz	g_{b}/Hz	g_{hole}/Hz
0.2	6.9945	-0.15882	-0.08242	-0.32032	0.16120	0.00042	0.50816
0.3	6.9945	-0.20824	-0.15067	0.14893	0.21136	0.00124	0.07471
0.4	6.9944	-0.24740	-0.23712	0.25059	0.25111	0.00247	0.15803
0.5	6.9944	-0.28099	-0.37211	0.25710	0.28520	0.00412	0.25374
0.2	6.0005	-0.16368	-0.07566	-0.29133	0.16590	0.00048	0.45719
0.3	6.0005	-0.21461	-0.13815	0.15471	0.21753	0.00141	0.07964
0.4	6.0005	-0.25497	-0.21690	0.25419	0.25843	0.00281	0.17585
0.5	6.0005	-0.28958	-0.33839	0.24661	0.29352	0.00468	0.28361
0.2	4.9890	-0.17110	-0.06843	-0.25716	0.17317	0.00056	0.40884
0.3	4.9891	-0.22434	-0.12481	0.16108	0.22706	0.00166	0.08650
0.4	4.9891	-0.26653	-0.19554	0.25456	0.26976	0.00330	0.19895
0.5	4.9891	-0.30272	-0.30350	0.22411	0.30639	0.00550	0.31530
0.2	3.9972	-0.18227	-0.06082	-0.25716	0.18420	0.00069	0.40884
0.3	3.9972	-0.23898	-0.11083	0.16108	0.24152	0.00203	0.08650
0.4	3.9972	-0.28392	-0.17331	0.25456	0.28694	0.00403	0.19895
0.5	3.9972	-0.32247	-0.26784	0.22411	0.32590	0.00671	0.31530
0.2	2.9930	-0.20060	-0.05229	-0.21853	0.20241	0.00090	0.36564
0.3	2.9930	-0.26303	-0.09522	0.16777	0.26540	0.00265	0.09605
0.4	2.9931	-0.31248	-0.14867	0.24780	0.31530	0.00528	0.22642
0.5	2.9931	-0.35491	-0.22891	0.18729	0.35811	0.00878	0.33975
0.2	1.9934	-0.23402	-0.04244	-0.17262	0.23571	0.00132	0.32493
0.3	1.9933	-0.30685	-0.07724	0.17433	0.30907	0.00390	0.11050
0.4	1.9932	-0.36456	-0.12043	0.22755	0.36719	0.00777	0.25713
0.5	1.9932	-0.41406	-0.18485	0.13686	0.41705	0.01293	0.34684
0.2	0.9957	-0.31517	-0.02986	-0.11572	0.31676	0.00259	0.28291
0.3	0.9957	-0.41325	-0.05432	0.17981	0.41533	0.00766	0.13483
0.4	0.9957	-0.49095	-0.08460	0.18390	0.49343	0.01527	0.28557
0.5	0.9954	-0.55768	-0.12951	0.07997	0.56050	0.02542	0.32655

Table D1.4 *Uncertainty contributions and result of speed of sound measurements in the 0.10%CO-0.90%N_2 mixture at T = 273.16 K.*

p/MPa	*u/m·s^{-1}*	$10^3 \cdot \left(\sum_{i=1}^{4} \frac{2\pi f_i}{4\upsilon_i}\right)^2 u^2(a) \Big/ m^2 \cdot s^{-2}$	$10^4 \cdot \sum_{i=1}^{4}\left(\frac{2\pi a}{4\upsilon_i}\right)^2 u^2(f_i) \Big/ m^2 \cdot s^{-2}$	$10^4 \cdot u^2_{disp}(u) / m^2 \cdot s^{-2}$	$10^2 \cdot u(u) / m \cdot s^{-1}$
9.95	361.7825	1.8	1.4	2.3	4.7
8.97	357.9527	1.8	1.1	1.9	4.5
8.02	354.5509	1.7	0.89	1.4	4.4
6.99	351.1970	1.7	0.73	1.1	4.3
6.00	348.2517	1.7	0.60	0.88	4.3
4.99	345.5726	1.6	0.56	0.67	4.2
4.00	343.2550	1.6	0.44	0.60	4.2
2.99	341.2070	1.6	0.30	0.43	4.1
1.99	339.4638	1.6	0.29	0.31	4.1
1.00	338.0267	1.6	0.36	0.16	4.0

D2

Measurements, corrections and uncertainties for X_{CO}=0.10 and X_{N_2}=0.90 mixture at T=325K.

Table D2.1 *Pressure, north and south hemisphere and average temperature, frequency of resonance, half-width of the resonance peak and frequency measured uncertainty in 0.10%CO-0.90%N_2 Mixture at T = 325 K.*

Mode	p/MPa	T_N/K	T_S/K	T_{ave}/K	*f*/Hz	*g*/Hz	u(*f*)/K
0.2	10.0063	324.9421	324.9335	324.9378	7024.0779	1.01665	0.76
0.3	10.0062	324.9421	324.9335	324.9378	12076.1335	1.28917	4.2
0.4	10.0062	324.9418	324.9332	324.9375	17044.3309	1.88501	6.3
0.5	10.0062	324.9418	324.9332	324.9375	21983.4161	2.03437	6.7
0.2	8.9627	324.9499	324.9422	324.9461	6958.6275	0.96427	1.2
0.3	8.9628	324.9499	324.9422	324.9461	11963.5580	1.20754	2.0
0.4	8.9628	324.9500	324.9423	324.9462	16885.6986	1.54727	6.5
0.5	8.9628	324.9500	324.9423	324.9462	21779.7656	1.72313	4.7
0.2	7.9960	324.9583	324.9517	324.9550	6900.9268	0.91774	1.4
0.3	7.9960	324.9585	324.9519	324.9552	11864.3604	1.12888	1.3
0.4	7.9959	324.9587	324.9521	324.9554	16745.9267	1.61981	3.5
0.5	7.9959	324.9587	324.9521	324.9554	21599.8472	1.57858	2.1
0.2	7.0005	324.9683	324.9635	324.9659	6844.4828	0.88249	2.4
0.3	7.0002	324.9679	324.9320	324.9500	11767.3179	1.11350	1.4
0.4	6.9968	324.9679	324.9632	324.9656	16608.6306	1.44350	9.9
0.5	6.9995	324.9674	324.9629	324.9652	21423.6316	1.44134	3.7
0.2	5.9978	324.9422	324.9361	324.9392	6790.3761	0.83547	0.76
0.3	5.9977	324.9422	324.9361	324.9392	11674.3132	0.97294	1.4
0.4	5.9978	324.9424	324.9363	324.9394	16477.6352	1.28951	7.1
0.5	5.9977	324.9424	324.9363	324.9394	21255.0699	1.39895	2.4
0.2	5.0020	324.9587	324.9540	324.9564	6740.3291	0.77915	0.58
0.3	5.0020	324.9587	324.9540	324.9564	11588.3126	0.94488	3.0
0.4	5.0020	324.9587	324.9540	324.9564	16356.3113	1.20757	5.3
0.5	5.0020	324.9587	324.9540	324.9564	21098.8016	1.36229	2.5
0.2	3.9975	324.9523	324.9471	324.9497	6692.8213	0.70861	2.0
0.3	3.9975	324.9523	324.9471	324.9497	11506.6080	1.01599	2.0
0.4	3.9975	324.9524	324.9472	324.9498	16241.0885	1.19127	7.6
0.5	3.9976	324.9527	324.9474	324.9501	20950.4936	1.38778	2.8

Mode	p/MPa	T_N/K	T_S/K	T_{ave}/K	*f*/Hz	*g*/Hz	u(*f*)/K
0.2	3.0024	324.9553	324.9504	324.9529	6649.0997	0.67530	1.2
0.3	3.0024	324.9553	324.9504	324.9529	11431.3352	0.87427	3.4
0.4	3.0024	324.9554	324.9505	324.9530	16135.0689	1.17836	4.4
0.5	3.0024	324.9555	324.9506	324.9531	20813.7691	1.32365	4.4
0.2	1.9889	324.9579	324.9529	324.9554	6608.1829	0.61630	0.46
0.3	1.9889	324.9580	324.9531	324.9556	11360.9882	0.76265	0.73
0.4	1.9889	324.9580	324.9531	324.9556	16035.8612	1.13534	6.0
0.5	1.9889	324.9581	324.9533	324.9557	20685.9141	1.28034	1.5
0.2	1.0011	324.9555	324.9513	324.9534	6570.9533	0.62830	0.37
0.3	1.0011	324.9555	324.9513	324.9534	11297.0757	0.76862	0.71
0.4	1.0011	324.9555	324.9513	324.9534	15945.6441	1.24144	0.98
0.5	1.0011	324.9555	324.9513	324.9534	20569.8033	1.34664	3.3
0.2	0.1171	324.9400	324.9346	324.9373	6539.8165	1.25483	12.
0.3	0.1171	324.9401	324.9349	324.9375	11244.0120	1.67447	3.7
0.4	0.1171	324.9401	324.9349	324.9375	15871.2980	2.27199	4.5
0.5	0.1171	324.9402	324.9351	324.9377	20473.8602	2.80573	6.2

***Table D2.2**. Parameters required for computing frequency corrections, thermal boundary layer length, viscous boundary layer length accommodation length and thermal boundary layer in sell side length in the 0.10%CO-0.90%N_2 mixture at T = 325 K.*

Mode	p/MPa	$10^6 \cdot \delta_{TH}$/m	$10^6 \cdot \delta_V$/m	$10^{11} \cdot l_{TH}$/m	$10^6 \cdot \delta_{TH,316L}$/m
0.2	10.0063	3.48246	3.03343	7.36426	13.53393
0.3	10.0062	2.65594	2.31348	7.36430	10.32178
0.4	10.0062	2.23560	1.94734	7.36433	8.68818
0.5	10.0062	1.96850	1.71468	7.36435	7.65017
0.2	8.9627	3.67449	3.19700	8.08319	13.59743
0.3	8.9628	2.80239	2.43823	8.08315	10.37023
0.4	8.9628	2.35883	2.05231	8.08311	8.72889
0.5	8.9628	2.07697	1.80707	8.08309	7.68585
0.2	7.9960	3.88834	3.37719	8.92952	13.65416
0.3	7.9960	2.96549	2.57565	8.92954	10.41349
0.4	7.9959	2.49612	2.16799	8.92959	8.76524
0.5	7.9959	2.19784	1.90891	8.92960	7.71780
0.2	7.0005	4.15673	3.60153	10.05932	13.71034
0.3	7.0002	3.17010	2.74669	10.05919	10.45634
0.4	6.9968	2.66910	2.31257	10.06414	8.80140
0.5	6.9995	2.34966	2.03582	10.06065	7.74947

Mode	p/MPa	$10^6 \cdot \delta_{TH}$/m	$10^6 \cdot \delta_V$/m	$10^{11} \cdot l_{TH}$/m	$10^6 \cdot \delta_{TH,316L}$/m
0.2	5.9978	4.49505	3.88276	11.59070	13.76486
0.3	5.9977	3.42820	2.96123	11.59072	10.49791
0.4	5.9978	2.88559	2.49253	11.59069	8.83631
0.5	5.9977	2.54069	2.19461	11.59075	7.78014
0.2	5.0020	4.93086	4.24374	13.73870	13.81586
0.3	5.0020	3.76058	3.23654	13.73880	10.53679
0.4	5.0020	3.16534	2.72425	13.73872	8.86903
0.5	5.0020	2.78699	2.39862	13.73872	7.80890
0.2	3.9975	5.52923	4.73867	17.00991	13.86481
0.3	3.9975	4.21692	3.61399	17.00991	10.57414
0.4	3.9975	3.54943	3.04194	17.00972	8.90043
0.5	3.9976	3.12512	2.67830	17.00953	7.83649
0.2	3.0024	6.40006	5.45915	22.43639	13.91032
0.3	3.0024	4.88109	4.16350	22.43639	10.60889
0.4	3.0024	4.10848	3.50447	22.43654	8.92962
0.5	3.0024	3.61734	3.08554	22.43633	7.86218
0.2	1.9889	7.89395	6.69748	33.58661	13.95332
0.3	1.9889	6.02045	5.10795	33.58693	10.64169
0.4	1.9889	5.06748	4.29941	33.58701	8.95720
0.5	1.9889	4.46171	3.78546	33.58708	7.88644
0.2	1.0011	11.17644	9.42794	66.25564	13.99279
0.3	1.0011	8.52383	7.19032	66.25564	10.67175
0.4	1.0011	7.17458	6.05216	66.25564	8.98251
0.5	1.0011	6.31687	5.32863	66.25544	7.90867
0.2	0.1171	32.82398	27.52961	563.20958	14.02606
0.3	0.1171	25.03294	20.99523	563.20521	10.69690
0.4	0.1171	21.07008	17.67157	563.20521	9.00352
0.5	0.1171	18.55123	15.55900	563.20554	7.92718

Table D2.3 *Values of calculated thermal boundary layer, shell motion and holes and ducts frequency corrections; and thermal boundary layer, bulk viscosity and ducts and holes half-width contributions to the resonance peaks in the 0.10%CO-0.90%N_2 mixture at T = 325 K.*

Mode	p/MPa	Δf_{th}/Hz	Δf_{shell}/Hz	Δf_{hole}/Hz	g_{th}/Hz	g_b/Hz	g_{hole}/Hz
0.2	10.0063	-0.16215	-0.11183	-0.29613	0.16495	0.00041	0.89792
0.3	10.0062	-0.21261	-0.20830	0.12878	0.21628	0.00122	0.07770
0.4	10.0062	-0.25259	-0.34190	0.21688	0.25695	0.00243	0.12171
0.5	10.0062	-0.28686	-0.60542	0.21842	0.29182	0.00404	0.15564

Mode	p/PMa	Δf_{th}/Hz	Δf_{shell}/Hz	Δf_{hole}/Hz	g_{th}/Hz	g_b/Hz	g_{hole}/Hz
0.2	8.9627	-0.16563	-0.10477	-0.29023	0.16830	0.00045	0.83125
0.3	8.9628	-0.21718	-0.19482	0.13153	0.22068	0.00133	0.08043
0.4	8.9628	-0.25801	-0.31847	0.21944	0.26217	0.00265	0.12818
0.5	8.9628	-0.29302	-0.55637	0.22323	0.29775	0.00441	0.16731
0.2	7.9960	-0.16989	-0.09807	-0.28316	0.17245	0.00049	0.76446
0.3	7.9960	-0.22276	-0.18209	0.13541	0.22611	0.00146	0.08368
0.4	7.9959	-0.26465	-0.29662	0.22345	0.26863	0.00291	0.13650
0.5	7.9959	-0.30057	-0.51237	0.22717	0.30509	0.00485	0.18067
0.2	7.0005	-0.17568	-0.09096	-0.27120	0.17812	0.00055	0.69393
0.3	7.0002	-0.23035	-0.16863	0.14128	0.23355	0.00164	0.08808
0.4	6.9968	-0.27371	-0.27369	0.22779	0.27751	0.00327	0.14740
0.5	6.9995	-0.31082	-0.46794	0.23016	0.31514	0.00543	0.19798
0.2	5.9978	-0.18351	-0.08347	-0.25351	0.18584	0.00063	0.62112
0.3	5.9977	-0.24061	-0.15454	0.14660	0.24367	0.00188	0.09369
0.4	5.9978	-0.28586	-0.25011	0.23119	0.28949	0.00374	0.16091
0.5	5.9977	-0.32466	-0.42348	0.23078	0.32879	0.00622	0.22030
0.2	5.0020	-0.19426	-0.07563	-0.22881	0.19649	0.00075	0.54864
0.3	5.0020	-0.25472	-0.13984	0.15434	0.25764	0.00221	0.10151
0.4	5.0020	-0.30261	-0.22567	0.23493	0.30608	0.00440	0.18021
0.5	5.0020	-0.34369	-0.37887	0.22579	0.34763	0.00733	0.24760
0.2	3.9975	-0.20991	-0.06709	-0.22881	0.21203	0.00092	0.54864
0.3	3.9975	-0.27523	-0.12392	0.15434	0.27802	0.00272	0.10151
0.4	3.9975	-0.32698	-0.19945	0.23493	0.33030	0.00541	0.18021
0.5	3.9976	-0.37137	-0.33227	0.22579	0.37514	0.00900	0.24760
0.2	3.0024	-0.23394	-0.05774	-0.19500	0.23597	0.00120	0.47782
0.3	3.0024	-0.30674	-0.10652	0.16318	0.30940	0.00356	0.11269
0.4	3.0024	-0.36442	-0.17104	0.23473	0.36759	0.00708	0.20586
0.5	3.0024	-0.41390	-0.28300	0.21009	0.41749	0.01179	0.27917
0.2	1.9889	-0.27733	-0.04668	-0.15124	0.27927	0.00179	0.40988
0.3	1.9889	-0.36363	-0.08604	0.17306	0.36618	0.00528	0.12952
0.4	1.9889	-0.43201	-0.13785	0.22547	0.43504	0.01052	0.23947
0.5	1.9889	-0.49067	-0.22667	0.17738	0.49410	0.01751	0.30823
0.2	1.0011	-0.37736	-0.03292	-0.09234	0.37922	0.00349	0.33844
0.3	1.0011	-0.49479	-0.06062	0.18551	0.49723	0.01033	0.16006
0.4	1.0011	-0.58783	-0.09693	0.19359	0.59074	0.02058	0.28374
0.5	1.0011	-0.66764	-0.15853	0.11871	0.67095	0.03425	0.32432
0.2	0.1171	-1.06902	-0.01120	-0.00793	1.07096	0.02946	0.27145
0.3	0.1171	-1.40165	-0.02062	0.18678	1.40427	0.08709	0.22209
0.4	0.1171	-1.66521	-0.03292	0.11844	1.66839	0.17351	0.30486
0.5	0.1171	-1.89124	-0.05359	0.05697	1.89492	0.28874	0.29168

Table D2.4 *Uncertainty contributions and result of speed of sound measurements in the 0.10%CO-0.90%N_2 mixture at T = 325 K.*

p/MPa	$u/m\cdot s^{-1}$	$10^3\cdot\left(\sum_{i=1}^{4}\frac{2\pi f_i}{4\upsilon_i}\right)^2 u^2(a)\Big/m^2\cdot s^{-2}$	$10^4\cdot\sum_{i=1}^{4}\left(\frac{2\pi a}{4\upsilon_i}\right)^2 u^2(f_i)\Big/m^2\cdot s^{-2}$	$10^4\cdot u_{disp}^2(u)/m^2\cdot s^{-2}$	$10^2\cdot u(u)/m\cdot s^{-1}$
10.01	394.8510	1.9	7.2	5.3	5.6
8.96	391.1656	1.8	5.2	3.2	5.1
8.00	387.9158	1.7	4.3	2.3	4.9
7.00	384.7326	1.7	4.8	1.8	4.8
6.00	381.6868	1.7	2.7	1.0	4.5
5.00	378.8670	1.6	2.2	0.74	4.4
4.00	376.1903	1.6	3.0	0.55	4.4
3.00	373.7251	1.5	1.8	0.44	4.2
1.99	371.4199	1.5	0.94	0.31	4.1
1.00	369.3268	1.6	0.41	0.16	4.0
0.12	367.6158	6.2	5.6	0.025	8.2

APPENDIX E

MEASUREMENTS, CORRECTIONS, AND UNCERTAINTIES FOR SYNTHETIC COAL MINE METHENE (CMM) MIXTURE

E1

Measurements, corrections and uncertainties for synthetic Coal Mine Methane (CMM) mixture at T=250K.

Table E1.1 *Pressure, north and south hemisphere and average temperature, frequency of resonance, half-width of the resonance peak and frequency measured uncertainty in CMM mixture at T = 250 K.*

Mode	p/MPa	T_N/K	T_S/K	T_{ave}/K	*f*/Hz	*g*/Hz	u(*f*)/K
0.2	7.9344	249.8940	249.8834	249.8887	5689.8612	0.29004	0.095
0.3	7.9331	249.8929	249.8816	249.8873	9781.8894	0.40893	0.15
0.4	7.9317	249.8929	249.8816	249.8873	13806.6237	0.61504	0.75
0.5	7.9307	249.8919	249.8816	249.8868	17810.4748	1.31260	0.84
0.2	6.9491	249.9350	249.9241	249.9296	5684.6134	0.26253	0.071
0.3	6.9481	249.9350	249.9241	249.9296	9772.9996	0.37600	0.13
0.4	6.9470	249.9338	249.9228	249.9283	13794.2461	0.57430	0.31
0.5	6.9456	249.9327	249.9214	249.9271	17794.8379	1.18191	0.55
0.2	6.0448	249.9318	249.9136	249.9227	5706.7644	0.25738	0.036
0.3	6.0438	249.9318	249.9136	249.9227	9811.1374	0.40071	0.081
0.4	6.0430	249.9326	249.9141	249.9234	13848.2275	0.56194	0.32
0.5	6.0421	249.9334	249.9146	249.9240	17864.4751	1.12475	0.27
0.2	4.8853	249.9800	249.9670	249.9735	5765.6165	0.24866	0.046
0.3	4.8831	249.9798	249.9667	249.9733	9912.4228	0.35902	0.11
0.4	4.8821	249.9798	249.9667	249.9733	13991.3067	0.59646	0.40
0.5	4.8810	249.9799	249.9667	249.9733	18049.0177	0.80767	0.21
0.2	3.9352	249.9949	249.9830	249.9890	5830.7615	0.29097	0.063
0.3	3.9343	249.9949	249.9828	249.9889	10024.4861	0.35938	0.073
0.4	3.9337	249.9951	249.9828	249.9890	14149.5048	0.63680	0.20
0.5	3.9329	249.9952	249.9828	249.9890	18252.8373	0.77932	0.18
0.2	2.9253	250.0169	250.0061	250.0115	5911.9934	0.27523	0.047
0.3	2.9250	250.0169	250.0061	250.0115	10164.0880	0.37026	0.097
0.4	2.9242	250.0168	250.0060	250.0114	14346.5284	0.70523	0.18
0.5	2.9237	250.0168	250.0060	250.0114	18507.2387	0.89524	0.31
0.2	1.9748	250.0021	249.9899	249.9960	5995.7643	0.31566	0.065
0.3	1.9746	250.0024	249.9904	249.9964	10308.1050	0.43410	0.090
0.4	1.9745	250.0026	249.9907	249.9967	14549.6875	0.80983	0.33
0.5	1.9742	250.0027	249.9910	249.9969	18769.1753	1.07566	0.32

Mode	p/MPa	T_N/K	T_S/K	T_{ave}/K	*f*/Hz	*g*/Hz	u(*f*)/K
0.2	0.9780	250.0160	250.0053	250.0107	6090.0578	0.38825	0.064
0.3	0.9779	250.0159	250.0052	250.0106	10470.2826	0.59889	0.12
0.4	0.9779	250.0160	250.0053	250.0107	14778.6038	1.06507	0.15
0.5	0.9778	250.0161	250.0052	250.0107	19064.3786	1.44000	0.17
0.2	0.1009	250.0079	249.9957	250.0018	6173.1242	1.39612	0.67
0.3	0.1009	250.0079	249.9957	250.0018	10613.4100	2.83883	1.1
0.4	0.1009	250.0081	249.9959	250.0020	14981.0843	5.09067	2.2
0.5	0.1008	250.0081	249.9959	250.0020	19325.3443	7.75256	3.8

Table E1.2*. Parameters required for computing frequency corrections, thermal boundary layer length, viscous boundary layer length accommodation length and thermal boundary layer in sell side length in the CMM mixture at T = 250 K.*

Mode	p/MPa	δ_{TH}(m)	δ_V(m)	l_{TH}(m)	$\delta_{TH,316L}$(m)
0.2	7.9344	2.72580	2.88695	4.32194	15.03723
0.3	7.9331	2.07912	2.20194	4.32233	11.46852
0.4	7.9317	1.75025	1.85356	4.32273	9.65328
0.5	7.9307	1.54114	1.63205	4.32302	8.49925
0.2	6.9491	2.99844	3.06496	4.67903	15.04417
0.3	6.9481	2.28705	2.33770	4.67945	11.47373
0.4	6.9470	1.92523	1.96780	4.67990	9.65761
0.5	6.9456	1.69529	1.73270	4.68052	8.50299
0.2	6.0448	3.29967	3.26854	5.15328	15.01494
0.3	6.0438	2.51683	2.49300	5.15389	11.45141
0.4	6.0430	2.11865	2.09853	5.15442	9.63877
0.5	6.0421	1.86555	1.84778	5.15497	8.48640
0.2	4.8853	3.78935	3.61544	6.08779	14.93811
0.3	4.8831	2.89086	2.75799	6.09006	11.39275
0.4	4.8821	2.43360	2.32168	6.09115	9.58936
0.5	4.8810	2.14297	2.04434	6.09229	8.44290
0.2	3.9352	4.32421	4.01383	7.32214	14.85443
0.3	3.9343	3.29839	3.06156	7.32368	11.32889
0.4	3.9337	2.77655	2.57715	7.32471	9.53560
0.5	3.9329	2.44490	2.26927	7.32591	8.39563
0.2	2.9253	5.13275	4.64277	9.57541	14.75202
0.3	2.9250	3.91483	3.54109	9.57647	11.25083
0.4	2.9242	3.29566	2.98097	9.57885	9.46990
0.5	2.9237	2.90191	2.62479	9.58022	8.33773
0.2	1.9748	6.36999	5.64148	13.86708	14.64861
0.3	1.9746	4.85834	4.30270	13.86798	11.17196
0.4	1.9745	4.08947	3.62176	13.86887	9.40355
0.5	1.9742	3.60084	3.18899	13.87063	8.27935

Mode	p/MPa	δ_{TH}(m)	δ_V(m)	l_{TH}(m)	$\delta_{TH,316L}$(m)
0.2	0.9780	9.21981	8.01158	27.44480	14.53476
0.3	0.9779	7.03173	6.11024	27.44589	11.08509
0.4	0.9779	5.91884	5.14319	27.44728	9.33044
0.5	0.9778	5.21142	4.52847	27.44894	8.21499
0.2	0.1009	29.12859	24.95564	261.94291	14.43664
0.3	0.1009	22.21270	19.03052	261.89108	11.01010
0.4	0.1009	18.70010	16.02113	261.99506	9.26717
0.5	0.1008	16.46545	14.10661	262.02100	8.15934

Table E1.3 *Values of calculated thermal boundary layer, shell motion and holes and ducts frequency corrections; and thermal boundary layer, bulk viscosity and ducts and holes half-width contributions to the resonance peaks in CMM mixture at T = 250 K.*

Mode	p/PMa	Δf_{th}/Hz	Δf_{shell}/Hz	Δf_{hole}/Hz	g_{th}/Hz	g_b/Hz	g_{hole}/Hz
0.2	7.9344	-0.19216	-0.07946	-0.13046	0.19798	0.00033	0.14664
0.3	7.9331	-0.25194	-0.14356	0.28540	0.25957	0.00098	0.15405
0.4	7.9317	-0.29929	-0.22063	-0.08368	0.30835	0.00195	0.43684
0.5	7.9307	-0.33991	-0.32812	-0.09678	0.35020	0.00325	0.18184
0.2	6.9491	-0.18343	-0.07427	-0.12855	0.18816	0.00036	0.14658
0.3	6.9481	-0.24050	-0.13417	0.28539	0.24670	0.00107	0.15582
0.4	6.9470	-0.28571	-0.20617	-0.08373	0.29307	0.00214	0.43175
0.5	6.9456	-0.32449	-0.30649	-0.09468	0.33285	0.00356	0.18077
0.2	6.0448	-0.17715	-0.06956	-0.12567	0.18106	0.00040	0.14747
0.3	6.0438	-0.23227	-0.12570	0.28637	0.23740	0.00119	0.15976
0.4	6.0430	-0.27594	-0.19332	-0.08349	0.28203	0.00237	0.42462
0.5	6.0421	-0.31340	-0.28790	-0.09149	0.32032	0.00395	0.18042
0.2	4.8853	-0.17256	-0.06319	-0.11867	0.17566	0.00048	0.14979
0.3	4.8831	-0.22626	-0.11431	0.28924	0.23032	0.00142	0.17055
0.4	4.8821	-0.26880	-0.17619	-0.08179	0.27363	0.00283	0.40886
0.5	4.8810	-0.30529	-0.26364	-0.08335	0.31077	0.00471	0.17919
0.2	3.9352	-0.17291	-0.05738	-0.11867	0.17549	0.00058	0.14979
0.3	3.9343	-0.22672	-0.10395	0.28924	0.23011	0.00172	0.17055
0.4	3.9337	-0.26936	-0.16063	-0.08179	0.27338	0.00343	0.40886
0.5	3.9329	-0.30593	-0.24169	-0.08335	0.31051	0.00570	0.17919
0.2	2.9253	-0.17974	-0.05019	-0.10843	0.18190	0.00077	0.15274
0.3	2.9250	-0.23568	-0.09108	0.29111	0.23851	0.00226	0.18573
0.4	2.9242	-0.28002	-0.14120	-0.07792	0.28337	0.00451	0.38682
0.5	2.9237	-0.31805	-0.21399	-0.07270	0.32186	0.00750	0.17872

Mode	p/PMa	Δf_{th}/Hz	Δf_{shell}/Hz	Δf_{hole}/Hz	g_{th}/Hz	g_b/Hz	g_{hole}/Hz
0.2	1.9748	-0.19796	-0.04185	-0.08952	0.19980	0.00112	0.15632
0.3	1.9746	-0.25957	-0.07608	0.28973	0.26198	0.00330	0.21253
0.4	1.9745	-0.30839	-0.11838	-0.06827	0.31125	0.00657	0.35181
0.5	1.9742	-0.35028	-0.18082	-0.05482	0.35353	0.01093	0.17806
0.2	0.9780	-0.25423	-0.02994	-0.05935	0.25580	0.00222	0.16065
0.3	0.9779	-0.33335	-0.05454	0.27566	0.33540	0.00657	0.25458
0.4	0.9779	-0.39604	-0.08520	-0.04853	0.39849	0.01309	0.30605
0.5	0.9778	-0.44983	-0.13136	-0.02770	0.45261	0.02179	0.17722
0.2	0.1009	-0.72613	-0.00976	0.00158	0.72755	0.02137	0.16780
0.3	0.1009	-0.95199	-0.01780	0.20531	0.95389	0.06316	0.31734
0.4	0.1009	-1.13124	-0.02791	-0.00196	1.13351	0.12589	0.24594
0.5	0.1008	-1.28487	-0.04341	0.02190	1.28748	0.20951	0.18157

Table E1.4 *Uncertainty contributions and result of speed of sound measurements in the CMM mixture at T = 250 K.*

p/MPa	$u/m\cdot s^{-1}$	$10^3\cdot\left(\sum_{i=1}^{4}\frac{2\pi f_i}{4\upsilon_i}\right)^2 u^2(a)\Big/m^2\cdot s^{-2}$	$10^4\cdot\sum_{i=1}^{4}\left(\frac{2\pi a}{4\upsilon_i}\right)^2 u^2(f_i)\Big/m^2\cdot s^{-2}$	$10^4\cdot u_{disp}^2(u)/m^2\cdot s^{-2}$	$10^2\cdot u(u)/m\cdot s^{-1}$
7.93	319.5408	1.07833	11.32004	0.51	3.5
6.95	319.2142	1.06649	4.03141	0.32	3.4
6.04	320.4591	1.09557	1.77274	0.26	3.4
4.88	323.7226	1.07733	2.31900	0.20	3.3
3.93	327.3650	1.09874	1.21223	0.15	3.4
2.92	331.9053	1.12418	1.52651	0.19	3.4
1.97	336.6156	1.15979	2.50324	0.16	3.5
0.98	341.9011	1.22644	1.24430	0.099	3.5

E2

Measurements, corrections and uncertainties for synthetic Coal Mine Methane (CMM) mixture at T=273K.

Table E2.1 *Pressure, north and south hemisphere and average temperature, frequency of resonance, half-width of the resonance peak and frequency measured uncertainty in CMM mixture at T = 273 K.*

Mode	p/MPa	T_N/K	T_S/K	T_{ave}/K	*f*/Hz	*g*/Hz	u(*f*)/K
0.2	5.5064	273.1571	273.1571	273.1571	6154.9465	0.26101	0.012
0.3	5.5064	273.1571	273.1571	273.1571	10581.6841	0.45009	0.090
0.4	5.5064	273.1572	273.1572	273.1572	14935.8197	0.61287	0.062
0.5	5.5064	273.1572	273.1572	273.1572	19267.6592	1.28995	0.36
0.2	4.9933	273.1609	273.1612	273.1611	6169.7707	0.26551	0.045
0.3	4.9934	273.1609	273.1612	273.1611	10607.1559	0.43299	0.067
0.4	4.9934	273.1609	273.1612	273.1611	14971.8200	0.61210	0.12
0.5	4.9933	273.1610	273.1612	273.1611	19313.7860	1.08037	0.21
0.2	4.5138	273.1683	273.1692	273.1688	6186.6981	0.26813	0.064
0.3	4.5138	273.1683	273.1692	273.1688	10636.2625	0.43734	0.080
0.4	4.5138	273.1683	273.1692	273.1688	15012.9445	0.60662	0.077
0.5	4.5138	273.1683	273.1692	273.1688	19366.6547	0.99048	0.21
0.2	4.0051	273.1619	273.1610	273.1615	6207.0795	0.27331	0.031
0.3	4.0051	273.1620	273.1611	273.1616	10671.3151	0.42434	0.031
0.4	4.0051	273.1620	273.1611	273.1616	15062.4537	0.63406	0.067
0.5	4.0051	273.1620	273.1612	273.1616	19430.4141	0.94907	0.075
0.2	3.4914	273.1718	273.1721	273.1720	6230.7315	0.27733	0.031
0.3	3.4913	273.1718	273.1721	273.1720	10711.9854	0.42856	0.062
0.4	3.4914	273.1718	273.1721	273.1720	15119.8740	0.68012	0.11
0.5	3.4914	273.1718	273.1721	273.1720	19504.3839	0.98055	0.051
0.2	2.9971	273.1542	273.1533	273.1538	6255.6301	0.28866	0.032
0.3	2.9971	273.1543	273.1534	273.1539	10754.7925	0.44457	0.11
0.4	2.9971	273.1543	273.1534	273.1539	15180.2241	0.71807	0.047
0.5	2.9971	273.1543	273.1535	273.1539	19582.2938	1.09040	0.14
0.2	2.4914	273.1622	273.1623	273.1623	6283.4444	0.30516	0.017
0.3	2.4914	273.1622	273.1623	273.1623	10802.6386	0.46305	0.047
0.4	2.4913	273.1623	273.1624	273.1624	15247.7752	0.72910	0.10
0.5	2.4913	273.1623	273.1624	273.1624	19669.4220	1.15889	0.30

Mode	p/MPa	T_N/K	T_S/K	T_{ave}/K	*f*/Hz	*g*/Hz	u(*f*)/K
0.2	2.0056	273.1458	273.1449	273.1454	6311.4527	0.32897	0.023
0.3	2.0056	273.1459	273.1449	273.1454	10850.8088	0.50098	0.052
0.4	2.0057	273.1459	273.1449	273.1454	15315.8074	0.80244	0.068
0.5	2.0056	273.1458	273.1449	273.1454	19757.1801	1.27665	0.15
0.2	1.4855	273.1691	273.1684	273.1688	6346.5974	0.37262	0.029
0.3	1.4855	273.1691	273.1685	273.1688	10911.2600	0.57376	0.036
0.4	1.4855	273.1691	273.1685	273.1688	15401.1624	0.93149	0.085
0.5	1.4856	273.1691	273.1685	273.1688	19867.2426	1.52722	0.072
0.2	0.9988	273.1564	273.1543	273.1554	6377.6099	0.44553	0.037
0.3	0.9988	273.1564	273.1543	273.1554	10964.6231	0.70949	0.063
0.4	0.9989	273.1565	273.1543	273.1554	15476.5103	1.17406	0.11
0.5	0.9989	273.1565	273.1543	273.1554	19964.3340	1.78591	0.72
0.2	0.4986	273.1710	273.1702	273.1706	6410.3061	0.62907	0.045
0.3	0.4986	273.1711	273.1703	273.1707	11020.9404	1.09616	0.087
0.4	0.4986	273.1711	273.1703	273.1707	15556.0241	1.83986	0.15
0.5	0.4986	273.1712	273.1704	273.1708	20067.1403	2.84972	0.39

***Table E2.2**. Parameters required for computing frequency corrections, thermal boundary layer length, viscous boundary layer length accommodation length and thermal boundary layer in sell side length in the CMM mixture at T = 273 K.*

Mode	p/MPa	$10^6 \cdot \delta_{TH}$/m	$10^6 \cdot \delta_V$/m	$10^{11} \cdot l_{TH}$/m	$10^6 \cdot \delta_{TH,316L}$/m
0.2	5.5064	3.63230	3.31270	7.61715	14.45794
0.3	5.5064	2.77023	2.52648	7.61714	11.02659
0.4	5.5064	2.33173	2.12656	7.61710	9.28120
0.5	5.5064	2.05295	1.87231	7.61713	8.17154
0.2	4.9933	3.84806	3.47376	8.27666	14.44056
0.3	4.9934	2.93478	2.64931	8.27661	11.01334
0.4	4.9934	2.47023	2.22995	8.27662	9.27003
0.5	4.9933	2.17492	1.96336	8.27665	8.16178
0.2	4.5138	4.08039	3.64953	9.03814	14.42079
0.3	4.5138	3.11198	2.78338	9.03815	10.99826
0.4	4.5138	2.61939	2.34280	9.03821	9.25733
0.5	4.5138	2.30623	2.06271	9.03812	8.15063
0.2	4.0051	4.36861	3.87052	10.05523	14.39710
0.3	4.0051	3.33181	2.95193	10.05531	10.98018
0.4	4.0051	2.80440	2.48466	10.05528	9.24210
0.5	4.0051	2.46915	2.18763	10.05526	8.13725

Mode	p/MPa	$10^6 \cdot \delta_{TH}$/m	$10^6 \cdot \delta_V$/m	$10^{11} \cdot l_{TH}$/m	$10^6 \cdot \delta_{TH,316L}$/m
0.2	3.4914	4.71873	4.14248	11.39617	14.36975
0.3	3.4913	3.59882	3.15934	11.39623	10.95932
0.4	3.4914	3.02914	2.65923	11.39614	9.22454
0.5	3.4914	2.66703	2.34134	11.39617	8.12180
0.2	2.9971	5.13312	4.46842	13.13090	14.34112
0.3	2.9971	3.91486	3.40791	13.13091	10.93749
0.4	2.9971	3.29518	2.86848	13.13095	9.20618
0.5	2.9971	2.90125	2.52556	13.13087	8.10563
0.2	2.4914	5.67502	4.89953	15.63445	14.30934
0.3	2.4914	4.32816	3.73672	15.63457	10.91324
0.4	2.4913	3.64306	3.14524	15.63464	9.18577
0.5	2.4913	3.20758	2.76927	15.63493	8.08766
0.2	2.0056	6.37204	5.46004	19.24183	14.27756
0.3	2.0056	4.85976	4.16421	19.24201	10.88899
0.4	2.0057	4.09041	3.50497	19.24128	9.16534
0.5	2.0056	3.60145	3.08599	19.24155	8.06968
0.2	1.4855	7.46071	6.34414	25.74682	14.23797
0.3	1.4855	5.68993	4.83838	25.74615	10.85878
0.4	1.4855	4.78923	4.07248	25.74598	9.13991
0.5	1.4856	4.21667	3.58561	25.74547	8.04729
0.2	0.9988	9.16305	7.73930	37.99043	14.20331
0.3	0.9988	6.98824	5.90241	37.98968	10.83233
0.4	0.9989	5.88194	4.96802	37.98849	9.11763
0.5	0.9989	5.17874	4.37408	37.98752	8.02770
0.2	0.4986	13.06234	10.96083	75.54128	14.16704
0.3	0.4986	9.96214	8.35940	75.54177	10.80461
0.4	0.4986	8.38517	7.03614	75.54162	9.09430
0.5	0.4986	7.38274	6.19498	75.54121	8.00711

Table E2.3 *Values of calculated thermal boundary layer, shell motion and holes and ducts frequency corrections; and thermal boundary layer, bulk viscosity and ducts and holes half-width contributions to the resonance peaks in CMM mixture at T = 273 K.*

Mode	p/PMa	Δf_{th}/Hz	Δf_{shell}/Hz	Δf_{hole}/Hz	g_{th}/Hz	g_b/Hz	g_{hole}/Hz
0.2	5.5064	-0.16410	-0.07192	-0.29654	0.16694	0.00040	0.49018
0.3	5.5064	-0.21516	-0.13118	0.15171	0.21889	0.00118	0.08047
0.4	5.5064	-0.25563	-0.20553	0.24990	0.26005	0.00234	0.16592
0.5	5.5064	-0.29034	-0.31911	0.25179	0.29536	0.00390	0.26970
0.2	4.9933	-0.16468	-0.06866	-0.28467	0.16731	0.00043	0.47316
0.3	4.9934	-0.21592	-0.12527	0.15472	0.21937	0.00129	0.08339
0.4	4.9934	-0.25652	-0.19641	0.25187	0.26062	0.00256	0.17418
0.5	4.9933	-0.29136	-0.30542	0.24705	0.29601	0.00442	0.27956

Mode	p/PMa	Δf_{th}/Hz	Δf_{shell}/Hz	Δf_{hole}/Hz	g_{th}/Hz	g_{b}/Hz	g_{hole}/Hz
0.2	4.5138	-0.16600	-0.06546	-0.27162	0.16845	0.00050	0.45747
0.3	4.5138	-0.21766	-0.11949	0.15769	0.22088	0.00146	0.08670
0.4	4.5138	-0.25859	-0.18749	0.25297	0.26241	0.00292	0.18291
0.5	4.5138	-0.29370	-0.29209	0.24086	0.29804	0.00486	0.28974
0.2	4.0051	-0.16848	-0.06188	-0.25538	0.17075	0.00058	0.44503
0.3	4.0051	-0.22091	-0.11300	0.15996	0.22389	0.00173	0.09075
0.4	4.0051	-0.26245	-0.17747	0.25152	0.26599	0.00344	0.19124
0.5	4.0051	-0.29808	-0.27709	0.23213	0.30211	0.00572	0.29644
0.2	3.4914	-0.17245	-0.05801	-0.23612	0.17457	0.00066	0.42885
0.3	3.4913	-0.22612	-0.10598	0.16309	0.22889	0.00197	0.09605
0.4	3.4914	-0.26864	-0.16663	0.24941	0.27193	0.00392	0.20226
0.5	3.4914	-0.30511	-0.26085	0.22052	0.30886	0.00652	0.30527
0.2	2.9971	-0.17822	-0.05397	-0.21574	0.18019	0.00077	0.40846
0.3	2.9971	-0.23368	-0.09866	0.16813	0.23626	0.00227	0.10341
0.4	2.9971	-0.27762	-0.15530	0.24741	0.28069	0.00453	0.21840
0.5	2.9971	-0.31532	-0.24380	0.20506	0.31881	0.00754	0.32004
0.2	2.4914	-0.18702	-0.04944	-0.21574	0.18886	0.00092	0.40846
0.3	2.4914	-0.24522	-0.09043	0.16813	0.24763	0.00272	0.10341
0.4	2.4913	-0.29133	-0.14253	0.24741	0.29419	0.00542	0.21840
0.5	2.4913	-0.33089	-0.22447	0.20506	0.33414	0.00901	0.32004
0.2	2.0056	-0.19982	-0.04457	-0.18897	0.20153	0.00114	0.38594
0.3	2.0056	-0.26200	-0.08157	0.17299	0.26425	0.00336	0.11269
0.4	2.0057	-0.31126	-0.12874	0.24054	0.31394	0.00669	0.23615
0.5	2.0056	-0.35352	-0.20343	0.18331	0.35657	0.01113	0.33002
0.2	1.4855	-0.22205	-0.03858	-0.15815	0.22365	0.00153	0.36294
0.3	1.4855	-0.29114	-0.07067	0.17774	0.29325	0.00451	0.12486
0.4	1.4855	-0.34589	-0.11173	0.22810	0.34839	0.00899	0.25532
0.5	1.4856	-0.39285	-0.17730	0.15695	0.39569	0.01497	0.33480
0.2	0.9988	-0.25974	-0.03180	-0.11387	0.26125	0.00226	0.30488
0.3	0.9988	-0.34057	-0.05829	0.19688	0.34255	0.00668	0.15245
0.4	0.9989	-0.40461	-0.09229	0.19683	0.40696	0.01331	0.31161
0.5	0.9989	-0.45953	-0.14702	0.08526	0.46221	0.02215	0.35004
0.2	0.4986	-0.35239	-0.02259	-0.06307	0.35381	0.00451	0.27726
0.3	0.4986	-0.46205	-0.04144	0.19946	0.46392	0.01333	0.18552
0.4	0.4986	-0.54893	-0.06572	0.14826	0.55116	0.02656	0.32188
0.5	0.4986	-0.62346	-0.10513	0.05376	0.62600	0.04420	0.31879

Table E2.4 *Uncertainty contributions and result of speed of sound measurements in the CMM mixture at T = 273 K.*

p/MPa	$u/m\cdot s^{-1}$	$10^4\cdot\left(\sum_{i=1}^{4}\frac{2\pi f_i}{4\upsilon_i}\right)^2 u^2(a)\Big/m^2\cdot s^{-2}$	$10^6\cdot\sum_{i=1}^{4}\left(\frac{2\pi a}{4\upsilon_i}\right)^2 u^2(f_i)\Big/m^2\cdot s^{-2}$	$10^5\cdot u^2_{disp}(u)/m^2\cdot s^{-2}$	$10^2\cdot u(u)/m\cdot s^{-1}$
5.51	345.6945	0.9992	8.3269	5.3	1.3
4.99	346.5196	1.0040	7.7914	5.2	1.3
4.51	347.4617	1.0095	8.5249	4.9	1.3
4.01	348.6087	1.0162	2.0150	4.5	1.2
3.49	349.9270	1.0239	3.2245	4.2	1.2
3.00	351.3351	1.0321	4.9587	4.1	1.2
2.49	352.8903	1.0413	6.5194	3.9	1.2
2.01	354.4741	1.0506	3.2354	3.1	1.2
1.49	356.4315	1.0624	2.3122	2.4	1.2
1.00	358.1830	1.0728	24.0330	1.7	1.2
0.50	360.0148	1.0838	15.8317	0.68	1.1

Universidad de **Valladolid**

ESCUELA DE INGENIERÍAS INDUSTRIALES

DPTO. INGENIERÍA ENERGÉTICA Y FLUIDOMECÁNICA

TESIS DOCTORAL:

DESARROLLO DE UN TÉCNICA AVANZADA DE RESONANCIA ACÚSTICA EN GASES PARA LA DETERMINACIÓN DE PROPIEDADES Y CONSTANTES TERMODINÁMICAS DE IMPORTANCIA.

Presentada por

FERNANDO JOSÉ PÉREZ SANZ

para optar al grado de doctor por la universidad de Valladolid

Dirigida por:

Dr. JOSÉ JUAN SEGOVIA PURAS

Dra. MARÍA DEL CARMEN MARTÍN GONZALEZ

Valladolid, Octubre 2014

Agradecimientos

El autor quiere dedicar unas líneas para agradecer la colaboración en la elaboración de esta tesis a:

José Juan Segovia Puras y María del Carmen Martín Gonzalez, por ayudarme y dirigirme durante la experimentación y la redacción de la tesis, además de ayudarme dentro y fuera del laboratorio.

A todo el equipo del grupo de investigación Termocal, que siempre están dispuestos a ayudar, aportar una idea y tomarse un café para despejarse.

A Roberto Gavioso del INRiM, por toda su ayuda durante mi estancia en Turín, fue desde el principio más amigo que jefe.

A mis padres y mis hermanos, que queriendo o sin querer han ayudado a forjarme como investigador y como persona.

A Ana, por estar a mi lado y aguantarme durante todo este tiempo.

Y por último al ministerio de economía por proporcionarme el apoyo económico para realizar esta tesis.

ÍNDICE

Capítulo 1:

INTRODUCCIÓN Y OBJETIVOS

1.1 MOTIVACIÓN DEL ESTUDIO

A través de la determinación de la velocidad del sonido en gases se pueden obtener propiedades termodinámicas de dichos gases, se puede comparar los resultados con los predichos por ecuaciones de estado, medir constantes termodinámicas y otras aplicaciones.

En el caso de este estudio, las medidas de la velocidad del sonido en gases se utilizan para determinar propiedades termodinámicas y la definición del nuevo Kelvin. A continuación se presenta la definición de la unidad de temperatura y su escala, desde un punto de vista histórico, y asimismo se justifica la necesidad de estudiar fuentes de energía no convencionales.

1.1.1 Definición del nuevo kelvin

La humanidad ha utilizado unidades de medida desde la antigüedad, para informar de lugares de caza o recolección, limites de territorios…

Inicialmente estaban relacionadas con partes del cuerpo humano: pies, codos, pulgadas… o periodos de tiempo como estaciones, ciclos lunares, etc. Estas unidades empezaron a estandarizarse cuando la población empezó a negociar mercancías. Estas unidades eran principalmente de volumen, peso, longitud y superficie. La temperatura todavía no era importante aunque si eran conscientes de ella y de sus cambios. No obstante estas medidas eran muy subjetivas ya que no requerían mucha precisión.

El primer artefacto que se uso como termómetro llegó de la mano de Galileo en 1592. El primer termómetro moderno fue desarrollado por el duque de Toscana en 1614, con una configuración idéntica a las de hoy en día, un capilar unido a un bulbo lleno de alcohol; más tarde en 1716 Fahrenheit sustituyó el alcohol por mercurio.

Cuando se realizaron los primeros prototipos de metro en 1878, se fabricaron también dos termómetros de mercurio Estos termómetros se relacionaban con temperaturas termodinámicas gracias a termómetros de volumen constante utilizando hidrógeno y otros gases como fluido de trabajo. Entre 1884 y 1887 la Oficina Internacional de Pesos y Medidas (BIMP) a adoptó la escala de hidrógeno con temperatura de fusión y ebullición del agua como puntos fijos.

Desde este momento se empiezan a realizar y definir distintas escalas de temperatura que fueron evolucionando mediante cambios de los puntos fijos, rangos de medida e incluso cambiando la técnica y las herramientas empleadas; hasta llegar a la escala actual ITS-90.

Esta escala de temperatura establece el kelvin como la unidad de temperatura y lo define conforme al punto triple del agua, su límite inferior disminuye hasta 0.68 K y el superior queda abierto a la máxima medida posible por radiación. Los rangos en los que está dividida esta escala a veces se solapan pero ambas definiciones conllevan al mismo valor o a una diferencia despreciable.

Los cuatro rangos de la ITS-90 son:

- De 0.65 K a 5 K, definida mediante la presión de vapor de He^3 y He^4.
- De 3 K a 24.5561 K, termometría de gas en helio.
- De 13.8032 K a 961.78^{0}C, medido con resistencias de platino.
- Temperaturas mayores a 961.78^{0}C se miden mediante la ley de radiación de Planck.

Así mismo establece una serie de puntos fijos para la definición de la escala como se muestra en la figura 1.4 del manuscrito completo en inglés.

1.1.1.1 *Definición actual del kelvin, problemas y desacuerdos.*

Existen siete magnitudes fundamentales: tiempo, longitud, masa, corriente eléctrica, temperatura termodinámica, cantidad de sustancia e intensidad lumínica; con sus siete unidades correspondientes: segundo (s), metro (m), kilogramo (kg), amperio (A), kelvin (K), mol y candela (cd). De estas siete unidades, kg, A, K y mol se definen conforme prototipos o artefactos que no se pueden preservar inalterables en el tiempo y, por tanto, el valor de estas unidades varía.

Varios proyectos tratan de solucionar este problema cambiando la definición de dichas unidades, refiriéndose a constantes termofísicas como la velocidad de la luz en el vacío, el número de Avogadro, etc. y no a sustancias o artefactos. Por ello es muy importante determinar el valor de estas constantes con gran precisión para que también sean precisas las unidades.

La definición del kelvin depende del punto triple del agua como muestra la ecuación 1.1.

$$K = \frac{1}{273.16} T_{WTP} \tag{1.1}$$

De esta manera el kelvin depende de las propiedades del agua, las cuales pueden cambiar con el tiempo debido a contaminación con el envase. Además es necesaria una caracterización isotópica del agua, la cual debe ser igual a la estandarizada (Viena Standard Mean Ocean Water) o determinar el factor de corrección debido a esta diferencia.

Estos pequeños problemas se intentan evitar con una nueva definición del kelvin. El proyecto "New Determinations of the Boltzmann Constant" finiciado por Euramet, cuyo objetivo es la redeterminación de la constante de Boltzmann mediante al menos tres técnicas termométricas distintas. En él han participado distintas universidades y laboratorios nacionales de metrología de distintos países: PTB (Alemania), NPL (Gran Bretaña), INRiM (Italia), LNE-INM/Cnam (Francia), Universidad de Paris Norte, Segunda Universidad de Nápoles, la Universidad Politécnica de Milán.EL laboratorio TERMOCAL junto con el Centro Español de Metrología (CEM) también ha participado con la determinación de la constante mediante resonancia acústica.

Cuando se realice la nueva definición será importante introducirlo en la escala de temperaturas, para ello es importante entender cómo funciona la escala ITS-90. La cual se basa en los denominados puntos fijos como puntos de fusión, solidificación y puntos triples. Debido a la definición, toda la escala pivota alrededor del punto triple del agua, haciendo necesarias medidas de este punto para medidas de temperaturas muy altas o muy bajas. Para el cambio de escala motivado por la redefinición del kelvin, se ha iniciado un proyecto europeo "Implementing the new kelvin" donde de nuevo participa TERMOCAL en colaboración con el CEM y donde se medirán, mediante termometría acústica, los valores del punto triple del mercurio, el agua y los puntos de fusión del galio y el indio.

1.1.2 Determinación de propiedades termodinámicas de nuevos gases energéticos.

En este estudio se utiliza la técnica de resonancia acústica para determinar capacidades caloríficas a presión y volumen constante entre otras propiedades termodinámicas

Las actividades cotidianas de los seres humanos (ducharse, cocinar, transporte…) requieren energía para realizarse. Esta energía se obtiene de distintas fuentes. Las cuales han

ido cambiando a lo largo de la historia. Antes de la revolución industrial el uso de madera como fuente de energía causo la devastación de los bosques cercanos a las grandes ciudades. La aparición del carbón como combustible redujo el consumo de madera, su fácil extracción y alto contenido energético hacen que siga siendo muy utilizado actualmente. Otro ejemplo es el petróleo, que tomó importancia con la aparición del motor de combustión interna.

A día de hoy existen muchas y distintas fuentes de energía, pero la mayoría son combustibles fósiles como petróleo, carbón o gas natural. Estas fuentes no son renovables, como la solar, eólica… por lo que las reservas actuales se agotarán en un futuro. El desarrollo de la humanidad va ligado al consumo de energía y, por ello, el consumo y la producción de petróleo, carbón y gas han crecido en los últimos años. Las reservas de estos combustibles se agotaran en un futuro, a pesar del aumento de las reservas motivado por el progreso de las técnicas de extracción y tratamiento, así como el incremento de los precios de los combustibles, lo cual parece lo contrario al ver la figura 1.7. Este efecto es debido a que las reservas solo contabilizan yacimientos que es rentable explotar, y estos aumentan con el cómo se observa en la figura 1.8.

1.1.2.1 *Nuevos combustibles*

Debido a que los combustibles fósiles no son una fuente de energía renovable y a que están relacionados con problemas medioambientales como el calentamiento global y el efecto invernadero se tiende a sustituir por otros combustibles menos dañinos.

Los nuevos combustibles suelen generarse como subproductos de otros procesos como tratamientos biológicos, aunque también se está trabajando en un mejor aprovechamiento y eficiencia de los procesos ya empleados, como es la utilización de los humos de combustión de calderas de carbón que aún pueden ser aprovechados.

Los combustibles procedentes de procesos biológicos no aumentan la producción de CO_2 ya que entran en el ciclo del CO_2 y al proceder de fuentes renovables no hay riesgo de que se agoten.

1.1.2.2 *Importancia de las propiedades termodinámicas de los nuevos gases.*

Es necesario conocer las propiedades termodinámicas de los gases con los que se trabaja para mejorar la eficiencia de los procesos de transporte, almacenaje, producción, etc. Existen ecuaciones de estado que describen bien el comportamiento de estas mezclas de gases pero es necesario comprobar los valores no solo de la ecuación de estado, también propiedades

como las capacidades caloríficas. Conocidos estos datos los procesos de diseño se simplificarán y ajustarán para dar mayor rendimiento.

1.2 OBJETIVOS

Los objetivos de esta tesis se describen a continuación:

Determinación del valor de la constante de Boltzmann con una incertidumbre tan baja como sea posible, como parte del proyecto europeo "New Determination of the Boltzmann's Constant", para ello se han de realizar algunas mejoras en el resonador acústico esférico que será utilizado como termómetro acústico de gases.

Adaptación del equipo para la caracterización termodinámica de mezclas gaseosas. La técnica de resonancia acústica se puede utilizar también para la caracterización de mezclas gaseosas. Este objetivo se puede cumplir utilizando una cavidad resonante diferente que debe caracterizarse calibrando su radio interno a diferentes presiones.

Determinación de la velocidad del sonido en mezclas gaseosas para la obtención del coeficiente adiabático, las capacidades caloríficas y los coeficientes del virial acústicos. En este trabajo se quieren medir algunos parámetros para la caracterización termodinámica de mezclas cuyos componentes suelen estar presentes en gases energéticos no convencionales. Se necesitan los datos de este tipo de mezclas para predecir y estimar el comportamiento de mezclas más complejas. También se medirán mezclas sintéticas de gases no convencionales como metano de mina de carbón (gas grisú).

Evaluación de las ecuaciones de estado de referencia utilizadas actualmente para el gas natural. Todos los datos recogidos en este estudio se compararán con la ecuación de estado GERG-2008, esta ecuación es comúnmente empleada en el ámbito del gas natural. Se comprobará si es válida para las mezclas estudiadas y los datos obtenidos pasarán a formar parte de la base de datos de propiedades termodinámicas.

Capítulo 2:

FUNDAMENTO TEÓRICO

2.1 INTRODUCCIÓN

La relación de las propiedades termodinámicas y la constante de Boltzmann con la velocidad del sonido en el gas se explica con la teoría cinética. La energía cinética de las moléculas se relaciona con la constante de Boltzmann como indica la ecuación 2.1, y la velocidad media de las moléculas se puede relacionar con la velocidad del sonido como muestra la ecuación 2.2. Al combinar estas dos se obtiene la ecuación 2.3, y está se puede modificar para dar la ecuación 2.4 utilizando la definición de la constante de Boltzmann.

Las capacidades caloríficas se calculan mediante la relación de Mayer (2.5) a partir del coeficiente adiabático.

El problema de la teoría cinética es que solo es válida para gases ideales. Para solventar este inconveniente en este trabajo se hace una extrapolación a presión cero, ya que los gases se comportan como ideales a presiones próximas a cero. Para ello se utiliza una ecuación del virial acústica manteniendo la temperatura constante. Esta ecuación puede ser en función de la densidad (2.6-a) o la presión (2.6-b) del gas. Los coeficientes de ambas ecuaciones están relacionados como se muestra en 2.7 y 2.8. A partir del valor de la coordenada en el origen A_0 (2.9) se puede calcular la constante de Boltzmann si se conoce la masa molar y el coeficiente adiabático como gas perfecto del gas; o con la masa molar se puede determinar el coeficiente adiabático.

En el estudio de la constante de Boltzmann se utiliza argón cuyas propiedades son bien conocidas.

2.2 RESONANCIA ACÚSTICA.

No se mide directamente la velocidad del sonido si no la frecuencia de resonancia en la cavidad y se calcula a partir de esta conociendo el radio interno de resonador, como se indica en la ecuación 2.10.

Esta ecuación es válida solo en condiciones ideales, donde no existe capa límite térmica, la densidad del gas no varía por el paso de la onda de sonido, no hay acoplamiento de la superficie interna del resonador con la vibración acústica ni existen tubos que modifiquen el volumen de resonancia. Todas estas no idealidades deben corregirse.

Otro parámetro importante es la anchura a la semialtura, cuyas contribuciones vienen dadas por estas no-idealidades. Es necesario calcularlas ya que la diferencia entre el valor

teórico y en valor experimental es un factor que se ha de tener en cuenta para el cálculo de incertidumbre

2.3 RESONANCIA MAGNÉTICA

El radio interno del resonador es una variable muy importante que debe determinarse con precisión ya que influye en la incertidumbre con la que se calcula la velocidad del sonido y las propiedades derivadas de ésta. Tiene especial interés para el cálculo de la constante de Boltzmann ya que requiere una muy baja incertidumbre.

Para este cálculo se han descrito y desarrollado múltiples procesos, como picnometría con mercurio (la cual no se realiza actualmente por los problemas que conlleva el uso de mercurio), a través de la ecuación de estado de un gas bien conocido (técnica que se utiliza en este trabajo para el cálculo de propiedades termodinámicas) o la resonancia de microondas que proporciona la precisión requerida para la determinación de la constante de Boltzmann.

Esta técnica es muy parecida a la resonancia acústica, salvo que al utilizarse modos de resonancia degenerados los autovalores seleccionados son distintos y la velocidad que se emplea en este caso es la de la luz en el medio calculada mediante la ecuación de Maxwell (2.27).

La resonancia electromagnética también necesita de ciertas correcciones por no idealidades. La primera es debida a que la superficie interna del resonador no tiene una conductividad infinita y la segunda es debida a que esta superficie no es perfectamente esférica (en el caso de un resonador desalineado no hay estudios para calcular esta corrección).

Además de estas correcciones debidas al modelo teórico es necesario corregir las medidas experimentales en presión y temperatura por las pequeñas diferencias entre las condiciones de medida y las condiciones deseadas, para ello se calcula un factor de corrección (2.28).

Capítulo 3:

TÉCNICA EXPERIMENTAL

3.1 TÉCNICA EXPERIMENTAL

La medida de la velocidad del sonido es una técnica de alta precisión que requiere un preciso control de presión y temperatura además de técnicas para la determinación del radio.

Los aparatos y procesos para llevar a cabo este estudio se describen a continuación.

3.1.1 Resonador

En este estudio se utilizaron dos resonadores, ambos consisten en dos semiesferas unidas por el ecuador, uno mediante soldadura (resonador A) y el otro con tornillos alrededor de la unión ecuatorial (resonador B).

El resonador A se utiliza para medir propiedades termodinámicas, el B para la determinación de la constante de Boltzmann. Esto es así ya que el resonador B está diseñado para realizar resonancia acústica y de microondas al mismo tiempo, además las dos semiesferas pueden desalinearse en mayor o menor cantidad para obtener mejor definición de los picos de resonancia electromagnética.

El resonador utilizado se acopla a una estructura en la cual hay establecidos una serie de sistemas de control de presión y temperatura.

3.1.2 Medida y control de la temperatura.

La temperatura del resonador se mide con dos resistencias Pt-25 CSPRT Rosemount 162D mediante un puente ASLF18 que mide variaciones de hasta 0.25mK. Las resistencias se localizan en la superficie externa del resonador separadas lo más posible para distinguir posibles gradientes de temperatura. Estos termómetros fueron calibrados en las instalaciones de calibración de TERMOCAL, los resultados pueden verse en las tablas 3.1 y 3.2.

El control de temperatura se hace mediante varios dispositivos. Todo el dispositivo se encuentra sumergido en un baño que mantiene la temperatura a unos 10 ó 20 grados por debajo de la temperatura de trabajo del resonador. De esta forma el resto de controladores solo se usa para aumentar la temperatura.

Existen tres sistemas para aumentar la temperatura, el primero y más directo está situado en el bloque de cobre que sujeta el resonador donde, mediante una termoresistencia Pt-25 y una resistencia de cobre, se controla la temperatura de este bloque, calentando mediante conducción el resonador.

Si solo existiese este control se establecería un gradiente entre la parte superior e inferior del resonador. Por ello se realizan otros dos controles, en los que se establece un flujo de calor por radiación desde las paredes y el fondo de la vasija en la que está el resonador, muy similares al situado en bloque de cobre.

Para evitar que exista flujo por convección, tanto el resonador como la vasija que controla el flujo de radiación se introducen en una segunda vasija en la que se produce un alto vacio gracias a dos bombas en serie, (Bomba centrifuga Leybold Trivac B8B y una bomba turbomolecular Leybold Turbovac SL300). Esta vasija está sellada con una junta de indio e inmersa en el baño termostático de etanol dentro de un vaso dewar que es enfriado gracias a un equipo Julabo FP89

Las termorresistencias para el control de temperatura en el bloque de cobre, el lateral y el fondo de la vasija de radiación se calibraron en la instalaciones de TERMOCAL, el resultado de estas calibraciones se pueden ver en las tablas 3.3, 3.4 y 3.5.

3.1.3 Medida y control de la presión.

La presión se mide mediante dos transductores de presión marca Paroscientific, el modelo 200 para presiones de 2 a 20 MPa y el modelo 20 para presiones inferiores a 2MPa. Al igual que los termómetros fueron calibrados en las instalaciones de TERMOCAL y los resultados de calibración se pueden ver en las tablas 3.6 y 3.7.

El control de la presión se realiza mediante un conjunto de cilindro y pistón con el que se varía el volumen del conjunto y por tanto su presión. Este cilindro está dispuesto en paralelo con otro de mayor volumen que se utiliza para subir la presión del sistema manualmente en caso de que la presión de la botella sea insuficiente para alcanzar la presión requerida.

3.1.4 Medida de resonancia de microondas.

Para la resonancia electromagnética se desarrollaron unas antenas de hilo de cobre OFHC de 0.125 mm de diámetro en forma de solenoide.

Para determinar las frecuencias de resonancia es necesario un analizador de redes “Network Analyzer Agilent N5230C PNA-L” el cual es capaz de generar y medir frecuencias de hasta 13.5 GHz.

3.2 PROCEDIMIENTO EXPERIMENTAL.

El procedimiento completo lleva varias partes. El primer proceso será determinar el radio del resonador ya que es un parámetro requerido para las demás mediciones.

3.2.1 Determinación del radio usando resonancia de microondas.

La determinación del radio por microondas solo es necesaria para la medida de la constante de Boltzmann, y se ha realizado para caracterizar dimensionalmente el resonador B. Este proyecto solo requiere medidas a 273.16 K y en el rango de presiones de 0 a 0.9 MPa.

Para empezar se realiza vacio dentro del resonador eliminando la presencia de gases no deseados. Se introduce un poco de argón en el circuito y se hace vacio otra vez para desplazar y eliminar las posibles trazas de gases, este proceso se repite varias veces. Después se llena hasta la presión deseada 0.9 MPa, ajustando si es necesario con el sistema de cilindro y pistón, se deja que alcance la temperatura y si es necesario se corrige presión de nuevo, este proceso también se repetirá las veces necesarias. Si fuese necesario se ajustarán las temperaturas de los controladores de temperatura descritos anteriormente para disminuir el gradiente de temperatura si lo hubiese. Todo este proceso se repite constantemente para eliminar las posibles variaciones con respecto a las condiciones deseadas.

Una vez se tienen las condiciones se realiza la medición de los modos de resonancia electromagnética, es una técnica muy compleja en la que es necesario realizar la medición varias veces ya que el valor de los picos puede variar ligeramente según los parámetros iniciales.

Tras tener las medidas de los 5 modos se reduce la presión para medir el siguiente punto, es necesario realizar los ajustes necesarios de presión y temperatura como se ha indicado antes. Se realiza esto para cada presión hasta alcanzar 0.1 MPa.

3.2.2 Resonancia acústica.

También se determina el radio mediante resonancia acústica, en este caso se utiliza para medir propiedades termodinámicas empleando el resonador A. Pero ahora se necesita conocer el radio en el intervalo de presiones y temperaturas a los que se realizarán las medidas de las mezclas.

El procedimiento es muy parecido al de resonancia de microondas. Primero se llena el resonador con un gas del que se conoce bien su ecuación de estado, en este caso argón, hasta que se alcanzan 20 MPa. Se ajusta la presión y la temperatura del mismo modo que en la técnica de microondas. Se hace un barrido de los 4 modos de resonancia para localizar, sin

mucha precisión, la frecuencia entorno a la que están los picos de resonancia y después se mide el pico de resonancia de cada modo de manera más precisa.

Para hacer esto se requieren dos transductores capacitivos, uno emisor y otro receptor unidos a un sintetizador (HP 3325B) y un analizador (SRS SR850 DPS). Además de dos programas para el barrido y detección de las frecuencias de resonancia.

Tras medir los 4 picos, se reduce la presión al siguiente punto y se repite el proceso. Se redujo la presión en escalones de 1 MPa hasta 1MPa y una última medida se tomó a 0.1 MPa.

Al terminar una isoterma se repite de nuevo todo el proceso a otra temperatura.

Cuando se realizan medidas en otros gases el proceso es el mismo al descrito hasta ahora cambiando el gas en el resonador y las condiciones de presión a las que se realizan las medidas siendo distintas para cada caso.

3.3 ANÁLISIS DE INCERTIDUMBRES.

Se realizaron dos estudios distintos uno para la determinación de la constante de Boltzmann y otro para la determinación de las propiedades de los gases.

3.3.1 Análisis de incertidumbres para la constante de Boltzmann.

Este análisis se realizó de acuerdo al realizado por Roberto Gavioso en el INRiM, de esta forma los resultados pueden ser comparados con los realizados por otros laboratorios implicados en este proyecto.

Las contribuciones a la incertidumbre se separan en dos tipos aquellas relacionadas con la incertidumbre de las medidas acústicas y todas las demás, como la masa molar del gas, temperatura y la constante de Avogadro. Todos tienen un coeficiente de sensibilidad de 1.

La incertidumbre relativa de la constante de Avogadro se obtiene de la bibliografía $u(N_A)=4.49\cdot10^{-8}$.

La incertidumbre debida a la masa molar se calcula a partir de los porcentajes de impurezas descritos por el proveedor, con un coeficiente de sensibilidad de 1.

Por último, la temperatura cuyo coeficiente de sensibilidad también es de uno se calcula como suma de incertidumbres de las contribuciones de calibración, gradiente y dispersión de las medidas.

El otro grupo de contribuciones (medidas acústicas) se divide a su vez en dos, las relacionadas con las propias medidas acústicas y aquellas debidas a la determinación del radio.

Las dos contribuciones principales debidas a la determinación del radio tienen sensibilidad de 2 y son las causadas por las diferencias entre la semi-anchura del pico de resonancia teórico y el real, y por la dispersión de modos de resonancia medidos.

Estas dos últimas contribuciones se dan del mismo modo en el caso de resonancia acústica.

Y la última contribución, la causada por la extrapolación a presión cero, se hace utilizando distintos modelos de ajuste y observando los cambios que este produce en el valor independiente de la presión.

3.3.2 Incertidumbre de las propiedades de mezclas de gases.

La primera propiedad obtenida es el coeficiente adiabático como gas ideal. Las fuentes de incertidumbre son la incertidumbre en la masa molar, en la constante de los gases ideales, en la medida de la temperatura y en el factor de extrapolación a presión cero.

La incertidumbre en la masa molar se hace mediante suma de incertidumbres de fracción molar de cada uno de los componentes. Para la constante de los gases ideales se utilizan datos bibliográficos, $u(R)=0.0000075\ J\cdot mol^{-1}K^{-1}$. La incertidumbre en temperatura se obtiene como en el caso anterior.

El caso de la extrapolación a cero el cálculo es más complejo. Se realiza una simulación de Montecarlo introduciendo los distintos valores de velocidad del sonido, presión y sus respectivas incertidumbres, se realizan varias simulaciones y se obtiene la incertidumbre del término independiente de la presión.

Para obtener la incertidumbre de los datos de velocidad del sonido es necesario tener en cuenta tres contribuciones: la dispersión de los modos, la incertidumbre en la frecuencia de los modos de resonancia y la incertidumbre en la determinación del radio.

La primera se calcula como la desviación estándar de los resultados obtenidos con cada modo. La incertidumbre en la determinación de la frecuencia es obtenida junto con la medida

y, por último, el radio interno. Al determinarse éste mediante resonancia acústica necesita un análisis más profundo.

Las contribuciones para la determinación del radio interno del resonador son similares a las de la velocidad del sonido, una componente causada por la dispersión de los modos, otra relacionada con la incertidumbre en la medida de la frecuencia y la que en este caso es distinta la debida a la velocidad del sonido determinada por la ecuación de estado utilizada y obtenida de la bibliografía.

Las capacidades caloríficas son calculadas a partir de la ecuación de Mayer, por lo que vuelve a influir la incertidumbre de la constante de los gases ideales y de la constante adiabática calculada anteriormente.

Por último, se calculan los coeficientes del virial acústicos. Estos coeficientes se dan en función de la densidad, y el ajuste desarrollado en este estudio es en función de la presión. Pero estos coeficientes están relacionados como se muestra en las ecuaciones 3.24 y 3.25. Para calcular las incertidumbres de estos parámetros son necesarios los datos obtenidos de la simulación de Montecarlo y, obviamente, vuelven a influir las incertidumbres de la constante de los gases ideales y la temperatura.

Capítulo 4:

RESULTADOS

Todos los datos medidos o calculados en este estudio están disponibles en los anexos. No obstante en los capítulos del 4 al 7 de la versión completa en inglés, se presentan una pequeña sección de los datos para entender las tendencias.

El capítulo 4 muestra las medidas de resonancia acústica y electromagnética realizadas así como las correcciones a estas frecuencias y las propiedades necesarias para estas correcciones, los resultados de medidas de radios y las velocidades del sonido. Por último, los cálculos necesarios para la determinación de la constante de Boltzmann y su incertidumbre.

El capítulo 5 muestra una parte de las medidas tomadas para la determinación del radio interno del resonador, es decir, las medidas de las frecuencias de resonancia acústica, las correcciones necesarias a esta frecuencia así como parámetros que estas correcciones requerían para ser calculadas. También se muestran los distintos valores de radio obtenidos a las distintas presiones y temperaturas así como los valores de los modelos cuadráticos que representan el radio a las distintas temperaturas. Por último, este capítulo presenta los cálculos de incertidumbre de estas medidas.

En el capítulo 6 se muestran parte de los resultados obtenidos para dos mezclas CO + N_2 (x_{CO}=0.05 + x_{N2}=0.95) y . (x_{CO}=0.10 + x_{N2}=0.90). Estos resultados comprenden los valores medidos de frecuencia de resonancia acústica, las correcciones que se aplican y también los parámetros que se han utilizado para calcular las correcciones, los valores obtenidos de velocidad del sonido, los parámetros del modelo virial acústico desarrollado, una comparación de la ecuación de estado GERG-2008 con el modelo desarrollado y con los datos experimentales, los valores del coeficiente adiabático, las capacidades caloríficas a presión y volumen constante y los coeficientes del virial acústico. Todos estos datos obtenidos se exponen para todo el rango de presiones medido a las dos temperaturas observadas. El capítulo se cierra con los cálculos de incertidumbres de todos estos datos y una discusión de los resultados obtenidos.

En el capítulo 7, utilizando la misma estructura que en el anterior se presentan los resultados para una mezcla sintética de metano de mina de carbón (gas grisú) de diez componentes.

Capítulo 5:

CONCLUSIONES

1. Se llevó a cabo una mejora de una técnica avanzada para la medida de la velocidad del sonido para la determinación de la constante de Boltzmann. Se incorporaron nuevas antenas de microondas en un nuevo resonador desalineado. Estas antenas se conectaban a un analizador de redes que cubre un rango de 0 a 13.5 GHz, para medir su radio interno con baja incertidumbre.

2. Se añadieron filtros cromatográficos y se cambiaron las tuberías previas a la entrada del resonador para purificar el argón, eliminando agua, oxígeno y asegurando que la concentración de monóxido de carbono, dióxido de carbono, hidrógeno y compuestos orgánicos fuera inferior a la especificada.

3. Se diseñó un nuevo preamplificador, más pequeño que el anterior, que redujo el ruido y mejoró la calidad de la señal. Con todas estas mejoras se determinó la constante de Boltzmann, k_B=1.380650·10^{-23} J·K^{-1}, con una incertidumbre relativa de ± 20 10^{-6} J·K^{-1}/J·K^{-1}. La diferencia con el codata de 2010 es de -5.3 10^{-6} J·K^{-1}/J·K^{-1}

4. Se utilizó una cavidad esférica diferente para determinación de algunas propiedades termodinámicas como el coeficiente adiabático, las capacidades caloríficas y los coeficientes del virial acústicos, a partir de lavelocidad del sonido para distintas mezclas gaseosas.

5. Se caracterizó el resonador acústico utilizando argón como gas de referencia para determinar su radio interno a diferentes presiones y temperaturas. La incertidumbre relativa estándar fue menor de ± 100·10^{-6} m·m^{-1}.

6. Se utilizaron distintas resistencias de referencia en el puente de resistencias, permitiendo así trabajar a mayores temperaturas, el uso de un nuevo equipo de refrigeración permitió trabajar a temperaturas de -40^{0}C. Se añadió un cilindro compresor que permite aumentar la presión del resonador por encima de la proporcionada por la botella.

7. Se midió la velocidad del sonido de las mezclas gaseosas (5%CO + 95%N_2) y (10%CO + 90%N_2) a dos temperaturas T = 273.16 K y T = 325.00 K comenzando a un presión de 10 MPa y disminuyendo hasta la presión de 0.1 MPa. Las principales fuentes de incertidumbre son debidas a la incertidumbre en la determinación del radio y a la dispersión de los diferentes modos acústicos medidos. La incertidumbre relativa estándar de la medidas de velocidad del sonido es mejor de ± 150 10^{-6} m·s^{-1}/m·s^{-1}

8. Se determinó el valor y las incertidumbres de otras propiedades termodinámicas a partir de los datos de la velocidad del sonido para dichas mezclas. Las incertidumbres de estas propiedades se calcularon mediante el método de Monte Carlo. Una de estas propiedades es el coeficiente adiabático cuya incertidumbre es menor a ± 300 10^{-6} para ambas temperaturas. Las otras propiedades y sus incertidumbres dependen del valor y de la incertidumbre del coeficiente adiabático. El coeficiente de sensibilidad de las capacidades caloríficas respecto coeficiente adiabático hace que aumenten sus incertidumbres; estando sus incertidumbres relativas estándar alrededor de ± 1000·10^{-6} J·$mol^{-1}K^{-1}$/J·mol^{-1} K^{-1}.También se obtuvieron el segundo y tercer coeficientes del virial acústicos con incertidumbres relativas estándar menores al ±2.5%.

9. Se realizaron medidas en una mezcla sintética de metano de mina de carbón (gas grisú)de 10 componentes a dos temperaturas T = 250 K y T = 273.16 K hasta presiones de p = 8 MPa. La incertidumbre relativa estándar de las medidas de velocidad del sonido es mejor de ± 110 10^{-6} m·s^{-1}/m·s^{-1}. La masa molar tiene un peso importante en el cálculo de incertidumbre debido a la complejidad de la muestra. La incertidumbre relativa estándar del coeficiente adiabático es menor a ± 380 10^{-6} para ambas temperaturas. Las capacidades caloríficas a presión y temperatura constantes tienen una incertidumbre relativa estándar en torno a ± 1500 10^{-6} J·$mol^{-1}K^{-1}$/J·mol^{-1} K^{-1}. También se calcularon el segundo y tercer coeficiente del virial acústico con una incertidumbre relativa estándar inferior al ± 1.3%.

10. Se comparó el comportamiento de todas las mezclas con el estimado por la ecuación de estado GERG-2008. Se observó una buena concordancia entre los valores experimentales de velocidad del sonido y los obtenidos por esta ecuación. La desviación relativa de velocidad del sonido de las mezclas de CO y N_2 es siempre menor de ± 250 10^{-6} m·s^{-1}/m·s^{-1}. En el caso de la mezcla sintética de metano de mina de carbón las desviaciones relativas de la velocidad del sonido no superaban los ± 900 10^{-6} m·s^{-1}/m·s^{-1}